

# **Synthesis of mackinawite and tochilinite analogues and investigations on carbon fixation in a prebiotic context**

## **Dissertation**

**zur Erlangung des akademischen Grades doctor rerum naturalium**

**(Dr. rer. Nat.)**

**vorgelegt dem Rat der Chemisch-Geowissenschaftlichen Fakultät der  
Friedrich-Schiller-Universität Jena**

**von M.Sc. Robert Bolney**

**geboren am 05.09.1989 in Nordhausen**

**Gutachter:**

**1. Prof. Dr. Christian Robl**, Friedrich-Schiller-Universität Jena,  
Chemisch-Geowissenschaftliche Fakultät, Institut für Anorganische und  
Analytische Chemie, Humboldtstrasse 8, 07743 Jena

**2. Prof. Dr. Wolfgang Weigand**, Friedrich-Schiller-Universität Jena,  
Chemisch-Geowissenschaftliche Fakultät, Institut für Anorganische und  
Analytische Chemie, Humboldtstrasse 8, 07743 Jena

**3. Prof. Dr. Thomas Schleid**, Universität Stuttgart, Chemische Fakultät,  
Institut für Anorganische Chemie, Pfaffenwaldring 55, 70569 Stuttgart

**Tag der Verteidigung: 19.01.2022**

## **Selbstständigkeitserklärung**

Ich erkläre, dass ich die vorliegende Arbeit selbständig und unter Verwendung der angegebenen Hilfsmittel, persönlichen Mitteilungen und Quellen angefertigt habe.

Jena, 01.06.2021

Robert Bolney

## Abstract

This thesis was created with the motivation to increase the knowledge about the possible impact of iron sulfides on the prebiotic chemistry. The long-known reactivity of elemental iron and elemental sulfur was used to synthesize the metastable iron sulfide mackinawite with remarkable purity. This work is the first to investigate the reactivity between transition metals and sulfur under mild conditions as a means for metal sulfide formation so far and maybe mark the beginning of an increasing interest in transition metal sulfides on the early earth's surface. Experiments with nickel, copper but first and foremost iron gave additional information on the course of this reaction and the solid phases that are accessible. This new approach offered the possibility to investigate the influence of different salts on the mackinawite formation and a new behavior of mackinawite nanoparticles in aqueous suspension was observed. If mackinawite is synthesized in a saline solution, iron ions are released as the sodium ions are able to replace them on the particle's surface. Deeper investigations of this phenomenon led to the development of a new model for the mackinawite-solution-interaction which is able to explain some inconsistent observations reported in the literature. This model not only explains how sodium ions can replace iron ions in mackinawite particles, but also some controversial issues regarding its interlayer spacing and surface charge. The evaluation of the scientific literature regarding the composition of the early earth's surface led to the conclusion that the formation of transition metal sulfides from elemental metals and elemental sulfur far off from deep sea vents is prebiotically plausible and could have been significant. As great amounts of different transition metals have been delivered by cosmic impacts, a broad spectrum of transition metal sulfides could have been available on the early earth's surface to an extent, that is much greater than assumed so far. The characteristics of the mackinawite particles resemble those of precipitated mackinawite which has been vastly discussed in regard of hydrothermal vents. The dried mackinawite powder is highly pyrophoric but cautious oxidation of its surface is a suitable way to deactivate it and preserve its structure. The freshly formed and carefully oxidized mackinawite still shows a very small fraction of  $\text{Fe}^{3+}$  in Mößbauer analysis.

As reported multiple times over the last 30 years, iron sulfides and especially mackinawite are expected to have played a role in prebiotic carbon fixation. This view is mainly supported by the frequent appearance of iron sulfide clusters in active sites of modern redox-

enzymes like nitrogenases. Mackinawite has not been studied for the activation and/or reduction of CO<sub>2</sub>. Our experiments show that the reduction of adsorbed carbonate was coupled to the oxidation of mackinawite that occurred at a temperature around 160 °C. The oxidation products are mainly greigite accompanied by small amounts of magnetite and sulfur. Volatile reduction products were determined by GC-MS analysis and mostly contain methane thiol but also C-C-coupled sulfur-containing compounds.

Tochilinite is a layered hybrid form of mackinawite that also contains layers of hydroxides with a brucite-like structure. Mixed layer sulfides like tochilinite may have also been much more abundant on the early earth than today. Nowadays, tochilinite is mainly found in meteorites and rarely occurs at sulfide ore deposits. This work shows, that tochilinite forms from nanoparticulate mackinawite in basic environments rich in di- and trivalent metal ions like Mg<sup>2+</sup> and Al<sup>3+</sup>. To investigate their catalytic potential, three different well defined tochilinite analogues were synthesized that differ in their structure, composition and stability. Novel tochilinite syntheses were established that use hydrothermal conditions and carefully chosen starting materials to kinetically control the concentrations of the involved solutes. The proper characterization of these misfit layered materials is challenging, which is why the syntheses had to be optimized to lead to pure tochilinite samples. In this regard, the side products of the reaction systems used were investigated thoroughly and conditions/methods established for their suppression or removal. Mößbauer and compositional data show that the compositions of the obtained materials fit well to natural tochilinite. Powder diffraction and TEM/SEM data also support a tochilinite-like structure. As tochilinite is much more stable than mackinawite, high temperature Fischer-Tropsch-type reactions were carried out with the most stable tochilinite analogue for CO<sub>2</sub> reduction. These experiments show that the material is able to activate CO<sub>2</sub> and H<sub>2</sub> and catalyze the formation of typical Fischer-Tropsch products like alcohols and long chain alkanes at temperatures above 200 °C. The material used partially decomposed at these temperatures leading to the formation of magnetite, magnesioferrite and pyrrhotite. This work underlines the potential role of iron sulfides for prebiotic carbon fixation and reduction reactions in general. Even if the formation of iron sulfides from elemental iron and sulfur may be rare, it still could have been significant in local areas.

## Zusammenfassung

In dieser Arbeit wurde der mögliche Einfluss von Eisensulfiden auf die präbiotische Chemie und die Entstehung des Lebens untersucht. Die bereits seit mehreren Hundert Jahren bekannte Reaktion zwischen Eisen und Schwefel wurde weiter erforscht, was zur Etablierung der Synthese von Mackinawit-Nanopartikeln aus den Elementen führte. Damit ist diese Arbeit die erste, die die Mackinawitsynthese aus den Elementen ausführlich beschreibt. Die Charakteristika der Partikel ähneln denen von gefällttem Eisensulfid in Bezug auf Größe und Struktur. Unter Ausschluss von Sauerstoff getrockneter Mackinawit ist sehr pyrophor und es konnte gezeigt werden, dass die vorsichtige Oxidation der Oberfläche zur Stabilisierung der Partikel führt und dennoch der Anteil an  $\text{Fe}^{3+}$  in den Partikeln relativ klein bleibt. Die Synthese von Mackinawit aus den Elementen ermöglichte die Untersuchung des Einflusses der umgebenden Lösung auf die entstehenden Partikel. Diese zeigte, dass die Zugabe von NaCl zu einer Mackinawitsuspension zum Anstieg der Konzentration an freien Eisenionen führt. Eingehendere Untersuchungen dieses Phänomens führten zur Entwicklung eines neuen Modells zur Beschreibung der Wechselwirkungen zwischen Mackinawit und der umgebenden Lösung das in der Lage ist, Unstimmigkeiten in bisherigen Veröffentlichungen bezüglich der Partikeleigenschaften von gefällttem Mackinawit zu erklären. Untersuchungen der Reaktivität anderer Metalle gegenüber Schwefel unter den gleichen Bedingungen haben gezeigt, dass weitere Sulfide wie beispielsweise CuS, NiS und  $\text{CuFeS}_2$  aus den Elementen herstellbar sind. Die Evaluierung der Fachliteratur zur Zusammensetzung der Oberfläche der frühen Erde und dem Eintrag von elementaren Metallen durch Meteorite lässt den Schluss zu, dass die Bildung von Übergangsmetallsulfiden auf der Erdoberfläche sehr wahrscheinlich ist. Im Kontext der präbiotischen Chemie wurde die Reaktivität von Eisen- und Nickelsulfiden bisher hauptsächlich für hydrothermale Umgebungen diskutiert. Es ist zu erwarten, dass das Vorhandensein signifikanter Mengen dieser Sulfide auf der Erdoberfläche in kommenden Arbeiten zur präbiotischen Kohlenstofffixierung berücksichtigt wird. Eisensulfide wurden innerhalb der letzten 30 Jahre häufiger als potentielle präbiotische Katalysatoren diskutiert, da Eisensulfidcluster in den aktiven Zentren von redox-aktiven Enzymen wie der Nitrogenase vorkommen. Reduktionsexperimente mit Mackinawit wurden jedoch bisher nicht mit dem Ziel der Kohlenstofffixierung durchgeführt. Die Experimente in dieser Arbeit zeigen, dass  $\text{CO}_2$  Gas bzw. gelöste Carbonate ohne Zusatz eines Elektronendonors

an Mackinawit reduziert werden können. Die Reduktion adsorbierter Carbonate fand bei einer Temperatur von ca. 160 °C statt, wobei sich Greigit, Magnetit und Spuren von elementarem Schwefel bildeten. Die leichtflüchtigen Reaktionsprodukte wurden mittels GC-MS analysiert und es stellte sich heraus, dass Methanthiol mit Abstand am häufigsten auftrat, aber es wurden auch C-C-verknüpfte Produkte gefunden.

Tochilinit ist ein Schichtmineral, das neben mackinawitartigen auch brucitartige Schichten enthält. Komplexe Schichtminerale wie Tochilinit waren auf der frühen Erdoberfläche wahrscheinlich häufiger anzutreffen, als es heutzutage der Fall ist, denn sie kommen vorrangig in Meteoriten und selten in Sulfidlagerstätten vor. Die Ergebnisse in dieser Arbeit zeigen, dass sich Tochilinit aus Mackinawit-Nanopartikeln in basischer Umgebung bilden kann, wobei die Zusammensetzung von den vorhandenen Konzentrationen verschiedener Metallionen wie  $Mg^{2+}$  und  $Al^{3+}$  abhängt. Zur Untersuchung des katalytischen Potentials dieser Minerale, wurden Proben mit verschiedenen Zusammensetzungen und Reaktivitäten hergestellt und charakterisiert. Für die Charakterisierung sind verlässliche Ergebnisse aus der Elementaranalyse und der Mößbauerspektroskopie von entscheidender Bedeutung. Dazu mussten zunächst Methoden entwickelt werden, die die Synthese von Tochilinit ohne signifikante Mengen von Verunreinigungen ermöglichen. Durch die Kontrolle der Konzentrationen der gelösten Ionen und dem nachträglichen Entfernen von magnetischem Material konnten sehr saubere Proben erhalten werden. Die ermittelten Zusammensetzungen entsprechen den zu erwarteten Werten bei Annahme einer Tochilinitstruktur. TEM- und REM-Aufnahmen der synthetisierten Tochilinitproben zeigen sehr große Ähnlichkeiten zu Aufnahmen früherer synthetischer Arbeiten. Da Tochilinit thermisch stabiler als Mackinawit ist und als Katalysator fungieren könnte, wurden Reduktionsexperimente bei höheren Temperaturen durchgeführt. In einer Atmosphäre aus  $CO_2$  Gas und  $H_2$  Gas konnten oberhalb von 200 °C Produkte wie Methanol, Ethanol und langkettige Alkane gefunden werden, wie sie auch aus Fischer-Tropsch-Reaktionen erhalten werden. Die Tochilinitproben zersetzten sich bei den verwendeten Temperaturen teilweise wobei die zu erwartenden Zerfallsprodukte Magnetit bzw. Magnesioferrit und Pyhrotin gefunden wurden. Diese Arbeit unterstreicht die präbiotische Relevanz von Eisensulfidmineralen, in dem sie einen bisher unbeachteten Bildungsweg beschreibt und das Potential zur Kohlenstofffixierung aufzeigt.

## Acknowledgements

To work in the field of prebiotic chemistry on a rather unexplored topic felt like being on a roller coaster with many ups and downs without knowing what waits behind the next turn. Many experiments have been carried out and many ideas have been developed, some of them were misleading, but some indeed led to a deeper understanding of iron sulfide and the origin-of-life chemistry. I want to thank Prof. Dr. Robl for giving me the opportunity to work on this fascinating topic and to let me find my way and take my time. I also want to thank Prof. Dr. Weigand for severe support and for occasionally letting me be part of his group (here I have to refer to the yearly Schrottwichteln event at the Christmas party and of course the trips to Singen and Seon). In this regard, I also thank the whole Weigand group for letting me be part in their ranks.

The most important influence on my work came from my colleague and friend, Mario Grosch. After the first year of my PhD thesis, he started to work on a topic related to mine and in the years that followed we have been working like a team. It was priceless to have a like-minded scientist at my side to evaluate and discuss so many aspects of our work. Scientific contributions to this work that have to be assigned to Mario are:

- 1) The (re)discovery of the reactivity between iron and sulfur at room temperature
- 2) The implementation and maintenance of the GC-MS and the method development
- 3) Development of the acidic treatment of the iron powder to remove carbonaceous material from the surface
- 4) Synthesis and deactivation of a mackinawite sample for Mößbauer analysis

Thank you very much for all the great time we had during the last years and hopefully for all the years to come.

Additional scientific exchange arose in a collaboration with the group of Prof. Dr. Trapp at the LMU in Munich and especially Sophia Peters. Sophia and me decided to work together on the catalytic CO<sub>2</sub> fixation on tochilinite analogues. As she left Germany before the experiments had been finished, Christoph Seifert continued our project during his master thesis. Scientific contributions to this work that have to be assigned to Sophia and Christoph are:

- 1) CO<sub>2</sub>-fixation experiments with H<sub>2</sub> gas on tochilinite samples at high temperatures and under high pressures



- 2) Implementation of the distillation procedure to collect the products formed which has been adapted for my CO<sub>2</sub>-fixation experiments on mackinawite
- 3) Qualitative and quantitative GC-MS analysis of the products formed in the tochilinite-CO<sub>2</sub> experiments

I want to thank Sophia for our pleasant collaboration and the great time at hers during my visit at the LMU and of course Sophia and Christoph for the experiments that underline the potential relevance of iron sulfides on the early earth.

Fuelled by the need for Mößbauer spectroscopic data, additional collaborations were set up with Dr. Christoph Göbel from the inorganic chemistry department of the University of Bayreuth in the group of Prof. Dr. Birgit Weber and Mario Winkler from the physical chemistry department of the University of Stuttgart in the group of Prof. Dr. van Slageren. The Mößbauer analysis of Toch\_MgAl\_11 was provided by Dr. Christoph Göbel and all other Mößbauer data were obtained and analyzed by Mario Winkler. I really want to thank both for the fruitful and pleasant collaborative work.

As a variety of different analytical methods was used during my work and I want to acknowledge and thank all who have provided measurements and their expertise. First of all, I want to thank Antje Wermann who was involved in many aspects of my work and provided PXRD and TGA/DSC data. She also supplied me with sweet treats whenever we met at her office what I cannot appreciate enough. Steffi Ebbinghaus was also very important for the preparation of this work as she did the PXRD measurements for most of my samples. SEM images and EDX data were collected by Steffi Stumpf and TEM images by Dr. Stephanie Höppener. I would also like to thank Dr. Johannes Buchheim and Dr. Oluseun Akintola for providing the BET surface analyses of my samples. ICP-AES analyses were carried out by Dr. Dirk Merten and Ines Kamp. I also want to thank Melanie Sauer and Mohamad Bahrou for their contributions to this work.

Last but definitely not least I want to thank my beautiful wife Mareike who supported me in my efforts and raised me up in times of struggle. I really appreciate the patience and encouragement over the last years.

# Content

<b>Selbstständigkeitserklärung</b> .....	<b>i</b>
<b>Abstract</b> .....	<b>ii</b>
<b>Zusammenfassung</b> .....	<b>iv</b>
<b>Acknowledgements</b> .....	<b>vi</b>
<b>Content</b> .....	<b>viii</b>
<b>List of figures</b> .....	<b>xi</b>
<b>List of tables</b> .....	<b>xvii</b>
<b>List of abbreviations</b> .....	<b>xix</b>
<b>1 Introduction to iron sulfides and carbon fixation</b> .....	<b>1</b>
1.1 Iron sulfide minerals – an overview .....	1
1.2 Mackinawite – a versatile iron sulfide.....	2
1.2.1 General information.....	2
1.2.2 Redox activity.....	4
1.2.3 Adsorption .....	5
1.2.4 Intercalation.....	7
1.2.5 Summary.....	8
1.3 Tochilinite – a mixed layered mineral.....	9
1.4 Activation and hydrogenation of CO <sub>2</sub> .....	15
1.4.1 Overview .....	15
1.4.2 Carbon fixation under hydrothermal conditions.....	17
1.4.3 The iron sulfur world by G. Wächtershäuser .....	19
1.4.4 Iron-sulfur centers in modern enzymes .....	21
1.4.5 Potential role of mackinawite and tochilinite.....	22
<b>2 Materials and methods</b> .....	<b>25</b>
2.1 Materials .....	25
2.1.1 Miscellaneous .....	25
2.1.2 Iron sulfide synthesis.....	25
2.1.3 Carbon fixation experiments .....	25
2.2 Methods .....	26
2.2.1 Syntheses .....	26
2.2.2 Carbon fixation experiments with mackinawite.....	28
2.2.3 Carbon fixation experiments with tochilinite.....	28

2.3	Elemental analysis via ICP-AES .....	29
2.4	Powder X-ray diffraction (PXRD) .....	30
2.5	Rietveld refinement of PXRD patterns.....	30
2.6	Mößbauer spectroscopy .....	31
2.7	Scanning electron microscopy (SEM).....	31
2.8	Energy-dispersive X-ray spectroscopy (EDX).....	31
2.9	High resolution transmission electron microscopy (TEM) .....	31
2.10	Gas chromatography coupled to mass spectrometry (GC-MS).....	31
2.11	BET surface area .....	32
2.12	TGA / DSC analysis .....	32
<b>3</b>	<b>Synthesis and characterization of mackinawite.....</b>	<b>34</b>
3.1	Synthesis of mackinawite .....	34
3.1.1	Mechanism .....	34
3.1.2	Kinetics.....	41
3.2	Characterization of mackinawite.....	43
3.2.1	Structure and morphology .....	43
3.2.2	Composition .....	47
3.2.3	Stability and oxidation behavior.....	48
3.2.4	Comparison to other syntheses routes .....	57
3.3	“Charged layer” model.....	59
<b>4</b>	<b>Synthesis of other metal sulfides from the elements.....</b>	<b>69</b>
<b>5</b>	<b>Carbon fixation with nano-mackinawite.....</b>	<b>77</b>
5.1	Activation and reduction of CO <sub>2</sub> .....	77
5.2	Experimental conditions .....	78
5.3	Mackinawite from iron and sulfur without pretreatment .....	80
5.4	Mackinawite from pretreated iron and sulfur .....	83
5.5	Mackinawite from (NH <sub>4</sub> ) <sub>2</sub> Fe(SO <sub>4</sub> ) <sub>2</sub> and Na <sub>2</sub> S.....	88
5.6	Conclusions .....	89
<b>6</b>	<b>Synthesis and characterization of tochilinite analogues .....</b>	<b>91</b>
6.1	State of the art.....	91
6.2	Determination of structure and composition .....	91
6.3	Reaction conditions and preliminary experiments .....	98
6.3.1	Synthesis with precipitated iron sulfide .....	98
6.3.2	Synthesis with solid starting materials .....	100

6.4	Controlled synthesis of tochilinite analogues.....	100
6.4.1	Overview .....	100
6.4.2	Mg-Al-tochilinite.....	102
6.4.3	Mg-Fe(III)-tochilinite .....	112
6.4.4	Fe(II)-Fe(III)-tochilinite (ferrotochilinite).....	117
6.4.5	Fe(II)-Al-tochilinite .....	119
6.5	Characterization of Tochilinite analogues.....	121
6.5.1	Particle characteristics .....	121
6.5.2	Stability.....	124
6.5.3	Composition and Mößbauer data.....	126
<b>7</b>	<b>Carbon fixation with tochilinite analogues .....</b>	<b>132</b>
<b>8</b>	<b>A plausible prebiotic scenario .....</b>	<b>135</b>
8.1	Introduction .....	135
8.2	Surface “black smokers” .....	137
<b>9</b>	<b>Summary and outlook.....</b>	<b>140</b>
<b>10</b>	<b>Experimental section .....</b>	<b>144</b>
10.1	Metal sulfide syntheses.....	144
10.1.1	Standard procedure .....	144
10.1.2	Iron sulfides .....	144
10.2	Binary sulfide synthesis from Fe, Cu, Ni and S .....	153
10.3	CO <sub>2</sub> / carbonate reduction experiments .....	155
10.4	Syntheses of tochilinite analogues.....	166
10.4.1	MgAl-tochilinite .....	166
10.4.2	MgFe-tochilinite .....	178
10.4.3	FeFe-tochilinite.....	187
10.4.4	FeAl-tochilinite.....	191
	<b>Appendix.....</b>	<b>195</b>
	<b>References.....</b>	<b>337</b>
	<b>Curriculum vitae.....</b>	<b>345</b>

## List of figures

Figure 1: Unit cell of mackinawite. ....	3
Figure 2: Tochilinite on calcite found at the Otamo dolomite quarry. ....	9
Figure 3: Unit cell of the isometric tochilinite variety as described by Organova <i>et al.</i> ....	10
Figure 4: Unit cell of brucite.....	11
Figure 5: Mg <sup>2+</sup> arrangement of brucite in the a-b-plane with the original unit cell.....	12
Figure 6: Mg <sup>2+</sup> arrangement of the brucite substructure of tochilinite in the a-b-plane and the tochilinite unit cell. ....	12
Figure 7: Fe <sup>2+</sup> arrangement of mackinawite in the a-b-plane with the original unit cell.....	12
Figure 8: Fe <sup>2+</sup> arrangement of the mackinawite sub-structure of tochilinite in the a-b-plane.....	13
Figure 9: Fe <sup>2+</sup> arrangement of the mackinawite substructure of tochilinite in the a-b-plane. ....	13
Figure 10: Extracted pictures from video footage of the reaction between sulfur grains and an iron plate. ....	36
Figure 11: SEM image of the iron plate after the reaction between sulfur grains and the iron plate showing severe pitting corrosion. ....	37
Figure 12: Image of the experimental setup investigated by SEM imaging and EDX. ....	38
Figure 13: SEM image of the on top view of the interface between the iron plate and sulfur after the reaction. ....	39
Figure 14: EDX mapping of the on top view of the interface between the iron plate and sulfur after the reaction. ....	39
Figure 15: SEM image of the side view of the interface between the iron plate and sulfur after the reaction. ....	40
Figure 16: EDX mapping of the side view of the interface between the iron plate and sulfur after the reaction. ....	40
Figure 17: Series of PXRD patterns and plot of the sulfur content of a reaction mixture of iron and sulfur after the reaction in pure water at different times.....	41
Figure 18: PXRD pattern of nanoparticulate mackinawite from reaction FeS_1.....	43
Figure 19: PXRD pattern of a mackinawite sample prepared from iron, sulfur. Rietveld fit using the iron, sulfur and mackinawite crystal structures.....	44
Figure 20: SEM image of a deactivated mackinawite sample prepared from iron and sulfur in a 0.01 M sodium chloride solution for 12 hours.....	45
Figure 21: TEM images of a deactivated mackinawite sample prepared from iron and sulfur in a 0.01 M sodium chloride solution for 12 hours.....	46
Figure 22: TEM investigation of the visible lattice fringes of a deactivated mackinawite sample prepared from iron and sulfur.....	46
Figure 23: TGA/DSC analysis of a freshly prepared nano-mackinawite sample that was dried in a stream of air with 50 ml/min. ....	49

Figure 24: TGA/DSC analysis of a freshly prepared mackinawite sample that was dried under N <sub>2</sub> for one hour.....	49
Figure 25: TGA/DSC analysis of a freshly prepared mackinawite sample that was dried under N <sub>2</sub> .....	50
Figure 26: TGA/DSC analysis of a pre-oxidized mackinawite sample.....	52
Figure 27: SEM image of a mackinawite sample stored open to the atmosphere for one month at room temperature. ....	53
Figure 28: SEM images of a deactivated mackinawite sample heated at 80 °C in CO <sub>2</sub> atmosphere for 3 days. ....	53
Figure 29: TGA/DSC investigation of a mackinawite sample. After drying in a CO <sub>2</sub> gas flow for 10 hours, the sample was exposed to air.....	54
Figure 30: TGA/DSC investigation of a mackinawite sample. After drying in a N <sub>2</sub> gas flow for 10 hours, the sample was exposed to air.....	54
Figure 31: SEM images of mackinawite particles synthesized from elemental iron in a 5 M sodium sulfide solution at 160 °C for three days. ....	57
Figure 32: PXRD pattern of a mackinawite sample synthesized from elemental iron in a 5 M sodium sulfide solution at 160 °C for three days. ....	58
Figure 33: SEM image and EDX analysis of a mackinawite sample synthesized from iron and sulfur in a 0.01 M sodium chloride solution. ....	62
Figure 34: Na-content in mackinawite samples (ICP-AES). ....	65
Figure 35: Plot of the pH value of the solution of a mackinawite synthesis versus the sodium chloride concentration. ....	65
Figure 36: PXRD pattern of a mackinawite sample prepared from iron and sulfur which was aged for one week at 80 °C. ....	66
Figure 37: SEM image of MB_7. ....	72
Figure 38: SEM image of MB_7. ....	72
Figure 39: SEM image of MB_23. ....	75
Figure 40: SEM image of MB_23. ....	75
Figure 41: Gas chromatogram of RED_6. ....	82
Figure 42: Gas chromatogram of RED_7. ....	83
Figure 43: PXRD pattern of the untreated powder of elemental iron.....	84
Figure 44: SEM images and EDX analysis of the untreated iron powder.....	85
Figure 45: Calculated PXRD pattern using Organova's isometric tochilinite crystal structure without strain or size effects. ....	92
Figure 46: View of the unit cell of Organova's isometric tochilinite along the b axis. ....	93
Figure 47: Calculated PXRD pattern using the structure of the isometric tochilinite variety described by Organova with a formula of 6 FeS * 5 Mg(OH) <sub>2</sub> .....	94
Figure 48: Calculated PXRD pattern using the structure of the isometric tochilinite variety described by Organova with a formula of 6 Fe <sub>0.9</sub> S * 5 Mg(OH) <sub>2</sub> .....	94
Figure 49: Calculated PXRD pattern using the crystal structure of the isometric tochilinite variety described by Organova with a formula of 6 Fe <sub>0.8</sub> S * 5 Mg(OH) <sub>2</sub> . ....	95

Figure 50: Calculated PXRD pattern using the crystal structure of the isometric tochilinite variety described by Organova with a formula of $6 \text{Fe}_{0.7}\text{S} * 5 \text{Mg}(\text{OH})_2$ .	95
Figure 51: Calculated PXRD pattern using the crystal structure of the isometric tochilinite variety described by Organova with a formula of $6 \text{Fe}_{0.67}\text{S} * 5 \text{Mg}(\text{OH})_2$ .	96
Figure 52: PXRD pattern of Toch_3.	99
Figure 53: Mößbauer spectrum of Toch_MgAl_11.	106
Figure 54: SEM images of Toch_MgFe_18.	122
Figure 55: SEM images of Toch_FeFe_11.	122
Figure 56: SEM images of Toch_FeAl_6.	122
Figure 57: TEM images of Toch_MgFe_18.	123
Figure 58: TGA/DSC analysis of Toch_MgFe_18 in a nitrogen gas atmosphere.	124
Figure 59: TGA/DSC analysis of Toch_FeAl_6 in a nitrogen gas atmosphere.	125
Figure 60: TGA/DSC analysis of Toch_FeFe_11 in a nitrogen gas atmosphere.	125
Figure 61: Mößbauer spectra at room temperature of different tochilinite analogues.	127
Figure 62: Mößbauer spectrum of deactivated mackinawite prepared from iron and sulfur following the standard synthetic procedure.	129
Figure 63: Powder diffraction pattern of FeS_1.	195
Figure 64: Powder diffraction pattern of FeS_2.	196
Figure 65: Powder diffraction pattern of FeS_NaCl_1.	197
Figure 66: Powder diffraction pattern of FeS_NaCl_2.	198
Figure 67: Powder diffraction pattern of FeS_NaCl_3.	199
Figure 68: Powder diffraction pattern of FeS_NaCl_4.	200
Figure 69: Powder diffraction pattern of FeS_NaCl_4.	201
Figure 70: Powder diffraction pattern of FeS_Ox_3.	202
Figure 71: Powder diffraction pattern of FeS_Ox_4.	203
Figure 72: Powder diffraction pattern of FeS_Ox_5.	204
Figure 73: Powder diffraction pattern of FeS_Ox_6.	205
Figure 74: Powder diffraction pattern of FeS_Ox_9.	206
Figure 75: Powder diffraction pattern of FeS_Ox_10.	207
Figure 76: Powder diffraction pattern of FeS_Ox_11.	208
Figure 77: Powder diffraction pattern of CoS_1.	209
Figure 78: Powder diffraction pattern of CoS_2.	210
Figure 79: Powder diffraction pattern of CuS_1.	211
Figure 80: Powder diffraction pattern of MnS_1.	212
Figure 81: Powder diffraction pattern of MnS_2.	213
Figure 82: Powder diffraction pattern of MoS_1.	214
Figure 83: Powder diffraction pattern of NiS_1.	215
Figure 84: Powder diffraction pattern of NiS_1.	216
Figure 85: Powder diffraction pattern of WS_1.	217

Figure 86: Powder diffraction pattern of ZnS_1.....	218
Figure 87: Powder diffraction pattern of ZnS_2.....	219
Figure 88: Powder diffraction pattern of MB_1.....	220
Figure 89: Powder diffraction pattern of MB_2.....	221
Figure 90: Powder diffraction pattern of MB_3.....	222
Figure 91: Powder diffraction pattern of MB_4.....	223
Figure 92: Powder diffraction pattern of MB_5.....	224
Figure 93: Powder diffraction pattern of MB_6.....	225
Figure 94: Powder diffraction pattern of MB_7.....	226
Figure 95: Powder diffraction pattern of MB_8.....	227
Figure 96: Powder diffraction pattern of MB_9.....	228
Figure 97: Powder diffraction pattern of MB_10.....	229
Figure 98: Powder diffraction pattern of MB_11.....	230
Figure 99: Powder diffraction pattern of MB_12.....	231
Figure 100: Powder diffraction pattern of MB_13.....	232
Figure 101: Powder diffraction pattern of MB_14.....	233
Figure 102: Powder diffraction pattern of MB_15.....	234
Figure 103: Powder diffraction pattern of MB_16.....	235
Figure 104: Powder diffraction pattern of MB_17.....	236
Figure 105: Powder diffraction pattern of MB_18.....	237
Figure 106: Powder diffraction pattern of MB_19.....	238
Figure 107: Powder diffraction pattern of MB_20.....	239
Figure 108: Powder diffraction pattern of MB_21.....	240
Figure 109: Powder diffraction pattern of MB_22.....	241
Figure 110: Powder diffraction pattern of MB_23.....	242
Figure 111: Powder diffraction pattern of Toch_1.....	243
Figure 112: Powder diffraction pattern of Toch_2.....	244
Figure 113: Powder diffraction pattern of ELT_1.....	245
Figure 114: Powder diffraction pattern of Toch_4.....	246
Figure 115: Powder diffraction pattern of Toch_5.....	247
Figure 116: Powder diffraction pattern of Toch_6.....	248
Figure 117: Powder diffraction pattern of Toch_7.....	249
Figure 118: Powder diffraction pattern of Toch_8.....	250
Figure 119: Powder diffraction pattern of Toch_9.....	251
Figure 120: Powder diffraction pattern of TochMgAl_1.....	252
Figure 121: Powder diffraction pattern of TochMgAl_2.....	253
Figure 122: Powder diffraction pattern of TochMgAl_3.....	254
Figure 123: Powder diffraction pattern of TochMgAl_4.....	255
Figure 124: Powder diffraction pattern of TochMgAl_5.....	256
Figure 125: Powder diffraction pattern of TochMgAl_6.....	257



Figure 126: Powder diffraction pattern of TochMgAl_7.....	258
Figure 127: Powder diffraction pattern of TochMgAl_8.....	259
Figure 128: Powder diffraction pattern of TochMgAl_9.....	260
Figure 129: Powder diffraction pattern of TochMgAl_10.....	261
Figure 130: Powder diffraction pattern of TochMgAl_11.....	262
Figure 131: Powder diffraction pattern of TochMgAl_12.....	263
Figure 132: Powder diffraction pattern of TochMgAl_13.....	264
Figure 133: Powder diffraction pattern of TochMgAl_14.....	265
Figure 134: Powder diffraction pattern of TochMgAl_15.....	266
Figure 135: Powder diffraction pattern of TochMgAl_16.....	267
Figure 136: Powder diffraction pattern of TochMgAl_17.....	268
Figure 137: Powder diffraction pattern of TochMgAl_18.....	269
Figure 138: Powder diffraction pattern of TochMgAl_19.....	270
Figure 139: Powder diffraction pattern of TochMgAl_20.....	271
Figure 140: Powder diffraction pattern of TochMgAl_21.....	272
Figure 141: Powder diffraction pattern of TochMgAl_22.....	273
Figure 142: Powder diffraction pattern of TochMgAl_23.....	274
Figure 143: Powder diffraction pattern of TochMgAl_24.....	275
Figure 144: Powder diffraction pattern of TochMgAl_25.....	276
Figure 145: Powder diffraction pattern of TochMgAl_26.....	277
Figure 146: Powder diffraction pattern of TochMgAl_27.....	278
Figure 147: Powder diffraction pattern of TochMgFe_1.....	279
Figure 148: Powder diffraction pattern of TochMgFe_2.....	280
Figure 149: Powder diffraction pattern of TochMgFe_3.....	281
Figure 150: Powder diffraction pattern of TochMgFe_4.....	282
Figure 151: Powder diffraction pattern of TochMgFe_5.....	283
Figure 152: Powder diffraction pattern of TochMgFe_6.....	284
Figure 153: Powder diffraction pattern of TochMgFe_7.....	285
Figure 154: Powder diffraction pattern of TochMgFe_8.....	286
Figure 155: Powder diffraction pattern of TochMgFe_9.....	287
Figure 156: Powder diffraction pattern of TochMgFe_10.....	288
Figure 157: Powder diffraction pattern of TochMgFe_11.....	289
Figure 158: Powder diffraction pattern of TochMgFe_12.....	290
Figure 159: Powder diffraction pattern of TochMgFe_13.....	291
Figure 160: Powder diffraction pattern of TochMgFe_14.....	292
Figure 161: Powder diffraction pattern of TochMgFe_15.....	293
Figure 162: Powder diffraction pattern of TochMgFe_16.....	294
Figure 163: Powder diffraction pattern of TochFeFe_1.....	295
Figure 164: Powder diffraction pattern of TochFeFe_2.....	296
Figure 165: Powder diffraction pattern of TochFeFe_3.....	297

Figure 166: Powder diffraction pattern of TochFeFe_4.....	298
Figure 167: Powder diffraction pattern of TochFeFe_5.....	299
Figure 168: Powder diffraction pattern of TochFeFe_6.....	300
Figure 169: Powder diffraction pattern of TochFeFe_7.....	301
Figure 170: Powder diffraction pattern of TochFeFe_8.....	302
Figure 171: Powder diffraction pattern of TochFeFe_9.....	303
Figure 172: Powder diffraction pattern of TochFeFe_10.....	304
Figure 173: Powder diffraction pattern of TochFeFe_11.....	305
Figure 174: Powder diffraction pattern of TochFeAl_1.....	306
Figure 175: Powder diffraction pattern of TochFeAl_2.....	307
Figure 176: Powder diffraction pattern of TochFeAl_3.....	308
Figure 177: Powder diffraction pattern of TochFeAl_4.....	309
Figure 178: Powder diffraction pattern of TochFeAl_5.....	310
Figure 179: Powder diffraction pattern of TochFeAl_6.....	311
Figure 180: Gas chromatogram of RED_1.....	312
Figure 181: Gas chromatogram of RED_2.....	313
Figure 182: Gas chromatogram of RED_3.....	314
Figure 183: Gas chromatogram of RED_4.....	315
Figure 184: Gas chromatogram of RED_5.....	316
Figure 185: Gas chromatogram of RED_6.....	317
Figure 186: Gas chromatogram of RED_7.....	318
Figure 187: Gas chromatogram of RED_8.....	319
Figure 188: Gas chromatogram of RED_9.....	320
Figure 189: Gas chromatogram of RED_10.....	321
Figure 190: Gas chromatogram of RED_11.....	322
Figure 191: Gas chromatogram of RED_12.....	323
Figure 192: Gas chromatogram of RED_13.....	324
Figure 193: Gas chromatogram of RED_14.....	325
Figure 194: Gas chromatogram of RED_15.....	326
Figure 195: Gas chromatogram of RED_16.....	327
Figure 196: Gas chromatogram of RED_17.....	328
Figure 197: Gas chromatogram of RED_18.....	329
Figure 198: Gas chromatogram of RED_19.....	330
Figure 199: Gas chromatogram of Toch_Red_1.....	331
Figure 200: Gas chromatogram of Toch_Red_1.....	332
Figure 201: Gas chromatogram of Toch_Red_2.....	333
Figure 202: Gas chromatogram of Toch_Red_2.....	334
Figure 203: Gas chromatogram of Toch_Red_3.....	335
Figure 204: Gas chromatogram of Toch_Red_3.....	336

## List of tables

Table 1: Compositions reported for natural tochilinite samples. ....	14
Table 2: Literature data for mackinawite compositions and (001) d-values. ....	60
Table 3: Products of the reactions between different metals and elemental sulfur at room temperature or 80 °C, respectively. ....	69
Table 4: Reaction products of a mixture of nickel and sulfur under different reaction conditions. ....	71
Table 5: Products of reactions between copper, iron and sulfur at different sodium chloride concentrations, temperatures, reaction times and starting mixtures. ....	73
Table 6: Reaction conditions of CO <sub>2</sub> reduction reactions and the assigned codes. ....	78
Table 7: Reaction conditions and products of the reactions between mackinawite and CO <sub>2</sub> /carbonate using untreated iron powder. ....	81
Table 8: Reaction conditions and products of the reactions between mackinawite and CO <sub>2</sub> /carbonate using pretreated iron powder. ....	86
Table 9: Reaction temperatures and solid products of the reaction of adsorbed carbonate on freshly prepared mackinawite in a nitrogen atmosphere. ....	87
Table 10: Reaction conditions and products of the reactions between precipitated mackinawite and CO <sub>2</sub> /carbonate. ....	88
Table 11: Compositions of natural tochilinite analogues. ....	96
Table 12: Theoretical compositions of the tochilinite analogues that are the aim of the syntheses of tochilinite analogues in this work. ....	101
Table 13: Sources of the necessary elements in different starting mixtures for the Mg-Al-tochilinite syntheses. ....	102
Table 14: Fitting parameters of the Mößbauer spectrum of Toch_MgAl_11. The parameters fitted are the center shift $\delta$ , the quadrupole splitting $\Delta E_Q$ , the width at half maximum $\Gamma$ and the area of the peaks $A$ . ....	106
Table 15: Absolute diffraction peak areas from different products in Mg-Al-tochilinite syntheses with identical PXRD settings. ....	107
Table 16: Absolute diffraction peak areas from different products in Mg-Al-tochilinite syntheses with identical PXRD settings. ....	108
Table 17: Absolute diffraction peak areas from different products in Mg-Al-tochilinite syntheses with decreasing relative amounts of sulfur using identical PXRD settings. ....	110
Table 18: Sources of the necessary ions in different starting mixtures for the Mg-Fe(III)-tochilinite syntheses. ....	112
Table 19: Absolute diffraction peak areas from different products in Mg-Fe(III)-tochilinite syntheses with identical PXRD settings. ....	114
Table 20: Absolute diffraction peak areas from different products in Mg-Fe(III)-tochilinite syntheses with identical PXRD settings. ....	115
Table 21: Correlation between the used mass of FeO(OH) and the removed magnetic material in Mg-Fe(III)-tochilinite syntheses. ....	117

Table 22: Sources of the necessary ions in different starting mixtures for the Fe(II)-Fe(III)-tochilinite syntheses. ....	118
Table 23: Correlation between the used mass of sulfur and the removed magnetic material in Fe(II)-Fe(III)-tochilinite syntheses. ....	119
Table 24: Overview of the ratio of the starting materials for Fe(II)-Al-tochilinite syntheses at a constant amount of sulfur.....	120
Table 25: Overview of side product free tochilinite analogues for in depth analysis. .	121
Table 26: BET surface areas and mean pore volumes of the different tochilinite analogues determined by adsorption isotherms of argon gas at 87 K.....	124
Table 27: Compositions of tochilinite analogs obtained by ICP-AES. ....	126
Table 28: Mößbauer data for tochilinite analogues without side products.....	127
Table 29: Fit parameters for Toch_FeAl_6. ....	128
Table 30: Fit parameters for Toch_MgFe_18.....	128
Table 31: Fit parameters for Toch_FeFe_11. ....	128
Table 32: Final normalized compositions for tochilinite analogues without side products.....	130
Table 33: Comparison of the theoretical composition of Organova’s isometric tochilinite variety and the obtained tochilinite analogues in this work.....	130
Table 34: Reaction conditions for FTT reactions carried out with Toch_MgFe_18....	132
Table 35: Reduction products obtained from FTT reactions on Toch_MgFe_18. C <sub>n</sub> represent saturated alkanes, linear and branched, with the corresponding chain length. ....	133
Table 36: Turn-Over-Numbers (TON) for the formation of alcohols and alkanes for the different FTT experiments. ....	133
Table 37: Proportions of the decomposition products of Toch_MgFe_18 under FTT conditions, without H <sub>2</sub> gas and under nitrogen atmosphere, respectively. ....	134
Table 38: Reaction times for the kinetic investigation of mackinawite formation from iron and sulfur. ....	145
Table 39: Amounts of sodium chloride in the syntheses of mackinawite samples FeS_NaCl_1 to FeS_NaCl_5 from iron and sulfur.....	146
Table 40: Sodium chloride concentration, reaction temperatures and times for experiments MB_1 to MB_8. ....	153
Table 41: Sodium chloride concentration, reaction temperatures and times for experiments MB_9 to MB_17. ....	154
Table 42: Sodium chloride concentration, reaction temperatures and times for experiments MB_18 to MB_23. ....	155

## List of abbreviations

PXRD	Powder X-ray diffraction
SEM	Scanning electron microscopy
TEM	Transmission electron microscopy
ICP-AES	Inductively coupled plasma atomic emission spectroscopy
DCM	Dichloromethane
LDH	Layered double hydroxide

# 1 Introduction to iron sulfides and carbon fixation

## 1.1 Iron sulfide minerals – an overview

The mineral class of iron sulfides is very diverse, and many different crystal structures and morphologies are known. In this chapter a short introduction on each iron sulfide mineral including their formation conditions will be given. Iron sulfides are a significant group of minerals that play key roles in biogeochemical processes, especially in marine systems.<sup>1</sup> They are a part of the global sulfur cycle and act as a sink for sulfide species due to their low solubility in water.<sup>2</sup>

**Pyrite** ( $\text{FeS}_2$ ) is the most abundant iron sulfide on the earth's surface. Compared to the other iron sulfide minerals, it has a remarkable stability and is the only one that does not dissolve in diluted mineral acids.<sup>1,3</sup> The structure of pyrite has been solved as one of the first in the history of X-ray structure determination.<sup>4</sup> It consists of  $\text{Fe}^{2+}$  and disulfide ions that are arranged in a NaCl-structure. Pyrite is widespread in marine sediments and forms in the oxic-anoxic transition zone. The formation mechanism of pyrite has been a topic of continuous debate as the poor reproducibility of experimental findings causes uncertainties.<sup>1</sup> Precipitated iron sulfide is very sensitive to oxidation and varies in its properties with the conditions of precipitation and aging procedures. As a result, multiple formation mechanisms are proposed and there is still doubt whether an additional oxidizing agent is needed for the formation of pyrite from precipitated  $\text{FeS}$  and  $\text{H}_2\text{S}$ .<sup>3,5-7</sup> In the context of prebiotic and origin of life chemistry, pyrite is mainly mentioned in the context of the iron-sulfur-world theory by Günther Wächtershäuser that will be covered later in detail.

**Marcasite** ( $\text{FeS}_2$ ) is a polymorph of pyrite. It has the same composition but a different structure and does not play a significant role in earth's biogeochemistry. Marcasite only forms at pH values below 3 and is less stable than pyrite.<sup>3</sup>

**Greigite** ( $\text{Fe}_3\text{S}_4$ ) belongs to the thiospinel group. It crystallizes in a cubic cell with the space group  $\text{Fd}\bar{3}\text{m}$ . The sulfide ions form a cubic close packed lattice in which tetrahedral and octahedral sites are occupied by iron ions. It is a mixed valence compound with  $\text{Fe}^{2+}$  and  $\text{Fe}^{3+}$  in a ratio of 1:2. Greigite forms from mackinawite upon oxidation. Lennie *et al.*

described in their work from 1997 that the transformation from mackinawite to greigite is a topotactic process. The iron ions rearrange in the sulfide structure without the need for dissolution and reprecipitation.<sup>8</sup> Greigite can be found in recent and relicts of ancient marine sediments. It is considered to be an intermediate in the oxidative transformation from mackinawite to pyrite.<sup>9–11</sup> The structure of greigite resembles the structure of certain iron-sulfur clusters that are found in modern biochemistry. Therefore, some attention was paid to the investigation of the electrochemistry of greigite surfaces and the incorporation of greigite particles into biomolecules<sup>12–14</sup> and it has been used as catalyst for CO<sub>2</sub> fixation.<sup>15,16</sup>

**Pyrrhotite** (Fe<sub>1-x</sub>S) is rather uncommon in marine environments but acts as a rock forming mineral. It can be found as a major constituent in sulfide ore deposits and in meteorites.<sup>17,18</sup> It is a non-stoichiometric compound with iron vacancies that are distributed in an ordered way leading to a series of possible superstructures. Several polytypes are known with compositions ranging from Fe<sub>7</sub>S<sub>8</sub> to Fe<sub>11</sub>S<sub>12</sub>. Pyrrhotite can have a hexagonal or a monoclinic symmetry.<sup>19,20</sup> As pyrrhotite is the most stable iron sulfide under reduced conditions, it may have been more abundant than pyrite on the early earth.

**Troilite** (Fe<sub>1-x</sub>S) can be regarded as the endmember of the pyrrhotite series with a composition very close to FeS. The troilite structure has hexagonal symmetry. It is a constituent of meteorites and in rare cases of terrestrial rocks.<sup>21,22</sup>

**Mackinawite** (FeS) and **tochilinite** (Fe<sub>1-e</sub>S\*x(Mg,Al,Fe)(OH)<sub>2</sub>) are the major topics of this work and the next chapters will give detailed information on their structures and properties.

## 1.2 Mackinawite – a versatile iron sulfide

### 1.2.1 General information

Mackinawite crystallizes with tetragonal symmetry in the space group P 4/nmm and therefore is often called tetragonal iron sulfide. The cell parameters are  $a = 3.66 \text{ \AA}$  and  $c = 5.03 \text{ \AA}$ .<sup>23</sup> The sulfide ions form a distorted cubic close packed lattice with iron ions occupying one-half of the tetrahedral sites with a Fe-Fe distance very close to the one in the  $\alpha$ -iron crystal structure. Mackinawite has a layered structure as filled and empty layers

alternate. The interlayer space in natural mackinawite is nonpolar and interlayer attraction is mainly caused by Van der Waals forces.<sup>24,25</sup>

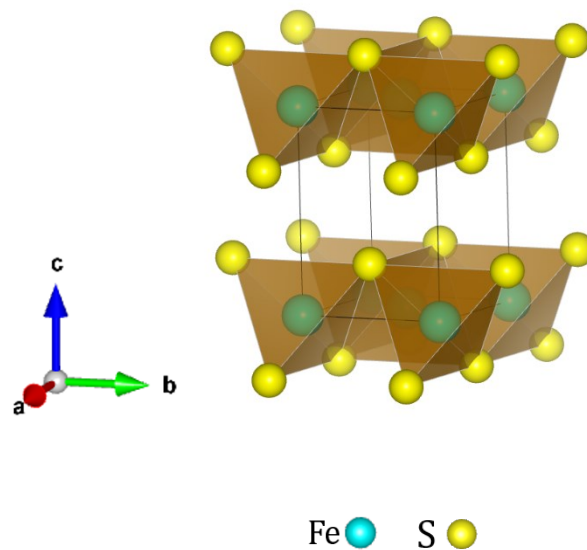


Figure 1: Unit cell of mackinawite.

Mackinawite is the least stable iron sulfide that crystallizes first from solution following Ostwald's step rule. Under most natural conditions, it is metastable and rapidly transforms into other iron sulfides although under anoxic low temperature conditions it can be stable for months. Upon heating without an oxidizing agent, it transforms to troilite or pyrrhotite. This transformation has not been studied exhaustively compared to the formation of greigite or pyrite but has been shown to occur in solution as well as in the dry state at moderate temperatures.<sup>19</sup> At more oxidizing conditions greigite forms within days even at room temperature and slowly converts to pyrite. In marine sediments mackinawite forms by precipitation of  $\text{Fe}^{2+}$  in hydrogen sulfide bearing solutions that primarily originates from sulfate reducing bacteria.<sup>1,3</sup> It is also the first corrosion product of iron or steel in anoxic sulfide or sulfur containing solutions.<sup>26</sup>

The formation and characteristics of mackinawite have been studied from different points of view. Earth scientists have been investigating the mackinawite formation in laboratory and field studies to explore its role in natural biogeochemical processes. Their focus has been led on the solubility and the transformations of precipitated mackinawite.<sup>1,2,8-10,24,27-</sup>

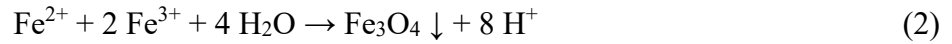
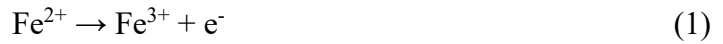
<sup>30</sup> Related to these studies are the investigations on the pronounced adsorption capabilities



i.e. for heavy and rare earth metals that are of interest from environmental and economical points of view.<sup>31–33</sup> Organic chemists have studied the reducing power towards organic nitro and chlorinated compounds what may be used in organic syntheses and waste water treatment.<sup>34–36</sup> The intrinsic physical properties like electrical conductivity and superconductivity have been investigated by material scientists. With this, the intercalation chemistry of mackinawite received some attention and experiments have been carried out to modify the interlayer space and to tune its electrical properties.<sup>37–41</sup> Examinations of corrosion processes of iron metal in sulfide and sulfur containing solutions led to the discovery of mackinawite formation on metal surfaces. Corrosion scientists were nonetheless more interested in the fate of the corroding metal than in the sulfides produced.<sup>26,42–49</sup> From these accounts it is apparent that the chemistry of iron sulfides with mackinawite structure is a very interesting topic with much potential for various applications and doubtless many more features to discover. In prebiotic chemistry, mackinawite has not attracted much attention but this work will give good reasons to consider it for future studies.

### 1.2.2 Redox activity

Mackinawite is composed of  $\text{Fe}^{2+}$  and  $\text{S}^{2-}$  ions, which both can be oxidized, and act as a reducing agent. The standard redox potential for the  $\text{Fe}^{2+}/\text{Fe}^{3+}$  redox couple has been determined to be  $E^\circ_{\text{pH}=0} (\text{Fe}^{2+}/\text{Fe}^{3+}) = 0,771 \text{ V (SHE)}$ . The standard potential for the oxidation of sulfide ions is hard to be determined because the oxidation in basic solutions leads to a complex mixture of polysulfide species. Therefore, the redox potential of sulfide ions depends on the concentrations of several species and especially on the pH value. Still, values for the standard redox potentials for sulfide ions in acidic as well as basic solutions are given in “Standard potentials in aqueous solution” from 1985:  $E^\circ_{\text{pH}=0} (\text{H}_2\text{S}/\text{S}^0) = 0,144 \text{ V (SHE)}$  and  $E^\circ_{\text{pH}=14} (\text{S}^{2-}/\text{S}^0) = - 0,52 \text{ V (SHE)}$ .<sup>50</sup> Sulfide ions in solution can be oxidized to variable extents leading to the formation of different sulfur species depending on the oxidizing agent and the pH value of the solution. Polysulfides, sulfites/ $\text{SO}_2$ , thio-sulfates and sulfates/ $\text{SO}_3$  occur in sulfide oxidation processes.

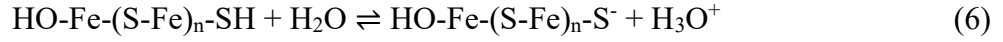
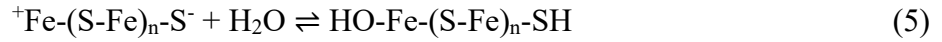


The formation of insoluble products increases the reducing power of mackinawite by changing the equilibrium concentrations of  $\text{Fe}^{2+}$  and  $\text{S}^{2-}$ . Pyrite, greigite, iron oxides or hydroxides and elemental sulfur have small solubilities and can form upon oxidation. Moreover, Mackinawite particles can be oxidized without changing their structure immediately. Mullet *et al.* reported, that mackinawite particles can have up to 20 % of their  $\text{Fe}^{2+}$  oxidized to  $\text{Fe}^{3+}$  and remain stable for at least 24 hours at room temperature open to the atmosphere.<sup>30</sup> The oxidation of mackinawite is favorable in basic solutions what should be taken into account when evaluating mackinawite oxidation reactions in a prebiotic scenario.

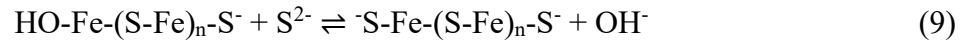
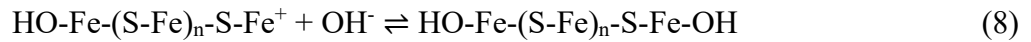
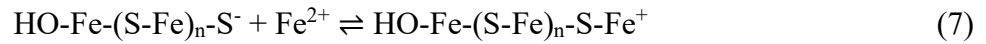
### 1.2.3 Adsorption

The adsorption capability of nanoparticulate mackinawite has been the focus of many studies over the last 30 years.<sup>31–33,51–55</sup> The removal of toxic metal ions like  $\text{Cr}^{3+}$ ,  $\text{Pb}^{2+}$  and  $\text{Cd}^{2+}$  is a crucial step in waste water treatment and investigations of mackinawite have been carried out in this regard. The adsorption of transition metals and their incorporation into the mackinawite structure offer effective routes for the capture of these metal ions from solution. Bebie *et al.* explored the behavior of the iron sulfide surface groups in an aqueous environment in 1997. The iron ions on the surface are Lewis acids and are coordinated by hydroxide ions. The sulfide ions act as bases and can be protonated. As the SH surface groups are more acidic than the OH surface groups, the SH groups are mainly deprotonated at basic conditions and the OH groups get protonated first upon the addition of acid. In neutral solutions, the major part of the sulfide ions is deprotonated and negatively charged. In acidic solutions, the hydroxide groups can get partially protonated. At the point of zero charge, the number of deprotonated and protonated surface groups is similar and the particles become uncharged. The points of zero charge of pyrite,

pyrrhotite, greigite, natural mackinawite and other transition metal sulfides have been determined to be at pH values around  $\text{pH}_{\text{pzc}} = 3$ .<sup>56</sup>



In contrast to this value, the point of zero charge of freshly precipitated nano-mackinawite in has been determined to be at  $\text{pH}_{\text{pzc}} \approx 7.5 - 8$ .<sup>57,58</sup> The discrepancy compared to the  $\text{pH}_{\text{pzc}}$  of natural mackinawite has not been resolved yet. Wolthers argues that oxidation of the surface or undiscovered surface reactions like the intercalation of protons or hydroxide ions could lead to higher  $\text{pH}_{\text{pzc}}$  values. The different  $\text{pH}_{\text{pzc}}$  for nano-mackinawite and greater mackinawite particles will be addressed in the surface model covered later. The addition of divalent metal ions like  $\text{Fe}^{2+}$  or  $\text{Ni}^{2+}$  leads to an increased number of metal surface sites and thus of hydroxide surface sites, whereas additional sulfide ions can replace coordinated hydroxide groups.<sup>55</sup>



As mentioned above, there are two different ways reported to retain metal ions by mackinawite. They can be incorporated into the mackinawite structure and they can be adsorbed onto the mackinawite surface. The incorporation of metal ions into the mackinawite structure keeps them firmly bound and prevents them from being released again into the solution. This is valid for metals whose sulfides are less soluble than mackinawite like NiS or CdS but not for the more soluble MnS. The increasing insolubility of some metal sulfides follows  $\text{MnS} < \text{mackinawite} < \text{NiS} < \text{CoS} < \text{ZnS} < \text{CdS} < \text{PbS} < \text{CuS}$ .<sup>33,59</sup> The adsorption energies of metal cations depend on many factors like the charge, size and the affinity towards sulfide ions. It is suggested by the Pearson acid-base concept, that “soft” metal ions like  $\text{Cd}^{2+}$  and  $\text{Pb}^{2+}$  should bind stronger than “hard” ones like  $\text{Na}^+$ .

The adsorption properties of mackinawite towards organic molecules have not been investigated extensively. In 2008, Hatton and Rickard investigated the adsorption behavior of different transition metal sulfides. Their “study demonstrates that double and single

stranded nucleic acid polymers as well as adenine and the nucleoside and nucleotide derived from it bind to copper, iron and zinc sulfides”<sup>60</sup>. A very recent publication by Picard *et al.* covers the adsorption of unspecified organic compounds by freshly precipitated mackinawite particles.<sup>61</sup> Organic molecules have been adsorbed during the formation of mackinawite in the presence of living sulfate reducing bacteria and this association persisted for at least two years. Amino acids, carbohydrates and lipids were especially bound by the mackinawite particles. They conclude that “biogenic iron sulfide minerals therefore represent a potential strong protectant for proteinaceous organic carbon as long as anoxic conditions are preserved in low temperature surface environments”. This is a very crucial statement for the potential role of mackinawite in prebiotic chemistry and maybe for the chemistry that led to the origin of life. There is also a publication by Dzade *et al.* concerning the theoretical interactions of methylamine and the mackinawite surface studied by DFT calculations that support the role of iron containing minerals for adsorption processes. They report that methylamine binds strongly to the (011) and (111) surfaces through the interaction of the lone pair of the nitrogen atom and the iron surface sites.<sup>62</sup> As mackinawite can offer not only very acidic but also very basic surface sites depending on the surrounding solution, a versatile adsorption chemistry of organics is expected. As low concentrations of the organic feedstock are a major obstacle for the origin of life, pronounced selective adsorption on mineral surfaces may be a crucial mechanism to provide higher concentrations especially for condensation reactions.

#### **1.2.4 Intercalation**

Clays like montmorillonite have attracted much attention in the prebiotic chemistry. As an example, Horowitz *et al.* have studied the intercalation as a means to suppress cyclization and promote polymerization of base-pairing oligonucleotides in a prebiotic world.<sup>63</sup> Intercalation chemistry is one of the most important features of clays and makes them a very interesting mineral class. Mackinawite also has a layered structure and is able to intercalate ions or molecular species into its interlayer space. Thus, intercalation chemistry may similarly be a very important feature of mackinawite but has not yet been extensively investigated. Only a few investigations are concerned with the requirements and possibilities of mackinawite intercalation reactions. To tune the critical temperature at which a material gets super conductive, intercalation is a tool that is used for a lot of different systems. As superconductivity has been observed in certain mackinawite

samples, intercalation compounds were synthesized and characterized to tune the electronic and magnetic properties. The obtained intercalation compounds are related to the mineral tochilinite whose structure and characteristics will be discussed in more detail in the following chapter. It has been shown that alkali metal hydroxides like NaOH and LiOH can be intercalated between the iron sulfide layers.<sup>38,64–66</sup> It is also possible to stabilize neutral molecules like dimethylhydrazine in the interlayer space.<sup>67</sup> In an experimental study on the preparation of mackinawite intercalation compounds, Peng *et al.* were able to intercalate cationic iron complexes of bipyridine, phenanthroline and other amino bases. These investigations on the mackinawite intercalation chemistry show, that it can intercalate cations and neutral molecules, which may be of relevance for the origin of life as the intercalation of organic molecules and their cationic complexes can increase their local concentrations and offer new reactivities. The prebiotic plausible formation of porphyrin may act as an example. A porphyrin ring can be formed by condensation of pyrrole and aldehydes as described by Almog *et al.* in 1975.<sup>68</sup> The synthesis of porphyrin affords high concentrations as four equivalents of pyrrole and four equivalents of a suitable aldehyde are needed to form one equivalent of porphyrin. Pyrrole may act as a ligand for iron ions in a cationic complex that can enter the interlayer space of mackinawite and bring pyrrole molecules in close contact. The addition of the aldehydes may lead to the formation of porphyrin rings without the risk of pyrrole polycondensation. This hypothesis is investigated in our laboratory but could not be confirmed yet.

### 1.2.5 Summary

In summary, mackinawite offers a high reducing potential that could have led to the reduction of C1 species like CO<sub>2</sub>, CO or HCN to provide an organic feedstock for the formation of the molecules necessary for the origin of life. Reduction reactions were also important regarding organics with multiple carbon atoms like the reductive amination of  $\alpha$ -ketoacids that may have led to the formation of amino acids as has been shown by Huber *et al.*<sup>69</sup> Moreover, mackinawite is a very effective adsorbent for most metal ions and organics. It offers a negatively charged surface in a wide pH region and surface areas up to 400 m<sup>2</sup>/g.<sup>70,71</sup> Toxic metal cations can replace iron ions in the mackinawite structure or be adsorbed onto the surface. The point of zero charge of mackinawite is around  $\text{pH}_{\text{pzc}} = 3$  and many sulfide groups are deprotonated at neutral pH what supports the surface complexation of metal cations. In a prebiotic context the adsorption of heavy metals

is important because the absence of soluble toxic heavy metals is one of nine key requirements for the origin of life as stated in a recent publication by Maruyama *et al.*<sup>72</sup> The adsorption of organic molecules is strong if they contain basic nitrogen atoms like peptides and nucleobases. This could lead to high local concentrations of these organics to promote condensation reactions and peptide or RNA/DNA formation. The adsorption could have stabilized these polymers and the iron sulfide core may have functioned as the active site as known from modern enzymes. The intercalation chemistry of mackinawite offers additional abilities for concentrating organics and polymerization reactions that still need to be explored.

### 1.3 Tochilinite – a mixed layered mineral

Tochilinite is a very rare mineral that occasionally occurs in areas associated with ultramafic rock. More important is its occurrence in carbonaceous chondrites where it often acts as a major constituent. It is regarded as a product of aqueous alteration of other iron sulfides and iron oxides.<sup>73–75</sup> It is named after M. Tochilin who was a professor for mineralogy at the Voronezh University in Russia and occurs in aggregates of cylindrical



Figure 2: Tochilinite on calcite found at the Otamo dolomite quarry, Siikainen, Sataku. © mindat.org.

acicular crystals and as thin coatings as shown in the picture above. Tochilinite was first discovered in 1970 by Harris *et al.* and its structure was determined by Organova *et al.* only a few years later.<sup>76–78</sup> Tochilinite is a complex hybrid mineral composed of mackinawite-like and brucite-like layers. Both layers are slightly distorted compared to the natural minerals. The hydroxide ions in the brucite substructure do not form regular

octahedra and the distance between the iron ions in the mackinawite substructure is longer compared to natural mackinawite. The different layers are reported to alternate in an A-B-A-B fashion. Organova describes two varieties of tochilinite, an isometric and an acicular one based on their morphology and crystal structure. An investigation of the crystal structures of both varieties by electron diffraction experiments leads to the conclusion, that the crystal structure of the isometric variety differs only in the distribution of the iron vacancies of the mackinawite-like substructure compared to the acicular one. The solution of structures of misfit-layered materials is a difficult and time-consuming task, which is why the structures for the different layers are often given independently. Consequently, Organova did determine a supercell for the combined mackinawite-like and brucite-like lattices for the isometric variety but not for the acicular one. Hence, the structure of the isometric tochilinite shall be used as the reference in this work and will be described below. The structure of the isometric variety was determined to have triclinic symmetry with monoclinic lattice constants. The space group is P1 with  $a = 5.37 \text{ \AA}$ ,  $b = 15.65 \text{ \AA}$ ,  $c = 10.72 \text{ \AA}$ ;  $\alpha = \beta = 90^\circ$  and  $\gamma = 95^\circ$ .

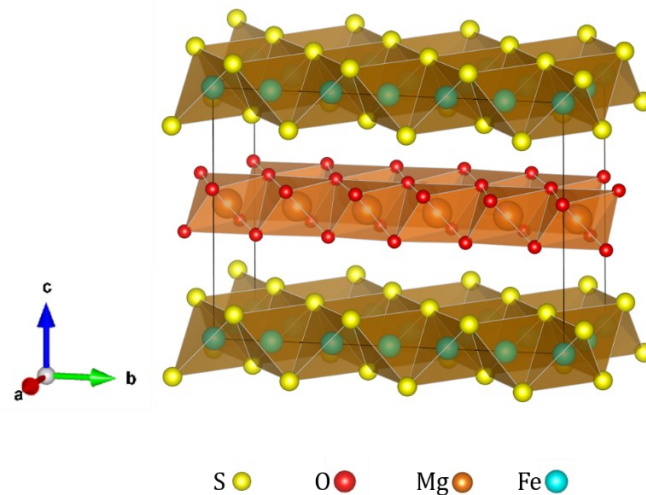


Figure 3: Unit cell of the isometric tochilinite variety as described by Organova *et al.*

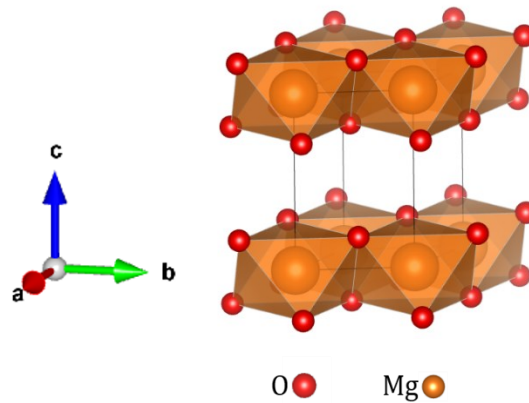


Figure 4: Unit cell of brucite.

The structure of isometric tochilinite as described by Organova is shown in figure 3 and the structures of mackinawite and brucite are shown in figure 1 and 4, respectively. Mackinawite crystallizes with tetragonal symmetry in the space group  $P 4/nmm$  with cell parameters of  $a = 3.66 \text{ \AA}$  and  $c = 5.03 \text{ \AA}$ .<sup>23</sup> Brucite,  $Mg(OH)_2$ , is the mineral form of magnesium hydroxide that can be described as a hexagonal close packing of hydroxide ions with the magnesium ions occupying one half of the octahedral sites. It has trigonal symmetry with space group  $P-3m1$  and lattice parameters of  $a = 3.15 \text{ \AA}$  and  $c = 4.77 \text{ \AA}$  ( $Z=1$ ).<sup>79</sup> The tetragonal lattice of mackinawite and the trigonal lattice of brucite cannot easily be aligned and multiples of the lattice parameters are needed to find a common set of lattice parameters for tochilinite.

To show how the structure of tochilinite corresponds to the mackinawite and brucite structures it is convenient to only consider the cation arrangements in the a-b-plane. The mackinawite and brucite structures in the a-b-plane and the corresponding unit cells are shown in figures 5 and 7. In mackinawite, the a and the b parameters are the same but the mackinawite substructure in tochilinite has lattice parameters of  $a_t = 2.68 \text{ \AA}$  and  $b_t = 2.60 \text{ \AA}$ . The distance between two  $Mg^{2+}$  in the brucite substructure of tochilinite is slightly increased from  $3.15 \text{ \AA}$  to  $3.21 \text{ \AA}$  in the b-direction and slightly decreased in a-direction from  $5.43 \text{ \AA}$  to  $5.37 \text{ \AA}$  compared to the brucite crystal structure.



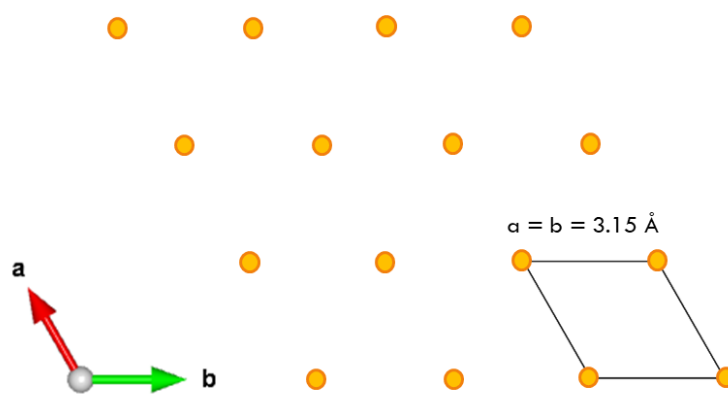


Figure 5:  $\text{Mg}^{2+}$  arrangement of brucite in the a-b-plane with the original unit cell.

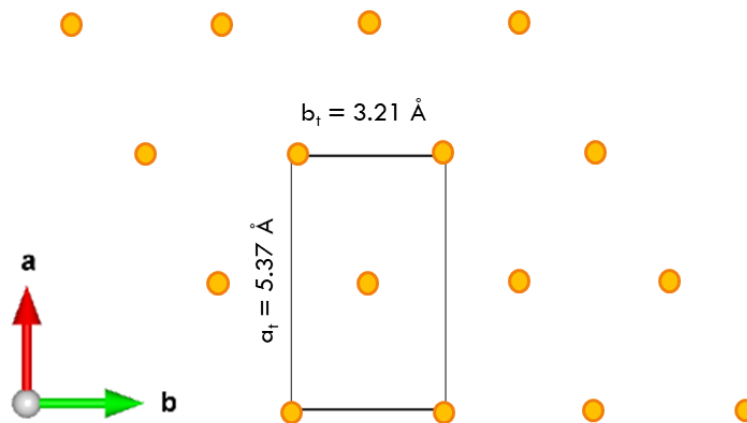


Figure 6:  $\text{Mg}^{2+}$  arrangement of the brucite substructure of tochilinite in the a-b-plane and the tochilinite unit cell.

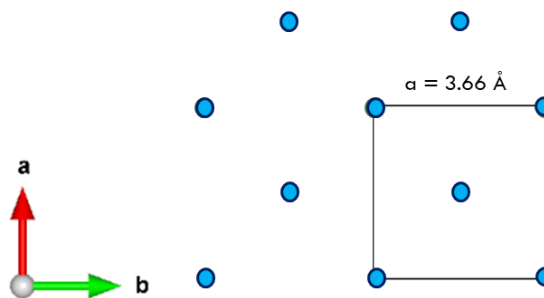


Figure 7:  $\text{Fe}^{2+}$  arrangement of mackinawite in the a-b-plane with the original unit cell.

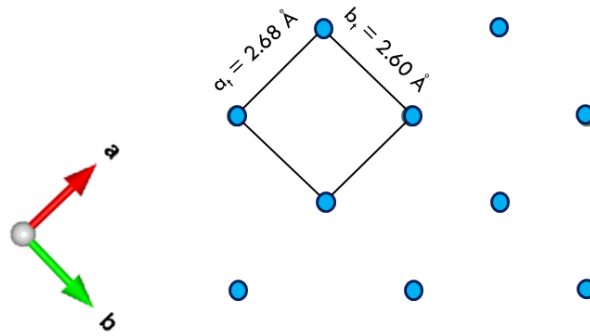


Figure 8:  $\text{Fe}^{2+}$  arrangement of the mackinawite sub-structure of tochilinite in the a-b-plane.

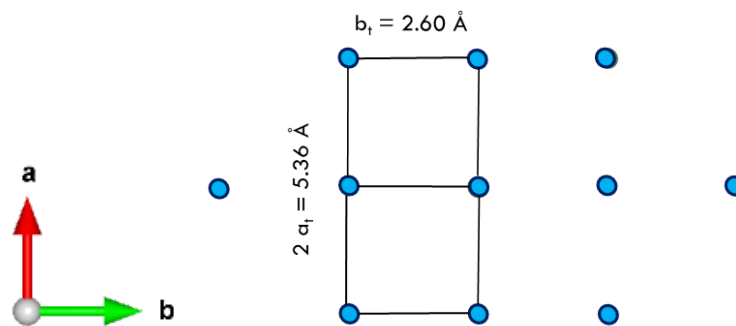


Figure 9:  $\text{Fe}^{2+}$  arrangement of the mackinawite substructure of tochilinite in the a-b-plane.

The lattice parameters of the brucite and the mackinawite substructures correspond with the lattice parameters of the tochilinite crystal structure by the following equations:

$$a_t (\text{brucite}) = 2 a_t (\text{mackinawite}) = a (\text{tochilinite})$$

$$5 b_t (\text{brucite}) = 6 b_t (\text{mackinawite}) = b (\text{tochilinite})$$

The composition of tochilinite is very versatile. Organova *et al.* determined the composition to be  $6 (\text{Fe}_{0.9}\text{S}) * 5 [\text{Mg}_{0.71}\text{Fe}_{0.29}(\text{OH})_2]$  after correction for gibbsite impurities. The ideal composition as expected from structural analysis is  $6 (\text{Fe}_{0.94}\text{S}) * [\text{Mg}_x\text{Fe}_y(\text{OH})_2]$  what fits well to the one obtained. This formula shows that there are iron vacancies in the mackinawite substructure and that iron ions occupy magnesium positions in the brucite substructure. Some of these iron ions are  $\text{Fe}^{3+}$  to balance the negative charge of the

mackinawite substructure. A great diversity of different compositions for tochilinite samples has been reported and some representative examples are shown in table 1.

Table 1: Compositions reported for natural tochilinite samples.

Formula	Reference
$6 (\text{Fe}_{0.8}\text{S}) * 5 [\text{Mg}_{0.71}\text{Fe}_{0.29}(\text{OH})_2]$	Organova <i>et al.</i> (1974) <sup>76</sup>
$6 (\text{Fe}_{0.9}\text{S}) * 4.47 [\text{Mg}_{0.53}\text{Fe}_{0.47}(\text{OH})_2]$	Harris and Vaughan (1972) <sup>80</sup>
$6 (\text{Fe}_{0.9}\text{S}) * 4.92 [\text{Mg}_{0.23}\text{Fe}_{0.71}(\text{OH})_2]$	Harris and Vaughan (1972) <sup>80</sup>
$6 (\text{Fe}_{0.78}\text{S}) * 4.71 [\text{Mg},\text{Fe}(\text{OH})_2]$	Organova <i>et al.</i> (1974) <sup>77</sup>
$6 (\text{Fe}_{0.81}\text{S}) * 5.37 [\text{Mg}_{0.79}\text{Al}_{0.21}(\text{OH})_2]$	Jambor (1976) <sup>81</sup>
$6 (\text{Fe}_{0.63}\text{Cu}_{0.24}\text{S}) * 4.95 [\text{Mg}_{0.78}\text{Al}_{0.29}\text{Ca}_{0.01}(\text{OH})_2]$	Muramatsu and Nambu (1980) <sup>82</sup>
$6 (\text{FeS}) * 5 [\text{Fe}(\text{OH})_2]$	Pekov <i>et al.</i> (2012) <sup>83</sup>

There are some more tochilinite-like minerals that do not have the same structure or composition as the Organova isometric tochilinite but may be also mentioned here to give a deeper insight into this mineral class. Valleriite is the most prominent layered hybrid mineral composed of sulfide and hydroxide layers. The main difference to the tochilinite structure is the arrangement of the sulfide tetrahedra and that it contains a significant amount of copper ions. Its composition is reported by Evans to be  $(\text{Fe}_{1.07}\text{Cu}_{0.93}\text{S}_2) * 1,526 [\text{Mg}_{0.68}\text{Al}_{0.32}(\text{OH})_2]$ <sup>84</sup>. The structure requires a large superlattice like tochilinite but has been defined in terms of two separate sublattices: a rhombohedral one corresponding to the sulfide layers and a hexagonal one corresponding to the hydroxide layers. The iron and copper ions are distributed randomly within the sulfide layers.<sup>84</sup> Yushkinite is a mixed layered mineral with a brucite-like hydroxide layer alternating with a berndtite-type sulfide layer. It has a composition of  $(\text{VS}_2) * [\text{Mg}_{0.71}\text{Al}_{0.36}\text{V}_{0.03}(\text{OH})_{2.18}\text{O}_{0.02}]$ .<sup>85</sup> Haapalaite is a mineral with the composition of  $(\text{Fe}_{1.36}\text{Ni}_{0.74}\text{S}_2) * 1.610 [\text{Fe}_{0.16}\text{Mg}_{0.84}(\text{OH})_2]$ . The structure still needs to be determined in detail but preliminary analyses indicate that is related

to the valleriite structure.<sup>86</sup> A calcium rich example is vyalsovite containing  $\text{Ca}(\text{OH})_2$  and  $\text{Al}(\text{OH})_3$  in the hydroxide layers. Ekplexite  $[(\text{Nb},\text{Mo})\text{S}_2] * [\text{Mg}_{1-x}\text{Al}_x(\text{OH})_{2+x}]$ , kaskasite  $[(\text{Nb},\text{Mo})\text{S}_2] * [\text{Mg}_{1-x}\text{Al}_x(\text{OH})_{2+x}]$  and the manganese rich equivalent manganokaskasite  $[(\text{Nb},\text{Mo})\text{S}_2] * [\text{Mn}_{1+x}\text{Al}_x(\text{OH})_{2+x}]$  are three quite new valleriite-group minerals described by Pekov *et al.* in 2014.<sup>87</sup>

This list shows how diverse the group of layered hybrid sulfides is and that the structures and compositions can differ within a great range. Therefore, the crystal structure of any natural or synthetic tochilinite-like sample needs to be evaluated thoroughly what may prove as a very tough task. Many of these minerals are quite rare and do not form massive aggregates what makes high-resolution crystal structure solution impossible.

Consequently, investigations on chemical reactivities and further properties of these hybrid minerals have not been carried out yet and offer a huge field for future studies.

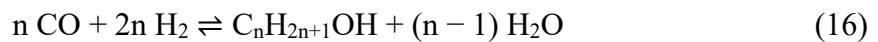
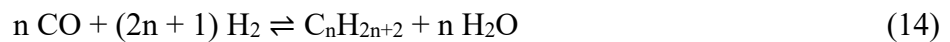
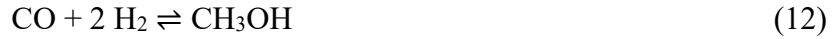
## 1.4 Activation and hydrogenation of $\text{CO}_2$

### 1.4.1 Overview

$\text{CO}_2$  is one of the simplest carbon compounds and universally available but also insignificant for laboratory and industrial chemical synthesis. Indeed, the use of  $\text{CO}_2$  as chemical feedstock is limited to a few industrial processes like the synthesis of urea and its derivatives, salicylic acid and carbonates.<sup>88</sup> The reason is that  $\text{CO}_2$  is inert and intrinsically stable with  $\Delta G_{f0} = -394.4 \text{ kJ}\cdot\text{mol}^{-1}$  and thus a great amount of energy is required for its activation. Heterogeneous and homogenous catalysts are used to reduce the activation barrier and promote any further reaction.<sup>89</sup> Several tools that can lead to the activation of  $\text{CO}_2$  have been reported that include bending or stretching of the linear  $\text{CO}_2$  molecule and charge transfer processes altering the electronic states.<sup>90,91</sup> Widespread heterogeneous catalyst systems use pure metals like Cu, Co and Fe that are coupled with promoters like Ce, Mn, Na and K and prepared on oxide supports like  $\text{Al}_2\text{O}_3$ ,  $\text{SiO}_2$ ,  $\text{CeO}_2$  or  $\text{TiO}_2$ . Iron and cobalt initially form carbides with  $\text{CO}_2$  that act as the main active phases. The promoters enhance the resistance towards deactivation / poisoning and improve the reaction rates and selectivity. The different oxide supports also offer multiple features that promote the reduction of  $\text{CO}_2$ . For example, MgO and  $\text{Al}_2\text{O}_3$  exhibit surface OH-groups, which favor the adsorption of reaction intermediates and enhance the reduction kinetics.

Their great surface areas help to disperse the metal particles and to prevent their agglomeration.<sup>89</sup> The mechanism of CO<sub>2</sub> reduction on heterogenous catalysts is a highly topical issue and still under extensive debate. The activation energy and the product selectivity for the reduction of CO<sub>2</sub> and carbonates depend on many aspects especially the adsorption on the catalyst surface but also on the influence of the surrounding solution.<sup>92,93</sup>

The reduction of CO<sub>2</sub> needs to be coupled to a suitable oxidation reaction that offers enough reducing power. In a heterogeneous system this is usually done catalytically without permanently changing the state of the solid catalyst. For catalysis, the use of hydrogen gas as reducing agent has attracted much attention as it acts as a source of electrons and protons at the same time. In Fischer-Tropsch-type reactions, the reduction of CO<sub>2</sub> by H<sub>2</sub> is considered to be a multi-step process with CO as the key intermediate formed by a reversed water gas shift reaction. The formed CO is further reduced yielding different carbohydrates depending on the reaction conditions.<sup>89,90</sup>



A direct reduction without the formation of CO has been also proposed, but could not be verified so far.<sup>94</sup> Like CO<sub>2</sub>, hydrogen also needs to be activated due to its intrinsic stability. Metals have been known for many years to activate elemental hydrogen by chemisorption. Particularly palladium, ruthenium and copper show high activities and are therefore the major materials used for modern heterogeneous hydrogen activation.<sup>89,95,96</sup> Catalytic activity is also observed for some semiconductor oxides like Cr<sub>2</sub>O<sub>3</sub> and NiO and a number of sulfides including MoS<sub>2</sub>, WS<sub>2</sub> and CoS but not for FeS, CuS or NiS.<sup>97,98</sup> A

recent publication shows that  $Zn_xCd_{1-x}S$  based materials show great catalytic activity towards the activation of hydrogen.<sup>99</sup>

In the case of a non-catalytic heterogeneous reduction reaction using iron sulfides, the particles themselves are oxidized and sufficient amounts of  $H^+$  need to be available for protonation. As already outlined in the previous chapter, iron sulfides can be oxidized in different ways e.g. by oxidation of the  $Fe^{2+}$  or  $S^{2-}$  depending on the reaction conditions. The protonation of the reduced carbon species may be possible by the presence of water alone and can be increased by the addition of acids. Several reports show that the pH-value of the reaction solution in  $CO_2$ -reduction reactions defines the reaction mechanism and in consequence the required redox potential and the product selectivity.<sup>92,93</sup>

#### **1.4.2 Carbon fixation under hydrothermal conditions**

Today, iron sulfides are highly abundant in certain marine sediments. Therefore, origin-of-life-theories considering iron sulfides as key participants are located at the bottom of the ocean. In Wächtershäuser's theory, only pyrite and its characteristics are important and the other iron sulfides do not contribute more than being a sole source for pyrite formation and  $H_2S$  oxidation. The catalytic potential and the redox chemistry of mackinawite, pyrrhotite and greigite were considered in other theories and most important at hydrothermal vents. Russel, Martin and many more contributed much to the prominence of this theory and explained the geological and thermodynamic background. Until now, only little experimental support was given for the hydrothermal vent chemistry of iron sulfides what also applies to the iron-sulfur-world theory by Wächtershäuser.<sup>13,16,100–102</sup>

Origin of life theories in a hydrothermal setting gained increasing attention after the discovery of submarine hydrothermal vents that release sulfide rich exhalations. The released sulfide ions precipitate with metal ions in the surrounding acidic seawater and form black sulfides that accumulate in chimney-like structures. Thus, these hydrothermal vents are called "black smokers" and are the trigger for the rise of prebiotic hydrothermal vent theories. Hydrothermal vents exhibit a great variety of dissolved species and pH and temperature ranges, but they are only the "tip of the iceberg". The underlying hydrothermal systems offer an even more versatile and complex chemistry.<sup>103</sup> Ancient hydrothermal fluids are expected to be highly reduced and carry great amounts of hydrogen gas with

them. The hydrogen gas is produced by serpentinization, an alteration process that generates serpentinites from minerals like olivine and pyroxene.<sup>104,105</sup>



Any carbon species like CO<sub>2</sub>, CO or HCN can be reduced in this environment and the major product found in hydrothermal environments is methane. Longer carbon chains are rather rare as they would probably form by Fischer-Tropsch-type reactions requiring appropriate catalysts and conditions. The investigation of hydrothermal CO<sub>2</sub> reduction with elemental iron by Deng *et al.*<sup>106</sup> showed that methane is the major product and longer carbohydrates are found only up to butane. These findings are supported by the later works of Hardy and Gillham<sup>107</sup> as well as McCollom and Seewald<sup>108</sup>. Elemental iron is used as a catalyst in Fischer-Tropsch reactions and may be found under strongly reduced hydrothermal conditions as shown by Chamberlain *et al.* and Schwarzenbach *et al.*<sup>109,110</sup>

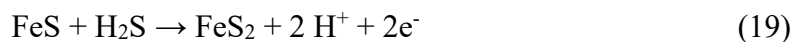
In current reports on theories and setting for the origin of life, the reduction of C1 species is thought to deliver small reactive water-soluble molecules like formic and acetic acid, aldehydes, pyruvate and amino acids that can later form more complex molecules under the appropriate conditions.<sup>111-113</sup> Preiner *et al.* very recently showed, that greigite, magnetite and awaruite can catalyze the reduction of CO<sub>2</sub> by H<sub>2</sub> under hydrothermal conditions mainly forming formate and acetate.<sup>16</sup> The formation of long chain hydrocarbons is not in the focus of many origin-of-life theories, although the appearance of long chain fatty acids is crucial for the formation of membranes and vesicles. The chain lengths of hydrocarbons at hydrothermal conditions is limited and has not reached C<sub>12</sub>.<sup>113,114</sup>

A second basic feature of hydrothermal models is the contact of hot water from the earth's mantle and the colder seawater that leads to steep pH, redox and temperature gradients. After the discovery of stable iron sulfide formations that looked like bubbles, Russel and Hall proposed the idea of iron sulfide membranes that separate the two regimes in hydrothermal vents. These conducting membranes should have enabled the emergence of a proton motive force offering additional redox potential. It has been proposed, that mackinawite and greigite that mainly constitute this membrane could have acted as the catalytic surfaces for CO<sub>2</sub> reduction as they share a similar structure with the active centers of modern enzymes.<sup>13</sup> A major problem of deep sea carbon fixation is the available

concentration of the carbon feedstock like CO and CO<sub>2</sub>. If iron sulfides would have been present on the earth's surface, the access to these gases would have been much easier.

### 1.4.3 The iron sulfur world by G. Wächtershäuser

In this chapter, a brief summary of the most relevant features of the iron sulfur world by G. Wächtershäuser is presented. He published a theory on the autotrophic origin of life in the 1980's and early 1990's. Wächtershäuser divides the metabolic character of the first living organism into two possibilities: a heterotrophic organism dependent on the carbon nutrients in its surrounding and an autotrophic organism capable of synthesizing all its carbon nutrients from C1 substrates. In his theory, the only plausible scenario is the origin of a chemoautotrophic organism utilizing a chemical source of reducing power. His theory focuses on the reduction of carbon species like CO<sub>2</sub>, CO or HCN and the origin of a surface bound metabolism. The power to reduce these carbon species is provided by the oxidation of hydrogen sulfide and the formation of pyrite.<sup>115</sup>

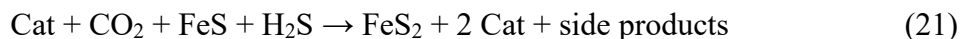
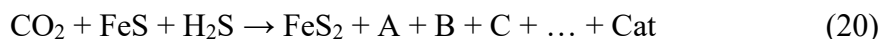


$$\Delta_{\text{R}}G^{\circ} = -38.4 \text{ kJ/mol}$$

In this reaction the Fe<sup>2+</sup> ions are not oxidized while two sulfide ions form a disulfide ion and release two electrons or hydrogen gas, respectively.<sup>7</sup> This reaction only takes place in acidic solutions following the pH dependency of the redox potential of sulfide ions.<sup>116</sup> The generation of hydrogen gas is kinetically hindered and shows a very small rate even at 100 °C.<sup>6</sup> This kinetic barrier is a key feature for the iron-sulfur-world theory. A reduction reaction with a small activation barrier would rapidly consume all nutrients without the ability to develop a self-sustaining reaction network. The continuous flow of H<sub>2</sub>S, CO<sub>2</sub> and Fe<sup>2+</sup> towards the pyrite surface leads to the growth of the pyrite crystal and the constant production of organic molecules. Bound to the pyrite surface, these organic species react with each other forming more and more complex species. These increasingly complex molecules at some point become catalytically active towards the pyrite pulled formation of them and implement the first autocatalytic cycle. In the chemical equation below "A", "B" and "C" represent organic molecules that are formed by pyrite pulled CO<sub>2</sub> reduction. "A" and "B" react on the pyrite surface to form a catalytically active



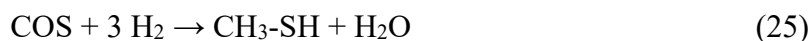
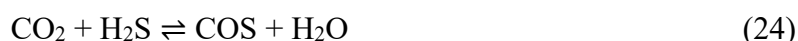
species “Cat”. This species is able to influence the pyrite pulled reduction to increase the formation of itself.



This process would be the origin of the first self-sustaining cycle or network that features chemical evolution. The next step Wächtershäuser describes is the formation of long chain fatty acids that could lead to self-compartmentation of pyrite particles. If a nitrogen source like ammonia is present, amino acids and peptides could form and mark the origin of enzymes. These enzymes may offer completely new reactivities and could kick off the formation of nucleotides and start the RNA/DNA chemistry. This would mark the beginning of the modern biochemistry. The matured and very topical RNA world theory can give insights into the next steps towards the origin of a real Last Universal Common Ancestor (LUCA). There is much more detail in Wächtershäuser's theory to be presented but that would exceed the scope of this chapter. Experimental findings regarding the pyrite pulled carbon fixation are presented below.

In 1995 and 1997, Heinen and Lauwers published two studies on the pyrite pulled reduction of  $\text{CO}_2$ . They found that in an aqueous  $\text{H}_2\text{S}$  environment iron sulfide converts to pyrite and  $\text{CO}_2$  is reduced to thiols.

For the reaction sequence they give following equations:



Regarding the C-C bond formation, they do not go into mechanistic detail. Other products of this system are  $\text{CS}_2$ , dimethyl disulfide and hydrogen gas. They also showed that  $\text{CO}_2$  reacts with  $\text{H}_2$  and  $\text{H}_2\text{S}$  to form thiols without iron sulfide but in the presence of elemental iron. In summary, they report the formation of thiols with low yields that stagnate already after a couple of days: “At temperatures below 25 °C, thiol formation never proceeded

for more than 7 days at low level, after this it collapsed totally". These findings were hardly promising and have not been pursued by any further investigation.

Regarding all the features of iron sulfide chemistry, these investigations can only be viewed as a first step towards an understanding of the pyrite pulled carbon fixation. Heinen and Lauwers did not look for other products than sulfur containing nonpolar volatiles. Any products that are highly soluble in aqueous solution would have been overlooked like carbonic acids that are key compounds for Wächtershäuser's theory. The use of commercial iron sulfide with pyrrhotite structure may lack reactivity and freshly precipitated mackinawite should be much more reactive.

#### 1.4.4 Iron-sulfur centers in modern enzymes

Modern organisms use specific enzymatic systems that allow for an effective conversion of different substrates to specific products. Many of these utilize active sites containing metal ions like  $\text{Fe}^{2+}$  and  $\text{Ni}^{2+}$  and a ligand sphere incorporated into a complex protein scaffold. Regarding carbon and nitrogen fixation, the most interesting enzymes are nitrogenases, hydrogenases and the carbon monoxide dehydrogenase.

Nitrogenases catalyze the reversible reduction of nitrogen:



Hydrogenases catalyze the reversible oxidation of hydrogen:



The carbon monoxide dehydrogenase catalyzes the reversible reduction of  $\text{CO}_2$ :



Hydrogenases are divided into three different types based on the active site metal ions. There are iron-iron hydrogenases and nickel-iron hydrogenases with very similar active sites and iron hydrogenases with only a mononuclear active site and no iron-sulfur clusters. The hydrogenases with binuclear active sites catalyze the oxidation of  $\text{H}_2$  whereas the iron hydrogenases catalyze the heterolytically cleavage of molecular hydrogen.



Common to the iron-iron and the nickel-iron hydrogenases are iron-sulfur clusters that act as electron mediators. [4Fe-4S] and [3Fe-4S] clusters are active in electron transfer from and to the active sites.<sup>117</sup> The coordination environment of the iron ions in these clusters is comparable to the one found in greigite. The active site of carbon monoxide dehydrogenase is also composed of analogous metal-sulfur clusters. It contains three [4Fe-4S] clusters, of which two are connected to nickel ions. It catalyzes the formation of acetyl-coenzyme A from CO bound to iron and a CH<sub>3</sub>- group bound to nickel. Similar abiotic reactions have been proposed to take place on the surfaces of iron-nickel sulfides.<sup>118,119</sup> Moreover, the mackinawite structure shows similarities to the active site of [FeFe]-hydrogenases. It has been determined that nitrogenases are two-component systems composed of a molybdenum-iron protein and an iron-containing electron-transfer protein. The coordination environment of the iron and molybdenum ions in these substructures also shows similarities to iron sulfide minerals. All these similarities make iron sulfides the most probable candidates as predecessors of crucial parts of modern enzymes that catalyze reduction reactions.<sup>120,121</sup>

Zhang *et al.* investigated the catalytic activity of different iron and nickel containing sulfides towards electrochemical CO<sub>2</sub> reduction. They found that: “Although Fe<sub>3</sub>S<sub>4</sub> inefficiently reduces CO<sub>2</sub>, the efficiency of CO and CH<sub>4</sub> production was substantially improved by the substitution of Fe with Ni to form violarite (FeNi<sub>2</sub>S<sub>4</sub>). Ni-containing greigite (NiFe<sub>5</sub>S<sub>8</sub>), and violarite (FeNi<sub>2</sub>S<sub>4</sub>) share structural similarity to nickel-iron hydrogenases, the C-cluster in carbon monoxide dehydrogenases and the Acetyl-coenzyme A synthetase active site A-cluster, respectively”.<sup>122</sup> A study of Roldan *et al.* has shown that greigite is able to catalyze the electrochemical reduction of CO<sub>2</sub> under ambient conditions into methanol, formic acetic and pyruvic acid. They found that a pH value of 6.5 is the optimum pH for the reduction experiments.<sup>15</sup>

#### **1.4.5 Potential role of mackinawite and tochilinite**

To examine the potential role of mackinawite and tochilinite for prebiotic carbon fixation, reduction reactions need to be done to show their reactivity and selectivity. It has to be clarified if the mackinawite structure supports the activation of CO<sub>2</sub> as the most crucial step for prebiotic carbon fixation. A theoretical investigation by Dzade *et al.* shows that

CO<sub>2</sub> can be activated on the mackinawite surface. The adsorption energies differ between the (001), (011) and (111) surfaces and are greatest on the (111) surface. Their calculations even show that the dissociation of the CO<sub>2</sub> molecule on the (011) and the (111) surface into a surface bound CO and an oxide anion while oxidizing Fe<sup>2+</sup> can be energetically favorable. The (001) surface is the most stable one and chemically inert compared to the other surfaces.<sup>123–125</sup> As mackinawite has a layered structure and forms thin platelets, the (001) surface is much more pronounced than the (011) and the (111) surfaces, but the use of freshly prepared nanoparticulate mackinawite may circumvent this issue.

Additionally, mackinawite offers the possibility to incorporate other transition metal ions into its structure. It has been shown that, among others, Ni<sup>2+</sup>, Cu<sup>2+</sup> and Co<sup>2+</sup> can replace Fe<sup>2+</sup> ions in mackinawite to a certain degree without changing its structure.<sup>55,126</sup> As the interatomic distances and the electronic structure of the surface sites strongly affect the catalytic activity, there is a lot of potential for optimization. Russel and Martin have reported that iron ions at the iron sulfide surface are suited to bind C-O species and that nickel ions are better at binding CH<sub>3</sub>-groups.<sup>13</sup> Different carbon species on the surface can react and form molecules that are more complex. Thus, the products of carbon fixation reactions strongly depend on the composition of the mackinawite surface. In general, the catalytic activity of heterogeneous catalysts depends on various factors. Surface area, active site concentration and chemical stability are very important factors. Regarding mackinawite, chemical stability is the main problem. As described in previous chapters it is very sensitive to oxidation and phase transformations at higher temperatures. Still, the catalytic activity of mackinawite is an interesting and promising topic that is still rather unexplored. In this regard, tochilinite also offers very interesting catalytic potential for the activation and reduction of CO<sub>2</sub>. For one part, it contains mackinawite-like layers that theoretically are able to activate CO<sub>2</sub>, but it should be much more stable than mackinawite. That is why it could be suited for reactions at higher temperatures to overcome crucial activation barriers. In modern systems for CO<sub>2</sub> reduction with H<sub>2</sub> multiple phases are used simultaneously that fulfill different tasks. When using tochilinite analogues, the reduction of CO<sub>2</sub> and the oxidation of H<sub>2</sub> can take place on similar surface sites but it is also possible, to have reduction and oxidation separated from one another. This has not been examined for tochilinite, but for other layered misfit structures it was reported, that a charge transfer between the different layers is possible.<sup>127</sup> As tochilinite contains sulfide

surface groups as well as hydroxide surface groups, a more versatile acid-base chemistry can be expected than for mackinawite or brucite alone. The close contact of the different layers can promote CO<sub>2</sub> adsorption and proton, electron, or CO transfer. The possibility to incorporate different transition metal ions in the sulfide layers like Ni<sup>2+</sup>, Co<sup>2+</sup> or Cu<sup>2+</sup> gives additional potential to increase the catalytic activity. The acidity and the redox behavior of the hydroxide layers may be adjusted by the content of Al<sup>3+</sup>, Mg<sup>2+</sup>, Ca<sup>2+</sup>, Fe<sup>2+</sup> and Fe<sup>3+</sup>. Therefore, tochilinite like solids may be able to catalyze a broad range of redox reactions and offer a high degree of adaptability.

The main questions that were investigated during this work regarding the reduction of CO<sub>2</sub> consequently are: Can mackinawite and/or tochilinite activate CO<sub>2</sub> as predicted by Dzade *et al.* and is there an activation of hydrogen at any of them to form reduced hydrocarbon species? What is the influence of the tochilinite composition on its stability and activity? The reduction of CO<sub>2</sub> can lead to the formation of various products that differ significantly in their physical and chemical properties. Therefore, it is necessary to establish an analytical method for any class of product that is of interest. As has been shown by Heinen and Lauwers<sup>128</sup>, thiols are a class of compounds that is expected in CO<sub>2</sub> reduction experiments using iron sulfides. As the low temperature reduction of CO<sub>2</sub> usually leads to the formation of small organic molecules like carbon monoxide, methane, methanol and formic acid, these are to be expected as well. To show that CO<sub>2</sub> can be reduced on mackinawite surfaces, gas chromatography coupled with mass spectrometry (GC-MS) was the method of choice for this work as it can separate any gaseous products and offer well established ways for their identification. A shortcoming of GC-MS is that H<sub>2</sub> and highly water-soluble products like carbonic acids, short chain alcohols or amino acids may be overlooked. Therefore, it is helpful to analyze the iron sulfides used after the reactions to investigate the formation of oxidized solid phases.

## **2 Materials and methods**

### **2.1 Materials**

#### **2.1.1 Miscellaneous**

Any salts used in this work were bought from Sigma-Aldrich in high purity and used as obtained. The same applies to organic solvents like EtOH and acetone. For GC-MS analysis, the solvents were bought in GC-MS grade and additionally distilled twice. Deionized water was provided by our in-house supply. In some reactions, ultra-pure water (HPLC grade) was used which was bought from Thermo Fisher Scientific. To deaerate the water before the syntheses, it was filled into a 250 ml 3-neck flask and purged with nitrogen gas for at least 12 hours. If the water additionally needed to be free of dissolved carbonates, all dissolved gases were removed by the freeze-pump-thaw technique.

#### **2.1.2 Iron sulfide synthesis**

For the sulfide syntheses, powders of elemental metals (iron, magnesium, aluminum, copper, nickel, zinc, manganese, chromium, cobalt, molybdenum and tungsten) were used as received. They were bought from Sigma-Aldrich. Purity for every metal was at least 99.5 % and the elemental iron was additionally investigated for impurity phases.

Elemental sulfur was bought from Sigma-Aldrich with a purity of 99.998 % and used as received.

#### **2.1.3 Carbon fixation experiments**

For carbon fixation experiments, iron sulfides were prepared from elemental iron and elemental sulfur as described above.

The carbon sources used are  $^{13}\text{C}$  sodium carbonate bought from Merck or Eurisotope or gaseous  $\text{CO}_2$  bought from Linde and used as received. When working with enriched gaseous  $^{13}\text{CO}_2$ , the carbonates were weighed into a 25 ml microwave vial and charged with concentrated phosphorous or hydrochloric acid after setting the vial under reduced pressure. The released  $^{13}\text{CO}_2$  was transferred into the reaction vial/flask using a syringe.

The water used for carbon fixation experiments was ultra-pure water (HPLC grade) that was bought from Thermo Fisher Scientific. Before the use in carbon fixation experiments, it was either deaerated by purging with nitrogen gas or all dissolved gases were removed by the freeze-pump-thaw technique.

Fischer-Tropsch-type (FTT) reactions were carried out in the group of Prof. Dr. Trapp at the LMU Munich by Sophia Peters and Christoph Seifert. All gas bottles used in these experiments were bought from Linde with a purity of at least 99.5 %. The DCM used for extraction was purified in a rotary condenser prior to the experiments.

## **2.2 Methods**

### **2.2.1 Syntheses**

#### **2.2.1.1 Synthesis of metal sulfides**

Metal sulfides were mainly synthesized from the elements. The elemental metals and sulfur were weighed into a beaker in the desired ratio and transferred into an automated mortar (Fritsch "Pulverisette", made in Germany) and ground thoroughly for one hour. The obtained homogeneously colored powders were stored in powder bottles.

The desired amount of metal-sulfur-mixture and any additional salts were filled into 25 ml microwave vials and sealed with aluminum caps with a polypropylene septum. The vials were repeatedly evacuated and filled with nitrogen gas using a Schlenk line connected via a cannula. Then, between 0.5 and 25 ml of deaerated water were added with a syringe. The reaction times and temperatures were set depending on the actual experiment.

After the reactions had finished, the product suspensions were further processed depending on their further use. If they were to be dried and analyzed, a standard procedure was established as follows. As many metal sulfides are pyrophoric at air contact, they need to be deactivated cautiously. Therefore, the lid was removed from the vials and the metal sulfide suspensions were quickly transferred into a glass frit. A funnel was used to direct nitrogen gas into the frit and to exclude air contact. The water was then removed through the frit and the wet metal sulfide particles were either dried overnight in this setup or previously washed successively with ethanol, acetone and diethyl ether to increase the

drying speed. When the particles were dry, the nitrogen flow was reduced to let air get into the frit and allow cautious oxidation. Thereby, the frit in most cases got warm, as the oxidation reactions are exothermic. To prevent a thermal runaway, the sulfides were immediately cooled again by increasing the nitrogen flow until they reached room temperature. This procedure was repeated until they did not heat up again upon air contact.

To check if this procedure has an influence on the detectable phases by PXRD, mackinawite was synthesized from iron and sulfur as described above and transferred as a wet paste onto a PXRD sample holder and frozen with liquid nitrogen. The frozen sample was allowed to melt slightly on the top and was then transferred into the instrument for measurement. No differences were observed in the PXRD patterns between deactivated and non-oxidized samples.

If the metal sulfides were used for the syntheses of tochilinite analogues without previous oxidation, the wet samples were transferred directly into steel autoclaves with Teflon inlets together with their surrounding solution as described below.

If the metal sulfides were to be used for carbon reduction experiments, air contact was thoroughly prevented and they were either used together with the surrounding solution or dried in their vial under reduced pressure for 12 to 48 hours.

#### **2.2.1.2 Synthesis of tochilinite analogues**

Tochilinite-like sulfides were prepared at temperatures above 100 °C under autogenous pressure in steel autoclaves. These autoclaves contained a 50 ml Teflon inlet with a Teflon lid and are safe to be used up to 180 °C. All solid starting materials were ground thoroughly in an automated mortar (Fritsch “Pulverisette”, made in Germany) for one hour. The solids were then weighed into the Teflon inlet and charged with 20 ml of water. This procedure was carried out open to the atmosphere.

If freshly prepared mackinawite was used, it was prepared previously either by precipitation or from the elements. The other reagents were weighed into the Teflon inlet and charged with the mackinawite suspension and additional water to reach a total volume of 20 ml. The solids were mixed with a glass rod until a homogenous mixture was obtained. Afterwards, the reactors were sealed and placed in an oven at the desired temperature.



### 2.2.2 Carbon fixation experiments with mackinawite

The carbon fixation experiments that were carried out during this work can be divided in high (above 100 °C), medium (80 °C) and low temperature (room temperature) runs.

The low and medium temperature runs were carried out in 25 ml microwave vials. The mackinawite intended for reduction experiments was prepared following the standard procedure and then used as synthesized in the initial vials. Deaerated solutions of the carbon source and any additional salts were added via a syringe to minimize the contamination with oxygen. If gaseous carbon sources were used, the atmosphere in the vials was removed under reduced pressure and the desired gas added through a cannula. After the reactions had finished, the solid, the solution and the gas phase were analyzed separately.

The high temperature runs were carried out in a distillation apparatus. A 20 ml flask was connected via a distillation bridge to a 10 ml flask using Teflon connectors. The former one was heated in an oil bath and the latter cooled in a DCM/liquid nitrogen cooling bath. Mackinawite with adsorbed carbonates was transferred into the 20 ml flask and 1 ml of DCM was transferred into the 10 ml flask. The reaction mixture was heated for several hours in which all nonpolar volatiles dissolved in the cooled liquid DCM phase.

### 2.2.3 Carbon fixation experiments with tochilinite

Fischer-Tropsch-type (FTT) reactions were carried out in a high-pressure stainless-steel autoclave with a 200 mL glass insert with digital pressure gauges, a fine throttling valve, and a temperature sensor. The autoclaves were tightened with silver gasket. The temperature was adjusted by a heating jacket. The autoclaves were purchased from Carl Roth, Karlsruhe, Germany. The autoclaves could be connected via a valve to a pipe system connecting a vacuum pump and gas bottles of N<sub>2</sub>, H<sub>2</sub> and CO<sub>2</sub>. The atmosphere in the autoclaves was removed to a pressure of at least 10<sup>-3</sup> bar and filled according to the experiments with the desired gases. The autoclaves were heated in heating jackets and after cooling down cooled to around -180 °C. The frozen solid material was transferred into a flask connected to the glass distillation apparatus which was evacuated 3 times at 10<sup>-2</sup> mbar. Then, the flask of the distillation apparatus was heated to the reaction temperature and the evaporated compounds were condensed into a flask cooled with liquid nitrogen. After completion of the distillation process the apparatus was opened and the condensed

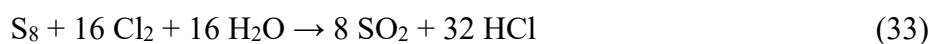
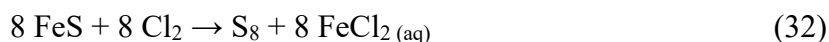
compounds were collected by adding dichloromethane (0.3 ml or 0.5 ml). All blank measurements showed no contamination, so it can be assumed that there are none of the targeted compounds present without the iron sulfides or without CO<sub>2</sub>.

### 2.3 Elemental analysis via ICP-AES

To determine the sulfide and metal content in the iron sulfide samples, they needed to be dissolved completely. As the acidic dissolution of iron sulfides leads to the formation of H<sub>2</sub>S that would be lost in an open system, a method had to be developed for how to deal with the H<sub>2</sub>S gas. Additionally, H<sub>2</sub>S in oxidizing acidic solutions quickly forms insoluble elemental sulfur that also has to be dealt with. To circumvent these issues, several approaches may be suitable. Rickard *et al.* published their extensive work on this topic in 2006 using a specially designed apparatus. They dissolved an iron sulfide sample in cold hydrochloric acid with an additional reducing agent and quantitatively released H<sub>2</sub>S from the solution and dissolved it again in a Cu<sup>2+</sup> containing solution whereby CuS precipitated. The remaining Cu<sup>2+</sup> in the solution was determined by back titration and the amount of released H<sub>2</sub>S could be calculated.



As the apparatus was not available, a different approach was developed using the oxidizing power of aqua regia that leads reproducibly to complete oxidation and dissolution of the sample.



To ensure the complete oxidation of the sulfide ions, high temperatures and high pressures would be beneficial. However, the use of high-pressure autoclaves for acidic digestion that are widely used for dissolution is difficult, as they cannot be charged with the FeS

sample and the acids without the loss of H<sub>2</sub>S before they can be closed. To circumvent this problem, the FeS samples were loaded into steel autoclaves with Teflon inlets and a Teflon lid and were charged with 10 ml of water to cover the sample completely. The water was frozen carefully with liquid nitrogen so that the FeS sample was protected by a cover of ice. On top of the ice surface, 10 ml of aqua regia was added and the autoclave sealed before the ice starts to melt. No smell of H<sub>2</sub>S was to be perceived in this process. The autoclaves were then heated to 130 °C overnight to obtain clear and deep orange solutions after they cooled down to room temperature. The solutions were transferred into a 250 ml volumetric flask and filled to the mark with distilled water. The obtained solutions were immediately transferred into polyethylene vials to reduce any contamination from the glass walls.

## **2.4 Powder X-ray diffraction (PXRD)**

Powder X-Ray diffraction patterns were collected at two different devices. Our in-house device is a STOE STADI P diffractometer equipped with a copper anode X-ray source and a Mythen 1K detector. As no additional monochromators are equipped, the patterns had a rather bad signal-to-noise ratio. Nevertheless, this device offers the possibility to analyze very small amounts of sample and was used occasionally. The other one is a tabletop Rigaku Mini-Flex 600 equipped with a copper anode with 0.6 kW and an energy dispersive detector to minimize effects of X-ray fluorescence.

## **2.5 Rietveld refinement of PXRD patterns**

Any Rietveld refinement was carried out with the software “Topas 5” by Bruker. The PXRD patterns for the refinements were collected at the Rigaku diffractometer. The instrumental parameters were determined with a LaB<sub>6</sub> standard by the fundamental parameters approach.<sup>129</sup> The background curve was also determined with this standard. The structures used for the refinements were taken from the American Mineralogist Crystal Structure Database.

## **2.6 Mössbauer spectroscopy**

Mössbauer spectra were obtained on a homemade spectrometer based on a RCPTM MS-96 Mössbauer spectrometer equipped with a Ritverc Co57 in a Rh-matrix source, a YAP:Ce scintillating crystal detector, and a Janis SVT-400 helium-bath cryostat. The samples (roughly 30 mg) were filled into weighing paper that was folded to squares, and parafilm was wrapped tightly around it. The sample was inserted into an Al sample holder, which was then inserted into the Mössbauer spectrometer. Spectra were calibrated against  $\alpha$ -iron at room temperature or 80 K and fitted using the MossWinn 4.01 program.

## **2.7 Scanning electron microscopy (SEM)**

Scanning electron microscopy (SEM) imaging was performed with a Sigma VP Field Emission Scanning Electron Microscope (Carl-Zeiss AG, Germany) using the InLens detector with an accelerating voltage of 6 kV.

## **2.8 Energy-dispersive X-ray spectroscopy (EDX)**

EDX was performed with an Oxford EDX system in combination with a Sigma VP Field Emission Scanning Electron Microscope (Carl-Zeiss AG, Germany).

## **2.9 High resolution transmission electron microscopy (TEM)**

TEM measurements were conducted with a FEI Tecnai G<sup>2</sup> 20 Transmission Electron Microscope. 15  $\mu$ L of the sample solution was blotted onto lacey carbon grids (Plano). Images were acquired at an acceleration voltage of 200 kV.

## **2.10 Gas chromatography coupled to mass spectrometry (GC-MS)**

GC-MS analyses of the reduction experiments on mackinawite were carried out on a Shimadzu GCMS-QP2010 SE equipped with an auto sampler for head-space and solution analysis. Gaseous samples were separated with a 30 m RT-Q-Bond column. The following temperature program was applied: Increasing the temperature from 35 °C to 200 °C with 10 °C/min and holding this temperature for 5 min. After this time, the temperature

was again increased with 10 °C/min to 250 °C and held for 20 min. The separation was performed under isobar conditions at 45 kPa using He gas as carrier.

Liquid samples were separated with a 60 m SH Rxi 624 SILMS column. The following temperature program was applied: Increasing the temperature from 40 °C to 250 °C with 7 °C/min and holding this temperature for 11 minutes. The separation was performed under isobar conditions at 100 kPa using He gas as carrier.

GC-MS analysis of the reduction experiments on tochilinite was carried out on a 25 m GE-SE-30 separation column. The following temperature program was applied: 4 min at 40 °C, heating to 180 °C at 4 °C / min staying at this temperature for 10 min. The separation was performed under isobar conditions at 80 kPa using He gas as carrier.

The products were identified using EI (70 eV) mass spectrometry. The EI mass spectra were measured by quadrupole ion trap (PolarisQ MS) or quadrupole (ISQ single quadrupole MS) MS. The compounds were identified by comparison of the fragmentation patterns of mass spectra in the NIST Database, based on retention times and measurements of reference compounds. These reference measurements were also used for quantification. Quantification was achieved by calibration with dilution series of (iso)alkanes and alcohols using FID detection.

## **2.11 BET surface area**

BET surface areas of mackinawite were determined with a Quantachrome ASiQwin. Mackinawite samples were pre-treated by outgassing under high vacuum at 0 °C for six hours. Sorption isotherms were then acquired at - 195.5 °C using N<sub>2</sub> as adsorbate.

Tochilinite samples were pretreated by outgassing under high vacuum at 130 °C for six hours. Sorption isotherms were then acquired at 87K using Ar as adsorbate on a Quantachrome iQSorb device.

## **2.12 TGA / DSC analysis**

TGA / DSC analyses were carried out with a Jupiter STA 449 F1 by Netsch. The device was equipped with a SiC oven, a high-performance Heat-Flux DSC with a nanogram-

resolution thermobalance and a Netsch Typ S sensor for measurements in corrosive atmospheres. The atmosphere in the device could be set to nitrogen gas, argon gas or gaseous CO<sub>2</sub> supplied from gas bottles bought from Linde.

## 3 Synthesis and characterization of mackinawite

### 3.1 Synthesis of mackinawite

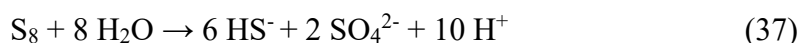
#### 3.1.1 Mechanism

The synthesis of mackinawite is usually carried out by precipitation. It has been repeatedly reported that an amorphous phase precipitates first and transforms into a more crystalline form upon aging.<sup>1,130</sup> Matamoros-Veloza *et al.* lately described a nanoparticulate precursor to the conventionally assumed initial precipitate in the iron sulfide system. This precursor contains  $\text{Fe}^{2+}$  tetrahedrally coordinated by sulfide and polysulfide species.<sup>131</sup> During further aging, it forms nano-sized mackinawite particles that grow following an aggregation-growth mechanism.<sup>132,133</sup> The crystallinity of freshly prepared mackinawite differs significantly depending on the conditions during the formation. In the early stages, the formed particles can appear amorphous in X-ray diffraction<sup>134,135</sup> but also show diffraction peaks<sup>71</sup> matching the d-values of highly ordered mackinawite. A yet undescribed way to make the formation conditions more controlled, is the reaction examined in this work. The reaction forming iron sulfides from wet elemental iron and elemental sulfur under very mild conditions has been known for over 300 years<sup>136</sup> but this knowledge has not yet found its way into the inorganic chemistry textbooks. In 1926, Alsen mentioned in a short notice, that iron sulfides can be synthesized from a wet homogenous mixture of iron and sulfur without going into any detail.<sup>137</sup>



The reactivity between iron and sulfur has mainly been studied by corrosion scientists and has not been used to synthesize mackinawite.<sup>26,42–49</sup> The mechanism has been clarified to a certain degree with the most extensive report published by Schmitt in 1991<sup>26</sup>. It was further extended by the work of Dowling in the following year.<sup>45</sup> The combined mechanisms propose the following steps:

- I) Elemental sulfur in contact to an iron surface is activated and disproportionates into sulfide and sulfate ions. Sulfur alone without the contact to the iron surface does only disproportionate considerably in hot alkaline solutions.



- II) The protons released by this reaction attack the iron surface that is covered by an oxide layer and promote the dissolution of the metal and the formation of hydrogen gas.



- III) The iron and hydrosulfide ions precipitate on the iron surface forming an initial layer of iron sulfide.



- IV) The iron sulfide layer prevents the re-passivation of the iron surface and leads to massively enhanced corrosion termed “sulfur assisted corrosion”. As the iron sulfide layers form in small areas, pitting corrosion is predominantly observed during this stage. Thereby the released iron ions lower the local pH value and enhance the metal dissolution speed even more.



For the final step experimental evidence is missing. Dowling suggests that an electrically conducting layer of iron sulfide is formed between the iron and the sulfur surface. The dissolution of iron releases  $\text{Fe}^{2+}$  and electrons that move through the iron sulfide and react with sulfur molecules on the surface. The sulfur molecules on the surface are reduced and form polysulfide ions. When the released iron ions reach the reduced sulfur species on the sulfur surface, iron sulfide is formed extending the conducting iron sulfide layer.



In order to examine the last step in more detail, the reaction was followed with a video camera and by SEM imaging. In figure 10 a series of photos extracted from the video is shown. For the experiment, an iron plate was placed on top of a sand bed in a round bottom flask. Some sulfur grains were placed on the iron plate and the flask was evacuated and filled with nitrogen gas for three times. Then, the flask was filled with a 0.001 M deoxygenated sodium chloride solution to half of the height of the sulfur grains. The



reaction was carried out under a permanent nitrogen flow to exclude any oxygen contamination. The flask was kept at room temperature for 9 hours.

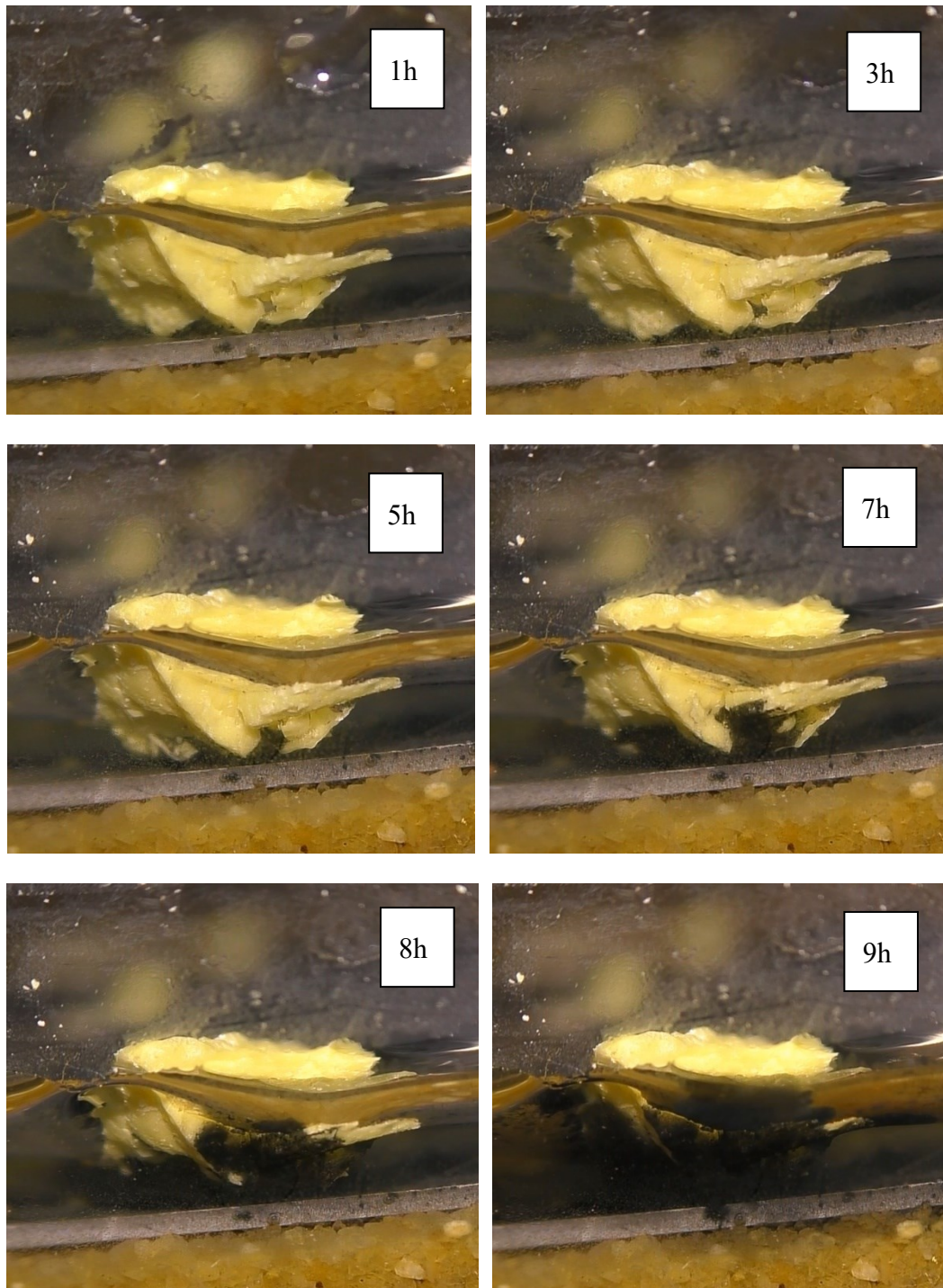


Figure 10: Extracted pictures from video footage of the reaction between sulfur grains and an iron plate in 0.001 M sodium chloride solution at room temperature.

In the images it can be seen that the formation of black iron sulfide starts at the interface between the iron plate and the sulfur grains. With time, the iron sulfide spreads over the surface of the sulfur particles. No iron sulfide is formed on the iron plates and new sulfide only forms as an extension of previously formed sulfide. This behavior corresponds to the electron transport from the metal surface through the already formed iron sulfide to the reaction front to reach the elemental sulfur. The iron sulfide formation stopped at the line, where the water covers the sulfur grains because the iron ions need to travel through the solution to reach the reaction front.

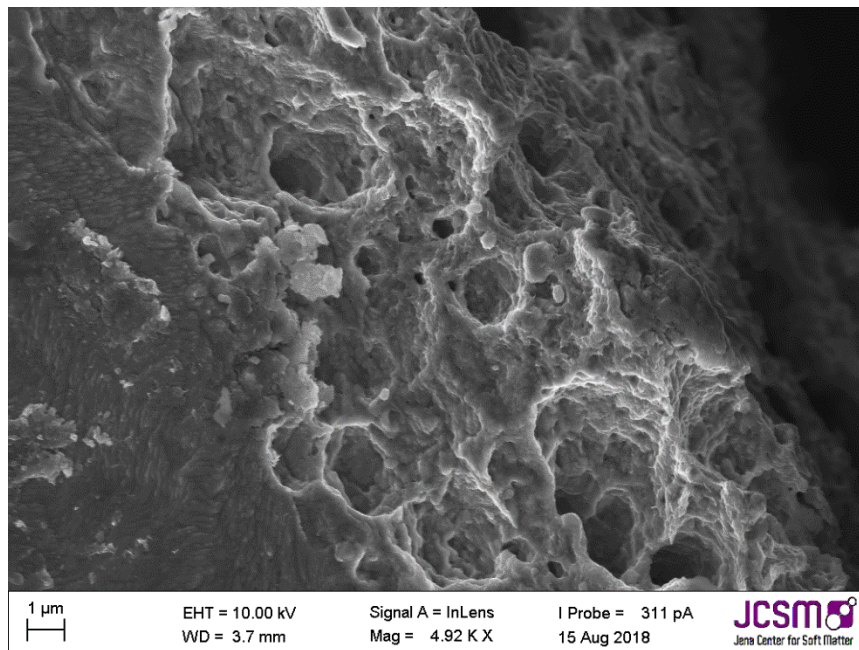


Figure 11: SEM image of the iron plate after the reaction between sulfur grains and the iron plate in 0.001 M sodium chloride solution at room temperature showing severe pitting corrosion.

After removing the sulfur crystal, the iron plate shows significant signs of pitting corrosion as can be seen from the SEM image in figure 11.

In a second SEM/EDX investigation, an iron plate was placed on a sticky SEM sample holder and molten sulfur was poured around it. The sample holder was placed in deoxygenated water on a sand bed for one day with the plate and the sulfur completely covered. After the reaction, a part of the sulfur was removed to investigate the interface. Some sand grains stick to the sample holder in front of the iron plate.



Figure 12: Image of the experimental setup investigated by SEM imaging and EDX.

Images from the interface were taken from different angles and EDX single point spectra and EDX mappings were recorded. Figure 13 shows the on top view of the interface. The tip of the sulfur is broken down during the preparation for SEM imaging. In the corresponding EDX mapping in figure 14 it can be seen that there is nearly no sulfur on the iron plate and that the iron content stretches into the middle of the broken fragment. Sulfur is an insulator and therefore SEM images can suffer from effects of accumulated charge and appear very bright. Figure 15 shows the side view of the interface and figure 16 shows the corresponding EDX mapping. The first feature to be mentioned is, that the sulfur in contact to the iron plate is cracked up but shows a closed surface at some distance from the interface. In the EDX mapping it can be seen, that in the cracked area a higher iron content can be observed, whereas in the smooth part there is only sulfur. This is reasonable because if iron sulfide formed at the interface, it would be wettable by water. During the drying of the sample the water evaporates and the iron sulfide would contract and crack. As sulfur is not wettable by water, it stays intact and smooth. The cracks could of course be only a result of the sample preparation, but the exact agreement with the iron content points towards a correlation.

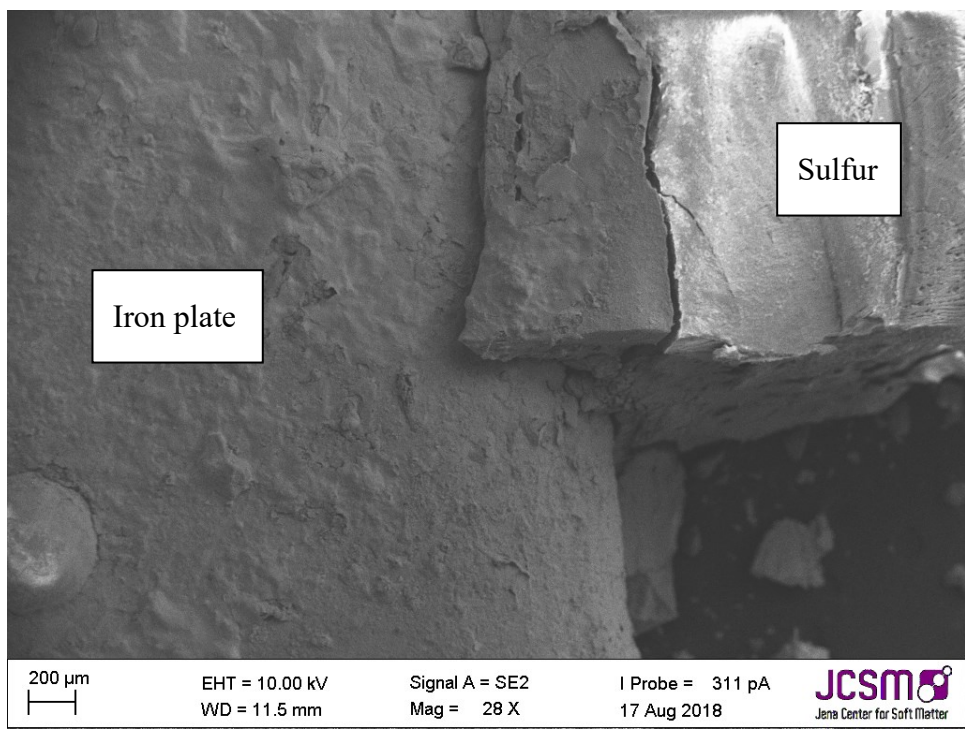


Figure 13: SEM image of the on top view of the interface between the iron plate and sulfur after the reaction.

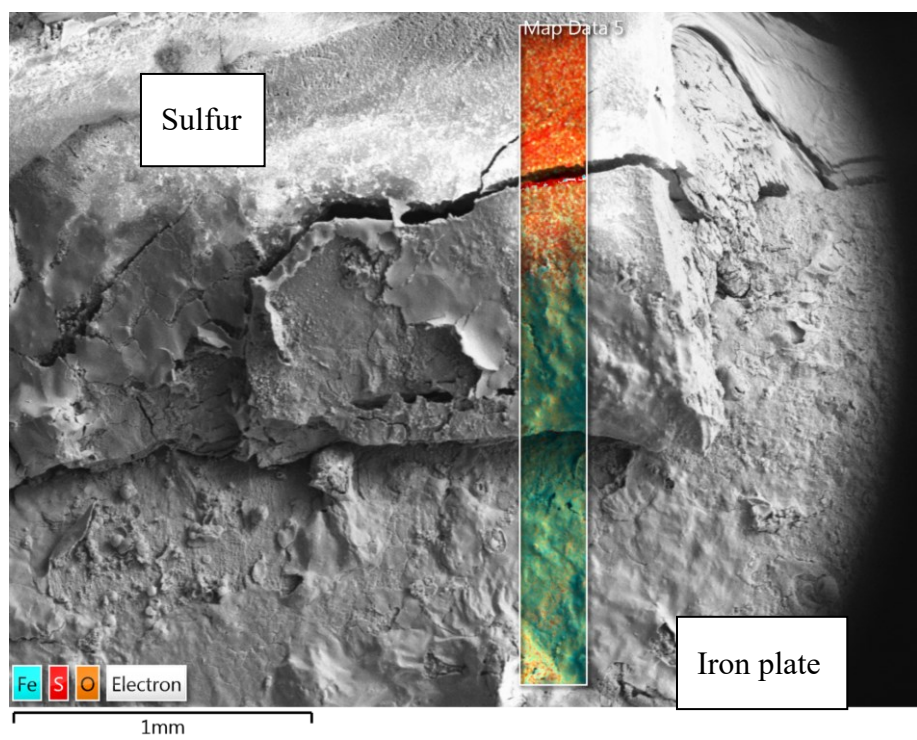


Figure 14: EDX mapping of the on top view of the interface between the iron plate and sulfur after the reaction.

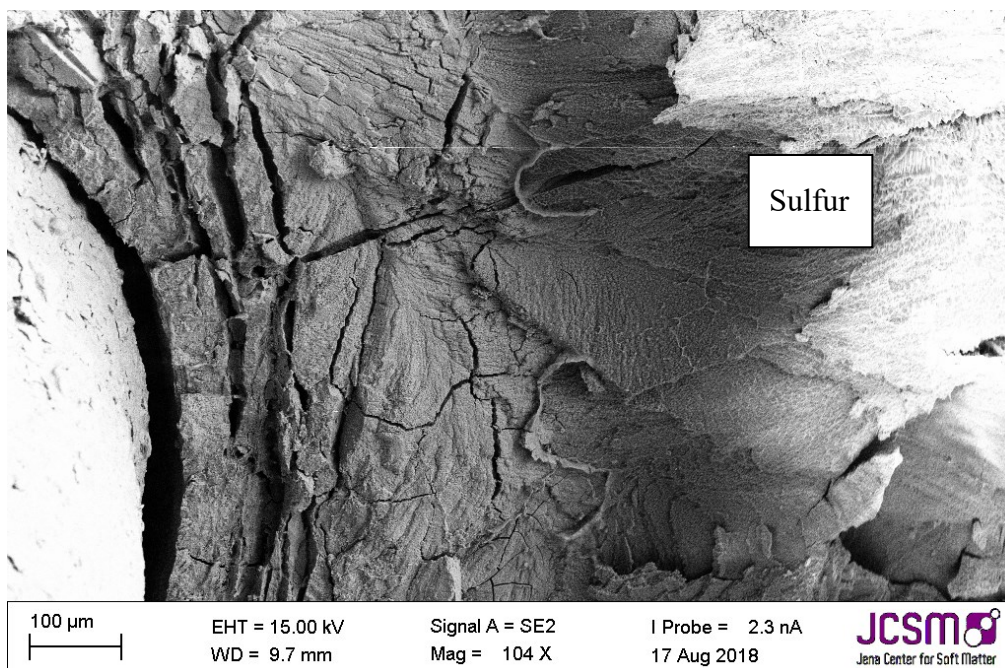


Figure 15: SEM image of the side view of the interface between the iron plate and sulfur after the reaction.

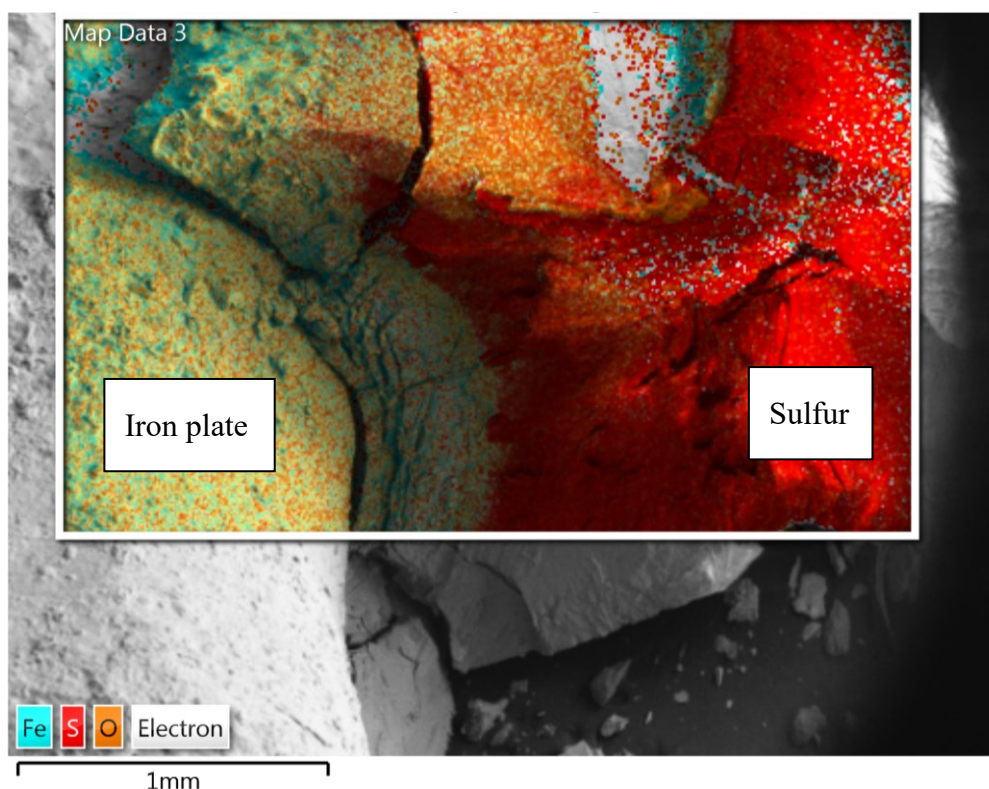


Figure 16: EDX mapping of the side view of the interface between the iron plate and sulfur after the reaction.

The examinations of the video and the SEM images agree with the proposed mechanism by Dowling. The electrons move through the conducting iron sulfide towards the sulfur surface. The reduction of the sulfur surface establishes an electrochemical potential that attracts the iron ions. Therefore, they follow the electrons through the solution along the wet iron sulfide surface and form new iron sulfide at the reaction front.

### 3.1.2 Kinetics

The rate of the corrosion of elemental iron in contact to elemental sulfur has been studied by several groups.<sup>26,42,46,138,139</sup> All investigations of the kinetic of the sulfur assisted corrosion report an induction period. During this period, only slow corrosion takes place and it is assumed, that this is the time needed for the disproportionation of sulfur and the formation of the initial iron sulfide layer. After this is established, sulfur assisted corrosion takes place that is much faster. This behavior was also observed in a kinetic study tracking the reaction by PXRD. For the investigation of the reaction rate, a fine ground mixture of iron and sulfur was placed in 25 ml vials and 10 ml deoxygenated water was added in a nitrogen atmosphere without additional salts. The vials were kept at room temperature for the assigned reaction times. The solids were isolated by filtration, dried in a nitrogen flow and cautiously deactivated to prevent a thermal runaway.

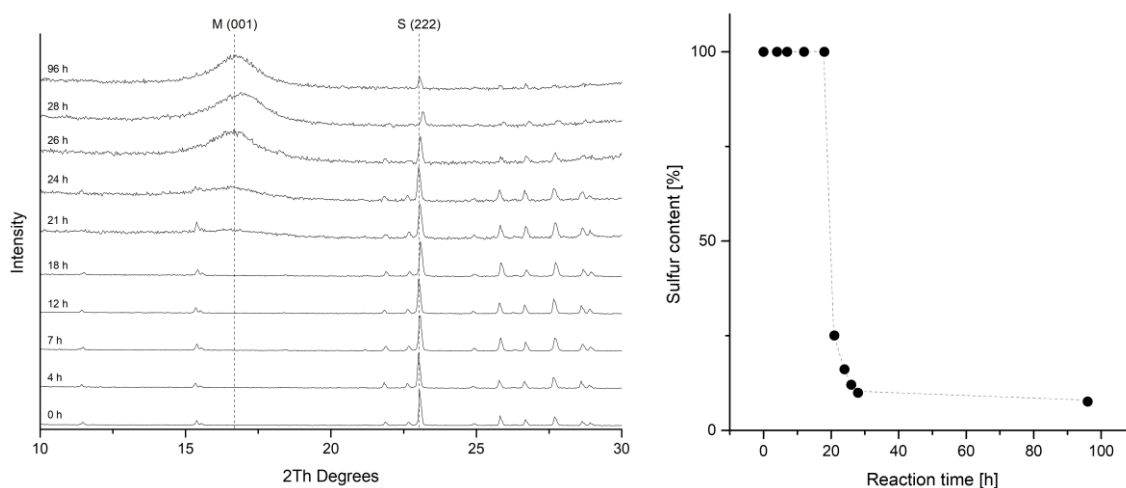


Figure 17: Left: Series of PXRD patterns of the reaction between iron and sulfur quenched and analyzed after different reaction times (experiments FeS\_k1 to FeS\_k10). Right: Plot of the sulfur content of a reaction mixture of iron and sulfur after the reaction in pure water at different times. The connection between the data points is shown for better visibility.

In the first PXRD pattern it can be seen that there are only diffraction peaks corresponding to elemental sulfur. After 21 hours, the signal to noise ratio gets worse and after 24 hours a broad hump around 5 Å d-spacing appears. This diffraction peak corresponds to the 001 diffraction peak of mackinawite. With further reaction time, this diffraction peak gets bigger but stays very broad. The sulfur diffraction peaks decrease in intensity and most of them completely disappear. A little amount of residual sulfur remains even after 96 hours. This is due to the separation of a small amount of sulfur from the elemental iron that floated on the water surface. As the formation of iron sulfide from elemental iron and sulfur is exothermic, the amount of the starting mixture needed to be small in kinetic experiments in order to keep the solution temperature constant.

The PXRD patterns were fitted using the mackinawite and the sulfur crystal structures and the mass fractions were determined. On the right in figure 17 the mass fractions of sulfur are plotted against the reaction time. The induction period in this setting at room temperature took around 20 hours. The following formation of mackinawite is relatively rapid and finished about 8 hours later. To increase the overall reaction rate, it is reasonable to use an additional electrolyte for a better conductivity of the solution. The addition of sodium chloride was used in most experiments to accelerate the reaction. Usually a 0.01 M solution was used to carry out the reaction with a yield of 100 % after 12 hours. The rate enhancement may not only be the result of a higher conductivity, but also of the influence of chloride ions on the general corrosion rate of elemental iron. To investigate the influence of different electrolytes, other common salts were used. The accelerating effect of small concentrations of KCl, NH<sub>4</sub>Cl, Na<sub>2</sub>SO<sub>4</sub>, KCN and NaHCO<sub>3</sub> were comparable to NaCl. The pH value of the solution also showed a significant influence on the reaction speed. The higher the pH value of the solution was, the slower was the overall reaction and at pH values above 10.5 no reaction occurred at all at room temperature. The low pH region was not investigated as in acidic systems pronounced hydrogen gas formation takes place, what makes these reactions hardly comparable to the neutral to basic ones. Higher pH values increase the stability of the passivating oxide layer on the iron surface what probably prevents the formation of the first iron sulfide and therefore the onset of sulfur-assisted corrosion. At higher temperatures, the reaction proceeded also at pH values above 10.5 but these conditions were also not investigated further. A rather unexpected observation was that upon washing with distilled water the mackinawite

samples prepared in basic solutions divided into smaller particles that were able to pass through the glass frits with a mesh of about 10-16  $\mu\text{m}$ . The dilution of the alkaline solution somehow led to a decrease in particle size. When washing with a sodium hydroxide solution with the same concentration as in the original reaction mixture, no such effect was observed and the particles stayed intact. The same observation could be made when mackinawite particles were synthesized at high concentrations of sodium chloride what points towards an agglomeration process of the particles that depends on the ionic strength of the solution.

## 3.2 Characterization of mackinawite

### 3.2.1 Structure and morphology

The morphological and structural properties of the mackinawite produced from the elements were determined by PXRD and TEM / SEM imaging. A representative PXRD pattern is shown in figure 18 (experiment FeS\_1).

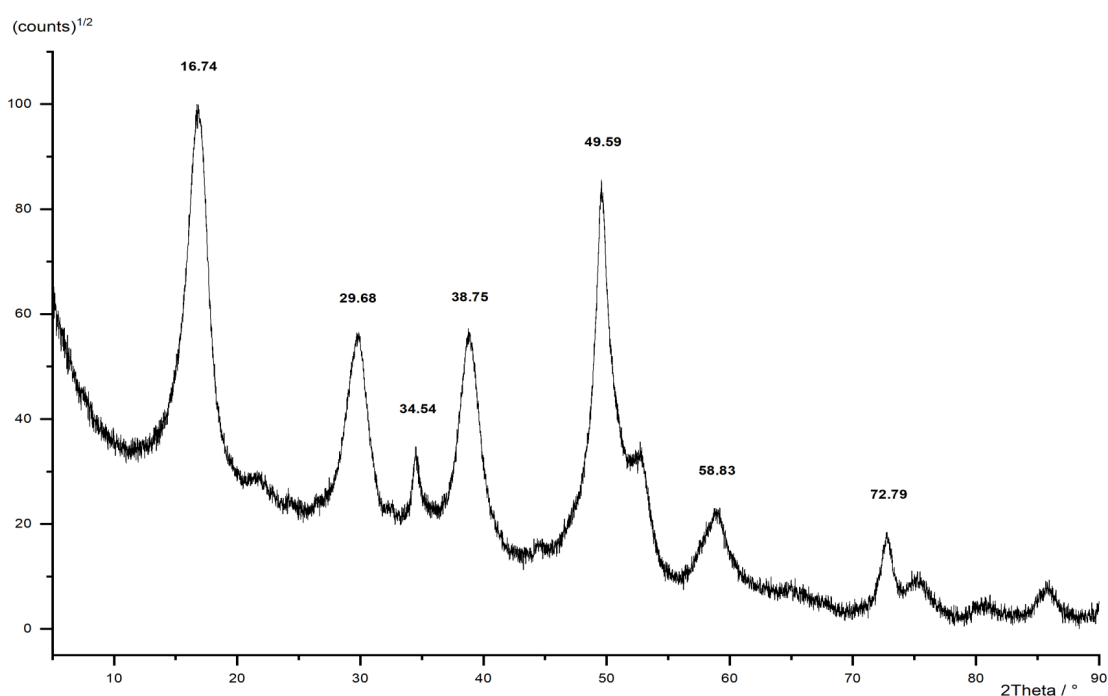


Figure 18: PXRD pattern of nanoparticulate mackinawite from reaction FeS\_1.



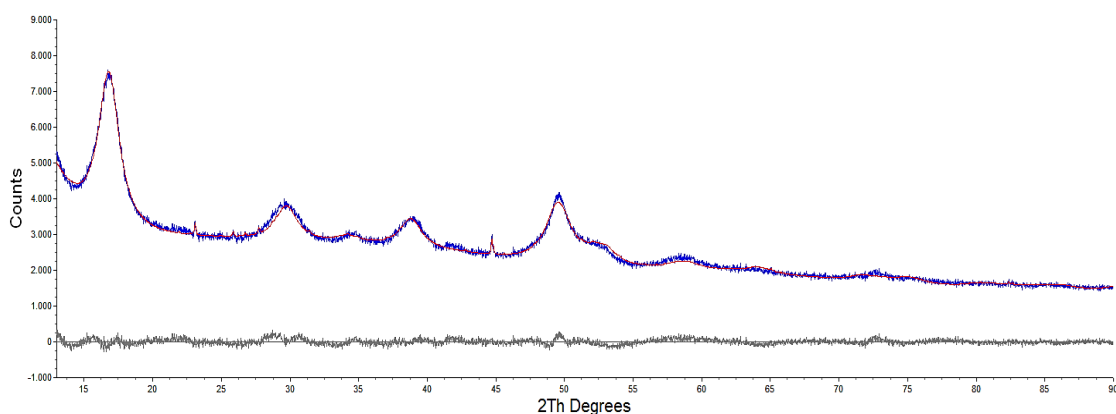


Figure 19: PXRD pattern of a mackinawite sample prepared from iron, sulfur in a 0.01 M sodium chloride solution for 12 h (blue line). Rietveld fit using the iron, sulfur and mackinawite crystal structures of the obtained pattern (red line). Differential plot between the pattern and the fitted curve (grey line).

A Rietveld refinement was carried out with the software “Topas 5” by Bruker. First, the instrument contribution to the PXRD pattern as well as the background function was determined with a  $\text{LaB}_6$  reference sample. Any displacement along the x-axes was corrected based on the positions of the residual sulfur and iron diffraction peaks. To fit the broadness of the mackinawite diffraction peaks, size and strain parameters were introduced that are reasonable in regard of the estimated particle size from SEM images and possible defects within the structure. The size parameter was fitted to a value corresponding to a particle size of less than 30 nm. Except for remaining iron and sulfur, no other phases than mackinawite can be identified in the PXRD pattern. The Rietveld-Refinement with  $R_{wp} = 0.02815$  using the mackinawite crystal structure gives lattice parameters of  $a = 3.6574 \pm 0.0007 \text{ \AA}$  and  $c = 5.2717 \pm 0.0011 \text{ \AA}$ . SEM and TEM images show curved platelets that form micrometer sized aggregates (fig. 20 and 21). The particles have a diameter of hundreds of nanometers with a thickness of only 5 to 30 nm.

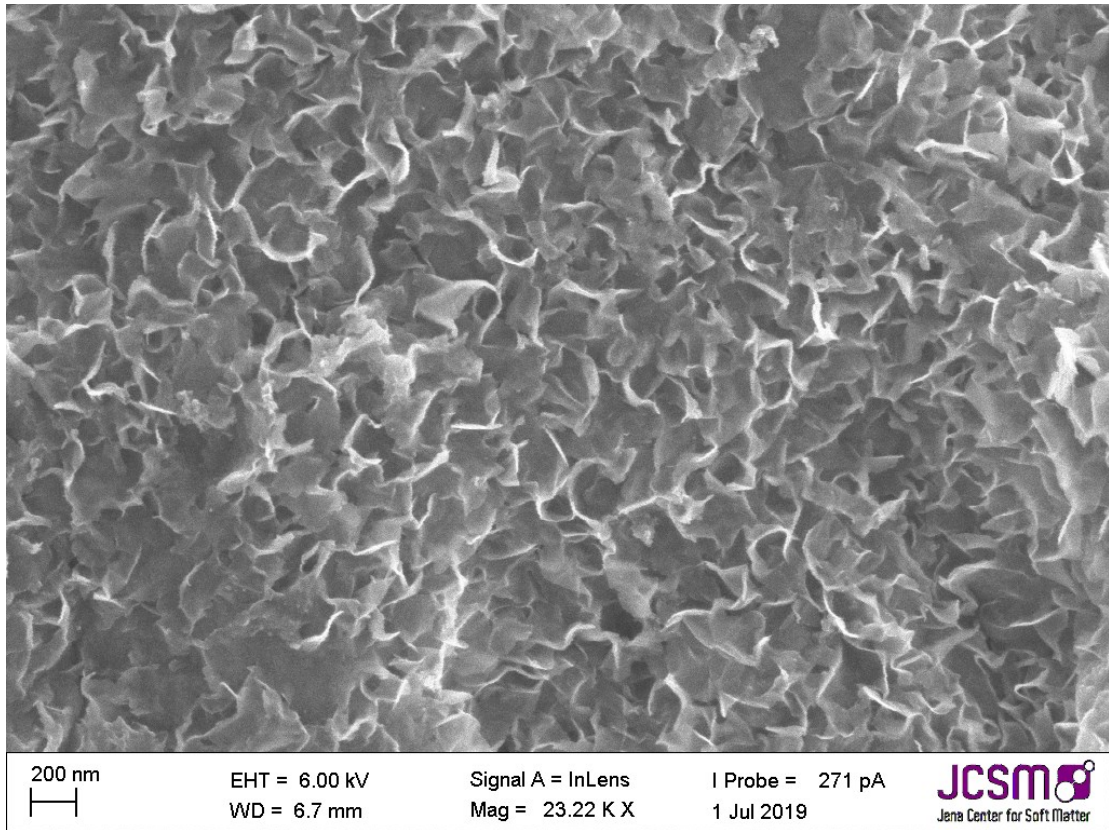


Figure 20: SEM image of a deactivated mackinawite sample prepared from iron and sulfur in a 0.01 M sodium chloride solution for 12 hours (FeS\_1).

The spacing of lattice fringes in the TEM images could be determined to be around 0.5 nm what corresponds to the interlayer spacing of the mackinawite structure.

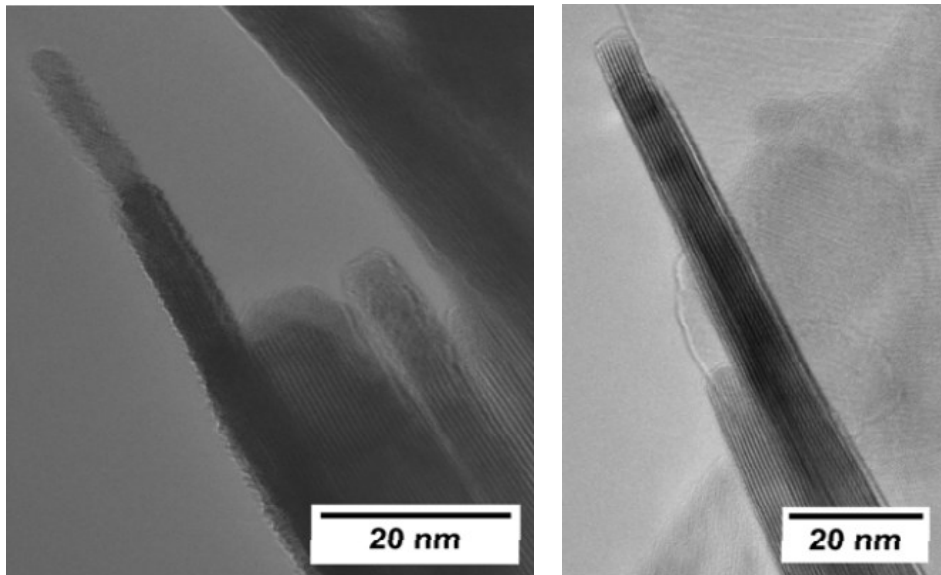


Figure 21: TEM images of a deactivated mackinawite sample prepared from iron and sulfur in a 0.01 M sodium chloride solution for 12 hours (FeS\_1).

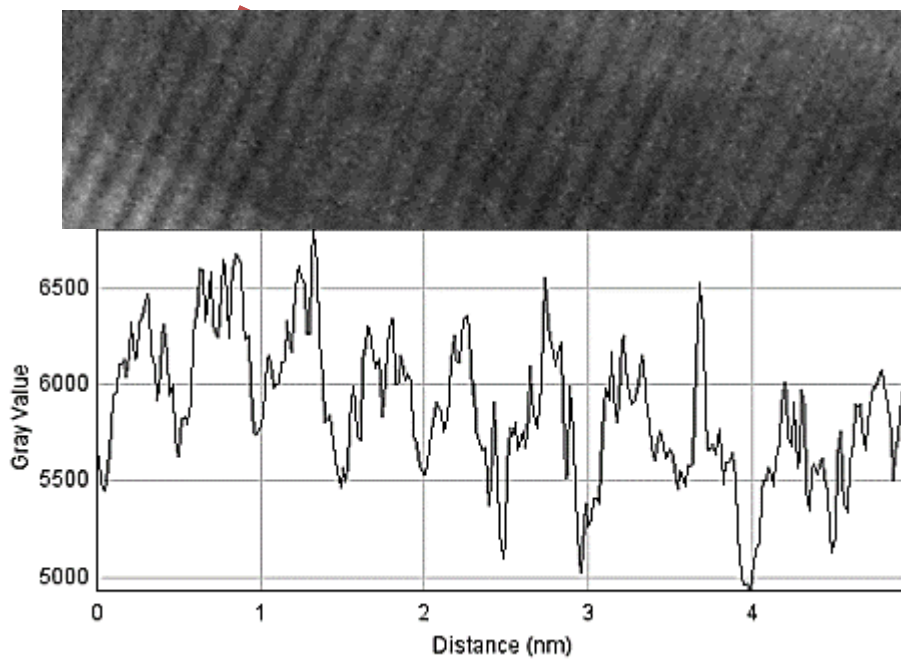


Figure 22: TEM investigation of the visible lattice fringes of a deactivated mackinawite sample prepared from iron and sulfur in a 0.01 M sodium chloride solution for 12 hours (FeS\_1). The lower picture shows the gray value along the line of the red arrow.

The BET surface area was determined by nitrogen gas adsorption to values between  $40 \text{ m}^2/\text{g}$  and  $80 \text{ m}^2/\text{g}$ . During the BET analysis additional cycles of loading and unloading

showed a decreased surface area. This may be caused by strong interactions of the nitrogen molecules with the dried mackinawite surface. The c-parameter with  $c = 5.27 \text{ \AA}$  is slightly higher compared to highly ordered mackinawite with a c-parameter of  $5.03 \text{ \AA}$  what will be addressed in more detail in section 4.3.

The mackinawite particles forming in the reaction between wet elemental iron and elemental sulfur at room temperature are very similar to mackinawite particles obtained by precipitation. They also consist of irregular curved platelets that are up to  $\sim 150 \text{ nm}$  large but only a few nanometers thick. The defects in the mackinawite structure that increase the broadness of the PXRD peaks may have multiple origins. One part is caused by point defects within the sheets like iron vacancies and partial oxidation. As the particles are in the nano regime, the surface structure and its composition have a significant influence on the interior of the particles. Additionally, misalignment of consecutive layers would also lead to broadened diffraction peaks.

### 3.2.2 Composition

The composition of mackinawite samples synthesized from the elements was determined with ICP-AES. Including the error of the method itself, the iron-sulfur-ratio was determined to be  $\text{Fe} : \text{S} = (1.010 \pm 0.004) : (1.000 \pm 0.003)$  with no residual elemental iron or sulfur or any other phase visible in the PXRD pattern. In the applied method of synthesis, this ratio can only change by dissolution of iron or sulfur species and their loss in the washing process. Very small residual iron and sulfur particles may not be visible in the PXRD pattern but still could influence the resulting composition. In this way, the accuracy of the composition given is limited more by the PXRD analysis than by the ICP-AES method and may have greater errors than given.

The water content of the samples was calculated by difference neglecting the sodium content as not significant. The samples that were dried by purging with cold nitrogen showed high water contents leading to compositions from FeS without water content to  $\text{FeS} \cdot 1.46 \text{ H}_2\text{O}$ . Heating the samples to  $80 \text{ }^\circ\text{C}$  under reduced pressure led to the release of water but not to a change in the PXRD patterns.

### 3.2.3 Stability and oxidation behavior

The stability of freshly prepared nano-mackinawite was investigated, as mackinawite is known to be readily oxidized and undergo phase transformations. Before any investigation of the reactivity or catalytic activity of mackinawite, it is crucial to ensure that the reaction conditions do not lead to the dissolution, transformation or deactivation of the mackinawite particles. The scientific literature on this topic gives some information regarding the stability of mackinawite in aqueous systems as well as in the dry state.<sup>120,121,110,117–119</sup>

#### 3.2.3.1 Dry state

Mackinawite transforms into greigite under oxidizing conditions and into pyrrhotite under reducing conditions upon heating in the dry state.<sup>8,19</sup> For the transformation into pyrrhotite, an activation energy of 493 kJ/mol and a frequency factor of  $3.7 * 10^{45} \text{ min}^{-1}$  have been determined.<sup>19</sup> Rapid transformation into pyrrhotite does not take place at temperatures below 453 K.<sup>19</sup> The transformation under oxidizing conditions into greigite is easier and already very fast at temperatures above 373 K.<sup>8</sup> Upon further heating, greigite transforms into pyrrhotite and magnetite. Therefore, nano-mackinawite can only be used as a catalyst in the dry state at low temperatures.

As there are some discrepancies regarding the properties of freshly prepared nano-mackinawite in the literature, TGA/DSC experiments were carried out to investigate the behavior of mackinawite synthesized from elemental iron and sulfur upon heating. The oxidation and transformations of mackinawite in solution are different compared to the dry state. The most prominent difference is the pyrophoricity of dried mackinawite. If mackinawite is prepared from elemental iron and sulfur and dried thoroughly in a stream of nitrogen gas, it starts to heat up very quickly upon air contact. If a certain temperature is not exceeded, the mackinawite structure stays intact and no other crystalline phases form, but if the sample gets too hot, it starts to glow brightly and in a vigorous reaction is oxidized to iron oxides, sulfur and SO<sub>2</sub>. The higher the mass of the mackinawite sample, the higher the temperature rises during the oxidation. Our investigations show that the initial oxidation reaction does not lead to the formation of iron oxides but to the oxidation of the surface of the mackinawite particles further denoted as FeSO<sub>x</sub>. Mullet *et al.* reported, that

mackinawite particles can have up to 20 % of their  $\text{Fe}^{2+}$  oxidized to  $\text{Fe}^{3+}$  without changing their structure significantly.<sup>30</sup>

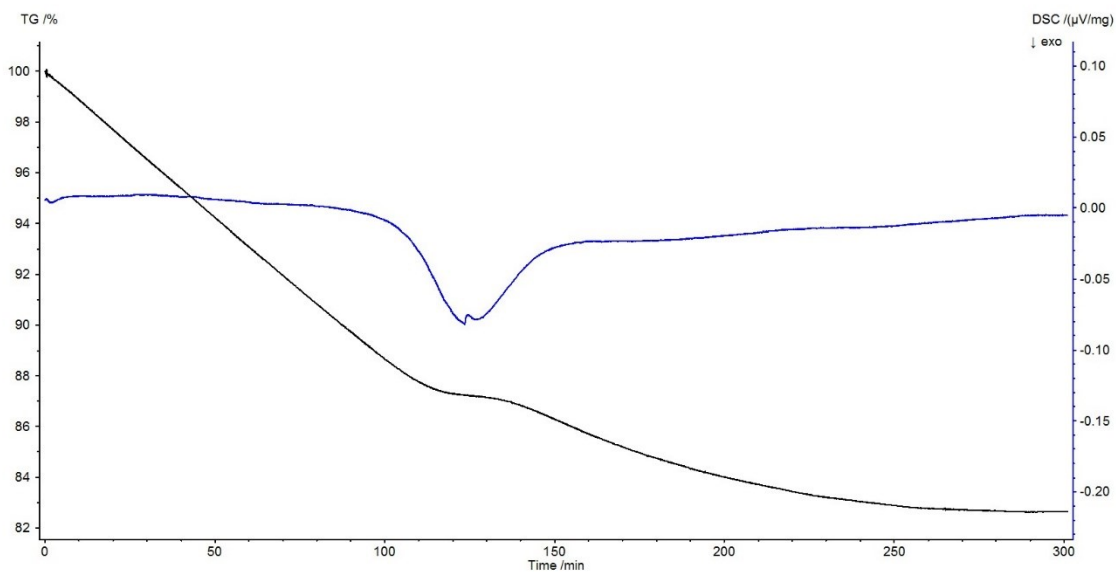


Figure 23: TGA/DSC analysis of a freshly prepared nano-mackinawite sample that was dried in a stream of air with 50 ml/min (exp. FeS\_Ox\_1).

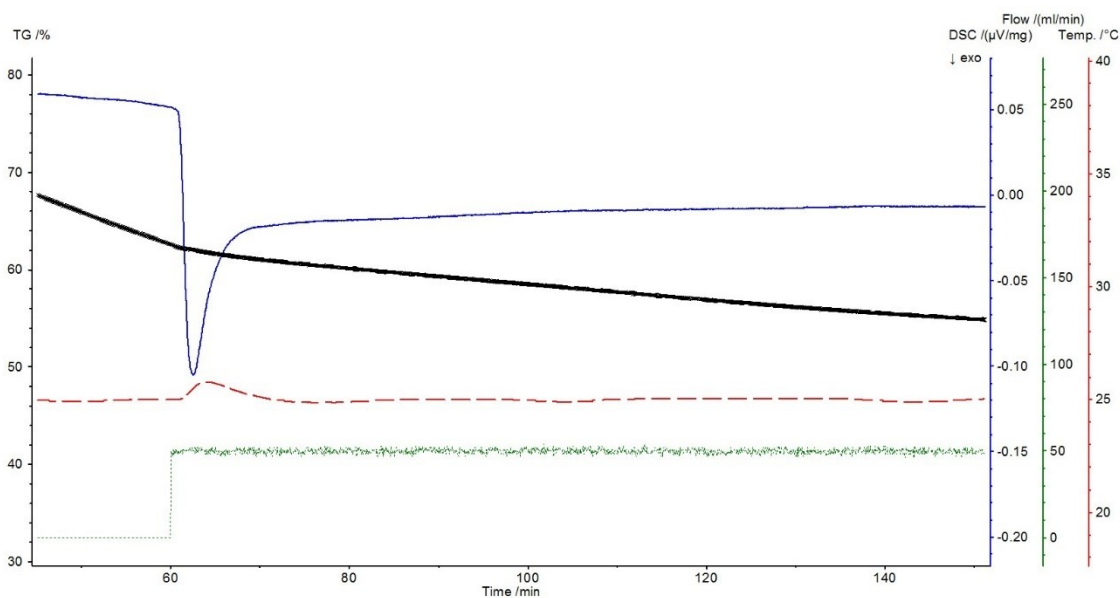


Figure 24: TGA/DSC analysis of a freshly prepared mackinawite sample that was dried under  $\text{N}_2$  for one hour (exp. FeS\_Ox\_2). Upon changing from  $\text{N}_2$ -atmosphere to air, an exothermic oxidation reaction immediately occurs with a detectable rise in temperature.

The extent of the oxidation depends on the sample mass and on the remaining water content. This behavior has also been followed by TGA/DSC analysis. A wet sample of freshly prepared mackinawite was transferred into the sample holder. The sample was dried in a stream of air with 50 ml/min (exp. FeS\_Ox\_1). The DSC shows that within the first two hours, no pronounced exothermic reaction takes place while the mass of the sample decreases by the loss of water. As soon as the sample dried to a certain degree, it oxidized rapidly in an exothermic reaction and the released heat caused a peak in the DSC curve and the sample mass increased (figure 23). The same behavior was observed when drying a sample in a stream of nitrogen gas and changing to air after one hour (figure 24).

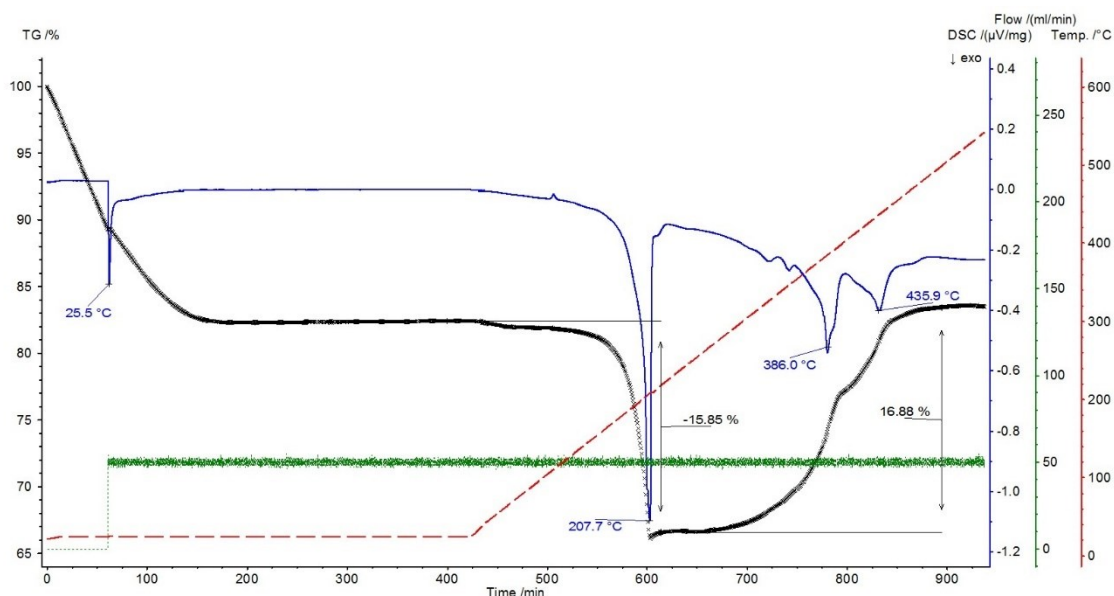
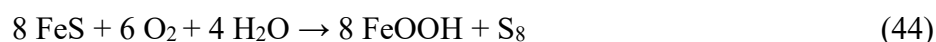
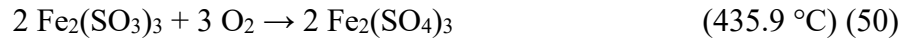
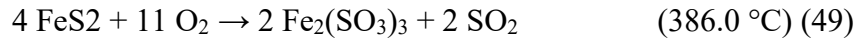
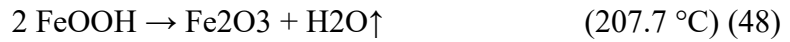
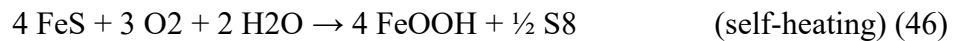
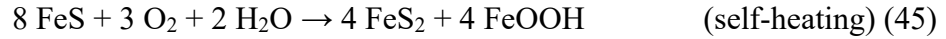


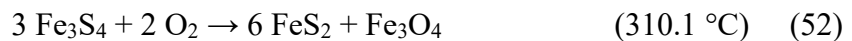
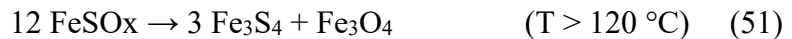
Figure 25: TGA/DSC analysis of a freshly prepared mackinawite sample that was dried under  $\text{N}_2$  (exp. FeS\_Ox\_3). Upon changing from  $\text{N}_2$  to air, an exothermic oxidation reaction immediately occurs. Increasing the temperature to 550 °C with 1K/min led to multiple oxidation events. The event at 207.7 °C was accompanied with a loss of around 16% of the sample mass. At higher temperatures, the mass increased again.

The oxidation of dry freshly prepared mackinawite upon air contact leads to the formation of lepidocrocite ( $\text{FeOOH}$ ), greigite and elemental sulfur (exp. FeS\_Ox\_3). Upon further

heating, a second oxidation event occurs at 207.7 °C, which is accompanied with a mass loss of approximately 16 %. Two less distinct oxidation events occur at 386.0 °C and 435.9 °C. As the final oxidation products are hematite with only a small fraction of Fe<sub>2</sub>(SO<sub>4</sub>)<sub>3</sub> with the crystal structure of mikasaite, sulfur has to be removed during the oxidation process what is expected to be in the form of SO<sub>2</sub> (exp. FeS\_Ox\_4). Taking together all the information obtained on iron sulfide oxidation from experiment and literature<sup>8,145</sup>, the oxidation process might be described in the following series:



Some of these reactions also occur when using dried and pre-oxidized mackinawite but the series of oxidation reactions is different (Fig. 26). The final oxidation products similarly are mikasaite, Fe<sub>2</sub>(SO<sub>4</sub>)<sub>3</sub>, and hematite. In contrast to the freshly prepared mackinawite, no FeOOH forms and no events occur where the mass of the sample decreases (exp. FeS\_Ox\_5). The sample steadily gets heavier and even at the pronounced exothermic reactions at 310.1 °C and 326.4 °C no significant mass change takes place. At the exothermic event at 392.6 °C the mass gain increases what is most likely caused by the formation of sulfate ions. Therefore, the series starting with the deactivated mackinawite FeSO<sub>x</sub> may be expressed like:





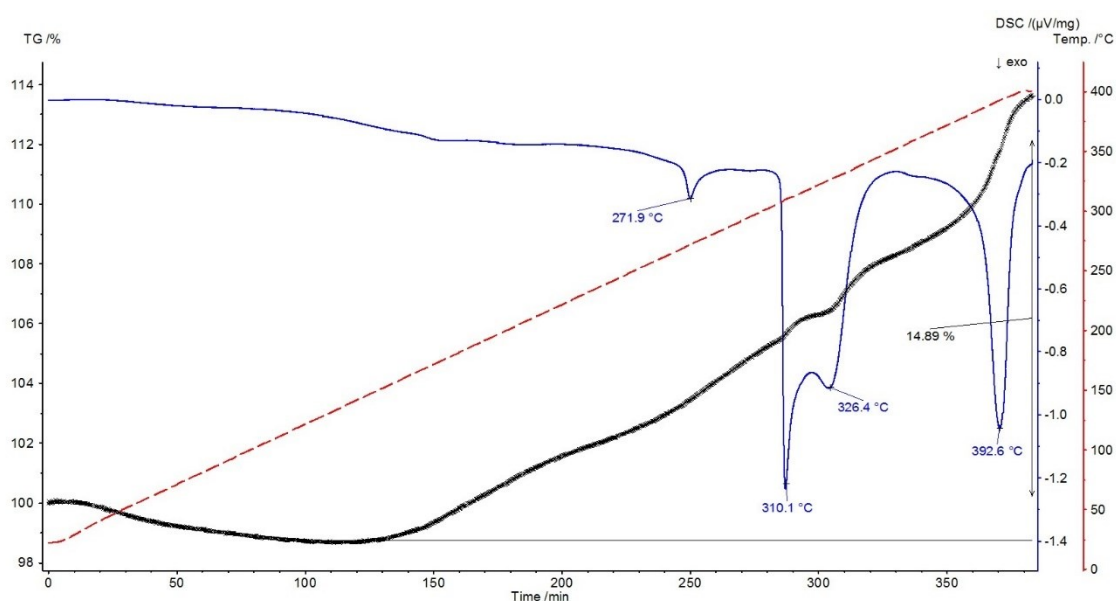


Figure 26: TGA/DSC analysis of a pre-oxidized mackinawite sample. Four distinct oxidation events occur when heating the sample under air (exp. FeS\_Ox\_5).

These experiments show that the oxidation behavior of dry mackinawite depends on the history of the sample. Freshly prepared mackinawite is oxidized via a different route compared to pre-oxidized mackinawite. The oxidation in both cases proceeds stepwise with different sulfide and oxide species forming with increasing temperature. The formation of elemental sulfur in the initial spontaneous oxidation is the key difference in the oxidation behavior. Another very interesting feature in the case of the pre-oxidized mackinawite is the section between 120 °C and 250 °C. The mass of the sample increases steadily without significant changes in the DSC curve. In this temperature area, the transformation from mackinawite to greigite occurs. The reason for the slow and steady oxidation might be the result of a deactivation-reativation process of the mackinawite surface. If the surface of mackinawite is once oxidized, it is quite stable. Mackinawite prepared from iron and sulfur did not change significantly after the deactivation, but storage open to the atmosphere at room temperature for one month led to the formation of greigite (exp. FeS\_Ox\_6). SEM investigations show that the particles get covered with a smooth greigite layer that reduces the available surface area determined by BET from around 80 m<sup>2</sup>/g to only 3 m<sup>2</sup>/g. The reactivation of the mackinawite particles can be achieved by the

crystallization of the smooth layer forming greigite and magnetite crystals as can be seen in figures 27 and 28.

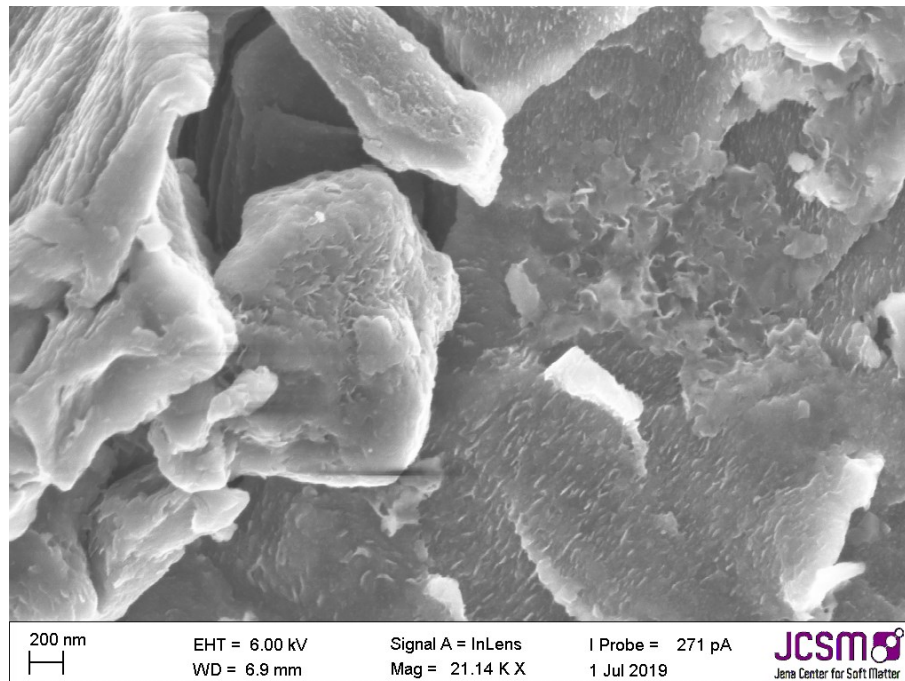


Figure 27: SEM image of a mackinawite sample stored open to the atmosphere for one month at room temperature. The mackinawite nanoparticles get covered by a smooth greigite layer.

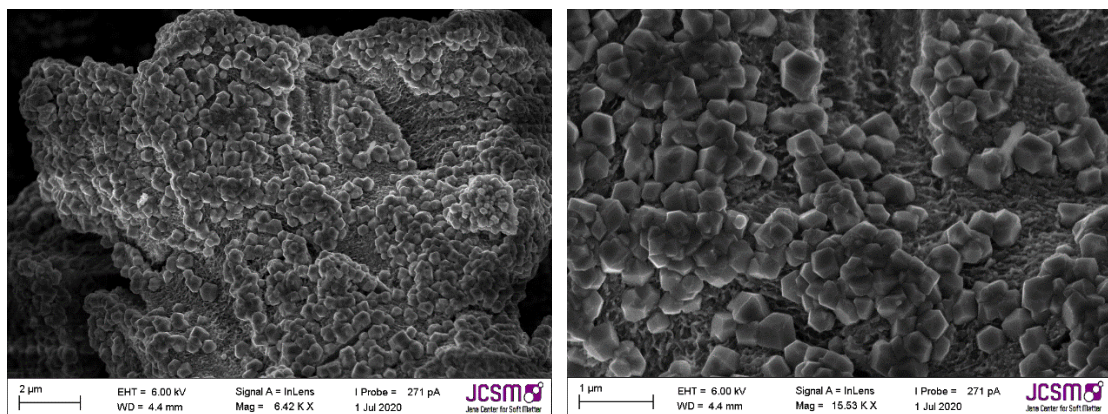


Figure 28: SEM images of a deactivated mackinawite sample heated at 80 °C in CO<sub>2</sub> atmosphere for 3 days. Comparable big greigite particles form on top of the mackinawite aggregates.

These SEM images show that on top of the mackinawite matrix much bigger particles formed.

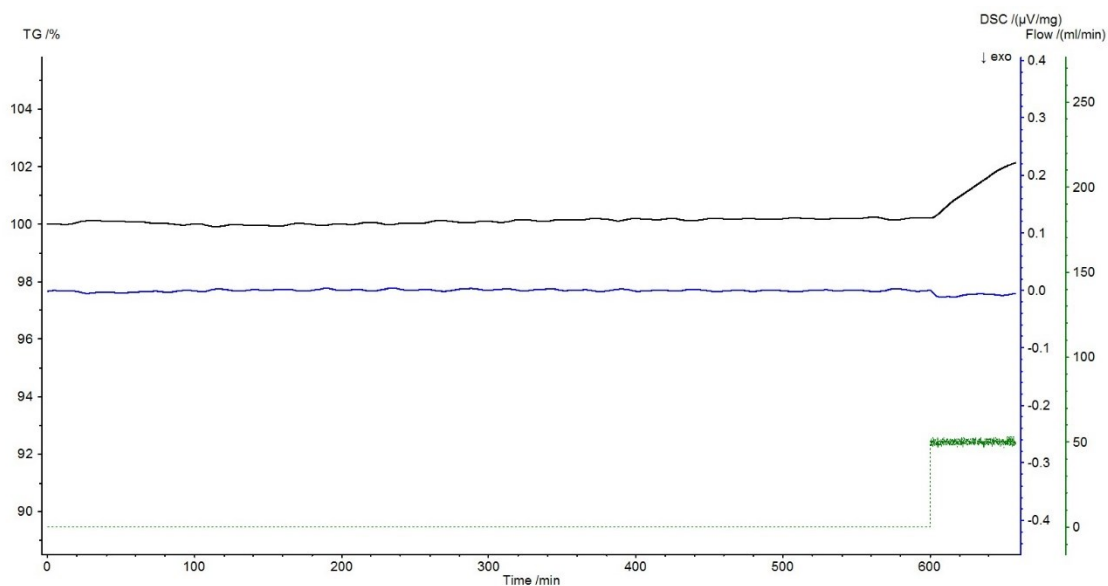


Figure 29: TGA/DSC investigation of a mackinawite sample (exp. FeS\_Ox\_7). After drying in a CO<sub>2</sub> gas flow for 10 hours, the sample was exposed to air.

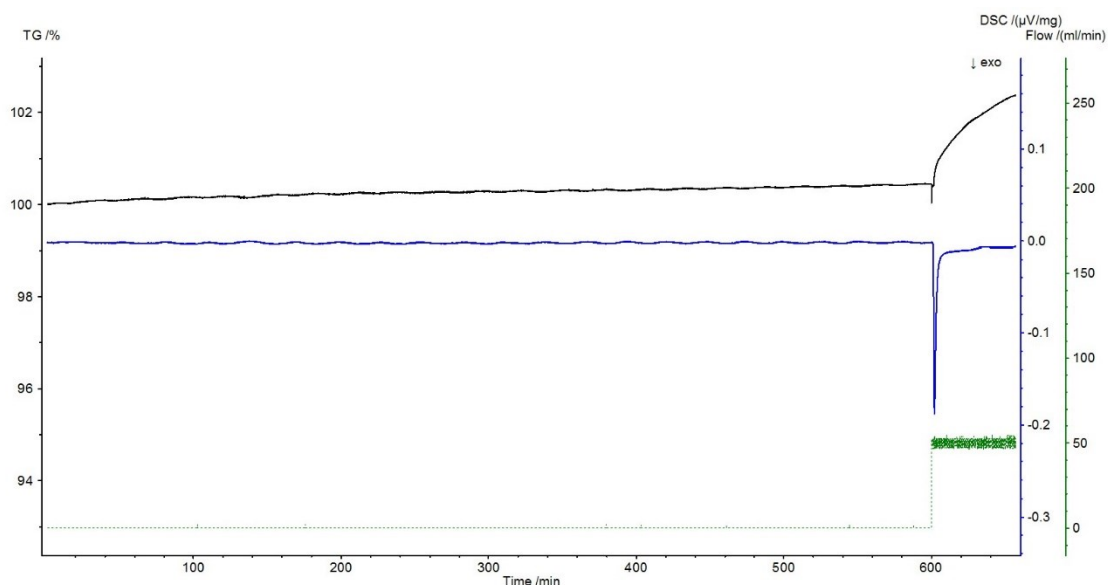


Figure 30: TGA/DSC investigation of a mackinawite sample (exp. FeS\_Ox\_8). After drying in a N<sub>2</sub> gas flow for 10 hours, the sample was exposed to air.

PXRD investigations imply that these particles consist of magnetite and greigite that formed by crystallization of the amorphous layer. This process uncovers reactive mackinawite underneath and leads to pyrophoric behavior again. The reactivation occurs in the dry state at higher temperatures but already at room temperature in aqueous solution. If

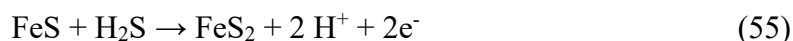
the cautious oxidation of the mackinawite surface leads to its deactivation, this behavior may be used as an indicator for the reduction of CO<sub>2</sub> on the mackinawite surface. As proposed by Dzade *et al.* in 2015<sup>124</sup>, the mackinawite surface may be oxidized by the chemisorption of CO<sub>2</sub>. Therefore, two experiments were carried out to investigate the mackinawite deactivation in CO<sub>2</sub> (exp. FeS\_Ox\_7) and N<sub>2</sub> (exp. FeS\_Ox\_8) atmosphere. Freshly prepared mackinawite was dried in the corresponding atmospheres before changing to air. The experiments clearly show that mackinawite dried under CO<sub>2</sub> does not react vigorously upon air contact but the mass of the sample still increases what may be explained by an incomplete deactivation of the mackinawite surface. Different surface sites may offer different reactivities and only the most reactive may be able to react with CO<sub>2</sub> and the remaining sites are then oxidized upon air contact.

### **Wet conditions**

Under wet and low temperature conditions open to the atmosphere, freshly prepared mackinawite slowly transforms into greigite and magnetite (exp. FeS\_Ox\_9). The dried solids were very pyrophoric and could hardly be isolated. Consequently, the formation of a passivating layer of greigite or iron oxide has to be prevented in aqueous systems and the material stays pyrophoric despite of its oxidation.

The transformation of mackinawite to troilite or pyrrhotite in solution depends on several parameters. At room temperature kept in the solution in which it has been prepared from elemental iron and sulfur, mackinawite stays stable and unchanged for several days. Even aged at 80 °C for three days mackinawite stays unchanged (FeS\_Ox\_10). At longer aging periods under these conditions, a reduction of the interlayer spacing and an increase in crystallinity can be observed (FeS\_Ox\_11). Mackinawite prepared from elemental iron in a basic sodium sulfide solution can be heated to 160 °C for several days and keep its structure without any signs of pyrrhotite formation (FeS\_2) but in neutral to slightly basic conditions it transforms completely to pyrrhotite at 130 °C within 3 days.

Another transformation of mackinawite is the formation of pyrite that takes place in acidic sulfide containing solutions or if elemental sulfur is present even at room temperature. As the oxidation of mackinawite leads to the release of sulfur, pyrite also forms in acidic solutions without soluble sulfide upon oxidation.<sup>1</sup>



## Summary

From the investigations regarding the stability of dry nano-mackinawite it can be concluded that it is very sensitive to oxidation and can only be handled under strictly inert conditions. The oxidation and deactivation of the surface leads to the formation of a passivating layer that is not visible with PXRD analysis. Prolonged storage open to the atmosphere leads to increased formation of greigite and reduces the BET surface drastically. The oxidation of mackinawite is a stepwise process leading with increasing temperatures to the formation of greigite, magnetite, sulfur and ultimately to hematite and iron(III)sulfate. A prolonged exposure to a CO<sub>2</sub> atmosphere suppresses the pyrophoric behavior what may be a sign for the oxidation of the mackinawite surface by CO<sub>2</sub>. The reactivation is possible by the crystallization of the amorphous layer what uncovers new reactive sites. This process is fast in aqueous solution but relatively slow in the dry state. The transformation to pyrrhotite without oxidation occurs at temperatures above 200 °C within hours.

In an aqueous system, nano-mackinawite is relatively stable at room temperature even under oxidizing conditions and does not change visibly for multiple days. Heating greatly accelerates its transformations into greigite and magnetite. The transformation to pyrrhotite in the wet state occurs at 130 °C under reducing conditions. Experiments on mackinawite reactivity should be carried out regarding these findings. If the mackinawite structure is to be maintained during the reaction, the temperatures need to be very low. If the mackinawite particles are meant to be oxidized as much as possible, higher temperatures are needed regarding the stepwise oxidation process. The deactivation of the surface prevents the complete oxidation and needs to be considered in experiments without an aqueous phase.

### 3.2.4 Comparison to other syntheses routes

Mackinawite prepared by the reaction of elemental iron and sulfur leads to the formation of nano-mackinawite that has a slightly increased c-parameter compared to the natural mineral. It forms very flat curved sheets that are only a few nanometers thick. The crystallites have some defects or dislocations that lead to very broad diffraction peaks in their PXRD patterns. All of these features also apply to nano-mackinawite prepared by precipitation. The very first phase isolated after the precipitation appears amorphous in PXRD analysis and starts to show the first diffraction peaks after a certain period of aging.<sup>130</sup> Thus, the mackinawite prepared from the elements is comparable to an aged precipitated mackinawite sample.

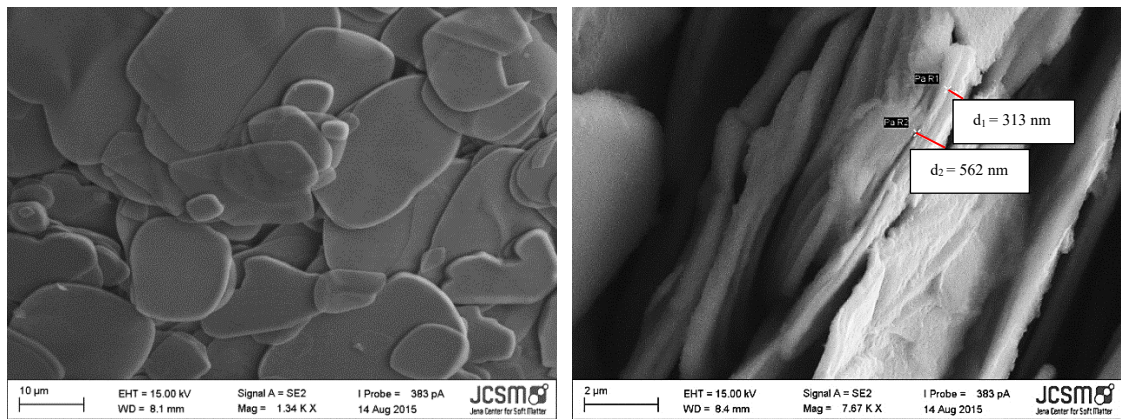


Figure 31: SEM images of mackinawite particles synthesized from elemental iron in a 5 M sodium sulfide solution at 160 °C for three days (exp. FeS\_2).

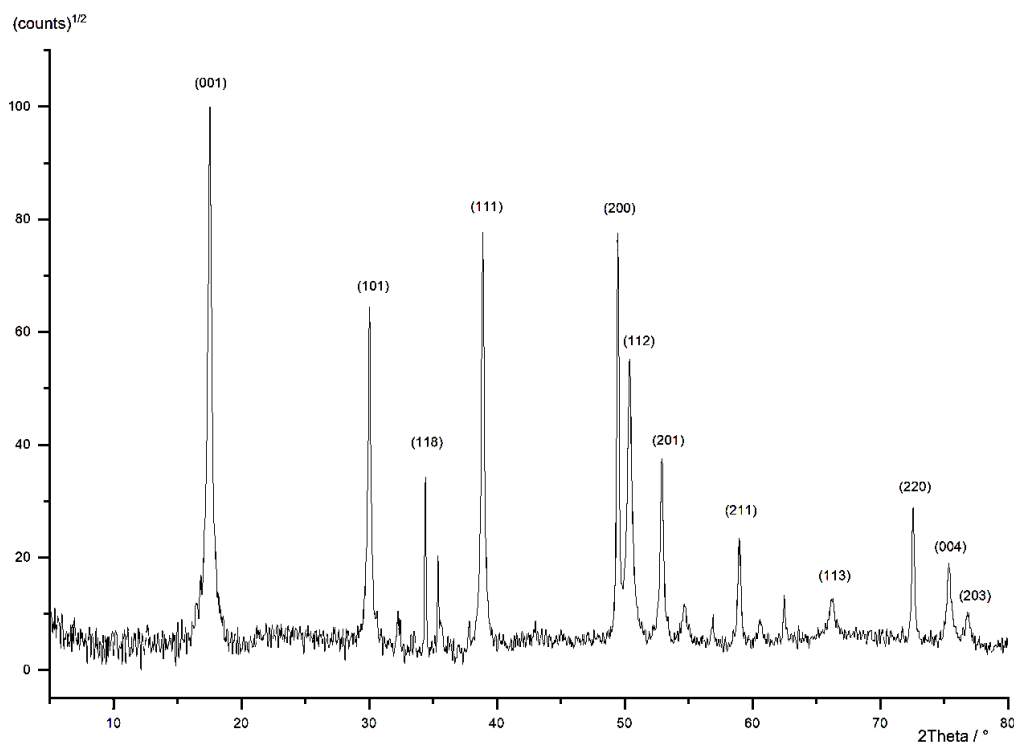


Figure 32: PXRD pattern of a mackinawite sample synthesized from elemental iron in a 5 M sodium sulfide solution at 160 °C for three days (exp. FeS\_2).

Mackinawite converts to pyrrhotite when prepared at higher temperatures in neutral solutions. However, at high sodium sulfide concentrations, highly ordered mackinawite can be synthesized at 160 °C from iron without the formation of pyrrhotite.<sup>37–41</sup> This synthesis was carried out for comparison and SEM images and the PRXD pattern are shown above (exp. FeS\_2). It is apparent that the mackinawite obtained at higher temperatures consists of much bigger sheets compared to the nano-mackinawite and shows much narrower diffraction peaks that correspond to a highly ordered structure.

The synthesis of mackinawite from the elements at low temperatures is an additional way to obtain nano-mackinawite particles that resemble the characteristics of mackinawite synthesized by precipitation. The particle structure, size, surface area and morphology are comparable but the synthesis itself is much more convenient. The advantages of the mackinawite synthesis from the elements are the following:

- No use of sensitive chemicals like  $\text{Fe}^{2+}$  salts or sulfides that are hardly purchased and stored without any traces of oxidation
- No use of toxic and environmentally harmful sulfur sources like  $\text{Na}_2\text{S}$  or  $\text{H}_2\text{S}$

- Much better control over the reaction conditions as any additional salt can be introduced very precisely prior to the reaction
- The use of solutions under anoxic conditions is very challenging and introduces higher errors than working with solids
- As the conditions during the precipitation of nanoparticles can have a huge influence on the structure and morphology, the synthesis of mackinawite from the elements is much more reliable

### 3.3 “Charged layer” model

#### 3.3.1.1 Basic idea

The literature concerned with mackinawite is full of inconsistencies regarding the composition, structure, stability and reactivity. A useful reference for the structure and composition is the natural mineral that is listed by the International Mineral Association (IMA). The composition was determined to be  $(\text{Fe,Ni})_{1+x}\text{S}$  ( $x = 0-0.07$ ).<sup>146</sup> This formula implies, that mackinawite is an iron sulfide with metal excess. Rickard *et al.* argue, that the determination of the composition of mackinawite is quite difficult and that most analyses are erroneous.<sup>126</sup> In his work he used a synthesized mackinawite sample and found a composition of Fe:S very close to 1:1. A detailed Rietveld investigation of the structure of synthetic mackinawite by Lennie *et al.* does also not support any surplus sulfur or iron within the structure.<sup>23</sup> This means that the Fe:S ratio at least of synthetic highly ordered mackinawite is very close to unity. These results are in contrast to other reported analyses of synthetic mackinawite with compositions ranging from  $\text{Fe}_{0.91}\text{S}$  to  $\text{Fe}_{1.15}\text{S}$ .<sup>126</sup>

The structure of mackinawite was determined in a Rietveld investigation of a synthetic mackinawite sample by Lennie *et al.* in 1995. The cell parameters reported in this publication are commonly used as the reference for synthetic and natural highly ordered mackinawite. Mackinawite has a layered structure with cell parameters of  $a = 3.6735(4) \text{ \AA}$  and  $c = 5.0328(7) \text{ \AA}$ . The value of the c-parameter is the same as for the interlayer spacing and therefore corresponds to the d-value of the 001 diffraction peak of mackinawite. The mackinawite sample in the work of Lennie *et al.* was synthesized in a buffered acetic acid solution from elemental iron and sodium sulfide at room temperature.



Below, a new model for the structure and composition of nano-mackinawite shall be described that is able to explain some inconsistent observations. The reaction of elemental iron with elemental sulfur offers completely new opportunities to study the formation and the characteristics of nano-mackinawite as the influence of the surrounding solution can be addressed independently. The reaction of elemental iron and sulfur does not require any additives and proceeds in distilled water in an inert atmosphere at room temperature. Therefore, the effects of different salts and their concentrations can be investigated. The elaborated model is called charged layer model as it divides mackinawite particles into two groups: a charged and a noncharged one. These groups represent two different states of mackinawite particles. The non-charged mackinawite is characterized by a relatively sharp 001 diffraction peak in X-ray diffraction that is mainly broadened by size effects and has an interlayer spacing close to 5.03 Å. The charged mackinawite is characterized by a very broad 001 diffraction peak due to pronounced strain effects and an interlayer spacing greater than 5.05 Å up to values of 5.7 Å.

Mackinawite with the characteristics of both states has been described in previous works on the precipitation of Fe<sup>2+</sup> ions and sulfide ions at very similar conditions. For now, it has not been investigated which conditions preferably lead to the formation of either state because there are a lot of parameters to be considered like local concentrations of sulfide ions, Fe<sup>2+</sup> ions, pH value, concentrations of counterions like Na<sup>+</sup>, NH<sub>4</sub><sup>+</sup>, NO<sub>3</sub><sup>-</sup>, SO<sub>4</sub><sup>2-</sup>, Cl<sup>-</sup>, temperature, purity of starting materials, oxygen contamination, mixing speed and any aging procedures that are often not given in detail. The following table shows the compositions of precipitated mackinawite and the determined d-values of the 001 diffraction peak in some reports on mackinawite.<sup>29,57,130,147–152</sup> The discrepancies in the literature may arise, as charged and non-charged mackinawite was not distinguished.

Table 2: Literature data for mackinawite compositions and (001) d-values. n.d. = not determined.

Reference	Experiment	Fe:S	d (001) [Å]
-----------	------------	------	-------------

Berner, 1964 <sup>130</sup>	Fe + H <sub>2</sub> S (RT)	1.05:1	5.03
Rickard, 1969 <sup>153</sup>	Fe <sup>2+</sup> + HS <sup>-</sup> (RT)	1:1,1	5.03
Lennie, 1995 <sup>149</sup>	Fe + HAc + Na <sub>2</sub> S (RT)	1.008:1	5.03
Mullet, 2002 <sup>150</sup>	Fe + HAc + Na <sub>2</sub> S (RT)	1:1	5.05
Wolthers, 2003 <sup>154</sup>	Fe <sup>2+</sup> + Na <sub>2</sub> S (RT)	n.d.	5.48
Michel, 2005 <sup>155</sup>	Fe <sup>2+</sup> + Na <sub>2</sub> S (RT)	n.d.	5.0X
Rickard, 2006 <sup>156</sup>	Fe <sup>2+</sup> + Na <sub>2</sub> S (RT)	1:1	n.d.
Ohfujii, 2006 <sup>151</sup>	Fe <sup>2+</sup> + Na <sub>2</sub> S (RT)	n.d.	5.19 (wet)
			5.08 (dried)
Jeong, 2008 <sup>71</sup>	Fe <sup>2+</sup> + Na <sub>2</sub> S (RT)	n.d.	5.20
Bourdoiseau, 2008 <sup>152</sup>	Fe <sup>2+</sup> + Na <sub>2</sub> S (RT)	n.d.	5.7
Bourdoiseau, 2011 <sup>29</sup>	Fe <sup>2+</sup> + Na <sub>2</sub> S (RT)	n.d.	5.05
Csákberényi-Malasics, 2012 <sup>157</sup>	Fe <sup>2+</sup> + C <sub>2</sub> H <sub>5</sub> NS (RT)	n.d.	5.88
	Fe <sup>2+</sup> + C <sub>2</sub> H <sub>5</sub> NS (120 °C)	n.d.	5.03
This work	Fe + S (RT)	1:1	5.26 - 5.29
	Fe + S (80 °C)		5.07 - 5.29

The charged mackinawite is considered to consist of nano sheets with a mackinawite structure with iron vacancies. Thus, the layers are negatively charged and repel each other what leads to an increased interlayer spacing. To balance the charge, the released iron ions are adsorbed onto the surface of the particles. The vacancies are not distributed evenly in the sheets what leads to curvature of the particles as can be seen in SEM images and peak broadening in its PXRD patterns. The iron ions on the charged mackinawite surfaces are bound quite loosely by electrostatic attraction. Consequently, other cations can replace these iron ions even those that are not able to enter an iron position of the mackinawite structure. In this regard, sodium chloride was used to show that sodium ions can replace iron ions on the mackinawite surface.

EDX analysis of a so prepared and chloride free washed mackinawite sample shows qualitatively that sodium is present without any chloride detectable.

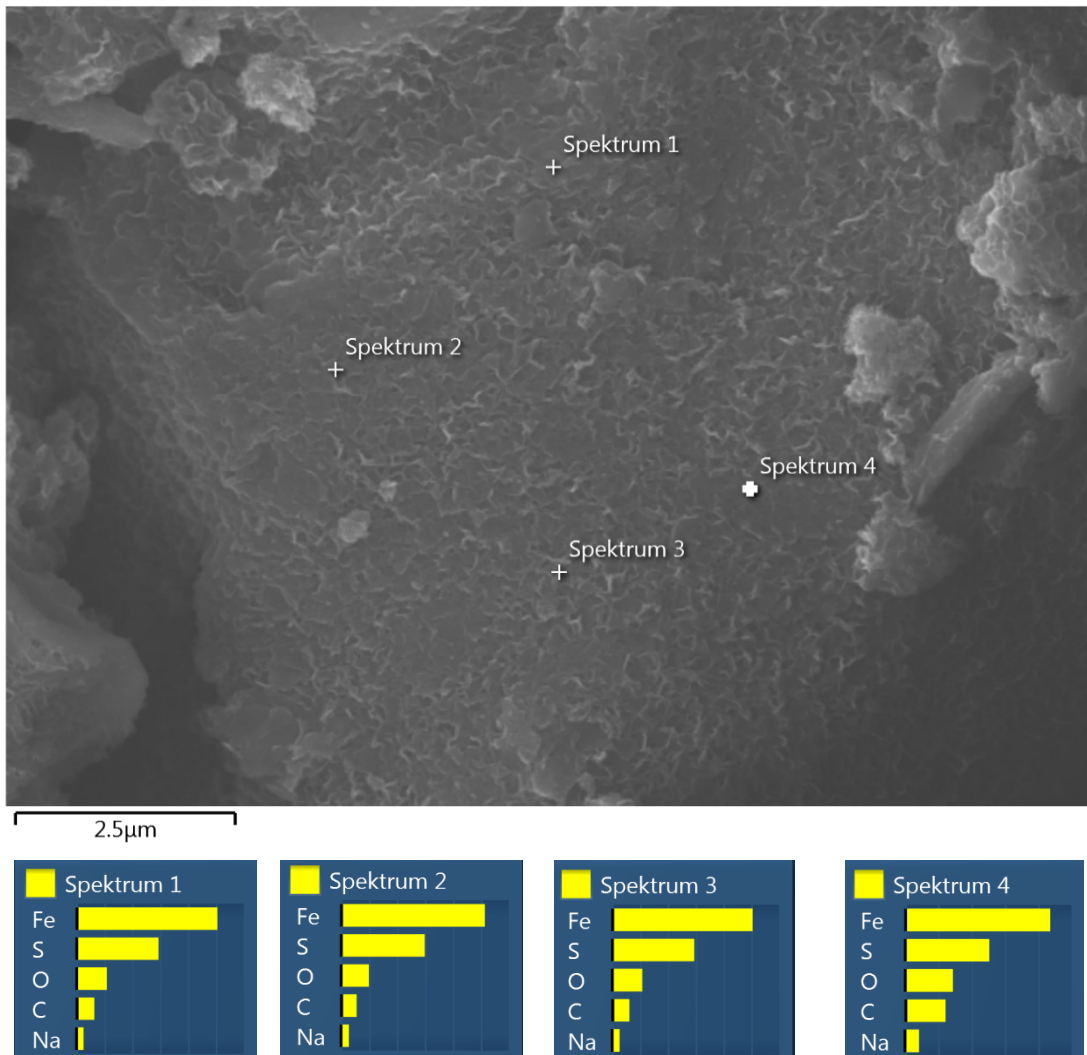


Figure 33: SEM image and EDX analysis of a mackinawite sample synthesized from iron and sulfur in a 0.01 M sodium chloride solution.

The carbon content is caused by the adsorption of CO<sub>2</sub> onto the surface and the oxygen content corresponds to CO<sub>2</sub> and partial oxidation of the mackinawite particles. The charged mackinawite can get uncharged by refilling the vacancies by Fe<sup>2+</sup> ions (or suitable other cations like Ni<sup>2+</sup>). It is expected that the reentering of Fe<sup>2+</sup> ions into the mackinawite structure is kinetically hindered and very slow at low temperatures. But particle growth with time will inevitably lead to noncharged mackinawite because the difference of charge on the surface of the particles compared to the interior creates an electrochemical potential. This potential would theoretically rise upon crystallite growth as with every

new layer more vacancies and corresponding cations are added to the same particle and more charge is accumulated. The rising potential forces the following layers to have ever fewer vacancies which is why the charged mackinawite is only expected to exist with very small particle sizes. It should also be possible to discharge the particles by oxidation, but that has not been shown experimentally yet. Even under conditions open to the atmosphere at room temperature for two days, the PXRD pattern of mackinawite did not change and only negligible amounts of iron oxides formed.

In summary, the new model proposes that there are two distinct states of nanoparticulate mackinawite, a charged and a noncharged one. The charged mackinawite particles have anionic sheets with iron vacancies and cations sitting on the particle surface to balance the charge. Mackinawite in this state has an increased interlayer spacing and shows broad diffraction peaks. Mackinawite in the noncharged state only contains few iron vacancies, if any. It has an interlayer spacing close to 5.03 Å and a comparable sharp 001 diffraction peak. In the following chapter, the assumptions of this model will be explained and experimental evidence will be presented.

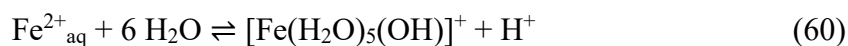
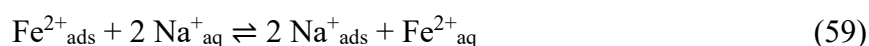
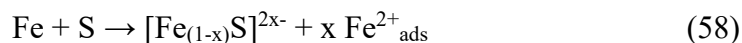
### **3.3.1.2 Experimental support**

It is assumed that mackinawite can have iron vacancies that lead to an anionic charge. This behavior for the mackinawite structure can be found in publications regarding the mineral tochilinite and synthetic analogues. The structure and characteristics of tochilinite have been described in chapter 1 with reference to the corresponding literature.

It was experimentally shown that sodium ions can replace iron ions from mackinawite particles. Because sodium ions cannot enter the iron sites in the mackinawite crystal structure, the replaced iron ions are expected to be adsorbed onto the particle surfaces and are mainly attracted by weak electrostatic forces. The adsorption energy of these  $\text{Fe}^{2+}$  needs to be in the same order of magnitude as the adsorption energy of dissolved  $\text{Na}^+$ . As iron sulfides and hydroxides are hardly soluble but sodium ions do not form any insoluble salts in the investigated systems, they have to be bound to the surface based on their positive charge.

Elemental analysis of mackinawite samples synthesized with increasing amounts of sodium chloride show an increasing amount of sodium in the final washed and dried sample. The data can be fitted by linear regression what is reasonable if the surface adsorbed

$\text{Fe}^{2+}_{\text{ads}}$  exchange with  $\text{Na}^{+}_{\text{aq}}$  in the solution and this process solely depends on the sodium chloride concentration (Fig. 34). The released amount of iron ions is too low to be confidently determined by the applied ICP-AES method but the pH value of the solution gives a simple way to access them indirectly. The addition of increasing amounts of sodium chloride to mackinawite synthesized from the elements leads to a lower pH at the end of the reaction which is a consequence of a rising  $\text{Fe}^{2+}$  ion concentration that act as a weak Lewis acid and release protons upon hydration.



It was experimentally shown, that the higher the sodium chloride concentration is, the more iron ions are released into the solution. This can be explained by an equilibrium process. The sodium ions reversibly replace the surface iron ions whereby the ratio of replaced to surface bound  $\text{Fe}^{2+}$  depends on the sodium concentration in solution.

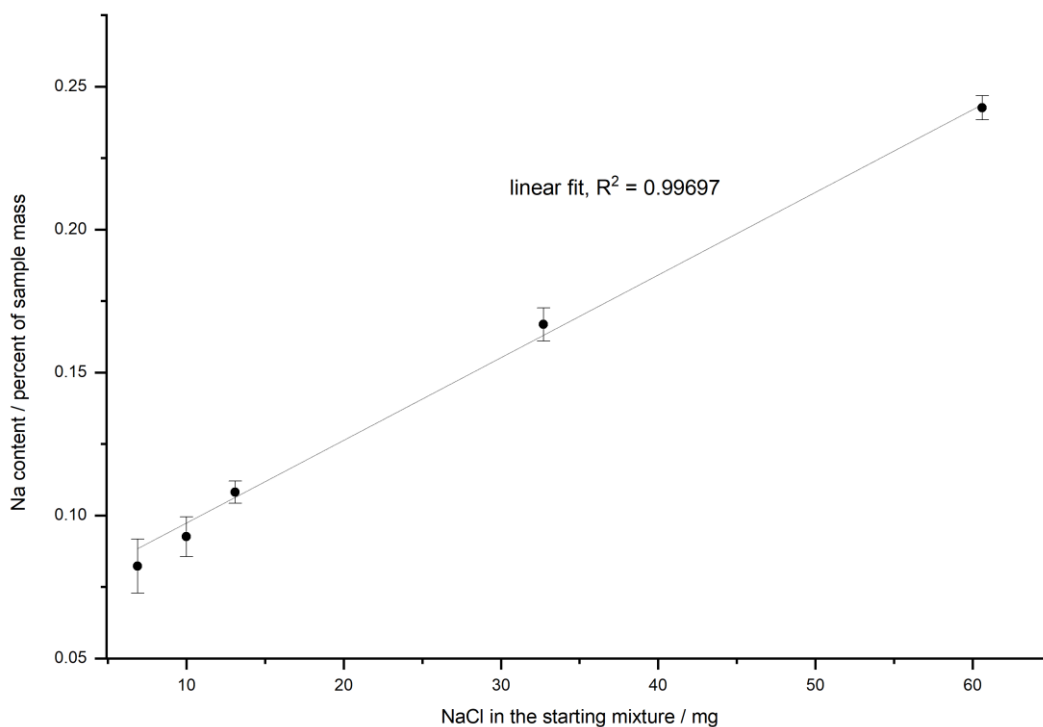


Figure 34: Na-content in mackinawite samples (ICP-AES) synthesized from iron, sulfur and sodium chloride in water at room temperature versus the amount of sodium chloride in the starting mixture.

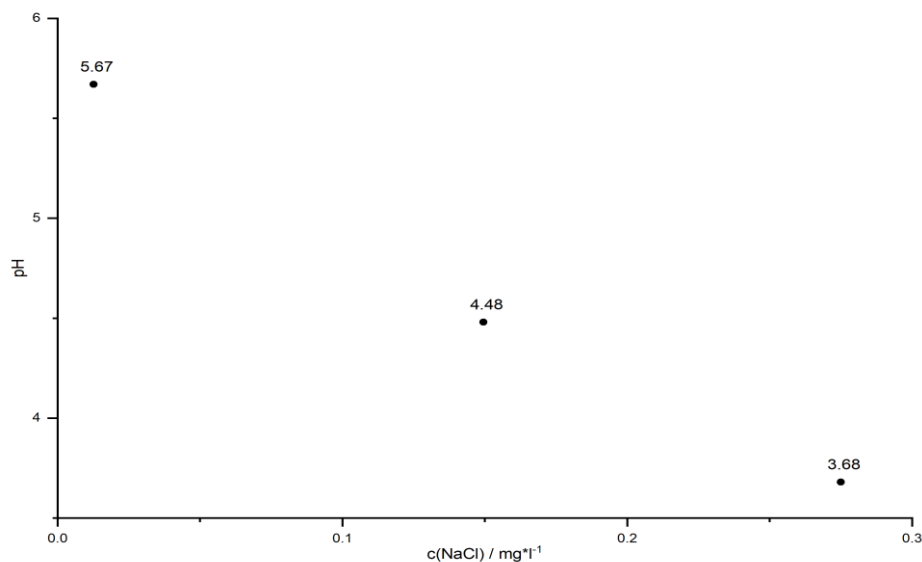


Figure 35: Plot of the pH value of the solution of a mackinawite synthesis from iron, sulfur and sodium chloride versus the sodium chloride concentration.

The model assumes, that the charged mackinawite will transform into the non-charged state upon aging. A sample of mackinawite aged in a solution with a low sodium chloride concentration ( $c_{\text{NaCl}} = 10 \text{ mmol/l}$ ) at  $80 \text{ }^\circ\text{C}$  for three days shows the appearance of a 001 reflection peak at  $d = 5.03 \text{ \AA}$  and a change in the shape of the other more intensive reflection peaks that is caused by the overlap of broad and narrow peaks at nearly the same  $d$ -values. This “tailing” of the diffraction peaks is a direct consequence of the change of the interlayer space and the transformation of charged into non-charged mackinawite upon aging.

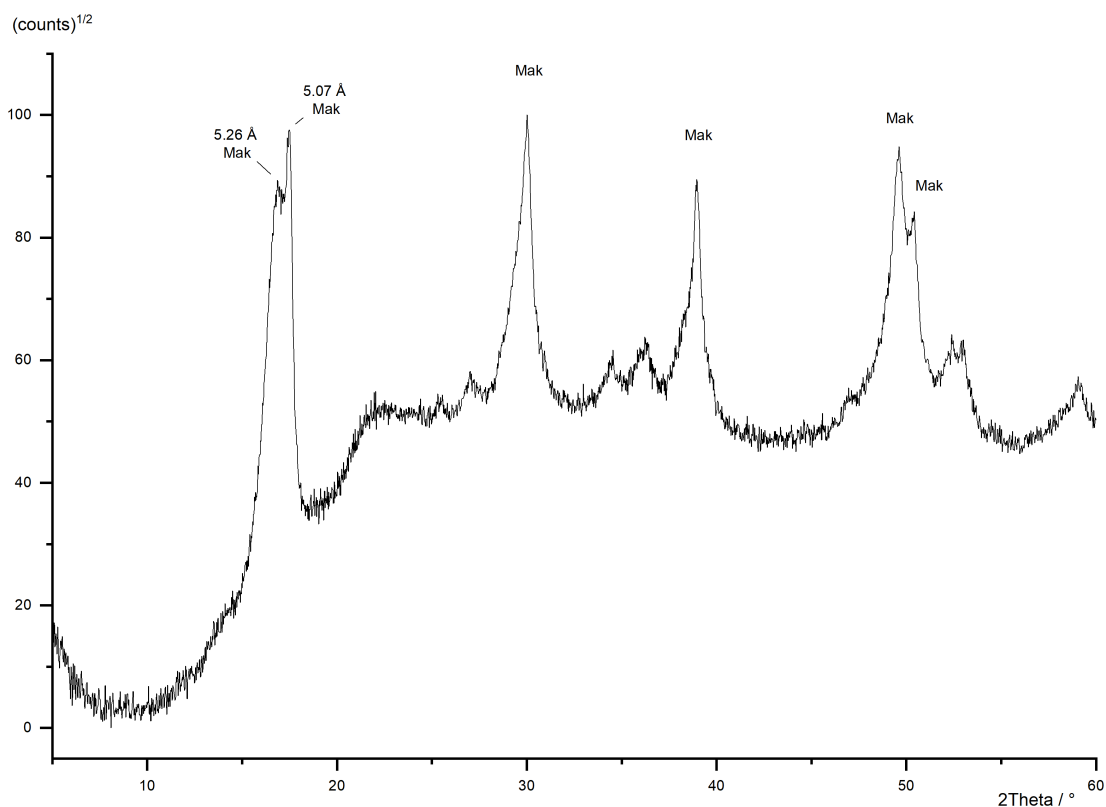


Figure 36: PXRD pattern of a mackinawite sample prepared from iron and sulfur which was aged for one week at 80 °C (exp. FeS\_Ox\_11).

The aging of freshly precipitated mackinawite leads simultaneously to lower interlayer distances and smaller widths at half maximum of the 001 diffraction peak. These changes upon aging also have been reported multiple times in the literature regarding freshly precipitated mackinawite.<sup>24,158</sup> There are no reports on mackinawite samples with large particles and an increased interlayer spacing. In the frequently quoted work of Wolthers *et al.* from 2003, an investigation of nanoparticulate mackinawite with low angle X-ray diffraction (LAXRD) was carried out. The LAXRD patterns showed very broad diffraction peaks and a d-value for the 001 diffraction peak greater than 5.5 Å. The LAXRD patterns was fitted using two mackinawite structures with different interlayer spacings as the fit was very poor when using only one set of lattice parameters. They stated that: “The fact that the patterns could be fitted with a minimum of two peak sets indicates that the material is a mixture of at least two disordered mackinawite phases, referred to as MkA and MkB, with varying d-spacing and crystallinity”.<sup>154</sup> It is apparent, that their sample may have contained multiple or even a nearly infinite number of different mackinawite

particles with different interlayer spacings. There is no reason to assume, that there are only two distinct forms MkA and MkB. This observation may be explained by the charged layer model because there is expected to be a distribution of different interlayer spacings. As there is a minimum value of around 5 Å, there might be an asymmetric distribution of interlayer spacings that would lead to “tailing” for the 001 diffraction peak in PXRD experiments. These observations clearly lead to the hypothesis, that in the absence of any oxidant the first mackinawite formed by precipitation in aqueous solution is always a charged mackinawite that transforms into a noncharged one upon aging. The charged mackinawite should be less stable but kinetically favored following Ostwald’s step rule. More support for this model can be found in the adsorption behavior of nano mackinawite and the determined points of zero charge. The adsorption of  $\text{Cd}^{2+}$  ions on the mackinawite surface follows an ion exchange mechanism replacing iron ions from the mackinawite surface as shown by Mustafa *et al.* 2010.<sup>31</sup> Such an adsorption behavior would be expected for charged mackinawite particles. As mentioned before, the point of zero charge of mackinawite was determined to be around  $\text{pH}_{\text{pzc}} = 3$ <sup>56</sup> on the one hand and around  $\text{pH}_{\text{pzc}} \approx 7.5 - 8$  on the other.<sup>57,58,159</sup> This discrepancy may arise from the different behaviors of charged and noncharged mackinawite. The mackinawite particles in these publications were not analyzed sufficiently to draw clear correlation between the  $\text{pH}_{\text{pzc}}$  and the structure. For charged mackinawite it is to be expected nonetheless, that the positively charged metal ions on the surface lead to a  $\text{pH}_{\text{pzc}}$  above 7 or at least higher than the non-charged one. The noncharged mackinawite surface is dominated by sulfide groups and should therefore show a  $\text{pH}_{\text{pzc}}$  around 3 like pyrite and pyrrhotite.

### 3.3.1.3 Implications for the mackinawite chemistry

Some consequences for the mackinawite chemistry that are to be expected from the charged layer model shall be explained below.

It is to be expected, that the adsorption of cationic species is dependent on the particle charge and therefore also on the particle size. The smaller the particles the more charge per particle is expected and relatively more iron ions can be replaced. This is especially interesting for cations that do not form insoluble sulfides but can nevertheless be bound to the mackinawite surface. The cationic layers around the particles should support the attraction of anions to form a double layer as known from metal surfaces. It has been observed that higher sodium chloride concentrations lead to an increase in the volume of



dispersed mackinawite in water what may be caused by the formation of a pronounced double layer that prevents the agglomeration of the nanoparticles.

The reactivity of charged mackinawite should be higher than for noncharged mackinawite, as the particles contain more defects and the surface iron ions are more exposed to the solution and probably get oxidized more easily.

The intercalation chemistry of mackinawite so far seems to be dependent on anionic iron sulfide layers and the ability to incorporate cations or cationic solid layers. As highly ordered mackinawite with very little vacancies is relatively stable, it should be difficult to introduce cationic guests into the interlayer space. It should be much easier to use charged mackinawite and introduce cationic guest species before the particles get too big. For noncharged guests it should be easier to use noncharged mackinawite. This prediction is supported by the fact, that any tochilinite synthesis during this work only succeeded when nanoparticulate mackinawite was used. When highly ordered mackinawite was used, the only iron sulfide formed was pyrrhotite.

## 4 Synthesis of other metal sulfides from the elements

In order to examine the possible reactivities of other elemental metals towards elemental sulfur, a series of reactions was carried out. In this series, Mg, Al, Mn, Co, Ni, Cu, Zn, Mo, Cd and W were mixed equimolar (two equivalents for Mo and W) with elemental sulfur and used in the same procedure as for the mackinawite synthesis at room temperature. The product mixtures were analyzed with PXRD and the phases identified using the Powder Diffraction Files database. Table 3 shows an overview of all experiments and the corresponding products. To evaluate if the temperature was just not high enough, the reactions where no or only little change was observed were repeated at 80 °C.

Table 3: Products of the reactions between different metals and elemental sulfur at room temperature or 80 °C, respectively.

Experiment	Metal	Products
MnS_1	Mn	Mn, S
CoS_1	Co	Co, S
NiS_1	Ni	Ni, S
CuS_1	Cu	Covellite, Chalcocite
ZnS_1	Zn	Zn, S
MoS_1	Mo	Mo, S, blue colored solution
CdS_1	Cd	orange CdS, no PXRD analysis
WS_1	W	Unknown phase
Mg_1	Mg	Mg-polysulfide complexes
Al_1	Al	Al, S
MnS_2	Mn (80 °C)	Mn, S
ZnS_2	Zn (80 °C)	Zn, S
CoS_2	Co (80 °C)	Co, S
NiS_2	Ni (80 °C)	Millerite, Heazlewoodite
Al_2	Al (80 °C)	Al, S

Iron, nickel, copper, wolfram, cadmium, magnesium and molybdenum do react with elemental sulfur at a maximum of 80 °C whereas aluminum, manganese, zinc and cobalt do not. The reactivity towards sulfur depends on several parameters that can be deduced from the reaction mechanism. Although copper is a noble metal, it is oxidized by sulfur what is also known for silver jewelry. Manganese and zinc are much more easily oxidized than these elements but do not react with elemental sulfur, what makes the redox potential of the metal a minor factor for the reactivity.

The mechanism shows that there is an equilibrium on the metal surface between the formation of a conducting sulfide layer and a passivating hydroxide layer. Therefore, the difference of the solubility of the metal sulfide to the metal hydroxide is a crucial feature. If the solubility of the sulfide is not low enough in respect to the solubility of the hydroxide, the formation of the first sulfide layer is very slow or impossible. MnS has a comparable high solubility and the highest in the investigated series. Therefore, it is reasonable to assume that the formation of an initial MnS layer on the Mn surface is hindered and the reaction cannot proceed. The same applies in the case of aluminum and magnesium but the latter forms relatively stable polysulfide complexes that lead to the dissolution of the metal. For zinc the reason needs to be another one, as ZnS has a much smaller molar solubility than Zn(OH)<sub>2</sub>. ZnS is the only transition metal sulfide that is colorless, as it possesses a great band gap and a low electrical conductivity. If an initial sulfide layer is formed on the metal surface, the next step in the mechanism is the transport of electrons through this sulfide layer towards the sulfur surface. If the conductivity of the sulfide is too low, the electron transport is hindered, and the reaction stops.

As nickel and copper show a sufficiently high reactivity towards elemental sulfur, these elements were investigated in more detail. Nickel and copper sulfides are highly interesting for prebiotic scenarios because they are found in the active sites in recent enzymes. The investigations of the reaction between iron and sulfur show that the addition of sodium chloride leads to an enormous increase of the reaction rate. Therefore, reactions were carried out at different temperatures and sodium chloride concentrations that are summarized in table 4. Powdered nickel and powdered sulfur were thoroughly mixed in a molar ratio of Ni:S = 3:2 and 2 g were used for each reaction following the standard procedure.

Table 4: Reaction products of a mixture of nickel and sulfur under different reaction conditions.

Exp.	NaCl / mol * l <sup>-1</sup>	Temp. / °C	Time / days	Products
MB_1	0	25	1	S, Ni
MB_2	0.01	25	1	S, Ni
MB_3	0	<b>80</b>	1	S, Ni, Millerite, Heazlewoodite
MB_4	0.01	<b>80</b>	1	S, Ni, Millerite, Heazlewoodite
MB_5	0	25	3	S, Ni
MB_6	0.01	25	3	S, Ni
MB_7	0.01	<b>80</b>	3	S, Ni, Millerite, Heazlewoodite
MB_8	0.17	25	3	S, Ni

From this reaction series it can be concluded that nickel and sulfur do not react at room temperature and that millerite and heazlewoodite form at 80 °C. Even higher concentrations of sodium chloride do not lead to a reaction at room temperature but increase the reaction speed at 80 °C. Sodium chloride only has influence on the latest step in the mechanism namely the transport of electrons and metal ions from the metal to the sulfur surface. Therefore, the reason for the lower reactivity of nickel compared to iron must come from the first steps in the reaction mechanism i.e. the promotion of the sulfur disproportionation or the formation of the first sulfide layer. SEM images of MB\_7 are shown in figure 37 and 38. The millerite and heazlewoodite particles are in the nano regime like the mackinawite particles formed from iron and sulfur.

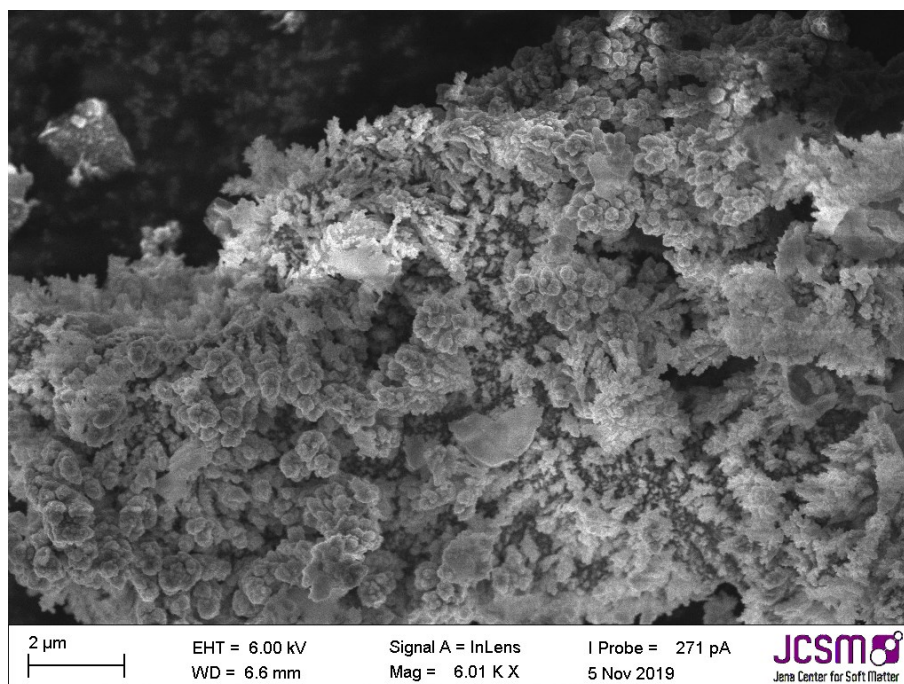


Figure 37: SEM image of MB\_7.

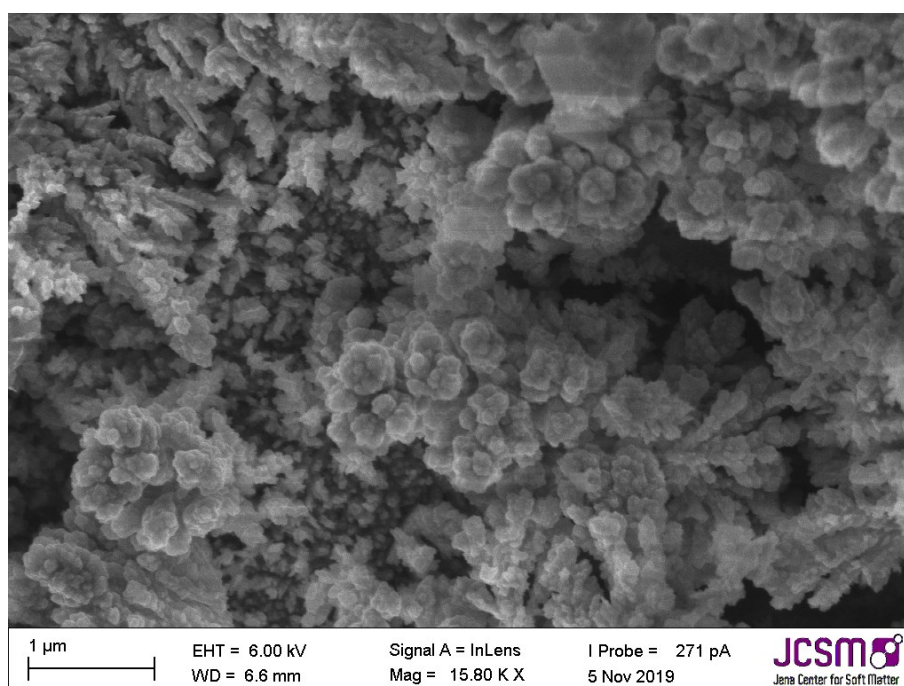


Figure 38: SEM image of MB\_7.

Copper readily reacts with sulfur forming covellite and chalcocite. As there are many mixed metal sulfides in the System Fe/Cu/S, a series of reactions was carried out to investigate if these may form or if the sulfides of copper and iron form independently. The

reactions carried out in this series are summarized in table 5. Powdered copper, powdered iron and powdered sulfur were thoroughly mixed in two different ratios and 2 g were used for each reaction following the standard procedure. From a mixture of iron, copper and sulfur a variety of phases forms. These phases have structures of pure iron sulfides like mackinawite, pyrrhotite and pyrite and pure copper sulfides like covellite, but the mixed metal sulfides chalcopyrite and bornite also form. Chalcopyrite seems to be the most stable phase under the applied conditions and forms as the major product independent of the ratio of nickel, iron and sulfur in the starting mixture. Elemental iron is consumed much faster than copper as the formation of mackinawite from iron and sulfur is much faster than the formation of covellite from copper and sulfur. Mackinawite and covellite are the first phases to form and transform into more stable sulfides, most of all chalcopyrite. At higher amounts of iron and sulfur in the starting mixture, relatively more iron sulfides form as would be expected. The presence of sodium chloride and higher reaction temperatures increase the reaction rates but do not alter the product distribution significantly. Unintended oxidation during the work up most probably was the reason for the formation of magnetite. As the diffraction peaks of the different phases are hard to be assigned confidently in the PXRD patterns, only these are listed in the table below that were undoubtedly identified and more may be present even if not listed.

Table 5: Products of reactions between copper, iron and sulfur at different sodium chloride concentrations, temperatures, reaction times and starting mixtures.

Exp.	Starting mixture	Concentration of NaCl / mol * l <sup>-1</sup>	Temp. / °C	Time / days	Products
MB_9	Cu : Fe : 2S	0	25	1	S, Cu, Mackinawite
MB_10	Cu : Fe : 2S	0.01	25	1	S, Cu, Mackinawite
MB_11	Cu : Fe : 2S	0	80	1	S, Cu, Chalcopyrite, Covellite, Mackinawite
MB_12	Cu : Fe : 2S	0.01	80	1	S, Cu, Chalcopyrite, Covellite, Pyrite, Bornite, Magnetite
MB_13	Cu : Fe : 2S	0	25	3	S, Cu, Chalcopyrite, Covellite, Mackinawite

MB_14	Cu : Fe : 2S	0.01	25	3	Cu, Covellite, Chalcopyrite, Mackinawite, Bornite, Pyrite, Magnetite
MB_15	Cu : Fe : 2S	0	80	3	Cu, Covellite, Chalcopyrite, Pyrrhotite, Bornite, Pyrite, Magnetite
MB_16	Cu : Fe : 2S	0.01	80	3	Cu, Covellite, Chalcopyrite
MB_17	Cu : Fe : 2S	0.17	25	3	S, Cu, Chalcopyrite, Covellite, Mackinawite
MB_18	Cu : 2Fe : 3S	0.01	25	1	S, Cu, Chalcopyrite, Covellite, Mackinawite, Pyrrhotite
MB_19	Cu : 2Fe : 3S	0.01	25	4	S, Cu, Chalcopyrite, Covellite, Mackinawite, Pyrrhotite
MB_20	Cu : 2Fe : 3S	0.01	25	10	Chalcopyrite, Covellite, Pyrite, Pyrrhotite, Magnetite
MB_21	Cu : 2Fe : 3S	0.01	80	1	S, Cu, Covellite, Mackinawite
MB_22	Cu : 2Fe : 3S	0.01	80	4	Cu, Chalcopyrite, Covellite, Bornite, Magnetite, Mackinawite, Pyrrhotite
MB_23	Cu : 2Fe : 3S	0.01	80	10	Chalcopyrite, Covellite, Pyrite, Magnetite

SEM images of the product mixture of reaction MB\_23 predominantly show chalcopyrite particles. These are nanoparticulate and have similar shapes and a narrow size distribution.

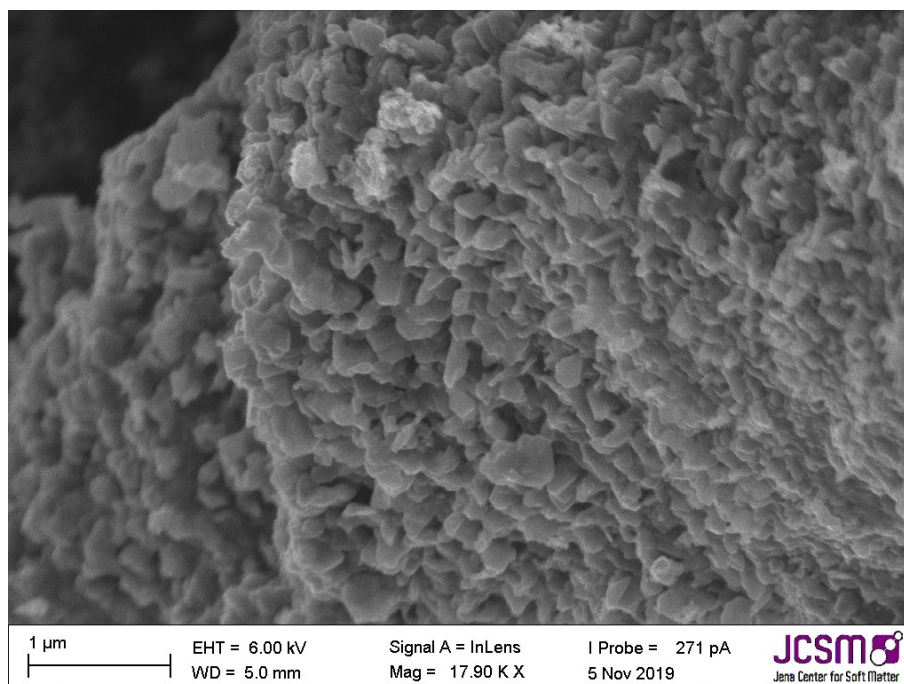


Figure 39: SEM image of MB\_23.

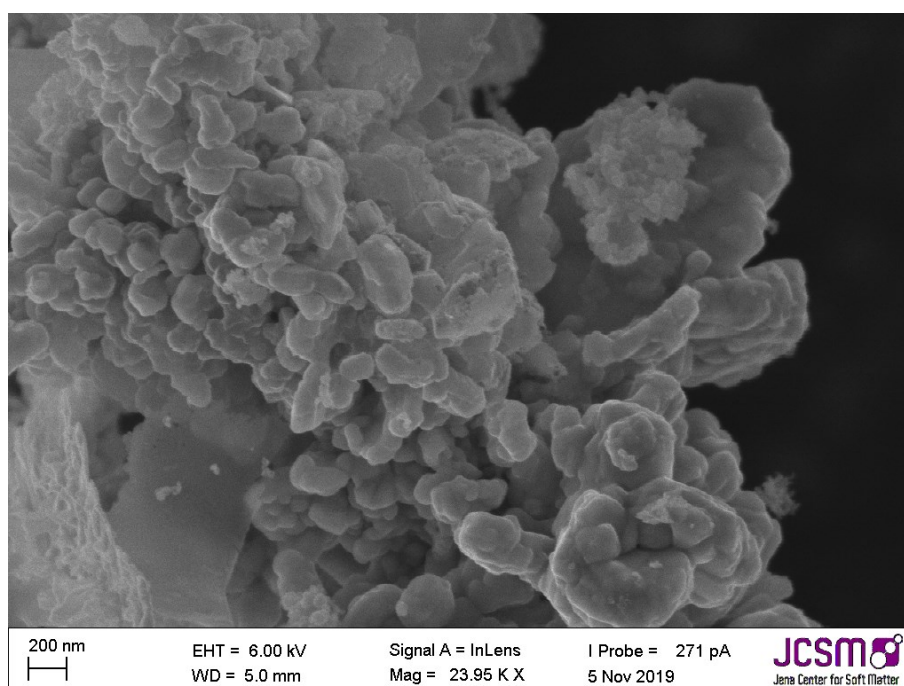


Figure 40: SEM image of MB\_23.

This series shows that the reactions between nickel, copper, iron and sulfur at low temperatures offer the possibility to synthesize metastable nano particulate phases that can have a variety of structures and compositions depending on the starting mixture and the



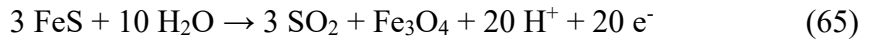
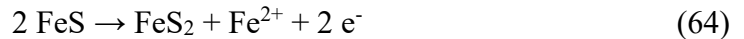
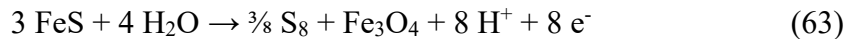
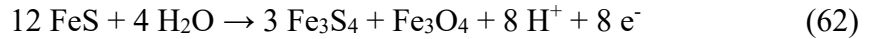
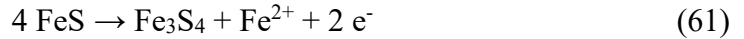
reaction conditions. Controlling the selectivity of reactions with copper and nickel seems to be challenging compared to the equimolar reaction between iron and sulfur forming only mackinawite. This problem may be addressed by first synthesizing CuS, NiS and FeS independently and mixing the sulfides in a subsequent reaction in appropriate ratios. For prebiotic chemistry, this feature allows the formation of highly reactive nanoparticulate sulfides with compositions and structures depending on the composition of the parent metal and adds a huge diversity to the possible mineral repertoire.

## 5 Carbon fixation with nano-mackinawite

### 5.1 Activation and reduction of CO<sub>2</sub>

The activation of CO<sub>2</sub> and the subsequent reduction are two different independent processes. There might be an activation of CO<sub>2</sub> on the iron sulfide surface e.g. by deformation of the CO<sub>2</sub> molecule without any electron transfer. It is also possible for electron transfers to occur without a previous activation of CO<sub>2</sub>, but this case is very unlikely due to the high potential that is needed. Therefore, it is reasonable to expect a CO<sub>2</sub> activation process if any reduction product is observed.

The standard redox potentials of Fe<sup>2+</sup> and S<sup>2-</sup> in solution can be vastly increased by the formation of stable solids like greigite, pyrite and iron oxides upon oxidation. As different oxidation reactions for mackinawite are possible, there is a range of potentials accessible that are depending on the actual oxidation reaction which in turn depends on several conditions especially the reaction temperature and the presence of an aqueous solution. From TGA/DSC/PXRD analysis the following reactions can be derived for mackinawite oxidation:



At low temperatures, the oxidation of nano-mackinawite predominantly leads to the oxidation of Fe<sup>2+</sup> to Fe<sup>3+</sup> and the formation of greigite and magnetite. The oxidation of the sulfide ions occurs at higher temperatures leading to the formation of elemental sulfur, SO<sub>2</sub>/SO<sub>3</sub><sup>2-</sup> and finally SO<sub>4</sub><sup>2-</sup>. The redox potential of the mackinawite nanoparticles is essentially unknown and depends on the band structure which in turn depends on many

parameters like the particle size, the surface groups and any deviations from the theoretical mackinawite crystal structure. Additionally, the redox potential is expected to change during the oxidation as  $\text{Fe}^{2+}$  are oxidized to  $\text{Fe}^{3+}$  and other phases form like greigite  $\text{Fe}_3\text{S}_4$  and magnetite  $\text{Fe}_3\text{O}_4$ . The redox potential will also be different for dry mackinawite compared to reactions in aqueous solution. As has been explained in chapter 1, the activation energy needed for the reduction of  $\text{CO}_2$  depends on many aspects and it is hard to predict, which conditions would be suited for the activation and reduction on nanoparticulate mackinawite. In this regard, different conditions were applied for the reduction experiments that are prebiotic plausible as explained in the following chapter.

## 5.2 Experimental conditions

The conditions of the early earth atmosphere are under permanent debate and the scientific view has changed several times over the last 100 years. Miller et al. for instance assumed a very reducing atmosphere containing greater amounts of  $\text{CH}_4$ . The faint-young-sun-problem demanded for an atmosphere containing higher levels of  $\text{CO}_2$  and it is also proposed that the atmospheric conditions could have changed periodically from more oxidizing to more reducing and back again.<sup>160-162</sup> Values for the temperature on the early earth's surface that are reported also vary significantly in a range of 26 °C to 85 °C and may have been much higher at hydrothermal settings.<sup>163,164</sup> Meteoritic impacts and volcanic eruptions have been common events and increase the range of possible conditions for prebiotic chemistry even further. Therefore, a set of different conditions was used to study the reaction between  $\text{CO}_2$  and nano-mackinawite as is summarized in table 6.

Table 6: Reaction conditions of  $\text{CO}_2$  reduction reactions and the assigned codes.

Name	Temp. / °C	Conditions
------	------------	------------

T1	40	0.1 M Carbonate containing solution at different pH values and autogenous CO <sub>2</sub> -pressure
M1	80	
T2	40	~ 2 atm CO <sub>2</sub> atmosphere saturated with water without a liquid phase
M2	80	
H1	160	Carbonate adsorbed onto a mackinawite sample and heated in a distillation setup
H2	160	~ 2 atm CO <sub>2</sub> atmosphere saturated with water without a liquid phase

As outlined before, the temperature is expected to have a high impact on the reactivity and the course of the reaction between CO<sub>2</sub> and mackinawite. However, the pH value of the reaction solutions may be similar important. The higher the pH value, the easier mackinawite can be oxidized but the harder it is to protonate reduced species. The main obstacle with high proton concentrations is the pronounced formation of H<sub>2</sub> and FeS<sub>2</sub> instead of reduced carbon species. Therefore, a compromise is required that enables Fe<sup>2+</sup> and S<sup>2-</sup> oxidation and CO<sub>2</sub> reduction without increased H<sub>2</sub> formation. A nearly neutral pH value has been reported to be the optimal pH region for the reduction of dissolved CO<sub>2</sub> on greigite surfaces.<sup>15</sup>

As the initial experiments showed, that the iron powder contained some organic material on its surface, the mackinawite syntheses were carried out in three different ways. The first experiments were carried out using the iron powder as received. My colleague Mario Grosch could show that all the organic material can be removed by washing the iron powder with diluted hydrochloric acid. Therefore, the second set of experiments was carried out with mackinawite synthesized using pretreated iron powder. In a third set of experiments, mackinawite was synthesized by precipitation from solutions of (NH<sub>4</sub>)<sub>2</sub>Fe(SO<sub>4</sub>)<sub>2</sub> and Na<sub>2</sub>S to exclude any impact from using elemental iron.

The evaluation of the reduction experiments needs some considerations regarding the methods of analysis and the results that can be deduced. Two different GC-MS methods were applied in regard of the experimental conditions. For the low and medium temperature reactions (T1, T2, M1, M2) and the high temperature reactions H2 the head space of

the reactions was transferred into a clean GC-MS vial and analyzed in a setup optimized for gaseous products like CO, CH<sub>4</sub>, C<sub>2</sub>H<sub>6</sub>, COS, CS<sub>2</sub>, CH<sub>3</sub>SH and CH<sub>3</sub>SSCH<sub>3</sub>. The high temperature reactions H1 were carried out and analyzed differently. A sample of mackinawite was stirred in a solution containing Na<sub>2</sub>CO<sub>3</sub> or NaHCO<sub>3</sub> and the pH value was adjusted with diluted acids. The carbonate ions adsorbed overnight onto the particles and the solid phase was isolated by filtration and transferred into a distillation setup. In this setup, the sample was placed in a 10 ml glass tube that was connected by a distillation bridge to a 10 ml glass flask which was filled with 1ml of DCM. To keep the DCM gas pressure during the distillation to a minimum it was cooled with a DCM/liquid nitrogen bath to around - 95 °C. The tube with the sample was heated for around 3 hours at 160 °C. Any volatiles that evaporated at these temperatures dissolved in the DCM which was then dried over Na<sub>2</sub>SO<sub>4</sub> and analyzed by GC-MS in a setup that was optimized for compounds with slightly higher boiling points like CH<sub>3</sub>SH and CH<sub>3</sub>SSCH<sub>3</sub>, C<sub>n</sub>H<sub>n+2</sub>S, carboxylic acids, higher alkanes and alcohols.

In general, the GC-MS analysis can only give information about compounds that are volatile at the temperatures used. The identification of the formed volatiles was achieved by reference samples for methane thiol, methane, ethane thiol, ethane, H<sub>2</sub>S and CO<sub>2</sub>. The structures of the other species that occurred have not been identified, but the compositions can be given by comparing the mass distributions with entries in the NIST database<sup>165</sup> and a publication by Levy and Stahl.<sup>166</sup> Strongly adsorbed or highly water soluble carbonaceous material or compounds with high boiling points could not have been detected in the low and medium temperature reactions. Analyses of the aqueous phases by NMR spectroscopy did not lead to comprehensive data. HPLC analysis should be viewed as essential for future investigations. Therefore, it is also important to investigate the solid phases after the reactions to see if the mackinawite shows any sign of oxidation even if no carbonaceous products were detected. Greigite occurred in many reactions whereas magnetite, pyrite, sulfur and siderite occurred occasionally depending on the reaction conditions.

### **5.3 Mackinawite from iron and sulfur without pretreatment**

The CO<sub>2</sub> reduction reactions that were carried out with mackinawite synthesized from untreated iron and sulfur are summarized in table 7. The conditions (T1, T2, M1, M2, H1

and H2) correspond to table 6. The solid reaction products were isolated by filtration, dried in nitrogen flow and cautiously exposed to air. Unfortunately, the solids were pyrophoric to such an extent, that they oxidized vigorously upon the first air contact. All PXRD patterns showed greigite and lepidocrocite as the main phases. Magnetite, sulfur and siderite occurred occasionally, but it is not clear to which extent these phases formed during the work up which is why the solid phases were not investigated any further.

Table 7: Reaction conditions and products of the reactions between mackinawite and CO<sub>2</sub>/carbonate using untreated iron powder.

Exp.	Conditions	Sum formulas of carbonaceous compounds
RED_1	T1, 4 days, pH=7, <sup>13</sup> C	N.D.
RED_2	T2, 4 days, <sup>13</sup> C	N.D.
RED_3	T2, 2 months, <sup>13</sup> C	<sup>12</sup> CH <sub>4</sub>
RED_4	M1, 4 days, pH=7, <sup>13</sup> C	<sup>12</sup> CH <sub>4</sub>
RED_5	M2, 4 days, <sup>13</sup> C	<sup>12</sup> CH <sub>4</sub> , <sup>12</sup> C <sub>2</sub> H <sub>4</sub> , <sup>12</sup> C <sub>2</sub> H <sub>6</sub>
RED_6	H1, 3 hours, pH=7, <sup>12</sup> C	<sup>12</sup> CH <sub>3</sub> SH, <sup>12</sup> C <sub>2</sub> H <sub>8</sub> S <sub>2</sub> , <sup>12</sup> C <sub>2</sub> H <sub>8</sub> S <sub>3</sub>
RED_7	H1, 3 hours, pH=7, <sup>13</sup> C	<sup>13</sup> CH <sub>3</sub> SH
RED_8	H1, 3 hours, pH=7, <sup>13</sup> C	<sup>12</sup> CH <sub>3</sub> SH, <sup>12</sup> C <sub>2</sub> H <sub>8</sub> S <sub>2</sub> , <sup>12</sup> C <sub>2</sub> H <sub>8</sub> S <sub>3</sub>
RED_9	H1, 3 hours, pH=7, <sup>12</sup> C	<sup>12</sup> C <sub>3</sub> H <sub>8</sub> S, <sup>12</sup> C <sub>4</sub> H <sub>10</sub> S, <sup>12</sup> C <sub>5</sub> H <sub>12</sub> S, <sup>12</sup> C <sub>6</sub> H <sub>12</sub> O, <sup>12</sup> C <sub>6</sub> H <sub>14</sub> S, <sup>12</sup> C <sub>3</sub> H <sub>8</sub> S <sub>2</sub> , <sup>12</sup> C <sub>5</sub> H <sub>12</sub> S <sub>2</sub> , <sup>12</sup> C <sub>6</sub> H <sub>14</sub> S <sub>2</sub>
RED_10	H2, 1 hour, <sup>13</sup> C	<sup>12</sup> CH <sub>4</sub> , <sup>12</sup> COS, <sup>12</sup> C <sub>2</sub> H <sub>4</sub> , <sup>12</sup> C <sub>2</sub> H <sub>4</sub> O, <sup>12</sup> C <sub>4</sub> H <sub>8</sub> , <sup>12</sup> C <sub>3</sub> H <sub>6</sub> O

The reactions were carried out first with <sup>12</sup>CO<sub>2</sub>/Na<sup>12</sup>CO<sub>3</sub>/NaH<sup>12</sup>CO<sub>3</sub> and if any products could be detected, they were repeated with <sup>13</sup>C starting materials. Reactions RED\_1 to RED\_5 were carried out with <sup>13</sup>CO<sub>2</sub> but only <sup>12</sup>C-compounds were detected by GC-MS. These experiments show, that <sup>13</sup>CO<sub>2</sub> does not form products detectable by GC-MS analysis in the reaction with mackinawite at 40 °C or 80 °C as well in solution as in the dry state in the experimental method applied. The <sup>12</sup>C-compounds that could be detected need

to have another origin what will be covered in the following section. In the high temperature reactions RED\_6 to RED\_9 the distillation procedure (H1) led to the formation of significant amounts of alkyl thiols and COS. Reaction RED\_7 is the only reaction in which reduced  $^{13}\text{C}$ -labeled compounds were identified in a reaction system of mackinawite and adsorbed  $^{13}\text{HCO}_3^-/^{13}\text{CO}_3^{2-}$ .

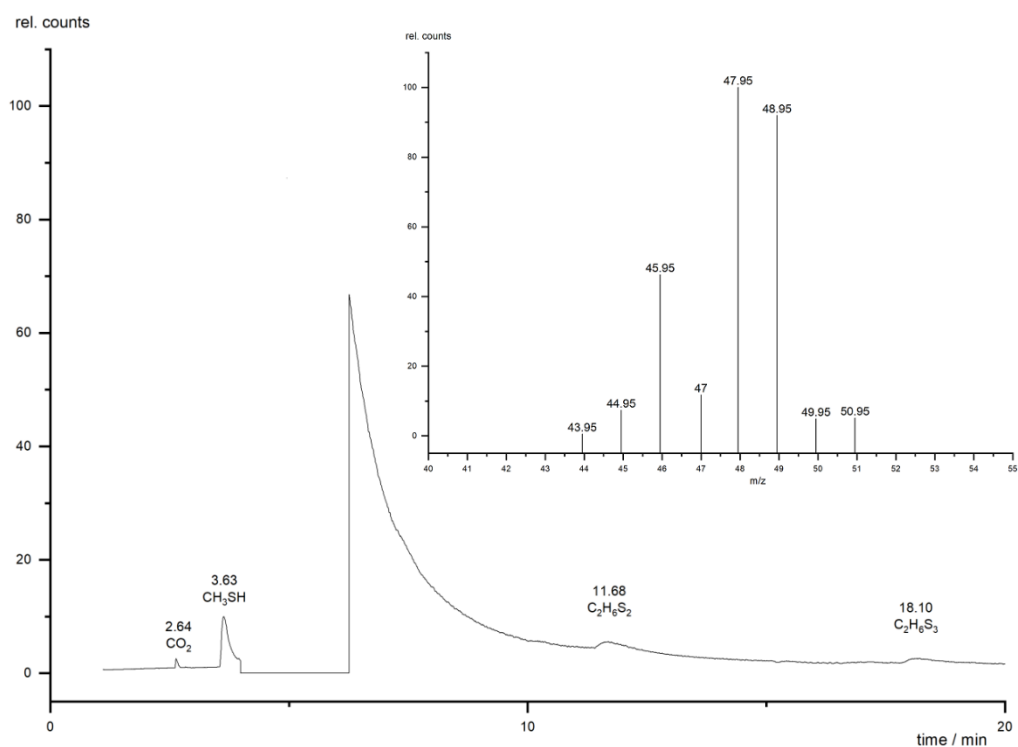


Figure 41: Gas chromatogram of RED\_6. The inset shows the m/z values of the  $^{13}\text{C}$  methane thiol peak at 3.63 minutes.

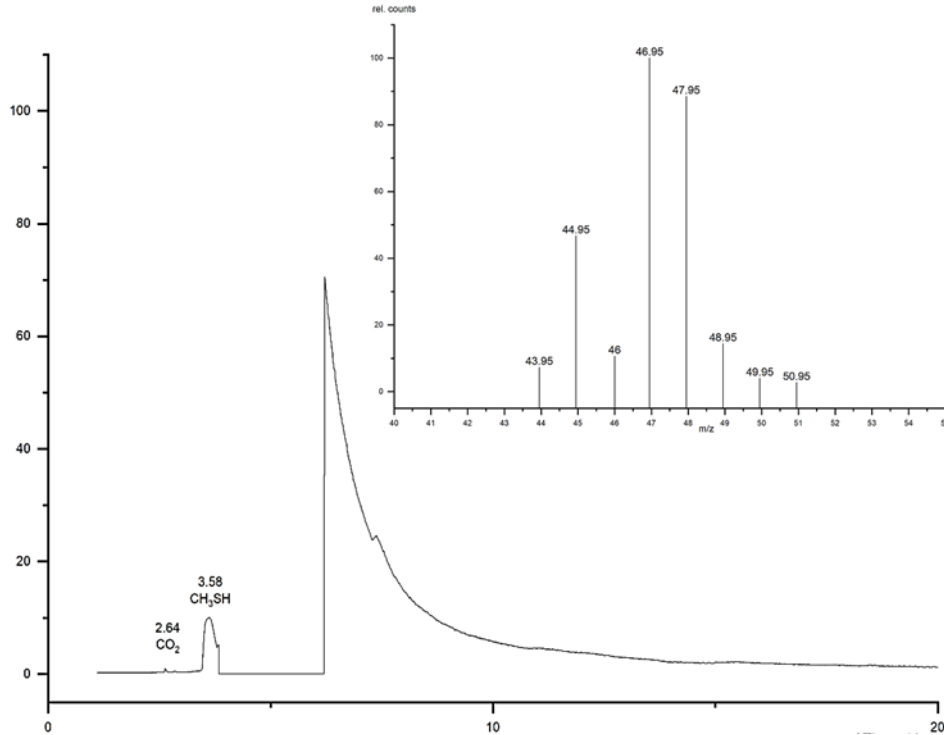
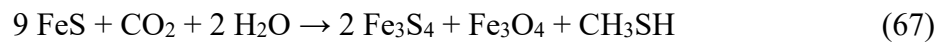


Figure 42: Gas chromatogram of RED\_7. The inset shows the m/z values of the methane thiol peak at 3.58 minutes.

The oxidation products are greigite, magnetite and sulfur what leads to the following reasonable equations for methane thiol formation:



The ratio of magnetite to greigite after the reactions is very small in the low and medium temperature runs but increases significantly in the high temperature runs. In addition, elemental sulfur only occurred at higher temperatures.

## 5.4 Mackinawite from pretreated iron and sulfur

In a system of Fe, S, H<sub>2</sub>O, NaCl and <sup>13</sup>CO<sub>2</sub>, <sup>12</sup>C-impurities most probably arise from carbonaceous material on the iron powder. The iron powder used was manufactured by a reduction process using a reduction mixture consisting of coke breeze blended with ground limestone and a pre-processed magnetite slick. The carbonaceous material in the



iron powder may consist of carbides, carbon or carbonates that are released during the mackinawite formation and become adsorbed again onto the mackinawite surface. In a  $^{13}\text{C}$  atmosphere, these  $^{12}\text{C}$ -compounds are reduced and lead to the formation of  $^{12}\text{CH}_4$ ,  $^{12}\text{C}_2\text{H}_6$ ,  $^{12}\text{COS}$ , greigite, magnetite and sulfur. The treatment of 5 g of the iron powder in a 25 ml GC-MS vial with diluted phosphorous acid and analyzing the headspace showed significant amounts of reduced carbon species namely methane, ethene, ethane, propene and propane (exp.  $\text{Fe}_2\text{H}_3\text{PO}_4$ ). The iron powder hence was analyzed in detail to see if the carbonaceous species can be identified. PXRD analysis shows, that there is another crystalline phase present but the diffraction peaks could not be assigned, neither to a carbide phase nor to a carbon or carbonate phase.

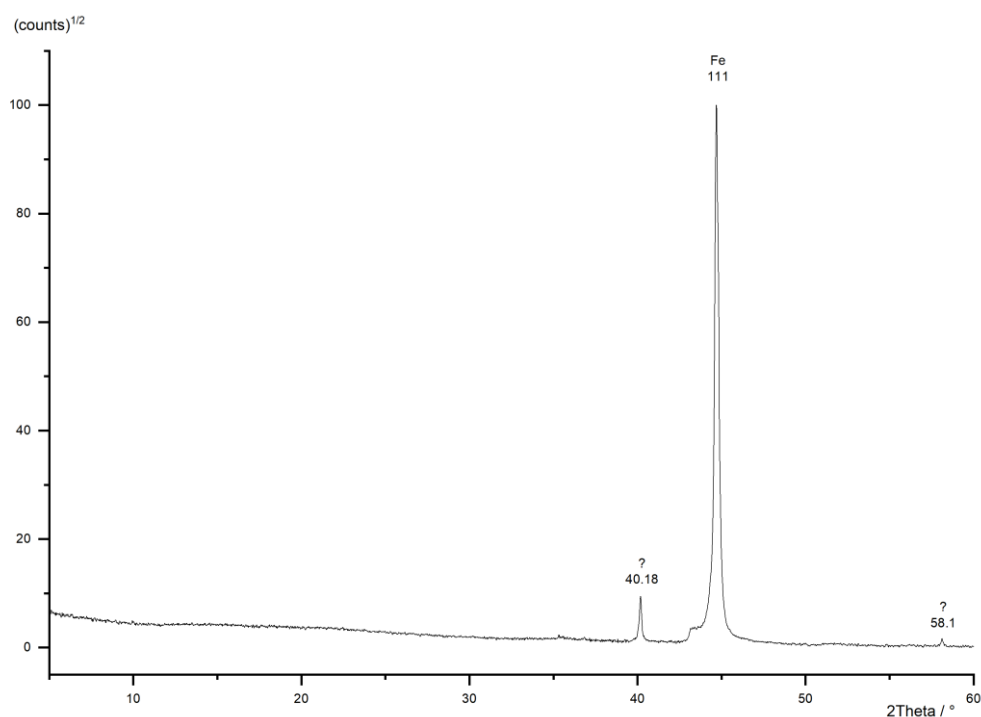


Figure 43: PXRD pattern of the untreated powder of elemental iron.

ICP-AES analysis gives a composition of  $100 \pm 0.01$  % iron with no sign of significant amounts of impurities but EDX shows, that there is a certain amount of carbon present at least at the particles' surface. Therefore, it was reasonable to try to remove the carbonaceous material by removing the surface of the iron particles with diluted hydrochloric acid. This treatment was developed by my colleague M. Grosch and he could show that after the acid treatment nearly no reduced carbon species emerged upon the addition of

diluted phosphorous acid. Cvetković *et al.* investigated the hydrocarbon formation from iron prepared from  $\text{Fe}(\text{CO})_5$  in alkaline solutions.<sup>167</sup> They suppose that carbide phases are present within the particles as they cleaned the particle surfaces by an acid treatment. They report that alkanes and alkenes, alcohols, aldehydes and carboxylic acids formed within 30 days at room temperature. The organic material on the surface of our iron powder could not be identified, but it is reasonable to assume it also to be composed of carbide phases. It could be removed by an acid treatment and no indissoluble part remained what excludes the presence of graphite. The reactions carried out with mackinawite from pre-treated iron and sulfur are summarized in table 8.

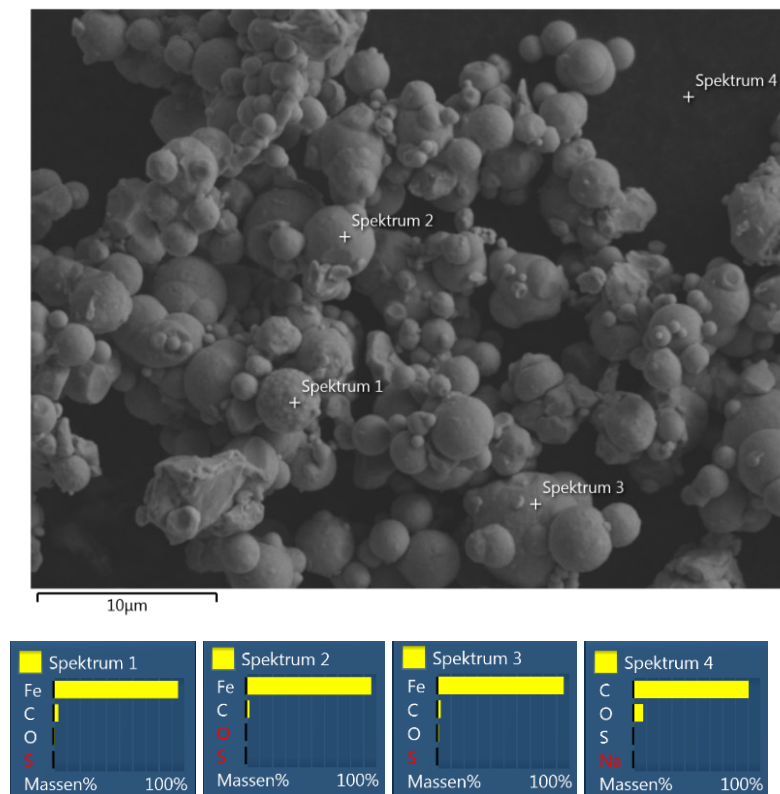


Figure 44: SEM images and EDX analysis of the untreated iron powder used for mackinawite synthesis.

Table 8: Reaction conditions and products of the reactions between mackinawite and CO<sub>2</sub>/carbonate using pretreated iron powder. Mak = mackinawite, Gre = greigite, Mag = magnetite, S = sulfur, Pyr = Pyrite.

Experiment	Conditions	Gaseous products	Solid phases
RED_11	T1, 2 weeks, <sup>12</sup> C	N.D.	Mak, Gre, Mag, Pyr
RED_12	M1, 4 days, pH < 3, <sup>12</sup> C	<sup>12</sup> CH <sub>3</sub> <sup>12</sup> CH <sub>3</sub> SH <sup>12</sup> COS H <sub>2</sub> S	Mak, Gre, Pyr
RED_13	M1, 4 days, pH < 3, <sup>13</sup> C	<sup>12</sup> CH <sub>3</sub> <sup>13</sup> COS	Mak, Gre, Pyr
RED_14	M2, 2 weeks, <sup>13</sup> C	<sup>12</sup> CH <sub>3</sub>	Mak, Gre, Mag, S

These experiments were carried out to investigate the low temperature conditions and to look for any <sup>13</sup>C reduced carbon species without the influence of carbon impurities from the iron surface. Furthermore, acidic conditions were applied following the experimental procedures by Heinen and Lauwers.<sup>128</sup> The low and medium temperature reactions RED\_11 and RED\_14 did not lead to the formation of volatile reduced carbon compounds what confirms that this is not possible in this temperature domain. Moreover, no <sup>13</sup>C thiols were detected in RED\_12 and RED\_13 what is in contrast to the observations by Heinen and Lauwers. The formation of pyrite in these reactions can be explained by the formation of H<sub>2</sub> what is known for iron sulfide in acidic environments.



The formation of <sup>13</sup>COS under acidic conditions is very interesting as this is not expected at these temperatures from H<sub>2</sub>S and CO<sub>2</sub> alone.<sup>168</sup>



It is therefore reasonable to assume a surface mediated formation of COS from CO<sub>2</sub> and H<sub>2</sub>S. COS is much more reactive than CO<sub>2</sub> and may be converted into organic compounds more easily. Moreover, it is reported to mediate the polycondensation of amino acids what is a very crucial step for the origin of life.<sup>169</sup>

In order to examine the phase transformations of mackinawite when heated in presence of carbonate with higher accuracy, an additional small series of experiments was carried out. Mackinawite was synthesized from pretreated iron and sulfur following the standard procedure. To the initial solution, 1 ml of a saturated NaHCO<sub>3</sub> solution was added and the solids kept at room temperature for 3 days. The solids were then isolated by filtration, dried in a stream of N<sub>2</sub> gas and heated to 140 °C, 180 °C and 250 °C in N<sub>2</sub> atmosphere for 2 hours, respectively (RED\_15 to RED\_17). The phases identified by PXRD are summarized in table 9.

Table 9: Reaction temperatures and solid products of the reaction of adsorbed carbonate on freshly prepared mackinawite in a nitrogen atmosphere. Mak = mackinawite, Gre = greigite, Pyh = pyrrhotite, Mag = magnetite.

Experiment	Temperature	Solid phases
RED_15	140 °C	Mak
RED_16	180 °C	Gre
RED_17	250 °C	Gre, Pyh, Mag

The temperature is a crucial condition for the reaction between adsorbed carbonates and mackinawite. Until 140 °C no reaction occurs in this setup and the mackinawite stays unchanged. At temperatures between 140 °C and 180 °C, an oxidation reaction takes place transforming the initial mackinawite completely to greigite. Magnetite is also expected but may be not visible in the PXRD patterns. After the reaction at 250 °C, magnetite diffraction peaks can be confidently identified and pyrrhotite forms. As the CO<sub>2</sub> reduction mechanism is highly depending on the available H<sup>+</sup> concentration, this temperature range may differ when changing the pH value during the adsorption process.

## 5.5 Mackinawite from $(\text{NH}_4)_2\text{Fe}(\text{SO}_4)_2$ and $\text{Na}_2\text{S}$

The reduction reactions using a  $^{13}\text{C}$  carbon source and pretreated iron in some cases still showed some  $^{12}\text{CH}_4$  from organic material on the iron surface. Therefore, a series of reactions was carried out using precipitated iron sulfide to exclude any influence of adsorbed carbonaceous material. A concentrated solution of sodium sulfide was added dropwise into an equimolar concentrated solution of ammonium iron sulfate whereby a black precipitate formed. The resulting suspension was centrifuged and the solution removed as much as possible. Reactions RED\_18 to RED\_20 were carried out in a carbonate solution that was added with a syringe and the pH was adjusted with hydrochloric acid. The precipitated iron sulfides in reactions RED\_21 to RED\_22 were dried under reduced pressure overnight and the reaction vials filled with  $\text{CO}_2$ .

Table 10: Reaction conditions and products of the reactions between precipitated mackinawite and  $\text{CO}_2$ /carbonate. Gre = greigite, Sid = siderite, S = sulfur, Lep = lepidocrocite, Mar = marcasite, The = thenardite, Moh = Mohr's salt, Pyr = pyrite.

Name	Conditions	Volatile products	Solid phases
RED_18	M1, 2 weeks, pH = 7, $^{12}\text{C}$	N.D.	Lep, Goe, The, FeCl <sub>3</sub> , Moh
RED_19	M1, 2 weeks, pH = 3, $^{12}\text{C}$	N.D.	S, Gre, Pyr
RED_20	M1, 2 weeks, pH < 3, $^{12}\text{C}$	$^{12}\text{COS}$ $^{12}\text{CH}_3\text{SH}$	S, Lep, Goe
RED_21	M2, 2 weeks, + 2 ml conc. HCl, $^{12}\text{C}$	$^{12}\text{COS}$ $^{12}\text{CH}_3\text{SH}$	S, Gre, FeCl <sub>3</sub> , The, Moh, Pyr
RED_22	H2 (110 °C), 2 weeks, no distillation, $^{12}\text{C}$	$\text{SO}_2$	Gre, FeCl <sub>3</sub> , The, Sid, Moh

At neutral and moderately acidic conditions, no volatiles have been detected by GC-MS analysis, although the occurrence of lepidocrocite, goethite, greigite and pyrite in these reactions show severe mackinawite oxidation. If  $\text{CO}_2$  is not reduced, sulfate ions or

protons may have acted as the electron acceptor. The oxides can also have been formed during the workup of the solids. At higher proton and H<sub>2</sub>S concentrations, COS and methane thiol were detected. These reduced carbon species occur coupled to the formation of sulfur, greigite and iron oxides. Under dry conditions at 110 °C only SO<sub>2</sub> was detected what may be caused by insufficient protonation of adsorbed reduced carbon compounds. In conclusion, the experiments carried out with precipitated mackinawite show that there is the possibility of thiol formation under moderate temperatures at least under acidic conditions. This confirms the results of the experiments of Heinen and Lauwers<sup>128</sup> and the mackinawite mediated CO<sub>2</sub> reduction. These experiments also show that using precipitated mackinawite without a severe pretreatment always involves unnecessary solutes and precipitated salts that can be excluded by synthesizing mackinawite from elemental iron and sulfur.

## 5.6 Conclusions

All experiments carried out to investigate the interaction of CO<sub>2</sub> and mackinawite lead to the conclusion, that mackinawite is able to activate and reduce CO<sub>2</sub> or carbonate, respectively. <sup>13</sup>C-labelled methane thiol and COS formed at 160 °C within a few hours from adsorbed CO<sub>2</sub>/carbonate. The reaction between precipitated mackinawite and CO<sub>2</sub> also led to the formation of methane thiol and COS under acidic conditions at 80 °C. C-C-bond formation has not been observed in the <sup>13</sup>C-labelled experiments, but in some <sup>12</sup>C-experiments like RED\_9. The formation of reduced carbon compounds from carbonaceous material on the iron surface is a major factor that has to be considered when using elemental iron as a starting material in carbon fixation experiments. The reduction of CO<sub>2</sub> and the formation of reduced carbon compounds is highly temperature and pH dependent. Adsorbed NaHCO<sub>3</sub> on a the mackinawite surface is not reduced at 140 °C and the mackinawite crystal structure stays unchanged. At around 160 °C to 180 °C though, greigite forms through mackinawite oxidation and reduced carbon compounds can be detected by GC-MS analysis. At 250 °C, the formed greigite transforms into pyrrhotite in a N<sub>2</sub> atmosphere. The required temperature of 160 °C is necessary to overcome the activation barrier of CO<sub>2</sub>/carbonate in the experimental setup used. As soon as the activation on the surface and the higher kinetic energy are sufficient, CO<sub>2</sub>/carbonate are reduced and the mackinawite surface is oxidized leading to the formation of greigite and magnetite. The

necessary temperature most probably depends on the degree of protonation of the mackinawite surface, as the formed intermediates in the CO<sub>2</sub> reduction depend on the available protons. The degree of protonation of the mackinawite surface and the availability of H<sub>2</sub>S is determined by the pH value of the solution. Under acidic conditions, thiol formation occurs what may be coupled to pyrite formation but which is no prerequisite as can be deduced from RED\_20. At very acidic conditions, proton reduction dominates over CO<sub>2</sub> reduction and no reduced carbon compounds could be detected. The difference between dry and wet systems and the overall role of water is not fully understood. Reactions carried out in solution did not at all lead to volatiles that could be detected by GC-MS as water may block the reactive surface sites and prevent CO<sub>2</sub>/carbonate reduction. Any thiols formed may also just dissolve in the solution and may not be found in sufficient concentrations in the head space, but without any water present, protonation could not have occurred.

## 6 Synthesis and characterization of tochilinite analogues

### 6.1 State of the art

The first syntheses of tochilinite analogues were carried out by Kakos *et al.* in 1994.<sup>170</sup> In their work they used a freshly precipitated Mg-Al-hydroxide gel and freshly precipitated iron sulfide that were combined and placed in an autoclave. At 2.5 bar of hydrogen gas pressure they heated this mixture for 2 days at 200 °C. The product contained a mixture of plates and rolled up multiwall tubes. The disordered nanocrystalline nature of the products posed difficulties both in characterization and adequate description. Nevertheless, they found, that the material consists of negatively charged mackinawite-like layers alternating in an incommensurate manner with hexagonal positively charged hydrotalcite-like layers with a layer spacing of 10.4 Å.

The composition was estimated by EDX to be  $6 (\text{Fe}_{0.79}\text{S}) * 5.76 [\text{Mg}_{0.69}\text{Al}_{0.31}(\text{OH})_2]$  for the tubes and  $6 (\text{Fe}_{0.71}\text{S}) * 4.92 [\text{Mg}_{0.70}\text{Al}_{0.30}(\text{OH})_2]$  for the plates based on the composition of previously described natural tochilinites. They did not investigate, if iron ions are incorporated in the hydroxide layers, but they assumed that this is not the case.

Later syntheses of tochilinite analogues include the works of Kozerenko *et al.* (1996, 2001)<sup>171,172</sup>, Chistyakova *et al.* (2006)<sup>173</sup>, Peng *et al.* (2007, 2009, 2014)<sup>39,73,174</sup> and two recent publications by Zhou *et al.* (2017) and Vacher *et al.* (2019)<sup>175</sup>. The syntheses of Kozerenko *et al.* and Chistyakov *et al.* were also carried out with magnesium and iron salts precipitated with sodium hydroxide and sodium sulfide, respectively. Peng *et al.* were the first to use pure elements as starting materials and Zhou *et al.* and Vacher *et al.* took up this approach. Because it is more convenient to use elemental iron instead of  $\text{Fe}^{2+}$  salts and elemental sulfur instead of  $\text{H}_2\text{S}$  or sulfide solutions, this approach was also pursued for tochilinite syntheses during this work. All publications on tochilinite syntheses point out, that proper characterization is a very tough task and suitable methods still need to be established.

### 6.2 Determination of structure and composition

The determination of the structure of a tochilinite sample is very challenging because the tochilinite structure is highly non-symmetrical, varies with its composition and diffraction



experiments suffer from defects and strain effects within the particles. Synthetic samples with a tochilinite-like structure have only been obtained in powder form from hydrothermal experiments. PXRD analysis can give some information on the structure of tochilinite analogues but needs to be complemented by other methods. Figure 45 shows a theoretical PXRD pattern calculated from Organova's isometric tochilinite with big crystallites and without any strain effects.

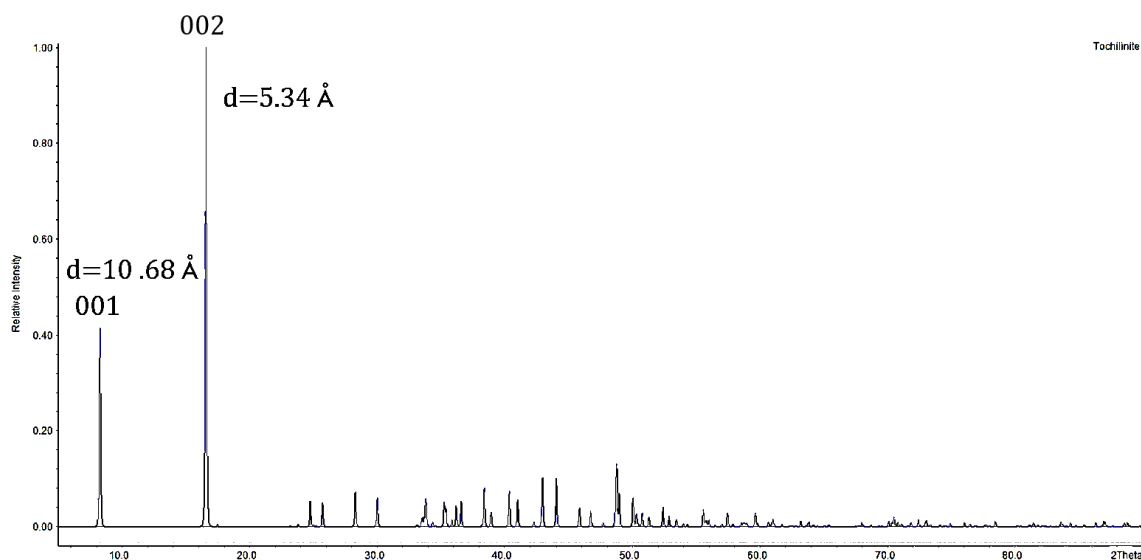


Figure 45: Calculated PXRD pattern using Organova's isometric tochilinite crystal structure without strain or size effects.

It is apparent, that the most intensive diffraction peaks are the 001 and 002 diffraction peaks caused by the reflections on the a-b-planes. The distance between two similar layers corresponds to the d-value of the 001 diffraction peak. The d-value can be calculated with the unit cell c parameter of 10.72 Å and  $\beta$ . All other diffraction peaks in the PXRD pattern are relatively weak with intensities lower than 10% of the 001 diffraction peak due to the absence of symmetry constraints. Peak broadening effects therefore lead to extensive overlapping of the smaller diffraction peaks what causes difficulties for indexing and the determination of their intensities. However, another problem arises from the variability of the tochilinite structure and its composition. It has multiply been reported that the hydrothermal synthesis leads to tochilinite crystallites with slightly different compositions and structures, what causes additional peak broadening and increases the overlap of the low intensity diffraction peaks. Defects in the stacking sequence may also be common as can be deduced from the simultaneous occurrence of nanotubes and flat sheets.

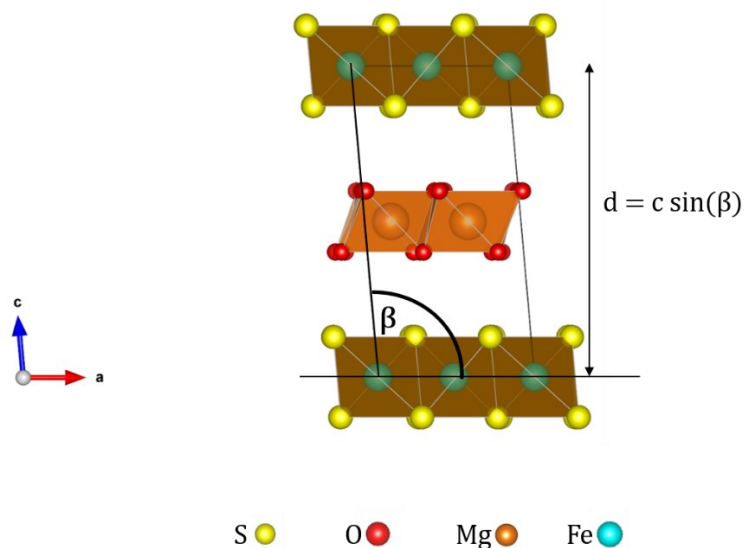


Figure 46: View of the unit cell of Organova's isometric tochilinite along the b axis.

The overlap of the 001 and 002 diffraction peaks is negligible as they are isolated in most cases. However, these two do not contain much structural information except for the layer spacings. An important feature of the 001 and the 002 diffraction peaks is, that their intensity ratio varies significantly upon changing the  $\text{Fe}^{2+}$  occupancy within the sulfide layer. In theoretical simulations (figures 47 to 51) it was found that the amount of iron vacancies in the sulfide part (parameter  $e$ ) has a great influence on the intensity ratio. If the metal sites in the hydroxide layer are assumed to be fully occupied, the difference in the PXRD patterns caused by variations in the metal ion content ( $\text{Fe}^{2+}$ ,  $\text{Fe}^{3+}$ ,  $\text{Mg}^{2+}$  and  $\text{Al}^{3+}$ ) has no significant influence on the diffraction peak intensities. In all calculated PXRD patterns, a random distribution of vacancies does not lead to the appearance of new peaks but an ordering of the vacancies leads to different structures. As an example, figure 51 shows a calculated PXRD pattern using the tochilinite crystal structure with a not random distribution of the iron vacancies.

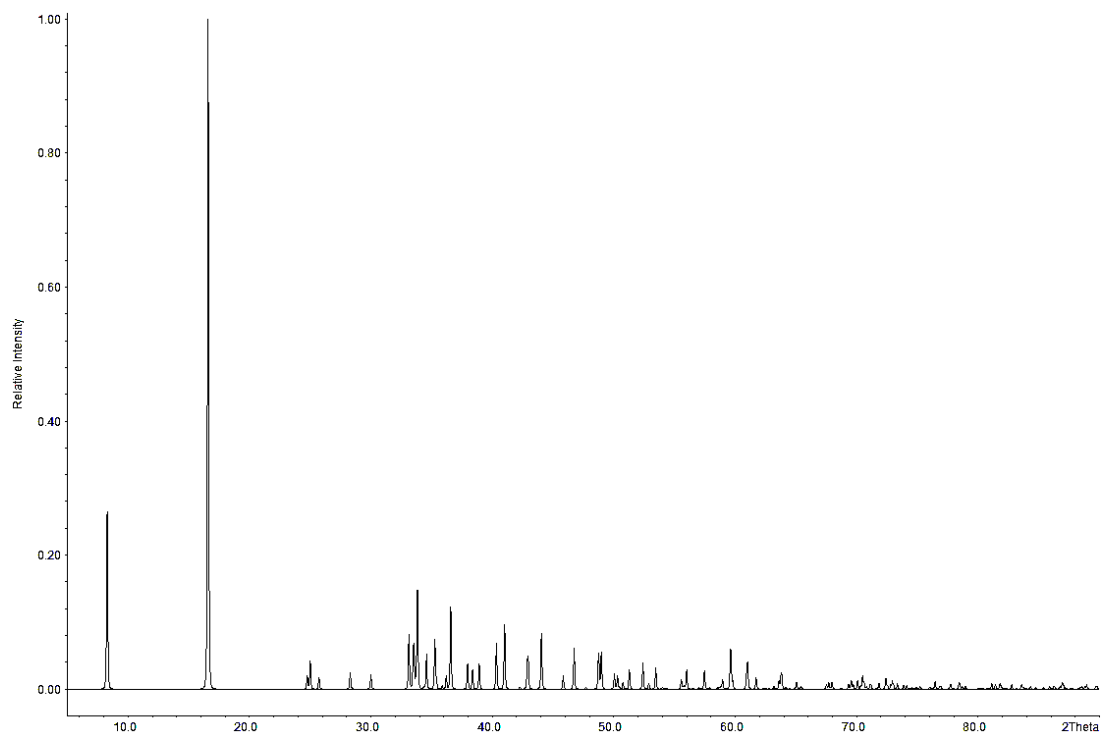


Figure 47: Calculated PXRD pattern using the structure of the isometric tochilinite variety described by Organova with a formula of  $6 \text{ FeS} * 5 \text{ Mg(OH)}_2$ .

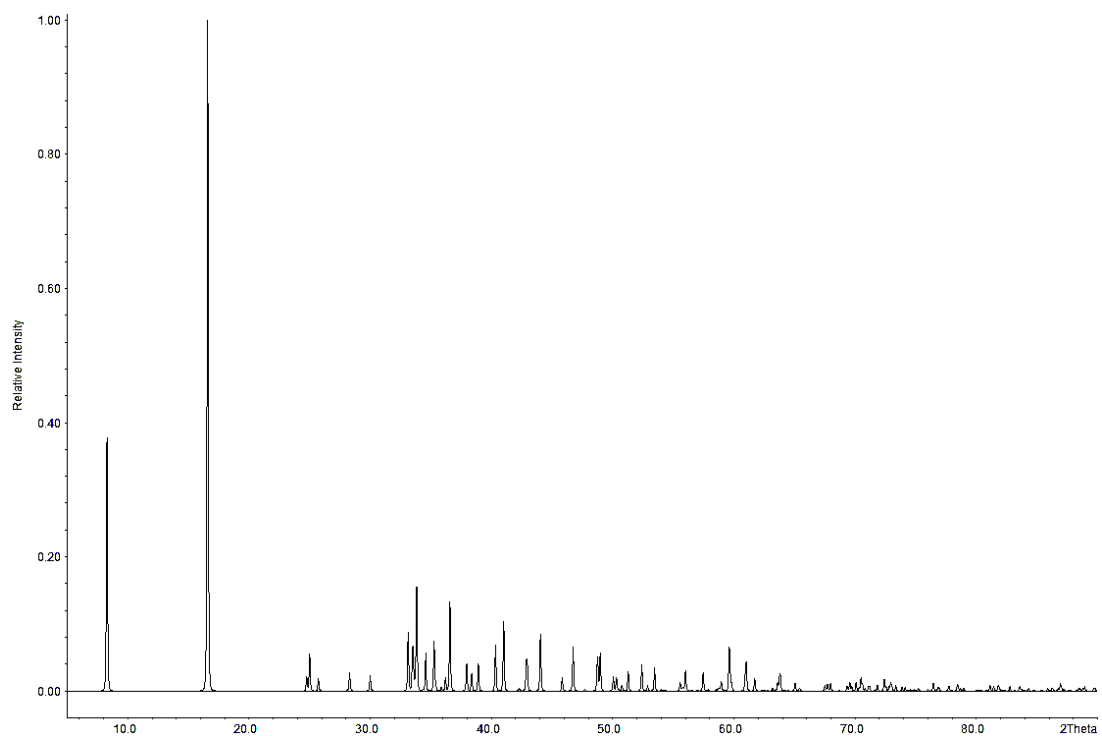


Figure 48: Calculated PXRD pattern using the structure of the isometric tochilinite variety described by Organova with a formula of  $6 \text{ Fe}_{0.9}\text{S} * 5 \text{ Mg(OH)}_2$ .

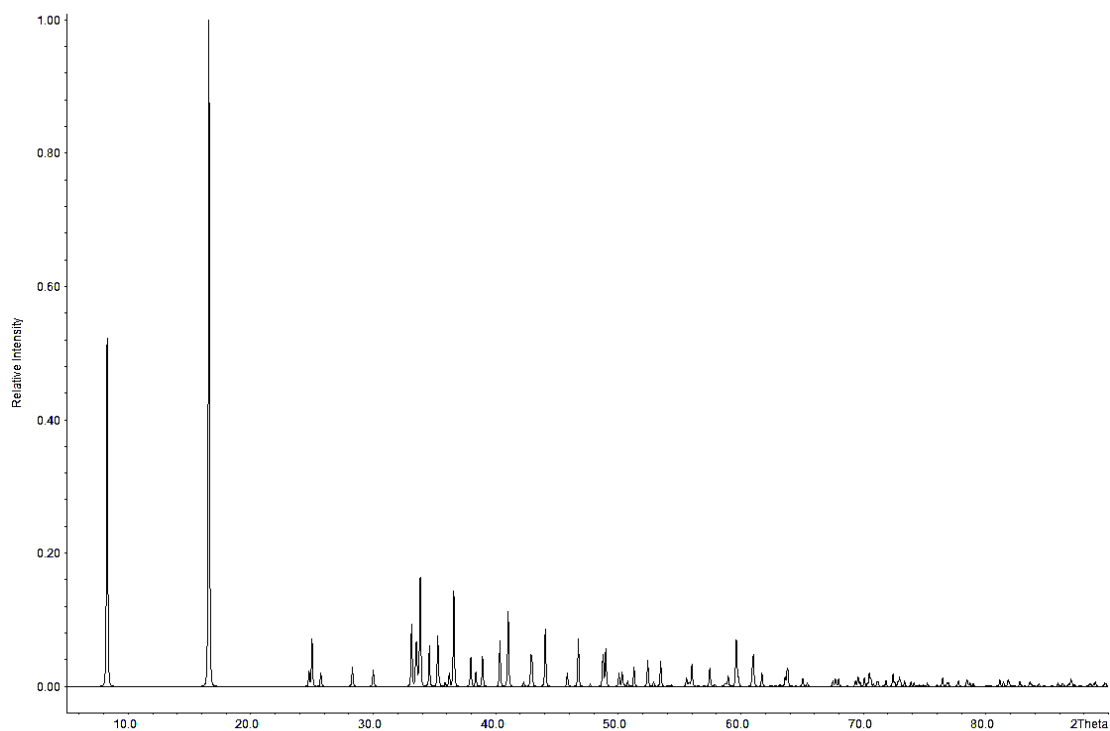


Figure 49: Calculated PXRD pattern using the crystal structure of the isometric tochilinite variety described by Organova with a formula of  $6 \text{Fe}_{0.8}\text{S} * 5 \text{Mg}(\text{OH})_2$ .

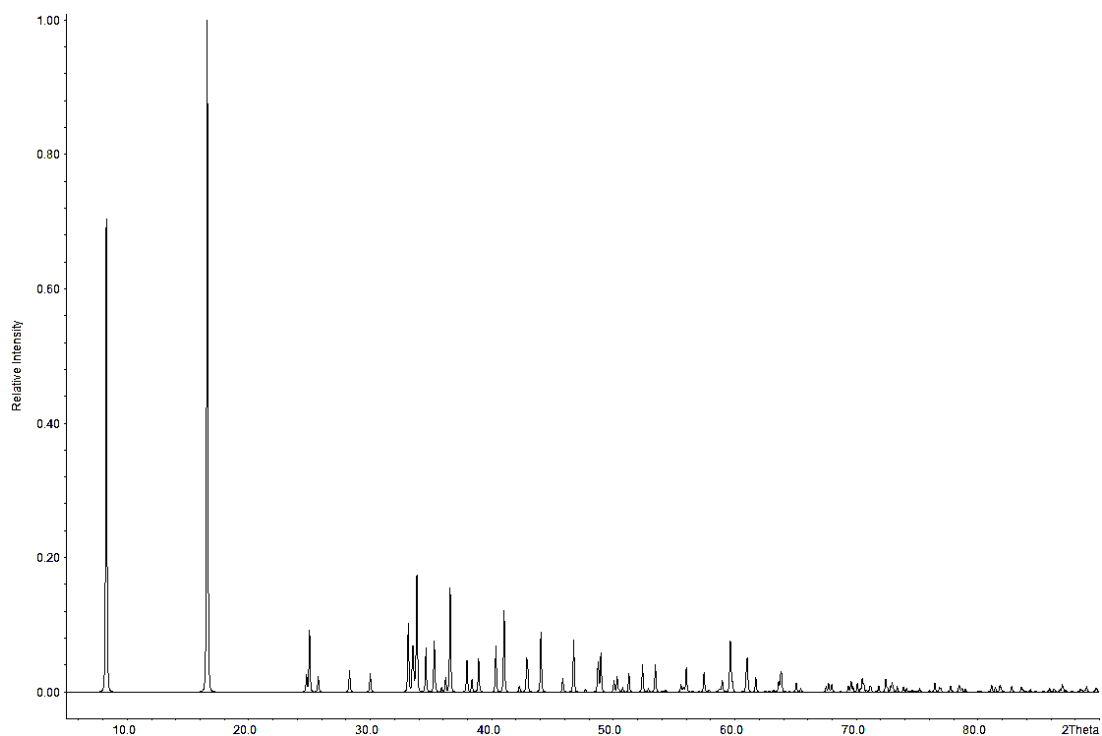


Figure 50: Calculated PXRD pattern using the crystal structure of the isometric tochilinite variety described by Organova with a formula of  $6 \text{Fe}_{0.7}\text{S} * 5 \text{Mg}(\text{OH})_2$ .

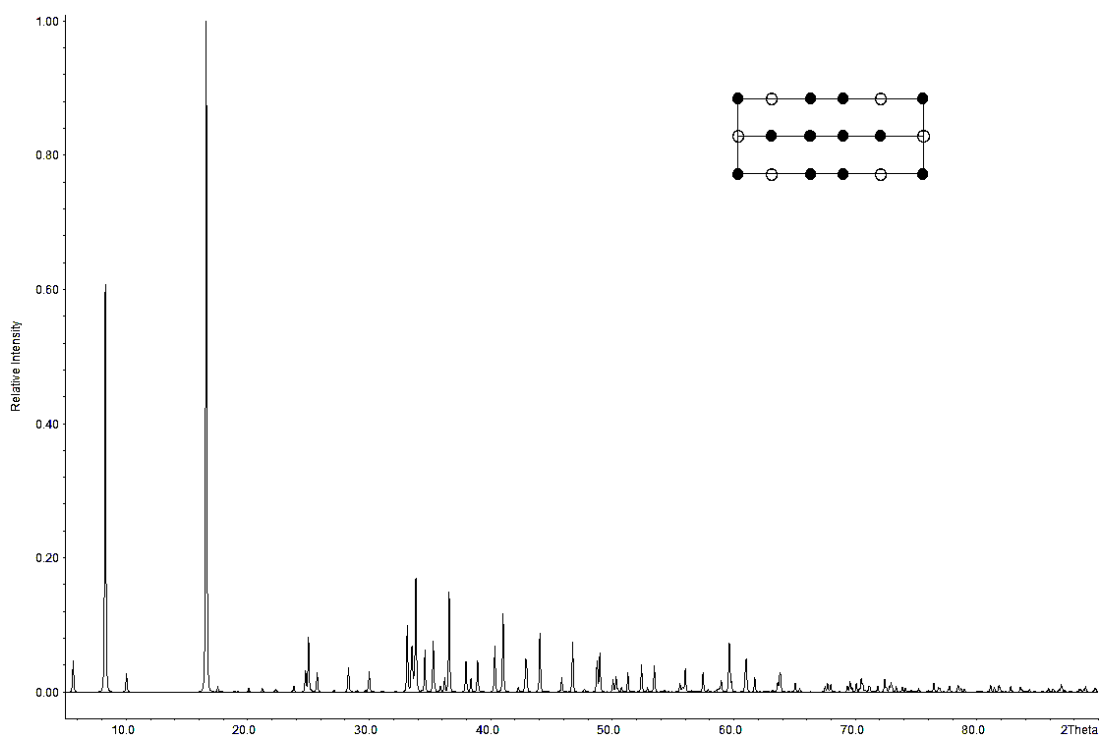


Figure 51: Calculated PXRD pattern using the crystal structure of the isometric tochilinite variety described by Organova with a formula of  $6 \text{Fe}_{0.67}\text{S} * 5 \text{Mg}(\text{OH})_2$  and a vacancy distribution as shown in the insert with full circles representing occupied and empty circles representing unoccupied iron positions.

As can be seen from table 11, the volume ratios of the sulfide and the hydroxide part can vary over a certain range due the expansion or contraction of the sub structures.

Table 11: Compositions of natural tochilinite analogues.

Formula	Reference
$6 (\text{Fe}_{0.8}\text{S}) * 5 [\text{Mg}_{0.71}\text{Fe}_{0.29}(\text{OH})_2]$	Organova <i>et al.</i> (1974) <sup>76</sup>
$6 (\text{Fe}_{0.9}\text{S}) * 4.47 [\text{Mg}_{0.53}\text{Fe}_{0.47}(\text{OH})_2]$	Harris and Vaughan (1972) <sup>80</sup>
$6 (\text{Fe}_{0.9}\text{S}) * 4.92 [\text{Mg}_{0.23}\text{Fe}_{0.71}(\text{OH})_2]$	Harris and Vaughan (1972) <sup>80</sup>
$6 (\text{Fe}_{0.78}\text{S}) * 4.71 [\text{Mg}_3\text{Fe}(\text{OH})_2]$	Organova <i>et al.</i> (1974) <sup>77</sup>
$6 (\text{Fe}_{0.81}\text{S}) * 5.37 [\text{Mg}_{0.79}\text{Al}_{0.21}(\text{OH})_2]$	Jambor (1976) <sup>81</sup>
$6 (\text{Fe}_{0.63}\text{Cu}_{0.24}\text{S}) * 4.95 [\text{Mg}_{0.78}\text{Al}_{0.29}\text{Ca}_{0.01}(\text{OH})_2]$	Muramatsu and Nambu (1980) <sup>82</sup>
$6 (\text{FeS}) * 5 [\text{Fe}(\text{OH})_2]$	Pekov <i>et al.</i> (2012) <sup>83</sup>

A theoretical formula containing the most prominent elements in natural samples is:

$$x (Mg_a^{II}; Fe_b^{II}; Fe_c^{III}; Al_d^{III} * OH_{(a+b+c+d)*2}) * 6 (Fe_{1-e}^{II} * S)$$

The value of x results from the volume ratio of the brucite to the mackinawite sub structure and mainly depends on the occupancy of metal sites in both sub structures when strictly alternating layers are assumed. As Guo *et al.* showed for mackinawite single crystals, the a-parameter decreases with decreasing iron occupancy in the mackinawite structure.<sup>176</sup> The volume of the brucite sub structure depends on the relative content of the different cations as the metal to metal distance varies slightly for Mg, Al, and Fe. Therefore, many different values for x are reported for natural samples. The volume ratio x would also change significantly if the layers would not alternate in an A-B-A-B but in an A<sub>n</sub>-B-A<sub>n</sub>-B pattern with n>1. The variables a, b, c, d and e are constrained by charge balancing. Every iron vacancy in the sulfide sub structure gives a charge of -2 if assumed that there are no Fe<sup>3+</sup> present. This charge needs to be compensated for by two trivalent metal ions in the hydroxide sub structure.

$$10x (c + d) = 6e \quad (71)$$

If e, c and d can be determined, the value of x can be calculated as follows:

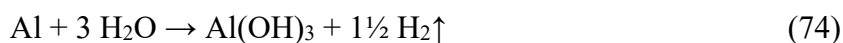
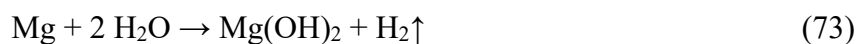
$$x = \frac{6e}{10 (c+d)} \quad (72)$$

The content of sulfur, aluminum, magnesium and total iron can be obtained by elemental analysis. The distinction between the iron species is more complicated, but the discrimination between Fe<sup>2+</sup> in the sulfide part and Fe<sup>2+</sup>/Fe<sup>3+</sup> in the hydroxide part is possible as their coordination environment is different. Fe<sup>2+</sup> and Fe<sup>3+</sup> in the hydroxide layers have different spin states and can thus also be determined separately. A suitable method to obtain this data is Mößbauer spectroscopy as it can discriminate quantitatively between Fe<sup>2+</sup> in the sulfide part and Fe<sup>2+</sup>/Fe<sup>3+</sup> in the hydroxide part. Mößbauer spectroscopy is not a direct method and cannot give absolute values on the ratio of Fe<sup>2+</sup> to Fe<sup>3+</sup> as the fits used for the obtained spectra need reasonable parameters. It is necessary to have a good estimate on how many iron species a sample contains and in which environment they are expected. Therefore, the tochilinite syntheses have to be carried out in a way, that the occurrence of Fe<sup>2+</sup> and Fe<sup>3+</sup> can realistically be estimated.

## 6.3 Reaction conditions and preliminary experiments

### 6.3.1 Synthesis with precipitated iron sulfide

The initial reactions to synthesize tochilinite analogues were carried out in a nitrogen atmosphere using freshly precipitated aluminum and magnesium hydroxide and iron sulfide following the procedure of Kakos *et al.* Because Kakos *et al.* and Kozerenko *et al.* reported reaction temperatures in the range of 80 °C to 320 °C, a temperature of 160 °C was chosen for these reactions. High pressure steel autoclaves with a 50 ml Teflon inlet were selected for the reactions which have a stability limit of 180 °C. Iron sulfide was precipitated by adding an ammonium disulfide solution to an ammonium iron sulfate solution in a glove box. Magnesium and aluminum hydroxide were prepared together in a beaker by adding sodium hydroxide solution to a solution of magnesium and aluminum nitrate. The hydroxides and the iron sulfide were mixed in the autoclave which was then filled to 25 ml with distilled oxygen free water. As the autoclaves did not have a gas inlet, no hydrogen atmosphere could be maintained. The autoclaves were sealed and heated in an oven for three days at 160 °C. The only products that could be isolated were magnetite and magnesioferrite, respectively (Toch\_1). The absence of oxygen was not sufficient to prevent the oxidation of  $\text{Fe}^{2+}$  to  $\text{Fe}^{3+}$  by water at 160 °C. Therefore, the temperature was lowered and reactions at 95 °C were carried out in a Schlenk flask in a nitrogen atmosphere. In two Schlenk flasks, the iron sulfide and the hydroxides were prepared by precipitation from ammonium iron sulfate and magnesium and aluminum nitrate as before. The sulfide suspension was then transferred into the hydroxide containing flask with a syringe and the obtained suspension stirred for one week at 95 °C. This procedure possibly has led to the formation of a tochilinite analogue as there is a strong diffraction peak that fits to the tochilinite 002 diffraction peak although the 001 diffraction peak is missing (Toch\_2). Additionally, reflections caused by silicate phases appear that are introduced into the system from the flask itself. Working at low temperatures in Schlenk flasks was not very promising and therefore no further investigations were carried out in this system. To be able to work at high temperatures and establish a reducing hydrogen atmosphere in situ, elemental magnesium and elemental aluminum were used instead.



The iron sulfide was precipitated like in the previous experiments and transferred together with magnesium and aluminum in the autoclaves which were then sealed and heated to 160 °C for three days. This approach clearly led to the synthesis of a tochilinite analogue that was identified by PXRD analysis as it exhibits the strong 001 and 002 diffraction peaks with d-values comparable to the ones reported in the literature. The diffraction peaks are sharp with a good signal to noise ratio (Toch\_3).

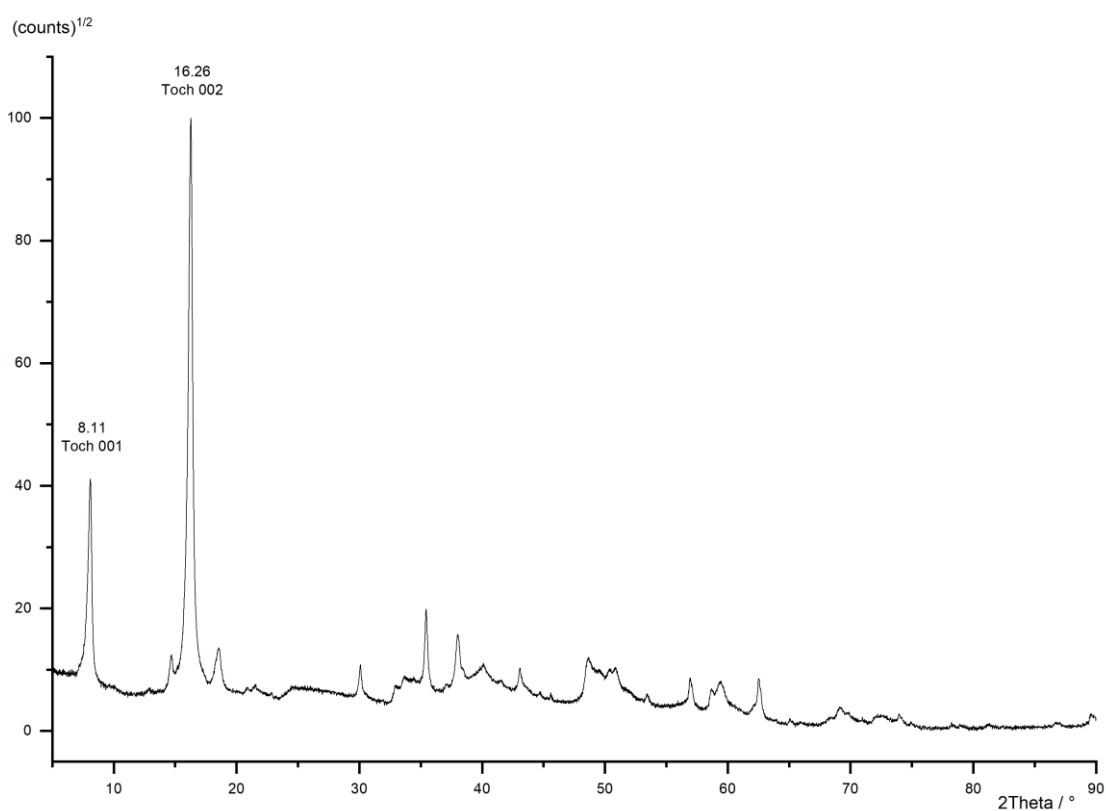


Figure 52: PXRD pattern of Toch\_3.

The only side products that could be identified are magnetite and brucite. Further reactions using this system led to comparable products, but the results were not very reproducible (Toch\_3, Toch\_4, Toch\_5, Toch\_6).



### 6.3.2 Synthesis with solid starting materials

To circumvent the difficulties of working with iron salts and  $(\text{NH}_4)\text{HS}$ -solutions and to increase the reproducibility, all further tochilinite syntheses should be carried out using only solid starting materials. Iron sulfide that shows similar characteristics to precipitated mackinawite could be synthesized from the elements as explained above. The mackinawite synthesis was carried out in 25 ml microwave vials from a mixture of elemental iron and sulfur at room temperature following the standard procedure. The reaction of a mixture of elemental iron, sulfur, aluminum, magnesium and water in the Teflon lined steel autoclaves at 160 °C led to the synthesis of a tochilinite analogue (Toch\_7). The same applies to the reaction of a mixture of magnesium and aluminum with pre-synthesized nano-mackinawite from elemental iron and sulfur (Toch\_8). The obtained PXRD patterns of the tochilinite analogues had a good signal to noise ratio and sharp diffraction peaks what made the investigated systems suitable for further tochilinite syntheses. The next step was to get more information on structure and composition of the synthesized tochilinite analogues but it was not possible to do a reliable indexation of the PXRD patterns as the diffraction peaks strongly overlap and only the positions of the 001 and 002 diffraction peaks could be determined. As stated earlier, elemental analysis combined with Mößbauer spectroscopy can give deeper insights into the structure. The samples contained a variety of side products that needed to be removed first to ensure a reliable elemental analysis and Mößbauer spectroscopy. Therefore, a lot of experimental effort was directed towards the correlations between the reaction conditions, the composition of the starting mixture and possible side products.

## 6.4 Controlled synthesis of tochilinite analogues

### 6.4.1 Overview

As shown before, there are many natural layered hybrid sulfides that have not attracted much attention what may be attributed to the difficulties in their controlled synthesis. This is why a systematic development of reaction conditions that are able to control the compositions of the different layers is highly desirable. As tochilinite analogues can contain different metal ions in the sulfide layers like  $\text{Fe}^{2+}$ ,  $\text{Ni}^{2+}$  and  $\text{Cu}^{2+}$  and even more in the hydroxide layers it was necessary to restrict the syntheses of tochilinite analogues to a

reasonable selection. Transition metal ions like  $\text{Cu}^{2+}$ ,  $\text{Ni}^{2+}$  and  $\text{Zn}^{2+}$  can replace iron ions in the hydroxide layers as well as in the sulfide part. This may cause difficulties for the syntheses because controlling the occupation of the desired metal positions is not easily achieved. Additionally, most transition metals form stable sulfides like CuS, NiS and ZnS what leads to massive side product formation as they are less soluble than FeS which has been observed in a reaction containing  $\text{Zn}^{2+}$  (Toch\_9).

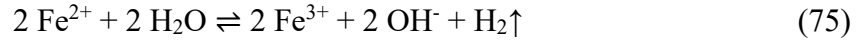
Most abundant natural tochilinite contains mainly  $\text{Fe}^{2+}$  in the sulfide layers and  $\text{Mg}^{2+}$ ,  $\text{Al}^{3+}$ ,  $\text{Fe}^{2+}$  and  $\text{Fe}^{3+}$  in the hydroxide layers. Therefore, this selection of ions was regarded to be of most importance and the corresponding metals were used for the controlled synthesis of tochilinite analogues. This leads to four possible tochilinite-like endmembers as shown in table 12 that should be synthesized during this work.

Table 12: Theoretical compositions of the tochilinite analogues that are the aim of the syntheses of tochilinite analogues in this work.

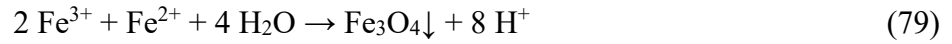
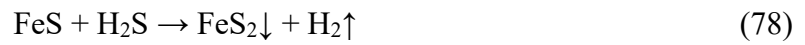
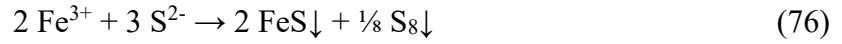
Name	Composition
Mg-Al-tochilinite	$x [ \text{Mg}_a^{\text{II}} ; \text{Al}_b^{\text{III}} * (\text{OH})_{(a+b)*2} ] * (\text{Fe}_{1-e}^{\text{II}} * \text{S})$
Mg-Fe-tochilinite	$x [ \text{Mg}_a^{\text{II}} ; \text{Fe}_b^{\text{III}} * (\text{OH})_{(a+b)*2} ] * (\text{Fe}_{1-e}^{\text{II}} * \text{S})$
Fe-Fe-tochilinite	$x [ \text{Fe}_a^{\text{II}} ; \text{Fe}_b^{\text{III}} * (\text{OH})_{(a+b)*2} ] * (\text{Fe}_{1-e}^{\text{II}} * \text{S})$
Fe-Al-tochilinite	$x [ \text{Fe}_a^{\text{II}} ; \text{Al}_b^{\text{III}} * (\text{OH})_{(a+b)*2} ] * (\text{Fe}_{1-e}^{\text{II}} * \text{S})$

In summary, the aim of the synthetic work was to develop the syntheses of these four tochilinite analogues in very pure form to carry out proper characterization. If the syntheses of these four endmembers could be established, all compositions in between these endmembers should also be realizable. As the exact structures and compositions of the desired materials are unknown, the first task was to find reasonable starting mixtures and reaction conditions. To investigate possible reaction conditions, the reactivity of several starting materials and their ratios, reaction temperatures and some additives were investigated. The reaction products were determined by PXRD analysis. As all patterns were obtained with the same measurement parameters, absolute diffraction peak areas of the least overlapping diffraction peaks were obtained by fitting with the same background function for comparison.

A universal reaction in the investigated systems is the oxidation of  $\text{Fe}^{2+}$  that takes place at high temperatures independent of the composition of the starting mixture.



The oxidation of  $\text{Fe}^{2+}$  to  $\text{Fe}^{3+}$  can lead to the formation of sulfur, pyrrhotite, pyrite and magnetite that are very stable and not easily removed.



A feasible way to prevent the oxidation is to shift the equilibrium of reaction 75 to the left side with an appropriate hydrogen gas pressure in the autoclave. Following this, the total mass of the starting mixture and the corresponding amount of hydrogen gas released is very important for the products formed.

#### 6.4.2 Mg-Al-tochilinite

The synthesis of Mg-Al-tochilinite was carried out with different starting materials and different ratios of the reactants, reaction temperatures and reaction times to explore the reactivity and the formation of side products. An important aim of the Mg-Al-tochilinite synthesis is the minimization of  $\text{Fe}^{2+}$  and  $\text{Fe}^{3+}$  incorporation into the hydroxide layers. The exclusion of  $\text{Fe}^{2+}/\text{Fe}^{3+}$  in the hydroxide layers is a tough task though, as they are omnipresent in the reaction systems. Proper reaction conditions may minimize their incorporation by controlling the concentrations of free iron ions. The variety of starting mixtures in this system is summarized in table 13.

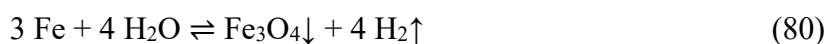
Table 13: Sources of the necessary elements in different starting mixtures for the Mg-Al-tochilinite syntheses.

Mixture	$\text{Fe}^{2+}$ source	$\text{S}^{2-}$ source	$\text{Mg}^{2+}$ source	$\text{Al}^{3+}$ source
<i>Mg-Al-A</i>	Fe	S	Mg	Al

<i>Mg-Al-B</i>	FeS	FeS	Mg	Al
<i>Mg-Al-C</i>	FeS	FeS	MgO	Al
<i>Mg-Al-D</i>	FeS	FeS	Mg	Al(OH) <sub>3</sub>

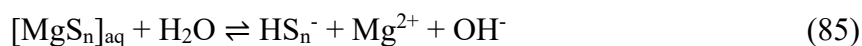
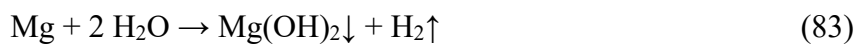
In the PXRD patterns from all obtained product mixtures, tochilinite-like diffraction peaks have been observed (Toch\_MgAl\_1, Toch\_MgAl\_2, Toch\_MgAl\_3, Toch\_MgAl\_4). In general, no difference was observed between the use of freshly prepared and dry stabilized iron sulfide (Toch\_3, Toch\_MgAl\_2). The side products identified in this system of H<sub>2</sub>O, Fe, S, Mg and Al at 130 °C and 160 °C are listed below with the corresponding reactions of formation.

I) Elemental iron; Fe



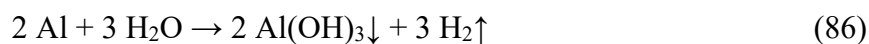
Residual elemental iron can be observed in the product mixture if the oxidation is incomplete as it is relatively stable in a hydrogen gas atmosphere. The oxidation of elemental iron is much faster, if it is oxidized by H<sub>2</sub>S/S<sub>8</sub> instead of H<sub>2</sub>O as can be deduced from the products of Toch\_MgAl\_5 and Toch\_MgAl\_6.

II) Magnesium hydroxide; Mg(OH)<sub>2</sub> with brucite structure



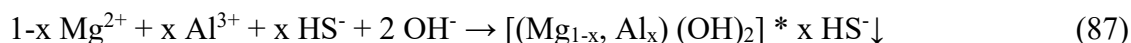
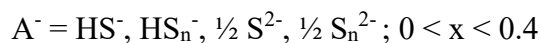
Magnesium is a very reactive compound that is oxidized by H<sub>2</sub>O already at moderate temperatures. If it is mixed with elemental sulfur, it even reacts at room temperature forming polysulfide complexes while increasing the pH value of the solution.

III) Aluminum hydroxide; Al(OH)<sub>3</sub> with bayerite structure



Aluminum is less reactive than magnesium and does not react with sulfur at room temperature in neutral solution. It is very sensitive to pH changes and thus can be oxidized at room temperature in acidic as well as basic solution.

IV) Layered double hydroxides  $[(\text{Mg}_{1-x}, \text{Al}_x) (\text{OH})_2]^{x+} * x \text{ A}^-$



Layered double hydroxides (LDHs) contain brucite-like layers in which some of the  $\text{Mg}^{2+}$  are replaced by trivalent cations like  $\text{Al}^{3+}$ . To balance the resulting positive charge, anions are intercalated between the sheets. In some tochilinite syntheses, diffraction peaks corresponding to layered double hydroxides have been observed. The PXRD patterns show one strong diffraction peak at  $d = 7.9 \text{ \AA}$  and a second one at  $d = 3.95 \text{ \AA}$ . A representative example is shown in figure 126 (Toch\_MgAl\_7). For comparison, a layered double hydroxide composed of magnesium hydroxide, aluminum hydroxide and sulfide interlayer anions was synthesized and the corresponding PXRD pattern fits well to the side product in the tochilinite syntheses (Toch\_MgAl\_8). Phases with diffraction peak positions in the same 2theta region have also been observed when using elemental magnesium and aluminum without any sulfur present (Toch\_MgAl\_9, Toch\_MgAl\_10). These phases could not be identified but could be suppressed by avoiding an excess of magnesium and aluminum.

V) Elemental sulfur; S

Elemental sulfur is rarely found as a side product and has only been observed at a reaction time of one day at  $130^\circ\text{C}$  as excess sulfur quantitatively forms pyrite with time.

VI) Iron sulfide; FeS with pyrrhotite structure

Pyrrhotite occurred in every tochilinite synthesis in the Mg-Al system. Mackinawite is the first iron sulfide phase that precipitates from aqueous solution and rapidly transforms to pyrrhotite at high temperatures under reducing conditions. Therefore, the occurrence of pyrrhotite is a kinetic problem and may only be minimized but never precluded completely.



Tochilinite cannot form from pyrrhotite what indicates that the solubility of pyrrhotite is lower than the solubility of tochilinite. To minimize the amount of pyrrhotite formed, the formation of tochilinite from mackinawite needs to be faster than its transformation to pyrrhotite. The formation of tochilinite depends on the simultaneous availability of all constituents ( $\text{Mg}^{2+}$ ,  $\text{Al}^{3+}$ ,  $\text{OH}^-$ ,  $\text{Fe}^{2+}$ ,  $\text{S}^{2-}$ ) and is therefore controlled by several parameters that will be discussed in more detail below.

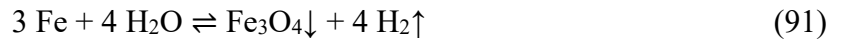
#### VII) Iron sulfide; $\text{FeS}_2$ with pyrite structure

Pyrite consists of  $\text{Fe}^{2+}$  and disulfide ions and forms from the reaction of iron or iron sulfide with elemental sulfur or  $\text{H}_2\text{S}$ .



#### VIII) Iron oxide; $\text{Fe}_3\text{O}_4$ with magnetite structure

Magnetite forms from elemental iron upon oxidation with water and has been formed in every tochilinite synthesis.



These eight side products need to be suppressed during the reaction or removed from the product mixture afterwards. Additionally, the incorporation of  $\text{Fe}^{2+}$  and  $\text{Fe}^{3+}$  into the hydroxide layer has to be prevented to ensure the desired composition of  $x [(\text{Mg}_a^{II}; \text{Al}_b^{III}) * (\text{OH})_{(a+b)*2}] * 6 (\text{Fe}_{1-e}^{II} * \text{S})$ . The exclusion of  $\text{Fe}^{2+}$  and  $\text{Fe}^{3+}$  seems not to be possible using pre-prepared mackinawite as was deduced from a Mößbauer investigation of Toch\_MgAl\_11 which is shown below.

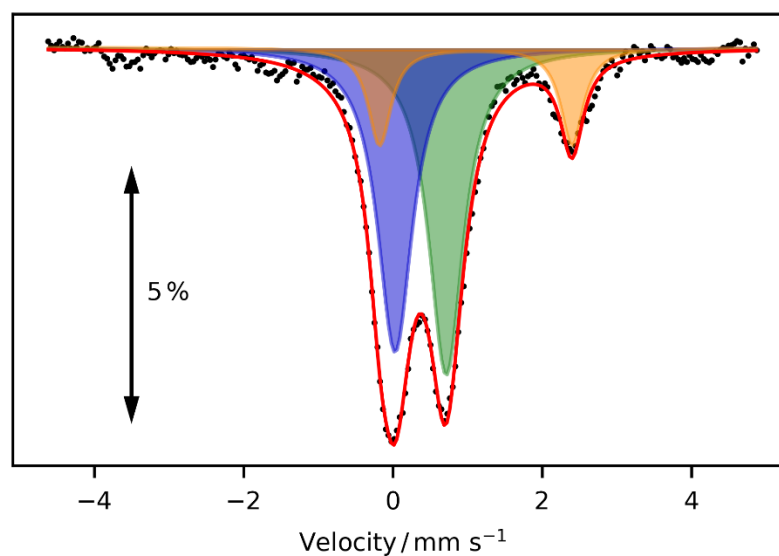


Figure 53: Mössbauer spectrum of Toch\_MgAl\_11. Orange: Fe<sup>2+</sup> in the hydroxide layers, dark blue: Fe<sup>3+</sup> in the hydroxide layers, green: Fe<sup>2+</sup> in the sulfide layers.

The parameters of the fit are summarized in table 14 and show high amounts of Fe<sup>2+</sup> and Fe<sup>3+</sup> in the hydroxide layers.

Table 14: Fitting parameters of the Mössbauer spectrum of Toch\_MgAl\_11. The parameters fitted are the center shift  $\delta$ , the quadrupole splitting  $\Delta E_Q$ , the width at half maximum  $\Gamma$  and the area of the peaks  $A$ .

Site	$\delta$ [mm/s]	$\Delta E_Q$ [mm/s]	$\Gamma$ [mm/s]	$A$ [%]
Fe <sup>2+</sup> Sulfide	0.71(1)	-	0.56(1)	43
Fe <sup>2+</sup> Hydroxide	1.11(1)	2.58(1)	0.37(2)	17
Fe <sup>3+</sup> Hydroxide	0.03(1)	-	0.57(1)	40

The Mössbauer analysis clearly shows that the tochilinite syntheses need to be controlled to achieve the desired distribution of iron ions in the hydroxide layers. Using pre-prepared mackinawite does not seem to be suited in a system with Mg and Al. A reasonable approach to exclude Fe<sup>2+</sup> and Fe<sup>3+</sup> from the hydroxide layers is the use of elemental iron in a hydrogen rich atmosphere that mainly oxidizes in the reaction with sulfur or hydrogen

sulfide to form mackinawite what minimizes the concentration of  $\text{Fe}^{2+}$  and  $\text{Fe}^{3+}$  in the solution.

The starting mixture Mg-Al-A is considered to be the most promising in excluding  $\text{Fe}^{2+}/\text{Fe}^{3+}$  from the hydroxide layers and was thus investigated in more detail. At first, the influence of the total mass, the reaction time and the reaction temperature were investigated. Four reactions with decreasing amounts of a fine ground mixture of Fe, S, Mg and Al were carried out at 160 °C for 6 days. The ratios of the elements correspond to the theoretical ratios of Organova's isometric tochilinite. The absolute values for the diffraction peak areas are shown in table 15.

Table 15: Absolute diffraction peak areas from different products in Mg-Al-tochilinite syntheses with identical PXRD settings. Bru = brucite, Fe = iron, Pyr = pyrite, Toch = tochilinite, LDH = layered double hydroxide, Mag = magnetite, Pyh = pyrrhotite.

Exp.	Total mass / g	Bru (001)	Fe (110)	Pyr (200)	Toch (002)	LDH (001)	Mag (311)	Pyh (228)
Toch_MgAl_7	0.50	30	201	0	100	7	26	0
Toch_MgAl_11	0.42	21	32	0	99	13	6	160
Toch_MgAl_12	0.34	8	51	1	94	0	14	28
Toch_MgAl_13	0.26	6	44	2	97	0	12	27

From these experiments it can be concluded that:

- Besides tochilinite, residual iron, layered double hydroxides, brucite, pyrite, magnetite and pyrrhotite are products of these reactions.
- With less starting mixture, less Mg and Al is oxidized what lowers the partial pressure of  $\text{H}_2$  during the reaction and the amount of brucite in the products.
- With less  $\text{H}_2$  in the system, more Fe is oxidized and the amount of residual Fe in the product mixture gets less but not linearly as it also depends on the sulfur species in the system.
- The amount of magnetite is related to the amount of residual iron and probably only forms on the iron surface and does not precipitate from solution.



- The lower the amount of starting material the more pyrite and pyrrhotite formed what may be attributed to increased iron oxidation.
- Pyrrhotite and the LDH are present in the same reaction although mackinawite as the pyrrhotite precursor can react with the LDH to form tochilinite. This observation can be explained by kinetic considerations. If the formation of tochilinite from LDH and mackinawite is not faster than the transformation of mackinawite to pyrrhotite, both side products appear simultaneously.
- In summary it is obvious, that small changes in the starting mixture can have a huge influence on the products formed and that it is very hard to predict the exact outcome of any changes of the starting mixture.

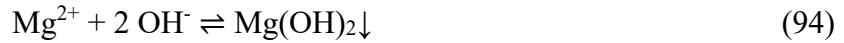
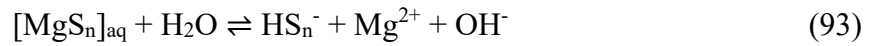
To investigate the influence of the reaction time, a series of reactions with the same amount of the same starting mixture at 130 °C with different reaction times was carried out (Toch\_MgAl\_14 to Toch\_MgAl\_17). This series also gives some additional mechanistic insights into this reaction system.

Table 16: Absolute diffraction peak areas from different products in Mg-Al-tochilinite syntheses with identical PXRD settings. Bru = brucite, Fe = iron, Pyr = pyrite, Toch = tochilinite, LDH = layered double hydroxide, Mag = magnetite, Pyh = pyrrhotite.

<b>Exp.</b>	<b>Time/ days</b>	<b>Bru (001)</b>	<b>Fe (110)</b>	<b>Pyr (200)</b>	<b>Toch (002)</b>	<b>LDH (001)</b>	<b>Mag (311)</b>	<b>Pyh (228)</b>
Toch_MgAl_16	1	3	19	3	0	0	0	0
Toch_MgAl_17	2	2	14	3	1	1	0	0
Toch_MgAl_18	3	1	6	2	1	0	0	0
Toch_MgAl_19	4	2	3	3	3	0	0	0

From the information of all reactions in this system it can be concluded that:

- The first reaction that occurs is the oxidation of magnesium coupled with the formation of a soluble magnesium polysulfide complex. The pH value of the solution increases significantly.



- With the rising pH value and temperature, aluminum oxidizes after magnesium what probably leads to the formations of amorphous layered double hydroxides consisting of (poly)sulfides,  $\text{Mg}(\text{OH})_2$  and  $\text{Al}(\text{OH})_3$ .
- After one day at 130 °C, no aluminum, magnesium or sulfur are present in the products whereas brucite and pyrite formed.
- Iron reacts with sulfur or polysulfides to form pyrite within the first day. The amount of pyrite that was present after one day did not change significantly with further reaction progress.
- With time Fe is oxidized either by sulfur or  $\text{H}_2\text{O}$  and iron sulfide is formed which reacts with dissolved magnesium, aluminum and  $\text{OH}^-$  to form tochilinite.
- The amounts of LDH and iron in the product mixture decrease upon further reaction. By dissolution of the LDH,  $\text{Al}^{3+}$  and  $\text{Mg}^{2+}$  are released again into the solution and additional brucite forms. The oxidation of Fe adds  $\text{Fe}^{2+}$  to the solution and together with sulfide ions more tochilinite is formed.
- The system of Mg, Al, Fe and S is very complex as some species linearly decrease or increase but others may form and get consumed again what may be attributed to changing concentrations of polysulfide species and in pH value.
- Therefore, it is crucial to keep the reaction time and temperature constant when varying the ratios of the starting materials to obtain reproducible results.
- The concentrations of all soluble species may rise and fall again during the reaction what definitely applies to brucite and LDH. Pyrite, pyrrhotite and tochilinite do not seem to dissolve again after they have once formed.

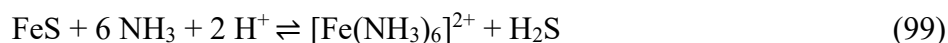
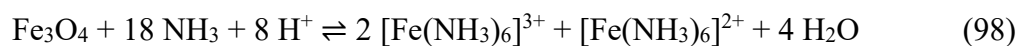
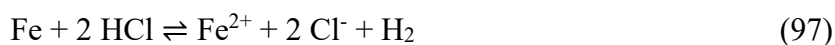
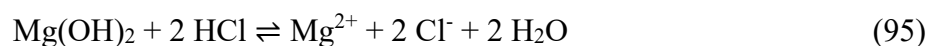
A reaction with the same starting mixture as for Toch\_MgAl\_16 was carried out at 160 °C for three days and showed much fewer side products relative to the tochilinite formed. Only brucite, iron, magnetite and a small amount of pyrrhotite could be identified besides

tochilinite (Toch\_MgAl\_20). As an interplay of the kinetics of the different reactions involved determines the side products formed, the increased reaction temperature has a huge impact. No pyrite nor LDHs were found in the product mixture as they did not form or were dissolved again during the reaction. Consequently, all following reactions were carried out at 160 °C for three days with the same total mass of the starting mixture. The ratios of Fe, S, Mg and Al seem to be close to an ideal one, but there is still potential to minimize brucite and pyrrhotite. The decrease of the relative amount of sulfur in the starting mixture led to a decrease in tochilinite formed and a rise in pyrrhotite (Toch\_MgAl\_20, Toch\_MgAl\_21).

Table 17: Absolute diffraction peak areas from different products in Mg-Al-tochilinite syntheses with decreasing relative amounts of sulfur using identical PXRD settings. Bru = brucite, Fe = iron, Pyr = pyrite, Toch = tochilinite, LDH = layered double hydroxide, Mag = magnetite, Pyh = pyrrhotite.

<b>Exp.</b>	<b>Sulfur / g</b>	<b>Bru (001)</b>	<b>Fe (110)</b>	<b>Pyr (200)</b>	<b>Toch (002)</b>	<b>LDH (001)</b>	<b>Mag (311)</b>	<b>Pyh (228)</b>
Toch_MgAl_20	0.30	15	22	0	101	0	22	5
Toch_MgAl_21	0.28	15	15	0	79	0	17	10

The complexity of this reaction system makes it a very time-consuming task to adjust the starting mixture and it may be impossible to carry out a completely side product free tochilinite synthesis in a system of Fe, S, Mg and Al. The reaction conditions of Toch\_MgAl\_20 seem to be very promising though. Instead of adjusting the starting mixture further it was more reasonable to find a way to remove the remaining side products after the reaction. As all of them are dissolvable in acid, a series of acidic treatments was carried out involving ammonium ions. Tochilinite is dissolvable in acidic solution as well and the yield may get lower during the treatment.



Any contamination by amorphous hydroxides or oxides that may not be visible in the PXRD pattern would be removed as well what is important for a reliable elemental analysis. The series includes the treatment with diluted HCl or NH<sub>4</sub>Cl or the addition of NH<sub>4</sub>Cl to the starting mixture. NH<sub>4</sub>Cl was chosen because NH<sub>3</sub> can form stable complexes with Fe<sup>2+</sup> and Fe<sup>3+</sup> and may dissolve FeS and Fe<sub>3</sub>O<sub>4</sub>. Magnetite was not the target of the acidic treatments as it can be removed with a magnet.

The treatment with HCl and NH<sub>4</sub>Cl led to similar observations as brucite and iron were removed in both cases but the amounts of pyrrhotite and magnetite were unchanged. If the treatments were carried out with high concentrations or increased temperatures pyrrhotite and magnetite were still unchanged but tochilinite dissolved instead. The same was observed if NH<sub>4</sub>Cl was present in the starting mixture (Toch\_MgAl\_23 to Toch\_MgAl\_26). In this regard, it was not possible to obtain a pure Mg-Al-tochilinite analogue without iron ions present in the hydroxide layers and the focus was shifted towards the other compositions that may be accessible more easily.

### 6.4.3 Mg-Fe(III)-tochilinite

For the synthesis of Mg-Fe(III)-tochilinite also different starting materials with different ratios, reaction temperatures and reaction times were used to explore their reactivity. The different starting mixtures in this system are summarized in table 18.

Table 18: Sources of the necessary ions in different starting mixtures for the Mg-Fe(III)-tochilinite syntheses.

Mixture name	Iron source	Sulfur source	Magnesium source	Fe <sup>3+</sup> source	Experiments
<i>Mg-Fe-A</i>	Fe	S	Mg	Fe	Toch_MgFe_1
<i>Mg-Fe-B</i>	Fe	S	Mg	FeO(OH)	Toch_MgFe_2
<i>Mg-Fe-C</i>	FeS	FeS	MgO	Fe/FeS	Toch_MgFe_3/4
<i>Mg-Fe-D</i>	FeS	FeS	Mg	FeO(OH)	Toch_MgFe_5

In the PXRD patterns of the products from all reactions in this system tochilinite-like diffraction peaks could be observed. The exclusion of Fe<sup>2+</sup> from the hydroxide layers is in principle possible by two approaches. Because the oxidation of elemental iron is slower than the oxidation of Fe<sup>2+</sup> to Fe<sup>3+</sup>, the concentration of Fe<sup>2+</sup> should be low under suitable oxidizing conditions in a system of Fe, S and Mg.



The second approach is to use FeO(OH) as the Fe<sup>3+</sup> source what would exclude any Fe<sup>2+</sup> if tochilinite formation is faster than the reduction of Fe<sup>3+</sup> to Fe<sup>2+</sup> which cannot be ruled out completely.

From the *Mg-Fe-A* mixture tochilinite can only form if iron is oxidized to Fe<sup>3+</sup> as no other trivalent cation is available. This oxidation determines the speed of tochilinite formation and is the key step using this mixture. In the corresponding reactions the following side products were identified. If nothing else is said, the same reactions and conditions apply that are specified in the Mg-Al-tochilinite system.

- I) Elemental iron; Fe
- II) Magnesium hydroxide  $\text{Mg}(\text{OH})_2$  with brucite crystal structure
- III) Iron sulfide FeS with pyrrhotite structure

Pyrrhotite occurred in every tochilinite synthesis with the *Mg-Fe-A* mixture like in all reactions towards Mg-Al-tochilinite. These systems are very similar and the occurrence of pyrrhotite is kinetically controlled and may not be precluded completely.

- IV) Iron sulfide  $\text{FeS}_2$  with pyrite structure

The side products that occur in the Mg-Al-tochilinite reactions are similar to the ones observed using this mixture, except for the formation of LDHs. Therefore, it is reasonable to suggest, that the formation of sulfide containing LDHs requires the availability of  $\text{Al}^{3+}$  and  $\text{Mg}^{2+}$  and is impossible from  $\text{Fe}^{2+}/\text{Fe}^{3+}$ .

To investigate the influence of the ratio of the three starting materials, two series were carried out at 160 °C with a reaction time of three days. In the first series the amount of iron and sulfur were kept constant whereas the amount of magnesium was lowered in small steps. In the second one, the amount of iron and magnesium were kept constant and the amount of sulfur was lowered in small steps. The corresponding PRXD patterns for the first series are shown in the figures 147 and 152 to 154 (Toch\_MgFe\_1, Toch\_MgFe\_6, Toch\_MgFe\_7, Toch\_MgFe\_8). The dependence of the product ratios is not intuitive and needs further explanation:

- With a decreasing amount of magnesium in the starting mixture, the amount of brucite in the products decreases whereas the amount of residual iron increases.
- The amounts of tochilinite, magnetite, pyrite and pyrrhotite are not proportional to the amount of magnesium in the starting mixture.
- This behavior may be explained by an interplay of the oxidation rate of iron to  $\text{Fe}^{2+}$  and the subsequent oxidation of  $\text{Fe}^{2+}$  to  $\text{Fe}^{3+}$ .

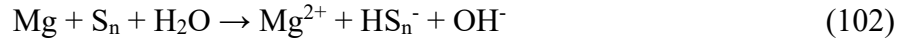


Table 19: Absolute diffraction peak areas from different products in Mg-Fe(III)-tochilinite syntheses with identical PXRD settings. Mg = magnesium, Bru = brucite, Fe = iron, Pyr = pyrite, Toch = tochilinite, Mag = magnetite, Pyh = pyrrhotite.

Exp.	Mg / mg	Bru (001)	Fe (110)	Pyr (200)	Toch (002)	Mag (311)	Pyh (228)
Toch_MgFe_1	50	107	36	0	62	9	87
Toch_MgFe_6	36	40	49	10	81	19	55
Toch_MgFe_7	20	21	80	6	53	0	60

- The amount of magnesium determines the pH value as it quantitatively reacts with sulfur forming basic polysulfide anions. The dissolution of elemental Fe is slowed down at higher pH values but increased at higher polysulfide concentrations.
- Therefore, small amounts of magnesium increase the pH and prevent iron oxidation and magnetite formation, but a higher magnesium content in the starting mixture leads to more polysulfide anions and increases the iron dissolution again.

The second series that was carried out to explore the influence of the sulfur shows a linear dependence of the system as can be seen from the corresponding PXRD patterns (Toch\_MgFe\_8 to Toch\_MgFe\_10) and table 20.

Table 20: Absolute diffraction peak areas from different products in Mg-Fe(III)-tochilinite syntheses with identical PXRD settings. Bru = brucite, Fe = iron, Pyr = pyrite, Toch = tochilinite, Mag = magnetite, Pyh = pyrrhotite.

<b>Exp.</b>	<b>Sulfur</b> / g	<b>Bru</b> <b>(001)</b>	<b>Fe</b> <b>(110)</b>	<b>Pyr</b> <b>(200)</b>	<b>Toch</b> <b>(002)</b>	<b>Mag</b> <b>(311)</b>	<b>Pyh</b> <b>(228)</b>
Toch_MgFe_8	0.12	10	25	9	45	9	57
Toch_MgFe_9	0.14	43	23	42	48	0	60
Toch_MgFe_10	0.17	71	8	136	15	0	36

As the amount of sulfur increases, the formation of pyrite is pronounced what leads to a decrease in tochilinite formation. Less tochilinite formed corresponds to more brucite that is present in the product mixture. As pyrite is very stable and cannot be removed, the amount of sulfur should be restricted to a necessary minimum in this system.

Fe-Mg-tochilinite synthesis with a mixture of Fe, S and Mg possibly prevents the incorporation of Fe<sup>2+</sup> into the hydroxide layer but leads to magnetite and especially pyrrhotite and pyrite that are hard to be removed. The main problem is the control of the oxidation of elemental iron and the formation of FeS. Therefore, experiments with previously prepared mackinawite (mixture *Mg-Fe-D*) were carried out using FeO(OH) as the Fe<sup>3+</sup> source and elemental Mg to maintain a hydrogen atmosphere.

The mixtures *Mg-Fe-B* and *Mg-Fe-C* were not investigated further as they also showed greater amounts of pyrrhotite and pyrite what is likely a consequence of the use of elemental iron.

With the *Mg-Fe-D* mixture tochilinite can form easily as all necessary ions are present from the start of the reaction but the solubility of FeO(OH) is very low which slows the formation of tochilinite down and offers time for side products to form. In the corresponding reactions the following side products were identified (Toch\_MgFe\_4) and if nothing else is said, the same reactions apply that are specified in the Mg-Al-tochilinite system.

- I) Magnesium hydroxide Mg(OH)<sub>2</sub> with brucite structure
- II) Iron sulfide FeS with pyrrhotite structure



Pyrrhotite occurred in some tochilinite synthesis with this mixture but could be suppressed if FeO(OH) was used in excess.

III) Iron oxide hydroxide FeO(OH) with goethite structure

Residual goethite was found in the product mixture if its excess used was too high.

IV) Iron oxide Fe<sub>3</sub>O<sub>4</sub> with magnetite structure

Magnetite was present in every reaction using the *Mg-Fe-D* mixture as it forms from Fe<sup>2+</sup> and FeO(OH).



As magnetite does not react with FeS and Mg(OH)<sub>2</sub> to form tochilinite, the solubility of magnetite is expected to be lower than that of tochilinite. This is very beneficial for the synthesis of Mg-Fe-tochilinite as any surplus Fe<sup>2+</sup> that is not incorporated into the sulfide layers can be bound by the formation of magnetite and does not enter the hydroxide part. The pre-prepared iron sulfide contains equimolar amounts of Fe<sup>2+</sup> and S<sup>2-</sup> but the tochilinite formation causes the release of Fe<sup>2+</sup> into the solution to create a certain amount of iron vacancies. These Fe<sup>2+</sup> would partly be incorporated into the hydroxide layer what has to be prevented. The formation of magnetite is a minor problem as it can be removed completely with a magnet. The use of excess sulfur in the iron sulfide synthesis did not work well as it led to increased amounts of pyrite in the products (Toch\_MgFe\_11). After adjusting the ratio of Mg to FeS, a sample was obtained that only contained magnetite as a side product (Toch\_MgFe\_12). The removal of the magnetic products with a Teflon coated neodymium magnet was very successful and led reproducibly to Mg-Fe-tochilinite samples without any side products identifiable in the PXRD patterns (Toch\_MgFe\_13).

The disadvantage of this method is that much more product is removed than iron and magnetite are present in the product mixture. This implies, that tochilinite is strongly attached to the magnetite in the mixture and is removed with it. It cannot easily be separated from the magnetite. Ultrasonication of the reaction mixture for one hour did not increase the tochilinite yield. The amount of magnetite formed depends on the amount of FeO(OH) in the starting mixture and decreases by lowering it. Therefore, a series of reactions was carried out with decreasing amounts of FeO(OH) that is summarized in table 21.

Table 21: Correlation between the used mass of FeO(OH) and the removed magnetic material in Mg-Fe(III)-tochilinite syntheses.

Experiment	Mass of FeO(OH) / g	Approx. removed product mass / %
Toch_MgFe_14	0.486	20
Toch_MgFe_15	0.409	10
Toch_MgFe_16	0.300	1
Toch_MgFe_17	0.221	0

The starting mixture of Toch\_MgFe\_16 is the best one in this series and probably the best one for the Mg-Fe-tochilinite system. Only a little amount of magnetite had to be removed and the PXRD pattern shows no signs of pyrrhotite or brucite. Using the starting mixture of Toch\_MgFe\_17 led to the formation of brucite as not enough Fe<sup>3+</sup> were present in the reaction system. The reaction is very reproducible and characterization was carried out with the product of reaction Toch\_MgFe\_18 using 0.31 g FeO(OH).

#### 6.4.4 Fe(II)-Fe(III)-tochilinite (ferrotochilinite)

A synthesis for tochilinite analogues exclusively containing Fe<sup>2+</sup> as the divalent cation in the hydroxide layers has not been reported in the literature. Pekov *et al.* reported on a natural Fe(II)-Fe(III)-tochilinite in 2012 that they called ferrotochilinite.<sup>83</sup> The synthesis of Fe(II)-Fe(III)-tochilinite was also carried out with different starting materials, ratios and reaction temperatures to explore their reactivity. The different starting mixtures in this system are summarized in table 22.

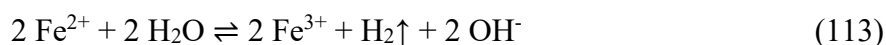
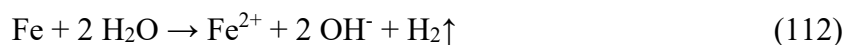
Table 22: Sources of the necessary ions in different starting mixtures for the Fe(II)-Fe(III)-tochilinite syntheses.

Mixture name	Fe <sup>2+</sup> source	Sulfur source	Fe <sup>3+</sup> source	Experiments
<i>Fe-Fe-A</i>	Fe	S	FeO(OH)	Toch_FeFe_1
<i>Fe-Fe-B</i>	Fe	FeS	FeO(OH)	Toch_FeFe_2
<i>Fe-Fe-C</i>	FeS	FeS	FeS	Toch_FeFe_3
<i>Fe-Fe-D</i>	Fe	S	Fe	Toch_FeFe_4

All reactions with the mixtures *Fe-Fe-A* to *Fe-Fe-C* were carried out at 160 °C as this reaction temperature worked well for Mg-Al-tochilinite and Mg-Fe-tochilinite syntheses but the only products found were residual iron, magnetite and pyrrhotite.



After several experiments it turned out, that lowering the reaction temperature is the key step for this system. An experiment at 130 °C using only a mixture of Fe and S led to the successful formation of Fe(II)-Fe(III)-tochilinite (Toch\_FeFe\_4). If the same reaction was carried out at 160 °C, again only pyrrhotite and magnetite were formed. This implies, that Fe-Fe-tochilinite has a stability limit during the synthesis of 130 °C in the reaction systems used. Lowering or increasing the total mass of the iron and sulfur starting mixture did not show significant differences in the products formed (Toch\_FeFe\_5, Toch\_FeFe\_6). The only side products found in this reaction were magnetite and traces of elemental iron. Iron and magnetite could be removed by a strong Teflon coated neodymium magnet. It was possible to attract all magnetite and residual iron to get a pure Fe(II)-Fe(III)-tochilinite sample (Toch\_FeFe\_7). The removal of the magnetic side products led to an even greater drop in tochilinite yield as observed in the Mg-Fe-tochilinite system. The yield dropped from approximately 95 % as estimated from the PXRD pattern to around 10 % after removing the magnetic part.



As the amount of magnetite should be reducible by increasing the amount of sulfur in the starting mixture, a series of reactions was carried out to find the optimum Fe to S ratio. The PXRD patterns of this series are presented in figures 166 and 169 to 172. (Toch\_FeFe\_7 to Toch\_FeFe\_10) and table 23 shows the composition of the starting mixture and the removed magnetic part.

Table 23: Correlation between the used mass of sulfur and the removed magnetic material in Fe(II)-Fe(III)-tochilinite syntheses.

Experiment	Mass of Fe / g	Mass of S / g	Approx. mass of removed magnetic material / %
Toch_FeFe_4	3.0	1	95
Toch_FeFe_7	3.0	1.1	10
Toch_FeFe_8	3.0	1.2	1
Toch_FeFe_9	3.0	1.3	0
Toch_FeFe_10	3.0	1.4	0

Pyrrhotite formed with increasing amounts of sulfur whereas the proportion of magnetite decreases. The ratio of Fe : S of 3.0 g : 1.1 g led to a product that does not show any impurities in its PXRD pattern. The reaction was repeated several times and always showed the same outcome.

#### 6.4.5 Fe(II)-Al-tochilinite

The knowledge gained from the previous tochilinite systems made clear, that Fe(II)-Al-tochilinite should be synthesized from a mixture of elemental iron, sulfur and aluminum

to prevent the formation of  $\text{Fe}^{3+}$  that could enter the hydroxide layers and to maintain an appropriate hydrogen gas pressure. As residual iron and any magnetite formed can be removed by a magnet, the use of an excess of elemental iron in this system is reasonable. The stability limit of 130 °C found for Fe(II)-Fe(III)-tochilinite was also expected for this system and therefore the reaction temperature was chosen in regard. Adopting the ratio of S to Al from the Mg-Al-System, the first experiments already led to a successful synthesis of very pure Fe(II)-Al-tochilinite (Toch\_Al\_1) after removing the magnetic side products. A comparatively high total mass of the starting mixture was chosen to ensure a high hydrogen gas pressure and minimize the concentration of  $\text{Fe}^{3+}$ . The yield was not lowered as drastically as in the Fe(II)-Fe(III)-tochilinite case by the removal of the magnetic part and it was suspected that there may be some pyrrhotite still present in the product mixture.

Table 24: Overview of the ratio of the starting materials for Fe(II)-Al-tochilinite syntheses at a constant amount of sulfur.

<b>Name of the reaction</b>	<b>Mass of Fe / g</b>	<b>Mass of S / g</b>	<b>Mass of Al / g</b>
Toch_Al_2	6.1	2.46	0.61
Toch_Al_3	6.2	2.46	0.62
Toch_Al_4	6.3	2.46	0.63
Toch_Al_5	6.4	2.46	0.64

Therefore, a reaction series was carried out with increasing amounts of Fe and Al in the starting mixture to find the optimal conditions. The compositions of the starting mixtures are summarized in table 24 and the corresponding PXDR patterns are shown in figures 175 to 178 (Toch\_Al\_2 to Toch\_Al\_5). The PXRD patterns in this series look very similar what indicates that the only side products are residual iron and magnetite that have been removed completely. In ELT\_175\_c and ELT\_175\_d a new diffraction peak appears that can be assigned to residual elemental aluminum that is not oxidized due to the high hydrogen gas pressure in the system. The reaction conditions of Toch\_Al\_2 are very reproducible and samples of Toch\_FeAl\_6 synthesized accordingly were used for characterization.

## 6.5 Characterization of Tochilinite analogues

From all experiments towards tochilinite analogues without side products, one sample for each variety was analyzed in detail. Table 25 summarizes their formation conditions. Aside the removal of magnetic material, no further purification was applied to the samples.

Table 25: Overview of side product free tochilinite analogues for in depth analysis.

Theoretical formula	Exp.	Starting materials and reaction conditions	Yield after purification
$x [ Mg_a^{II} ; Fe_b^{III} * (OH)_{(a+b)*2} ]$ $* (Fe_{1-e}^{II} * S)$	Toch_MgFe_18	FeS, Mg, FeOOH 160 °C, 3 days	~ 99 %
$x [ Fe_a^{II} ; Fe_b^{III} * (OH)_{(a+b)*2} ]$ $* (Fe_{1-e}^{II} * S)$	Toch_FeFe_11	Fe, S 130 °C, 3 days	~ 90 %
$x [ Fe_a^{II} ; Al_b^{III} * (OH)_{(a+b)*2} ]$ $* (Fe_{1-e}^{II} * S)$	Toch_FeAl_6	Fe, S, Al 130 °C, 3 day	~ 85 %

### 6.5.1 Particle characteristics

The obtained samples of the tochilinite analogues were investigated by SEM and TEM. All three samples show nanometer sized platelets and very few nano-tubes as has been reported for natural tochilinite.<sup>170,171</sup>

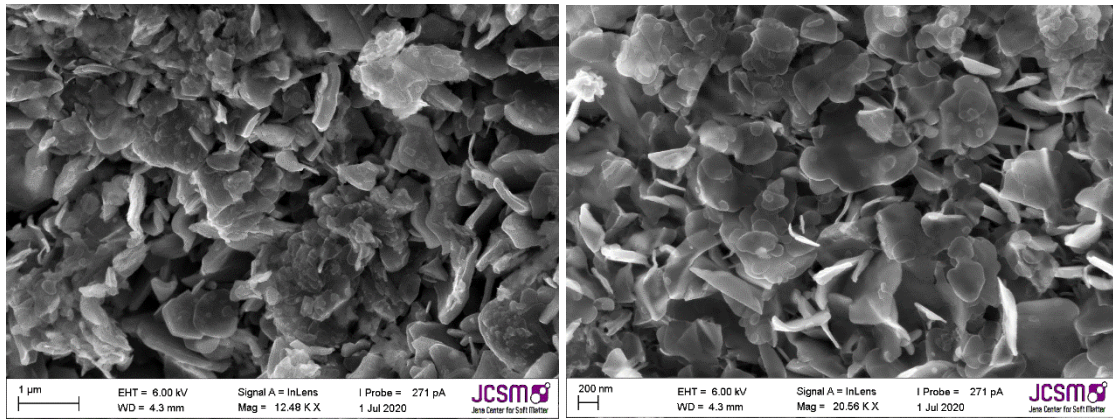


Figure 54: SEM images of Toch\_MgFe\_18.

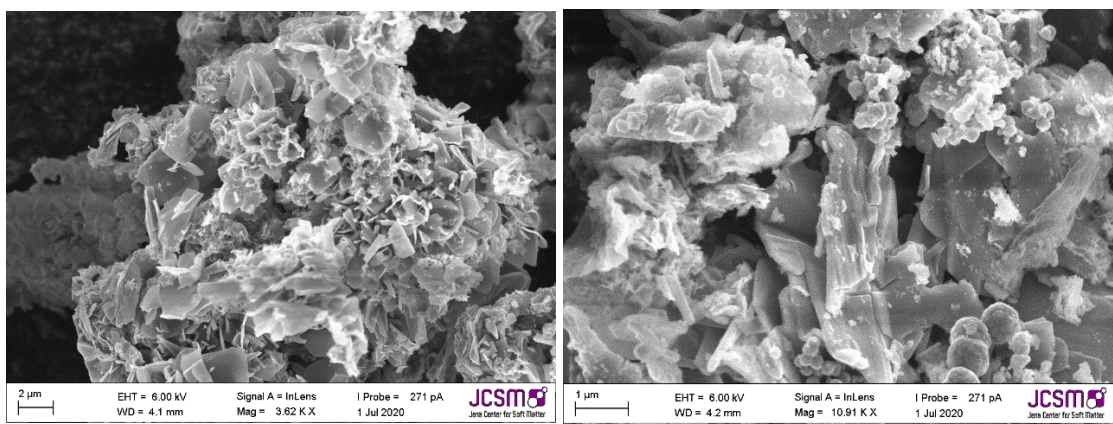


Figure 55: SEM images of Toch\_FeFe\_11.

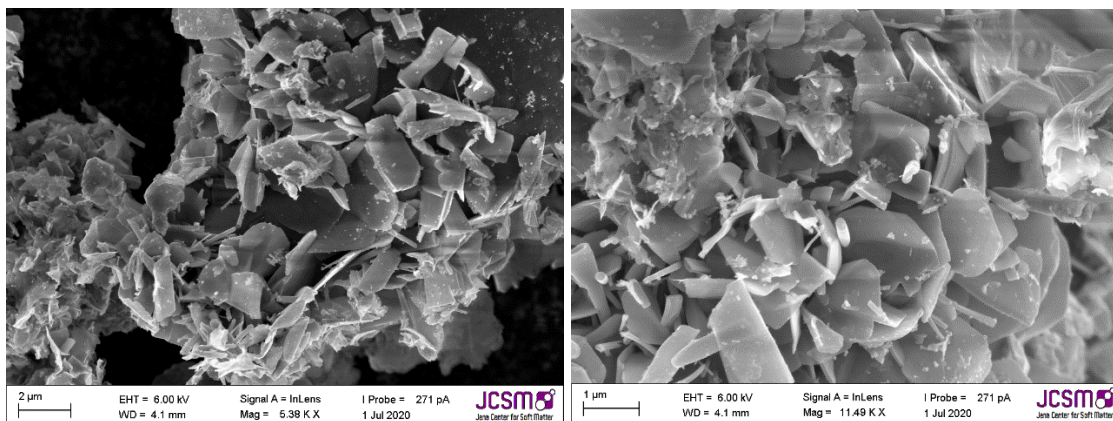


Figure 56: SEM images of Toch\_FeAl\_6.

The Toch\_MgFe\_18 and Toch\_FeAl\_6 samples seem to be very homogenous, whereas the Toch\_FeFe\_11 sample shows signs for oxidation during storage over time. A sample of Toch\_MgFe\_18 was also investigated by TEM. As the small particles form

micrometer-sized aggregates and could hardly be separated during TEM sample preparation, only the edges of these aggregates could be investigated. The images show a mixture of platelets and nano-tubes as has been reported for natural and synthetic tochilinite.<sup>177</sup>

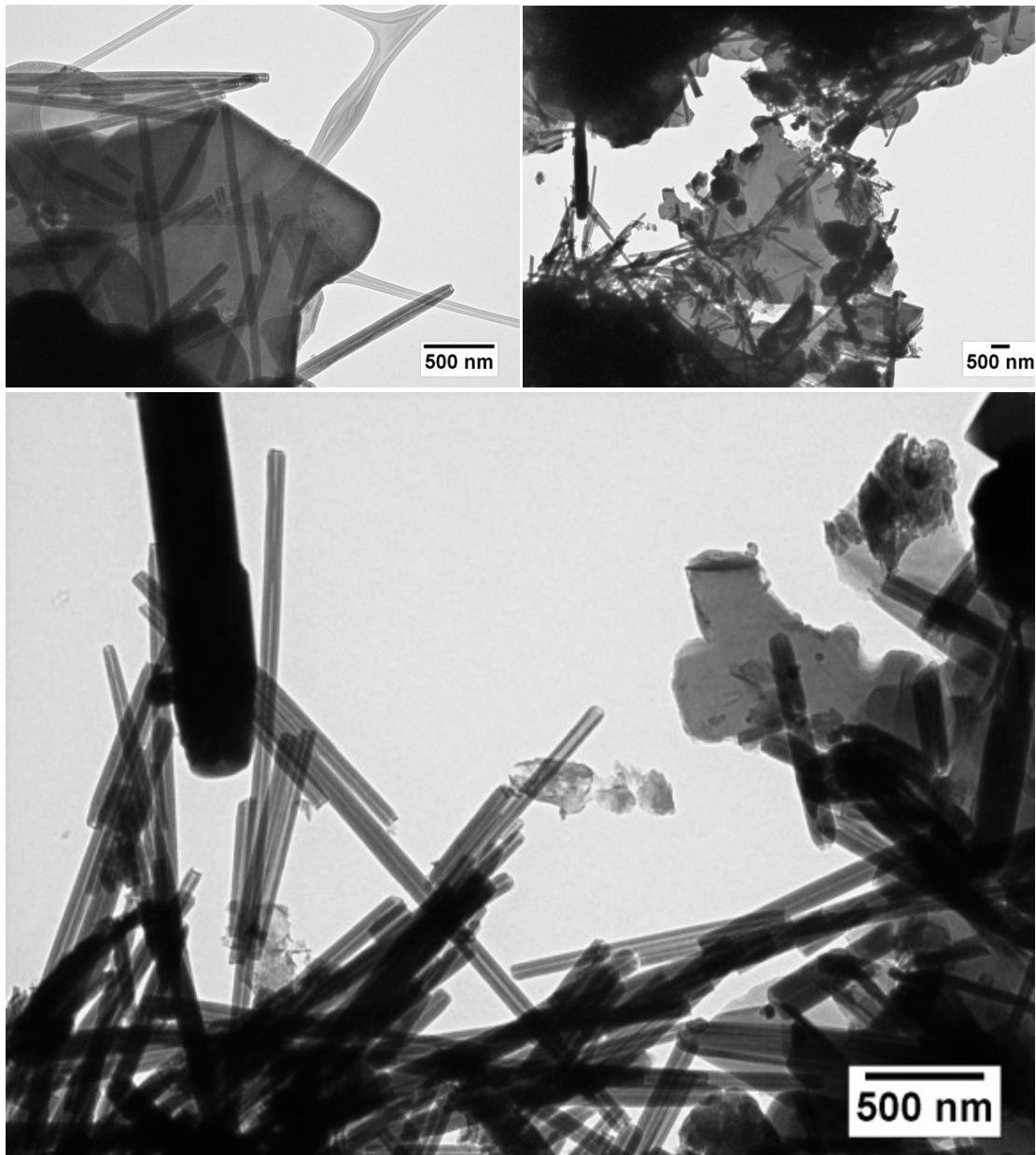


Figure 57: TEM images of Toch\_MgFe\_18 showing a mixture of platelets and nano-tubes.

The tubes may be a result of misalignment of the different layers that result in a pronounced curvature of the sheets. All analysis that has been carried out can therefore only give mean values for both tubes and platelets.



Table 26: BET surface areas and mean pore volumes of the different tochilinite analogues determined by adsorption isotherms of argon gas at 87 K.

Exp.	BET surface area / $\text{m}^2 \cdot \text{g}^{-1}$	Mean pore volume / $\text{cm}^3/\text{g}$
Toch_MgFe_18	40	0.090
Toch_FeAl_6	31	0.082
Toch_FeFe_11	23	0.100

BET surface areas were determined using adsorption isotherms of argon gas at 87 K. The samples were pretreated by outgassing under high vacuum at 130 °C for six hours. The determined surface areas are summarized in table 26.

### 6.5.2 Stability

Like for the mackinawite case, the thermal stability of the different tochilinite analogues was determined to evaluate the maximum temperature for CO<sub>2</sub> reduction reactions. The dried samples were heated in N<sub>2</sub> atmosphere and analyzed by TGA/DSC.

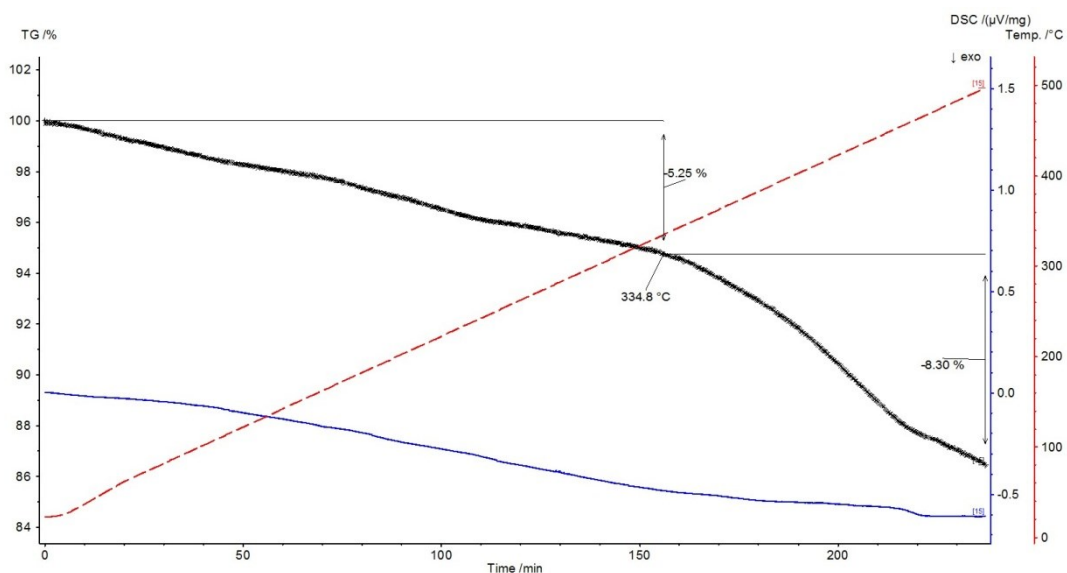


Figure 58: TGA/DSC analysis of Toch\_MgFe\_18 in a nitrogen gas atmosphere. The sample mass decreases from the start even at low temperatures but decreases faster at temperatures higher than 335 °C.

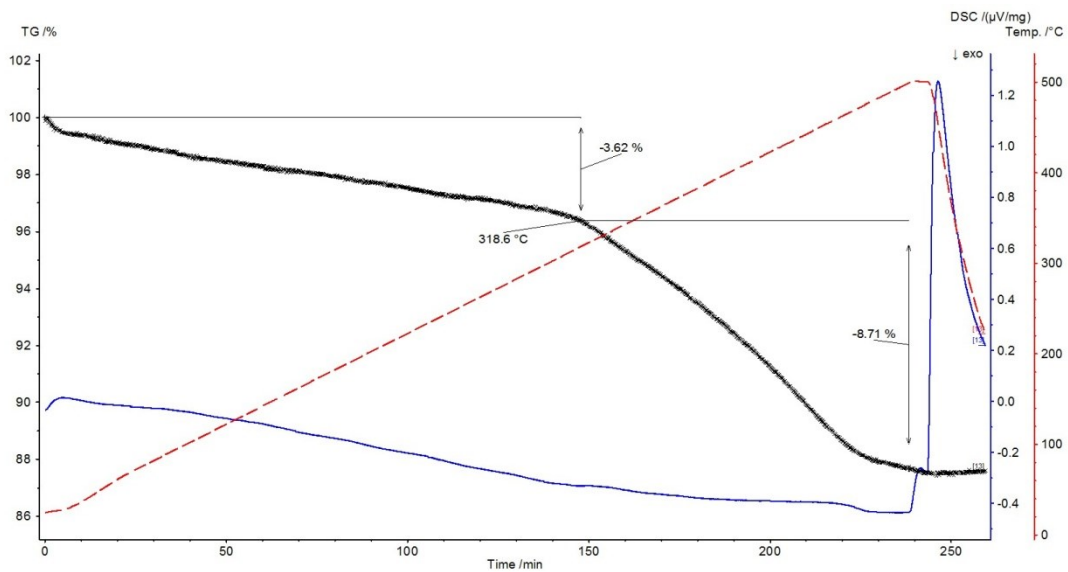


Figure 59: TGA/DSC analysis of Toch\_FeAl\_6 in a nitrogen gas atmosphere. The sample mass decreases from the start even at low temperatures but decreases faster at temperatures higher than 318 °C.

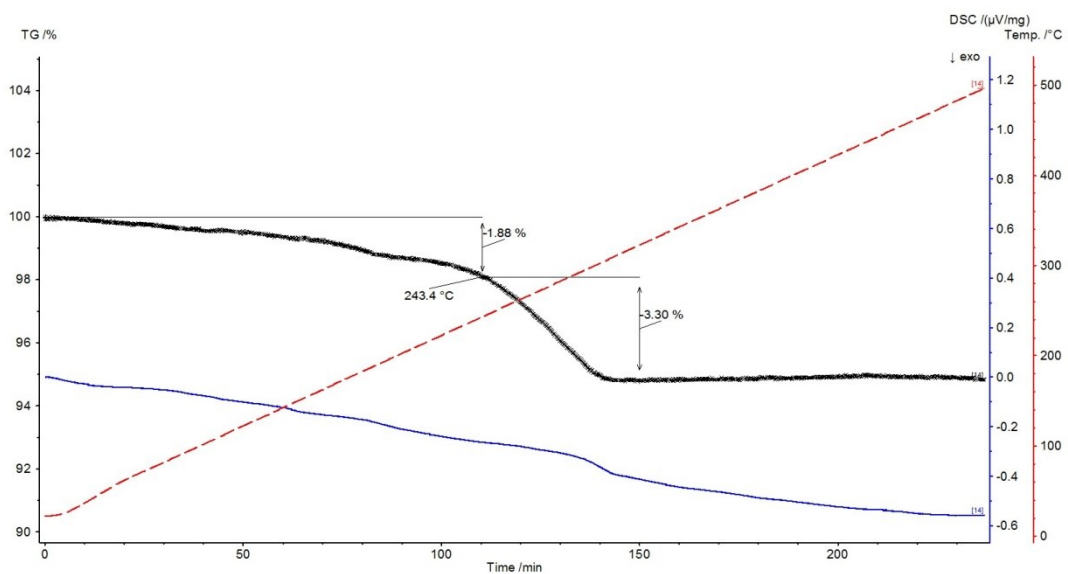


Figure 60: TGA/DSC analysis of Toch\_FeFe\_11 in a nitrogen gas atmosphere. The sample mass decreases from the start even at low temperatures but decreases faster at temperatures higher than 243 °C.

The TGA/DSC analysis shows, that the mass of all samples decreases from the start even at low temperatures. This may be attributed to a loss of adsorbed water as the samples

were used shortly after their synthesis without excessive drying. The pronounced loss of mass at higher temperatures is attributed to the decomposition and the formation of magnetite/magnesioferrite and pyrrhotite accompanied by the loss of water. The temperatures at which the decomposition starts is in the order Toch\_MgFe\_18 (335 °C) > Toch\_FeAl\_6 (318 °C) > Toch\_FeFe\_11 (243 °C). The stability of the tochilinite analogues clearly differs with their composition with the naturally most abundant analogue containing high amounts of Mg<sup>2+</sup> and Fe<sup>3+</sup> having the highest decomposition temperature. This observation corresponds to the temperatures range during the synthesis as it has been observed that the Fe-Fe-analogue does not form at temperatures above 130 °C.

### 6.5.3 Composition and Mößbauer data

The compositions of the samples were determined by ICP-AES. The samples were dissolved following the dissolution procedure described in the methods section. In short, around 300 mg of the samples were placed in a Teflon lined steel autoclave. The powdered sample was cautiously covered with water and placed in a fridge until the water was frozen. 10 ml of aqua regia was poured on top of the ice without contact to the sample. The autoclave was sealed and heated in an oven for more than 12 hours at 130 °C.

Table 27: Compositions of tochilinite analogs obtained by ICP-AES.

Name	Fe / mg	S /mg	Mg / mg	Al / mg	undefined / mg
Toch_MgFe_18	57.92	27.50	8.92	0.02	30.03
Toch_FeFe_11	63.25	24.25	0.03	0.37	23.20
Toch_FeAl_6	58.25	22.92	0.00	5.32	28.99

The sample mass that has not been assigned to the determined elements (undefined) is attributed to OH<sup>-</sup> and O<sup>2-</sup>. As sulfur is only expected in the form of sulfide ions, charge balancing was used to determine the ratio of these ions.

The Mößbauer data was obtained by fitting the Mößbauer spectrum for <sup>57</sup>Fe with three different iron species: Fe<sup>2+</sup> in tetrahedral sulfide environment (Fe<sup>2+</sup><sub>S</sub>) and Fe<sup>2+</sup> and Fe<sup>3+</sup> in octahedral hydroxide environment (Fe<sup>2+</sup><sub>H</sub>/Fe<sup>3+</sup><sub>H</sub>). The Mößbauer spectra were fitted

with a singlet for  $\text{Fe}^{2+}_{\text{S}}$  and  $\text{Fe}^{3+}_{\text{H}}$  and a doublet for  $\text{Fe}^{2+}_{\text{H}}$ . The proportions of the iron species are summarized in table 28.

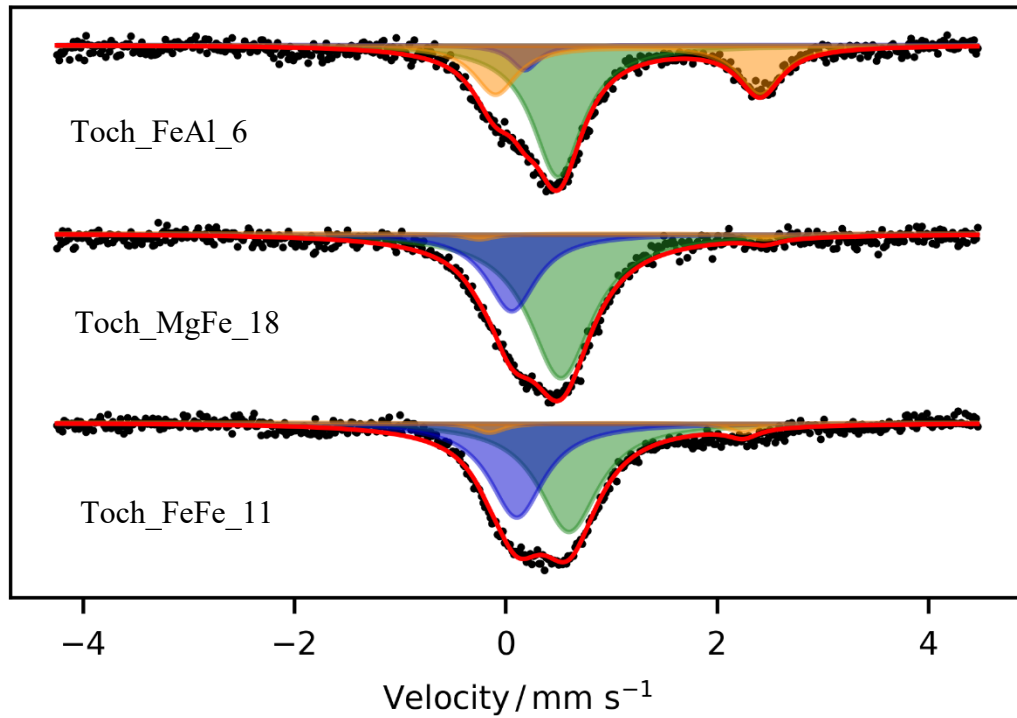


Figure 61: Mössbauer spectra at room temperature of different tochilinite analogues without side products. Green area:  $\text{Fe}^{2+}_{\text{S}}$ ; Blue area:  $\text{Fe}^{3+}_{\text{H}}$ ; Orange area:  $\text{Fe}^{2+}_{\text{H}}$ .

Table 28: Mössbauer data for tochilinite analogues without side products.

Exp.	$\text{Fe}^{2+}$ (sulfide) / %	$\text{Fe}^{2+}$ (hydroxide) / %	$\text{Fe}^{3+}$ (hydroxide) %
Toch_FeAl_6	$57 \pm 5$	$37 \pm 4$	$6 \pm 2$
Toch_MgFe_18	$69 \pm 5$	$3 \pm 2$	$29 \pm 3$
Toch_FeFe_11	$53 \pm 5$	$5 \pm 2$	$42 \pm 4$

The singlets for  $\text{Fe}^{2+}_{\text{S}}$  and  $\text{Fe}^{3+}_{\text{H}}$  overlap to a great extent what makes them interchangeable to a certain degree without lowering the goodness of the fit. Therefore, reasonable expected values for  $\text{Fe}^{2+}_{\text{S}}$  and  $\text{Fe}^{3+}_{\text{H}}$  were used for the fit and the fitting parameters were examined in regard of their plausibility.

Table 29: Fit parameters for Toch\_FeAl\_6. IS = Internal Shift, QS = Quadrupole Splitting, LW = Line width.

Iron ions	Color	IS / mm s <sup>-1</sup>	QS / mm s <sup>-1</sup>	LW / mm s <sup>-1</sup>
Fe <sup>2+</sup> <sub>S</sub>	green	0.49(1)	-	0.89(1)
Fe <sup>2+</sup> <sub>H</sub>	orange	1.15(1)	2.51(1)	0.50(1)
Fe <sup>3+</sup> <sub>H</sub>	blue	0.18(1)	-	0.32(3)

Table 30: Fit parameters for Toch\_MgFe\_18. IS = Internal Shift, QS = Quadrupole Splitting, LW = Line width.

Iron ions	Color	IS / mm s <sup>-1</sup>	QS / mm s <sup>-1</sup>	LW / mm s <sup>-1</sup>
Fe <sup>2+</sup> <sub>S</sub>	green	0.52(1)	-	0.74(2)
Fe <sup>2+</sup> <sub>H</sub>	orange	1.10(4)	2.70(9)	0.35(1)
Fe <sup>3+</sup> <sub>H</sub>	blue	0.05(1)	-	0.57(3)

Table 31: Fit parameters for Toch\_FeFe\_11. IS = Internal Shift, QS = Quadrupole Splitting, LW = Line width.

Iron ions	Color	IS / mm s <sup>-1</sup>	QS / mm s <sup>-1</sup>	LW / mm s <sup>-1</sup>
Fe <sup>2+</sup> <sub>S</sub>	green	0.60(1)	-	0.70(1)
Fe <sup>2+</sup> <sub>H</sub>	orange	1.05(2)	2.40(4)	0.35(4)
Fe <sup>3+</sup> <sub>H</sub>	blue	0.10(1)	-	0.63(1)

The obtained values for the internal shift are in the same order of magnitude for all three samples and are not in contradiction to literature values. As there is no Mößbauer investigation of natural or synthetic tochilinite at room temperature, the values need to be compared to low temperature ones. The internal shift gets lower at higher temperatures, what makes the obtained values reasonable compared to the shifts obtained by Chistyakova et.

al.<sup>173</sup> For comparison, my colleague Mario Grosch synthesized a mackinawite sample that was also analyzed by Mößbauer spectroscopy.

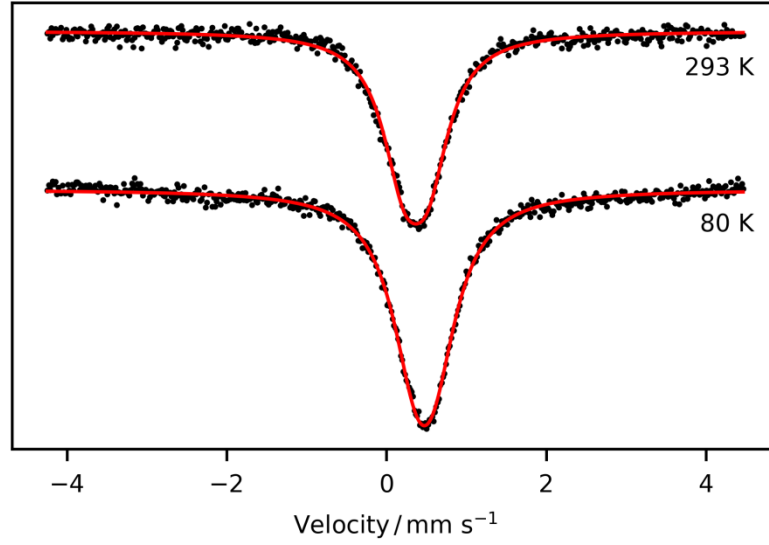


Figure 62: Mößbauer spectrum of deactivated mackinawite prepared from iron and sulfur following the standard synthetic procedure. The spectra were recorded at room temperature and at 80 K, respectively and differ only slightly in their center shift.

The Mößbauer spectrum was fitted with a singlet as has been done previously.<sup>143,178</sup> The fitted center shifts are  $0.37(1) \text{ mm s}^{-1}$  at room temperature and  $0.47(1) \text{ mm s}^{-1}$  at 80 K and are comparable to the obtained shifts for the  $\text{Fe}^{2+}$  attributed to the iron sulfide layers for all tochilinite analogues. The shifts in the tochilinite samples are slightly increased what may be caused by distortion of the sulfide tetrahedra.

The amounts of  $\text{OH}^-$  and  $\text{O}^{2-}$  in the tochilinite analogues can be calculated by comparing all negative to all positive ions available.

$$2 n_{\text{Fe}^{2+}} + 3 n_{\text{Fe}^{3+}} + 2 n_{\text{Mg}^{2+}} + 3 n_{\text{Al}^{3+}} = 2 n_{\text{S}^{2-}} + n_{\text{OH}^-} + 2 n_{\text{O}^{2-}} \quad (114)$$

Assuming that the undefined mass from the elemental analysis belongs to hydrogen and oxygen leads to:

$$m_{\text{undefined}} = m_{\text{OH}^-} + m_{\text{O}^{2-}} + m_{\text{H}_2\text{O}} \quad (115)$$

$$m_{\text{undefined}} = n_{\text{OH}^-} * M_{\text{OH}^-} + n_{\text{O}^{2-}} * M_{\text{O}^{2-}} + m_{\text{H}_2\text{O}} \quad (116)$$

The amount of OH<sup>-</sup> was calculated by first omitting any oxide ions and water assuming that the undefined mass is only attributed to OH<sup>-</sup>. In a second step, the amount of OH<sup>-</sup> was replaced by O<sup>2-</sup> to achieve charge balancing according to equation 114. As the complete undefined masses could be attributed to OH<sup>-</sup> and O<sup>2-</sup>, probably no water is present in the samples and the resulting compositions are presented in table 32.

Table 32: Final normalized compositions for tochilinite analogues without side products.

Exp.	Composition
Toch_MgFe_18	S <sub>1.00</sub> Fe <sub>1.13</sub> Mg <sub>0.43</sub> Al <sub>0.00</sub> OH <sub>1.63</sub> O <sub>0.00</sub>
Toch_FeFe_11	S <sub>1.00</sub> Fe <sub>1.50</sub> Mg <sub>0.00</sub> Al <sub>0.02</sub> OH <sub>1.24</sub> O <sub>0.24</sub>
Toch_FeAl_6	S <sub>1.00</sub> Fe <sub>1.46</sub> Mg <sub>0.00</sub> Al <sub>0.28</sub> OH <sub>1.76</sub> O <sub>0.03</sub>

To compare these compositions with the theoretical composition of Organova's isometric tochilinite variety it is useful to use similar writing. The parameter e corresponds to the iron vacancies in the sulfide layers and the parameter x corresponds to the volume ratio of the sulfide to hydroxide layers.

Table 33: Comparison of the theoretical composition of Organova's isometric tochilinite variety and the obtained tochilinite analogues in this work.

Exp.	Composition
Theoretical formula	Fe <sub>(1-e)</sub> S * x [Fe <sup>2+</sup> <sub>a</sub> Fe <sup>3+</sup> <sub>b</sub> Mg <sup>2+</sup> <sub>c</sub> Al <sup>3+</sup> <sub>d</sub> (OH) <sub>2</sub> ]
Organova's isometric tochilinite variety	Fe <sub>0.8</sub> S * 0.83 [Mg <sub>0.71</sub> Fe <sub>0.29</sub> (OH) <sub>2</sub> ]
Toch_MgFe_18	Fe <sub>0.82</sub> S * 0.82 [Fe <sup>2+</sup> <sub>0.04</sub> Fe <sup>3+</sup> <sub>0.43</sub> Mg <sup>2+</sup> <sub>0.53</sub> Al <sup>3+</sup> <sub>0.00</sub> (OH) <sub>1.99</sub> (O) <sub>0.01</sub> ]
Toch_FeFe_11	Fe <sub>0.79</sub> S * 0.73 [Fe <sup>2+</sup> <sub>0.11</sub> Fe <sup>3+</sup> <sub>0.85</sub> Mg <sup>2+</sup> <sub>0.02</sub> Al <sup>3+</sup> <sub>0.02</sub> (OH) <sub>1.68</sub> (O) <sub>0.32</sub> ]
Toch_FeAl_6	Fe <sub>0.83</sub> S * 0.90 [Fe <sup>2+</sup> <sub>0.59</sub> Fe <sup>3+</sup> <sub>0.09</sub> Mg <sup>2+</sup> <sub>0.00</sub> Al <sup>3+</sup> <sub>0.32</sub> (OH) <sub>1.96</sub> (O) <sub>0.04</sub> ]

These formulas show that the compositions obtained fit to theoretical compositions of tochilinite in regard of the amount of iron vacancies, the volume ratio of hydroxide to sulfide layers and the structures of the sulfide and hydroxide layers. From charge-balancing calculations it is concluded that a certain amount of oxides needs to be present in the hydroxide layers, but deprotonation of the hydroxide ions has not been reported so far. This may be explained by the work-up procedure of the samples, as they are pyrophoric like mackinawite. The deactivation with air has led to surface oxidation and consequently to the formation of oxides which results in a higher ratio of  $\text{Fe}^{3+}$  to  $\text{Fe}^{2+}$ . The tochilinite analogue containing mainly iron ions was the most pyrophoric sample and contains the highest amount of oxide ions.

The compositional data clearly show that the controlled synthesis of tochilinite analogues was successful. The oxidation state of iron ions could be controlled using appropriate reaction conditions within a small margin of error. Controlling the different ion concentrations by the kinetics of their release and consumption is a suitable approach to synthesize complex layered hybrid sulfide minerals. This may offer the exploration of synthetic analogues of other valleriite-group minerals like yushkinite, haapalaite vyalsovite, ekplexite and kaskasite. Additionally, the formation conditions described in these syntheses may offer a deeper insight into natural tochilinite formation in outer space as well as on the early earth.



## 7 Carbon fixation with tochilinite analogues

Tochilinite and mackinawite have comparable structure motives and may therefore be comparable in their catalytic behavior. As mackinawite is very unstable at higher temperatures compared to tochilinite, high temperature Fischer-Tropsch-type (FTT) reactions were carried out using the most stable tochilinite analogue. The reactions were carried out at the LMU in Munich at the group of Prof. Dr. Trapp by Sophia Peters and Christoph Seifert. In stainless steel autoclaves with a 200 ml glass inlet and a valve for gas supply FTT reactions were carried out at different temperatures with an atmosphere of CO<sub>2</sub> and H<sub>2</sub>. The products were analyzed by GC-MS in DCM solution obtained from a similar distillation method as used for the reduction experiments with mackinawite. After the reaction, the autoclaves were connected to a distillation bridge which had a 3 ml flask on the other side which was cooled in liquid nitrogen. The distillation was carried out at the same temperature as the reaction for one hour. The volatiles that condensed in the cooled flask were dissolved in DCM after removing the distillation bridge. The products were identified by comparing the retention time of reference samples with the retention times observed from the product solutions. The solid phases were analyzed by PXRD. A quantitative analysis was also carried out by comparing the GC peak areas to calibration curves for the different products formed. The reactions are summarized in table 34.

Table 34: Reaction conditions for FTT reactions carried out with Toch\_MgFe\_18.

<b>Exp.</b>	<b>Temperature / reaction time</b>	<b>pH<sub>2</sub> / pCO<sub>2</sub></b>	<b>Tochilinite mass / g</b>
Toch_Red_1	250 °C / 4 days	17.5 bar / 17.5 bar	0.999
Toch_Red_2	264 °C / 4 days	17.5 bar / 17.5 bar	0.655
Toch_Red_3	300 °C / 4 days	17.5 bar / 17.5 bar	1.003
Toch_Red_4	200 °C / 4 days	0 bar / 25 bar	1.006
Toch_Red_5	200 °C / 4 hours	1 bar N <sub>2</sub>	1.001

Table 35: Reduction products obtained from FTT reactions on Toch\_MgFe\_18. C<sub>n</sub> represent saturated alkanes, linear and branched, with the corresponding chain length.

Exp.	MeOH [mg]	EtOH [mg]	C <sub>6</sub> [mg]	C <sub>7</sub> [mg]	C <sub>8</sub> [mg]	C <sub>9</sub> [mg]	C <sub>10</sub> [mg]	C <sub>11</sub> [mg]	C <sub>12</sub> [mg]
Toch_Red_1	0.226	0.001	0.000	0.000	0.000	0.000	0.000	0.000	0.000
Toch_Red_2	0.251	0.020	0.012	0.008	0.106	0.019	0.021	0.001	0.042
Toch_Red_3	0.485	0.044	0.004	0.001	0.006	0.002	0.007	0.016	0.114

For a better comparison, turn-over-numbers (TON) were calculated in regard of the determined yields of methanol, ethanol and the alkanes. It is obvious that already at 250 °C CO<sub>2</sub> is reduced on Toch\_MgFe\_18 and MeOH and EtOH form. At 264 °C, the formation of alkanes is observed. The total TON at 300 °C is less than the one at 264 °C what may be attributed to increased decomposition of the catalyst.

Table 36: Turn-Over-Numbers (TON) for the formation of alcohols and alkanes for the different FTT experiments.

Name	TON MeOH + EtOH [g/kg*d]	TON alkanes [g/kg*d]	TON total [g/kg*d]
Toch_Red_1	0.056	0.000	0.056
Toch_Red_2	0.103	0.080	0.183
Toch_Red_3	0.132	0.037	0.170

This explanation is supported by comparing the amounts of decomposition products as shown in table 37. In a CO<sub>2</sub> atmosphere, siderite (FeCO<sub>3</sub>) is an additional decomposition product of tochilinite compared to the decomposition in N<sub>2</sub> atmosphere. The mass fractions of tochilinite, magnetite, pyrrhotite, pyrite and siderite were estimated by fitting suitable diffraction peaks and determining the corresponding peak areas. The areas are rough estimates as the peaks severely overlap and contain different contributions from

the tochilinite phase that are unknown. Nevertheless, the data is suitable to draw a clear trend in the decomposition behaviour in the different FTT reactions.

Table 37: Proportions of the decomposition products of Toch\_MgFe\_18 under FTT conditions, without H<sub>2</sub> gas and under nitrogen atmosphere, respectively. Toch = tochilinite, Mag = magnetite, Pyrr = pyrrhotite, Sid = siderite, Pyr = pyrite.

Name	Toch / %	Mag / %	Pyrr / %	Sid / %	Pyr / %
Toch_Red_3	35	11	52	1	0
Toch_Red_4	10	33	18	23	16
Toch_Red_5	93	7	0	0	0

The decomposition of Toch\_MgFe\_18 is negligible at 200 °C under nitrogen atmosphere but significant under CO<sub>2</sub> atmosphere. Only a small fraction of tochilinite is left after the reaction and pyrite formed due to its oxidation. In the presence of H<sub>2</sub> gas, no pyrite formed and the decomposition is less extensive. The absence of pyrite clearly supports the activation of hydrogen gas that has not been reported for any iron sulfide phase.

In summary, tochilinite analogues like Toch\_MgFe\_18 are able to catalyze FTT reactions between CO<sub>2</sub> and H<sub>2</sub>. At 250 °C, only methanol and ethanol formed after 4 days but already at 264 °C long chain alkanes were identified. Tochilinite analogues decompose at higher temperatures and therefore active material is lost during the reaction. The decomposition increases with temperature what leads to a decrease of the total TON already at 300 °C compared to 264 °C. Nevertheless, this is the first report of any iron sulfide catalyzing the reaction between CO<sub>2</sub> and H<sub>2</sub> in a FTT reaction.

## 8 A plausible prebiotic scenario

### 8.1 Introduction

Prebiotic chemistry covers all chemical processes that occurred before the onset of biological life. The prebiotic chemistry somehow provided all necessary molecules in appropriate concentrations under the right conditions to enable the emergence of the first living entity. There may have been multiple forms of life as life has not necessarily only emerged once, but the last universal common ancestor (LUCA) of modern life has to be based on DNA/RNA for information storage and enzymes composed of polypeptides for metabolic processes. There is a great amount of reports on reactions and chemical systems that lead to the formation of the building blocks of peptides and DNA / RNA under various conditions<sup>113,179,180</sup> and some that lead to sufficient prebiotic plausible polymerization of these building blocks depending on specific condensation agents.<sup>181</sup> The formation of the building blocks and their condensation depend on certain conditions that differ significantly for amino acids, nucleobases, sugars, nucleosides, nucleotides and membrane constituents.<sup>113,179</sup> Therefore, it is very hard if not impossible to find the right conditions in a “one-pot scenario” for the formation of all necessary species in sufficient concentrations. In this regard it is likely that the different building blocks originated in different “pots” and that their condensation or phosphorylation may have also occurred in a different environment than their formation.<sup>182,183</sup> At some point, all necessary molecules had to come together in appropriate concentrations and under the right conditions in a “final pot” that led to the emergence of the first living entity. A suitable geological setting may be realized by multiple “warm little ponds” on the early earth’s surface, as Charles Darwin called them, that are interconnected by water channels. This idea has already been proposed and elucidated by several authors.<sup>184–186</sup> Hydrothermal conditions are mainly discussed for submarine vents, but may also apply to hydrothermal fields on the earth’s surface.<sup>113,187</sup> Additionally, the chemistry of impacts, although investigated sparsely yet, offers promising pathways for the synthesis of crucial organics and phosphorylation reactions that may be unique in prebiotic chemistry. Schreibersite, an iron phosphide, that is abundant in iron meteorites is a very promising candidate to facilitate the phosphorylation reactions needed to form DNA or RNA.<sup>188–190</sup>

Life is expected to have emerged during the Eoarchean era spanning 400 million years from the end of the Hadean era 4000 million years ago to the beginning of the Paleoarchean Era 3600 million years ago. It is the first geological era for which the earth probably had a solid crust. The earth's surface likely was covered by liquid water and an atmosphere had formed that consisted mainly of CO<sub>2</sub> and N<sub>2</sub> without significant concentrations of O<sub>2</sub> and a pressure between 10 and 100 bar. Volcanic activity was considerably higher than today, with numerous lava eruptions for example in volcanic island arcs caused by the onset of plate tectonics.<sup>162</sup> The first 300 million years of this era are also the time when the Late Heavy Bombardment (LHB) is expected to have occurred. During this time, a vast number of meteorites stroke the earth even leading to the partial melting of the earth's crust. An unknown part of these meteorites have been iron or stony-iron meteorites composed of iron-nickel-alloys together with the lighter elements C, N, O, Si, P and S.<sup>190</sup> Regarding iron meteorite impacts, Bland and Artemieva reported that they “anticipate two 10<sup>3</sup> kg events at the Earth's surface every year, a 10<sup>5</sup> kg event every 100 years, a 10<sup>7</sup> kg event every 5,400 years, a 10<sup>9</sup> kg event every 40,000 years, and a 10<sup>11</sup> kg event every 130,000 years”. As these values are averaged over the earth's whole history, the impacts have probably been more frequent for the early earth. Compared to stony meteorites, iron meteorites are less abundant but more likely to survive the way through the atmosphere as they are much more resistant to ablation and extreme temperatures. Fragments of iron meteorites can have masses from less than one kilogram to multiple tons and are spread around the impact area.<sup>191</sup> They are also relative resistant to weathering and can stay intact for long periods of time depending on the atmospheric conditions.<sup>192,193</sup> As these fragments weather from the surface towards the core, a large portion protected by the surface oxides and carbonates may stay unaltered. Iron carbonates can act as a passivating layer under the right conditions that were favored by the high CO<sub>2</sub> pressure that is assumed on the early earth.<sup>194</sup> To form mackinawite from elemental iron, a sulfur source is needed. Sulfide containing solutions or H<sub>2</sub>S gas are suitable, but elemental sulfur released by volcanic activity can offer some advantages as discussed in the next chapter.

## 8.2 Surface “black smokers”

In a geological setting on the early earth’s surface where volcanic activity and elemental iron come together a unique combination of chemical reaction pathways becomes possible. Volcanoes offer a source for both very basic as well as very acidic conditions. Mafic or ultramafic volcanic rock contains basic metal oxides that leads to a basic environment upon dissolution whereas sour volcanic gases like SO<sub>2</sub> and SO<sub>3</sub> form sulfurous and sulfuric acid when dissolved in water. In this regard, prebiotic chemistry may benefit from either of these conditions and all pH regions in between. H<sub>2</sub>S may also be a volatile released by volcanic activity and can lead to the formation of elemental sulfur.



These processes have been examined, among others, in the works of Oppenheimer *et al.* regarding the Volcan Poas in Costa Rica.<sup>195</sup>

Elemental iron, although little abundant on the present earth’s surface, may have played a significant role in local areas on the early earth. Assuming an impact of a greater iron meteorite with multiple tons in weight, the chemistry in its surroundings would have been altered for a significant period of time. Iron offers catalytic activity for the reduction of CO<sub>2</sub> using H<sub>2</sub>, but more interestingly the ability to form freshly precipitated mackinawite. It is able to react with sulfur in all oxidation states specifically H<sub>2</sub>S / HS<sup>-</sup> / S<sup>2-</sup>, polysulfides, sulfur, H<sub>2</sub>SO<sub>3</sub> and H<sub>2</sub>SO<sub>4</sub> forming iron sulfides. The reaction with sulfide ions or elemental sulfur at low temperatures leads to the formation of mackinawite whereas the reaction with sulfite or sulfate ions leads to the comparable slow formation of pyrite. Mackinawite in submarine hydrothermal systems is subject to very fast phase transformations what leads to diminishing mackinawite equilibrium quantities and pyrite and pyrrhotite as the main iron sulfide phases.<sup>196</sup> Iron in contact to sulfur can be considered as a “surface black smoker” as it continuously releases nano-mackinawite in aqueous systems. Mackinawite formed from iron and sulfur at low temperatures offers a high surface area what is advantageous for prebiotic important adsorption and reduction processes. The adsorption of amino acids, peptides, carbohydrates and lipids as investigated by Picard *et al.*<sup>61</sup> could lead to increased concentrations on the mackinawite surface and support

condensation reactions that still remain a rather unsolved problem in prebiotic chemistry. The continuous release of only small quantities of nano-mackinawite at a time reduces the extent of agglomeration and preserves high surface areas. Elemental sulfur and iron can both be very resistant to weathering under the right conditions and could stay intact over extended periods of time. This makes it possible for iron and sulfur to accumulate in different areas before they get in contact leading to extensive mackinawite formation for many years. Therefore, even elemental iron that formed by mineralogical alteration processes may have acted as a means for iron sulfide formation. Serpentinization, for example, is a mineralogical alteration process that generates serpentinite minerals from olivine and pyroxene minerals while releasing hydrogen gas. High pressures of hydrogen gas could have led to the formation of elemental iron under suitable conditions.<sup>104,105</sup>

Because natural iron can contain significant amounts of nickel and other metals, the resulting mackinawite would incorporate the corresponding ions what alters its reactivity. As has been shown experimentally, a high nickel content could lead to the formation of other sulfide minerals like heazlewoodite, chalcopyrite or millerite that offer additional reactivities.

The investigations of the interaction between mackinawite and CO<sub>2</sub>/carbonates show that both get adsorbed onto the surface in the dry state and in solution, respectively. Temperatures around 160 °C lead to the formation of thiols while oxidizing the mackinawite particles. The necessary reaction temperature and the resulting reduced carbon species may be altered by the pH value of the solution and the surface composition in regard of other metal ions like Ni<sup>2+</sup> or Cu<sup>2+</sup>. As 160 °C is still a comparable low temperature for CO<sub>2</sub> reduction reactions, the activation of CO<sub>2</sub> by mackinawite as predicted by Dzade *et al.*<sup>124</sup> is very reasonable.

Tochilinite analogues may have formed in basic environments where mackinawite is present or as aqueous alteration products of sulfide minerals on the earth's surface as well as in meteorites. They may have been much more common than today and could have added to the catalytic inventory of the early earth's surface. The activation and reduction of CO<sub>2</sub> in the presence of nano-particulate mackinawite or tochilinite analogues has never been investigated experimentally before. The reduction of CO<sub>2</sub> should be considered as the first step of carbon fixation leading to a yet undefined pool of reduced carbon species depending on the actual conditions.

The subsequent reduction of some of the initial products on mackinawite has been investigated in previous studies that underline the potential of mackinawite in general. These reactions cover for example the reduction of CO<sup>197-199</sup>, aldehydes<sup>200</sup>, citric acid<sup>201</sup>, alpha-keto acids<sup>69</sup>, nitroarenes<sup>36</sup>, ethyne, acetaldehyde, thioglycolic acid, phenylpyruvate<sup>202</sup> and halogenated compounds<sup>34,35</sup>. In this regard, CO<sub>2</sub> should be considered to be only the tip of the iceberg, although very important and that reduction reactions coupled to mackinawite oxidation may have contributed significantly to certain stages during the emergence and evolution of life.



## 9 Summary and outlook

### Synthesis of mackinawite and characterization

A convenient and reliable synthesis for mackinawite nanoparticles has been developed based on the reaction between elemental sulfur and iron. A fine ground mixture of iron and sulfur converts completely to mackinawite within 12 hours at room temperature in a 0.01 M NaCl solution without any side products. This synthetic method offers multiple advantages to the common precipitation, as it enables the investigation of any additional solutes on the mackinawite formation. Moreover, the use of elemental sulfur and iron reduces unintended oxidation that is hardly excluded in the precipitation method. The particle characteristics of mackinawite synthesized from the elements resemble those observed for mackinawite synthesized by precipitation. They also consist of irregular curved platelets that are up to ~150 nm large but only a few nanometers thick. The BET surface area was determined to be between 40 and 80 m<sup>2</sup>/g. A Rietveld fit of the obtained PXRD pattern showed, that the interlayer distance is slightly increased compared to highly crystalline mackinawite. The observation that the addition of NaCl to a mackinawite suspension leads to the release of dissolved Fe<sup>2+</sup>, led to the proposal of a new model concerning the mackinawite-solution-interactions. This model assumes that nanoparticulate mackinawite consists of negatively charged layers due to the presence of iron vacancies within the mackinawite layers. This negative charge is compensated for by cations that are adsorbed onto the surfaces of the particles. The negative charge of the layers leads to increased interlayer spacings. Upon aging and particle growth, the interlayer distance gets smaller and approaches the value of around 5 Å as reported for natural mackinawite.

Further experimental effort may be directed to an understanding of the influence of different dissolved ions during the mackinawite formation and the influence of the formation conditions on its reactivity.

### Carbon fixation on mackinawite

Iron sulfides may have acted as catalysts for reduction reactions relevant for the origin of life and it has been proposed that they may be able to activate CO<sub>2</sub> for its conversion into organic molecules. In this regard, reduction experiments with CO<sub>2</sub> and dissolved carbonates have been carried out in solution and in the dry state. Reactions at temperatures below 80°C did not lead to reduction products detectable by the GC-MS methods applied.

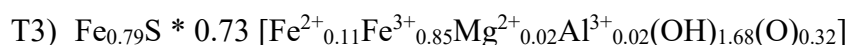
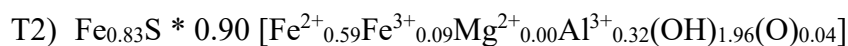
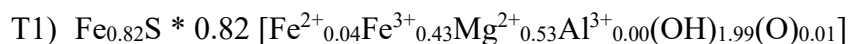
$^{13}\text{C}$ -labelled methane thiol and COS formed at 160 °C within a few hours from adsorbed  $\text{CO}_2$ /carbonate. The reaction between precipitated mackinawite and  $\text{CO}_2$  also led to the formation of methane thiol and COS under acidic conditions at 80 °C. C-C-bond formation has not been observed in the  $^{13}\text{C}$ -labelled experiments, but in some  $^{12}\text{C}$ -experiments. The oxidation products of mackinawite are mainly greigite accompanied by smaller amounts of magnetite and sulfur. These experiments show, that nanoparticulate mackinawite is able to activate and reduce  $\text{CO}_2$  not demanding for any additional electron donor. The oxidation of mackinawite to greigite has not been considered as a significant source of reducing power on the early earth but these results show, that this should be the case at least for the reduction of  $\text{CO}_2$ . Future studies should focus on the analysis of the solution to detect and quantify highly soluble organic molecules like acids and alcohols. As the pH value of the solution has a huge influence on the reduction of  $\text{CO}_2$  and the oxidation of mackinawite, this parameter also needs to be investigated in a comprehensive manner.

#### Synthesis and characterization of nickel and copper sulfides

Besides iron, many more transition metals may be able to react with sulfur in a similar manner. Therefore, experiments have been carried out to investigate the reactivity of different metals towards elemental sulfur at room temperature and at 80 °C. It has been found that iron, nickel, copper, wolfram, cadmium, magnesium and molybdenum do react with elemental sulfur at a maximum of 80 °C whereas aluminum, manganese, zinc and cobalt do not. As copper and nickel sulfides have also been proposed as prebiotic catalysts, experiments have been carried out to investigate the phases that form in systems of  $\text{Ni} + \text{S}$  and  $\text{Fe} + \text{Cu} + \text{S}$ . The results show that millerite and heazlewoodite form at 80 °C from Ni and S. In the ternary system, chalcopyrite is the main product, but a variety of phases forms. Controlling the selectivity of reactions with copper and nickel seems to be challenging compared to the equimolar reaction between iron and sulfur forming only mackinawite. For prebiotic chemistry, the observed reactivity allows the formation of highly reactive nanoparticulate sulfides with compositions and structures depending on the composition of the parent metal and adds a huge diversity to the possible mineral repertoire. Future studies should investigate the selectivity control of the reactions between different sulfides and the reactivity changes that result from the different structures and compositions.

### Synthesis of tochilinite analogues and characterization

Tochilinite is a complex hybrid mineral composed of mackinawite-like and brucite-like layers. Tochilinite analogues may have formed in basic environments where mackinawite was present or as aqueous alteration products of sulfide minerals on the early earth's surface. The theoretical formula for tochilinite is  $\text{Fe}_{(1-e)}\text{S} * x [\text{Fe}^{2+}_a\text{Fe}^{3+}_b\text{Mg}^{2+}_c\text{Al}^{3+}_d(\text{OH})_2]$  with  $\text{Fe}_{0.8}\text{S} * 0.83 [\text{Mg}_{0.71}\text{Fe}_{0.29}(\text{OH})_2]$  as an example for the mineral as described by Organova *et al.*<sup>76</sup> The synthesis of tochilinite has been described before but a proper characterization with an elemental analysis was missing. Moreover, the distribution of the ions in the hydroxide layers has not been investigated before. In this work, three different pure tochilinite analogues have been obtained by synthetic methods that allow for the control of the composition of the hydroxide layers. The determined formulas are shown below:



Elemental analysis and Mößbauer spectroscopy show that the compositions obtained fit to theoretical compositions of tochilinite in regard of the amount of iron vacancies, the volume ratio of hydroxide to sulfide layers and the structures of the sulfide and hydroxide layers. TEM and SEM investigations show that the obtained powders consist of nanoparticles with BET surface areas between 20 and 40 m<sup>2</sup>/g. The thermal stability was investigated by TGA/DSC analysis which declines from T1 to T3.

To complete this series of tochilinite analogues, future works should find a suitable synthetic method to obtain a Mg<sup>2+</sup> and Al<sup>3+</sup> rich sample what has not been achieved in this work. Furthermore, there are many complex hybrid sulfide minerals that have not been synthesized so far and that may be accessible by the synthetic methods elaborated here.

### Carbon fixation on tochilinite analogues

Like mackinawite, tochilinite analogues may offer the catalytic potential for the activation and reduction of CO<sub>2</sub>. As they are much more stable and therefore suited for reactions at higher temperatures, Fischer-Tropsch-type reactions have been carried out in an atmosphere of CO<sub>2</sub> and H<sub>2</sub> above 200°C at 35 bar total pressure. The experiments showed that tochilinite analogues are able to catalyze FTT reactions between CO<sub>2</sub> and H<sub>2</sub>. At 250 °C,

only methanol and ethanol formed after 4 days but already at 264 °C long chain alkanes were identified. The tochilinite analogues decomposed at higher temperatures and therefore active material was lost during the reaction. The decomposition increases with temperature what leads to a decrease of the total turnover numbers already at 300 °C compared to 264 °C. Nevertheless, this is the first report of any iron sulfide catalyzing the reaction between CO<sub>2</sub> and H<sub>2</sub> in a Fischer-Tropsch-type reaction.

#### Relevance to the prebiotic and origin of life chemistry

The reaction between metals and elemental sulfur may have been a rather unusual reaction on the early earth, but still has the potential to significantly contribute to the inventory of organic compounds. Impacts of greater iron meteorites have been common during earth's history and especially during the time of the Late Heavy Bombardment. Compared to stony meteorites, iron meteorites are less abundant but more likely to survive the way through the atmosphere as they are much more resistant to ablation and extreme temperatures. Fragments of iron meteorites can have masses from less than one kilogram to multiple tons and are spread around the impact area.<sup>191</sup> Volcanic activity is a common feature of prebiotic chemistry and can lead to the formation of elemental sulfur. If iron and sulfur get in contact, nanoparticulate mackinawite and probably tochilinite analogues will form that would lead to the reduction of CO<sub>2</sub> under appropriate conditions. The reduction of CO<sub>2</sub> should be considered as the first step of carbon fixation leading to a yet undefined pool of reduced carbon species depending on the actual conditions. The subsequent reduction of some of the initial products on mackinawite has been investigated in previous studies that underline the potential of mackinawite in general. These reactions cover for example the reduction of CO<sup>197-199</sup>, aldehydes<sup>200</sup>, citric acid<sup>201</sup>, alpha-keto acids<sup>69</sup>, nitroarenes<sup>36</sup>, ethyne, acetaldehyde, thioglycolic acid, phenylpyruvate<sup>202</sup> and halogenated compounds<sup>34,35</sup>. In this regard CO<sub>2</sub> should only be considered as the tip of the iceberg, although very important and that reduction reactions coupled to mackinawite oxidation may have contributed significantly to certain stages during the emergence and evolution of life.

## 10 Experimental section

### 10.1 Metal sulfide syntheses

#### 10.1.1 Standard procedure

0.88 g of a thoroughly ground mixture of powdered elemental iron (0.56 g, 10.0 mmol), powdered elemental sulfur (0.32 g, 10.0 mmol) and sodium chloride (0.06 g, 1.0 mmol) were filled into a 25 ml microwave vial and covered by an aluminum cap with a septum. The atmosphere was replaced by nitrogen gas for three times and deaerated water was added using a syringe. The resulting suspension was held at the desired temperature for the intended reaction time without any disturbance. When the reactions had finished, the solid phases were separated by filtration through a glass frit and washed either only with water or successively with water, ethanol, acetone and diethyl ether. The solids were dried under a stream of nitrogen gas passing through a funnel that completely covered the top of the frit. After the solids had dried, the funnel was removed very cautiously. If the solids turned warm upon air contact, the funnel was put back on the frit until it had cooled down again. This procedure was repeated until the sample stopped to heat up upon air contact.

#### 10.1.2 Iron sulfides

##### FeS\_1

Mackinawite was synthesized following the standard procedure overnight at room temperature. The obtained solids were washed only with distilled water.

##### FeS\_2

In a steel autoclave with a Teflon inlet iron (3.5 g, 62.67 mmol) and sodium sulfide nonahydrate (11.5 g, 95.8 mmol) were charged with 50 ml deionized water. The autoclave was sealed and heated to 160 °C for 3 days. After this time, the autoclave was left to cool down to room temperature. The solids were isolated by filtration through a glass frit and washed with water. The solids looked metallic and were dried in a stream of nitrogen gas.

### **FeS\_k\_1 to FeS\_k\_10**

0.88 g of a mixture of elemental iron (0.56 g, 10.0 mmol) and elemental sulfur (0.32 g, 10.0 mmol) were charged with 25 ml of deionized water following the standard procedure. The resulting suspension was held at room temperature for a certain period as is listed in table 38.

Table 38: Reaction times for the kinetic investigation of mackinawite formation from iron and sulfur.

Reaction	Reaction time / hours
FeS_k_1	0
FeS_k_2	4
FeS_k_3	7
FeS_k_4	12
FeS_k_5	18
FeS_k_6	21
FeS_k_7	24
FeS_k_8	26
FeS_k_9	28
FeS_k_10	96

### **FeS\_NaCl\_1 to FeS\_NaCl\_5**

0.88 g of a thoroughly ground mixture of powdered elemental iron (0.56 g, 10.0 mmol), powdered elemental sulfur (0.32 g, 10.0 mmol) and sodium chloride as listed in table 39 was charged with 20 ml of deionized water following the standard procedure. The resulting suspension was held at room temperature for 1 day. The obtained solids were washed successively with water, ethanol, acetone and diethyl ether.

Table 39: Amounts of sodium chloride in the syntheses of mackinawite samples FeS\_NaCl\_1 to FeS\_NaCl\_5 from iron and sulfur.

Reaction	NaCl / mg
FeS_NaCl_1	6
FeS_NaCl_2	9
FeS_NaCl_3	12
FeS_NaCl_4	30
FeS_NaCl_5	60

### **FeS\_KCl**

0.88 g of a thoroughly ground mixture of powdered elemental iron (0.56 g, 10.0 mmol), powdered elemental sulfur (0.32 g, 10.0 mmol) and potassium chloride (0.015 g, 0.2 mmol) was charged with 20 ml of deionized water following the standard procedure. The resulting suspension was held at room temperature for 1 day. The obtained solids were washed successively with water, ethanol, acetone and diethyl ether.

### **FeS\_Na<sub>2</sub>SO<sub>4</sub>**

0.88 g of a thoroughly ground mixture of powdered elemental iron (0.56 g, 10.0 mmol), powdered elemental sulfur (0.32 g, 10.0 mmol) and sodium sulfate (0.028 g, 0.2 mmol) was charged with 20 ml of deionized water following the standard procedure. The resulting suspension was held at room temperature for 1 day. The obtained solids were washed successively with water, ethanol, acetone and diethyl ether.

### **FeS\_NH<sub>4</sub>Cl**

0.88 g of a thoroughly ground mixture of powdered elemental iron (0.56 g, 10.0 mmol), powdered elemental sulfur (0.32 g, 10.0 mmol) and ammonium chloride (0.020 g, 0.4 mmol) was charged with 20 ml of deionized water following the standard procedure. The resulting suspension was held at room temperature for 1 day. The obtained solids were washed successively with water, ethanol, acetone and diethyl ether.

### **FeS\_KCN**

0.88 g of a thoroughly ground mixture of powdered elemental iron (0.56 g, 10.0 mmol), powdered elemental sulfur (0.32 g, 10.0 mmol) and potassium cyanide (0.013 g, 0.2 mmol) was charged with 20 ml of deionized water following the standard procedure. The resulting suspension was held at room temperature for 1 day. The obtained solids were washed successively with water, ethanol, acetone and diethyl ether.

### **FeS\_NaHCO<sub>3</sub>**

0.88 g of a thoroughly ground mixture of powdered elemental iron (0.56 g, 10.0 mmol), powdered elemental sulfur (0.32 g, 10.0 mmol) and potassium cyanide (0.017 g, 0.2 mmol) was charged with 20 ml of deionized water following the standard procedure. The resulting suspension was held at room temperature for 1 day. The obtained solids were washed successively with water, ethanol, acetone and diethyl ether.

### **FeS\_Ox\_1**

Mackinawite was synthesized following the standard procedure overnight at room temperature. A small sample was taken with a syringe and most of the contained water was removed with a PET filter. The sample was transferred quickly into a corundum sample holder and into the TGA device. The sample was dried in a stream of air without any heating.

### **FeS\_Ox\_2**

Mackinawite was synthesized following the standard procedure overnight at room temperature. A small sample was taken with a syringe and most of the contained water was removed with a PET filter. The sample was transferred quickly into a corundum sample holder and into the TGA device. The sample was dried in a stream of nitrogen gas and then exposed to air without external heating.



### **FeS\_Ox\_3**

Mackinawite was synthesized following the standard procedure overnight at room temperature. A small sample was taken with a syringe and most of the contained water was removed with a PET filter. The sample was transferred quickly into a corundum sample holder and into the TGA device. The sample was dried in a stream of nitrogen gas gas and then exposed to air.

### **FeS\_Ox\_4**

Mackinawite was synthesized following the standard procedure overnight at room temperature. A small sample was taken with a syringe and most of the contained water was removed with a PET filter. The sample was transferred quickly into a corundum sample holder and into the TGA device. The sample was dried in a stream of nitrogen gas gas and then heated with 1 K/min to 500 °C in air.

### **FeS\_Ox\_5**

Mackinawite was synthesized following the standard procedure overnight at room temperature. The sample was isolated by filtration and washed successively with water, ethanol, acetone and diethyl ether. A sample of around 30 mg was transferred into a corundum sample holder and into the TGA device. The sample was heated with 1 K/min to 500 °C in air.

### **FeS\_Ox\_6**

Mackinawite was synthesized following the standard procedure overnight at room temperature. The sample was isolated by filtration and washed successively with water, ethanol, acetone and diethyl ether. The deactivated sample was stored in a covered beaker for one month open to the atmosphere.

### **FeS\_Ox\_7**

Mackinawite was synthesized following the standard procedure overnight at room temperature. A small sample was taken with a syringe and most of the contained water was

removed with a PET filter. The sample was transferred quickly into a corundum sample holder and into the TGA device. The sample was dried in a stream of nitrogen gas for 10 hours and then exposed to air for one hour.

### **FeS\_Ox\_8**

Mackinawite was synthesized following the standard procedure overnight at room temperature. A small sample was taken with a syringe and most of the contained water was removed with a PET filter. The sample was transferred quickly into a corundum sample holder and into the TGA device. The sample was dried in a stream of nitrogen gas for 10 hours and then exposed to air for one hour.

### **FeS\_Ox\_9**

Mackinawite was synthesized following the standard procedure overnight at room temperature. Afterwards, the cap of the vial was removed and the vial was covered with a beaker and was left untouched for one week. During this time, iron sulfide attached to the vial walls above the solution turned brown but the bulk of the sample sitting on the bottom of the vial remained black.

### **FeS\_Ox\_10**

Mackinawite was synthesized following the standard procedure but using pretreated ion powder overnight at room temperature. On the next day, the vial was heated to 80 °C in the original solution for one day. Afterwards, the solids were removed by filtration, washed successively with water, ethanol, acetone and diethyl ether and dried and deactivated following the standard procedure.

### **FeS\_Ox\_11**

Mackinawite was synthesized following the standard procedure but using pretreated ion powder overnight at room temperature. On the next day, the vial was heated to 80 °C in the original solution for one week. Afterwards, the solids were removed by filtration,

washed successively with water, ethanol, acetone and diethyl ether and dried and deactivated following the standard procedure.

### **MnS\_1**

0.87 g of a thoroughly ground mixture of powdered elemental manganese (0.55 g, 10.0 mmol) and powdered elemental sulfur (0.32 g, 10.0 mmol) was charged with 20 ml of deionized water following the standard procedure. The resulting suspension was held at room temperature for 4 days. The isolated solids were washed only with distilled water. No change compared to the initial mixture was observed.

### **MnS\_2**

0.87 g of a thoroughly ground mixture of powdered elemental manganese (0.55 g, 10.0 mmol) and powdered elemental sulfur (0.32 g, 10.0 mmol) was charged with 20 ml of deionized water following the standard procedure. The resulting suspension was held at 80 °C for 4 days. The isolated solids were washed only with distilled water. No change regarding the start of the reaction was observed.

### **CoS\_1**

0.91 g of a thoroughly ground mixture of powdered elemental cobalt (0.59 g, 10.0 mmol) and powdered elemental sulfur (0.32 g, 10.0 mmol) was charged with 20 ml of deionized water following the standard procedure. The resulting suspension was held at room temperature for 4 days. The black isolated solids were washed only with distilled water.

### **CoS\_2**

0.91 g of a thoroughly ground mixture of powdered elemental cobalt (0.59 g, 10.0 mmol) and powdered elemental sulfur (0.32 g, 10.0 mmol) was charged with 20 ml of deionized water following the standard procedure. The resulting suspension was held at 80 °C for 4 days. The black isolated solids were washed only with distilled water.

### **NiS\_1**

0.95 g of a thoroughly ground mixture of powdered elemental nickel (0.585 g, 10.0 mmol) and powdered elemental sulfur (0.32 g, 10.0 mmol) was charged with 20 ml of deionized water following the standard procedure. The resulting suspension was held at room temperature for 4 days. The black isolated solids were washed only with distilled water.

### **NiS\_2**

0.95 g of a thoroughly ground mixture of powdered elemental nickel (0.585 g, 10.0 mmol) and powdered elemental sulfur (0.32 g, 10.0 mmol) was charged with 20 ml of deionized water following the standard procedure. The resulting suspension was held at 80 °C for 4 days. The black isolated solids were washed only with distilled water.

### **CuS\_1**

0.96 g of a thoroughly ground mixture of powdered elemental copper (0.64 g, 10.0 mmol) and powdered elemental sulfur (0.32 g, 10.0 mmol) was charged with 20 ml of deionized water following the standard procedure. The resulting suspension was held at room temperature for 4 days. The black isolated solids were washed only with distilled water.

### **ZnS\_1**

0.97 g of a thoroughly ground mixture of powdered elemental zinc (0.65 g, 10.0 mmol) and powdered elemental sulfur (0.32 g, 10.0 mmol) was charged with 20 ml of deionized water following the standard procedure. The resulting suspension was held at room temperature for 4 days. The isolated solids were washed only with distilled water. No change compared to the initial mixture was observed.

### **ZnS\_2**

0.97 g of a thoroughly ground mixture of powdered elemental zinc (0.65 g, 10.0 mmol) and powdered elemental sulfur (0.32 g, 10.0 mmol) was charged with 20 ml of deionized

water following the standard procedure. The resulting suspension was held at 80 °C for 4 days. The isolated solids were washed only with distilled water. No change compared to the initial mixture was observed.

### **MoS<sub>1</sub>**

1.0 g of a thoroughly ground mixture of powdered elemental molybdenum (0.96 g, 10.0 mmol) and powdered elemental sulfur (0.64 g, 20.0 mmol) was charged with 20 ml of deionized water following the standard procedure. The resulting suspension was held at room temperature for 4 days. Overnight, the solution in the vial had turned deep blue. The isolated solids were washed only with distilled water.

### **CdS<sub>1</sub>**

Chips of elemental cadmium (1.12 g, 10.0 mmol) were mixed with elemental sulfur (0.32 g, 10.0 mmol) in a mortar to ensure close contact between both solids. This mixture was transferred into a 25 ml microwave vial and charged with 20 ml of deionized water following the standard procedure. The resulting suspension was held at room temperature for 4 days. On the surface of the chips bright orange spots appeared overnight that nearly covered them completely after 4 days.

### **WS<sub>1</sub>**

1.0 g of a thoroughly ground mixture of powdered elemental tungsten (2.48 g, 10.0 mmol) and powdered elemental sulfur (0.64 g, 20.0 mmol) was charged with 20 ml of deionized water following the standard procedure. The resulting suspension was held at room temperature for 4 days. The dark grey isolated solids were washed only with distilled water.

### **Mg<sub>1</sub>**

0.55 g of a thoroughly ground mixture of powdered elemental magnesium (0.23 g, 10.0 mmol) and powdered elemental sulfur (0.32 g, 10.0 mmol) was charged with 20 ml of deionized water following the standard procedure. The resulting suspension was held at room temperature for 4 days. The solution quickly turned yellow and the pH increased.

After 4 days, the elemental sulfur nearly completely dissolved and the amount of magnesium had decreased substantially.

### Al\_1

0.59 g of a thoroughly ground mixture of powdered elemental aluminum (0.270 g, 10.0 mmol) and powdered elemental sulfur (0.32 g, 10.0 mmol) was charged with 20 ml of deionized water following the standard procedure. The resulting suspension was held at room temperature for 4 days. No change compared to the initial mixture was observed.

### Al\_2

0.95 g of a thoroughly ground mixture of powdered elemental nickel (0.585 g, 10.0 mmol) and powdered elemental sulfur (0.32 g, 10.0 mmol) was charged with 20 ml of deionized water following the standard procedure. The resulting suspension was held at 80 °C for 4 days. No change compared to the initial mixture was observed.

## 10.2 Binary sulfide synthesis from Fe, Cu, Ni and S

All syntheses towards binary sulfides from Fe, Cu, Ni and S were carried out following the standard procedure using fine ground mixtures of the starting materials. Reaction times, temperatures and the amounts of sodium chloride are summarized in tables 40 to 42. In experiments MB\_1 to MB\_8 two grams of a fine ground mixture of nickel (17.55 g, 300 mmol) and sulfur (6.4 g, 200 mmol) were used.

Table 40: Sodium chloride concentration, reaction temperatures and times for experiments MB\_1 to MB\_8.

Exp.	Concentration of NaCl / mol * l <sup>-1</sup>	Temperature / °C	Time / days
MB_1	0	25	1

MB_2	0.01	25	1
MB_3	0	80	1
MB_4	0.01	80	1
MB_5	0	25	3
MB_6	0.01	25	3
MB_7	0.01	80	3
MB_8	0.17	25	3

In experiments MB\_9 to MB\_17 two grams of a fine ground mixture of copper (6.35 g, 100 mmol), iron (5.56 g, 100 mmol) and sulfur (6.4 g, 200 mmol) were used.

Table 41: Sodium chloride concentration, reaction temperatures and times for experiments MB\_9 to MB\_17.

Exp.	Concentration of NaCl / mol * l <sup>-1</sup>	Temp. / °C	Time / days
MB_9	0	25	1
MB_10	0.01	25	1
MB_11	0	80	1
MB_12	0.01	80	1
MB_13	0	25	3
MB_14	0.01	25	3
MB_15	0	80	3
MB_16	0.01	80	3
MB_17	0.17	25	3

Table 42: Sodium chloride concentration, reaction temperatures and times for experiments MB\_18 to MB\_23.

Exp.	Concentration of NaCl / mol * l <sup>-1</sup>	Temp. / °C	Time / days
MB_18	0.01	25	1
MB_19	0.01	25	4
MB_20	0.01	25	10
MB_21	0.01	80	1
MB_22	0.01	80	4
MB_23	0.01	80	10

In experiments MB\_9 to MB\_17 two grams of a fine ground mixture of copper (6.35 g, 100 mmol), iron (11.12 g, 200 mmol) and sulfur (9.6 g, 300 mmol) were used.

### 10.3 CO<sub>2</sub> / carbonate reduction experiments

#### RED\_1

1.00 g of mackinawite was prepared following the standard procedure at room temperature overnight in 10 ml deoxygenated water. <sup>13</sup>C-labeled sodium carbonate (0.212 g, 2 mmol) was placed in another vial and the atmosphere was replaced by nitrogen gas. The carbonate was dissolved in 10 ml deoxygenated water and the obtained solution added to the mackinawite suspension. The pH value of the resulting suspension was adjusted with diluted phosphorous acid to a value around 7 and it was held at 40 °C for 4 days. A 25 ml GC-MS vial was evacuated through a canulla and the headspace of the reaction vial was transferred by connecting both vials with a double-edged canulla that has been previously purged with nitrogen gas. After around 5 minutes equilibrium pressure in both vials was reached and the GC-MS vial was removed. The head-space was analyzed in the GC-MS using the head-space sampler and subjected to the operation conditions as described in the materials section.



## **RED\_2**

1.00 g of mackinawite was prepared following the standard procedure at room temperature overnight in 2 ml deoxygenated water and dried under reduced pressure afterwards.  $^{13}\text{C}$ -labeled sodium carbonate (0.5 g, 5 mmol) was placed in another vial which was evacuated. The carbonate was charged with 10 ml concentrated phosphorus acid (ca. 30%) and the forming gas was collected with two 25 ml syringes. The evacuated mackinawite vial was filled with the  $^{13}\text{C}$ -labelled  $\text{CO}_2$  and held at 40 °C for 4 days. A 25 ml GC-MS vial was evacuated through a cannula and the headspace of the reaction vial was transferred by connecting both vials with a double-edged cannula that has been previously purged with nitrogen gas. After around 5 minutes equilibrium pressure in both vials was reached and the GC-MS vial was removed. The head-space was analyzed in the GC-MS using the head-space sampler and subjected to the operation conditions as described in the materials section.

## **RED\_3**

1.00 g of mackinawite was prepared following the standard procedure at room temperature overnight in 2 ml deoxygenated water and dried under reduced pressure afterwards.  $^{13}\text{C}$ -labeled sodium carbonate (0.5 g, 5 mmol) was placed in another vial which was evacuated. The carbonate was charged with 10 ml concentrated phosphorus acid (ca. 30%) and the forming gas was collected with two 25 ml syringes. The evacuated mackinawite vial was filled with the  $^{13}\text{C}$ -labelled  $\text{CO}_2$  and held at 40 °C for 2 months. A 25 ml GC-MS vial was evacuated through a cannula and the headspace of the reaction vial was transferred by connecting both vials with a double-edged cannula that has been previously purged with nitrogen gas. After around 5 minutes equilibrium pressure in both vials was reached and the GC-MS vial was removed. The head-space was analyzed in the GC-MS using the head-space sampler and subjected to the operation conditions as described in the materials section.

#### **RED\_4**

1.00 g of mackinawite was prepared following the standard procedure at room temperature overnight in 10 ml deoxygenated water.  $^{13}\text{C}$ -labeled sodium carbonate (0.212 g, 2 mmol) was placed in another vial and the atmosphere was replaced by nitrogen gas. The carbonate was dissolved in 10 ml deoxygenated water and the obtained solution added to the mackinawite suspension. The pH value of the resulting suspension was adjusted with diluted phosphorous acid to a value around 7 and it was held at 80 °C for 4 days. A 25 ml GC-MS vial was evacuated through a cannula and the headspace of the reaction vial was transferred by connecting both vials with a double-edged cannula that has been previously purged with nitrogen gas. After around 5 minutes equilibrium pressure in both vials was reached and the GC-MS vial was removed. The head-space was analyzed in the GC-MS using the head-space sampler and subjected to the operation conditions as described in the materials section.

#### **RED\_5**

1.00 g of mackinawite was prepared following the standard procedure at room temperature overnight in 2 ml deoxygenated water and dried under reduced pressure afterwards.  $^{13}\text{C}$ -labeled sodium carbonate (0.5 g, 5 mmol) was placed in another vial which was evacuated. The carbonate was charged with 10 ml concentrated phosphorus acid (ca. 30%) and the forming gas was collected with two 25 ml syringes. The evacuated mackinawite vial was filled with the  $^{13}\text{C}$ -labelled  $\text{CO}_2$  and held at 80 °C for 4 days. A 25 ml GC-MS vial was evacuated through a cannula and the headspace of the reaction vial was transferred by connecting both vials with a double-edged cannula that has been previously purged with nitrogen gas. After around 5 minutes equilibrium pressure in both vials was reached and the GC-MS vial was removed. The head-space was analyzed in the GC-MS using the head-space sampler and subjected to the operation conditions as described in the materials section.

#### **RED\_6**

1.00 g of mackinawite was prepared following the standard procedure at room temperature overnight in 10 ml deoxygenated water.  $^{12}\text{C}$  sodium carbonate (0.212 g, 2 mmol) was

placed in another vial and the atmosphere was replaced by nitrogen gas. The carbonate was dissolved in 10 ml deoxygenated water and the obtained solution added to the mackinawite suspension. The pH value of the resulting suspension was adjusted with diluted phosphorous acid to a value around 7 and it was held at room temperature for 1 day. A distillation apparatus was set up composed of a 10 ml oblong flask connected via a distillation to a 5 ml round bottom flask. The 5 ml flask was cooled in a DCM/liquid nitrogen cooling bath and filled with 1 ml of purified DCM. The mackinawite was isolated by filtration and quickly transferred into the 10 ml flask which was connected to the distillation bridge. The single parts were connected by Teflon sleeves. The mackinawite vial was heated to 160 °C for while all volatiles that were released could dissolve in the liquid DCM phase in the small vial. During the distillation some droplets of water formed in the distillation bridge. After three hours, the bridge was removed and the DCM solution transferred into a 1 ml GC-MS vial. The solution was analyzed in the GC-MS using the solution auto sampler and subjected to the operation conditions as described in the materials section.

## **RED\_7**

1.00 g of mackinawite was prepared following the standard procedure at room temperature overnight in 10 ml deoxygenated water. <sup>13</sup>C-labeled sodium carbonate (0.212 g, 2 mmol) was placed in another vial and the atmosphere was replaced by nitrogen gas. The carbonate was dissolved in 10 ml deoxygenated water and the obtained solution added to the mackinawite suspension. The pH value of the resulting suspension was adjusted with diluted phosphorous acid to a value around 7 and it was held at room temperature for 1 day. A distillation apparatus was set up composed of a 10 ml oblong flask connected via a distillation to a 5 ml round bottom flask. The 5 ml flask was cooled in a DCM/liquid nitrogen cooling bath and filled with 1 ml of purified DCM. The mackinawite was isolated by filtration and quickly transferred into the 10 ml flask which was connected to the distillation bridge. The single parts were connected by Teflon sleeves. The mackinawite vial was heated to 160 °C for while all volatiles that were released could dissolve in the liquid DCM phase in the small vial. During the distillation some droplets of water formed in the distillation bridge. After three hours, the bridge was removed and the DCM solution transferred into a 1 ml GC-MS vial. The solution was analyzed in the GC-MS using the

solution auto sampler and subjected to the operation conditions as described in the materials section.

### **RED\_8**

1.00 g of mackinawite was prepared following the standard procedure at room temperature overnight in 10 ml deoxygenated water.  $^{12}\text{C}$  sodium carbonate (0.212 g, 2 mmol) was placed in another vial and the atmosphere was replaced by nitrogen gas. The carbonate was dissolved in 10 ml deoxygenated water and the obtained solution added to the mackinawite suspension. The pH value of the resulting suspension was adjusted with diluted phosphorous acid to a value around 7 and it was held at room temperature for 1 day. A distillation apparatus was set up composed of a 10 ml oblong flask connected via a distillation to a 5 ml round bottom flask. The 5 ml flask was cooled in a DCM/liquid nitrogen cooling bath and filled with 1 ml of purified DCM. The mackinawite was isolated by filtration and quickly transferred into the 10 ml flask which was connected to the distillation bridge. The single parts were connected by Teflon sleeves. The mackinawite vial was heated to 160 °C for while all volatiles that were released could dissolve in the liquid DCM phase in the small vial. During the distillation some droplets of water formed in the distillation bridge. After three hours, the bridge was removed and the DCM solution transferred into a 1 ml GC-MS vial. The solution was analyzed in the GC-MS using the solution auto sampler and subjected to the operation conditions as described in the materials section.

### **RED\_9**

1.00 g of mackinawite was prepared following the standard procedure at room temperature overnight in 2 ml deoxygenated water and dried under reduced pressure afterwards.  $^{13}\text{C}$ -labeled sodium carbonate (0.5 g, 5 mmol) was placed in another vial which was evacuated. The carbonate was charged with 10 ml concentrated phosphorus acid (ca. 30%) and the forming gas was collected with two 25 ml syringes. The evacuated mackinawite vial was filled with the  $^{13}\text{C}$ -labelled  $\text{CO}_2$  and held at 160 °C for 1 hour. A 25 ml GC-MS vial was evacuated through a canulla and the headspace of the reaction vial was transferred by connecting both vials with a double-edged canulla that has been previously

purged with nitrogen gas. After around 5 minutes equilibrium pressure in both vials was reached and the GC-MS vial was removed. The head-space was analyzed in the GC-MS using the head-space sampler and subjected to the operation conditions as described in the materials section.

### **RED\_10**

Around 10 g of untreated iron powder was placed in a 25 ml microwave vial. The vial was evacuated and charged with 10 ml of concentrated phosphorous acid. A lot of gas emerged from the iron dissolution which was captured in two 25 ml syringes. The gas was transferred into an evacuated 25 ml GC-MS vial. The head-space was analyzed in the GC-MS using the head-space sampler and subjected to the operation conditions as described in the materials section.

### **RED\_11**

1.00 g of mackinawite was prepared following the standard procedure at room temperature overnight in 10 ml deoxygenated water. <sup>13</sup>C-labeled sodium carbonate (0.212 g, 2 mmol) was placed in another vial and the atmosphere was replaced by nitrogen gas. The carbonate was dissolved in 10 ml deoxygenated water and the obtained solution added to the mackinawite suspension. The pH value of the resulting suspension was adjusted with diluted hydrochloric acid to a value around 7 and it was held at 40 °C for 2 weeks. A 25 ml GC-MS vial was evacuated through a canulla and the headspace of the reaction vial was transferred by connecting both vials with a double-edged canulla that has been previously purged with nitrogen gas. After around 5 minutes equilibrium pressure in both vials was reached and the GC-MS vial was removed. The head-space was analyzed in the GC-MS using the head-space sampler and subjected to the operation conditions as described in the materials section.

### **RED\_12**

1.00 g of mackinawite was prepared following the standard procedure using pretreated iron powder at room temperature overnight in 10 ml deoxygenated water. Non-labelled sodium carbonate (0.212 g, 2 mmol) was placed in another vial and the atmosphere was

replaced by nitrogen gas. The carbonate was dissolved in 10 ml deoxygenated water and the obtained solution added to the mackinawite suspension. The pH value of the resulting suspension was adjusted with diluted hydrochloric acid to a value around 3 and it was held at 40 °C for 4 days. A 25 ml GC-MS vial was evacuated through a canulla and the headspace of the reaction vial was transferred by connecting both vials with a double-edged canulla that has been previously purged with nitrogen gas. After around 5 minutes equilibrium pressure in both vials was reached and the GC-MS vial was removed. The head-space was analyzed in the GC-MS using the head-space sampler and subjected to the operation conditions as described in the materials section.

### **RED\_13**

1.00 g of mackinawite was prepared following the standard procedure using pretreated iron powder at room temperature overnight in 10 ml deoxygenated water. <sup>13</sup>C-labelled sodium carbonate (0.212 g, 2 mmol) was placed in another vial and the atmosphere was replaced by nitrogen gas. The carbonate was dissolved in 10 ml deoxygenated water and the obtained solution added to the mackinawite suspension. The pH value of the resulting suspension was adjusted with diluted hydrochloric acid to a value around 3 and it was held at 40 °C for 4 days. A 25 ml GC-MS vial was evacuated through a canulla and the headspace of the reaction vial was transferred by connecting both vials with a double-edged canulla that has been previously purged with nitrogen gas. After around 5 minutes equilibrium pressure in both vials was reached and the GC-MS vial was removed. The head-space was analyzed in the GC-MS using the head-space sampler and subjected to the operation conditions as described in the materials section.

### **RED\_14**

1.00 g of mackinawite was prepared following the standard procedure at room temperature overnight in 2 ml deoxygenated water and dried under reduced pressure afterwards. <sup>13</sup>C-labeled sodium carbonate (0.5 g, 5 mmol) was placed in another vial which was evacuated. The carbonate was charged with 10 ml concentrated phosphorus acid (ca. 30%) and the forming gas was collected with two 25 ml syringes. The evacuated mackinawite vial was filled with the <sup>13</sup>C-labelled CO<sub>2</sub> and held at 80 °C for 2 weeks. A 25 ml GC-MS

vial was evacuated through a canulla and the headspace of the reaction vial was transferred by connecting both vials with a double-edged canulla that has been previously purged with nitrogen gas. After around 5 minutes equilibrium pressure in both vials was reached and the GC-MS vial was removed. The head-space was analyzed in the GC-MS using the head-space sampler and subjected to the operation conditions as described in the materials section.

### **RED\_15 to RED\_17**

1.00 g of mackinawite was prepared following the standard procedure using pretreated iron powder at room temperature overnight in 10 ml deoxygenated water. To the initial solution, 1 ml of a saturated  $\text{NaHCO}_3$  solution was added and the solids kept at room temperature for 3 days. The solids were then isolated by filtration, dried in a stream of  $\text{N}_2$  gas and heated to 140 °C, 180 °C and 250 °C in  $\text{N}_2$  atmosphere for 2 hours, respectively.

### **RED\_18**

Iron sulfide synthesis was carried out by precipitation from  $(\text{NH}_4)_2\text{Fe}(\text{SO}_4)_2$  (3.9213 g, 10 mmol) and sodium sulfide nonahydrate (2.402 g, 10 mmol) each dissolved in 12 ml deaerated water in a 25 ml microwave vial under nitrogen gas atmosphere. The solutions were combined and a black precipitate formed. The vials were centrifuged and the solutions removed with a syringe and pressure compensation by nitrogen gas. To the solid iron sulfide phase 20 ml of a 0.1 M deaerated solution of  $\text{NaHCO}_3$  was added and the resulting suspension kept at 80 °C for two weeks. A 25 ml GC-MS vial was evacuated through a canulla and the headspace of the reaction vial was transferred by connecting both vials with a double-edged canulla that has been previously purged with nitrogen gas. After around 5 minutes equilibrium pressure in both vials was reached and the GC-MS vial was removed. The head-space was analyzed in the GC-MS using the head-space sampler and subjected to the operation conditions as described in the materials section.

### **RED\_19**

Iron sulfide synthesis was carried out by precipitation from  $(\text{NH}_4)_2\text{Fe}(\text{SO}_4)_2$  (3.9213 g, 10 mmol) and sodium sulfide nonahydrate (2.402 g, 10 mmol) each dissolved in 12 ml de-aerated water in a 25 ml microwave vial under nitrogen gas atmosphere. The solutions were combined and a black precipitate formed. The vials were centrifuged and the solutions removed with a syringe and pressure compensation by nitrogen gas. To the solid iron sulfide phase 20 ml of a 0.1 M de-aerated solution of  $\text{NaHCO}_3$  was added and the pH value was adjusted with diluted hydrochloric acid to 3. The resulting suspension kept at 80 °C for two weeks. A 25 ml GC-MS vial was evacuated through a cannula and the headspace of the reaction vial was transferred by connecting both vials with a double-edged cannula that has been previously purged with nitrogen gas. After around 5 minutes equilibrium pressure in both vials was reached and the GC-MS vial was removed. The head-space was analyzed in the GC-MS using the head-space sampler and subjected to the operation conditions as described in the materials section.

#### **RED\_20**

Iron sulfide synthesis was carried out by precipitation from  $(\text{NH}_4)_2\text{Fe}(\text{SO}_4)_2$  (3.9213 g, 10 mmol) and sodium sulfide nonahydrate (2.402 g, 10 mmol) each dissolved in 12 ml de-aerated water in a 25 ml microwave vial under nitrogen gas atmosphere. The solutions were combined and a black precipitate formed. The vials were centrifuged and the solutions removed with a syringe and pressure compensation by nitrogen gas. To the solid iron sulfide phase 20 ml of a 0.1 M de-aerated solution of  $\text{NaHCO}_3$  was added and the pH value was adjusted with diluted hydrochloric acid to 3 and a little excess was added to ensure the presence of  $\text{H}_2\text{S}$ . The resulting suspension kept at 80 °C for two weeks. A 25 ml GC-MS vial was evacuated through a cannula and the headspace of the reaction vial was transferred by connecting both vials with a double-edged cannula that has been previously purged with nitrogen gas. After around 5 minutes equilibrium pressure in both vials was reached and the GC-MS vial was removed. The head-space was analyzed in the GC-MS using the head-space sampler and subjected to the operation conditions as described in the materials section.

#### **RED\_21**



Iron sulfide synthesis was carried out by precipitation from  $(\text{NH}_4)_2\text{Fe}(\text{SO}_4)_2$  (3.9213 g, 10 mmol) and sodium sulfide nonahydrate (2.402 g, 10 mmol) each dissolved in 12 ml de-aerated water in a 25 ml microwave vial under nitrogen gas atmosphere. The solutions were combined and a black precipitate formed. The vials were centrifuged and the solutions removed with a syringe and pressure compensation by nitrogen gas. The solid phase was dried under reduced pressure afterwards. Non-labeled sodium carbonate (0.5 g, 5 mmol) was placed in another vial which was evacuated. The carbonate was charged with 5 ml concentrated hydrochloric acid (ca. 15%) and the forming gas was collected with two 25 ml syringes. The evacuated mackinawite vial was filled with the  $\text{CO}_2$  and additional 2 ml of concentrated HCl and held at 80 °C for 4 days. A 25 ml GC-MS vial was evacuated through a cannula and the headspace of the reaction vial was transferred by connecting both vials with a double-edged cannula that has been previously purged with nitrogen gas. After around 5 minutes equilibrium pressure in both vials was reached and the GC-MS vial was removed. The head-space was analyzed in the GC-MS using the head-space sampler and subjected to the operation conditions as described in the materials section.

## **RED\_21**

Iron sulfide synthesis was carried out by precipitation from  $(\text{NH}_4)_2\text{Fe}(\text{SO}_4)_2$  (3.9213 g, 10 mmol) and sodium sulfide nonahydrate (2.402 g, 10 mmol) each dissolved in 12 ml de-aerated water in a 25 ml microwave vial under nitrogen gas atmosphere. The solutions were combined and a black precipitate formed. The vials were centrifuged and the solutions removed with a syringe and pressure compensation by nitrogen gas. Non-labeled sodium carbonate (0.5 g, 5 mmol) was placed in another vial which was evacuated. The carbonate was charged with 5 ml concentrated hydrochloric acid (ca. 15%) and the forming gas was collected with two 25 ml syringes. The evacuated mackinawite vial was filled with the  $\text{CO}_2$  and held at 110 °C for 2 weeks. A 25 ml GC-MS vial was evacuated through a cannula and the headspace of the reaction vial was transferred by connecting both vials with a double-edged cannula that has been previously purged with nitrogen gas. After around 5 minutes equilibrium pressure in both vials was reached and the GC-MS vial was removed. The head-space was analyzed in the GC-MS using the head-space sampler and subjected to the operation conditions as described in the materials section.

### **Toch\_Red\_1 to Toch\_Red\_5**

FTT reactions of CO<sub>2</sub> and H<sub>2</sub> were carried out at the LMU in Munich at the group of Prof. Dr. Trapp by Sophia Peters and Christoph Seifert. In 400 ml stainless steel autoclaves with a glass inlet and a valve for gas supply FTT reactions were carried out at different temperatures with an atmosphere of N<sub>2</sub>, CO<sub>2</sub> and H<sub>2</sub>. The products were analyzed by GC-MS in DCM solution obtained from a similar distillation method as used for the reduction experiments using mackinawite. After the reaction, the autoclaves were connected to a distillation bridge which had a 10 ml flask on the other side cooled in liquid nitrogen. The distillation was carried out at the same temperature as the reaction for one hour. The volatiles that condensed in the cooled flask were dissolved in DCM after removing the distillation bridge

<b>Name</b>	<b>Temperature / reaction time</b>	<b>pH<sub>2</sub> / pCO<sub>2</sub></b>	<b>Tochilinite mass / g</b>
Toch_Red_1	250 °C / 4 days	17.5 bar / 17.5 bar	0.999
Toch_Red_2	264 °C / 4 days	17.5 bar / 17.5 bar	0.655
Toch_Red_3	300 °C / 4 days	17.5 bar / 17.5 bar	1.003
Toch_Red_4	200 °C / 4 days	0 bar / 25 bar	1.006
Toch_Red_5	200 °C / 4 hours	1 bar N <sub>2</sub>	1.001

## 10.4 Syntheses of tochilinite analogues

### 10.4.1 MgAl-tochilinite

#### Toch\_1

All water used in this synthesis has previously been deionized and purged with nitrogen gas while boiling to remove carbonates and oxygen. Magnesium nitrate hexahydrate (1.00 g, 3.9 mmol) and aluminum nitrate nonahydrate (0.29 g, 0.8 mmol) were dissolved in 20 ml of water to obtain a clear colorless solution. A second solution was prepared by dissolving ammonium iron (II) sulfate hexahydrate (1.88 g, 4.8 mmol) in 20 ml of water. To the first solution 15 ml of an aqueous solution of sodium hydroxide (0.62 mol/l) was slowly added while stirring and a white precipitate formed. To the iron(II)-solution 1 ml of an ammonium hydrosulfide solution (5.10 mol/l; pH = 10) was slowly added while stirring and a black precipitate formed. Both colloidal suspensions were filtered and the solid residues washed with water. Afterwards these wet solids were transferred into a stainless-steel autoclave with a Teflon inlet. The autoclave was charged with 20 ml of water and mixed with a glass rod. The resulting black colloidal suspension was heated in an oven for one week at 160 °C without stirring.

After cooling down to room temperature, the black suspension was filtered under flowing nitrogen and the solid residue was washed with ethanol and dried in a stream of nitrogen gas to obtain a black solid.

#### Toch\_2

All water used in this synthesis has previously been deionized and purged with nitrogen gas while boiling to remove carbonates and oxygen. In a 50 ml Schlenk flask under nitrogen atmosphere magnesium nitrate hexahydrate (1.00 g, 3.9 mmol) and aluminum nitrate nonahydrate (0.29 g, 0.8 mmol) were dissolved in 20 ml of deaerated water to obtain a clear colorless solution. A second solution was prepared in a second Schlenk flask under a nitrogen atmosphere by dissolving ammonium iron (II) sulfate hexahydrate (1.88 g, 4.8 mmol) in 20 ml of deaerated water. To the first solution 15 ml of an aqueous solution of sodium hydroxide (0.62 mol/l) was slowly added while stirring and a white precipitate formed. To the iron(II)-solution 1 ml of an ammonium hydrosulfide solution (5.10 mol/l;

pH = 10) was slowly added while stirring and a black precipitate formed. Both colloidal suspensions were filtered and the solid residues washed with water. Afterwards these solids were transferred into a third Teflon flask that was flushed with nitrogen for at least 30 minutes. 20 ml of deaerated water was added and the resulting black colloidal suspension was heated for one week at 95 °C while stirred.

After cooling down to room temperature, the black suspension was filtered under flowing nitrogen and the solid residue was washed with ethanol and dried in a stream of nitrogen gas.

### **Toch\_3**

All water used in this synthesis has previously been deionized and purged with nitrogen gas while to remove dissolved oxygen. Powder of magnesium (0.1 g, 4.1 mmol) and aluminum (0.02 g, 0.8 mmol) were mixed in a steel autoclave with a Teflon inlet. Then a solution was prepared by dissolving ammonium iron (II) sulfate hexahydrate (1.98 g, 5.0 mmol) in 20 ml of deaerated water in a Schlenk flask in a nitrogen atmosphere. To this solution 1.1 ml of an ammonium hydrosulfide solution (5.1 mol/l; pH = 10) was quickly added while stirring and a black precipitate formed. The resulting colloidal suspension was filtered and the black solid residue was washed with water while under a nitrogen flow. After drying for a couple of minutes the iron sulfide was added to the magnesium and aluminum powder in the autoclave and charged with 20 ml of water. The autoclave was sealed and the resulting black colloidal suspension was heated in an oven for 3 days at 160 °C without stirring.

After cooling down to room temperature, the black suspension was filtered under air and the solid residue was washed with water and ethanol to obtain a black solid.

### **Toch\_4**

All water used in this synthesis has previously been deionized and purged with nitrogen gas while to remove dissolved oxygen. Powder of magnesium (0.1 g, 4.1 mmol) and aluminum (0.02 g, 0.8 mmol) were mixed in a steel autoclave with a Teflon inlet. Then a solution was prepared by dissolving ammonium iron (II) sulfate hexahydrate (1.98 g, 5.0

mmol) in 20 ml of deaerated water in a Schlenk flask in a nitrogen atmosphere. To this solution 1.1 ml of an ammonium hydrosulfide solution (5.1 mol/l; pH = 10) was quickly added while stirring and a black precipitate formed. The resulting colloidal suspension was filtered and the black solid residue was washed with water while under a nitrogen flow. After drying for a couple of minutes the iron sulfide was added to the magnesium and aluminum powder in the autoclave and charged with 20 ml of water. The autoclave was sealed and the resulting black colloidal suspension was heated in an oven for 4 days at 160 °C without stirring.

After cooling down to room temperature, the black suspension was filtered under air and the solid residue was washed with water and ethanol to obtain a black solid.

### **Toch\_5**

All water used in this synthesis has previously been deionized and purged with nitrogen gas while to remove dissolved oxygen. Powder of magnesium (0.1 g, 4.1 mmol) and aluminum (0.02 g, 0.8 mmol) were mixed in a steel autoclave with a Teflon inlet. Then a solution was prepared by dissolving ammonium iron (II) sulfate hexahydrate (1.98 g, 5.0 mmol) in 20 ml of deaerated water in a Schlenk flask in a nitrogen atmosphere. To this solution 1.1 ml of an ammonium hydrosulfide solution (5.1 mol/l; pH = 10) was quickly added while stirring and a black precipitate formed. The resulting colloidal suspension was filtered and the black solid residue was washed with water while under a nitrogen flow. After drying for a couple of minutes the iron sulfide was added to the magnesium and aluminum powder in the autoclave and charged with 20 ml of water. The autoclave was sealed and the resulting black colloidal suspension was heated in an oven for 4 days at 160 °C without stirring.

After cooling down to room temperature, the black suspension was filtered under air and the solid residue was washed with water and ethanol to obtain a black solid.

### **Toch\_6**

All water used in this synthesis has previously been deionized and purged with nitrogen gas while to remove dissolved oxygen. Powder of magnesium (0.1 g, 4.1 mmol) and aluminum (0.02 g, 0.8 mmol) were mixed in a steel autoclave with a Teflon inlet. Then a solution was prepared by dissolving ammonium iron (II) sulfate hexahydrate (1.98 g, 5.0 mmol) in 20 ml of deaerated water in a Schlenk flask in a nitrogen atmosphere. To this solution 1.1 ml of an ammonium hydrosulfide solution (5.1 mol/l; pH = 10) was quickly added while stirring and a black precipitate formed. The autoclave was sealed and the resulting black colloidal suspension was heated in an oven for 4 days at 160 °C without stirring.

After cooling down to room temperature, the black suspension was filtered under air and the solid residue was washed with water and ethanol to obtain a black solid.

### **Toch\_7**

Finely powdered magnesium (0.18 g, 7.41 mmol), powdered aluminum (0.16 g, 1.5 mmol), powdered iron (0.5 g, 8.89 mmol) and powdered sulfur (0.28 g, 8.89 mmol) were mixed in a steel autoclave with a Teflon inlet and charged with 20 ml of water. The autoclave was sealed and heated in an oven for 5 days at 160 °C without stirring.

After cooling down to room temperature, the black suspension was filtered under air and the solid residue was washed with water and ethanol to obtain a black solid.

### **Toch\_8**

A mixture of iron and sulfur with a molar ratio of 1:1 was grinded thoroughly in a mortar. 0.88 g (10 mmol sulfur, 10 mmol iron) of this mixture was transferred into a 25-ml vial with a septum. The air was replaced by nitrogen gas to keep the vial oxygen free. To this mixture 10 ml of degassed water was added and the resulting suspension was kept at room temperature overnight without stirring. The solids turned black within a couple of hours. In a steel autoclave with a Teflon inlet magnesium (0.24 g, 9.87 mmol) and aluminum (0.08 g, 2.96 mmol) were mixed with the iron sulfide suspension. The autoclave was sealed and heated in an oven for 3 days at 160 °C without stirring.

After cooling down to room temperature, the black suspension obtained was filtered under air and the solid residue was washed with water and ethanol to obtain a black solid. This solid was transferred into a Schlenk flask and charged with 20 ml of a nitrogen saturated solution of ammonium sulfate (1g/10 ml) and stirred at 80 °C overnight. The solids were isolated by filtration through a glass frit and washed successively with water, ethanol, acetone and diethyl ether and dried in a stream of nitrogen gas.

### **Toch\_9**

All water used in this synthesis has previously been deionized and purged with nitrogen gas while to remove dissolved oxygen. Powder of zinc (0.27 g, 4.1 mmol) and aluminum hydroxide (0.06 g, 0.8 mmol) were mixed in a steel autoclave with a Teflon inlet. Then a solution was prepared by dissolving ammonium iron (II) sulfate hexahydrate (1.98 g, 5.0 mmol) in 20 ml of deaerated water in a Schlenk flask in a nitrogen atmosphere. To this solution 1.1 ml of an ammonium hydrosulfide solution (5.1 mol/l; pH = 10) was quickly added while stirring and a black precipitate formed. The resulting colloidal suspension was filtered and the black solid residue was washed with water while under a stream of nitrogen. After drying for a couple of minutes the iron sulfide was added to the magnesium and aluminum powder in the autoclave and charged with 20 ml of water. The autoclave was sealed and the resulting black colloidal suspension was heated in an oven for 3 days at 160 °C without stirring.

After cooling down to room temperature, the black suspension was filtered under air and the solid residue was washed with water and ethanol to obtain a black solid.

### **Toch\_MgAl\_1**

Finely powdered magnesium (0.18 g, 7.41 mmol), powdered aluminum (0.16 g, 1.5 mmol), powdered iron (0.5 g, 8.89 mmol) and powdered sulfur (0.28 g, 8.89 mmol) were mixed in a steel autoclave with a Teflon inlet and charged with 20 ml of water. The autoclave was sealed and heated in an oven for 6 days at 160 °C without stirring.

After cooling down to room temperature, the black suspension was filtered under air and the solid residue was washed with water and ethanol to obtain a black solid.

### **Toch\_MgAl\_2**

Powdered magnesium (0.16 g, 6.67 mmol), powdered aluminum (0.05 g, 1.67 mmol) and FeS\_1 (0.88 g) were mixed in a steel autoclave with a Teflon inlet and charged with 20 ml of water. The autoclave was sealed and the resulting suspension was heated in an oven for 3 days at 160 °C without stirring.

After cooling down to room temperature, the black suspension was filtered under air and the solid residue was washed with water and ethanol to obtain a black solid.

### **Toch\_MgAl\_3**

All water used in this synthesis has previously been deionized and purged with nitrogen gas while to remove dissolved oxygen. Magnesium oxide (0.17 g, 4.2 mmol) and aluminum (0.02 g, 0.8 mmol) were mixed in a steel autoclave with a Teflon inlet. A solution was prepared by dissolving ammonium iron (II) sulfate hexahydrate (1.98 g, 5.0 mmol) in 20 ml of deaerated water in a 50 ml Schlenk flask under a nitrogen atmosphere. To this solution 1.1 ml of an ammonium hydrosulfide solution (5.1 mol/l; pH = 10) was quickly added while stirring and a black precipitate formed. The resulting suspension was filtered and the black solid residue was washed with ethanol while under a nitrogen flow. After drying for a couple of minutes the iron sulfide was added to the magnesium and aluminum powder in the autoclave and charged with 20 ml of water. The autoclave was sealed and the resulting suspension was heated in an oven for 6 days at 160 °C without stirring.

After cooling down to room temperature, the black suspension was filtered under air and the solid residue was washed with water and ethanol to obtain a black solid.

### **Toch\_MgAl\_4**



All water used in this synthesis has previously been deionized and purged with nitrogen gas while to remove dissolved oxygen. Powdered magnesium (0.10 g, 4.1 mmol) and powdered aluminum hydroxide (0.06 g, 0.8 mmol) were mixed in a steel autoclave with a Teflon inlet. A solution was prepared by dissolving ammonium iron (II) sulfate hexahydrate (1.98 g, 5.0 mmol) in 20 ml of deaerated water in a 50 ml Schlenk flask under a nitrogen atmosphere. To this solution 1.1 ml of an ammonium hydrosulfide solution (5.1 mol/l; pH = 10) was quickly added while stirring and a black precipitate formed. The resulting black suspension was filtered and the black solid residue was washed with ethanol while under a nitrogen flow. After drying for a couple of minutes the iron sulfide was added to the magnesium and aluminum powder in the autoclave and charged with 20 ml of water. The autoclave was sealed and the resulting black suspension was heated in an oven for 6 days at 160 °C without stirring.

After cooling down to room temperature, the black suspension was filtered under air and the solid residue was washed with water and ethanol to obtain a black solid.

#### **Toch\_MgAl\_5**

Powdered magnesium (0.05 g, 2.06 mmol), powdered iron (0.08 g, 1.4 mmol) and powdered sulfur (0.04 g, 1.3 mmol) were mixed in a steel autoclave with a Teflon inlet and charged with 20 ml of water. The autoclave was sealed and the resulting suspension was heated in an oven for 6 days at 160 °C without stirring.

After cooling down to room temperature, the black suspension was filtered under air and the solid residue was washed with water and ethanol to obtain a black solid.

#### **Toch\_MgAl\_6**

Powdered magnesium (0.05 g, 2.06 mmol), powdered iron (0.08 g, 1.4 mmol) and sodium hydroxide (0.04 g, 1.03 mmol) were mixed in a steel autoclave with a Teflon inlet and charged with 20 ml of water. The autoclave was sealed and the resulting suspension was heated in an oven for 6 days at 160 °C without stirring.

After cooling down to room temperature, the black suspension was filtered under air and the solid residue was washed with water and ethanol to obtain a black solid.

### **Toch\_MgAl\_7**

Powdered magnesium (0.08 g, 3.42 mmol), powdered iron (0.25 g, 4.48 mmol), powdered aluminum (0.02 g, 0.74 mmol) and powdered sulfur (0.14 g, 4.38 mmol) were mixed in a steel autoclave with a Teflon inlet and charged with 20 ml of water. The autoclave was sealed and the resulting suspension was heated in an oven for 3 days at 160 °C without stirring.

After cooling down to room temperature, the black suspension was filtered under air and the solid residue was washed with water and ethanol to obtain a black solid.

### **Toch\_MgAl\_8**

In a 100 ml Schlenk flask magnesium nitrate hexahydrate (2.5 g, 10.2 mmol) and aluminum nitrate nonahydrate (0.95 g, 2.53 mmol) were charged with 50 ml of deaerated water in a nitrogen atmosphere. In a second Schlenk flask a solution was prepared from sodium sulfide nonahydrate (2.4 g, 10.0 mmol) in 20 ml deaerated water. The sulfide solution was added to the first one drop wise using a syringe. Thereby, a light green precipitate formed. The obtained suspension was heated at 60 °C and stirred overnight. The solid phase was isolated by filtration through a glass frit and washed successively with water, ethanol and acetone and let dry open to the atmosphere.

### **Toch\_MgAl\_9**

Powdered magnesium (0.16 g, 6.6 mmol) and powdered aluminum (0.04 g, 1.3 mmol) were mixed in a steel autoclave with a Teflon inlet and charged with 20 ml of water. The autoclave was sealed and the resulting suspension was heated in an oven for 6 days at 160 °C without stirring.

After cooling down to room temperature, the white suspension was filtered under air and the solid residue was washed with water and ethanol to obtain a white solid.

### **Toch\_MgAl\_10**

Powdered magnesium (0.05 g, 2.06 mmol), powdered aluminum (0.06 g, 2.06 mmol) and sodium hydroxide (0.04 g, 1.03 mmol) were mixed in a steel autoclave with a Teflon inlet and charged with 20 ml of water. The autoclave was sealed and the resulting suspension was heated in an oven for 3 days at 160 °C without stirring.

After cooling down to room temperature, the white suspension was filtered under air and the solid residue was washed with water and ethanol to obtain a white solid.

### **Toch\_MgAl\_11**

Powdered magnesium (0.08 g, 3 mmol), powdered aluminum (0.02 g, 1 mmol), powdered iron (0.26 g, 4.61 mmol) and powdered sulfur (0.16 g, 4.61 mmol) were mixed in a steel autoclave with a Teflon inlet the autoclave and charged with 20 ml of water. The autoclave was sealed and the resulting suspension was heated in an oven for at 160 °C without stirring for 3 days.

After cooling down to room temperature, the black suspension was filtered under air and the solid residue was washed with water and ethanol to obtain a black solid.

### **Toch\_MgAl\_12**

Powdered magnesium (0.072 g, 2.96 mmol), powdered aluminum (0.016 g, 0.60 mmol) powdered iron (0.26 g, 4.70 mmol) and powdered sulfur (0.15 g, 4.68 mmol) were mixed in a steel autoclave with a Teflon inlet and charged with 20 ml of water. The autoclave was sealed and the resulting suspension was heated in an oven for at 160 °C without stirring for 3 days.

After cooling down to room temperature, the black suspension was filtered under air and the solid residue was washed with water and ethanol to obtain a black solid.

### **Toch\_MgAl\_13**

Powdered magnesium (0.04 g, 1.65 mmol), powdered aluminum (0.01 g, 0.33 mmol), powdered iron (0.29 g, 5.14 mmol) and powdered sulfur (0.16 g, 5.13 mmol) were mixed in a steel autoclave with a Teflon inlet and charged with 20 ml of water. The autoclave was sealed and the resulting suspension was heated in an oven for at 160 °C without stirring for 3 days.

After cooling down to room temperature, the black suspension was filtered under air and the solid residue was washed with water and ethanol to obtain a black solid.

#### **Toch\_MgAl\_14**

Powdered magnesium (0.18 g, 7.59 mmol), powdered aluminum (0.04 g, 1.52 mmol), powdered iron (0.48 g, 8.67 mmol) and powdered sulfur (0.29 g, 9.13 mmol) were mixed in a steel autoclave with a Teflon inlet and charged with 20 ml of water. The resulting suspension was heated in an oven for 2 days at 130 °C without stirring.

After cooling down to room temperature, the black suspension was filtered under air and the solid residue was washed with water and left to dry open to the atmosphere.

#### **Toch\_MgAl\_16**

Powdered magnesium (0.18 g, 7.59 mmol), powdered aluminum (0.04 g, 1.52 mmol), powdered iron (0.48 g, 8.67 mmol) and powdered sulfur (0.29 g, 9.13 mmol) were mixed in a steel autoclave with a Teflon inlet and charged with 20 ml of water. The resulting suspension was heated in an oven for 4 days at 130 °C without stirring.

After cooling down to room temperature, the black suspension was filtered under air and the solid residue was washed with water and left to dry open to the atmosphere.

#### **Toch\_MgAl\_17**

Powdered magnesium (0.18 g, 7.59 mmol), powdered aluminum (0.04 g, 1.52 mmol), powdered iron (0.48 g, 8.67 mmol) and powdered sulfur (0.29 g, 9.13 mmol) were mixed in a steel autoclave with a Teflon inlet and charged with 20 ml of water. The resulting suspension was heated in an oven for 7 days at 130 °C without stirring.

After cooling down to room temperature, the black suspension was filtered under air and the solid residue was washed with water and left to dry open to the atmosphere.

### **Toch\_MgAl\_18**

Powdered magnesium (0.18 g, 7.59 mmol), powdered aluminum (0.04 g, 1.52 mmol), powdered iron (0.48 g, 8.67 mmol) and powdered sulfur (0.29 g, 9.13 mmol) were mixed in a steel autoclave with a Teflon inlet and charged with 20 ml of water. The resulting suspension was heated in an oven for 9 days at 130 °C without stirring.

After cooling down to room temperature, the black suspension was filtered under air and the solid residue was washed with water and left to dry open to the atmosphere.

### **Toch\_MgAl\_19**

Powdered magnesium (0.18 g, 7.59 mmol), powdered aluminum (0.04 g, 1.52 mmol), powdered iron (0.48 g, 8.67 mmol) and powdered sulfur (0.24 g, 7.5 mmol) were mixed in a steel autoclave with a Teflon inlet and charged with 20 ml of water. The resulting suspension was heated in an oven for 3 days at 160 °C without stirring.

After cooling down to room temperature, the black suspension was filtered under air and the solid residue was washed with water and left to dry open to the atmosphere.

### **Toch\_MgAl\_20**

Powdered magnesium (0.18 g, 7.59 mmol), powdered aluminum (0.04 g, 1.52 mmol), powdered iron (0.48 g, 8.67 mmol) and powdered sulfur (0.29 g, 9.13 mmol) were mixed in a steel autoclave with a Teflon inlet and charged with 20 ml of water. The resulting suspension was heated in an oven for 3 days at 160 °C without stirring.

After cooling down to room temperature, the black suspension was filtered under air and the solid residue was washed with water and left to dry open to the atmosphere.

### **Toch\_MgAl\_21, Toch\_MgAl\_22, Toch\_MgAl\_23**

Samples of Toch\_MgAl\_19 were treated with diluted ammonium chloride solutions. Therefor 0.5 g of Toch\_MgAl\_19 and different amounts of ammonium chloride were dispersed in 25 ml of water in a two neck round bottom flask. To sustain oxygen free conditions and keep the particles in motion nitrogen was led through the solution with a glass tube. The samples were kept in the solutions overnight at room temperature. After this time, the solids were separated by filtration through a glass frit, washed multiple times with water and dried in the open air.

Toch\_MgAl\_21: 0.1 g ammonium chloride

Toch\_MgAl\_22: 0.5 g ammonium chloride

Toch\_MgAl\_23: 1.0 g ammonium chloride

#### **Toch\_MgAl\_24**

Powdered magnesium (0.18 g, 7.41 mmol), powdered aluminum (0.04 g, 1.48 mmol), ammonium sulfate (1.00 g, 7.5 mmol), powdered iron (0.50 g, 8.89 mmol) and powdered sulfur (0.28 g, 8.89 mmol) were mixed in a steel autoclave with a Teflon inlet and charged with 20 ml of water. The resulting suspension was heated in an oven for 6 days at 160 °C without stirring.

After cooling down to room temperature, the black suspension was filtered under air and the solid residue was washed with water and left to dry in the open air.

#### **Toch\_MgAl\_25**

Powdered magnesium (0.18 g, 7.41 mmol), powdered aluminum (0.04 g, 1.48 mmol), ammonium sulfate (2.00 g, 15 mmol), powdered iron (0.50 g, 8.89 mmol) and powdered sulfur (0.28 g, 8.89 mmol) were mixed in a steel autoclave with a Teflon inlet and charged with 20 ml of water. The resulting suspension was heated in an oven for 6 days at 160 °C without stirring.

After cooling down to room temperature, the black suspension was filtered under air and the solid residue was washed with water and left to dry in the open air.

### **Toch\_MgAl\_26**

Powdered magnesium (0.18 g, 7.41 mmol), powdered aluminum (0.04 g, 1.48 mmol), ammonium sulfate (3.00 g, 22.5 mmol), powdered iron (0.50 g, 8.89 mmol) and powdered sulfur (0.28 g, 8.89 mmol) were mixed in a steel autoclave with a Teflon inlet and charged with 20 ml of water. The resulting suspension was heated in an oven for 6 days at 160 °C without stirring.

After cooling down to room temperature, the black suspension was filtered under air and the solid residue was washed with water and left to dry in the open air.

### **Toch\_MgAl\_27**

Powdered magnesium (0.18 g, 7.41 mmol), powdered aluminum (0.04 g, 1.48 mmol), ammonium sulfate (4.00 g, 30 mmol), powdered iron (0.50 g, 8.89 mmol) and powdered sulfur (0.28 g, 8.89 mmol) were mixed in a steel autoclave with a Teflon inlet and charged with 20 ml of water. The resulting suspension was heated in an oven for 6 days at 160 °C without stirring.

After cooling down to room temperature, the black suspension was filtered under air and the solid residue was washed with water and left to dry in the open air.

## **10.4.2 MgFe-tochilinite**

### **Toch\_MgFe\_1**

Powdered magnesium (0.050 g, 2 mmol), powdered iron (0.132 g, 3 mmol) and powdered sulfur (0.09 g, 3 mmol) were mixed in a steel autoclave with a Teflon inlet and charged with 20 ml of water. The resulting suspension was heated in an oven for 4 days at 160 °C without stirring.

After cooling down to room temperature, the black suspension was filtered under air and the solid residue was washed successively with water and ethanol to obtain a black solid that was left to dry in the open air.

### **Toch\_MgFe\_2**

Powdered magnesium (0.188 g, 8 mmol), powdered iron oxide hydroxide (0.146 g, 2 mmol), powdered iron (0.480 g, 9 mmol) and powdered sulfur (0.291 g, 9 mmol) were mixed in a steel autoclave with a Teflon inlet and charged with 20 ml of water. The resulting suspension was heated in an oven for 3 days at 160 °C without stirring.

After cooling down to room temperature, the black suspension was filtered under air and the solid residue was washed with successively with water and ethanol to obtain a black solid that was left to dry in the open air.

### **Toch\_MgFe\_3**

All water used in this synthesis has previously been deionized and purged with nitrogen gas while to remove dissolved oxygen. Powdered magnesium oxide (0.170 g, 4 mmol) and powdered iron (0.055 g, 1 mmol) were mixed in a steel autoclave with a Teflon inlet. A solution was prepared by dissolving ammonium iron (II) sulfate hexahydrate (1.98 g, 5.0 mmol) in 20 ml of deaerated water in a 50 ml Schlenk flask under a nitrogen atmosphere. To this solution 1.1 ml of an ammonium hydrosulfide solution (5.1 mol/l; pH = 10) was quickly added while stirring and a black precipitate formed. The resulting suspension was filtered and the black solid residue was washed with ethanol while under a nitrogen flow. After drying for a couple of minutes the iron sulfide was added to the magnesium and aluminum powder in the autoclave and charged with 20 ml of water. The autoclave was sealed and the resulting mixture was heated in an oven for 6 days at 160 °C without stirring.

After cooling down to room temperature, the black suspension was filtered under air and the solid residue was washed with water and ethanol to obtain a black solid that was left to dry in the open air.

### **Toch\_MgFe\_4**



Powdered magnesium (0.166 g, 6 mmol), powdered iron oxide hydroxide (0.159 g, 2 mmol) and FeS<sub>1</sub> (0.880 g) were mixed in a steel autoclave with a Teflon inlet and charged with 20 ml of water. The resulting suspension was heated in an oven for 3 days at 160 °C without stirring.

After cooling down to room temperature, the black suspension was filtered under air and the solid residue was washed successively with water and ethanol to obtain a black solid that was left to dry in the open air.

### **Toch\_MgFe\_5**

88 g of a mixture of iron and sulfur with a molar ratio of 1:1 was ground thoroughly in an automated mortar. 0.88 g of this mixture containing powdered iron (0.560 g, 10 mmol) and powdered sulfur (0.320 g, 10 mmol) was transferred into a 25-ml microwave vial and sodium chloride (0.06 g, 1 mmol) was added. The vial was sealed and the air was replaced by nitrogen following the standard procedure to exclude oxygen. To this mixture 10 ml of degassed water was added and the resulting suspension was kept at room temperature overnight without stirring. The solids turned black within a couple of hours and the complete conversion of the starting materials was controlled with a strong magnet.

In a steel autoclave with a Teflon inlet powdered magnesium (0.240 g, 10 mmol) and powdered iron oxide hydroxide (0.270 g, 3 mmol) were mixed with the iron sulfide suspension. The reactor was sealed and heated in an oven for 3 days at 160 °C without stirring.

After cooling down to room temperature, the black suspension was filtered under a stream of nitrogen and the solid residue was washed successively with water and ethanol to obtain a black solid that was left to dry in the open air.

The solid products were transferred into a Schlenk flask and the air was replaced by nitrogen. 20 ml a deaerated solution of ammonium sulfate (1g/10 ml) was added and the resulting suspension stirred at 80 °C overnight. After cooling down to room temperature, the black suspension was filtered under a stream of nitrogen and the solid residue was washed successively with water, ethanol, acetone and diethyl ether and dried following the standard procedure

### **Toch\_MgFe\_6**

Powdered magnesium (0.036 g, 1 mmol), powdered iron (0.134 g, 3 mmol) and powdered sulfur (0.09 g, 3 mmol) were mixed in a steel autoclave with a Teflon inlet and charged with 20 ml of water. The resulting suspension was heated in an oven for 4 days at 160 °C without stirring.

After cooling down to room temperature, the black suspension was filtered under air and the solid residue was washed with successively with water and ethanol to obtain a black solid that was left to dry in the open air.

### **Toch\_MgFe\_7**

Powdered magnesium (0.020 g, 1 mmol), powdered iron (0.134 g, 3 mmol) and powdered sulfur (0.09 g, 3 mmol) were mixed in a steel autoclave with a Teflon inlet and charged with 20 ml of water. The resulting suspension was heated in an oven for 4 days at 160 °C without stirring.

After cooling down to room temperature, the black suspension was filtered under air and the solid residue was washed with successively with water and ethanol to obtain a black solid that was left to dry in the open air.

### **Toch\_MgFe\_8**

Powdered magnesium (0.053 g, 3 mmol), powdered iron (0.132 g, 3 mmol) and powdered sulfur (0.120 g, 4 mmol) were mixed in a steel autoclave with a Teflon inlet and charged with 20 ml of water. The resulting suspension was heated in an oven for 4 days at 160 °C without stirring.

After cooling down to room temperature, the black suspension was filtered under air and the solid residue was washed with successively with water and ethanol to obtain a black solid that was left to dry in the open air.

### **Toch\_MgFe\_9**

Powdered magnesium (0.051 g, 3 mmol), powdered iron (0.134 g, 3 mmol) and powdered sulfur (0.141 g, 4 mmol) were mixed in a steel autoclave with a Teflon inlet and charged with 20 ml of water. The resulting suspension was heated in an oven for 4 days at 160 °C without stirring.

After cooling down to room temperature, the black suspension was filtered under air and the solid residue was washed with successively with water and ethanol to obtain a black solid that was left to dry in the open air.

### **Toch\_MgFe\_10**

Powdered magnesium (0.049 g, 3 mmol), powdered iron (0.130 g, 3 mmol) and powdered sulfur (0.166 g, 5 mmol) were mixed in a steel autoclave with a Teflon inlet and charged with 20 ml of water. The resulting suspension was heated in an oven for 4 days at 160 °C without stirring.

After cooling down to room temperature, the black suspension was filtered under air and the solid residue was washed with successively with water and ethanol to obtain a black solid that was left to dry in the open air.

### **Toch\_MgFe\_11**

90 g of a mixture of iron, sulfur and sodium chloride were ground thoroughly in an automated mortar. 3.00 g of this mixture containing powdered iron (1.550 g, 28 mmol), powdered sulfur (1.066 g, 33 mmol) and powdered sodium chloride (0.383 g, 7 mmol) were transferred into a 25-ml microwave vial. The vial was sealed and the air was replaced by nitrogen following the standard procedure to exclude oxygen. To this mixture 10 ml of deaerated water was added and the resulting suspension was kept at room temperature overnight without stirring. The solids turned black within a couple of hours and the complete conversion of the starting materials was controlled with a strong magnet.

In a steel autoclave with a Teflon inlet powdered magnesium (0.510 g, 22 mmol) and powdered iron oxide hydroxide (0.480 g, 5 mmol) were mixed with the iron sulfide suspension and 10 ml of deionized water were added. The reactor was sealed and heated in an oven for 4 days at 160 °C without stirring.

After cooling down to room temperature, the black solid residue was isolated by filtration and washed successively with water and ethanol to obtain a black solid that was left to dry in the open air.

### **Toch\_MgFe\_12**

88 g of a mixture of iron and sulfur with a molar ratio of 1:1 was ground thoroughly in an automated mortar. 3.00 g of this mixture containing powdered iron (1.904 g, 34 mmol) and powdered sulfur (1.096 g, 34 mmol) was transferred into a 25-ml microwave vial and sodium chloride (0.191 g, 3 mmol) was added. The vial was sealed and the air was replaced by nitrogen following the standard procedure to exclude oxygen. To this mixture 10 ml of deaerated water was added and the resulting suspension was kept at room temperature overnight without stirring. The solids turned black within a couple of hours and the complete conversion of the starting materials was controlled with a strong magnet.

In a steel autoclave with a Teflon inlet powdered magnesium (0.122 g, 22 mmol) and powdered iron oxide hydroxide (0.302 g, 5 mmol) were mixed with the iron sulfide suspension and 10 ml of deionized water were added. The reactor was sealed and heated in an oven for 4 days at 160 °C without stirring.

After cooling down to room temperature, the obtained black suspension was transferred into a 500 ml beaker and charged with 200 ml deionized water. The suspension was stirred with a strong magnet for multiple minutes and all magnetic solids were removed. The residual solid was isolated by filtration and washed successively with water and ethanol to obtain a black solid that was left to dry in the open air.

### **Toch\_MgFe\_13**

88 g of a mixture of iron and sulfur with a molar ratio of 1:1 was ground thoroughly in an automated mortar. 3.00 g of this mixture containing powdered iron (1.904 g, 34 mmol) and powdered sulfur (1.096 g, 34 mmol) was transferred into a 25-ml microwave vial and sodium chloride (0.188 g, 3 mmol) was added. The vial was sealed and the air was replaced by nitrogen following the standard procedure to exclude oxygen. To this mixture 10 ml of deaerated water was added and the resulting suspension was kept at room

temperature overnight without stirring. The solids turned black within a couple of hours and the complete conversion of the starting materials was controlled with a strong magnet.

In a steel autoclave with a Teflon inlet powdered magnesium (0.363 g, 16 mmol) and powdered iron oxide hydroxide (0.300 g, 3 mmol) were mixed with the iron sulfide suspension and 10 ml of deionized water were added. The reactor was sealed and heated in an oven for 4 days at 160 °C without stirring.

After cooling down to room temperature, the obtained black suspension was transferred into a 500 ml beaker and charged with 200 ml deionized water. The suspension was stirred with a strong magnet for multiple minutes and all magnetic solids were removed. The residual solid was isolated by filtration, washed successively with water, ethanol, acetone and diethyl ether and dried under a stream of nitrogen.

#### **Toch\_MgFe\_14**

88 g of a mixture of iron and sulfur with a molar ratio of 1:1 was ground thoroughly in an automated mortar. 3.00 g of this mixture containing powdered iron (1.904 g, 34 mmol) and powdered sulfur (1.096 g, 34 mmol) was transferred into a 25-ml microwave vial and sodium chloride (0.181 g, 3 mmol) was added. The vial was sealed and the air was replaced by nitrogen following the standard procedure to exclude oxygen. To this mixture 10 ml of deaerated water was added and the resulting suspension was kept at room temperature overnight without stirring. The solids turned black within a couple of hours and the complete conversion of the starting materials was controlled with a strong magnet.

In a steel autoclave with a Teflon inlet powdered magnesium (0.36 g, 16 mmol) and powdered iron oxide hydroxide (0.486 g, 6 mmol) were mixed with the iron sulfide suspension and 10 ml of deionized water were added. The reactor was sealed and heated in an oven for 4 days at 160 °C without stirring.

After cooling down to room temperature, the obtained black suspension was transferred into a 500 ml beaker and charged with 200 ml deionized water. The suspension was stirred with a strong magnet for multiple minutes and all magnetic solids were removed. The residual solid was isolated by filtration, washed successively with water, ethanol, acetone and diethyl ether and dried under a stream of nitrogen.

### **Toch\_MgFe\_15**

88 g of a mixture of iron and sulfur with a molar ratio of 1:1 was ground thoroughly in an automated mortar. 3.00 g of this mixture containing powdered iron (1.904 g, 34 mmol) and powdered sulfur (1.096 g, 34 mmol) was transferred into a 25-ml microwave vial and sodium chloride (0.181 g, 3 mmol) was added. The vial was sealed and the air was replaced by nitrogen following the standard procedure to exclude oxygen. To this mixture 10 ml of deaerated water was added and the resulting suspension was kept at room temperature overnight without stirring. The solids turned black within a couple of hours and the complete conversion of the starting materials was controlled with a strong magnet.

In a steel autoclave with a Teflon inlet powdered magnesium (0.36 g, 16 mmol) and powdered iron oxide hydroxide (0.409 g, 5 mmol) were mixed with the iron sulfide suspension and 10 ml of deionized water were added. The reactor was sealed and heated in an oven for 4 days at 160 °C without stirring.

After cooling down to room temperature, the obtained black suspension was transferred into a 500 ml beaker and charged with 200 ml deionized water. The suspension was stirred with a strong magnet for multiple minutes and all magnetic solids were removed. The residual solid was isolated by filtration, washed successively with water, ethanol, acetone and diethyl ether and dried under a stream of nitrogen.

### **Toch\_MgFe\_16**

88 g of a mixture of iron and sulfur with a molar ratio of 1:1 was ground thoroughly in an automated mortar. 3.00 g of this mixture containing powdered iron (1.904 g, 34 mmol) and powdered sulfur (1.096 g, 34 mmol) was transferred into a 25-ml microwave vial and sodium chloride (0.181 g, 3 mmol) was added. The vial was sealed and the air was replaced by nitrogen following the standard procedure to exclude oxygen. To this mixture 10 ml of deaerated water was added and the resulting suspension was kept at room temperature overnight without stirring. The solids turned black within a couple of hours and the complete conversion of the starting materials was controlled with a strong magnet.

In a steel autoclave with a Teflon inlet powdered magnesium (0.36 g, 16 mmol) and powdered iron oxide hydroxide (0.300 g, 3 mmol) were mixed with the iron sulfide suspension and 10 ml of deionized water were added. The reactor was sealed and heated in an oven for 4 days at 160 °C without stirring.

After cooling down to room temperature, the obtained black suspension was transferred into a 500 ml beaker and charged with 200 ml deionized water. The suspension was stirred with a strong magnet for multiple minutes and all magnetic solids were removed. The residual solid was isolated by filtration, washed successively with water, ethanol, acetone and diethyl ether and dried under a stream of nitrogen.

### **Toch\_MgFe\_17**

88 g of a mixture of iron and sulfur with a molar ratio of 1:1 was ground thoroughly in an automated mortar. 3.00 g of this mixture containing powdered iron (1.904 g, 34 mmol) and powdered sulfur (1.096 g, 34 mmol) was transferred into a 25-ml microwave vial and sodium chloride (0.181 g, 3 mmol) was added. The vial was sealed and the air was replaced by nitrogen following the standard procedure to exclude oxygen. To this mixture 10 ml of deaerated water was added and the resulting suspension was kept at room temperature overnight without stirring. The solids turned black within a couple of hours and the complete conversion of the starting materials was controlled with a strong magnet.

In a steel autoclave with a Teflon inlet powdered magnesium (0.36 g, 16 mmol) and powdered iron oxide hydroxide (0.221 g, 3 mmol) were mixed with the iron sulfide suspension and 10 ml of deionized water were added. The reactor was sealed and heated in an oven for 4 days at 160 °C without stirring.

After cooling down to room temperature, the obtained black suspension was transferred into a 500 ml beaker and charged with 200 ml deionized water. The suspension was stirred with a strong magnet for multiple minutes and all magnetic solids were removed. The residual solid was isolated by filtration, washed successively with water, ethanol, acetone and diethyl ether and dried under a stream of nitrogen.

### **Toch\_MgFe\_18**

88 g of a mixture of iron and sulfur with a molar ratio of 1:1. was ground thoroughly in an automated mortar. 3.00 g of this mixture containing powdered iron (1.904 g, 34 mmol) and powdered sulfur (1.096 g, 34 mmol) was transferred into a 25-ml microwave vial and sodium chloride (0.181 g, 3 mmol) was added. The vial was sealed and the air was replaced by nitrogen following the standard procedure to exclude oxygen. To this mixture 10 ml of deaerated water was added and the resulting suspension was kept at room temperature overnight without stirring. The solids turned black within a couple of hours and the complete conversion of the starting materials was controlled with a strong magnet.

In a steel autoclave with a Teflon inlet powdered magnesium (0.36 g, 16 mmol) and powdered iron oxide hydroxide (0.30 g, 5 mmol) were mixed with the iron sulfide suspension and 10 ml of deionized water were added. The reactor was sealed and heated in an oven for 4 days at 160 °C without stirring.

After cooling down to room temperature, the obtained black suspension was transferred into a 500 ml beaker and charged with 200 ml deionized water. The suspension was stirred with a strong magnet for multiple minutes and all magnetic solids were removed. The residual solid was isolated by filtration, washed successively with water, ethanol, acetone and diethyl ether and dried under a stream of nitrogen.

### **10.4.3 FeFe-tochilinite**

#### **Toch\_FeFe\_1**

Powdered iron (0.630 g, 11 mmol), powdered iron oxide hydroxide (0.134 g, 2 mmol) and powdered sulfur (0.241 g, 8 mmol) were mixed in a steel autoclave with a Teflon inlet and charged with 20 ml of water. The resulting suspension was heated in an oven for 5 days at 160 °C without stirring. After cooling down to room temperature, the black suspension was filtered open to the air and the solid residue was washed with water and ethanol to obtain a black solid.

#### **Toch\_FeFe\_2**

Powdered iron (0.375 g, 7 mmol), powdered iron oxide hydroxide (0.153 g, 2 mmol) and FeS\_1 (0.88 g) were mixed in a steel autoclave with a Teflon inlet and charged with 20 ml



of water. The resulting suspension was heated in an oven for 5 days at 160 °C without stirring. After cooling down to room temperature, the black suspension was filtered open to the air and the solid residue was washed with water and ethanol to obtain a black solid.

### **Toch\_FeFe\_3**

Powdered iron (0.307 g, 5 mmol) and FeS\_1 (0.882 g) were mixed in a steel reactor with a Teflon inlet the reactor and charged with 20 ml of water. The resulting suspension was heated in an oven for 3 days at 160 °C without stirring. After cooling down to room temperature, the black suspension was filtered open to the air and the solid residue was washed with water and ethanol to obtain a black solid.

### **Toch\_FeFe\_4**

40 g of a mixture of iron and sulfur was ground thoroughly in an automated mortar. 4.000 g of this mixture containing powdered iron (3.000 g, 54 mmol) and powdered sulfur (1.000 g, 31 mmol) was transferred into a steel autoclave with a Teflon inlet and 20 ml of deionized water were added. The reactor was sealed and heated in an oven for 3 days at 130 °C without stirring.

After cooling down to room temperature, the obtained black solid was isolated by filtration and washed successively with water, ethanol, acetone and diethyl ether. As it got warm upon air contact, it was dried following the standard procedure to obtain a brownish dark powder.

### **Toch\_FeFe\_5**

40 g of a mixture of iron and sulfur was ground thoroughly in an automated mortar. 4.00 g of this mixture containing powdered iron (3.000 g, 54 mmol) and powdered sulfur (1.000 g, 31 mmol) was transferred into a steel autoclave with a Teflon inlet and 20 ml of deionized water were added. The reactor was sealed and heated in an oven for 5 days at 120 °C without stirring.

After cooling down to room temperature, the obtained black suspension was transferred into a 500 ml beaker and stirred with a strong magnet for 5 minutes and all magnetic

solids were removed. The solid was isolated by filtration and washed successively with water, ethanol, acetone and diethyl ether. As it got warm upon air contact, it was dried following the standard procedure to obtain a brownish dark powder.

#### **Toch\_FeFe\_6**

40 g of a mixture of iron and sulfur was ground thoroughly in an automated mortar. 1.00 g of this mixture containing powdered iron (1.000 g, 17 mmol) and powdered sulfur (0.333 g, 10 mmol) was transferred into a steel autoclave with a Teflon inlet and 20 ml of deionized water were added. The reactor was sealed and heated in an oven for 5 days at 120 °C without stirring.

After cooling down to room temperature, the obtained black suspension was transferred into a 500 ml beaker and stirred with a strong magnet for 5 minutes and all magnetic solids were removed. The solid was isolated by filtration and washed successively with water, ethanol, acetone and diethyl ether. As it got warm upon air contact, it was dried following the standard procedure to obtain a brownish dark powder.

#### **Toch\_FeFe\_7**

40 g of a mixture of iron and sulfur was ground thoroughly in an automated mortar. 4.00 g of this mixture containing powdered iron (3.000 g, 54 mmol) and powdered sulfur (1.000 g, 31 mmol) and additional powdered sulfur (0.111 g, 3 mmol) were transferred into a steel autoclave with a Teflon inlet and 20 ml of deionized water were added. The reactor was sealed and heated in an oven for 3 days at 130 °C without stirring.

After cooling down to room temperature, the obtained black suspension was transferred into a 500 ml beaker and stirred with a strong magnet for 5 minutes and all magnetic solids were removed. The solid was isolated by filtration and washed successively with water, ethanol, acetone and diethyl ether. As it got warm upon air contact, it was dried following the standard procedure to obtain a brownish dark powder.

#### **Toch\_FeFe\_8**

40 g of a mixture of iron and sulfur was ground thoroughly in an automated mortar. 4.00 g of this mixture containing powdered iron (3.000 g, 54 mmol) and powdered sulfur (1.000 g, 31 mmol) and additional powdered sulfur (0.214 g, 6 mmol) were transferred into a steel autoclave with a Teflon inlet and 20 ml of deionized water were added. The reactor was sealed and heated in an oven for 3 days at 130 °C without stirring.

After cooling down to room temperature, the obtained black suspension was transferred into a 500 ml beaker and stirred with a strong magnet for 5 minutes and all magnetic solids were removed. The solid was isolated by filtration and washed successively with water, ethanol, acetone and diethyl ether. As it got warm upon air contact, it was dried following the standard procedure to obtain a brownish dark powder.

### **Toch\_FeFe\_9**

40 g of a mixture of iron and sulfur was ground thoroughly in an automated mortar. 4.00 g of this mixture containing powdered iron (3.000 g, 54 mmol) and powdered sulfur (1.000 g, 31 mmol) and additional powdered sulfur (0.309 g, 9 mmol) were transferred into a steel autoclave with a Teflon inlet and 20 ml of deionized water were added. The reactor was sealed and heated in an oven for 3 days at 130 °C without stirring.

After cooling down to room temperature, the obtained black suspension was transferred into a 500 ml beaker and stirred with a strong magnet for 5 minutes and all magnetic solids were removed. The solid was isolated by filtration and washed successively with water, ethanol, acetone and diethyl ether. As it got warm upon air contact, it was dried following the standard procedure to obtain a brownish dark powder.

### **Toch\_FeFe\_10**

40 g of a mixture of iron and sulfur was ground thoroughly in an automated mortar. 4.00 g of this mixture containing powdered iron (3.000 g, 54 mmol) and powdered sulfur (1.000 g, 31 mmol) and additional powdered sulfur (0.406 g, 12 mmol) were transferred into a steel autoclave with a Teflon inlet and 20 ml of deionized water were added. The reactor was sealed and heated in an oven for 3 days at 130 °C without stirring.

After cooling down to room temperature, the obtained black suspension was transferred into a 500 ml beaker and stirred with a strong magnet for 5 minutes and all magnetic solids were removed. The solid was isolated by filtration and washed successively with water, ethanol, acetone and diethyl ether. As it got warm upon air contact, it was dried following the standard procedure to obtain a brownish dark powder.

#### **Toch\_FeFe\_11**

40 g of a mixture of iron and sulfur was ground thoroughly in an automated mortar. 4.00 g of this mixture containing powdered iron (3.000 g, 54 mmol) and powdered sulfur (1.000 g, 31 mmol) and additional powdered sulfur (0.111 g, 3 mmol) were transferred into a steel autoclave with a Teflon inlet and 20 ml of deionized water were added. The reactor was sealed and heated in an oven for 3 days at 130 °C without stirring.

After cooling down to room temperature, the obtained black suspension was transferred into a 500 ml beaker and stirred with a strong magnet for 5 minutes and all magnetic solids were removed. The solid was isolated by filtration and washed successively with water, ethanol, acetone and diethyl ether. As it got warm upon air contact, it was dried following the standard procedure to obtain a brownish dark powder.

#### **10.4.4 FeAl-tochilinite**

##### **Toch\_FeAl\_1**

90.6 g of a mixture of iron, sulfur and aluminum was ground thoroughly in an automated mortar. 9.06 g of this mixture containing powdered iron (6.000 g, 107 mmol), powdered sulfur (2.460 g, 44 mmol) and powdered aluminum (0.600 g, 22 mmol) were transferred into a steel autoclave with a Teflon inlet and 20 ml of deionized water were added. The reactor was sealed and heated in an oven for 3 days at 130 °C without stirring.

After cooling down to room temperature, the obtained black suspension was transferred into a 500 ml beaker and stirred with a strong magnet for 5 minutes and all magnetic solids were removed. The solid was isolated by filtration and washed successively with water, ethanol, acetone and diethyl ether. As it got warm upon air contact, it was dried following the standard procedure to obtain a black powder.

### **Toch\_FeAl\_2**

90.6 g of a mixture of iron, sulfur and aluminum was ground thoroughly in an automated mortar. 9.06 g of this mixture containing powdered iron (6.000 g, 107 mmol), powdered sulfur (2.460 g, 44 mmol) and powdered aluminum (0.600 g, 22 mmol) were transferred into a steel autoclave with a Teflon inlet.

Additional iron and aluminum was ground in a mortar and 0.1217 g of this mixture containing powdered iron (0.1106 g, 2.0 mmol) and powdered aluminum (0.0111 g, 0.4 mmol) was added to the steel autoclave. The solids were mixed and 20 ml of deionized water were added. The reactor was sealed and heated in an oven for 3 days at 130 °C without stirring.

After cooling down to room temperature, the obtained black suspension was transferred into a 500 ml beaker and stirred with a strong magnet for 5 minutes and all magnetic solids were removed. The solid was isolated by filtration and washed successively with water, ethanol, acetone and diethyl ether. As it got warm upon air contact, it was dried following the standard procedure to obtain a black powder.

### **Toch\_FeAl\_3**

90.6 g of a mixture of iron, sulfur and aluminum was ground thoroughly in an automated mortar. 9.06 g of this mixture containing powdered iron (6.000 g, 107 mmol), powdered sulfur (2.460 g, 44 mmol) and powdered aluminum (0.600 g, 22 mmol) were transferred into a steel autoclave with a Teflon inlet.

Additional iron and aluminum were ground in a mortar and 0.5603 g of this mixture containing powdered iron (0.5092 g, 9.1 mmol) and powdered aluminum (0.0511 g, 1.89 mmol) was added to the steel autoclave. The solids were mixed and 20 ml of deionized water were added. The reactor was sealed and heated in an oven for 3 days at 130 °C without stirring.

After cooling down to room temperature, the obtained black suspension was transferred into a 500 ml beaker and stirred with a strong magnet for 5 minutes and all magnetic solids were removed. The solid was isolated by filtration and washed successively with

water, ethanol, acetone and diethyl ether. As it got warm upon air contact, it was dried following the standard procedure to obtain a black powder.

#### **Toch\_FeAl\_4**

90.6 g of a mixture of iron, sulfur and aluminum was ground thoroughly in an automated mortar. 9.06 g of this mixture containing powdered iron (6.000 g, 107 mmol), powdered sulfur (2.460 g, 44 mmol) and powdered aluminum (0.600 g, 22 mmol) were transferred into a steel autoclave with a Teflon inlet.

Additional iron and aluminum were ground in a mortar and 0.3426 g of this mixture containing powdered iron (0.3113 g, 5.6 mmol) and powdered aluminum (0.0312 g, 1.2 mmol) was added to the steel autoclave. The solids were mixed and 20 ml of deionized water were added. The reactor was sealed and heated in an oven for 3 days at 130 °C without stirring.

After cooling down to room temperature, the obtained black suspension was transferred into a 500 ml beaker and stirred with a strong magnet for 5 minutes and all magnetic solids were removed. The solid was isolated by filtration and washed successively with water, ethanol, acetone and diethyl ether. As it got warm upon air contact, it was dried following the standard procedure to obtain a black powder.

#### **Toch\_FeAl\_5**

90.6 g of a mixture of iron, sulfur and aluminum was ground thoroughly in an automated mortar. 9.06 g of this mixture containing powdered iron (6.000 g, 107 mmol), powdered sulfur (2.460 g, 44 mmol) and powdered aluminum (0.600 g, 22 mmol) were transferred into a steel autoclave with a Teflon inlet.

Additional iron and aluminum were ground in a mortar and 0.7652 g of this mixture containing powdered iron (0.6954 g, 12.5 mmol) and powdered aluminum (0.0698 g, 2.6 mmol) was added to the steel autoclave. The solids were mixed and 20 ml of deionized water were added. The reactor was sealed and heated in an oven for 3 days at 130 °C without stirring.

After cooling down to room temperature, the obtained black suspension was transferred into a 500 ml beaker and stirred with a strong magnet for 5 minutes and all magnetic solids were removed. The solid was isolated by filtration and washed successively with water, ethanol, acetone and diethyl ether. As it got warm upon air contact, it was dried following the standard procedure to obtain a black powder.

### **Toch\_FeAl\_6**

90.6 g of a mixture of iron, sulfur and aluminum was ground thoroughly in an automated mortar. 9.06 g of this mixture containing powdered iron (6.000 g, 107 mmol), powdered sulfur (2.460 g, 44 mmol) and powdered aluminum (0.600 g, 22 mmol) were transferred into a steel autoclave with a Teflon inlet.

Additional iron and aluminum were ground in a mortar and 0.1217 g of this mixture containing powdered iron (0.1106 g, 2.0 mmol) and powdered aluminum (0.0111 g, 0.4 mmol) was added to the steel autoclave. The solids were mixed and 20 ml of deionized water were added. The reactor was sealed and heated in an oven for 3 days at 130 °C without stirring.

After cooling down to room temperature, the obtained black suspension was transferred into a 500 ml beaker and stirred with a strong magnet for 5 minutes and all magnetic solids were removed. The solid was isolated by filtration and washed successively with water, ethanol, acetone and diethyl ether. As it got warm upon air contact, it was dried following the standard procedure to obtain a black powder.

## Appendix

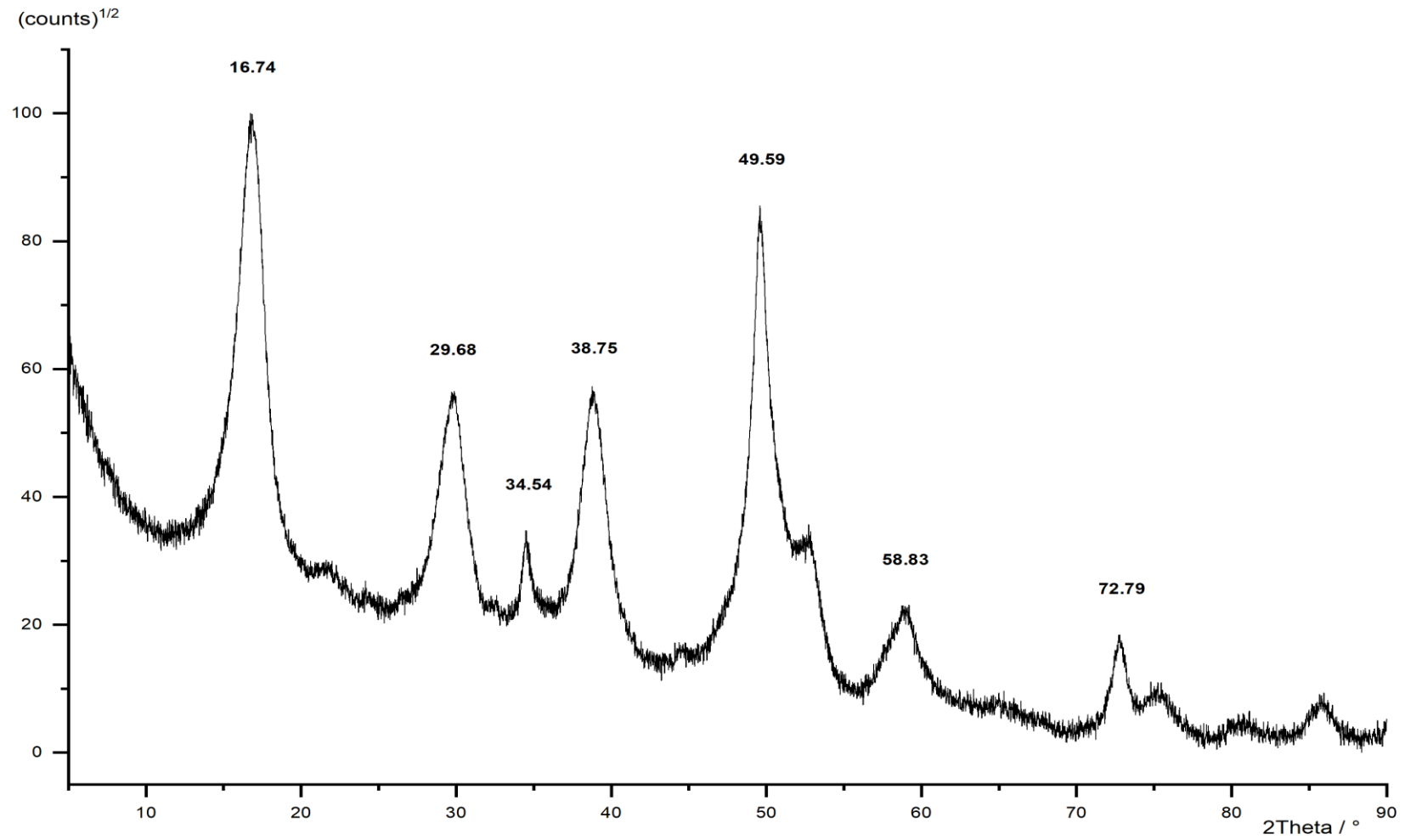


Figure 63: Powder diffraction pattern of FeS<sub>1</sub>.



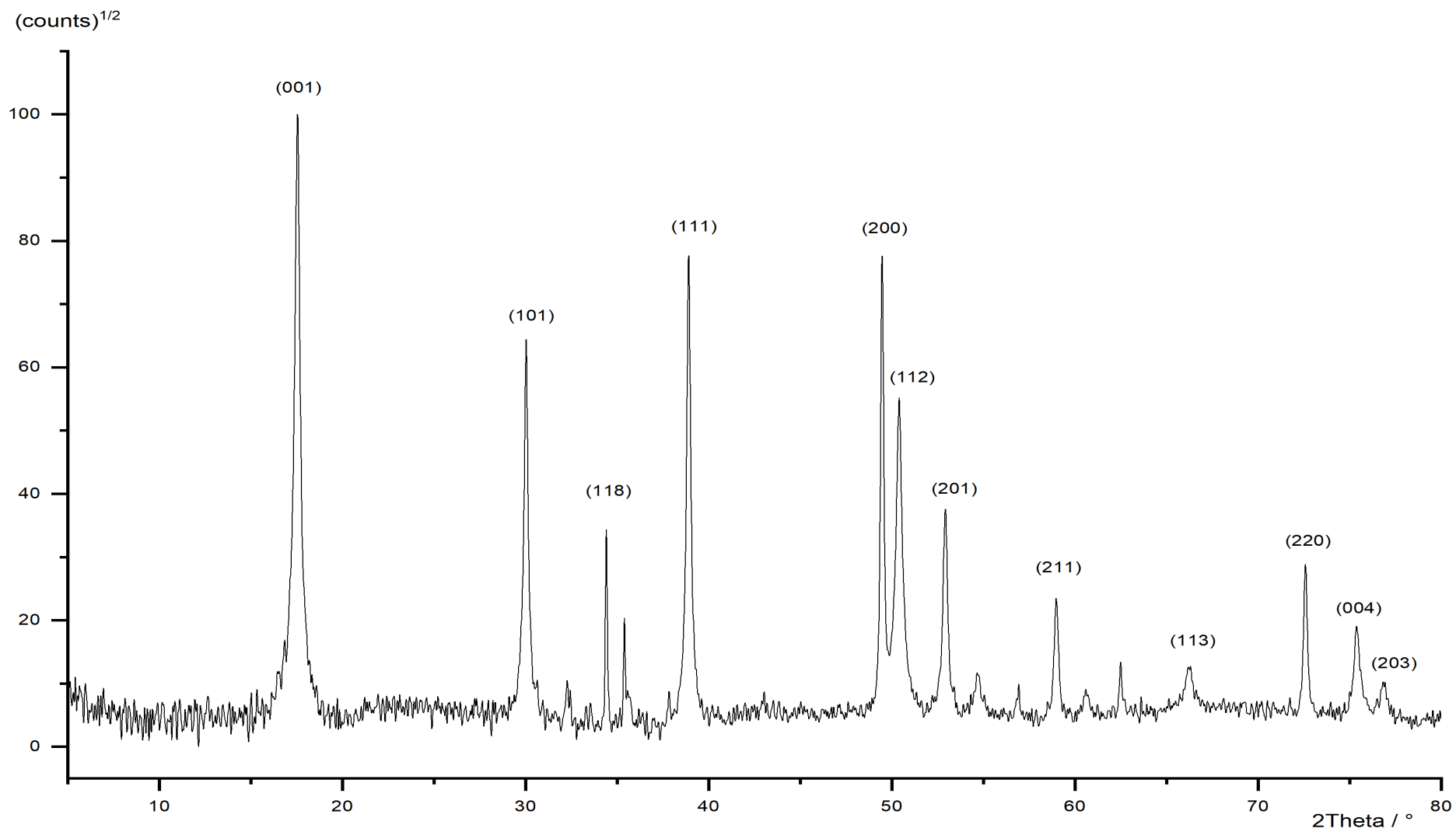


Figure 64: Powder diffraction pattern of FeS<sub>2</sub>. Mackinawite HKL value are assigned to the diffraction peaks.

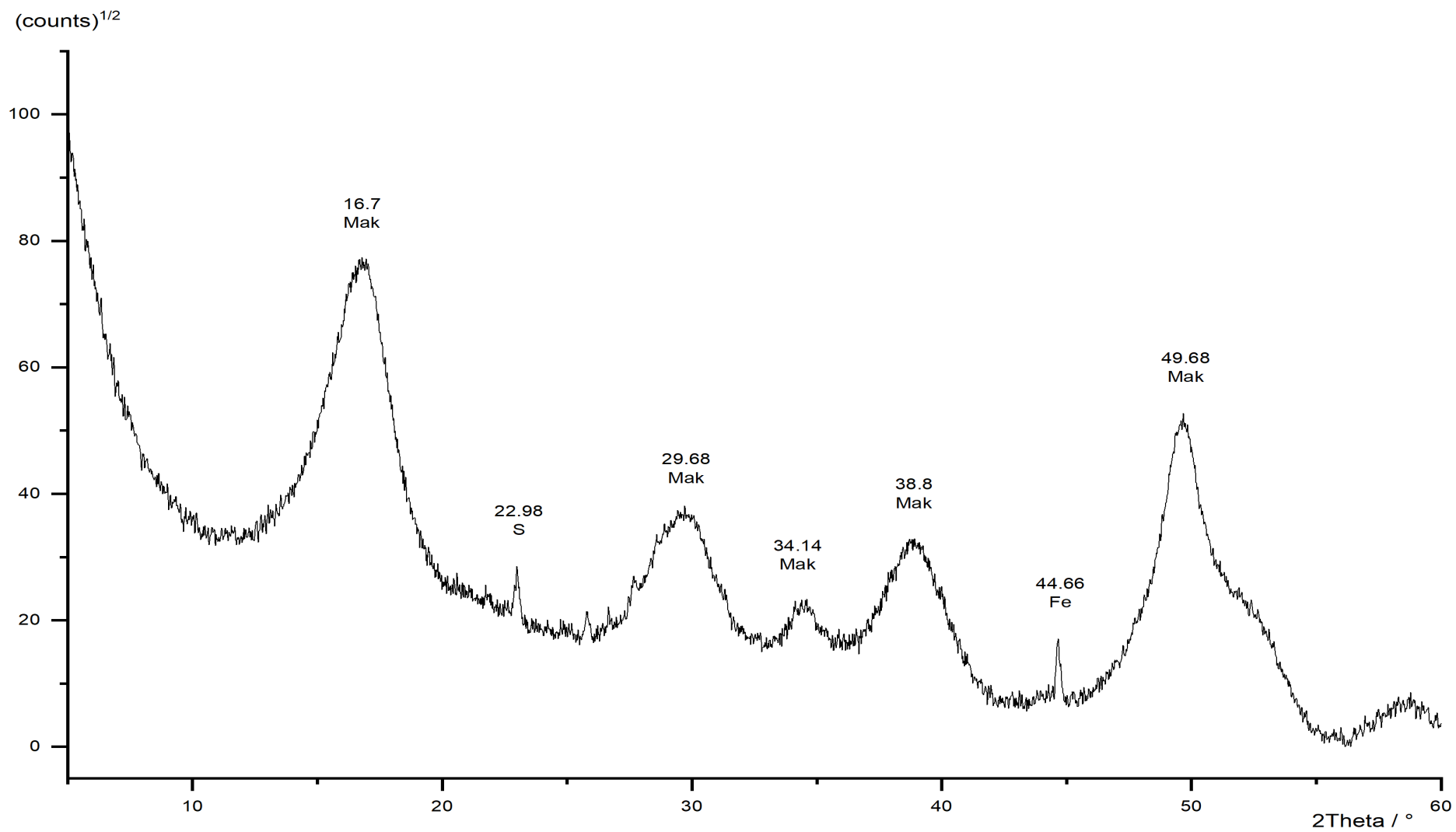


Figure 65: Powder diffraction pattern of FeS\_NaCl\_1. Mak = mackinawite, Fe = iron, S = sulfur.

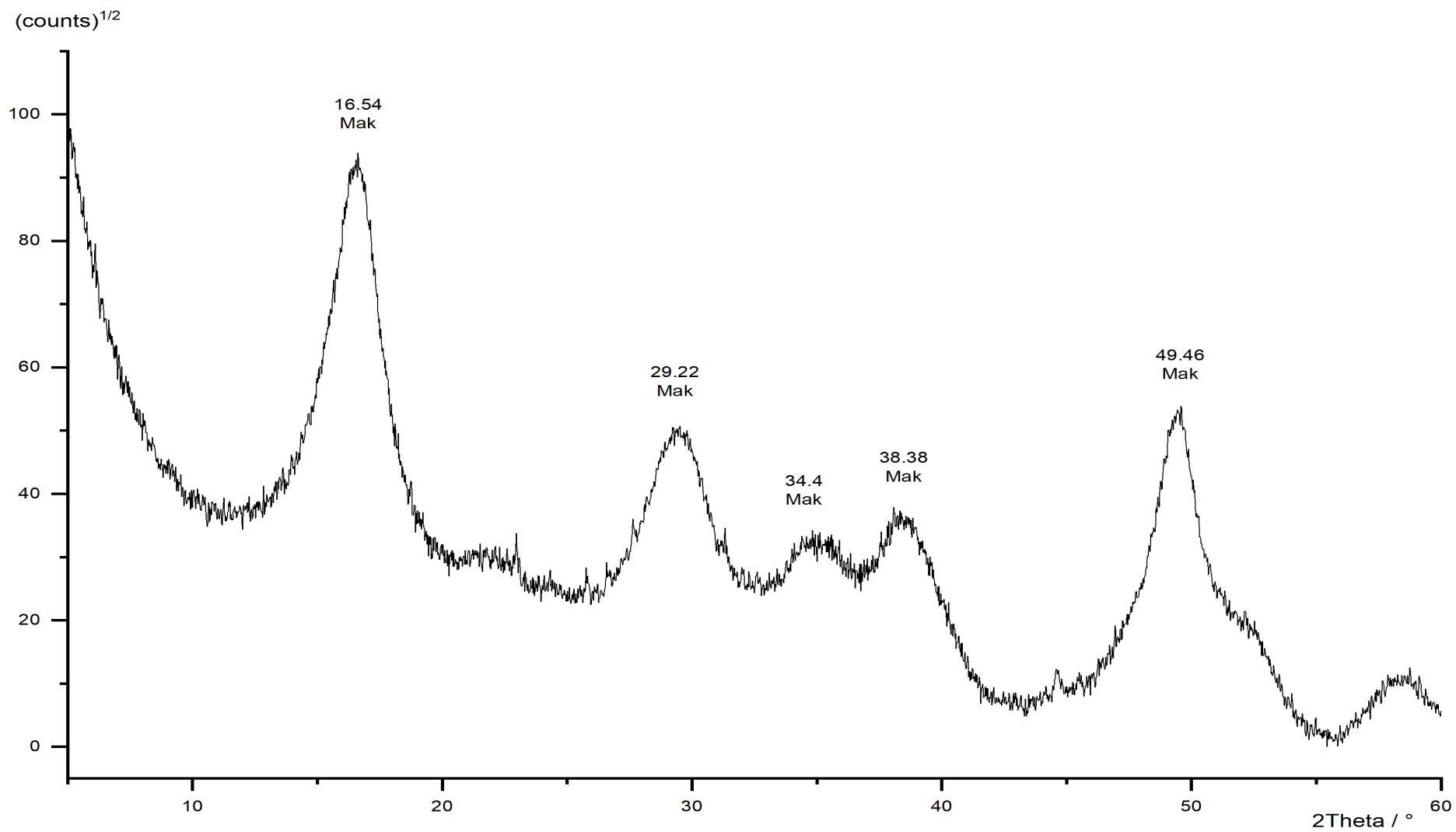


Figure 66: Powder diffraction pattern of FeS\_NaCl\_2. Mak = mackinawite.

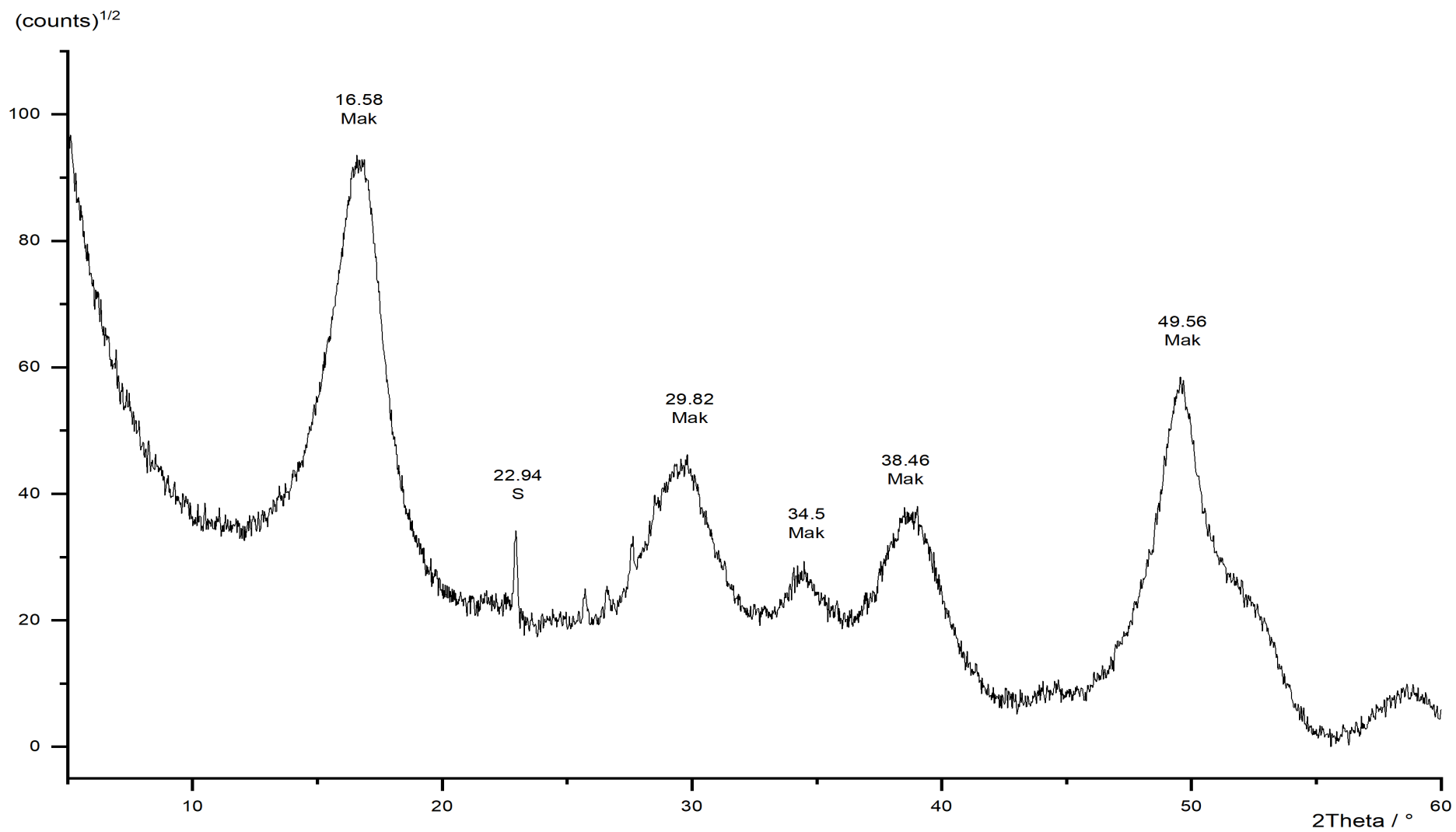


Figure 67: Powder diffraction pattern of  $\text{FeS}_{\text{NaCl}_3}$ . Mak = mackinawite, S = sulfur.

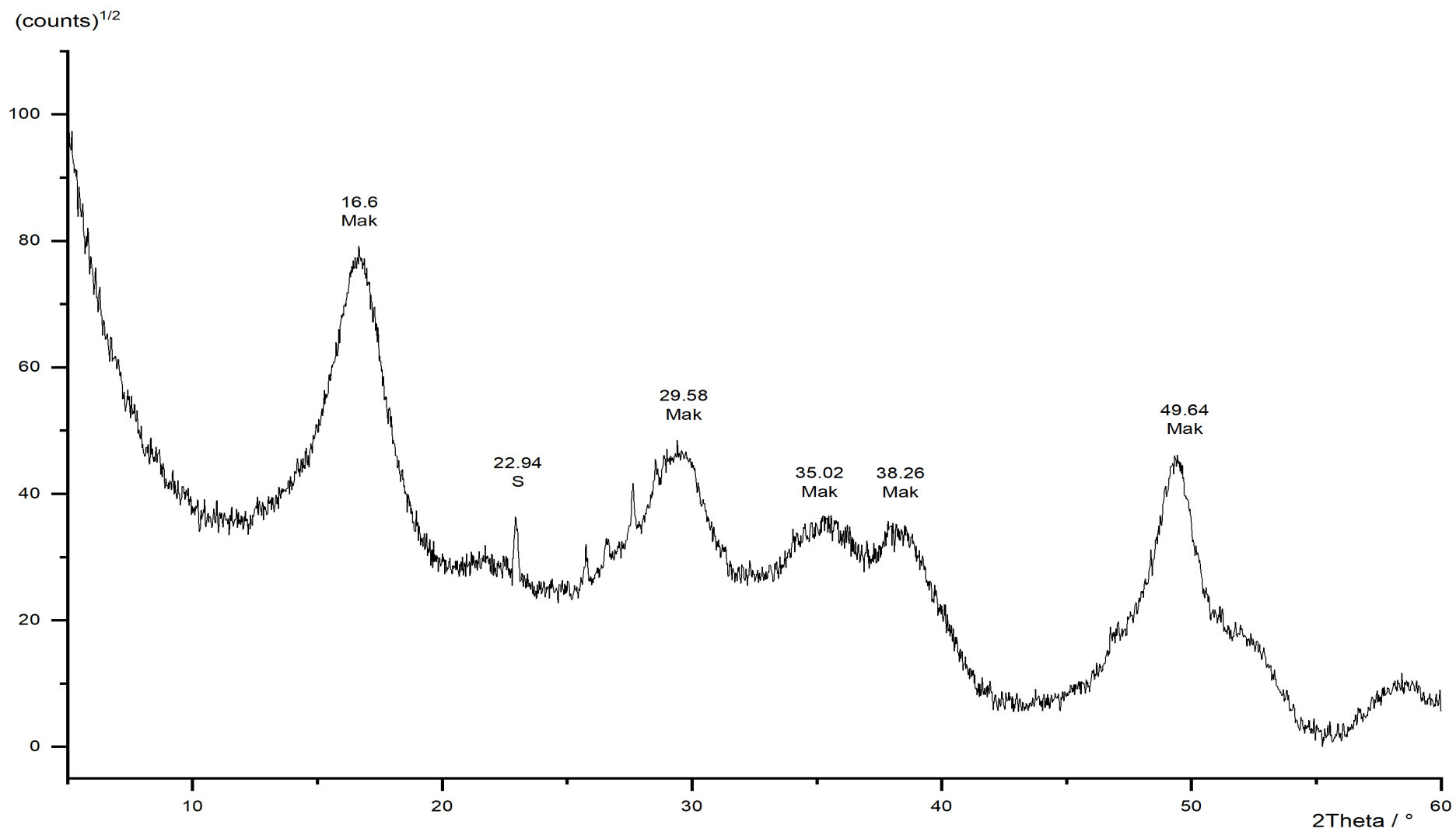


Figure 68: Powder diffraction pattern of FeS\_NaCl\_4. Mak = mackinawite, S = sulfur.

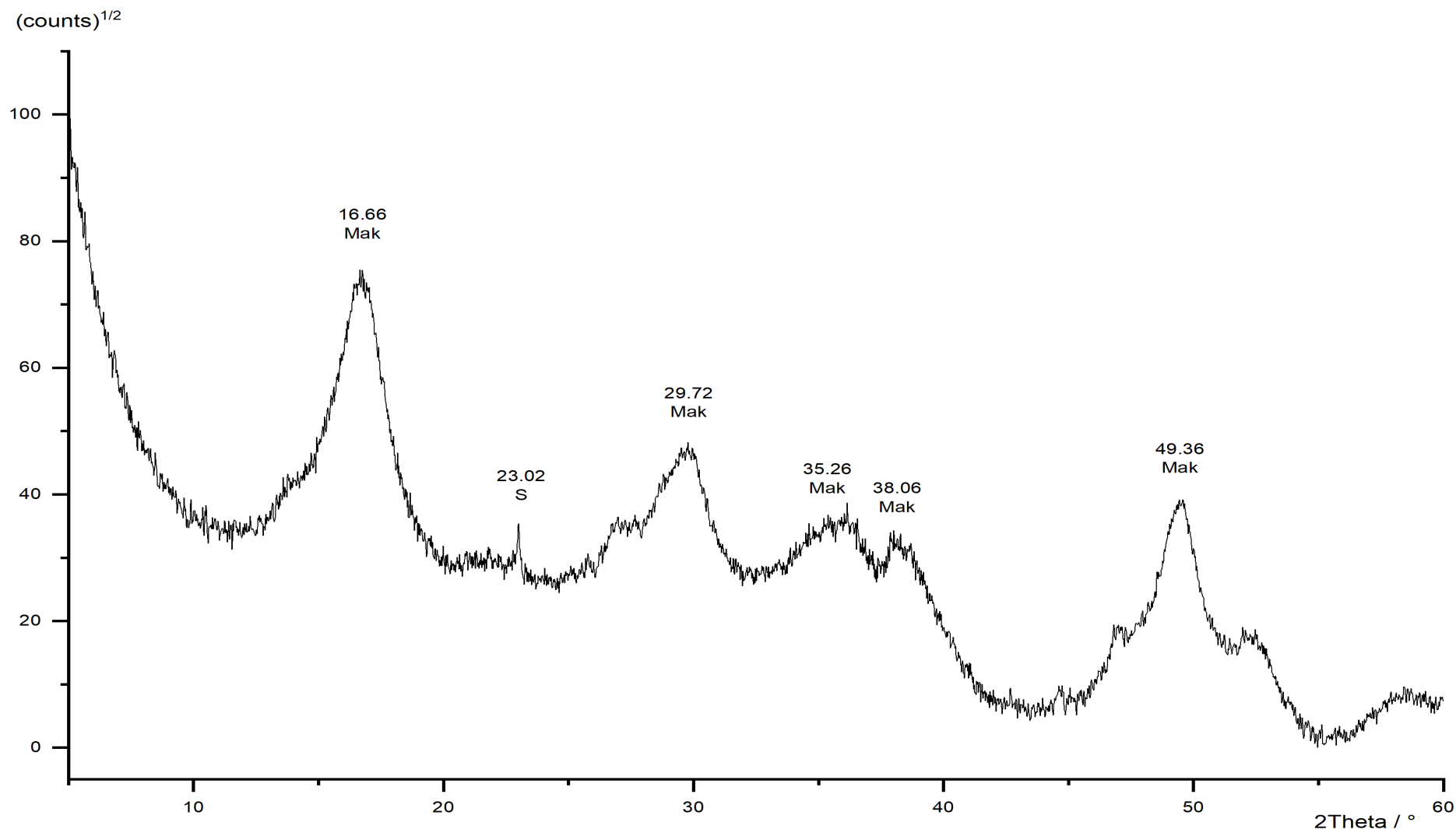


Figure 69: Powder diffraction pattern of  $\text{FeS}_{\text{NaCl}_4}$ . Mak = mackinawite, S = sulfur.

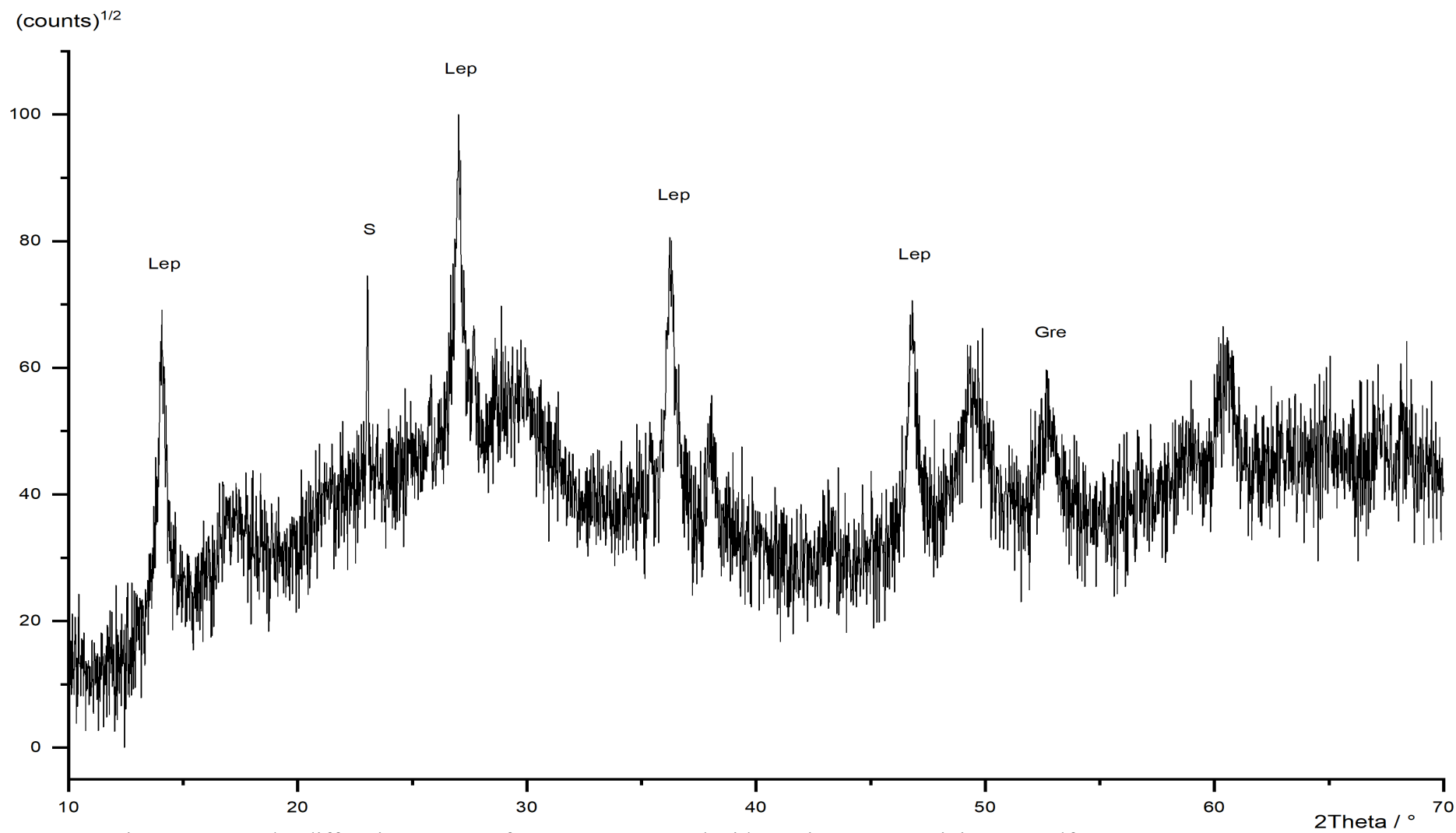


Figure 70: Powder diffraction pattern of FeS\_Ox\_3. Lep = lepidocrocite, Gre = greigite, S = sulfur.

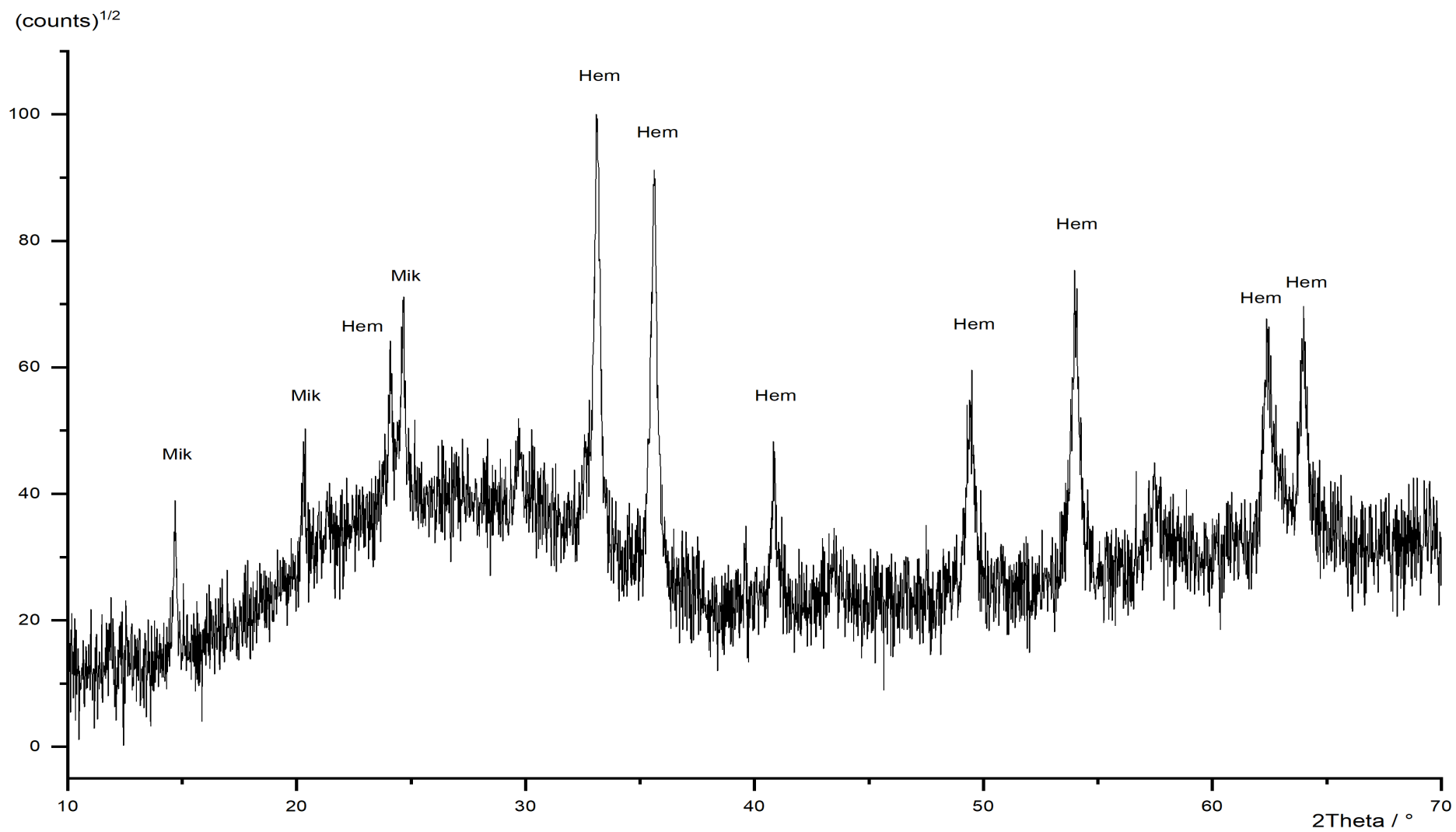


Figure 71: Powder diffraction pattern of FeS\_Ox\_4. Mik = Mikasaite, Hem = Hematite.



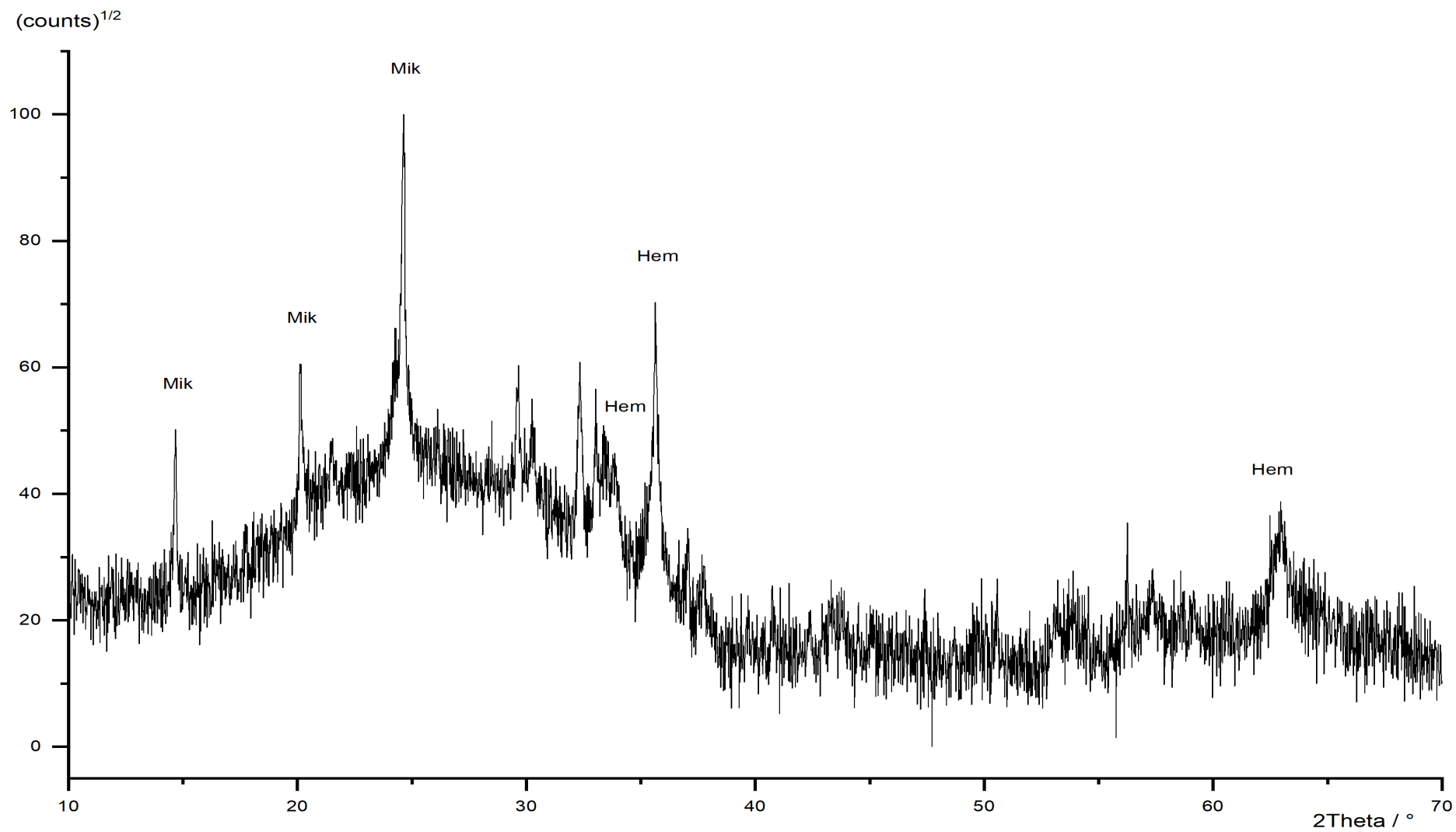


Figure 72: Powder diffraction pattern of FeS\_Ox\_5. Mik = Mikasaite, Hem = Hematite.

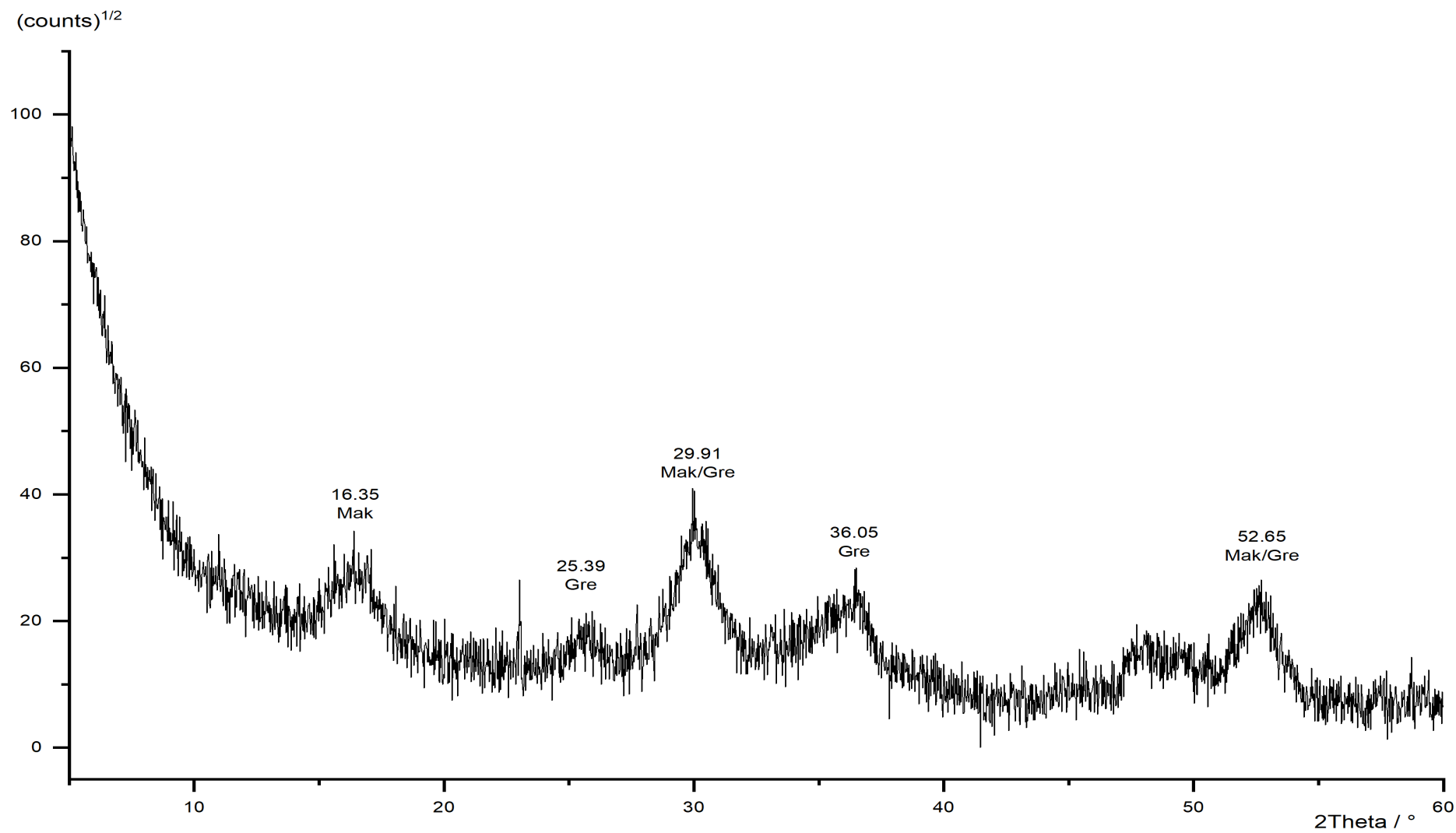


Figure 73: Powder diffraction pattern of FeS\_Ox\_6. Mak = mackinawite, Gre = greigite.

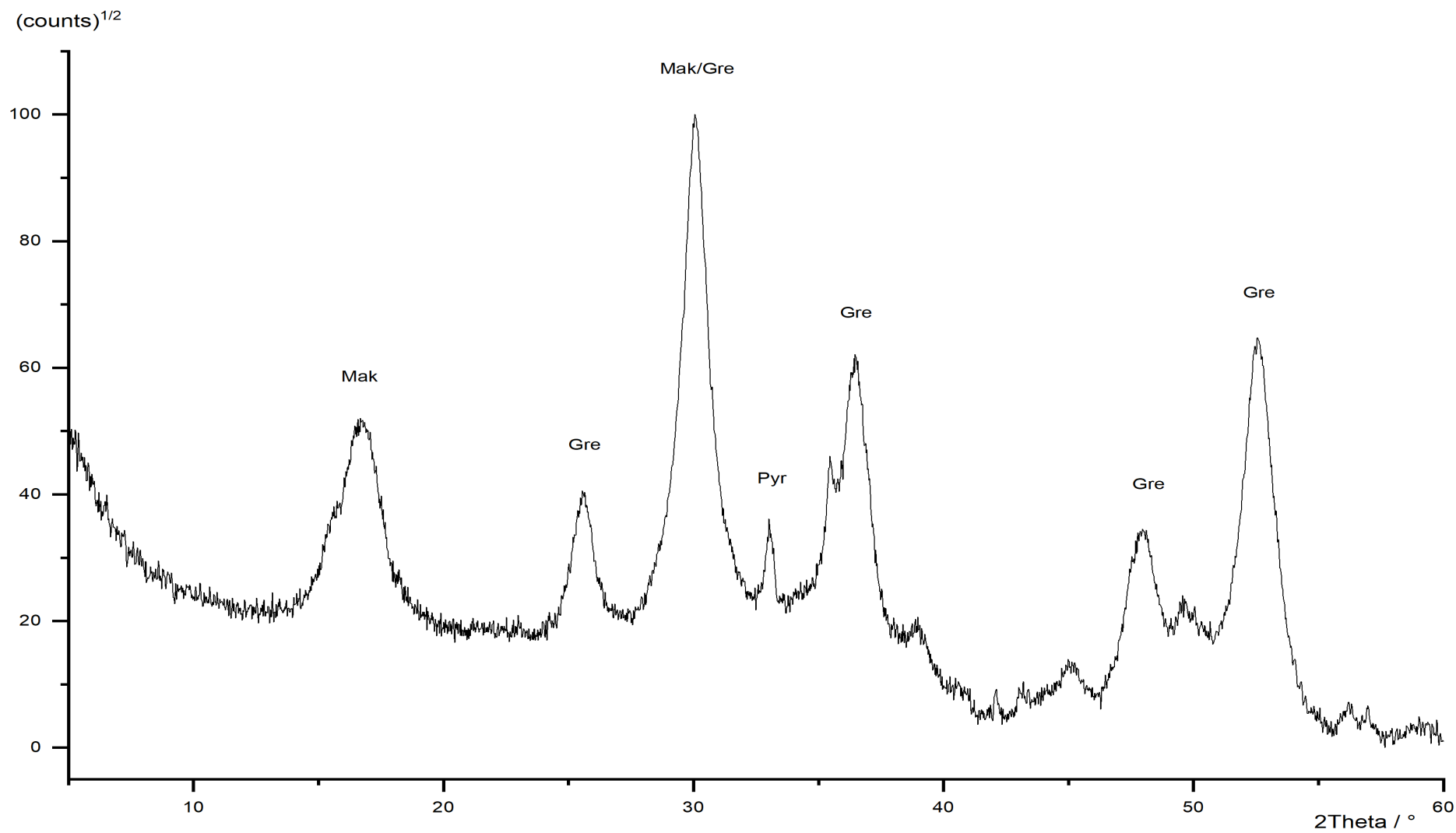


Figure 74: Powder diffraction pattern of FeS\_Ox\_9. Mak = mackinawite, Gre = greigite.

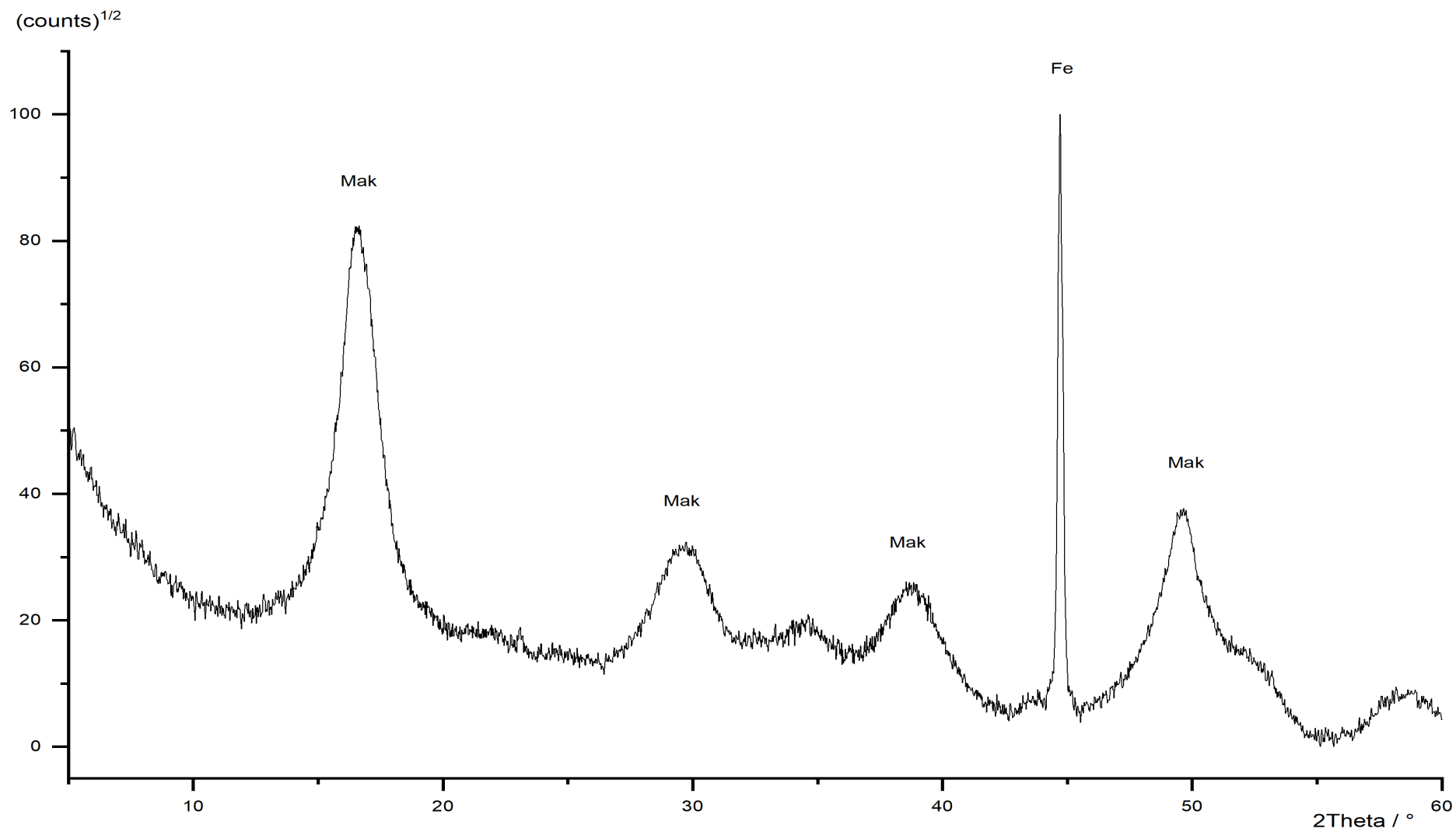


Figure 75: Powder diffraction pattern of FeS\_Ox\_10. Mak = mackinawite, Fe = iron.

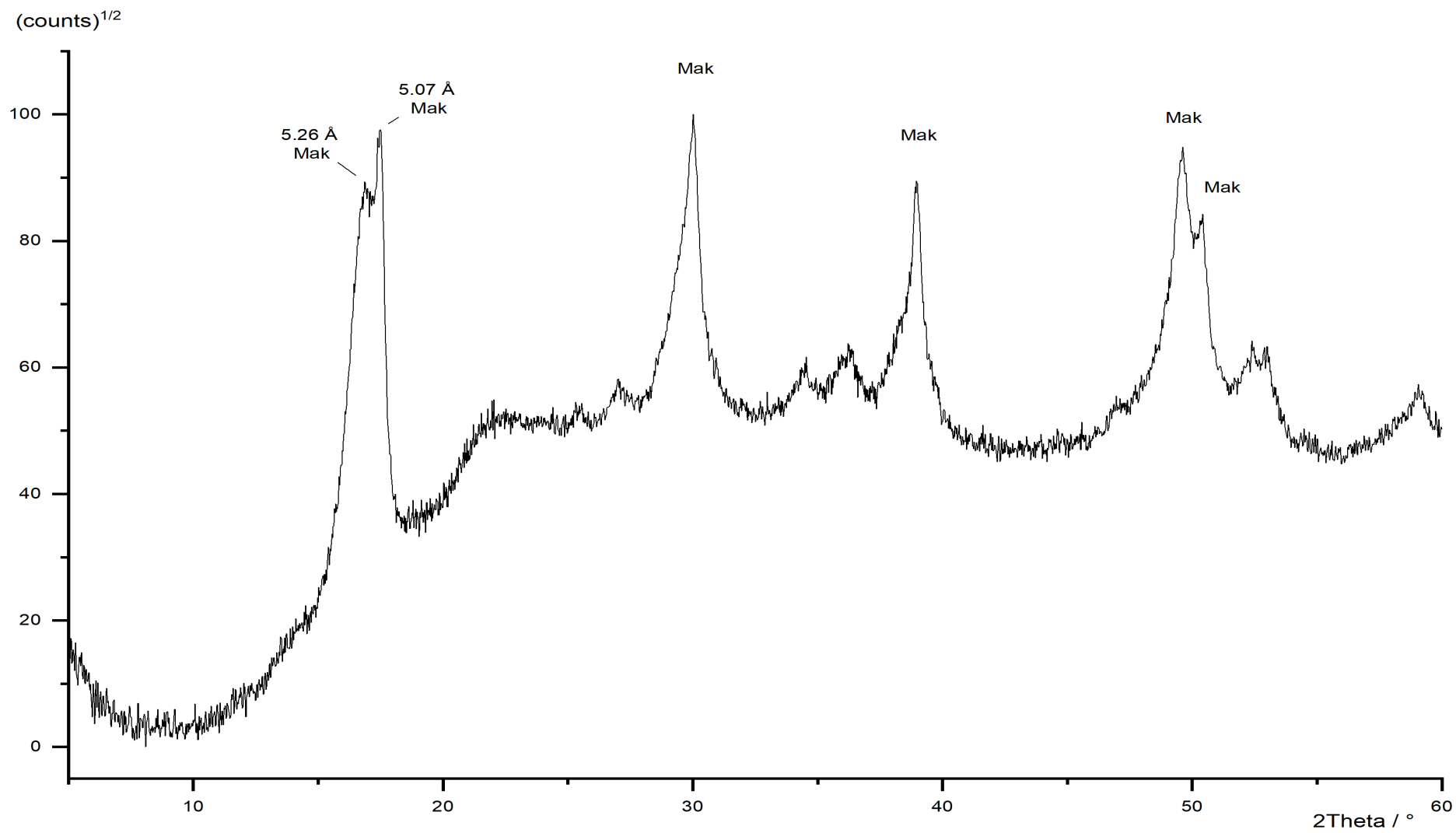


Figure 76: Powder diffraction pattern of FeS\_Ox\_11. Mak = mackinawite.

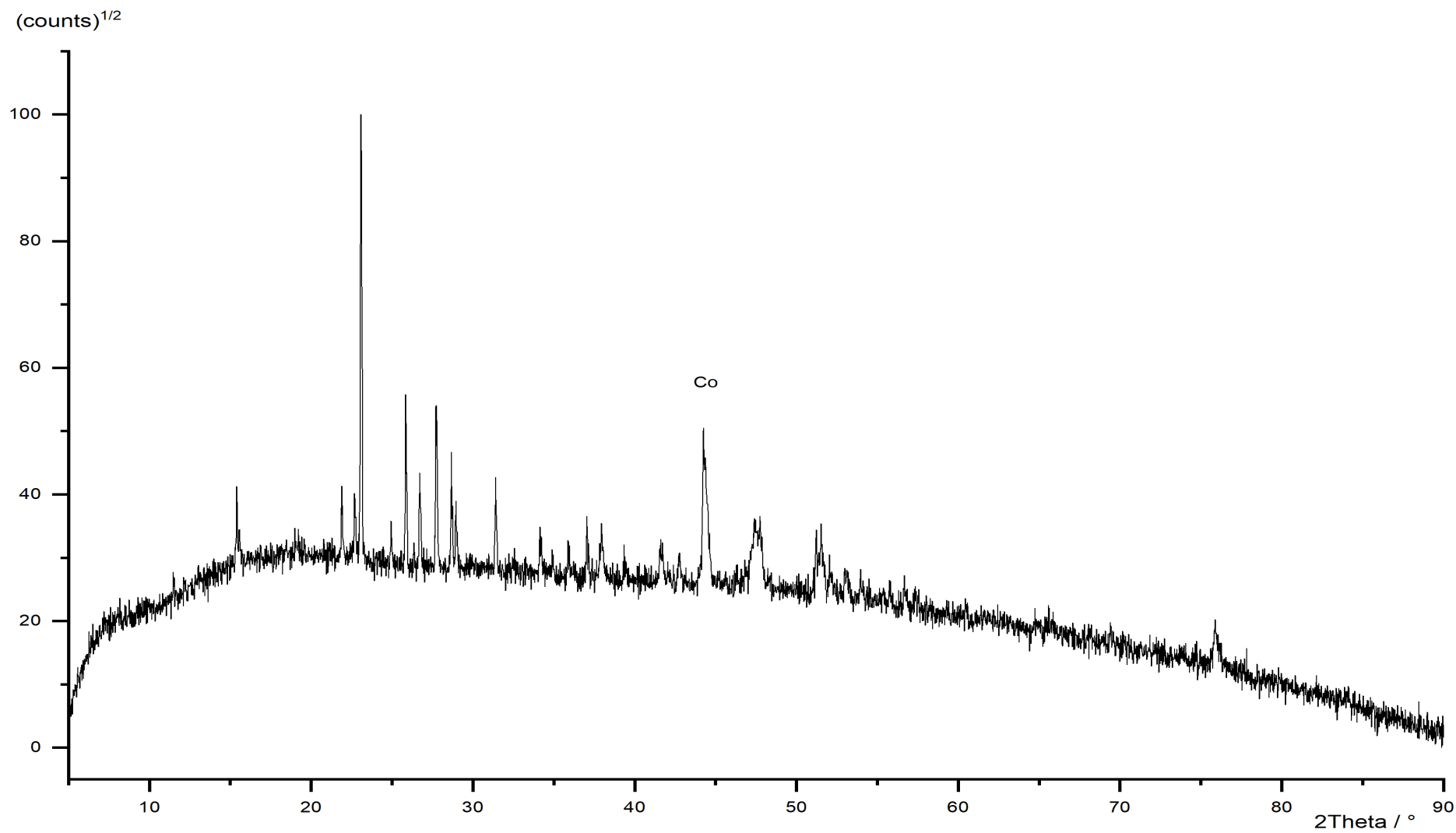


Figure 77: Powder diffraction pattern of CoS<sub>1</sub>. Co = cobalt. All other peaks can be assigned to elemental sulfur.

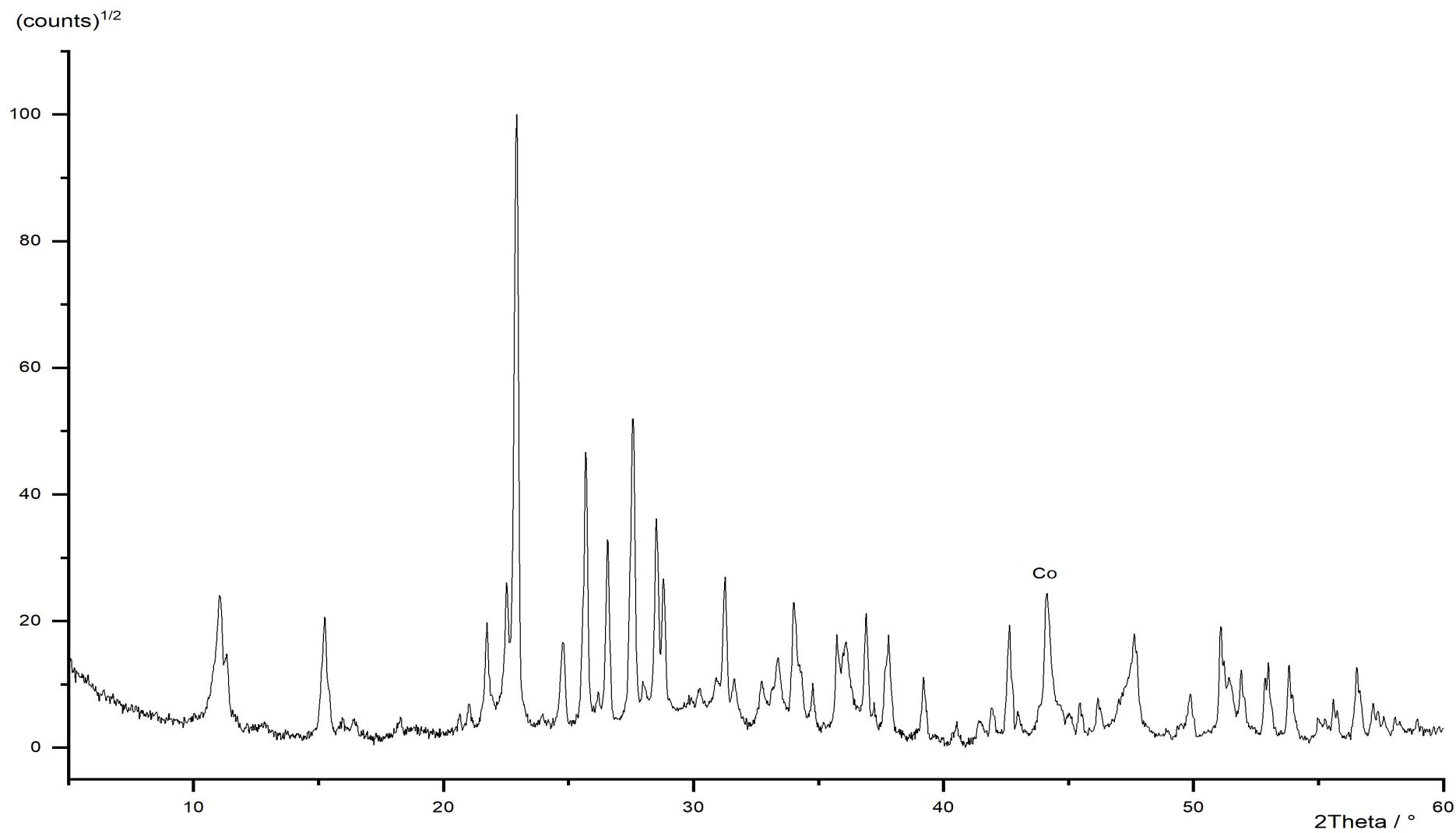


Figure 78: Powder diffraction pattern of CoS<sub>2</sub>. Co = cobalt. All other peaks can be assigned to elemental sulfur

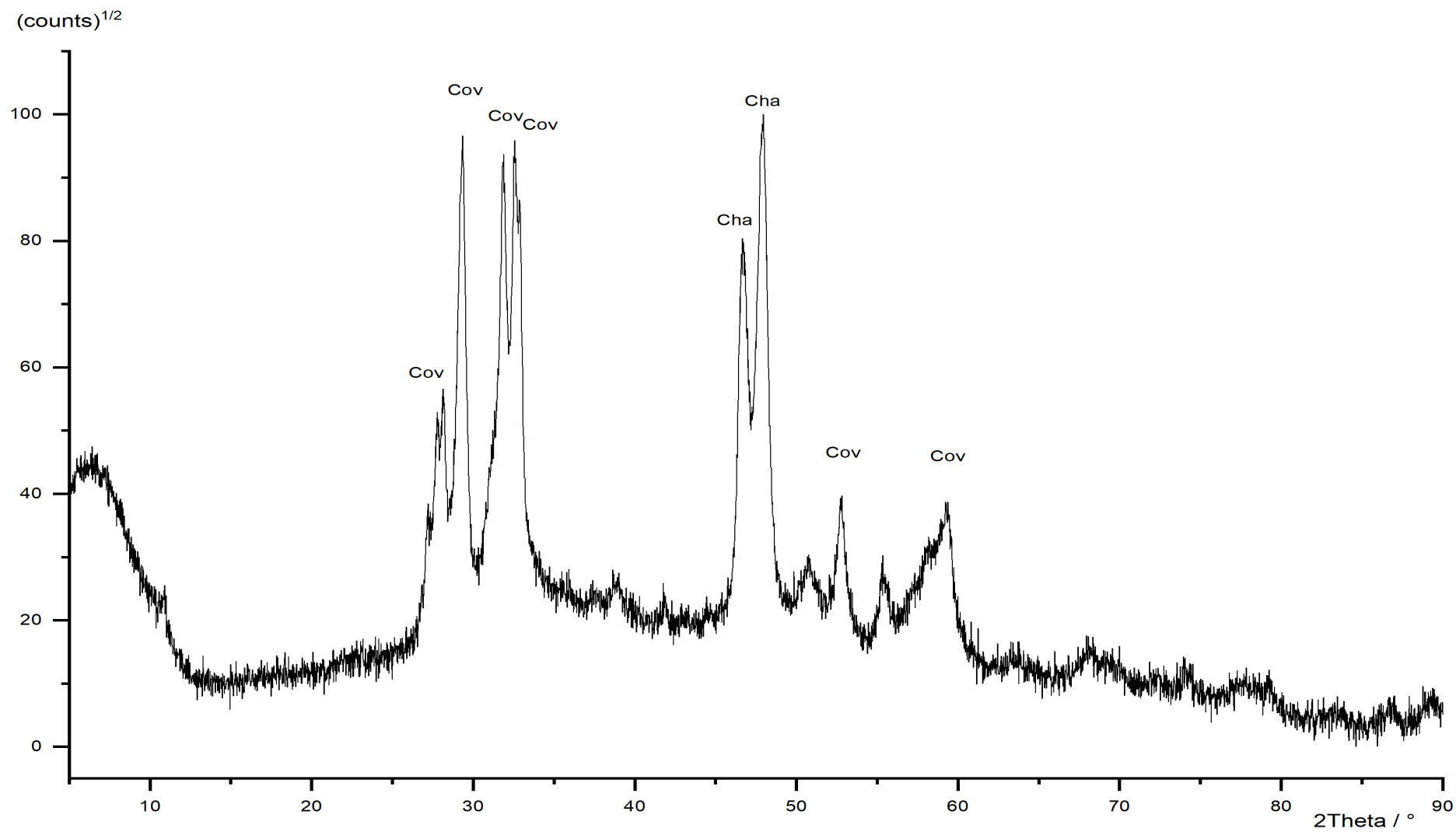


Figure 79: Powder diffraction pattern of CuS<sub>1</sub>. Cha = chalcopyrite, Cov = covellite.



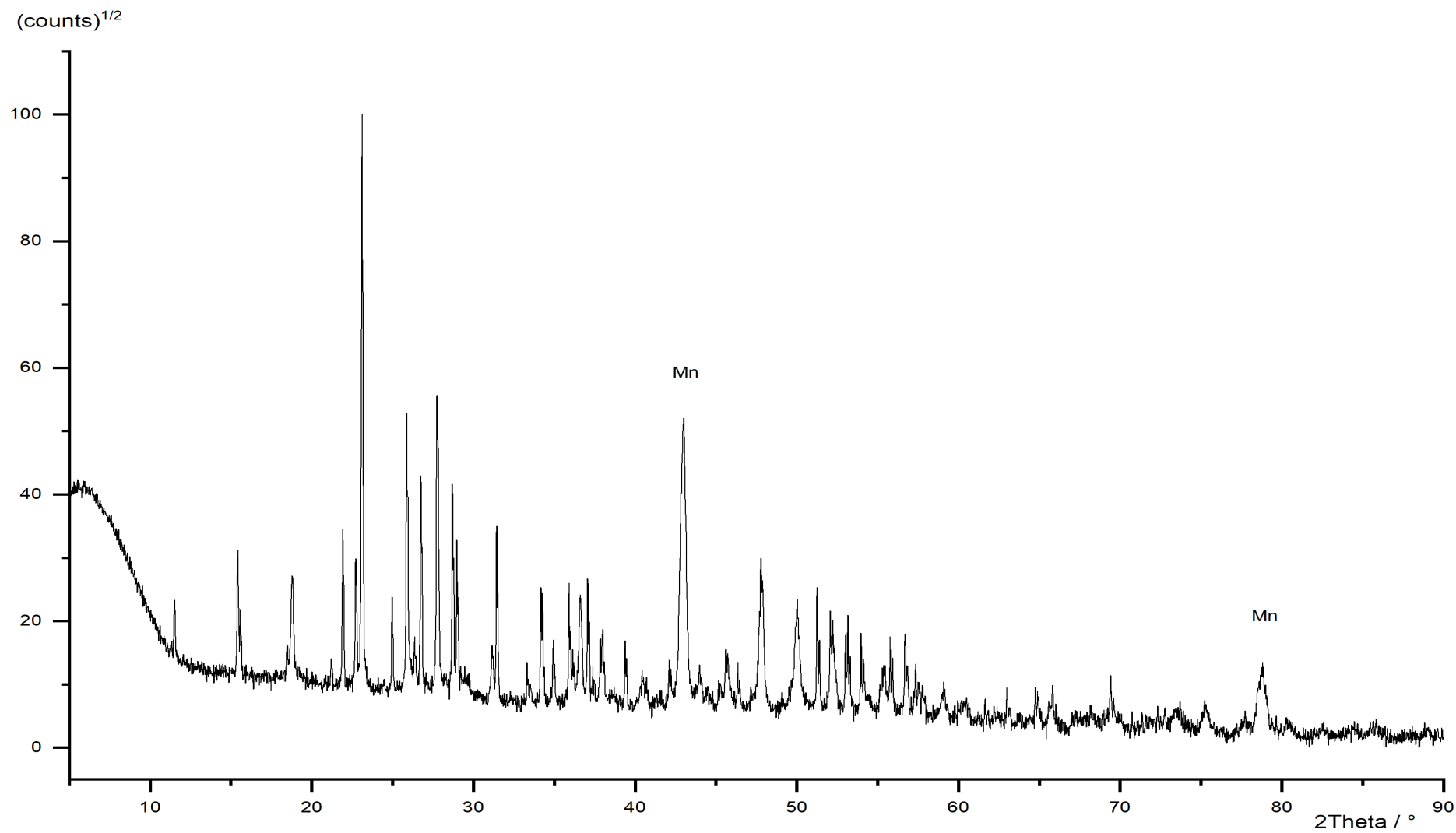


Figure 80: Powder diffraction pattern of MnS<sub>1</sub>. Mn = manganese, all other peaks can be assigned to sulfur.

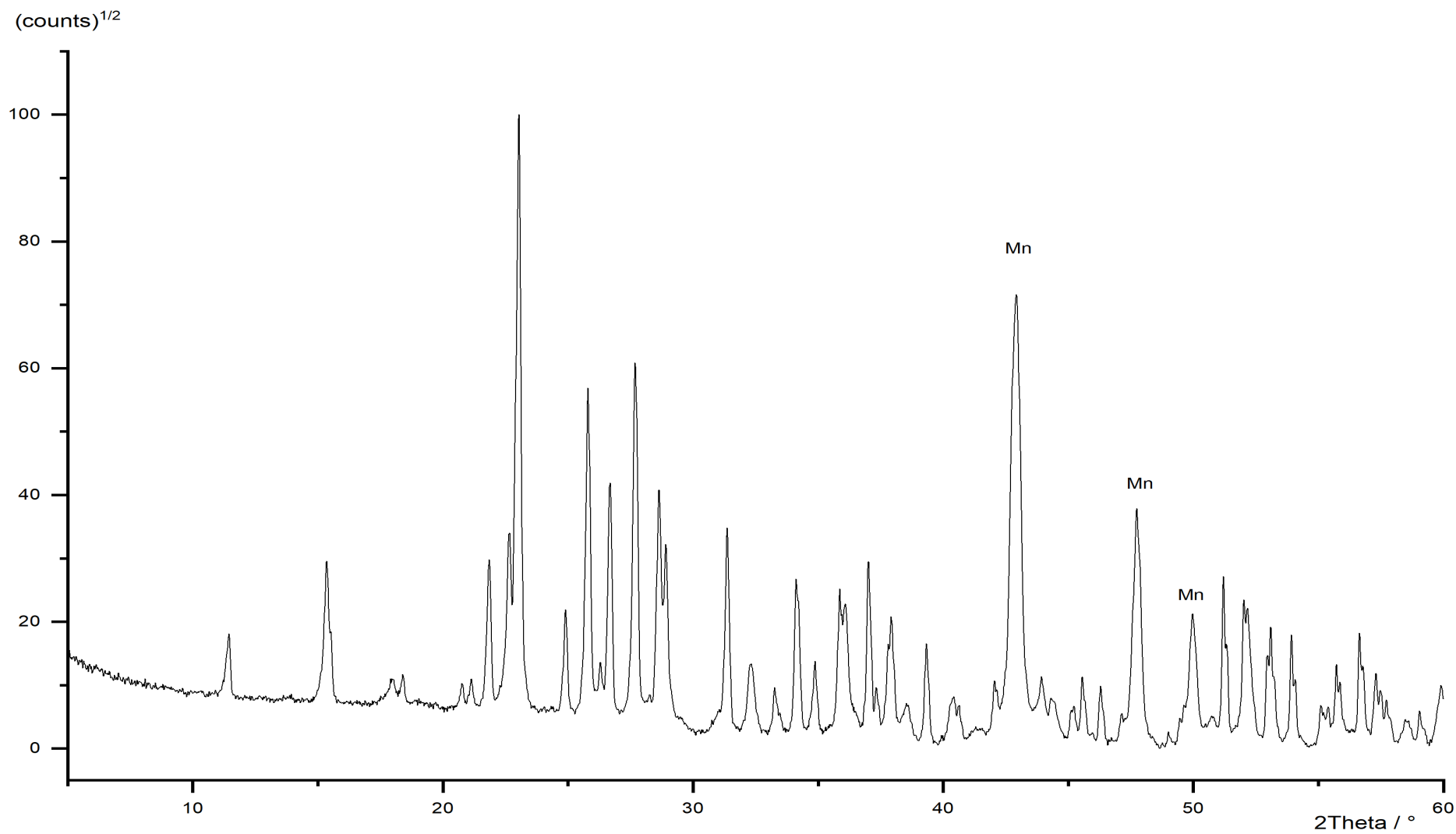


Figure 81: Powder diffraction pattern of MnS<sub>2</sub>. Mn = manganese, all other peaks can be assigned to sulfur.

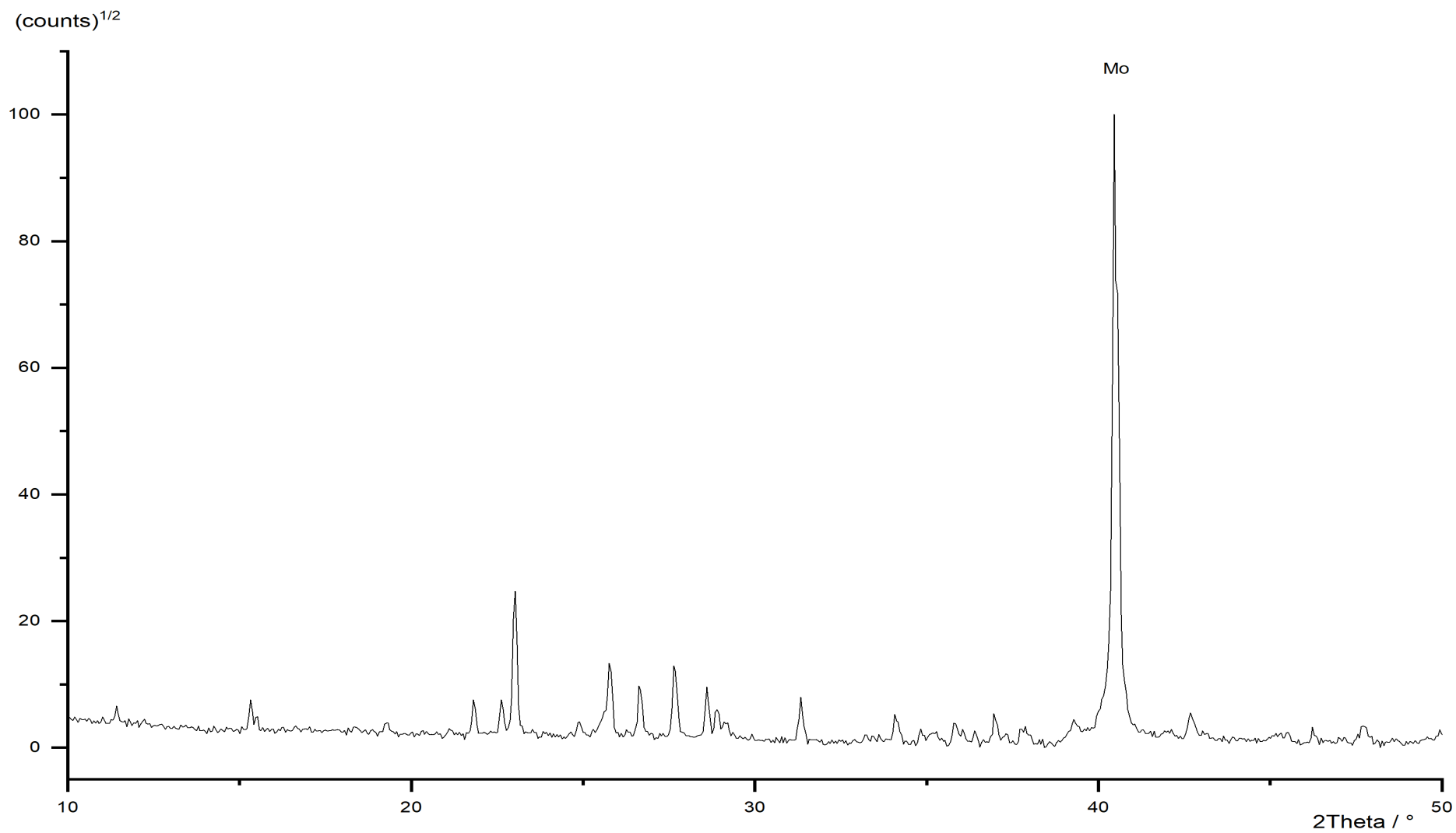


Figure 82: Powder diffraction pattern of MoS<sub>1</sub>. Mo = molybdenum, all other peaks can be assigned to sulfur.

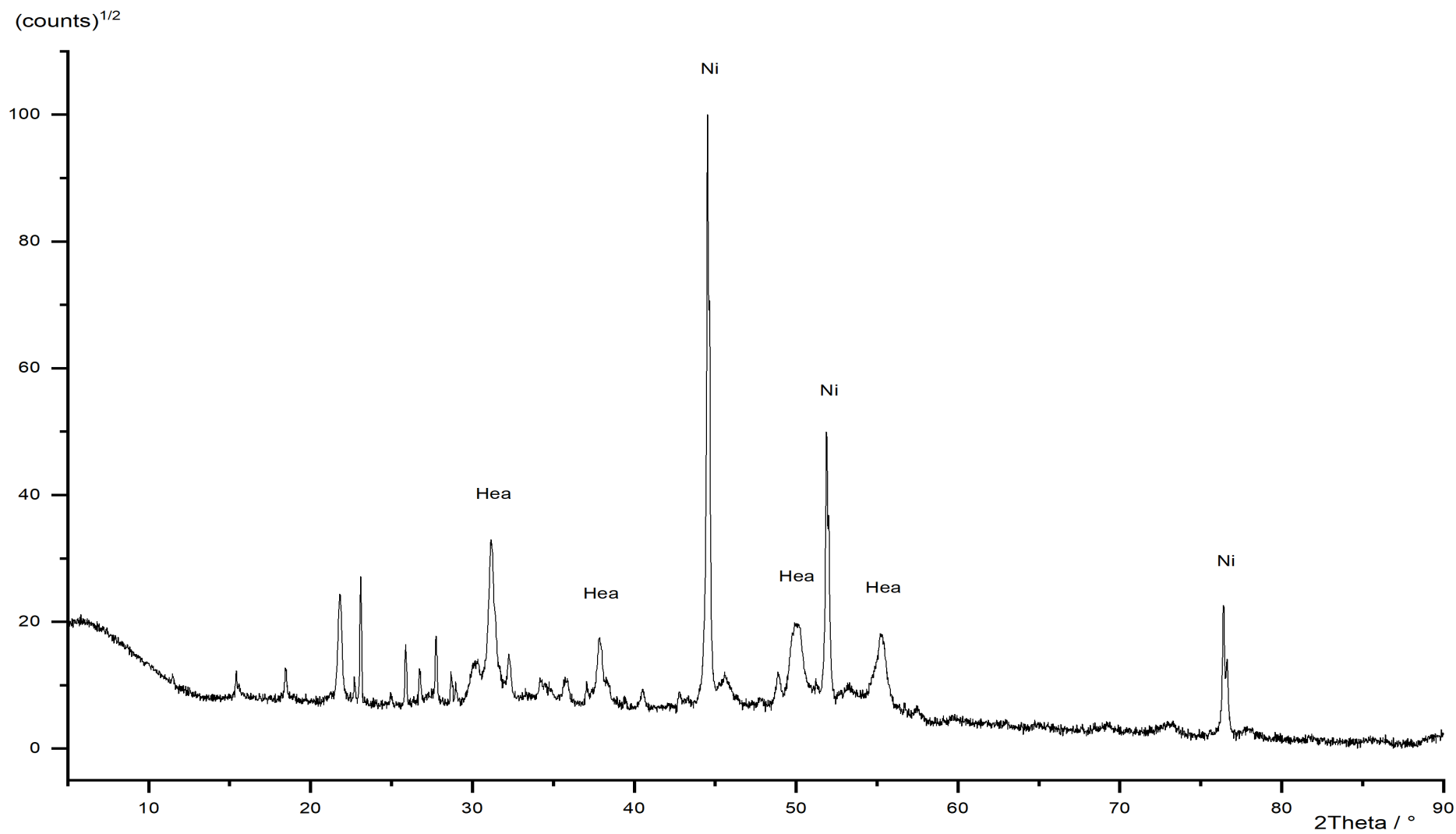


Figure 83: Powder diffraction pattern of NiS\_1. Ni = nickel, Hea = heazlewoodite.

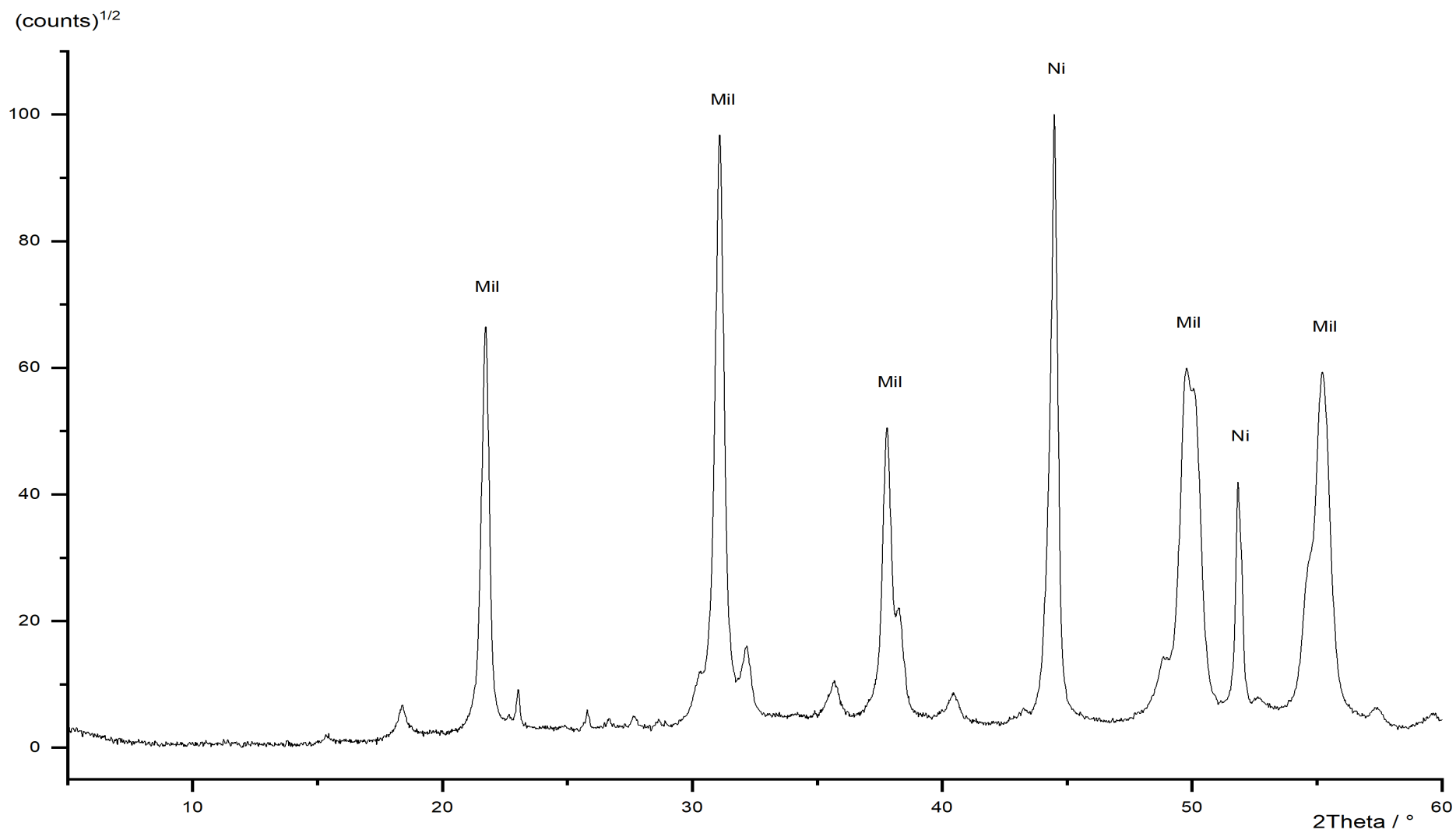


Figure 84: Powder diffraction pattern of NiS\_1. Ni = nickel, Hea = heazlewoodite.

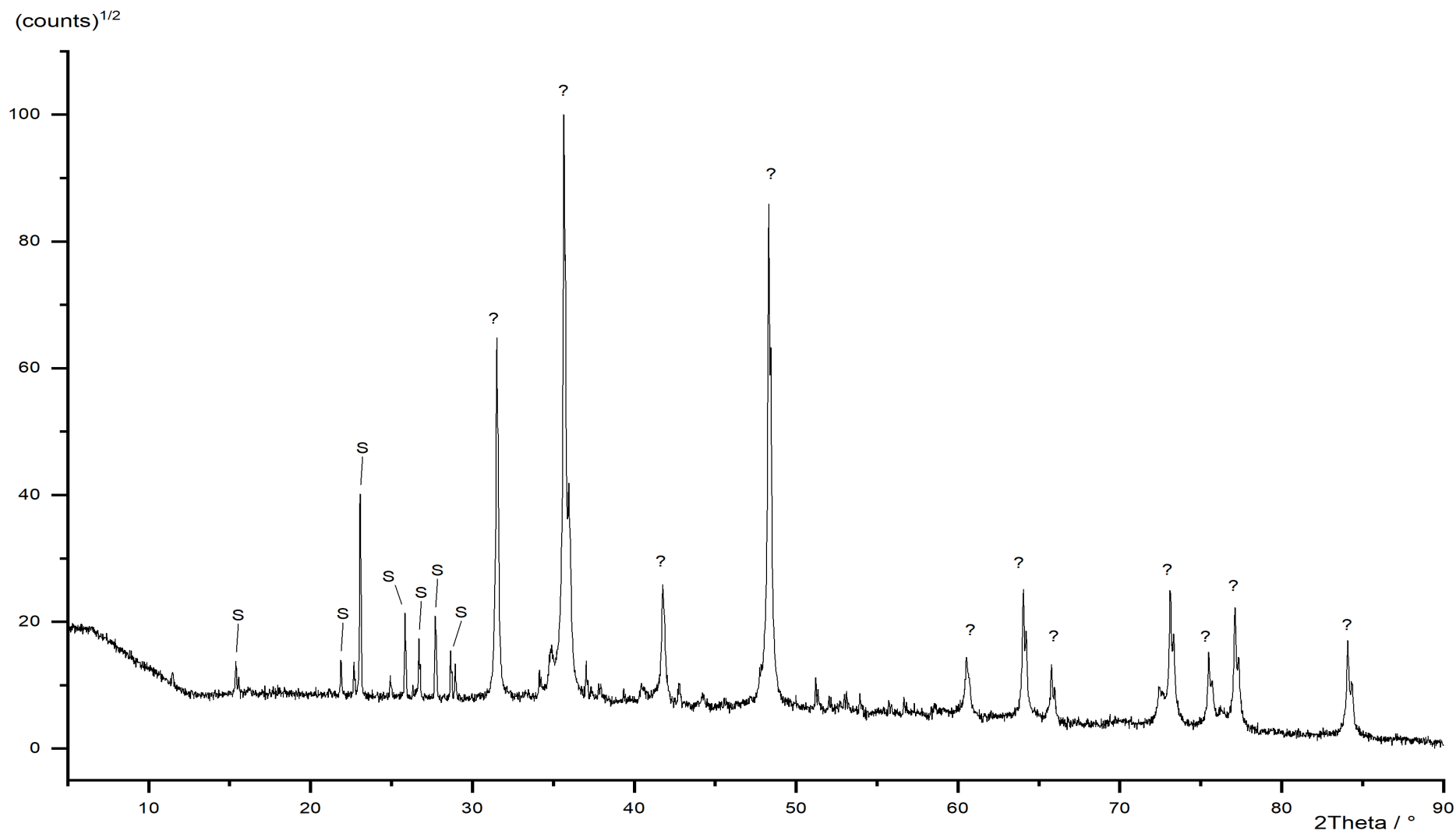


Figure 85: Powder diffraction pattern of WS<sub>1</sub>. S = sulfur, ? = unidentified.

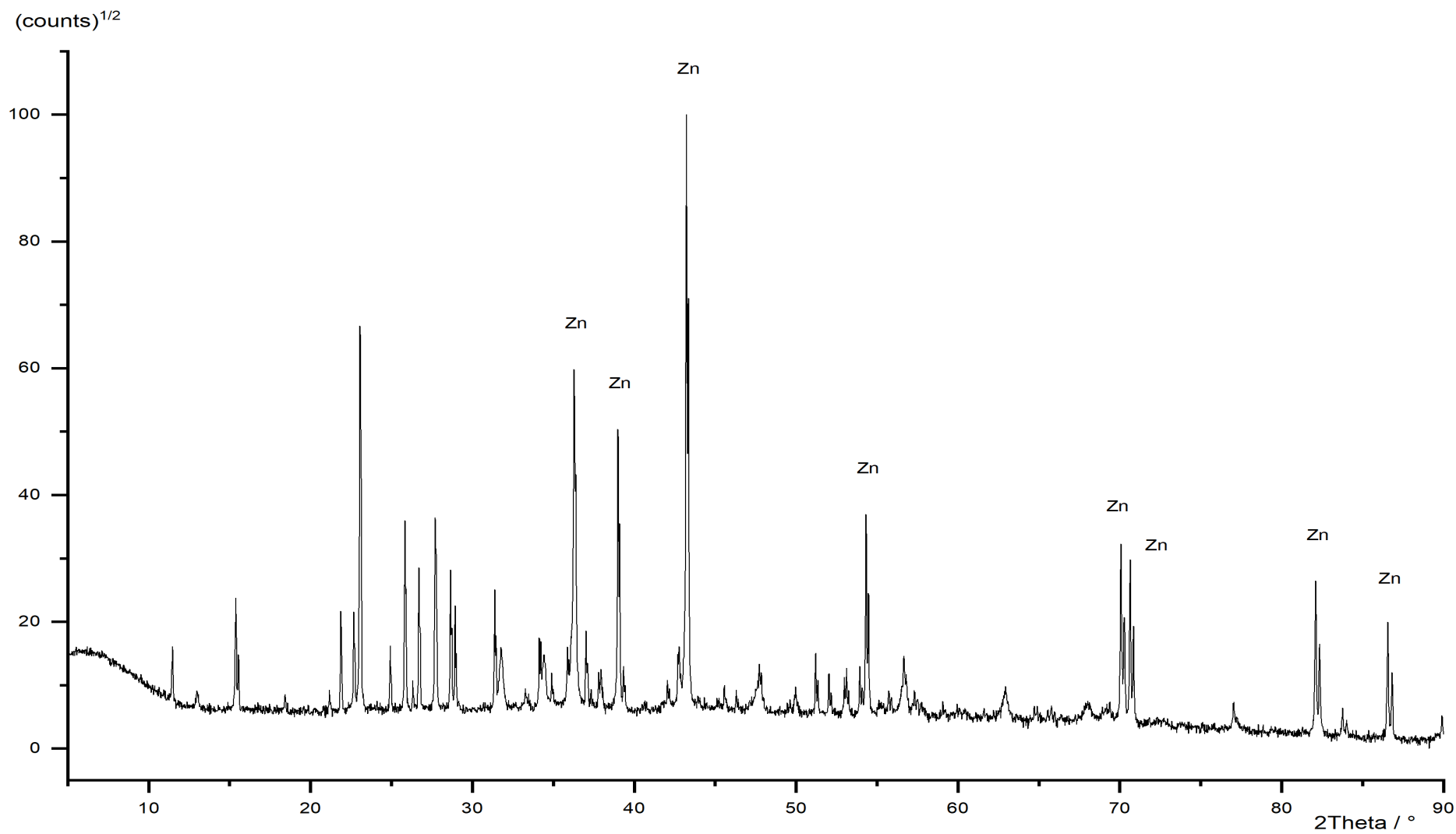


Figure 86: Powder diffraction pattern of ZnS<sub>1</sub>, Zn = zinc, all other peaks can be assigned to sulfur.

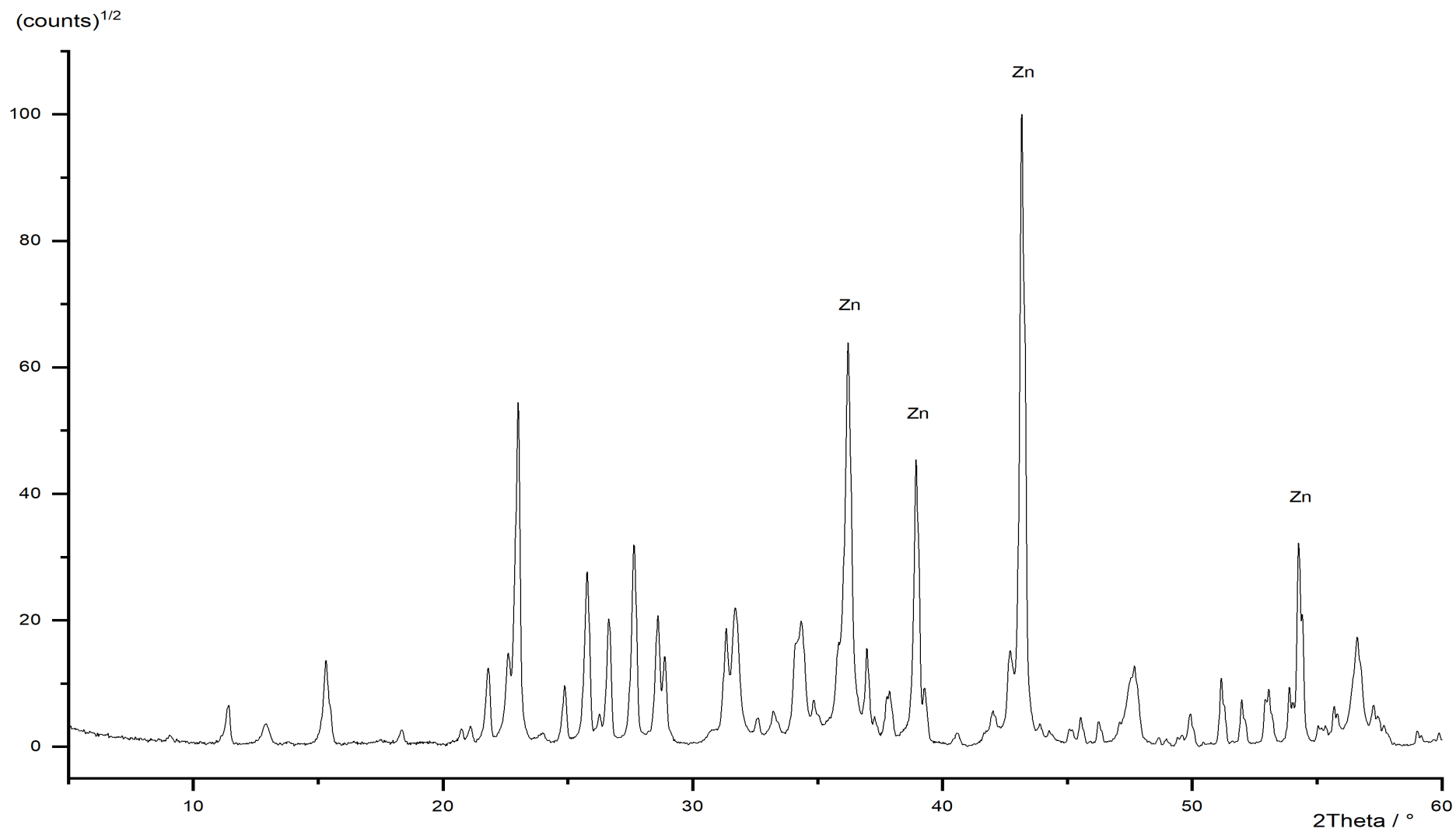


Figure 87: Powder diffraction pattern of ZnS<sub>2</sub>, Zn = zinc, all other peaks can be assigned to sulfur.



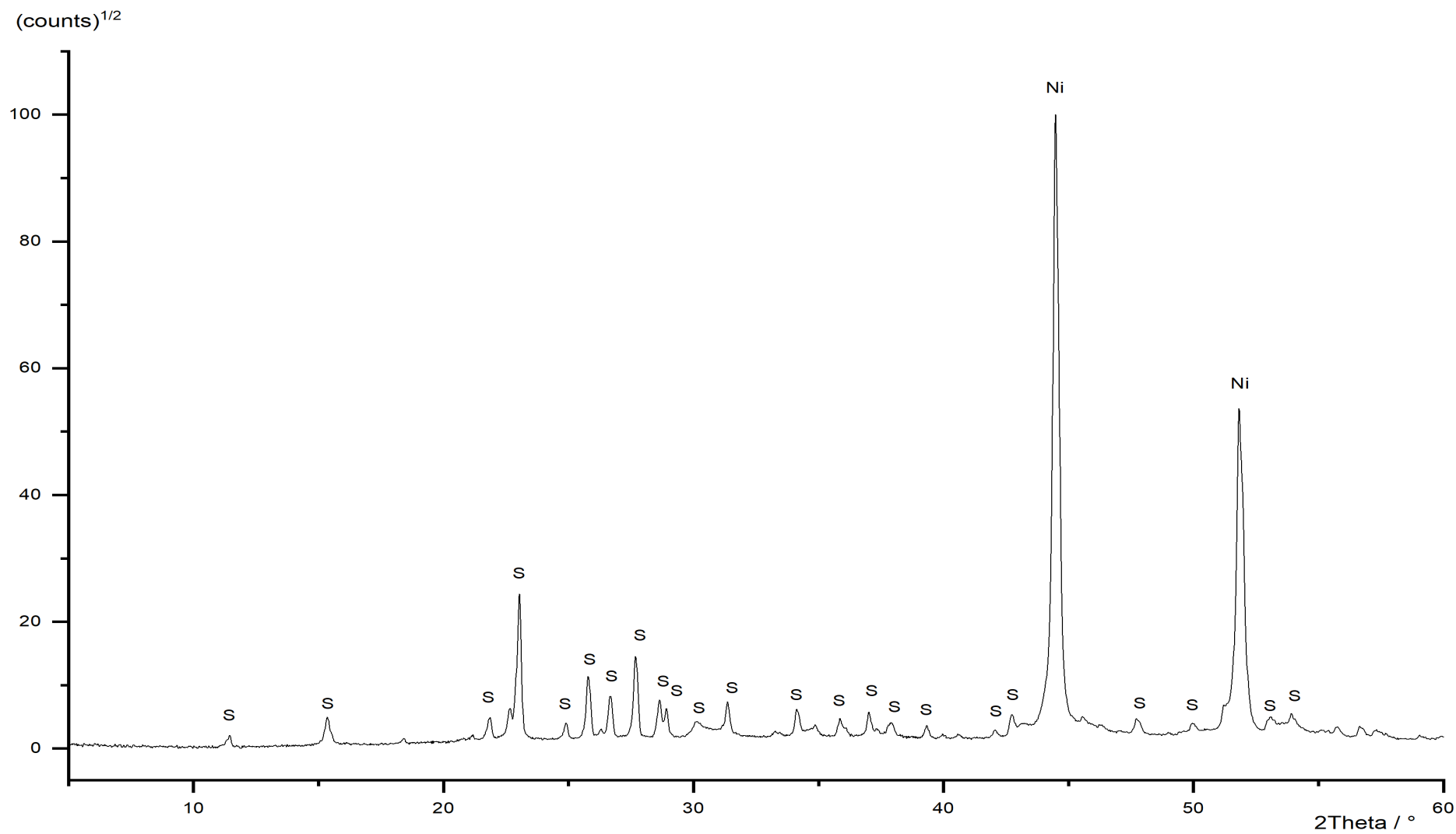


Figure 88: Powder diffraction pattern of MB\_1, S = sulfur, Ni = nickel.

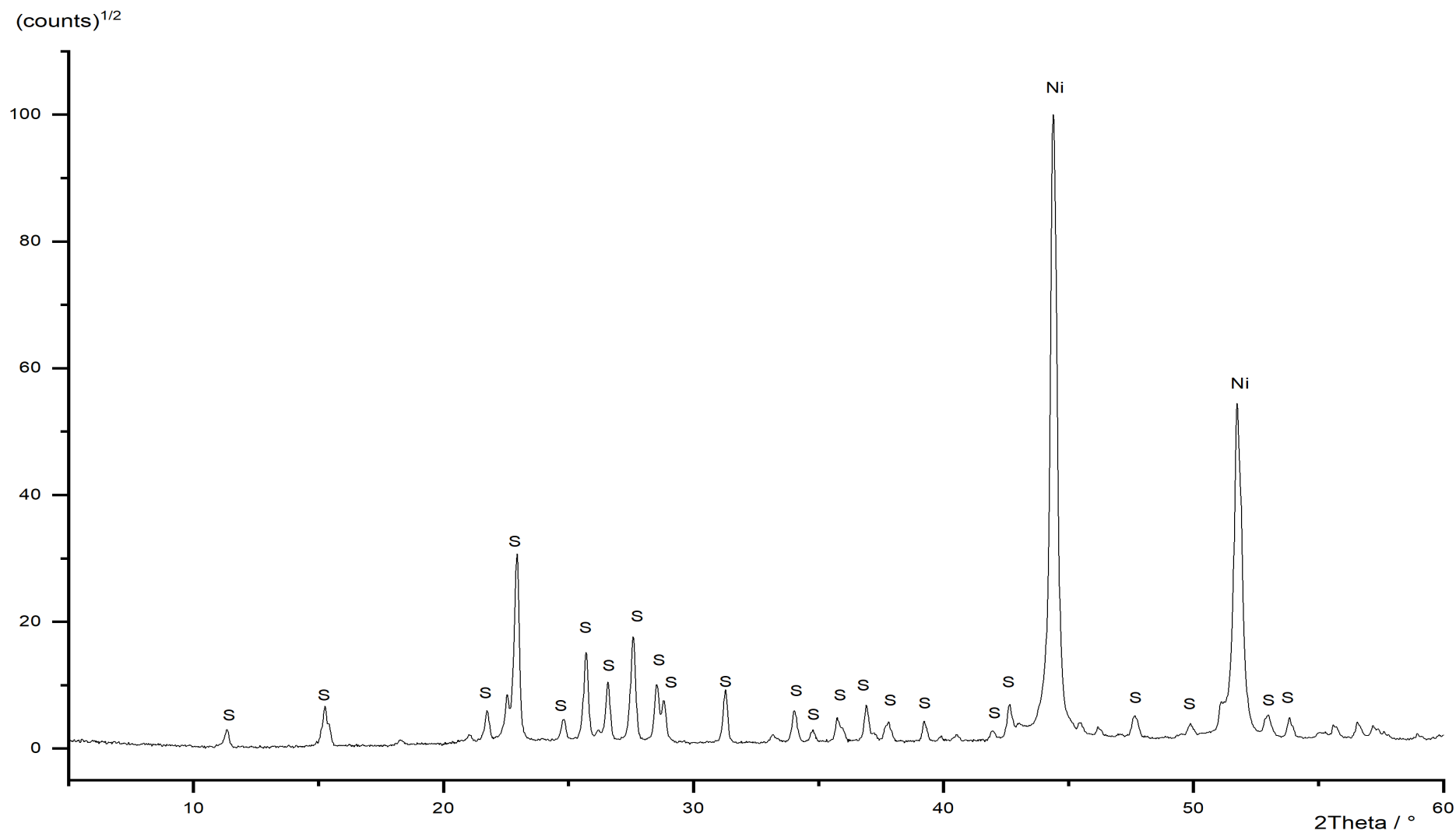


Figure 89: Powder diffraction pattern of MB\_2, S = sulfur, Ni = nickel.

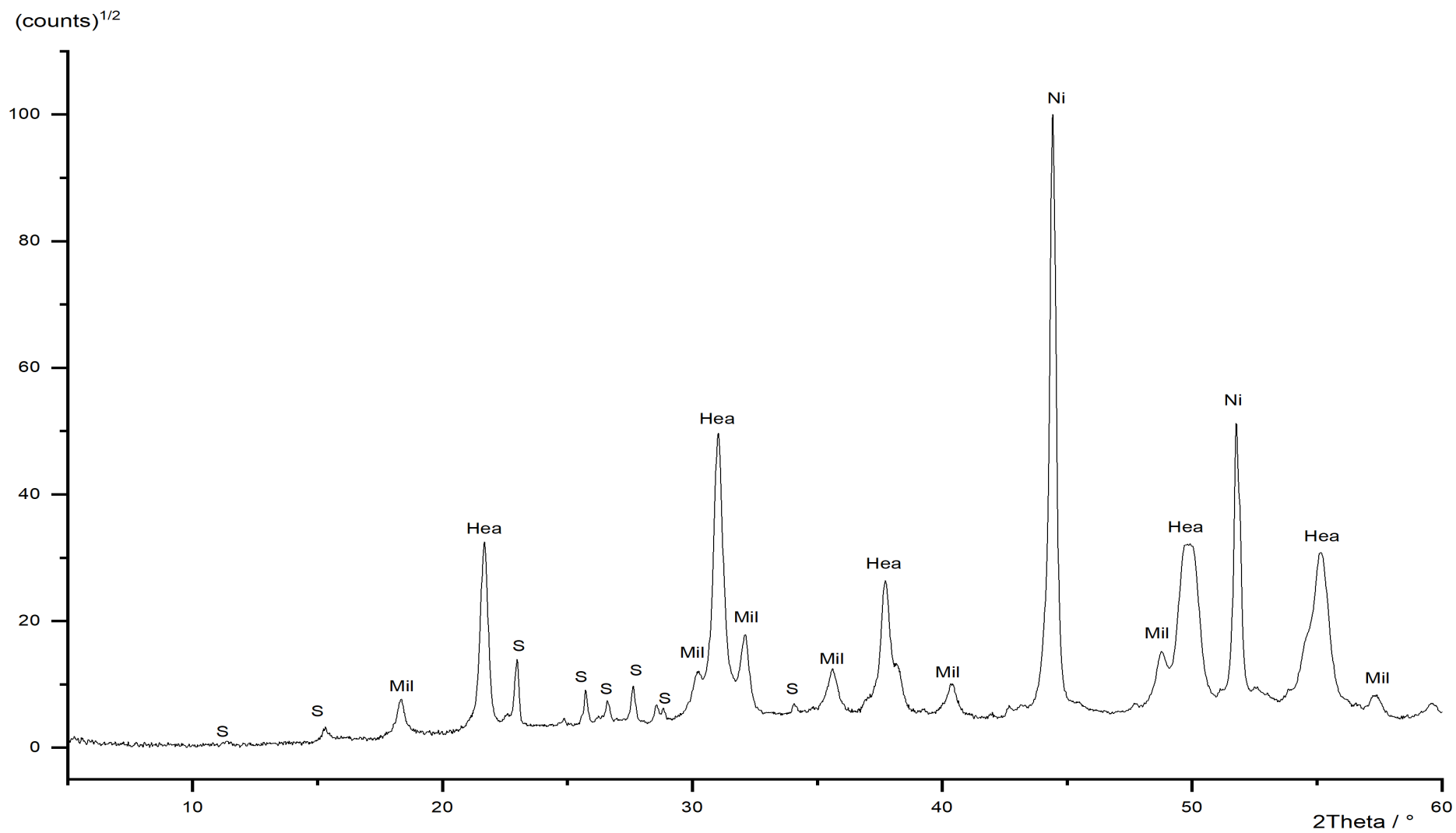


Figure 90: Powder diffraction pattern of MB\_3, S = sulfur, Ni = nickel, Mil = millerite, Hea = heazlewoodite.

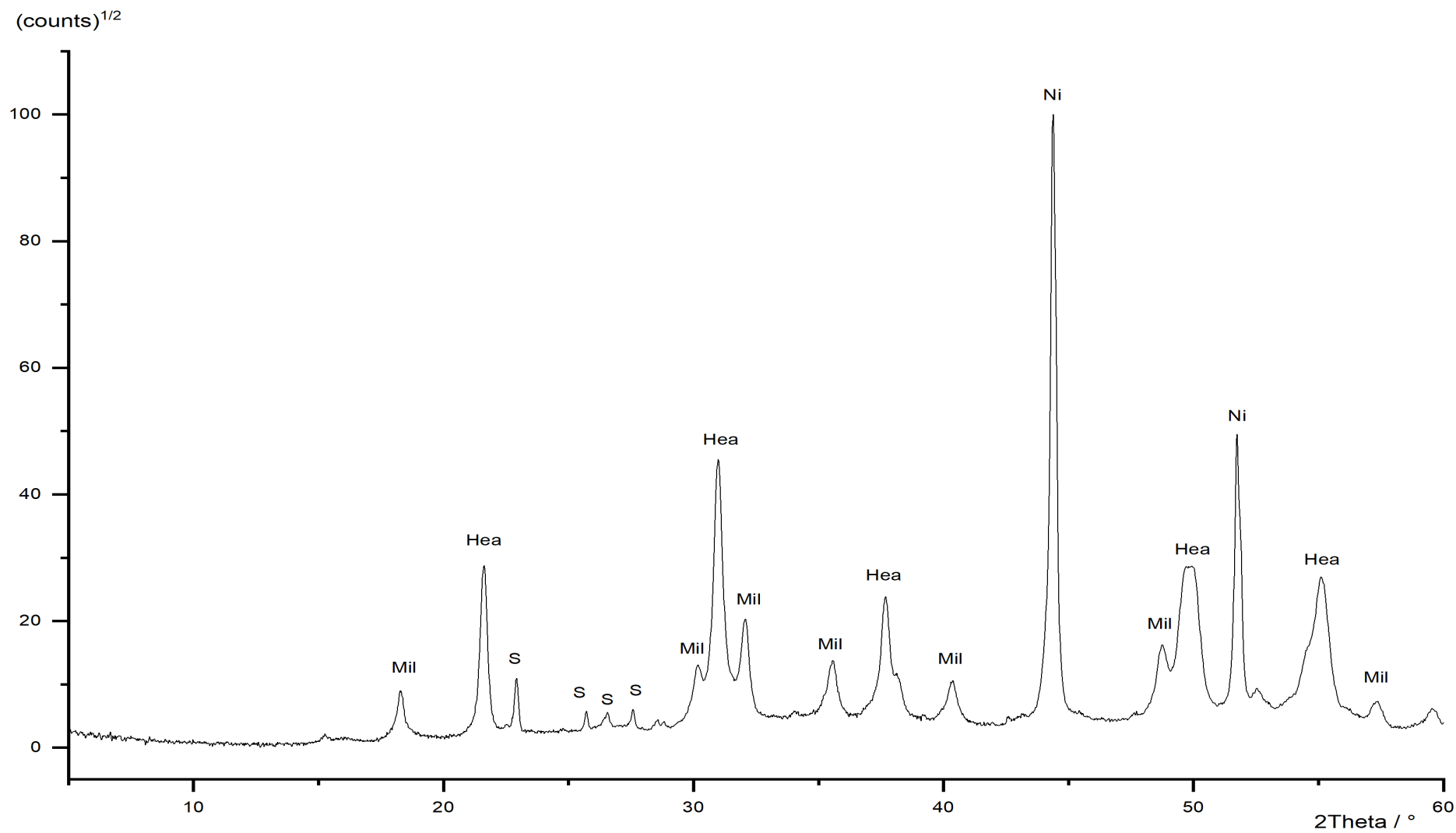


Figure 91: Powder diffraction pattern of MB\_4, S = sulfur, Ni = nickel, Mil = millerite, Hea = heazlewoodite.

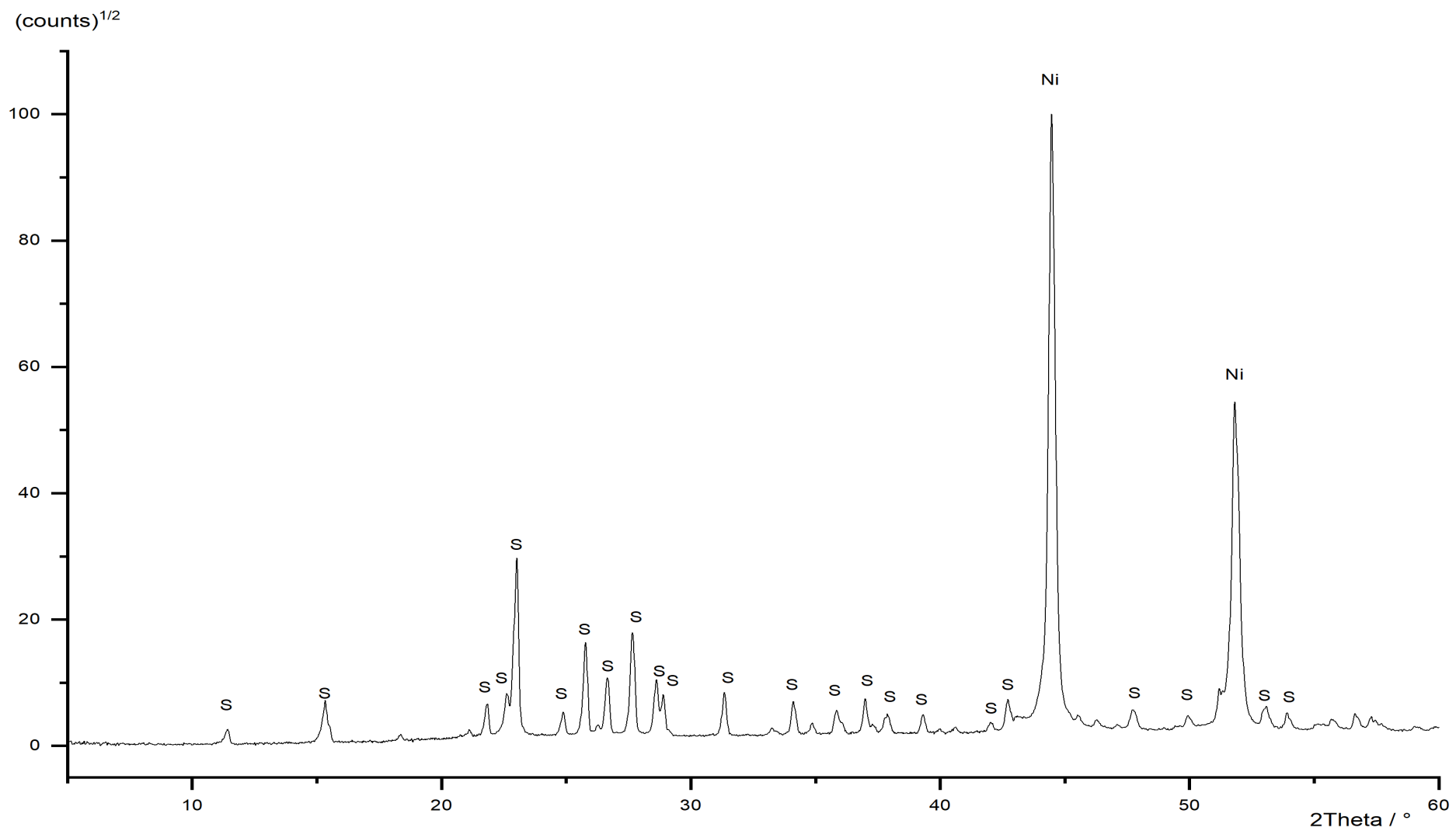


Figure 92: Powder diffraction pattern of MB\_5, S = sulfur, Ni = nickel.

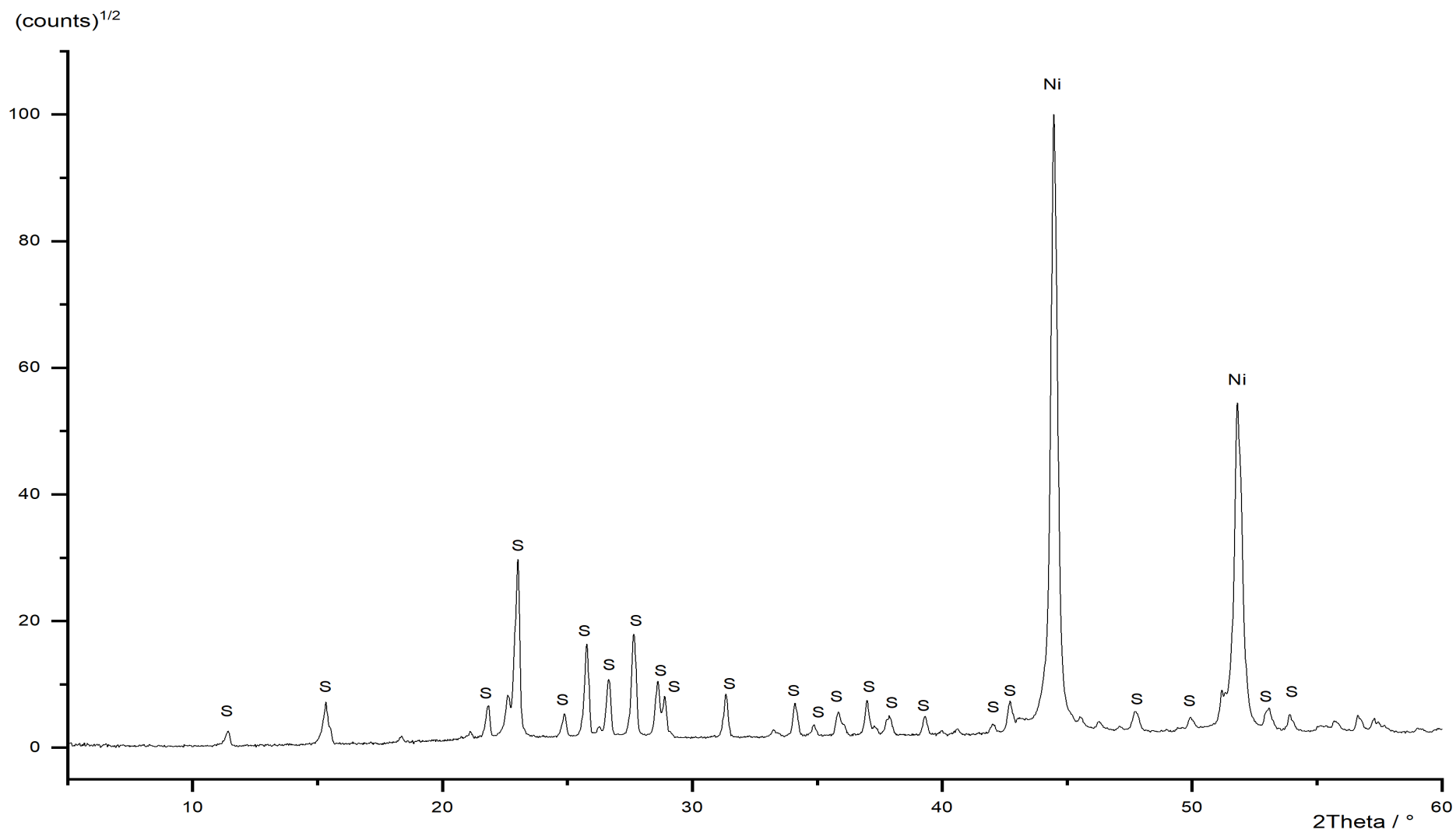


Figure 93: Powder diffraction pattern of MB\_6, S = sulfur, Ni = nickel.

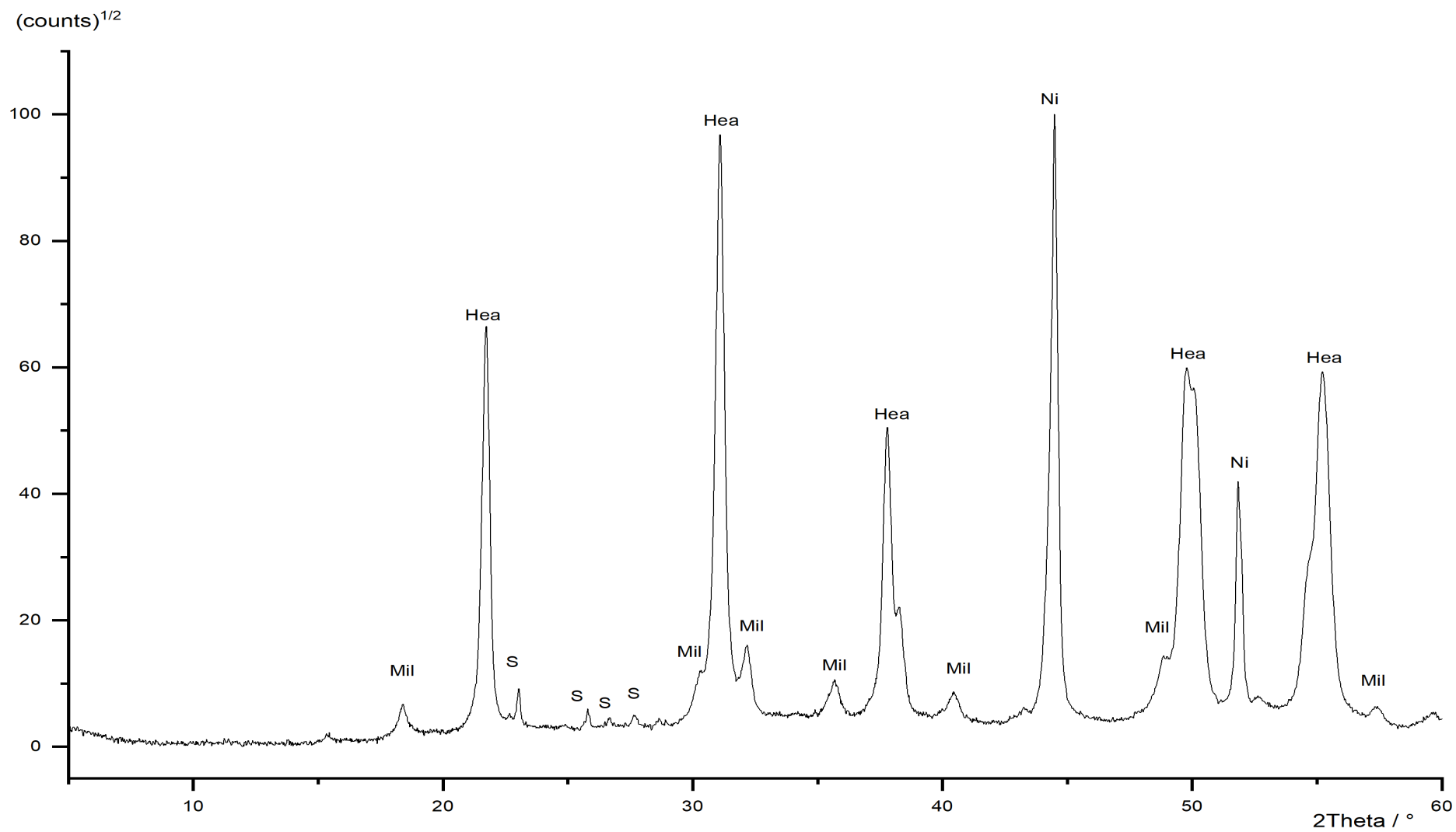


Figure 94: Powder diffraction pattern of MB\_7, S = sulfur, Ni = nickel, Mil = millerite, Hea = heazlewoodite.

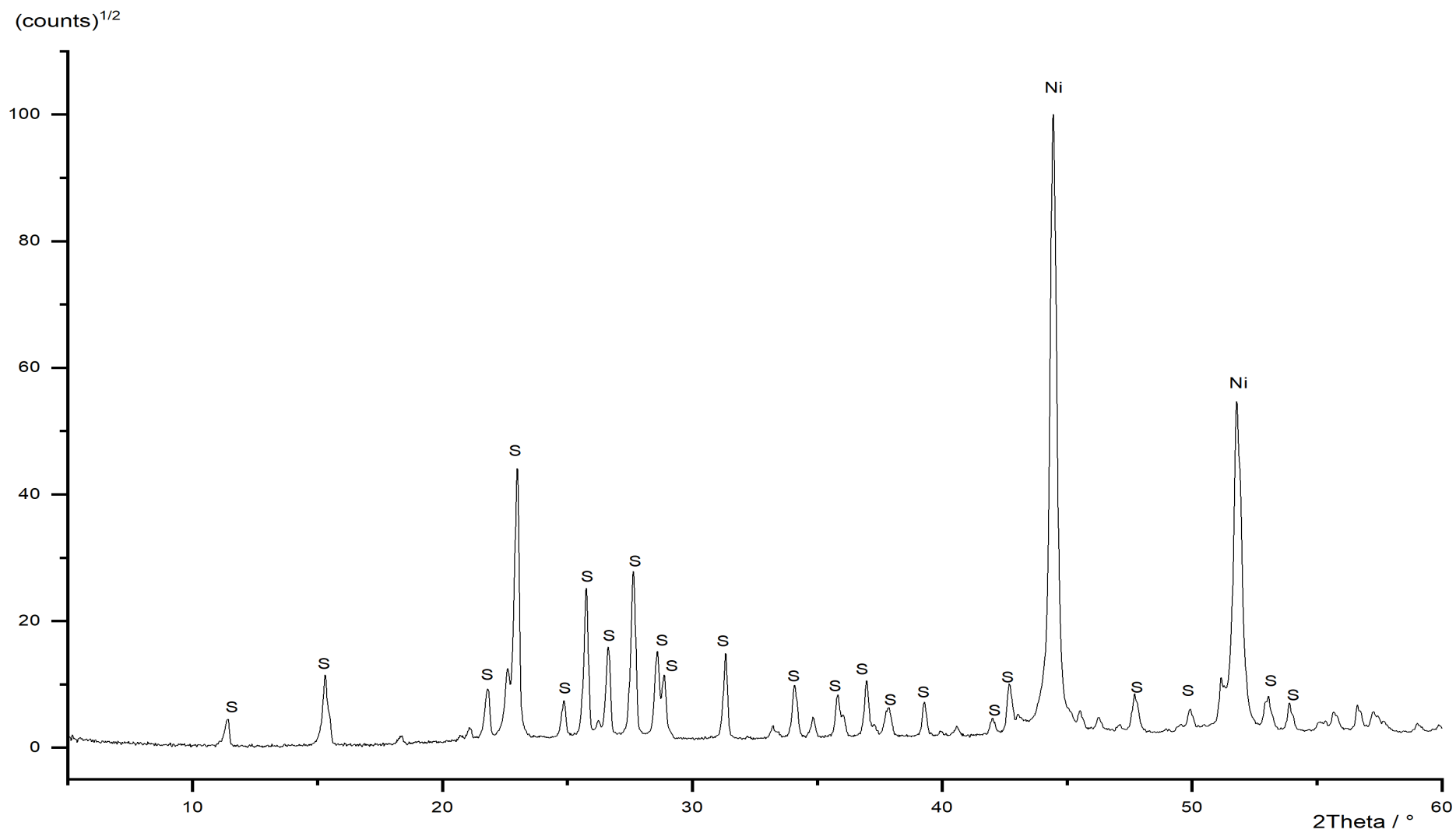


Figure 95: Powder diffraction pattern of MB\_8, S = sulfur, Ni = nickel.



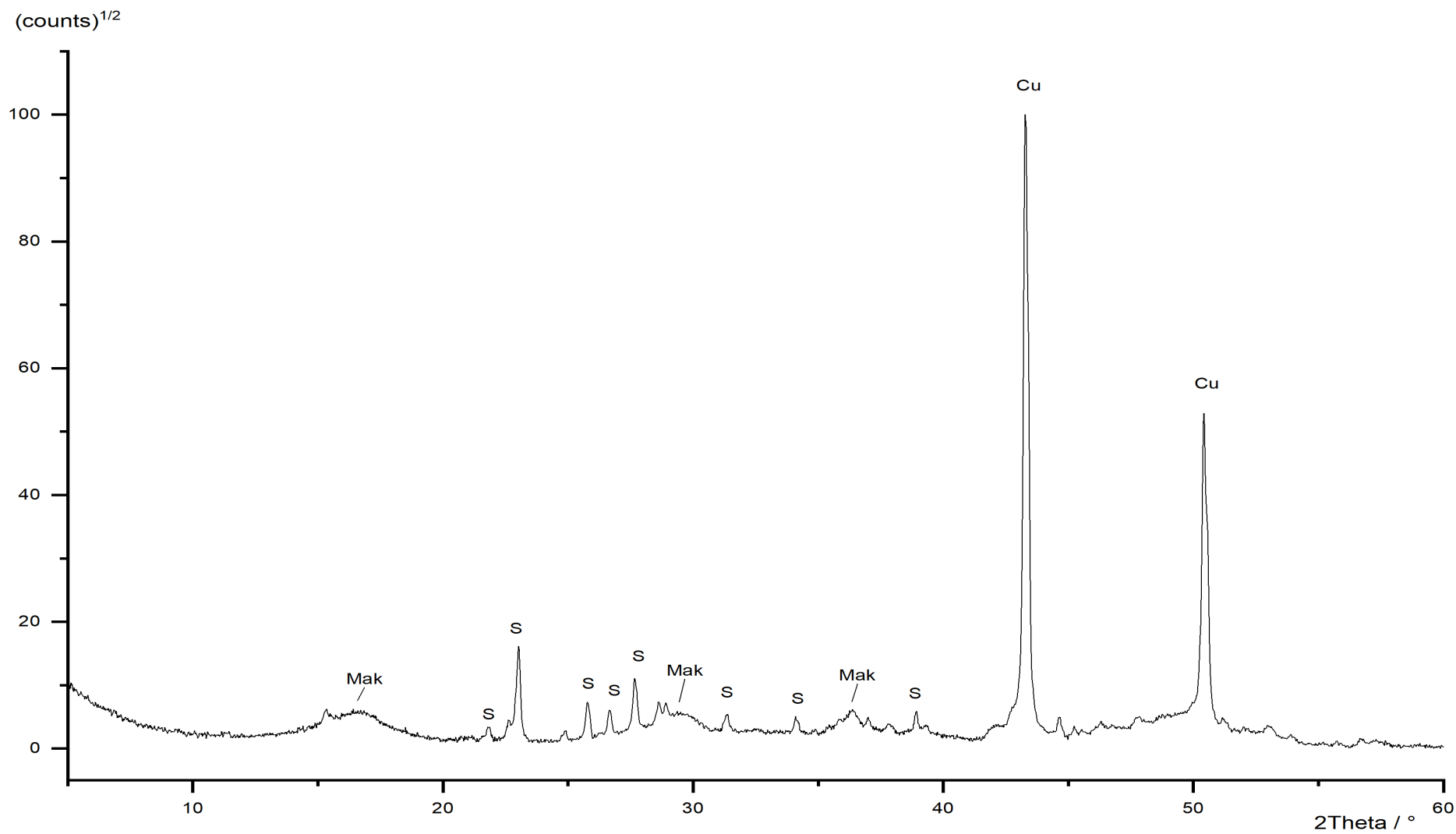


Figure 96: Powder diffraction pattern of MB\_9, S = sulfur, Mak = mackinawite, Cu = copper.

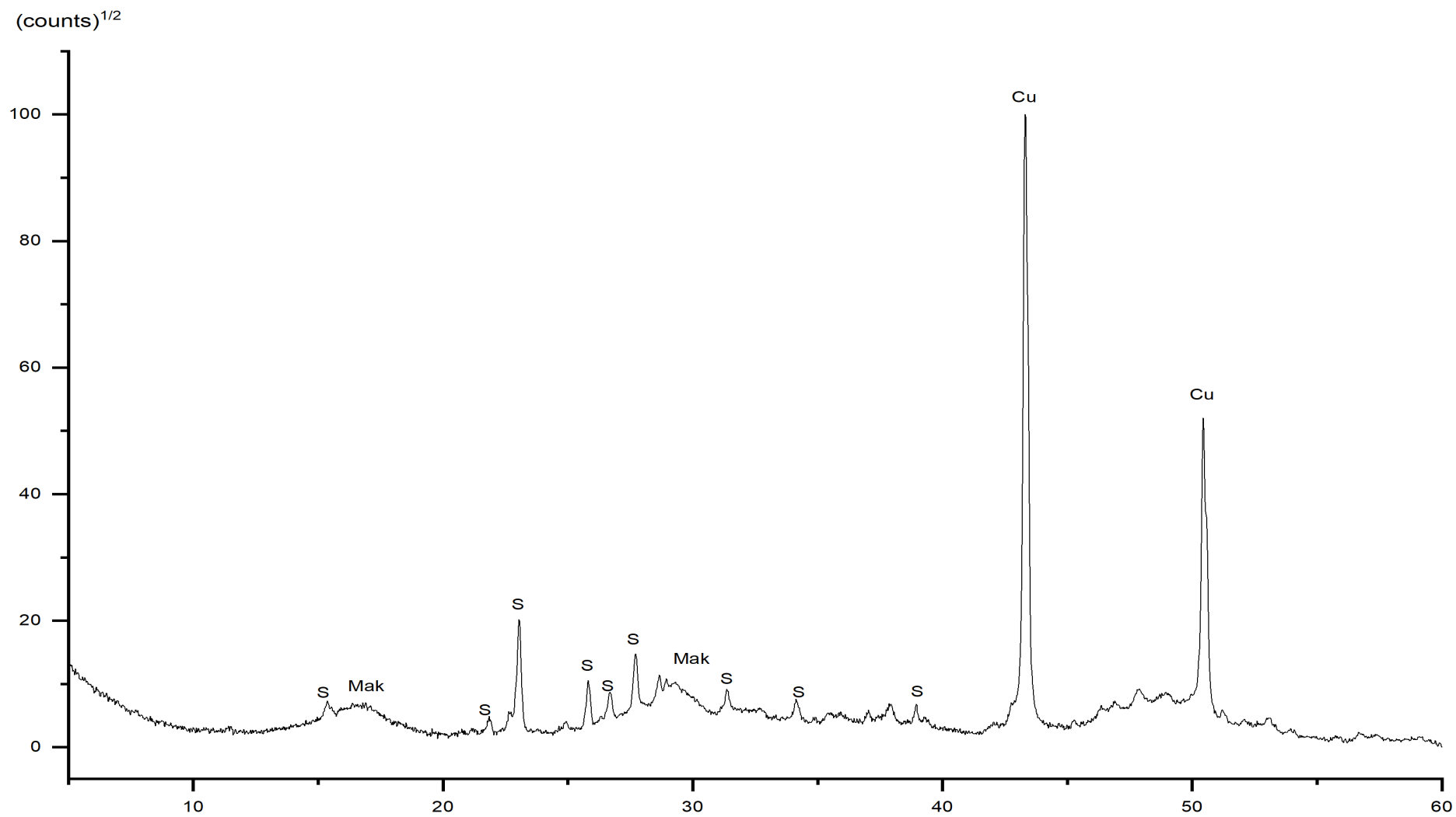


Figure 97: Powder diffraction pattern of MB\_10, S = sulfur, Mak = mackinawite, Cu = copper.

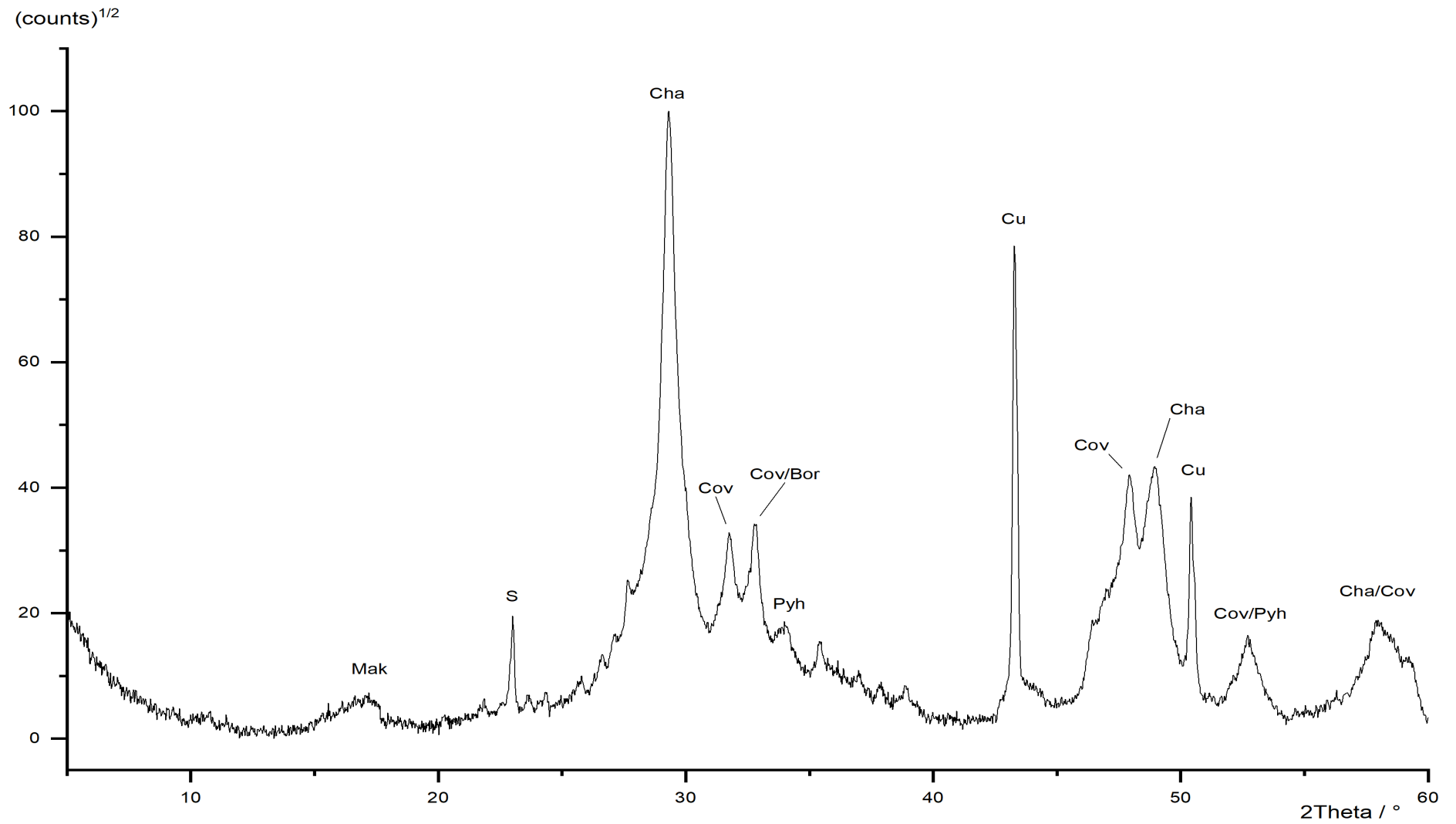


Figure 98: Powder diffraction pattern of MB\_11, S = sulfur, Mak = mackinawite, Cu = copper, Cov = covellite, Cha = chalcopyrite, Pyh = pyrrhotite.

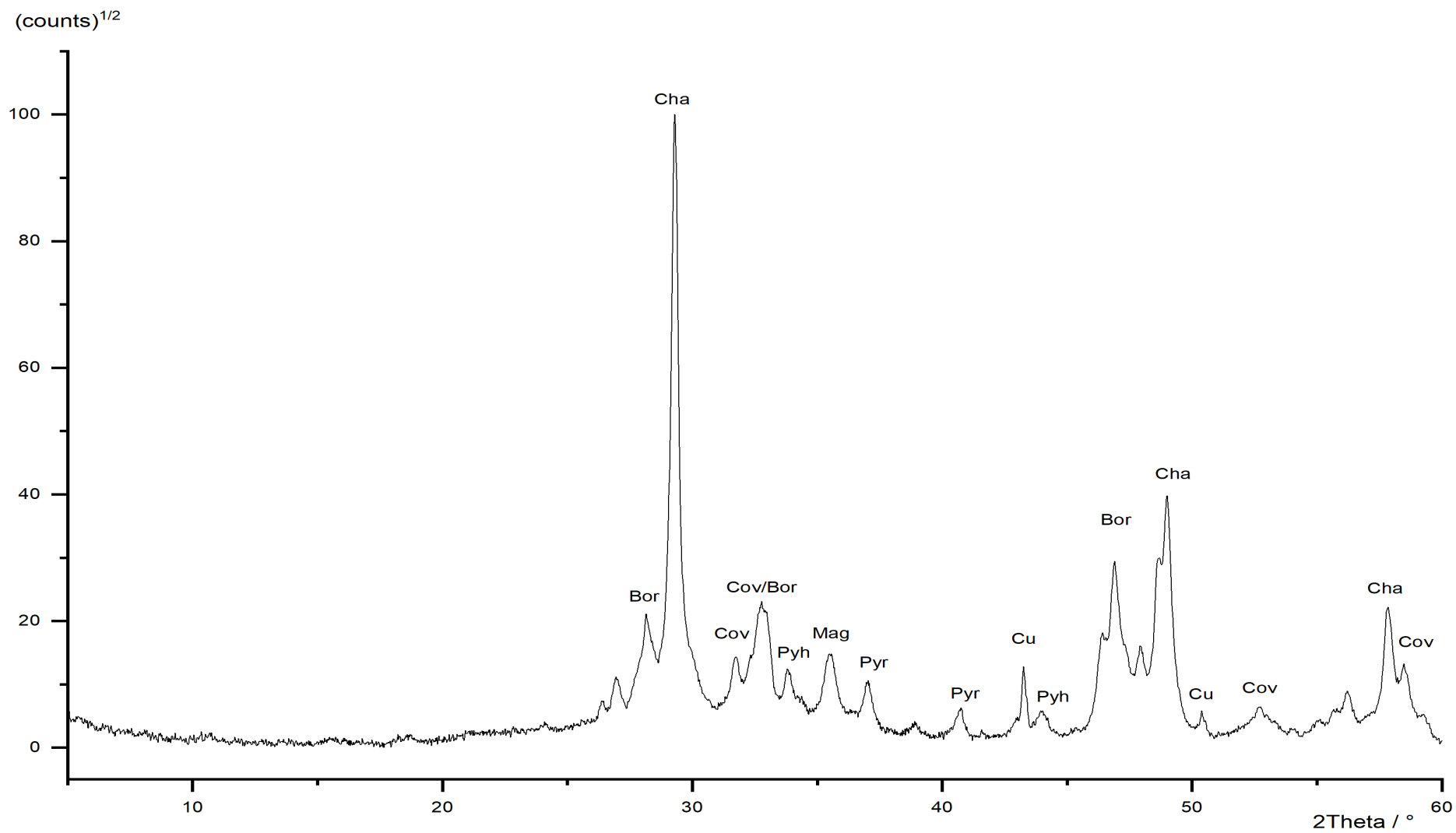


Figure 99: Powder diffraction pattern of MB\_12, Cu = copper, Cov = covellite, Cha = chalcopyrite, Pyh = pyrrhotite, bor = bornite, mag = magnetite.

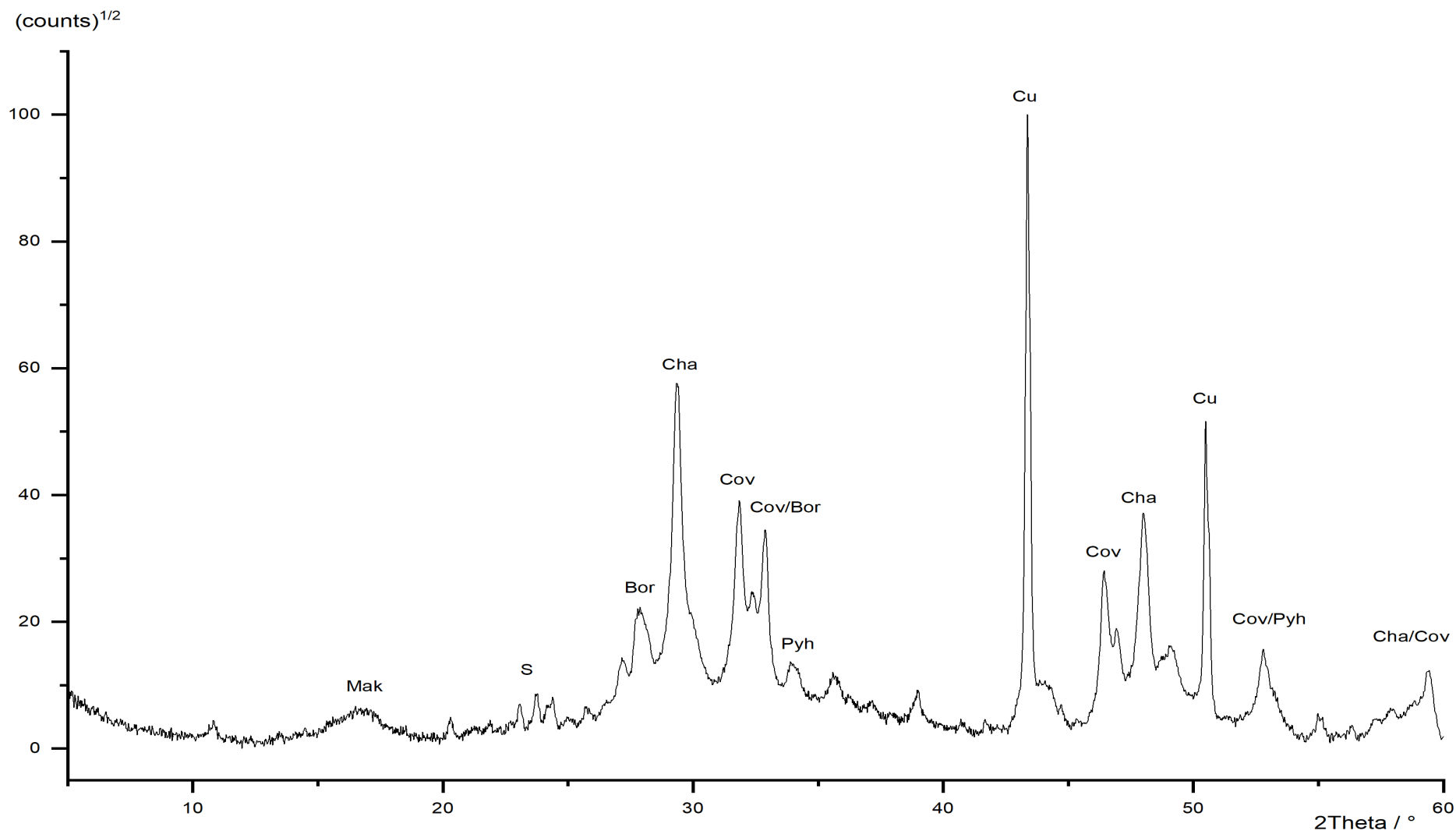


Figure 100: Powder diffraction pattern of MB\_13, S = sulfur, Mak = mackinawite, Cu = copper, Cov = covellite, Cha = chalcopyrite, Pyh = pyrrhotite.

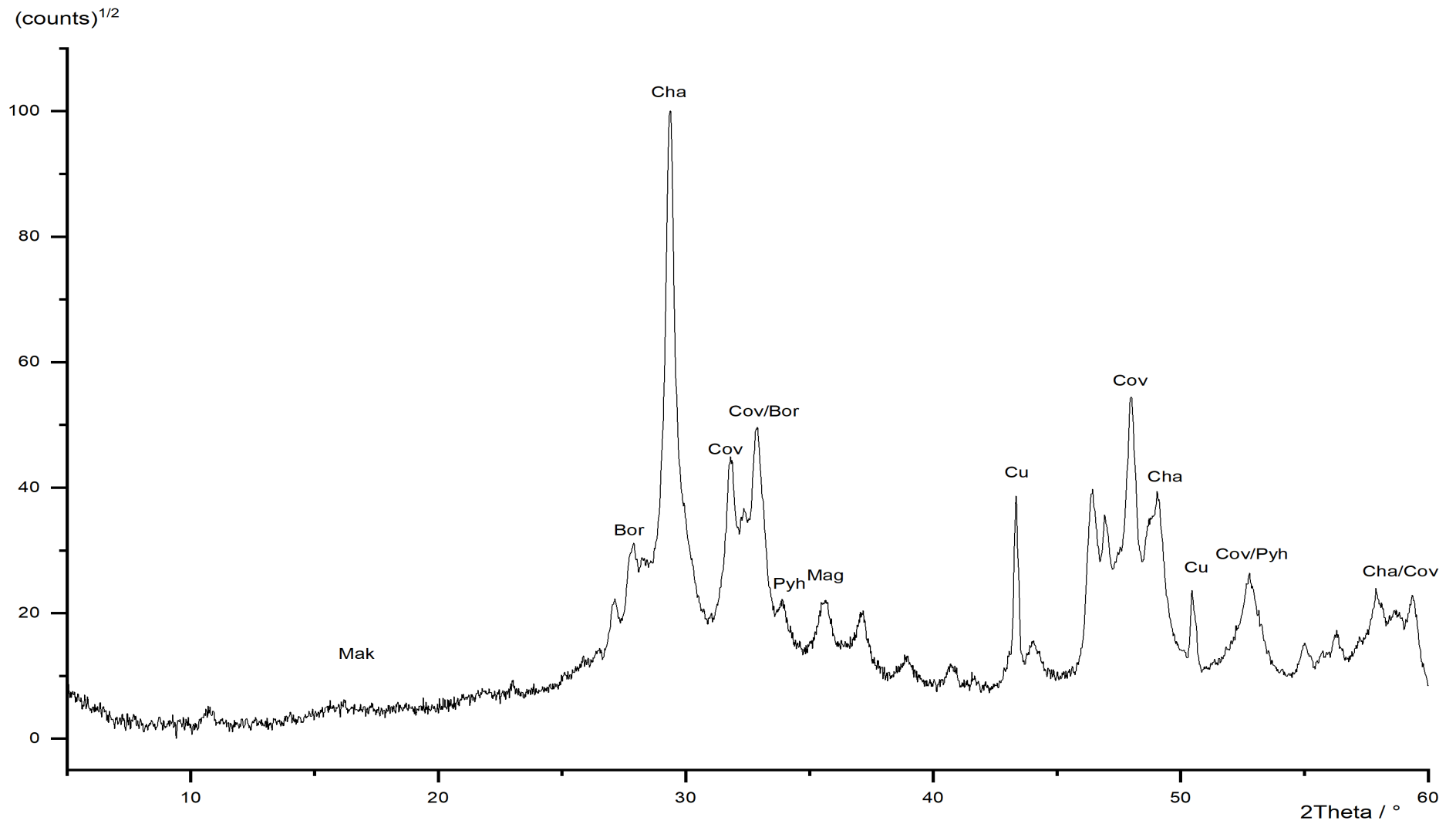


Figure 101: Powder diffraction pattern of MB\_14, S = sulfur, Mak = mackinawite, Cu = copper, Cov = covellite, Cha = chalcopyrite, Pyh = pyrrhotite.

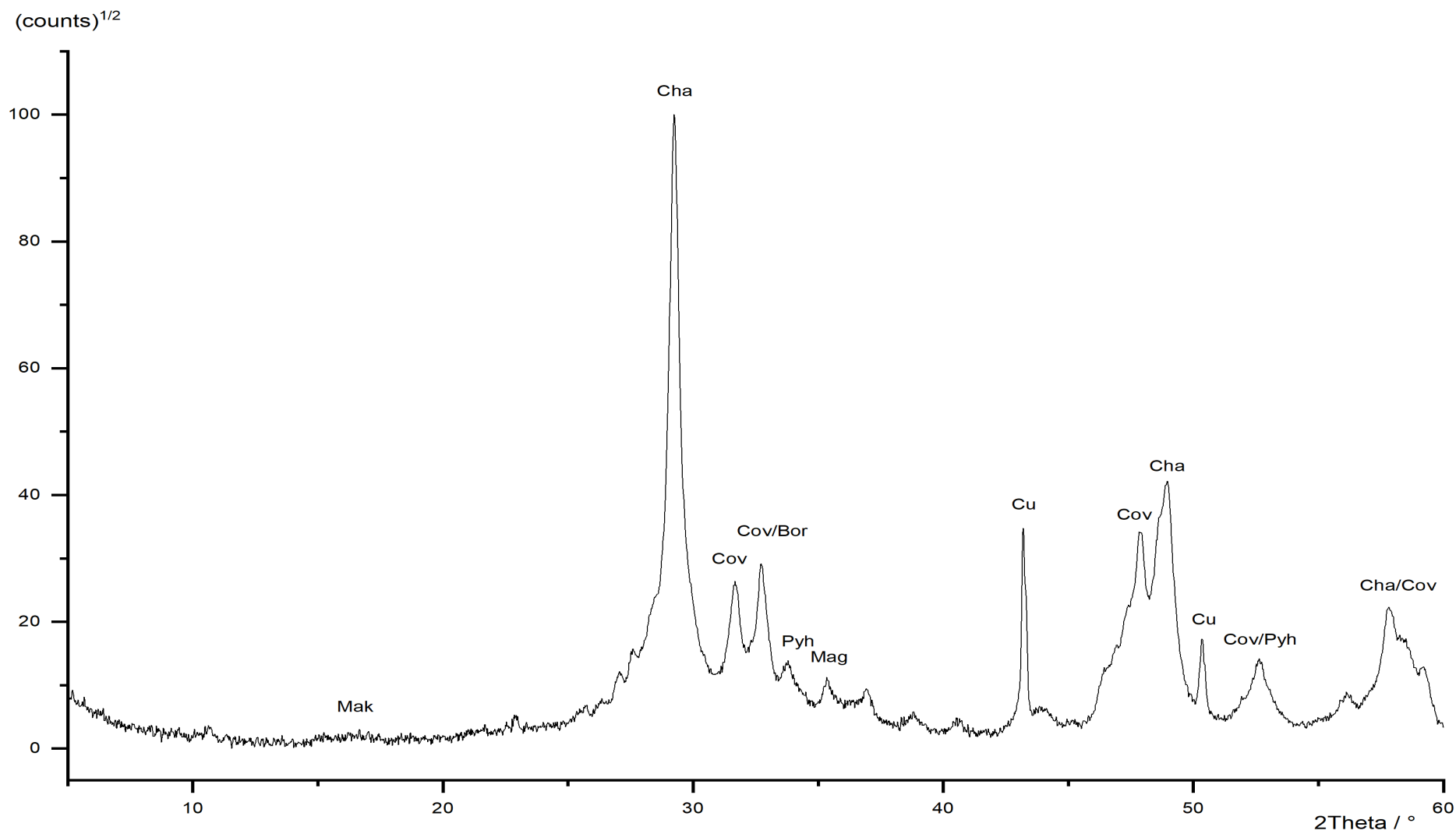


Figure 102: Powder diffraction pattern of MB\_15, S = sulfur, Mak = mackinawite, Cu = copper, Cov = covellite, Cha = chalcopyrite, Pyh = pyrrhotite.

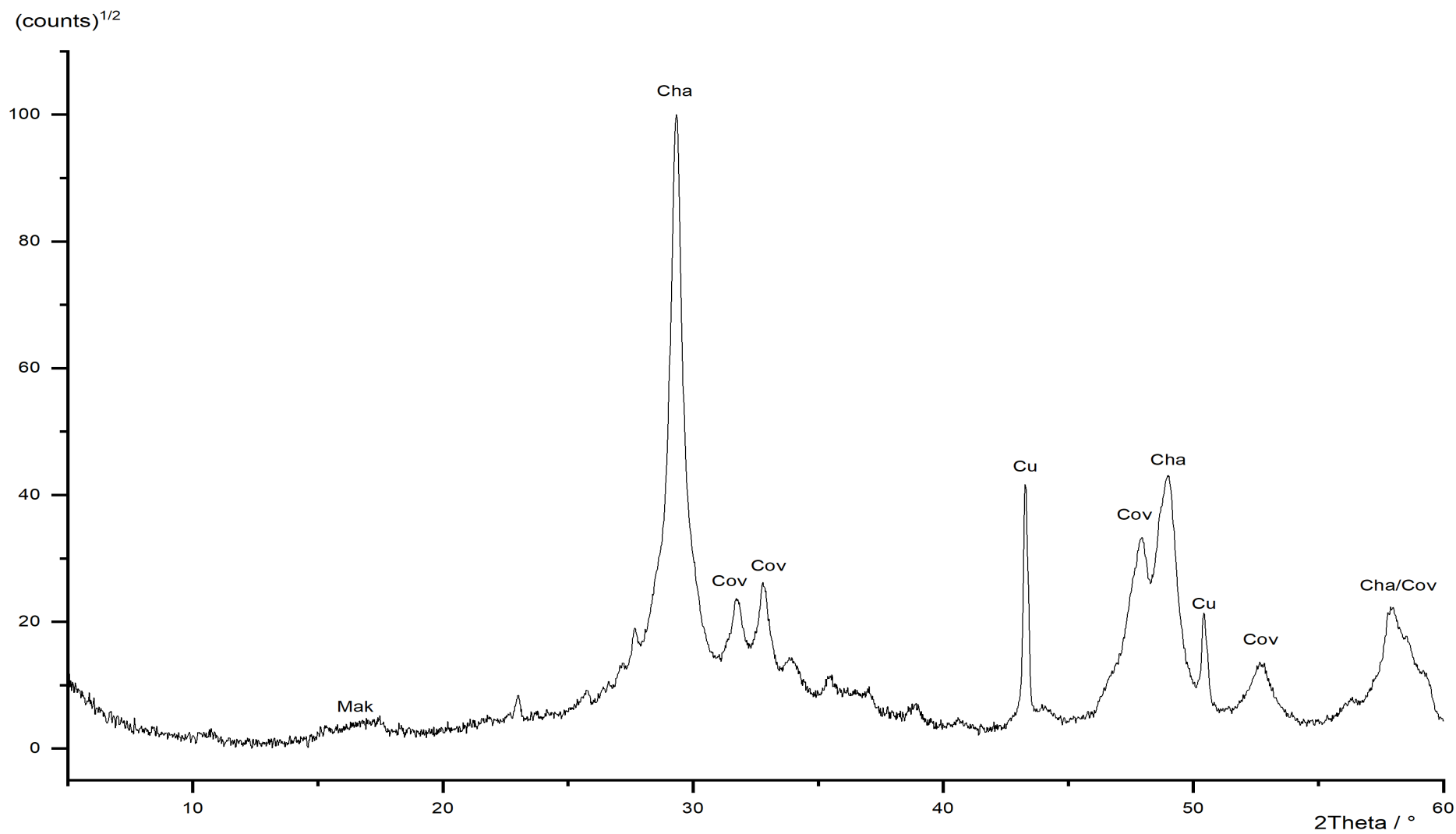


Figure 103: Powder diffraction pattern of MB\_16, Mak = mackinawite, Cu = copper, Cov = covellite, Cha = chalcopyrite.



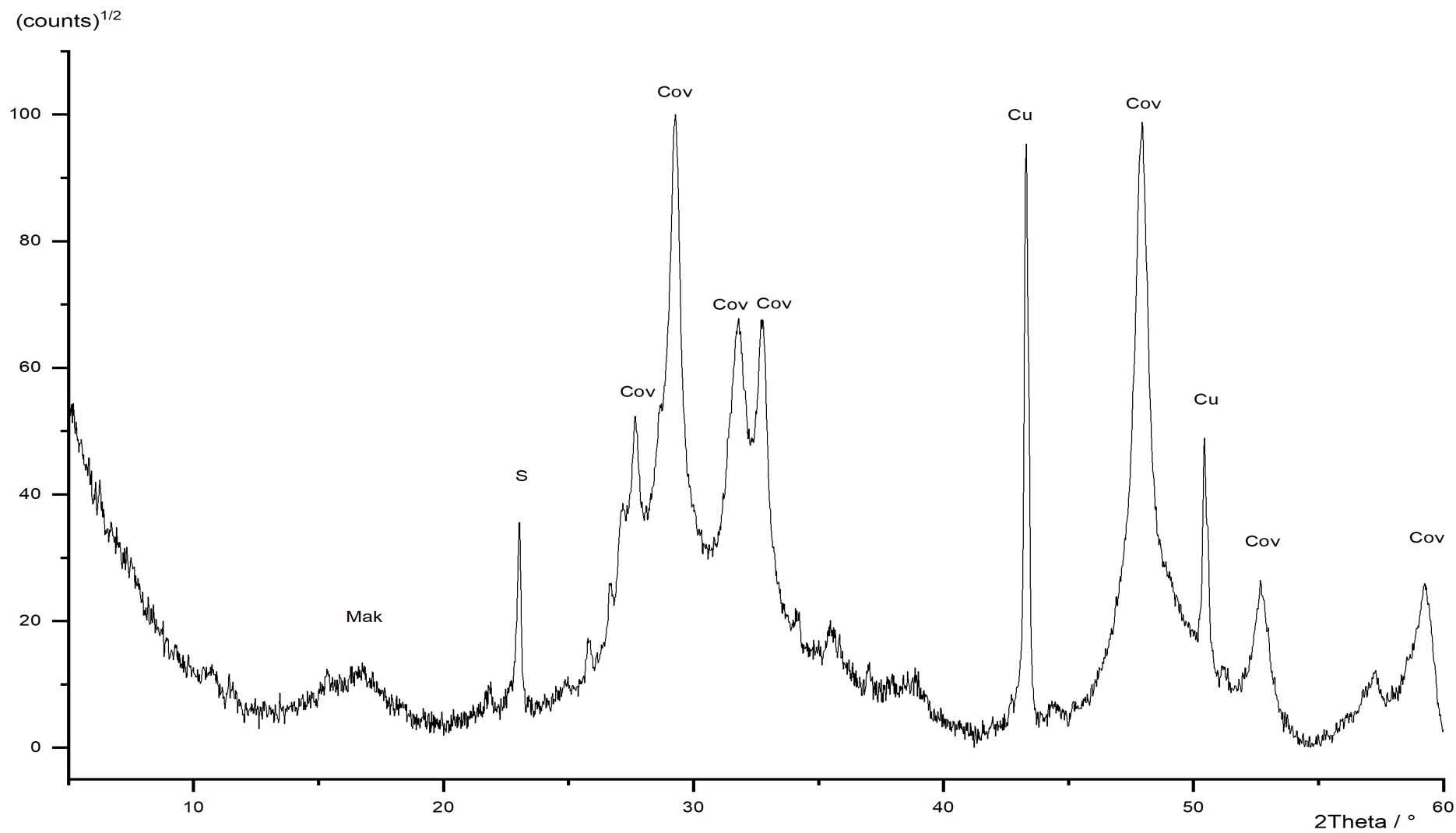


Figure 104: Powder diffraction pattern of MB\_17, Mak = mackinawite, S = sulfur, Cu = copper, Cov = covellite.

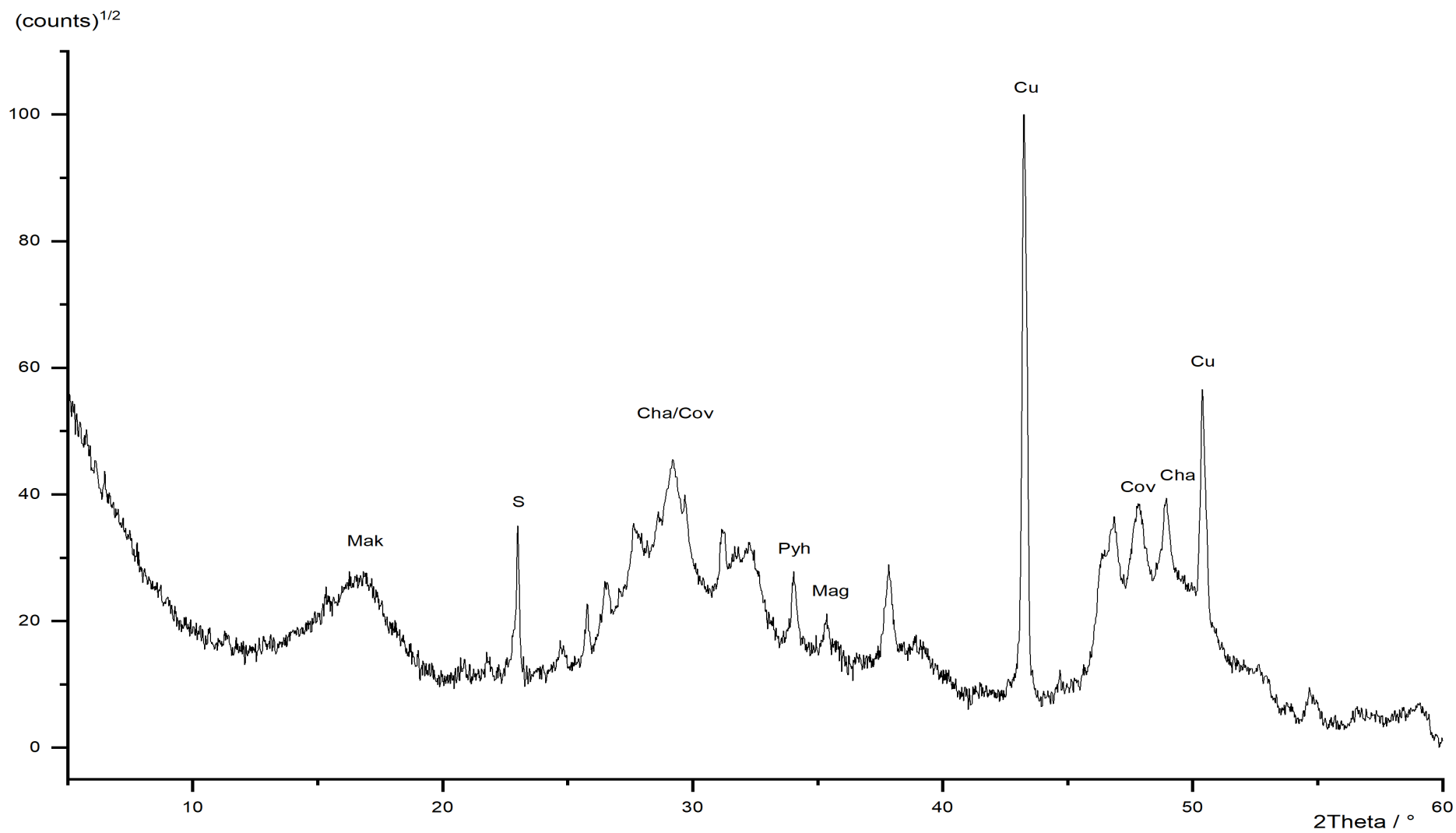


Figure 105: Powder diffraction pattern of MB\_18, Mak = mackinawite, S = sulfur, Mag = magnetite, Cu = copper, Cov = covellite, Cha = chalcopyrite.

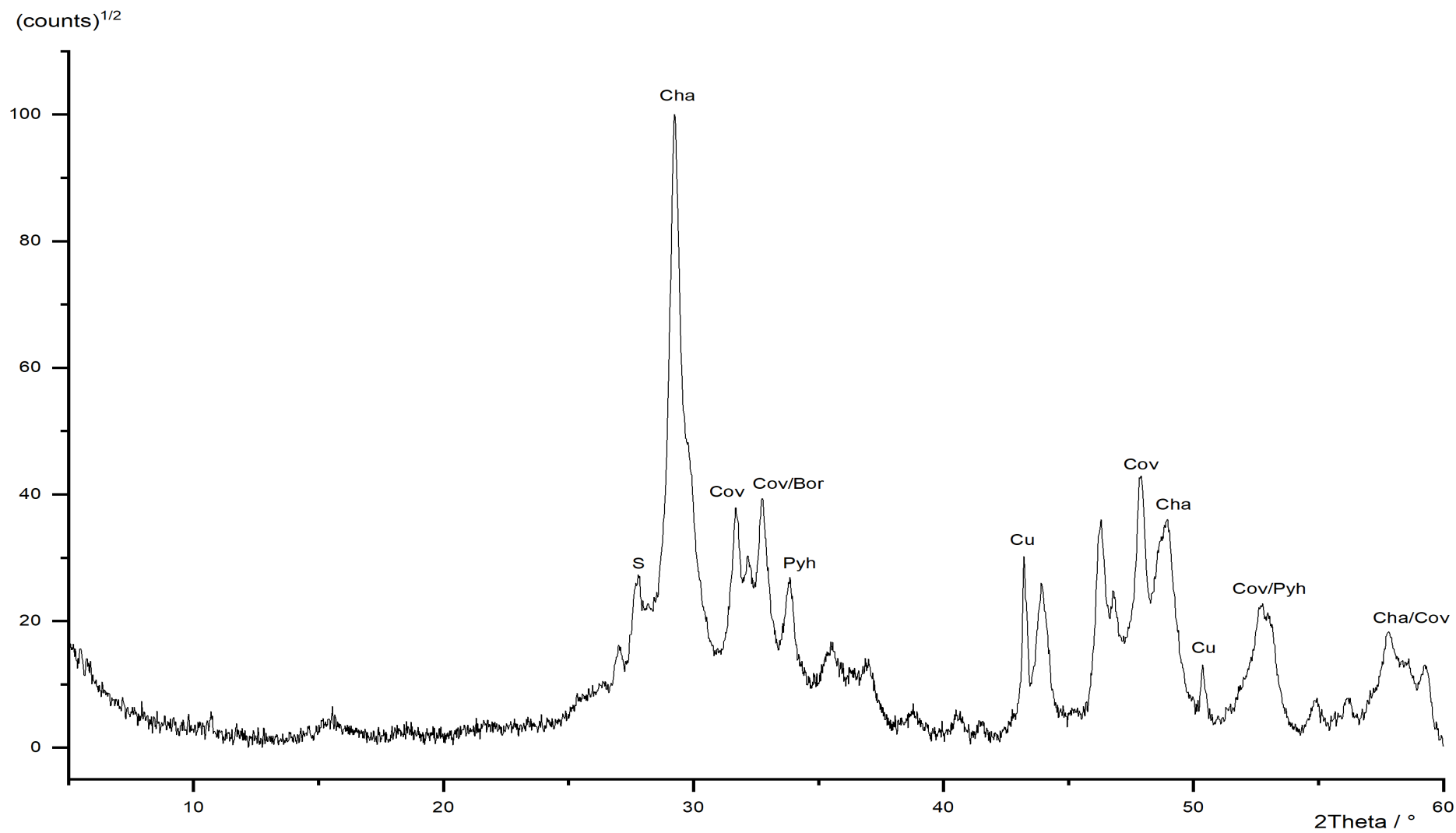


Figure 106: Powder diffraction pattern of MB\_19, Cu = copper, Cov = covellite, Cha = chalcopyrite, Pyh = pyrrhotite, bor = bornite.

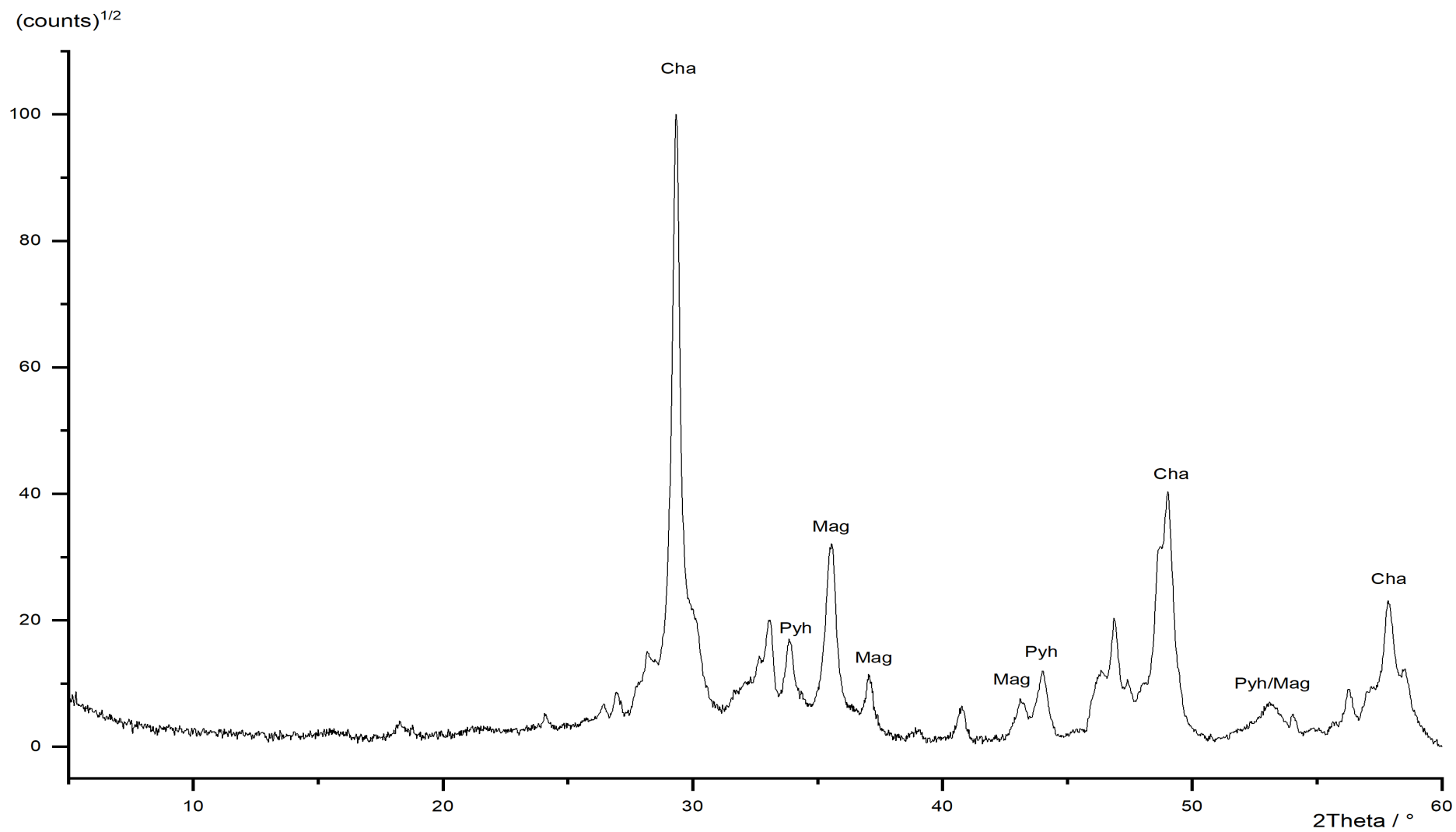


Figure 107: Powder diffraction pattern of MB\_20, Cu = copper, Cov = covellite, Cha = chalcopyrite, Pyh = pyrrhotite, Mag = magnetite.

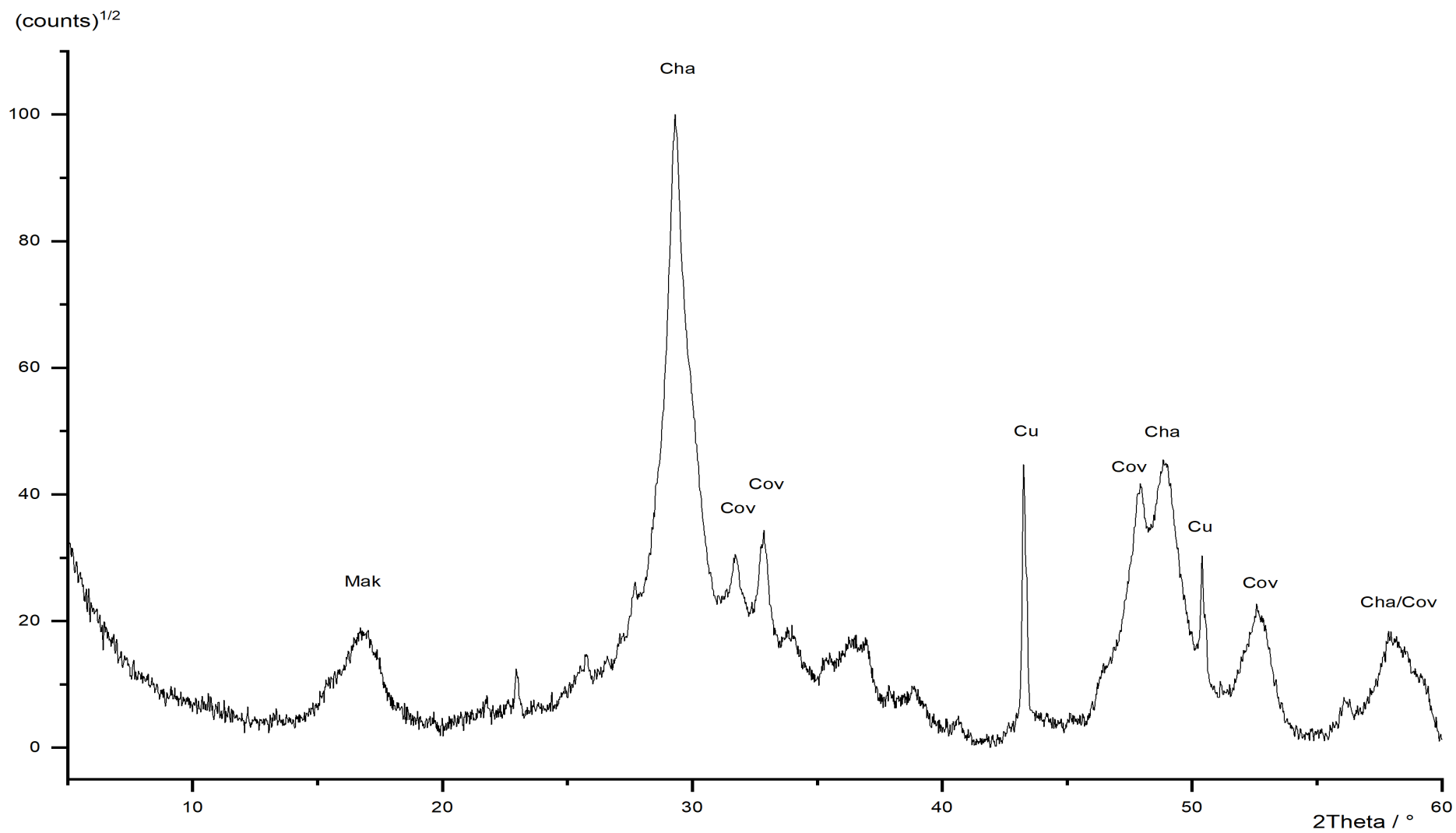


Figure 108: Powder diffraction pattern of MB\_21, Mak = mackinawite, Cu = copper, Cov = covellite, Cha = chalcopyrite.

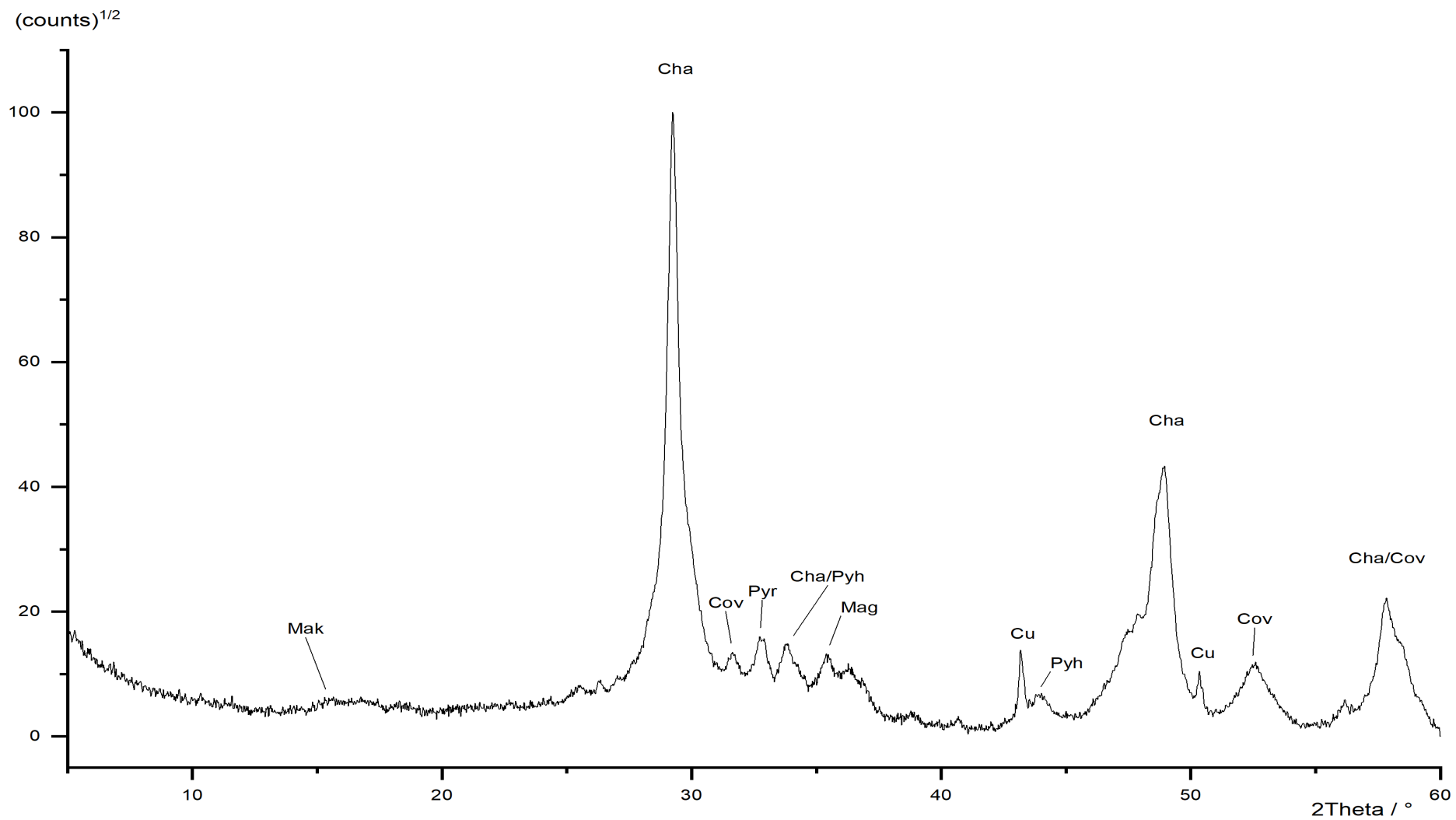


Figure 109: Powder diffraction pattern of MB\_22, Mak = mackinawite, Cu = copper, Cov = covellite, Cha = chalcopyrite, Mag = magnetite, Pyr = pyrite, Pyh = pyrrhotite.

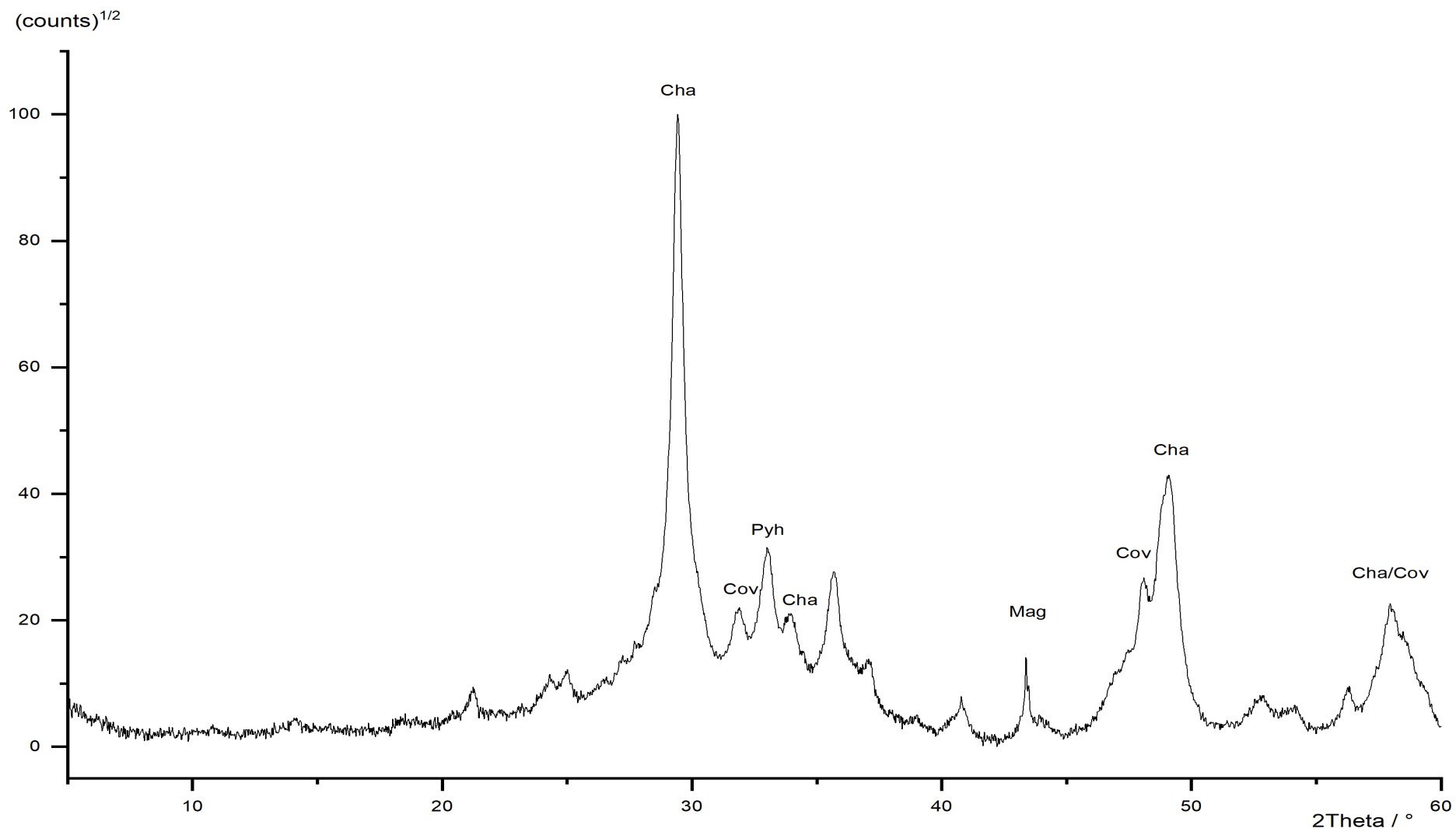


Figure 110: Powder diffraction pattern of MB\_23, Mak = mackinawite, Cu = copper, Cov = covellite, Cha = chalcopyrite, Mag = magnetite.

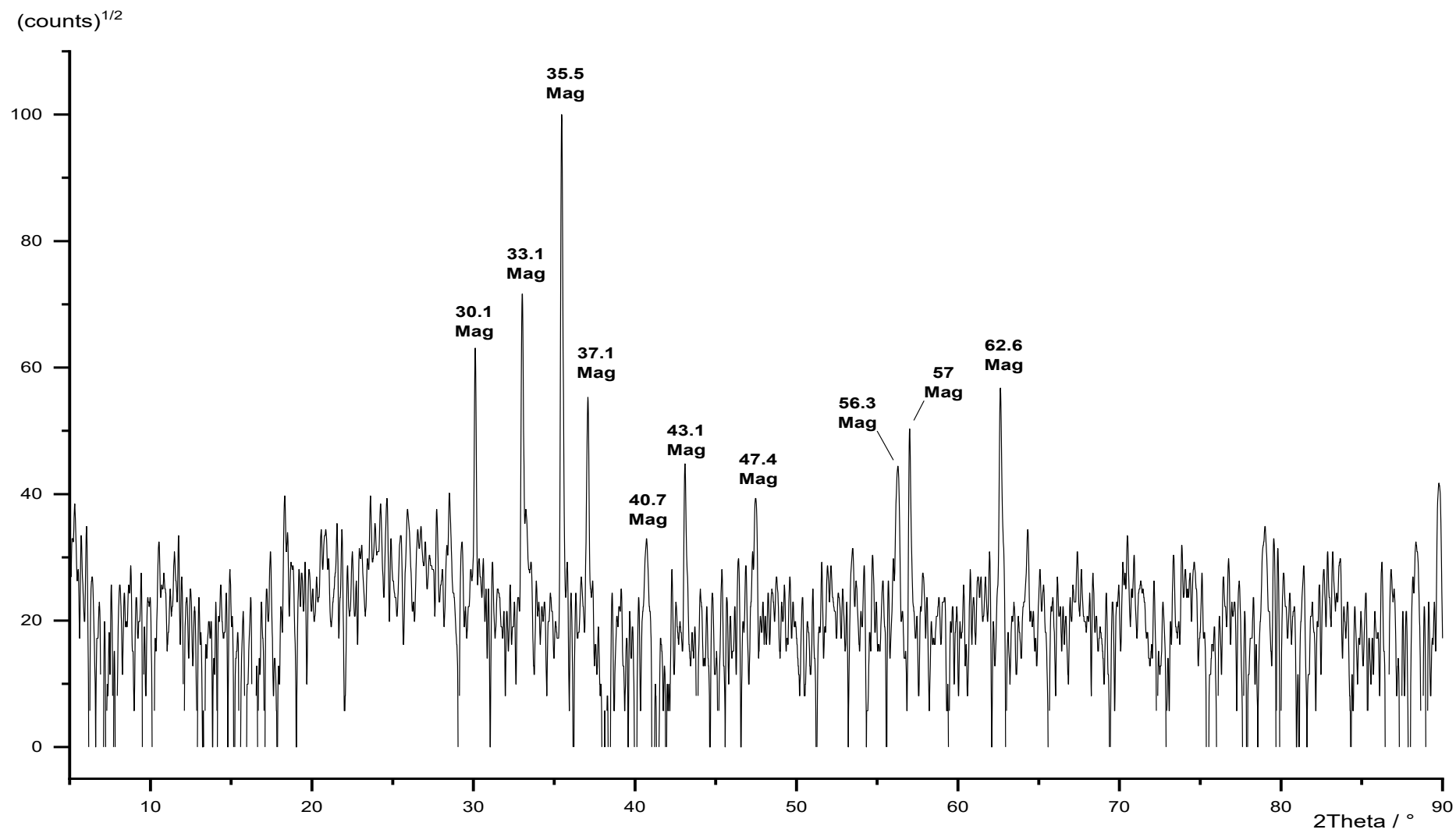


Figure 111: Powder diffraction pattern of Toch\_1. Mag = magnetite.



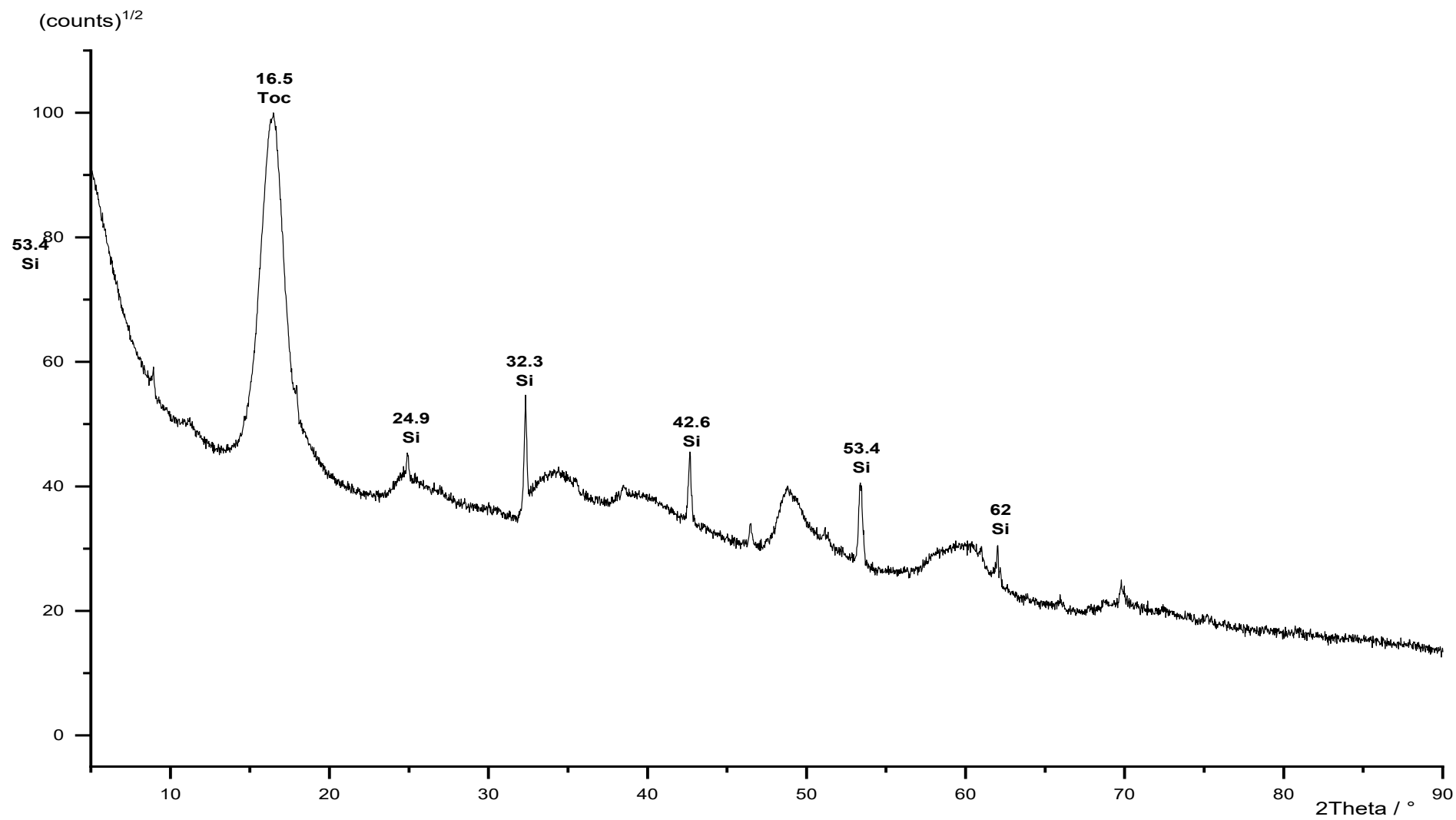


Figure 112: Powder diffraction pattern of Toch\_2. Toc = tochilinite, Si = silicates.

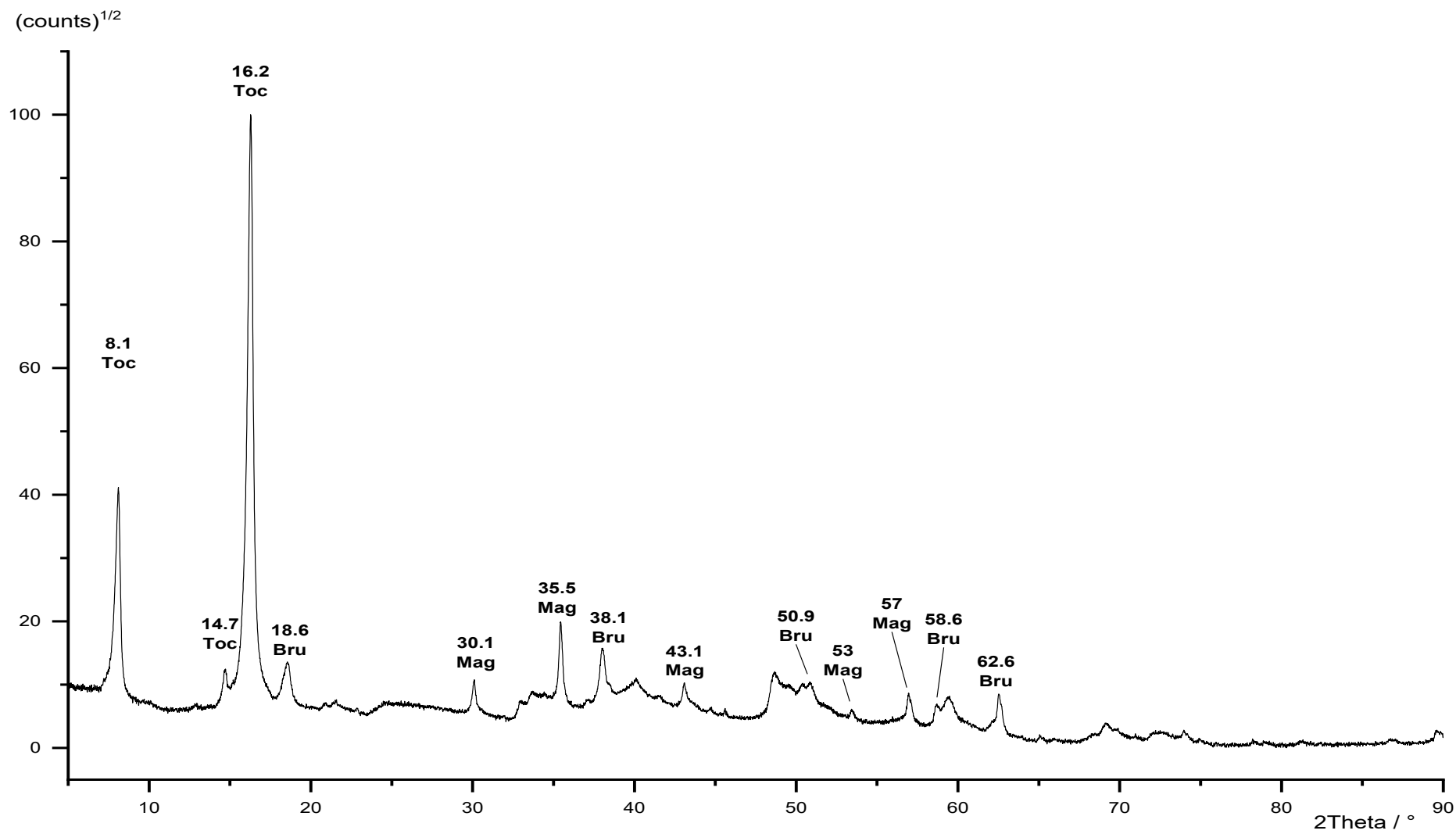


Figure 113: Powder diffraction pattern of ELT\_1. Toc = tochilinite, Mag = magnetite, Bru = brucite.

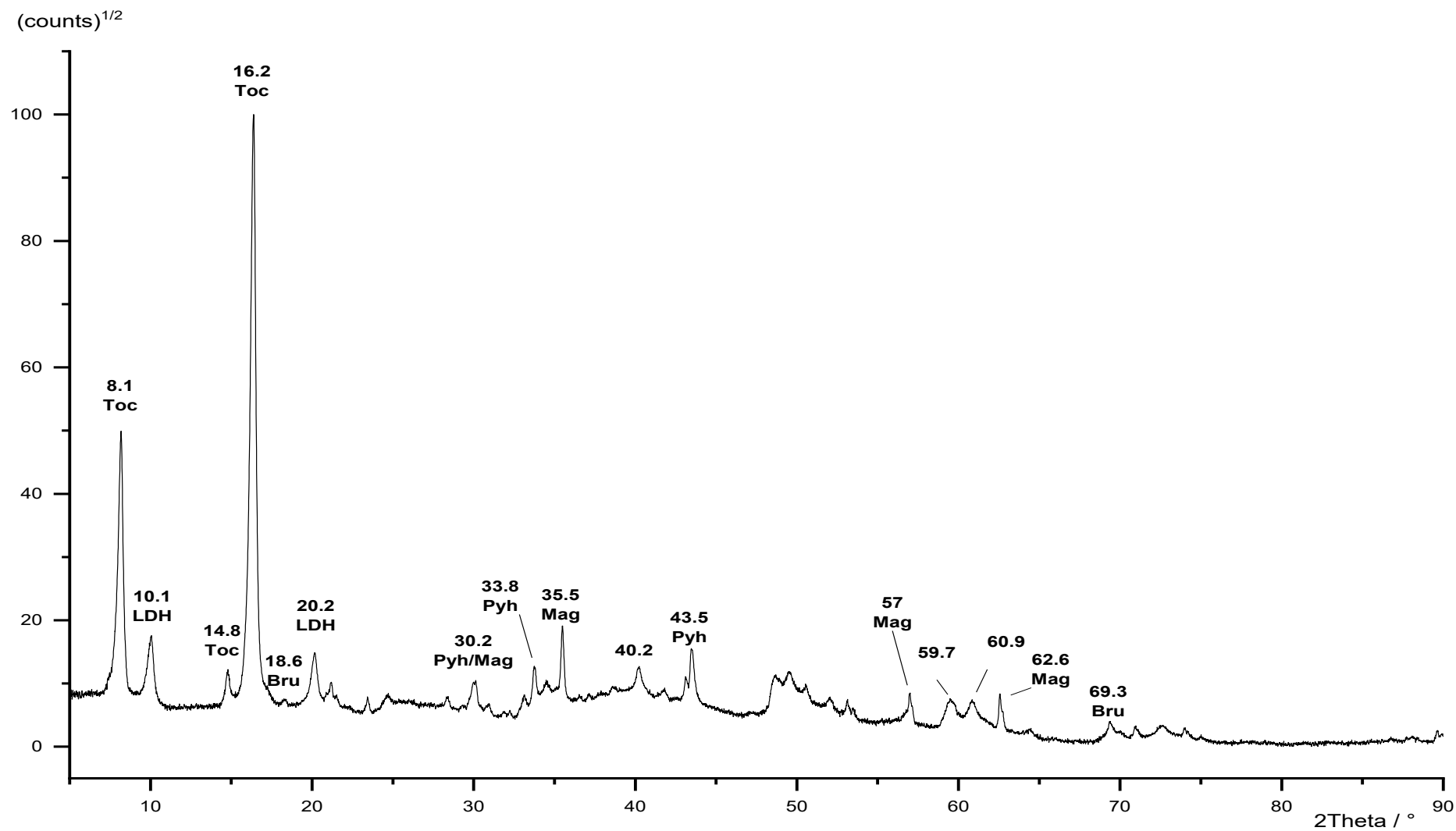


Figure 114: Powder diffraction pattern of Toch\_4. Toc = tochilinite, Mag = magnetite, Bru = brucite. Pyh = pyrrhotite, LDH = layered double hydroxide.

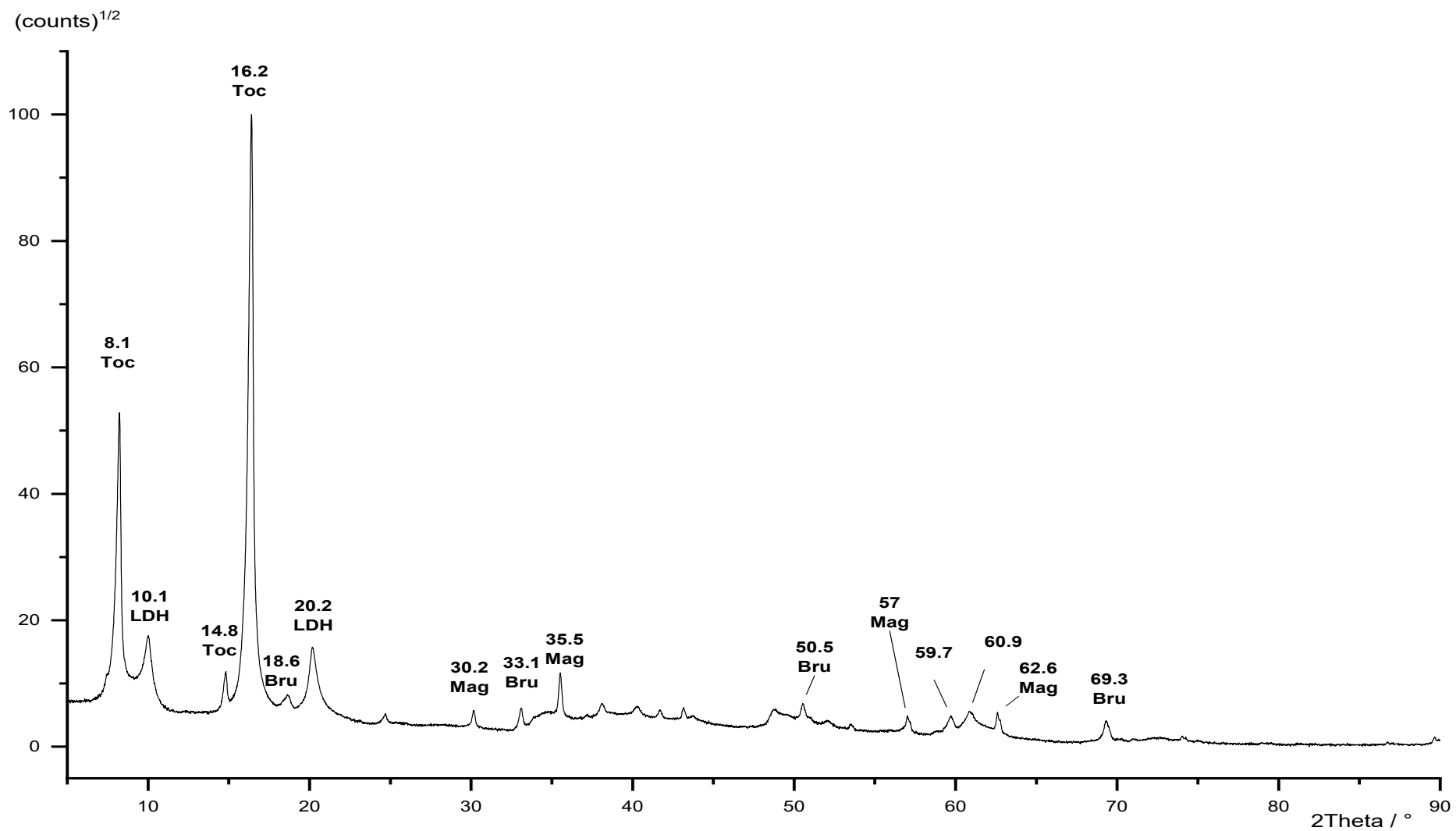


Figure 115: Powder diffraction pattern of Toch\_5. Toc = tochilinite, Mag = magnetite, Bru = brucite. Pyh = pyrrhotite, LDH = layered double hydroxide.

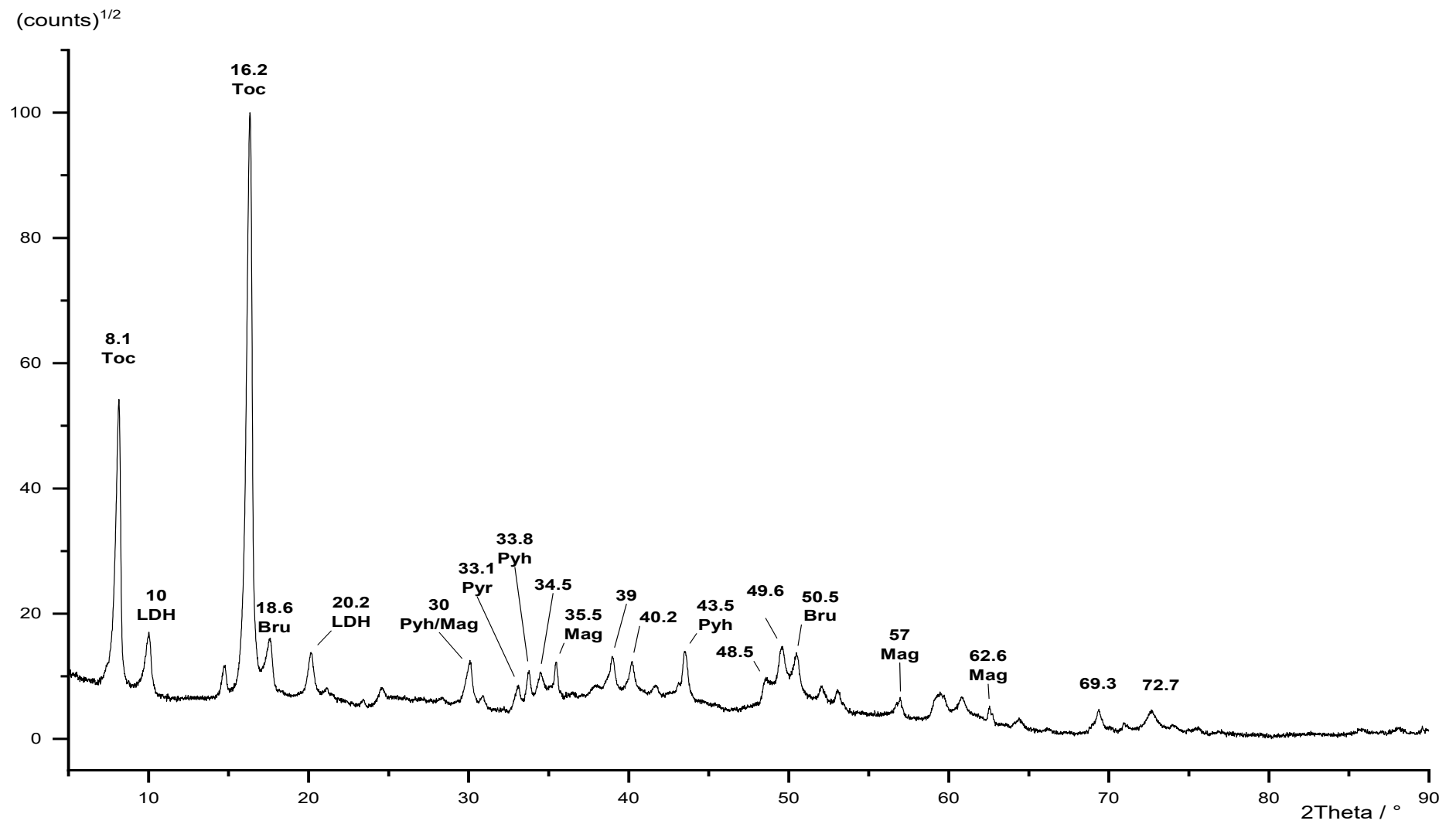


Figure 116: Powder diffraction pattern of Toch\_6. Toc = tochilinite, Mag = magnetite,  
Bru = brucite. Pyh = pyrrhotite, LDH = layered double hydroxide.

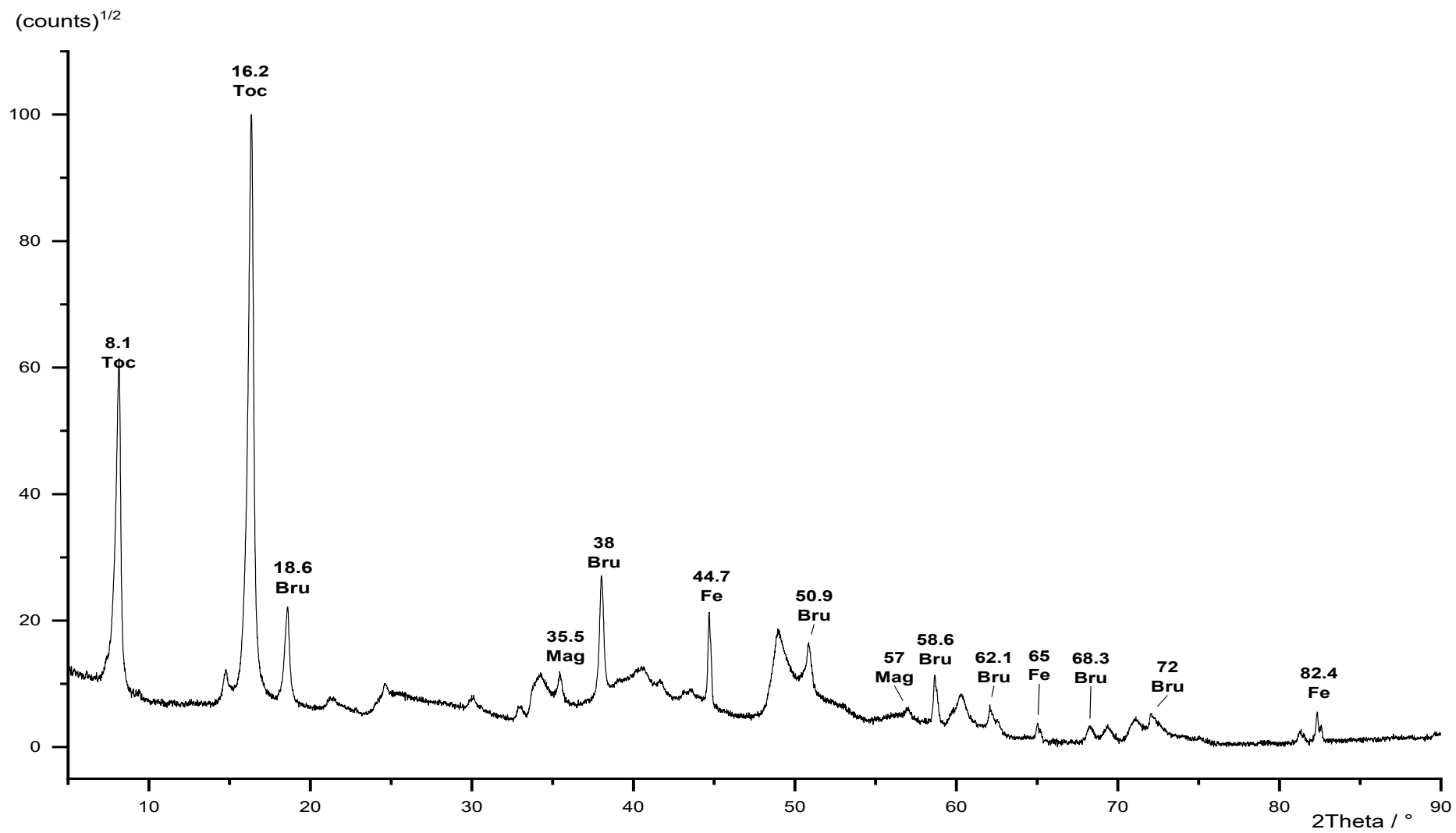


Figure 117: Powder diffraction pattern of Toch\_7. Toc = tochilinite, Mag = magnetite, Bru = brucite. Pyh = pyrrhotite, Fe = iron.

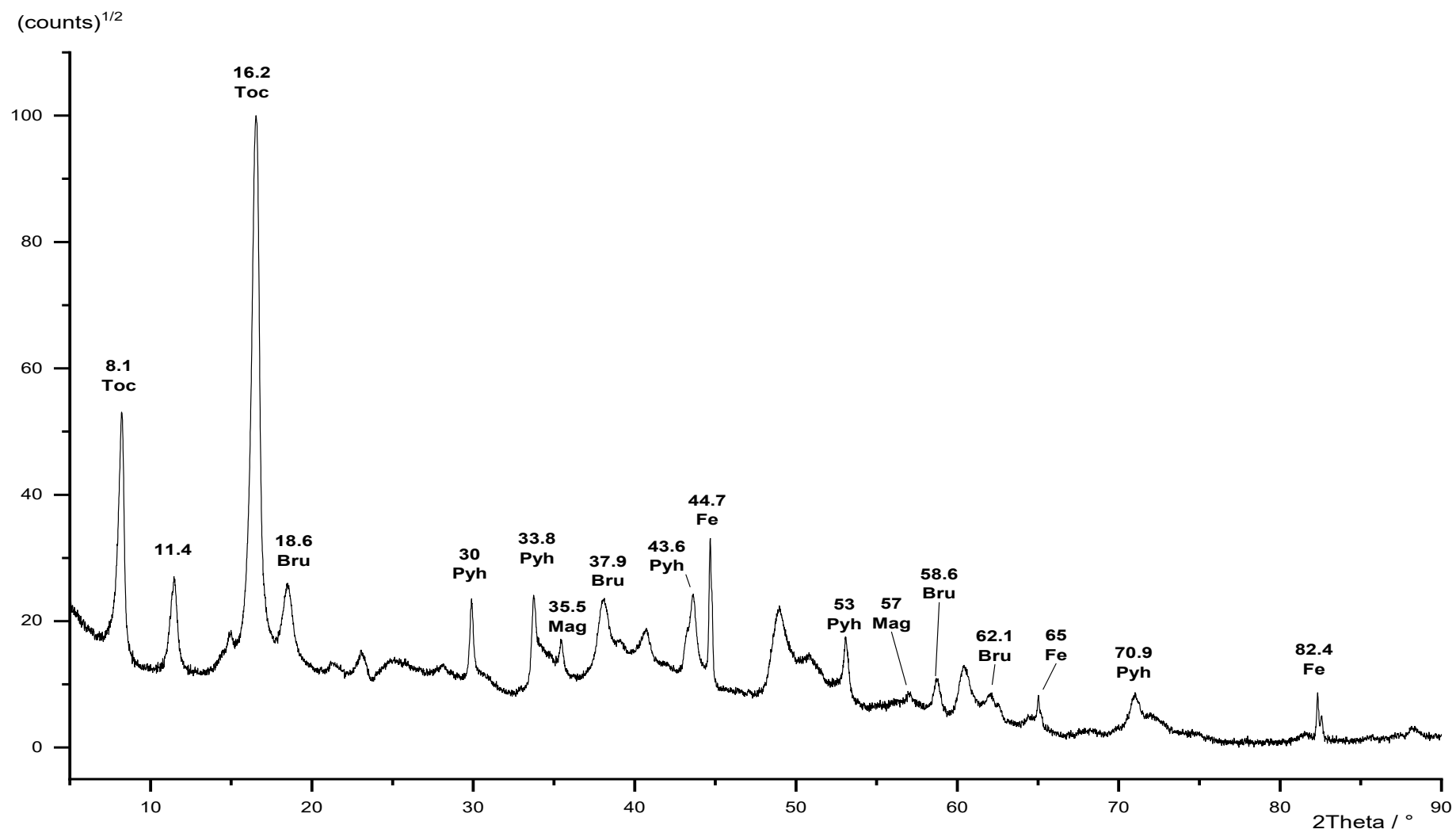


Figure 118: Powder diffraction pattern of Toch\_8. Toc = tochilinite, Mag = magnetite, Bru = brucite. Pyh = pyrrhotite, Fe = iron.

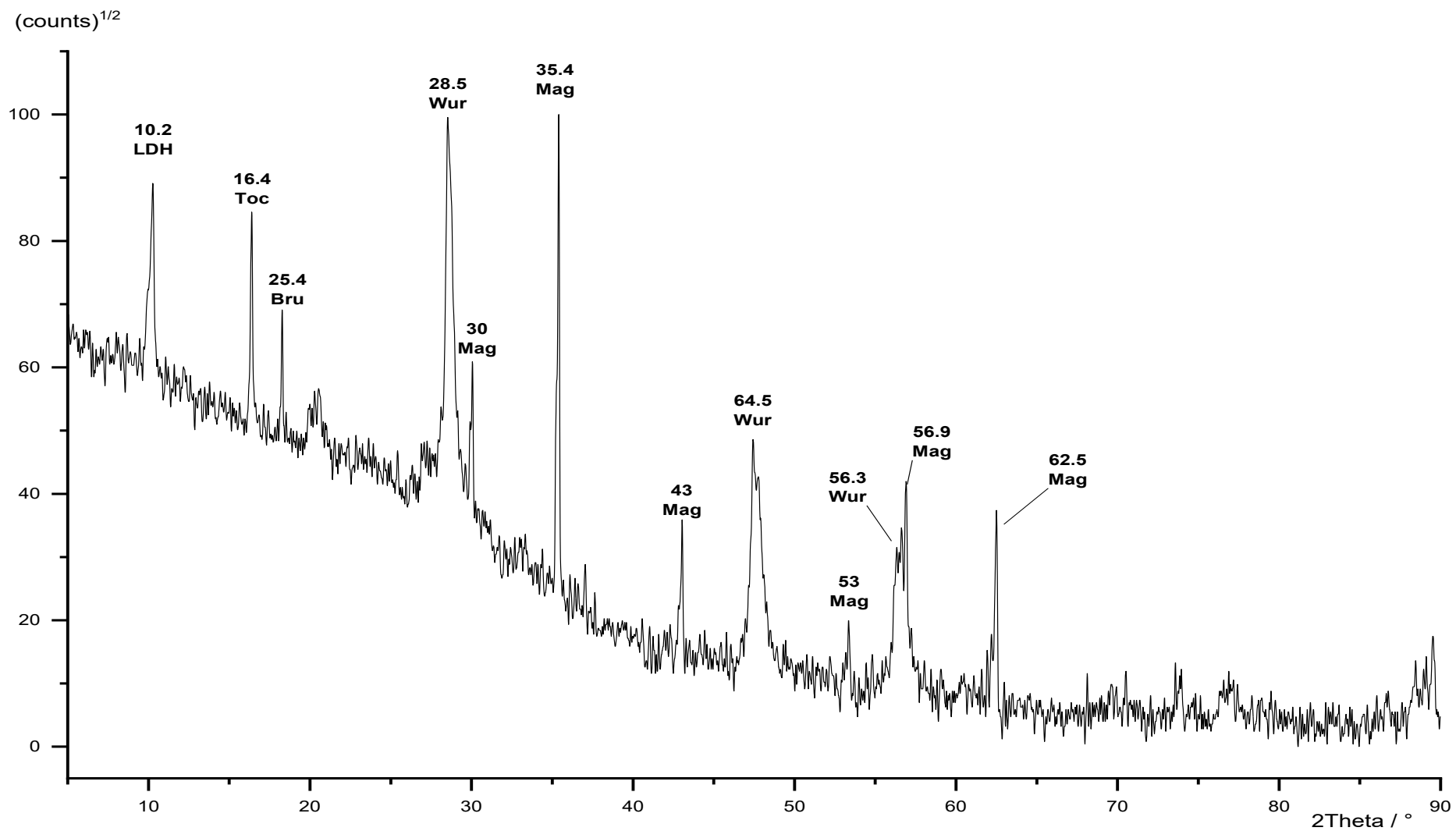


Figure 119: Powder diffraction pattern of Toch\_9. Toc = tochilinite, Mag = magnetite, Bru = brucite. Pyh = pyrrhotite, Wur = wurtzite.



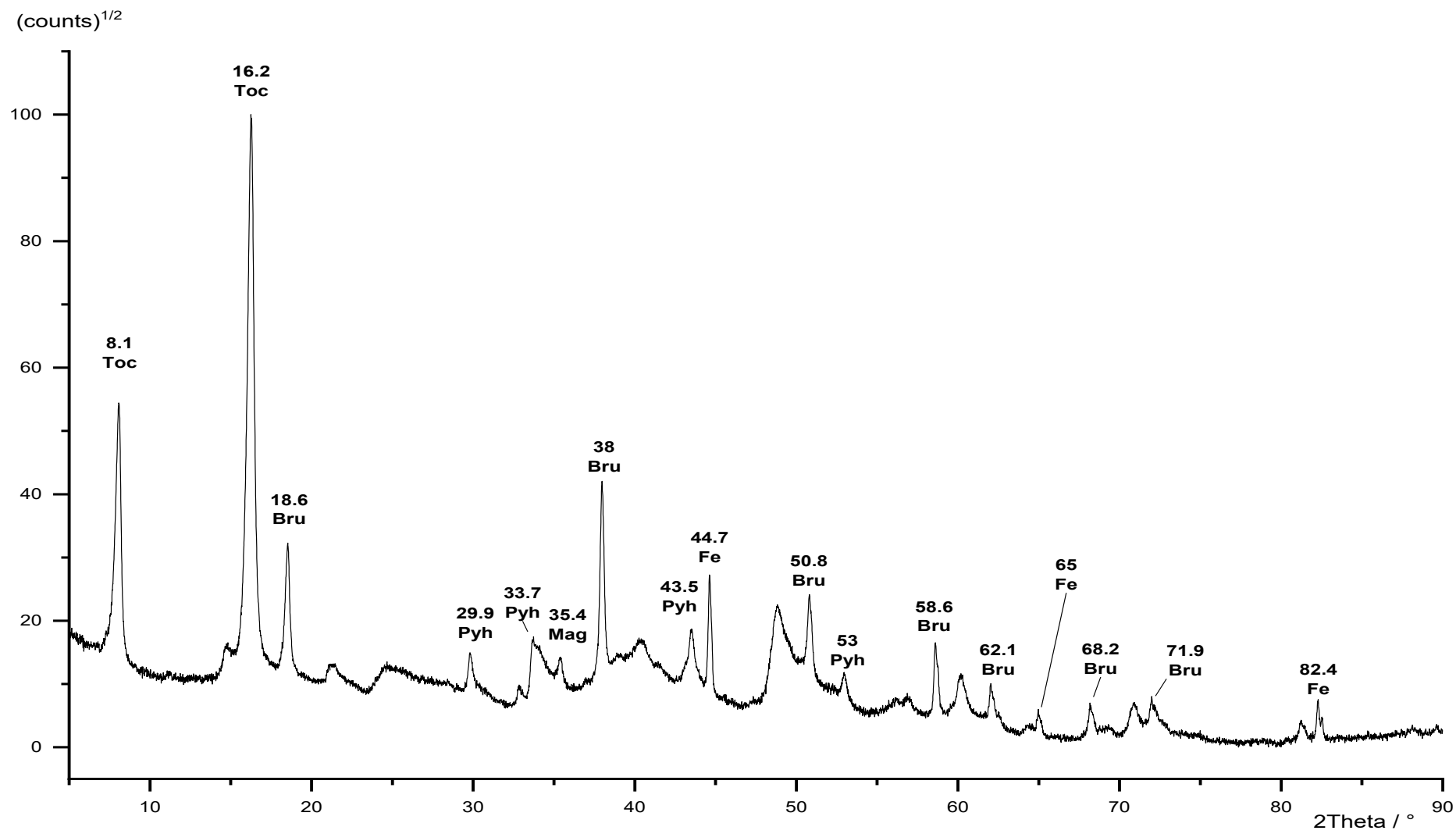


Figure 120: Powder diffraction pattern of TochMgAl\_1.

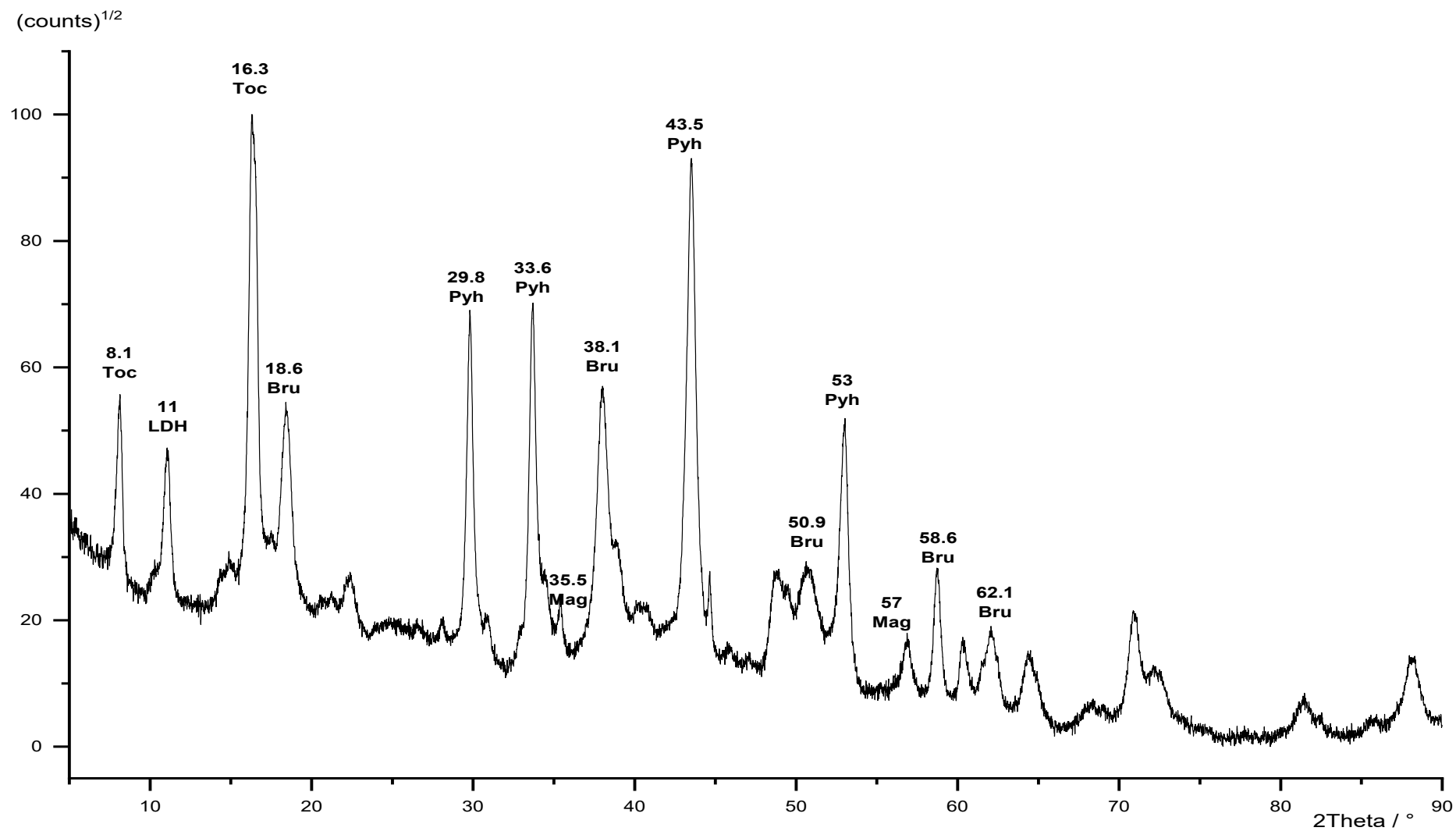


Figure 121: Powder diffraction pattern of TochMgAl<sub>2</sub>. Toc = tochilinite, Mag = magnetite,

Bru = brucite. Pyh = pyrrhotite, Fe = iron.

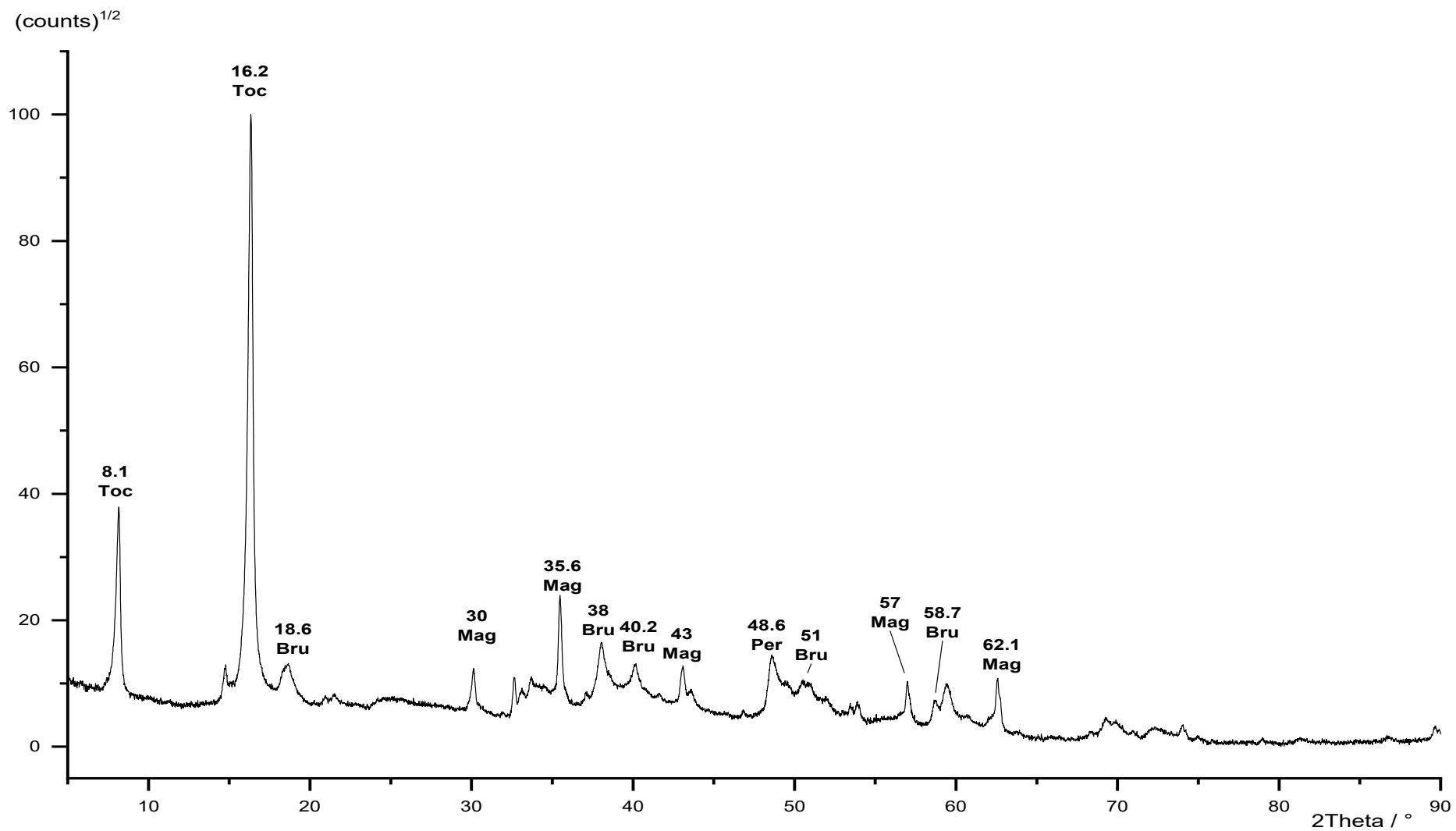


Figure 122: Powder diffraction pattern of TochMgAl<sub>3</sub>. Toc = tochilinite, Mag = magnetite, Bru = brucite. Pyh = pyrrhotite, Fe = iron.

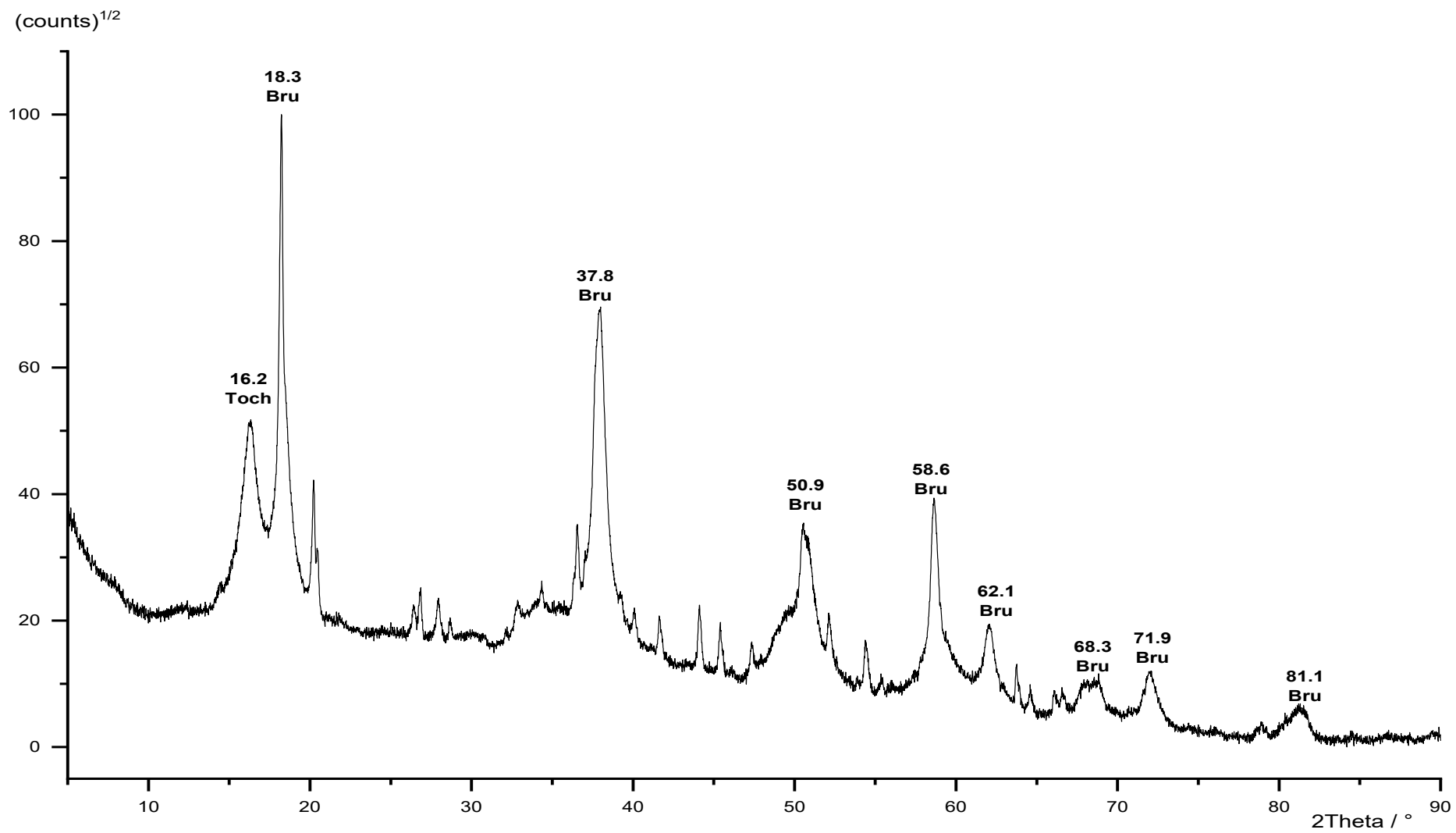


Figure 123: Powder diffraction pattern of TochMgAl<sub>4</sub>. Toc = tochilinite, Bru = brucite.

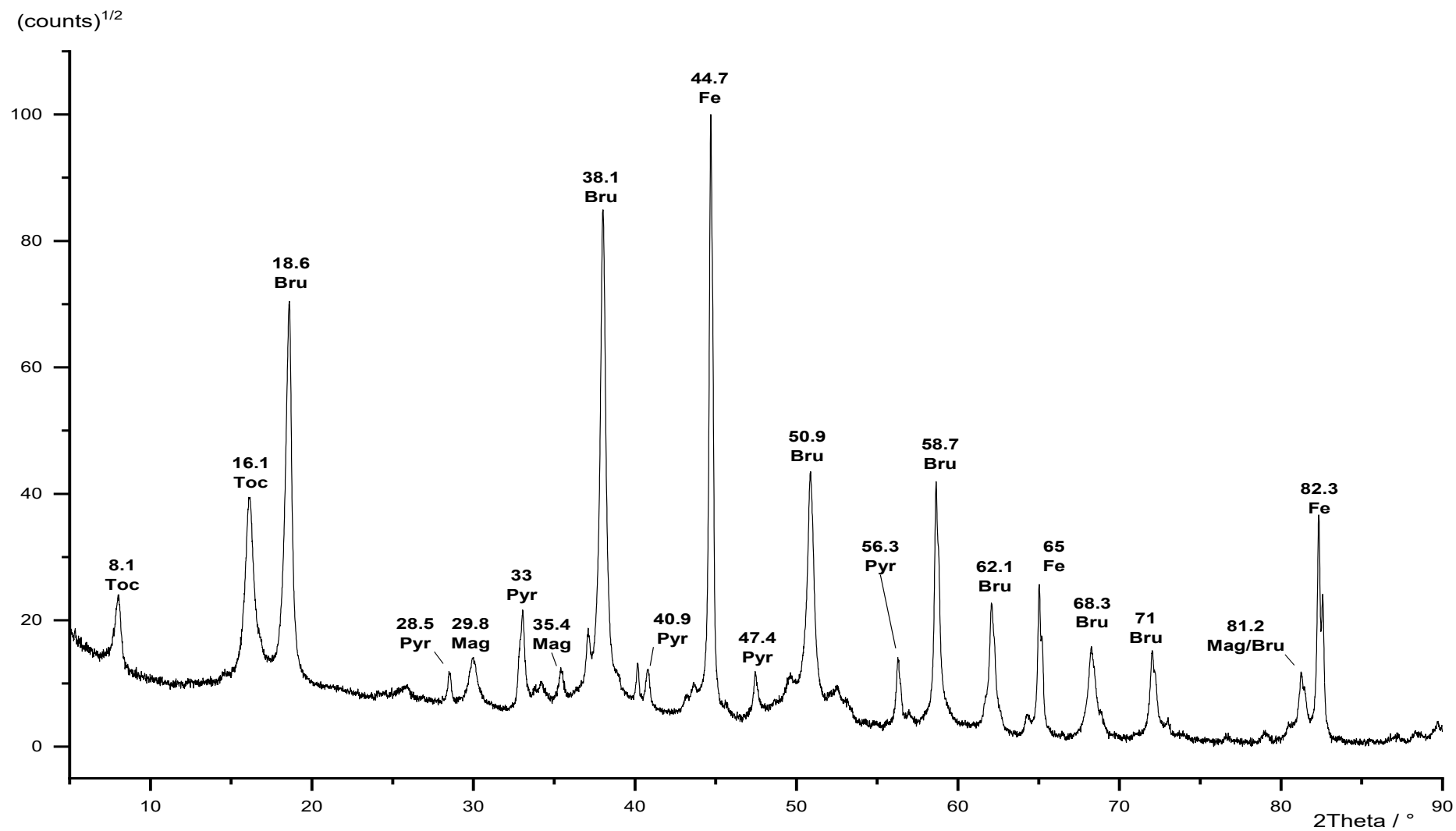


Figure 124: Powder diffraction pattern of TochMgAl<sub>5</sub>. Toc = tochilinite, Mag = magnetite, Bru = brucite. Pyh = pyrrhotite, Fe = iron.

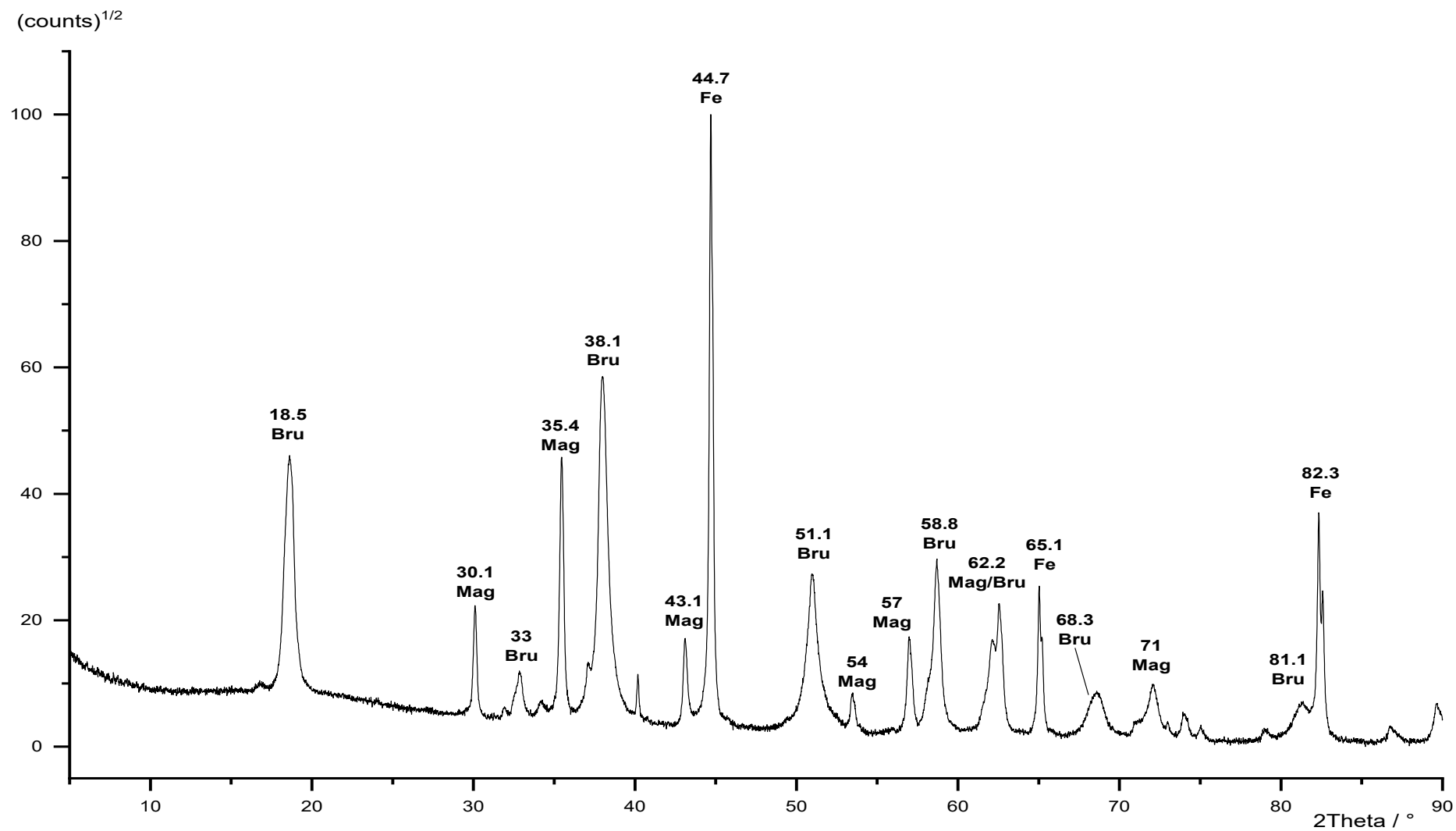


Figure 125: Powder diffraction pattern of TochMgAl\_6. Mag = magnetite, Bru = brucite. Pyh = pyrrhotite, Fe = iron.

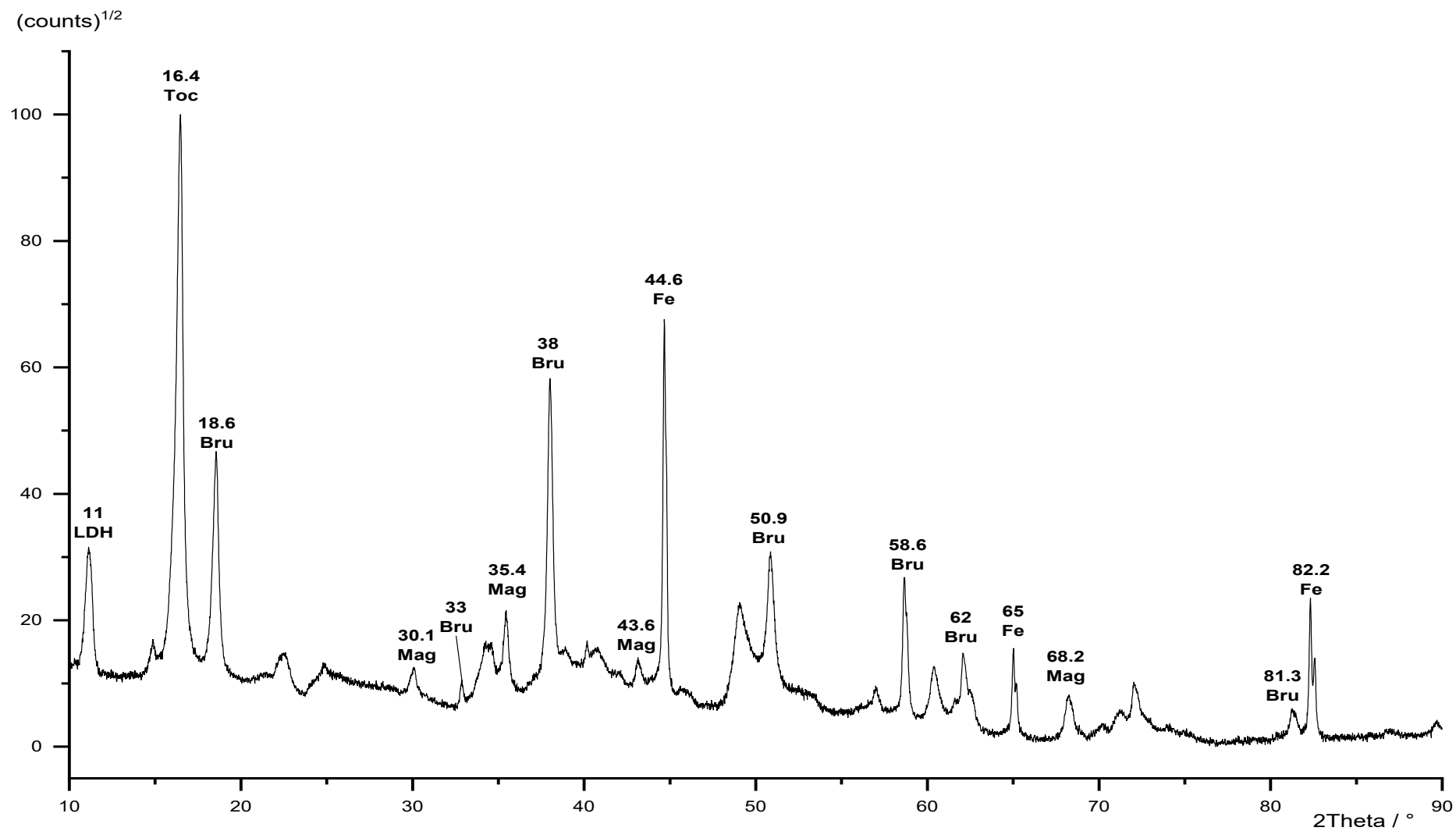


Figure 126: Powder diffraction pattern of TochMgAl<sub>7</sub>. Toc = tochilinite, Mag = magnetite, Bru = brucite. Pyh = pyrrhotite, Fe = iron, LDH = layered double hydroxide.

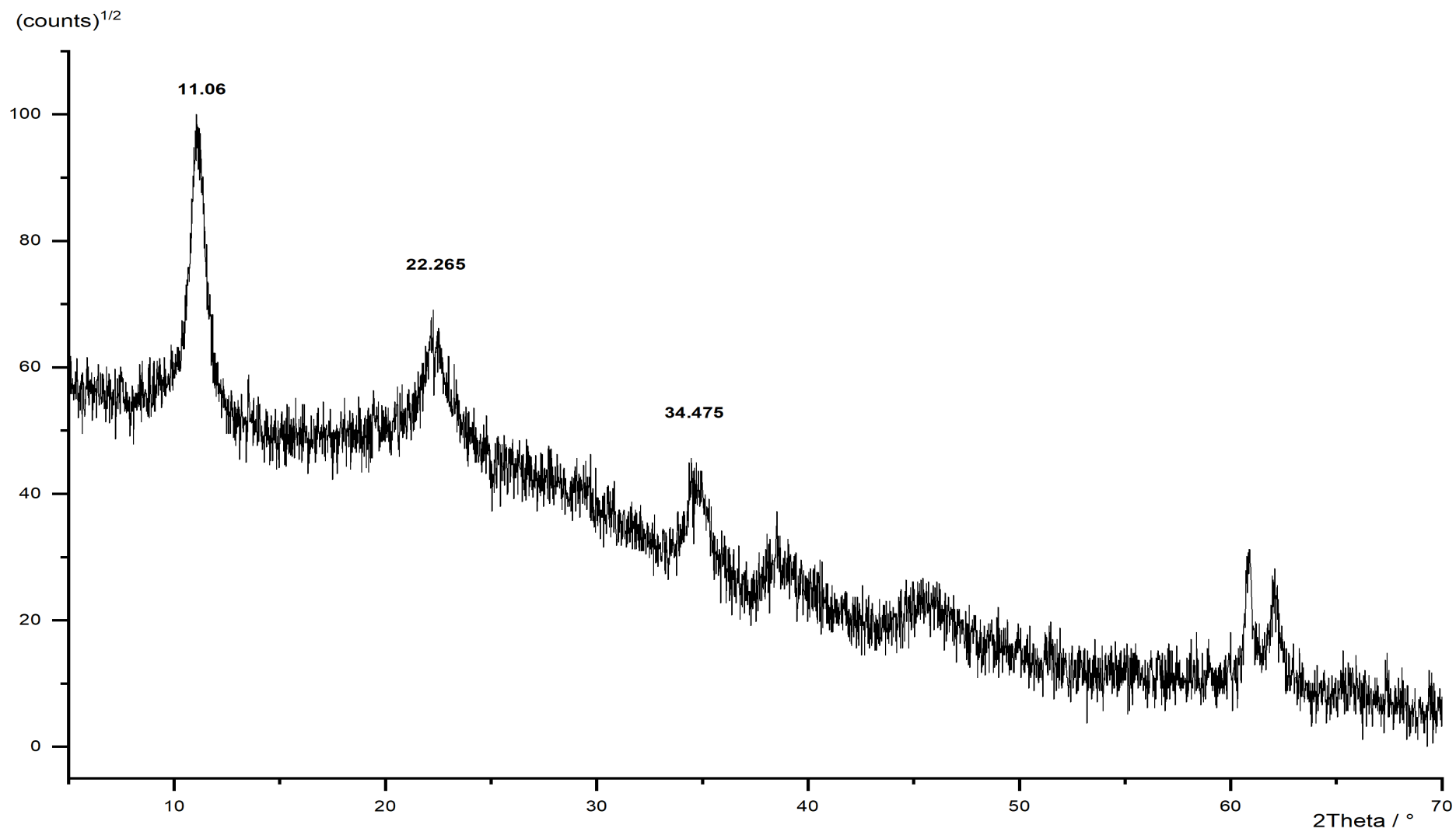


Figure 127: Powder diffraction pattern of TochMgAl<sub>8</sub>.



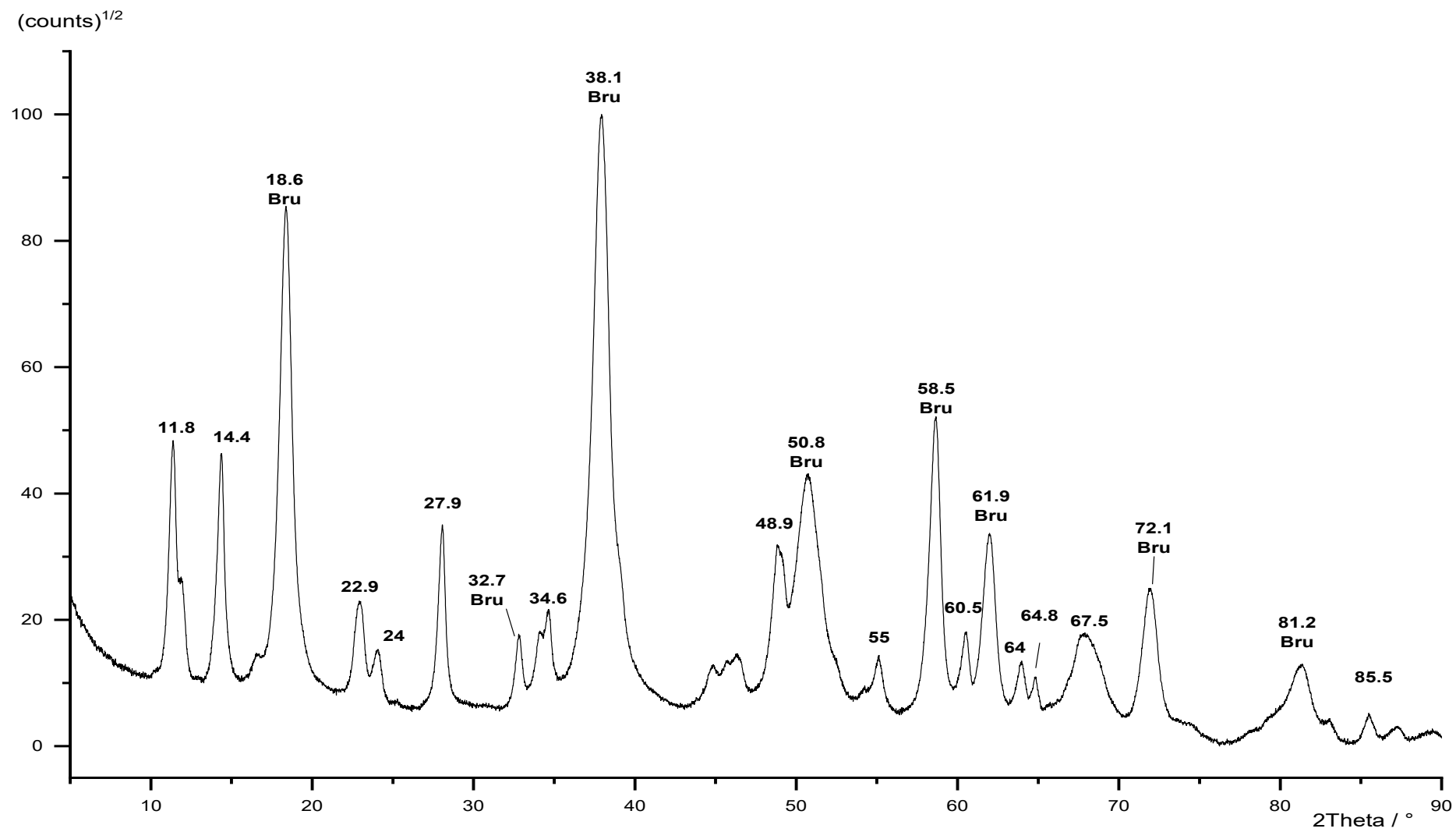


Figure 128: Powder diffraction pattern of TochMgAl\_9. Bru = brucite.

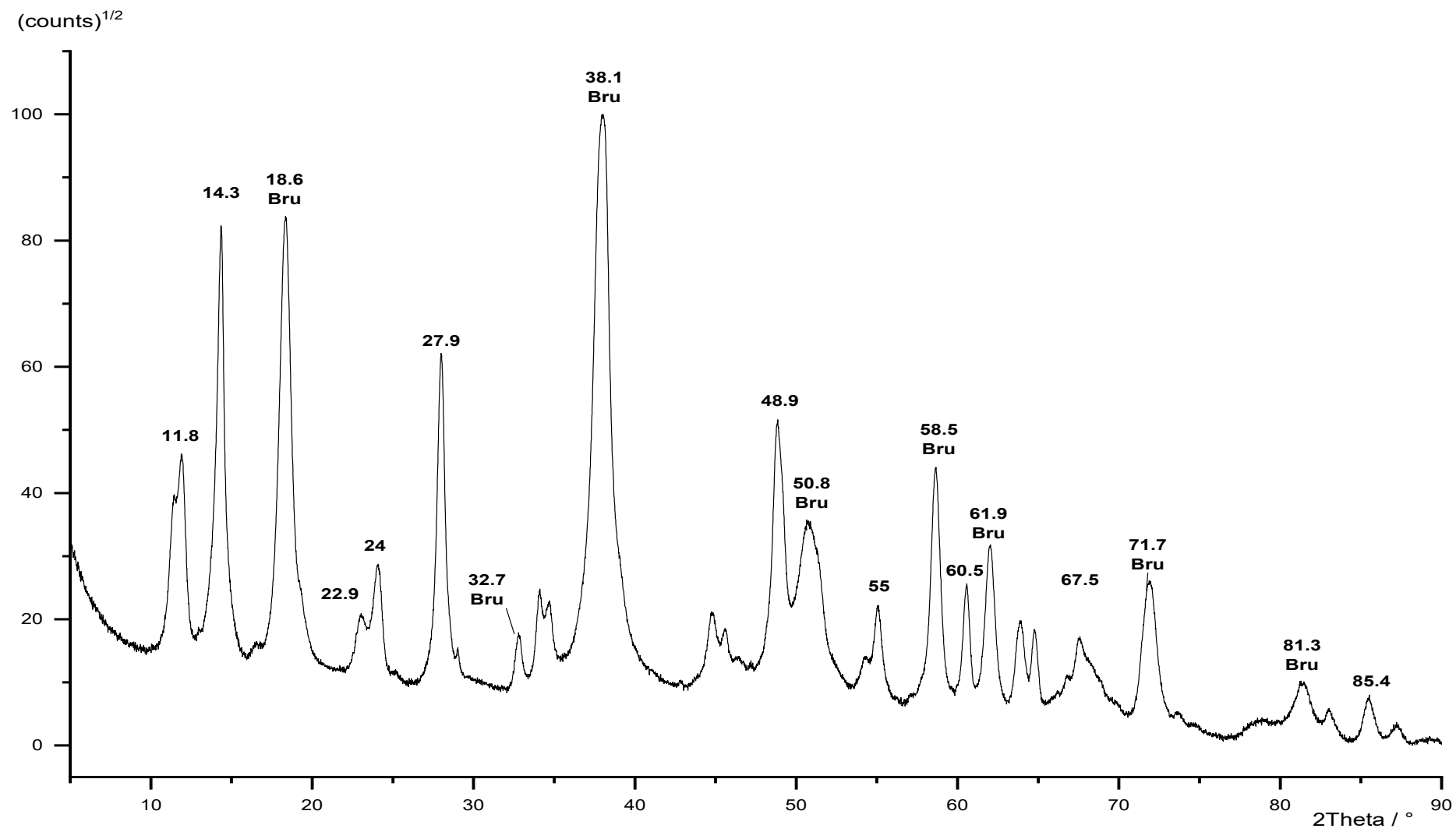


Figure 129: Powder diffraction pattern of TochMgAl\_10. Bru = brucite.

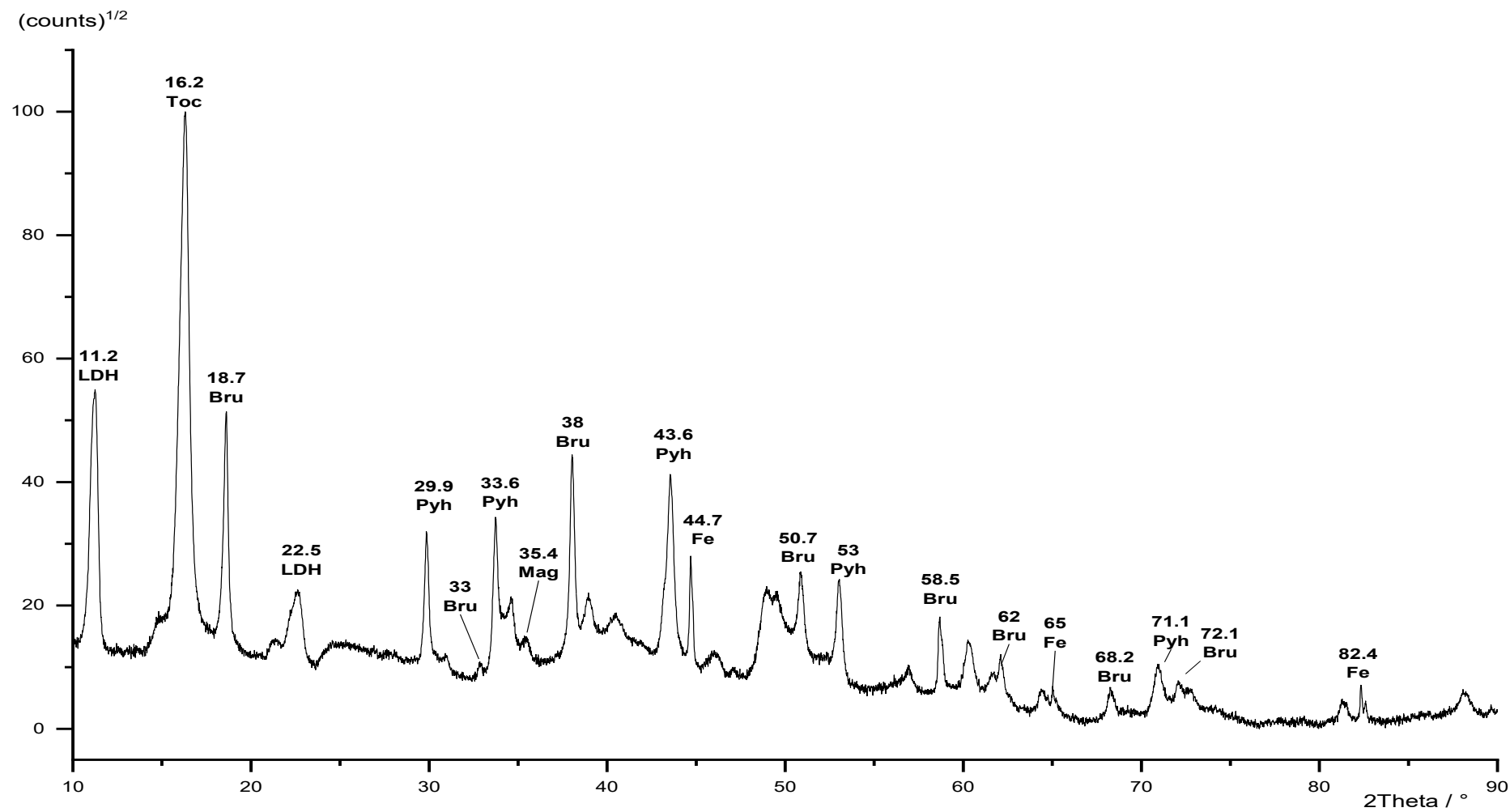


Figure 130: Powder diffraction pattern of TochMgAl<sub>11</sub>. Toc = tochilinite, Mag = magnetite, Bru = brucite. Pyh = pyrrhotite, Fe = iron, LDH = layered double hydroxide.

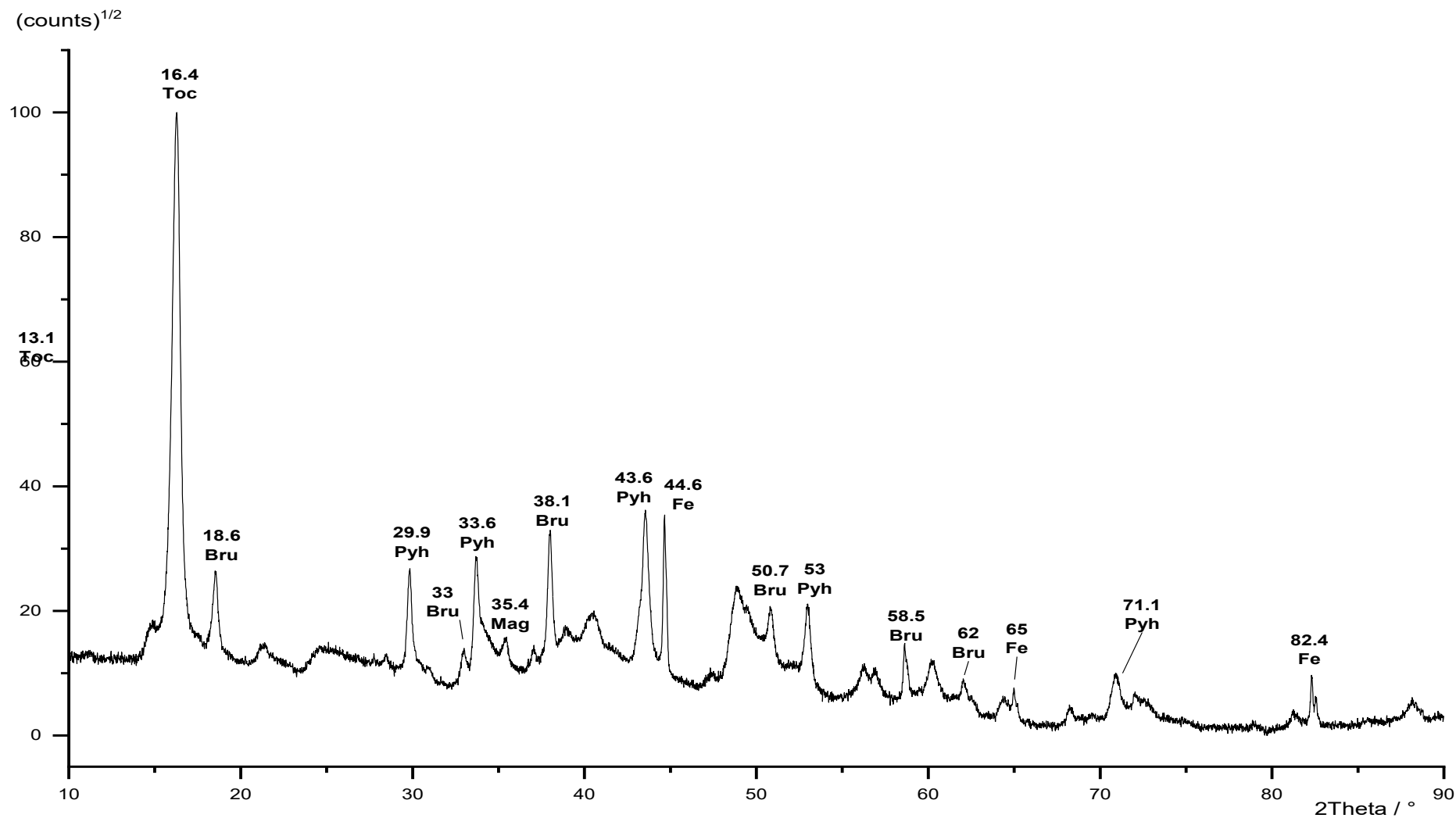


Figure 131: Powder diffraction pattern of TochMgAl<sub>12</sub>. Toc = tochilinite, Mag = magnetite, Bru = brucite. Pyh = pyrrhotite, Fe = iron.

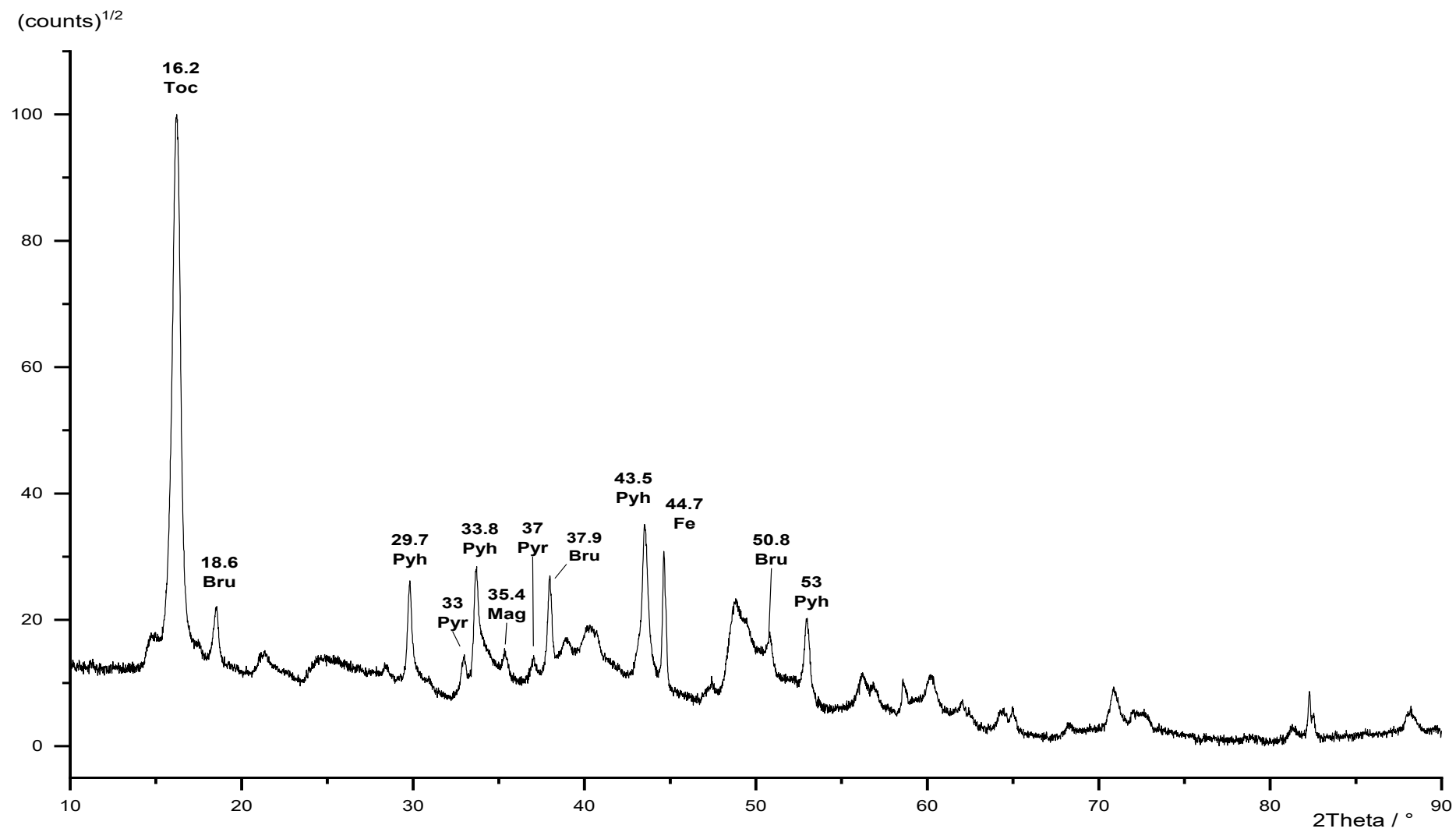


Figure 132: Powder diffraction pattern of TochMgAl\_13. Toc = tochilinite, Mag = magnetite,

Bru = brucite. Pyh = pyrrhotite, Fe = iron.

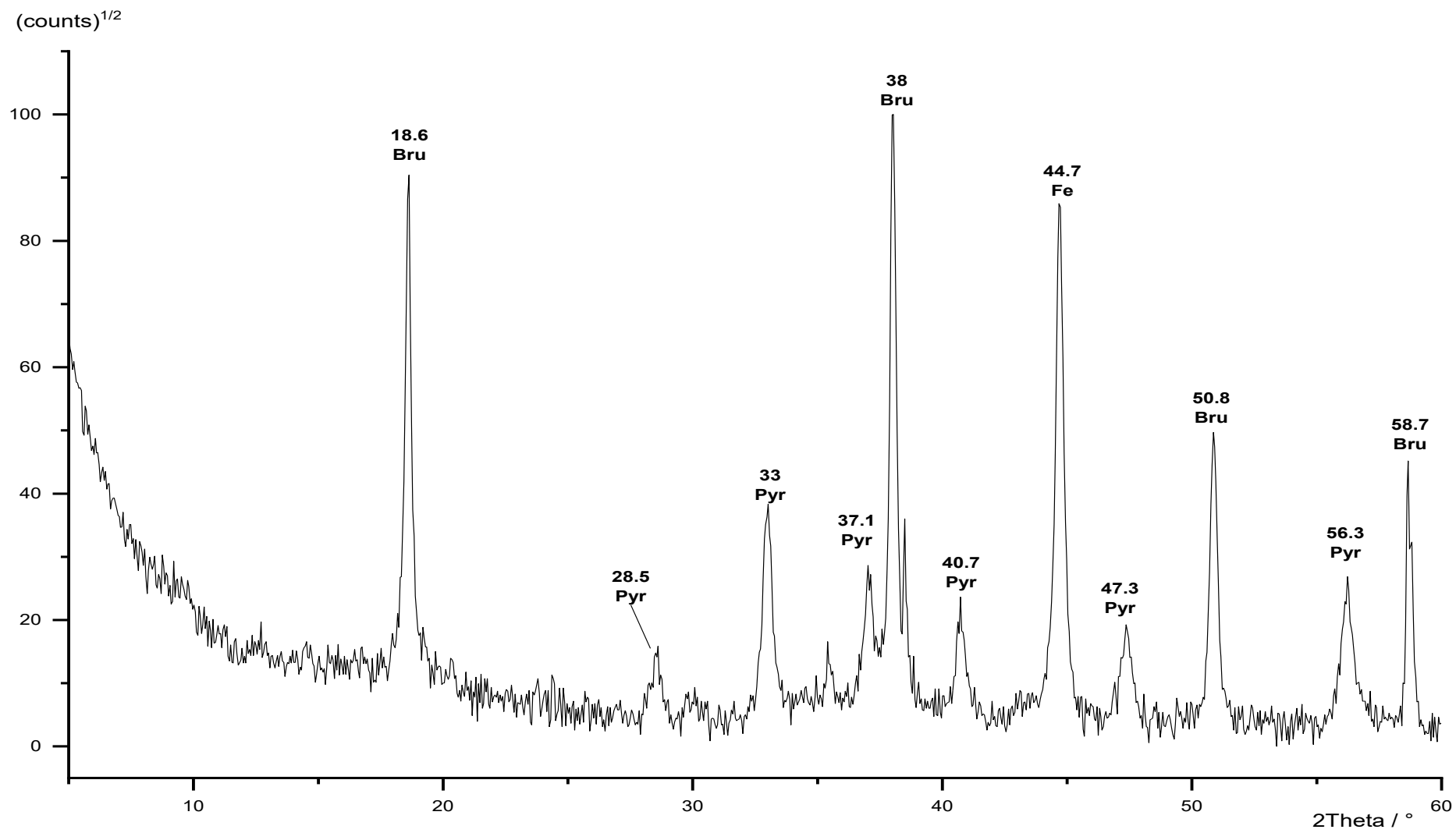


Figure 133: Powder diffraction pattern of TochMgAl<sub>14</sub>. Bru = brucite. Pyr = pyrrhotite, Fe = iron.

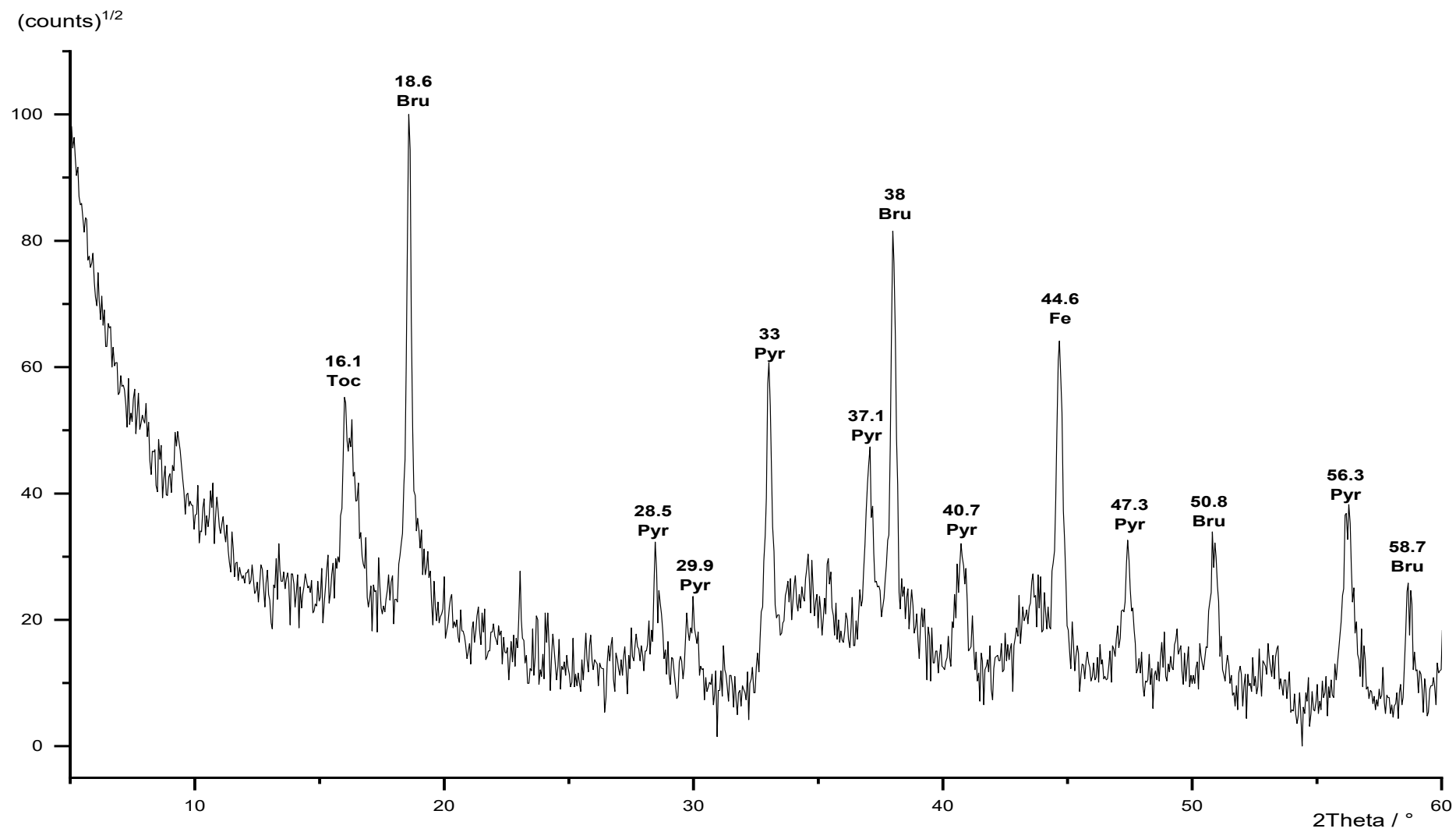


Figure 134: Powder diffraction pattern of TochMgAl\_15. Toc = tochilinite,  
Bru = brucite. Pyh = pyrrhotite, Fe = iron.

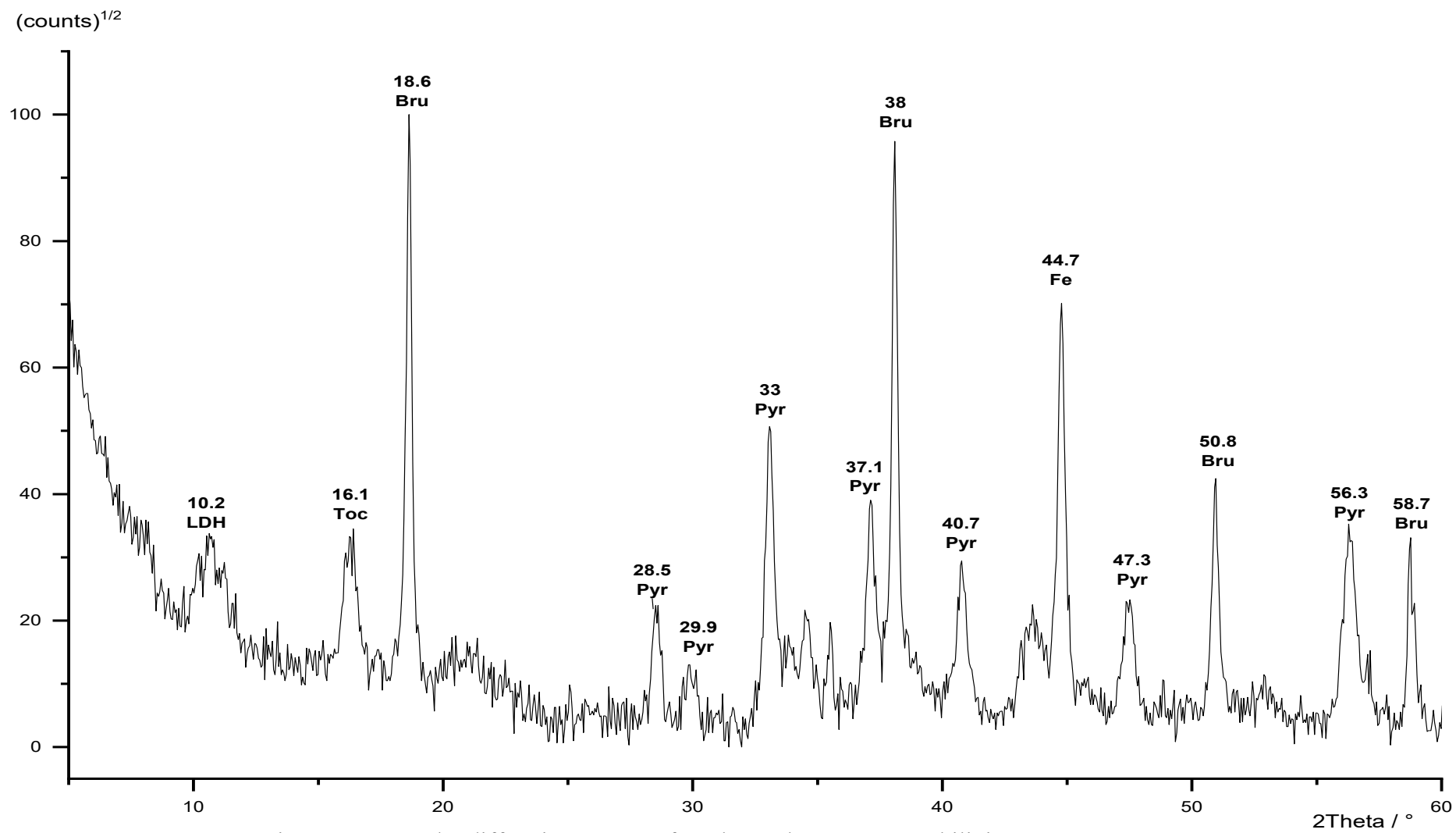


Figure 135: Powder diffraction pattern of TochMgAl<sub>16</sub>. Toc = tochilinite, Bru = brucite. Pyr = pyrrhotite, Fe = iron, LDH = layered double hydroxide.



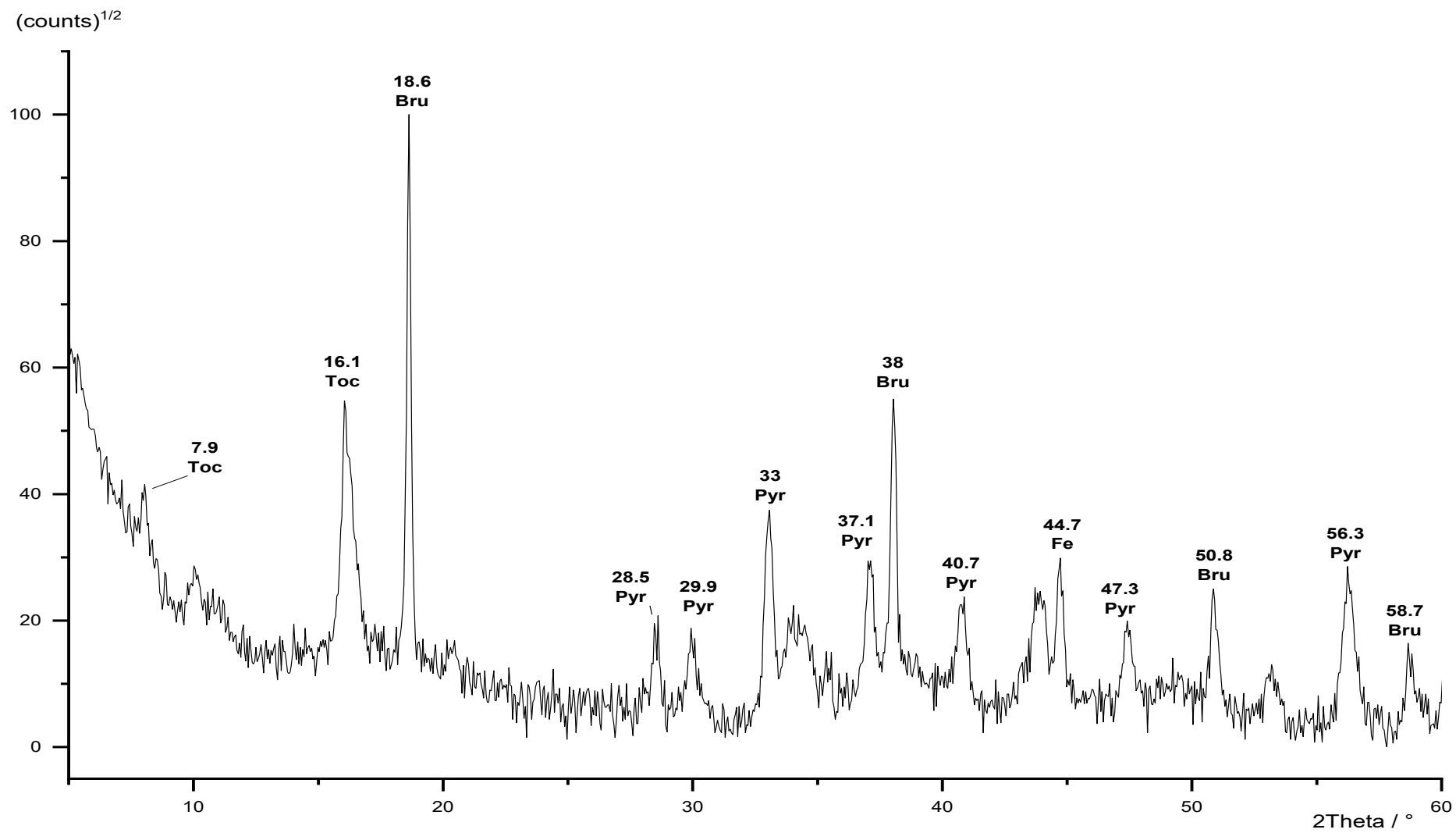


Figure 136: Powder diffraction pattern of TochMgAl\_17. Toc = tochilinite,  
 Bru = brucite. Pyh = pyrrhotite, Fe = iron..

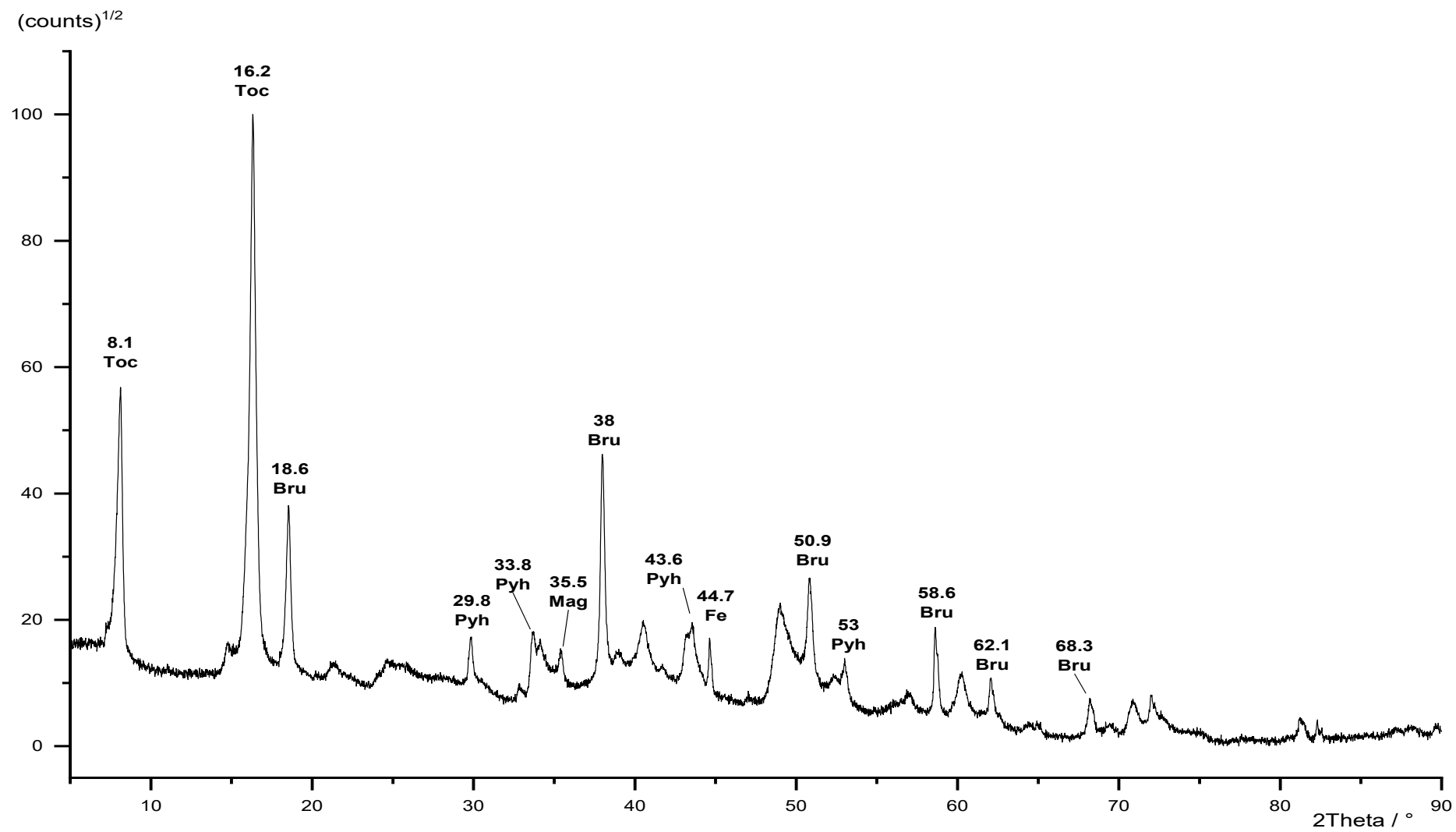


Figure 137: Powder diffraction pattern of TochMgAl<sub>18</sub>. Toc = tochilinite, Mag = magnetite, Bru = brucite. Pyh = pyrrhotite, Fe = iron.

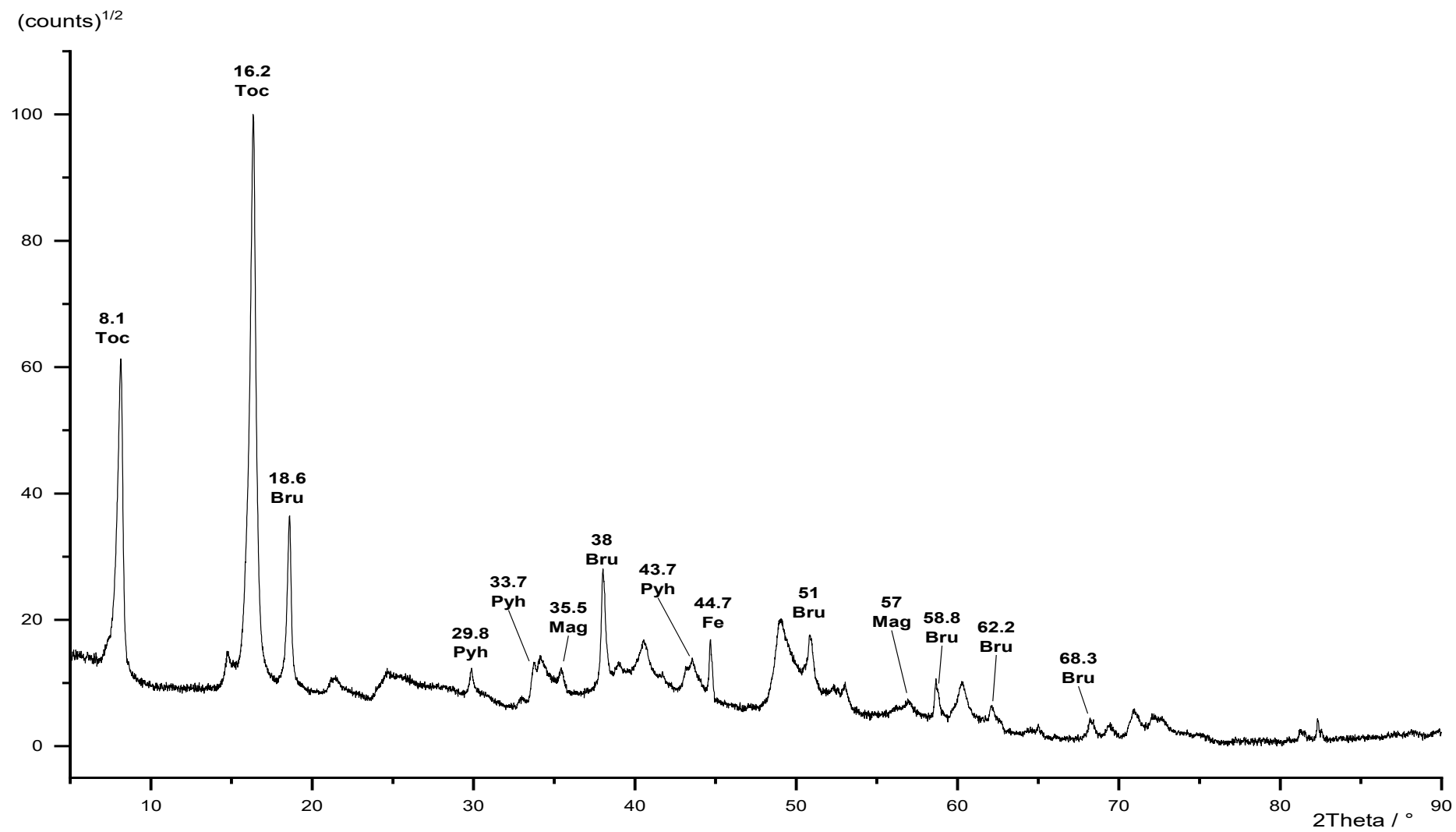


Figure 138: Powder diffraction pattern of TochMgAl<sub>19</sub>. Toc = tochilinite, Mag = magnetite, Bru = brucite. Pyh = pyrrhotite, Fe = iron.

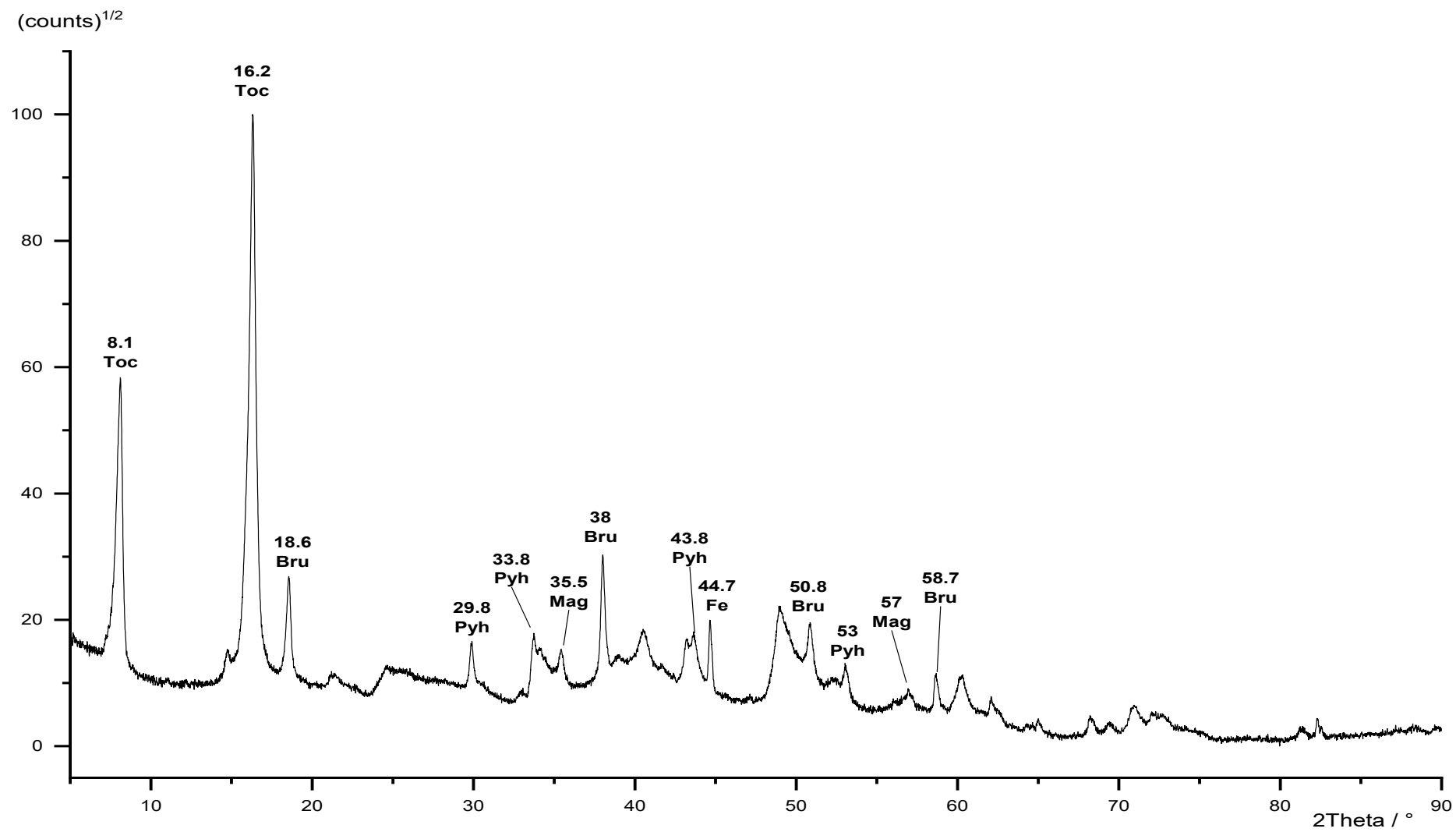


Figure 139: Powder diffraction pattern of TochMgAl<sub>20</sub>. Toc = tochilinite, Mag = magnetite, Bru = brucite. Pyh = pyrrhotite, Fe = iron.

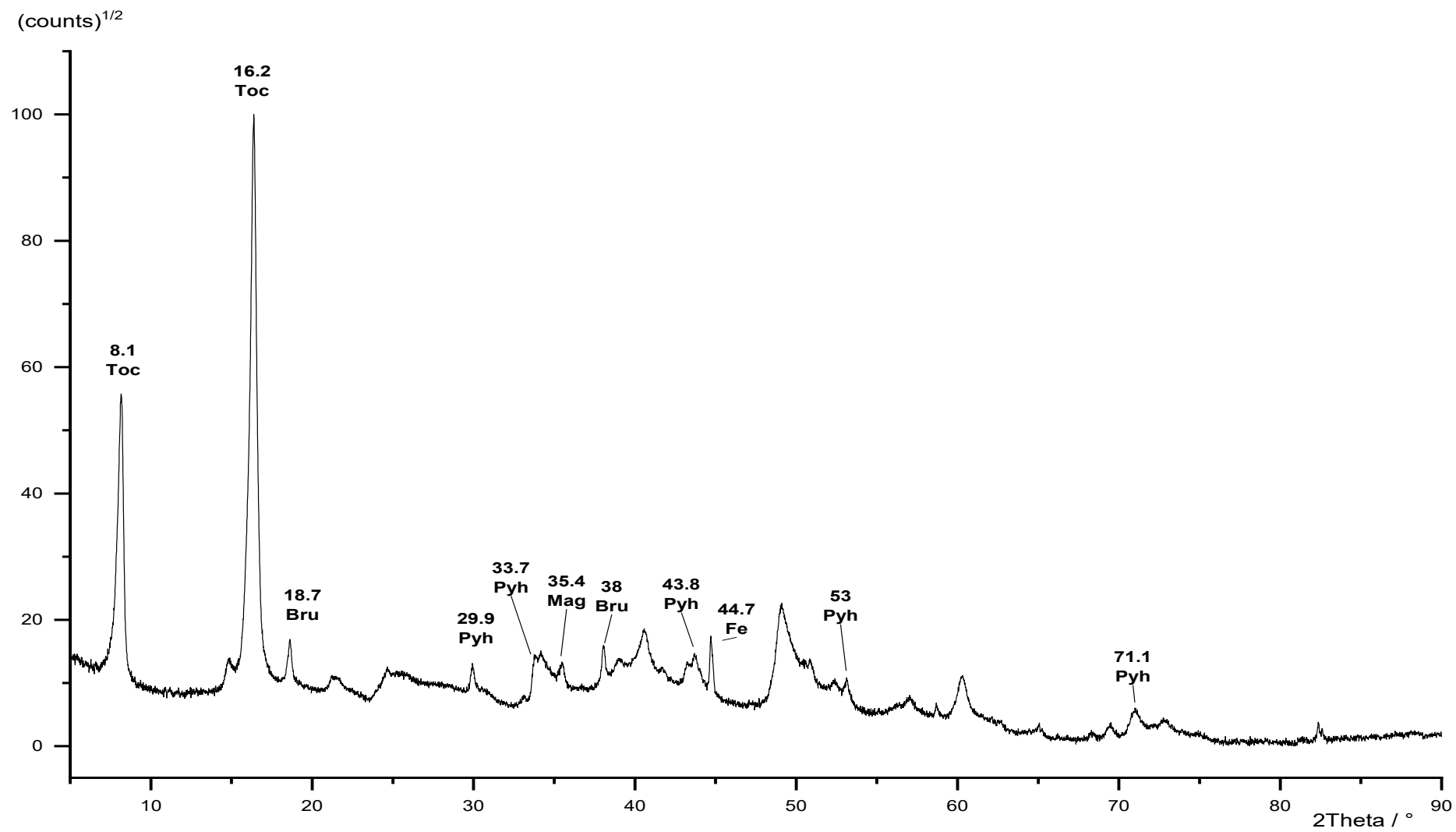


Figure 140: Powder diffraction pattern of TochMgAl<sub>21</sub>. Toc = tochilinite, Mag = magnetite, Bru = brucite. Pyh = pyrrhotite, Fe = iron.

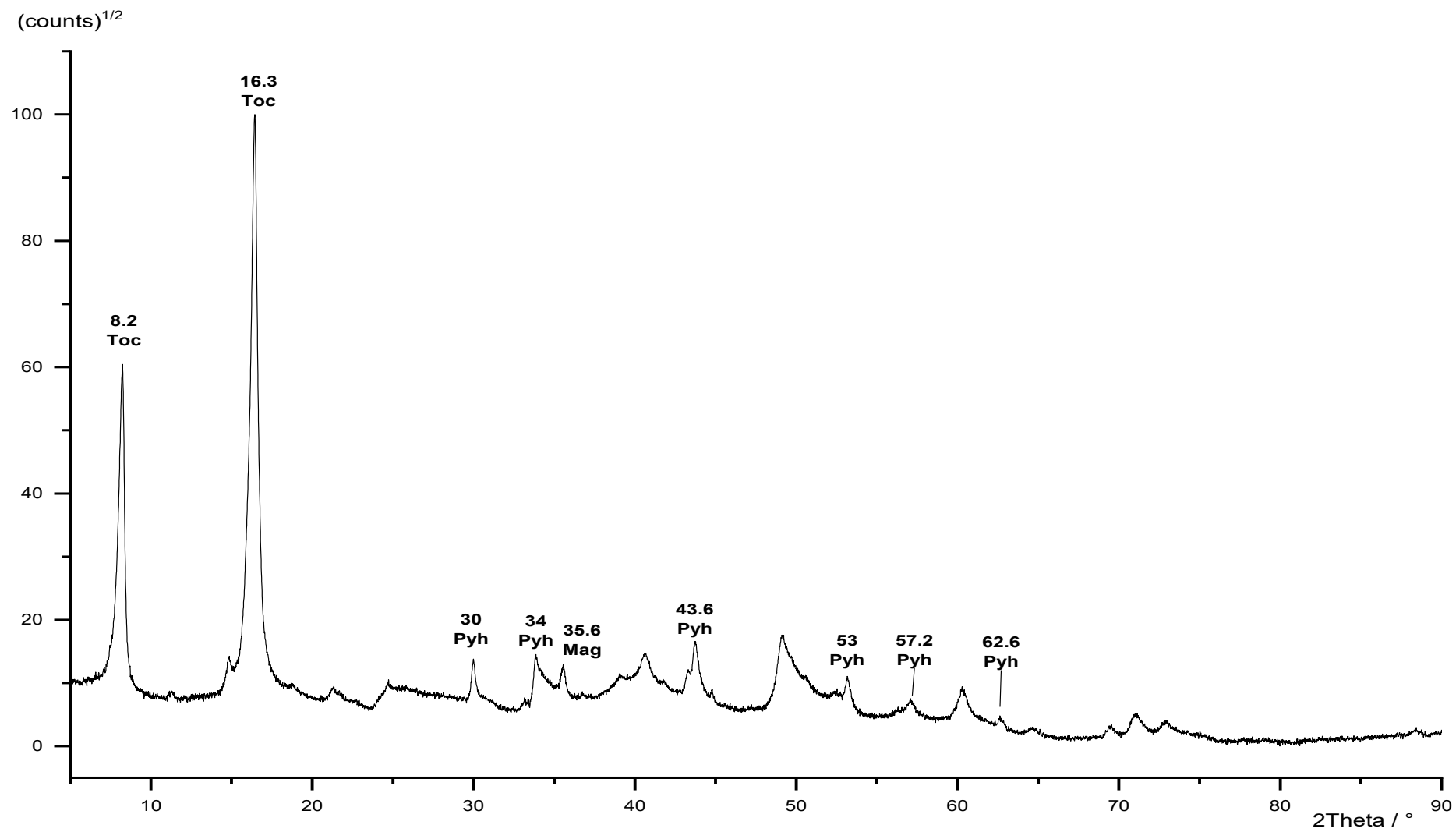


Figure 141: Powder diffraction pattern of TochMgAl<sub>22</sub>. Toc = tochilinite, Mag = magnetite, Pyh = pyrrhotite, Fe = iron.

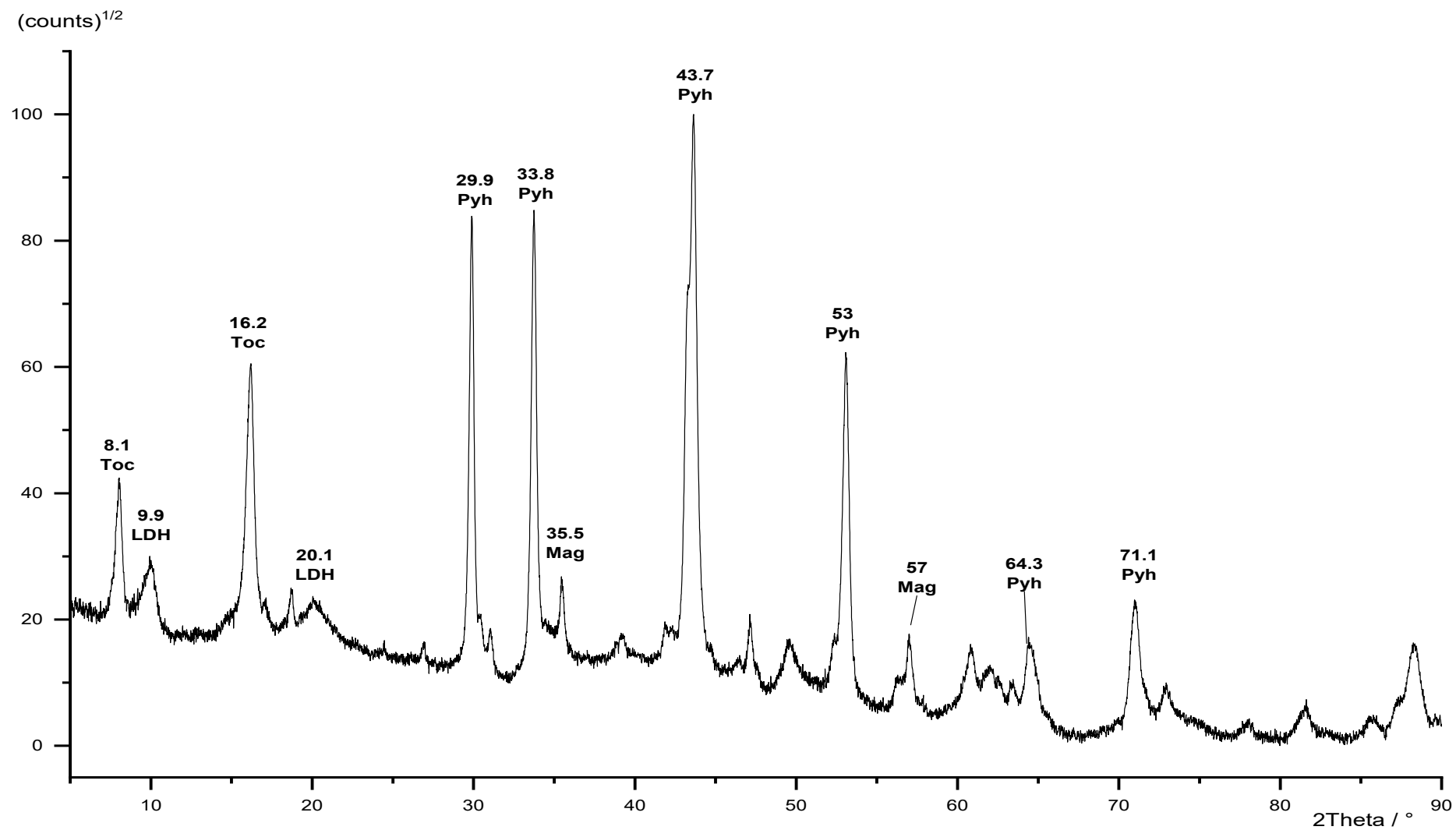


Figure 142: Powder diffraction pattern of TochMgAl<sub>23</sub>. Toc = tochilinite, Mag = magnetite, Bru = brucite. Pyh = pyrrhotite, Fe = iron, LDH = layered double hydroxide.

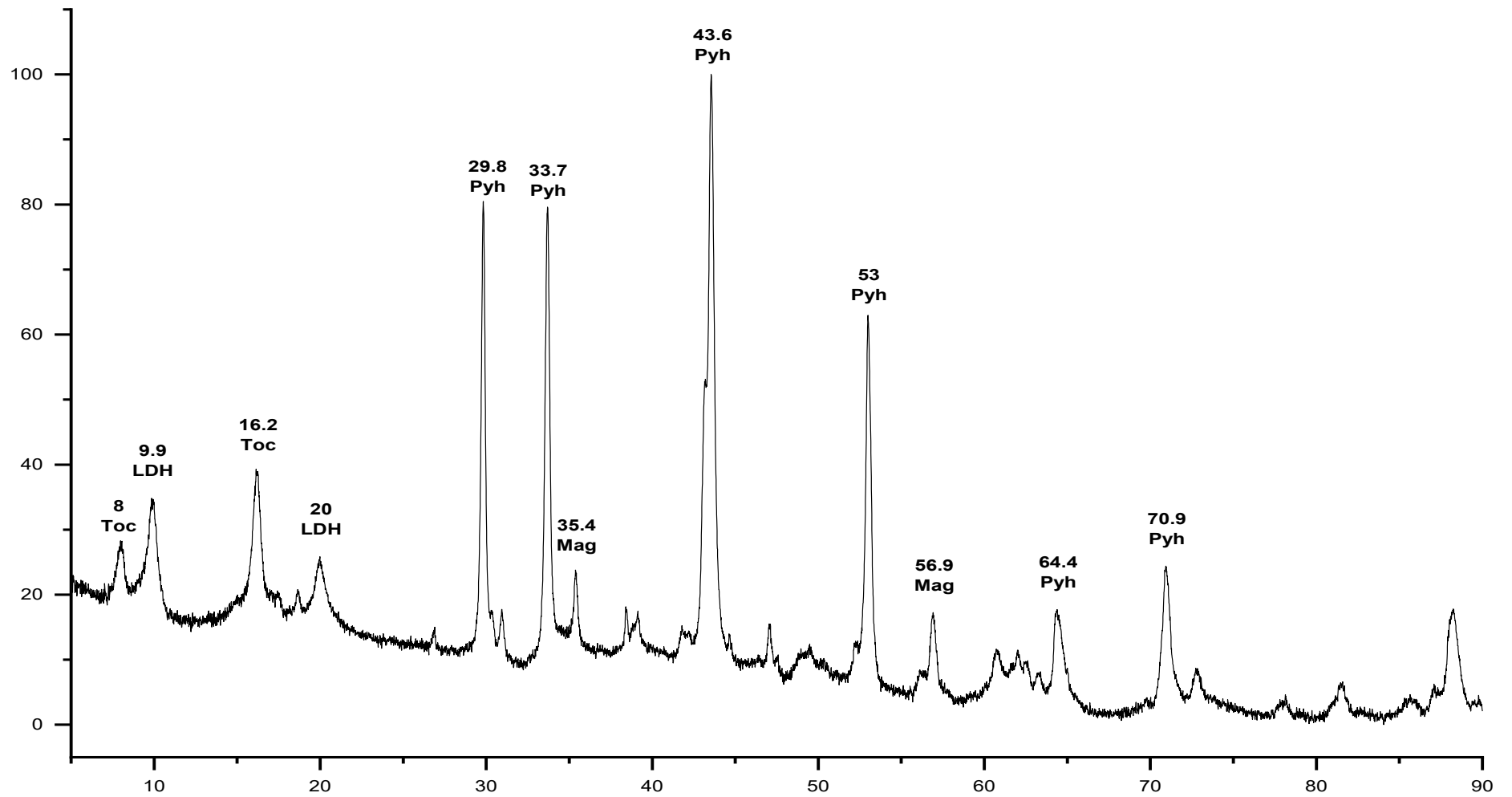


Figure 143: Powder diffraction pattern of TochMgAl<sub>24</sub>. Toc = tochilinite, Mag = magnetite, Bru = brucite. Pyh = pyrrhotite, Fe = iron, LDH = layered double hydroxide.



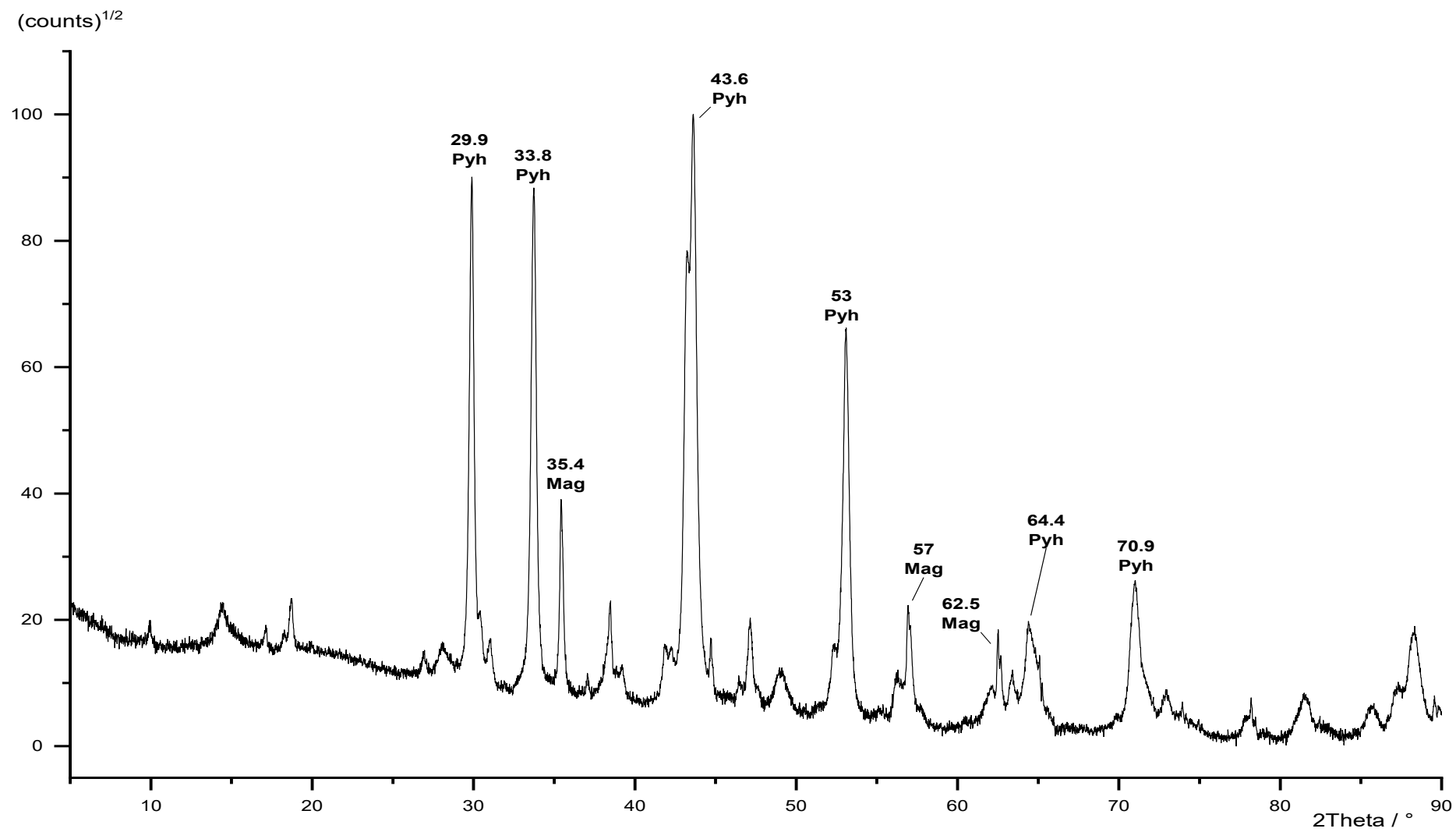


Figure 144: Powder diffraction pattern of TochMgAl\_25. Mag = magnetite.

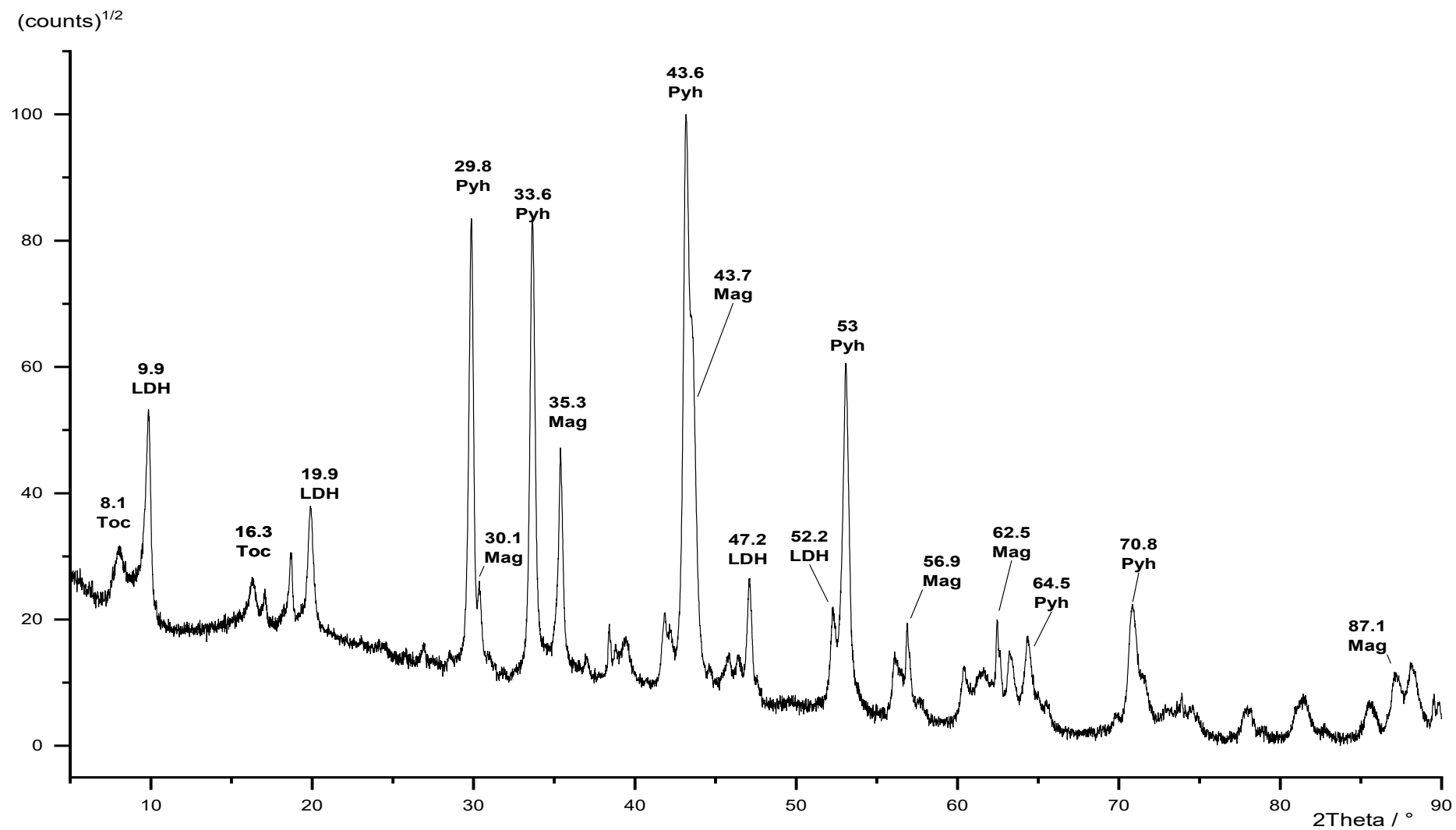


Figure 145: Powder diffraction pattern of TochMgAl<sub>26</sub>. Toc = tochilinite, Mag = magnetite, Bru = brucite. Pyh = pyrrhotite, Fe = iron, LDH = layered double hydroxide.

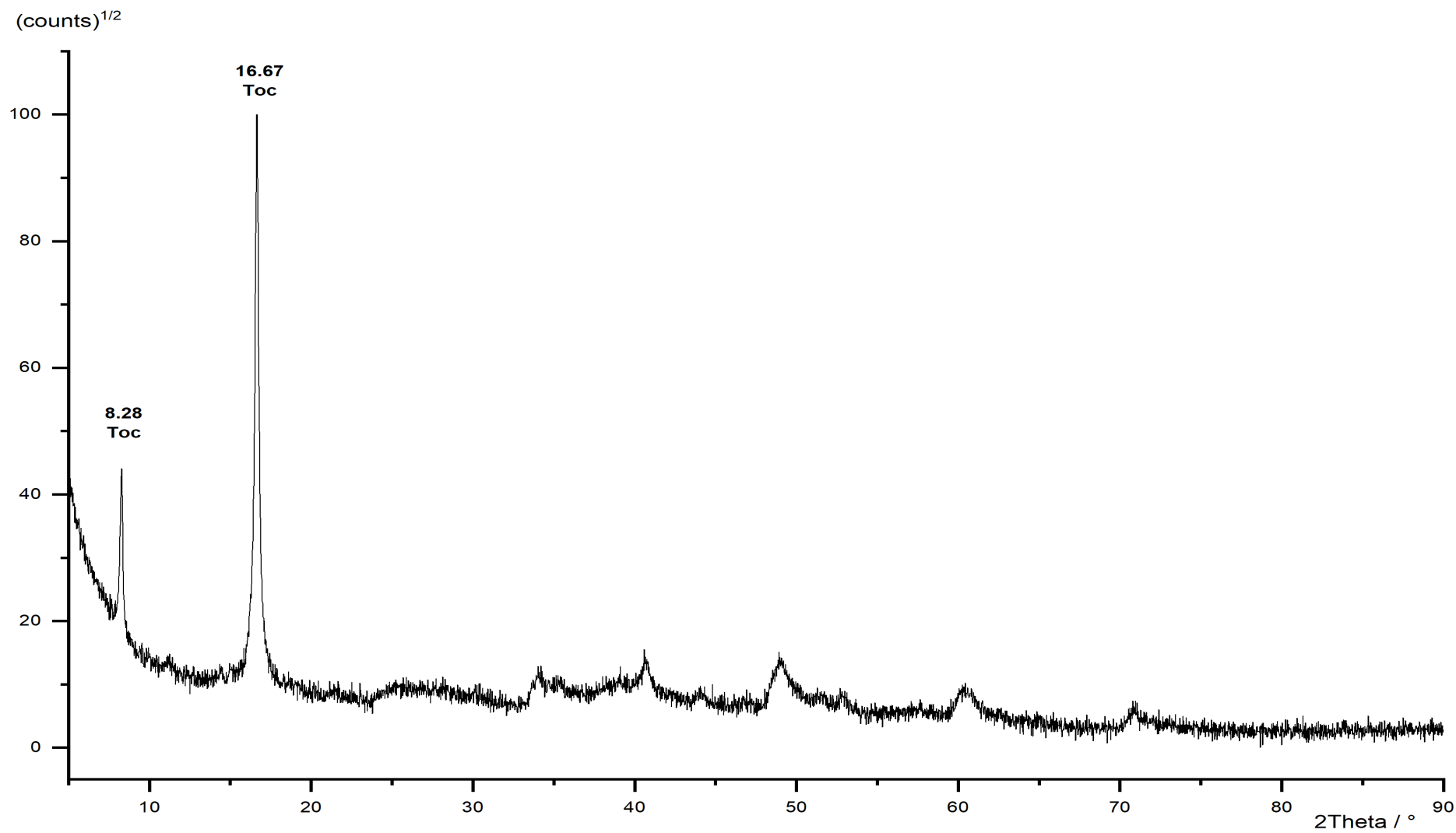


Figure 146: Powder diffraction pattern of TochMgAl<sub>27</sub>. Toc = tochilinite.

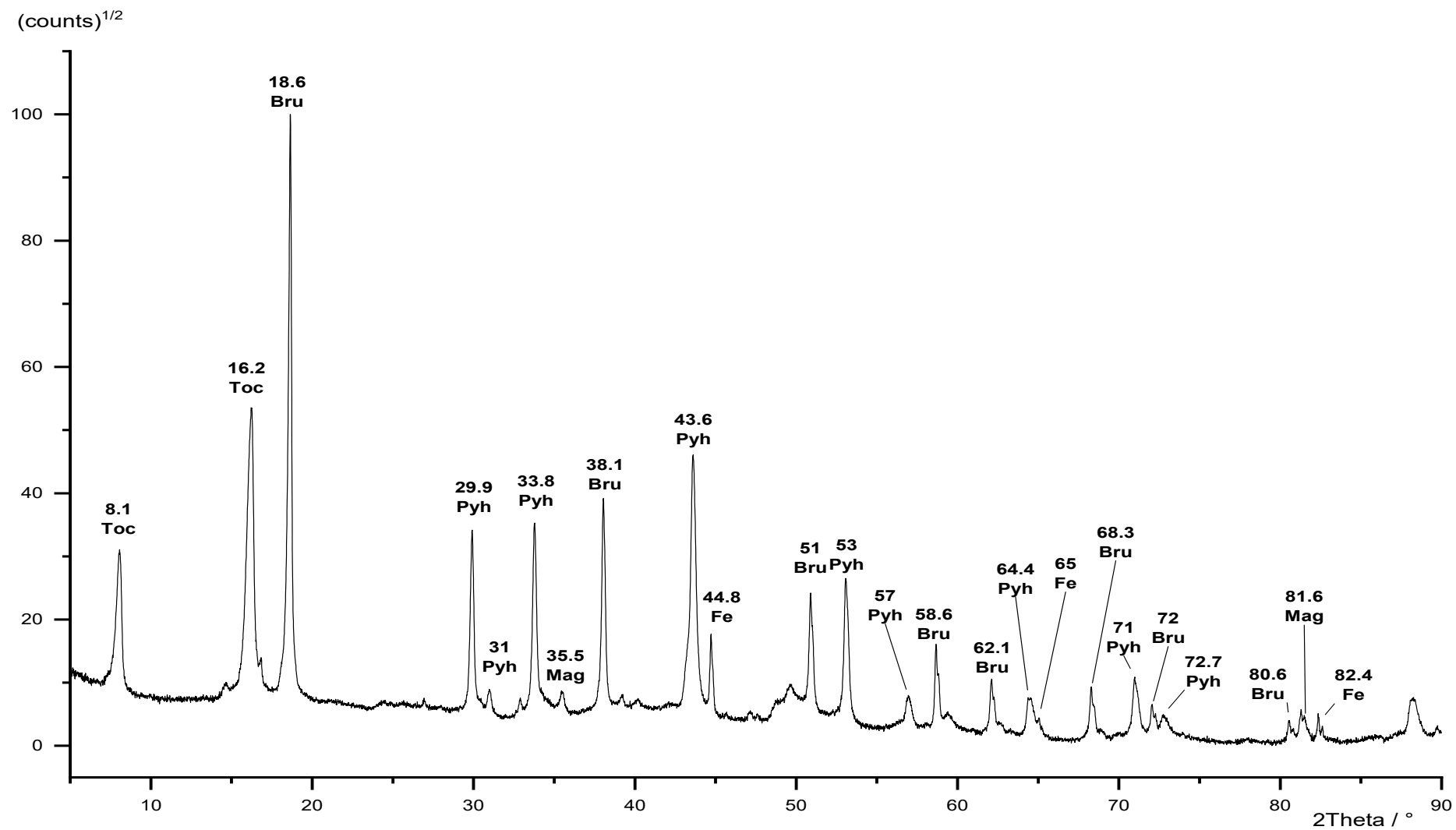


Figure 147: Powder diffraction pattern of TochMgFe\_1. Toc = tochilinite, pyh = pyrrhotite, mag = magnetite, bru = brucite, Fe = iron.

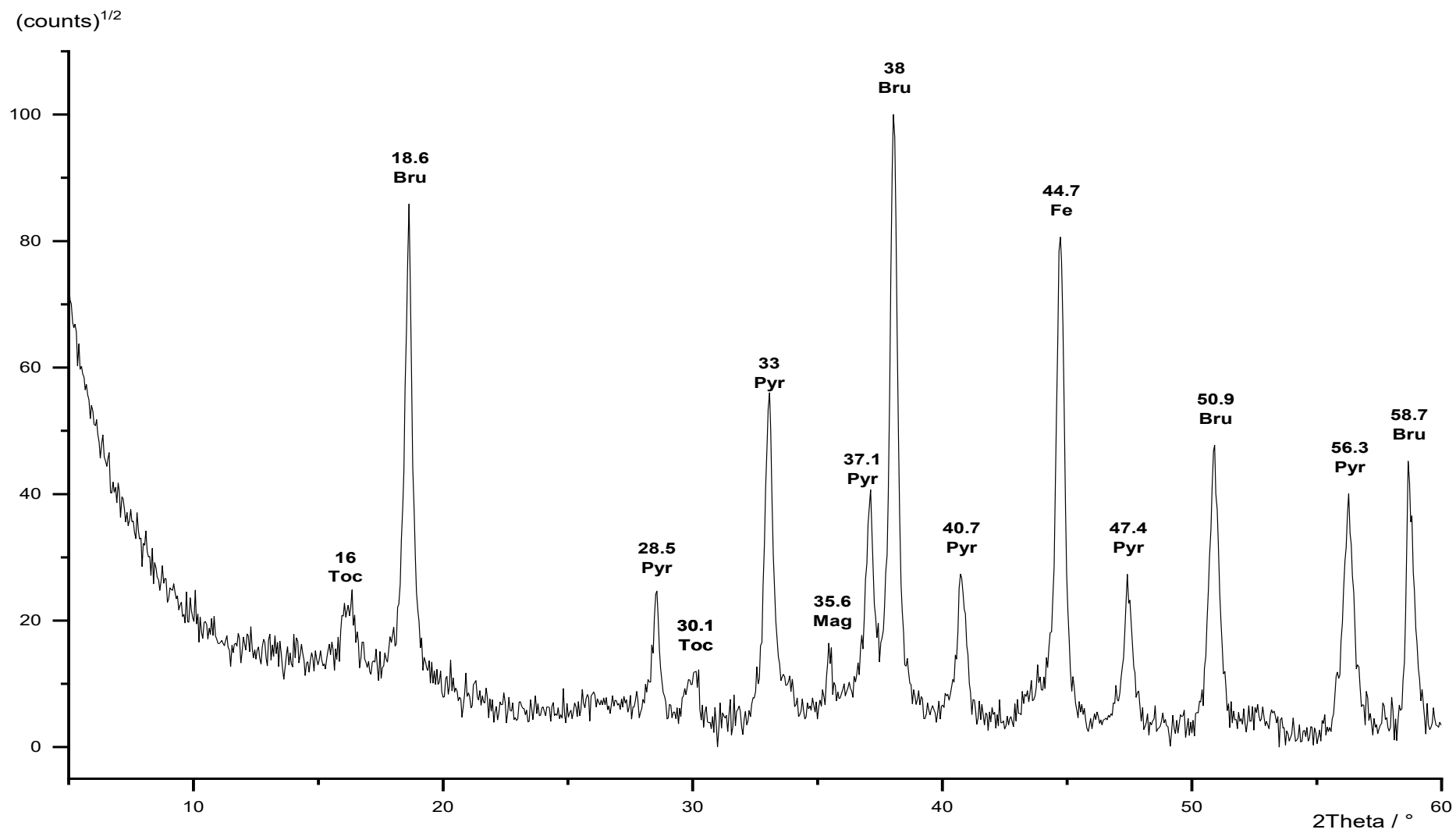


Figure 148: Powder diffraction pattern of TochMgFe\_2. Toc = tochilinite, pyh = pyrrhotite, mag = magnetite, bru = brucite, Fe = iron.

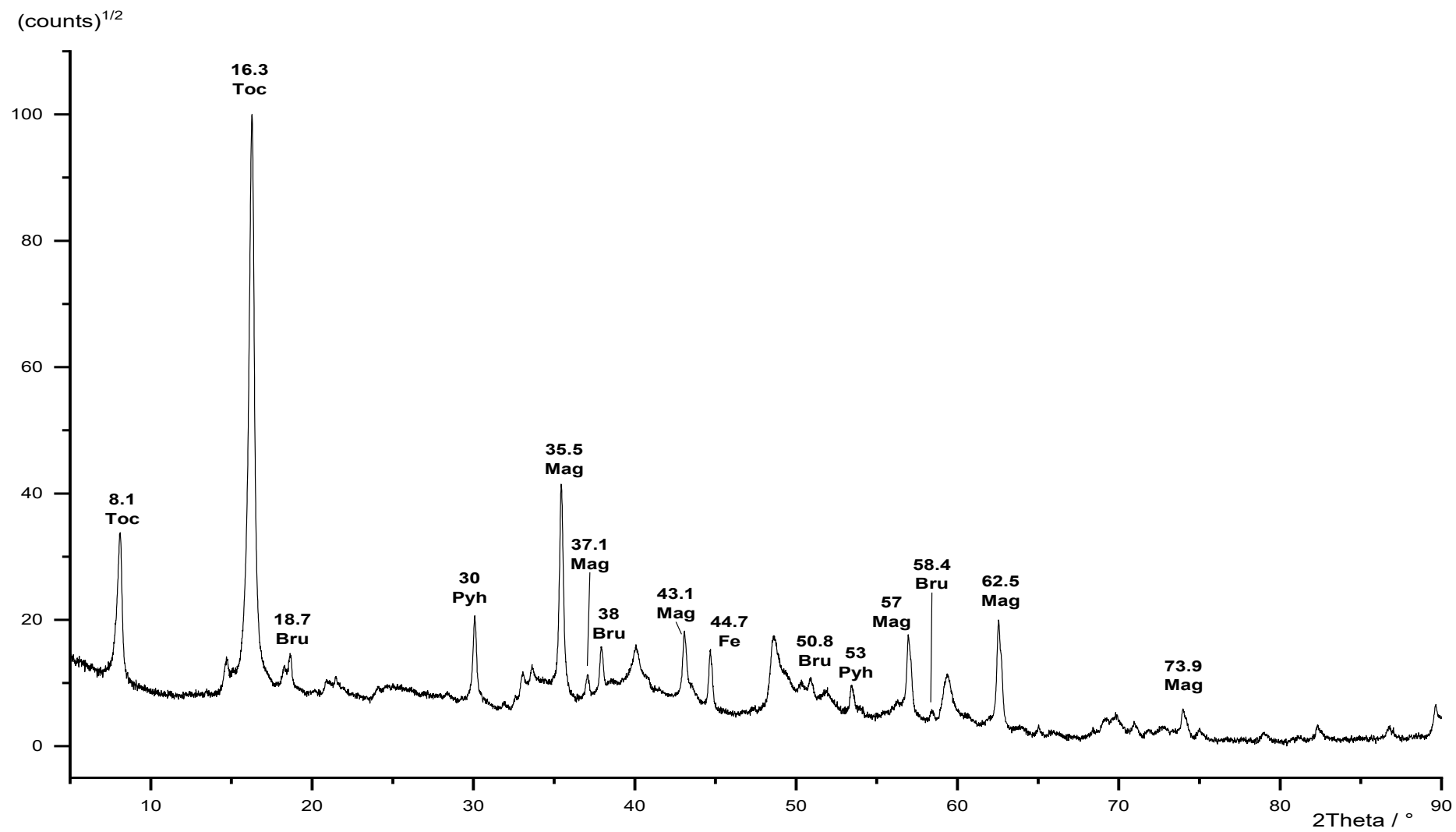


Figure 149: Powder diffraction pattern of TochMgFe\_3. Toc = tochilinite, pyh = pyrrhotite, mag = magnetite, bru = brucite, Fe = iron.

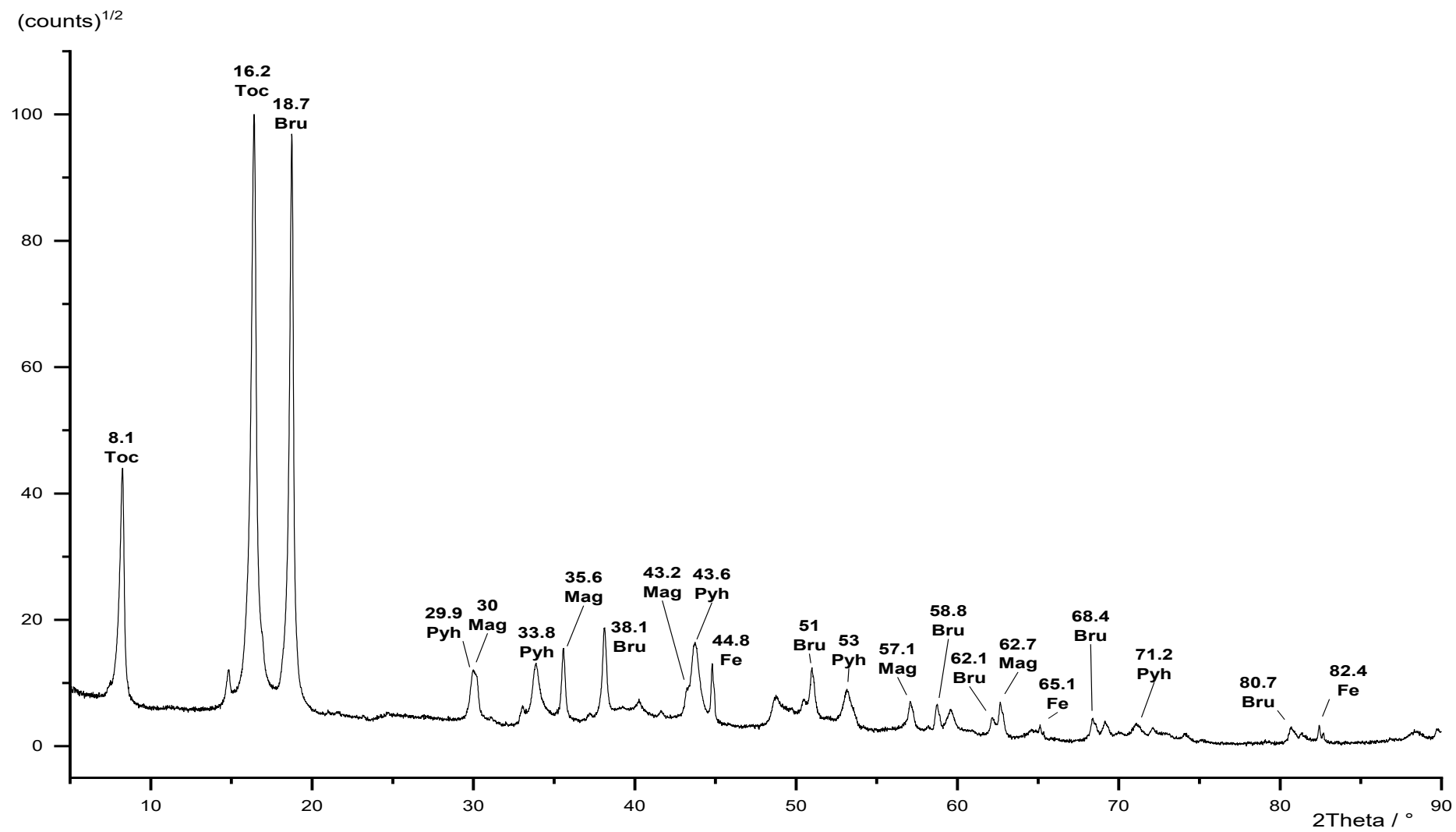


Figure 150: Powder diffraction pattern of TochMgFe\_4. Toc = tochilinite, pyh = pyrrhotite, mag = magnetite, bru = brucite, Fe = iron.

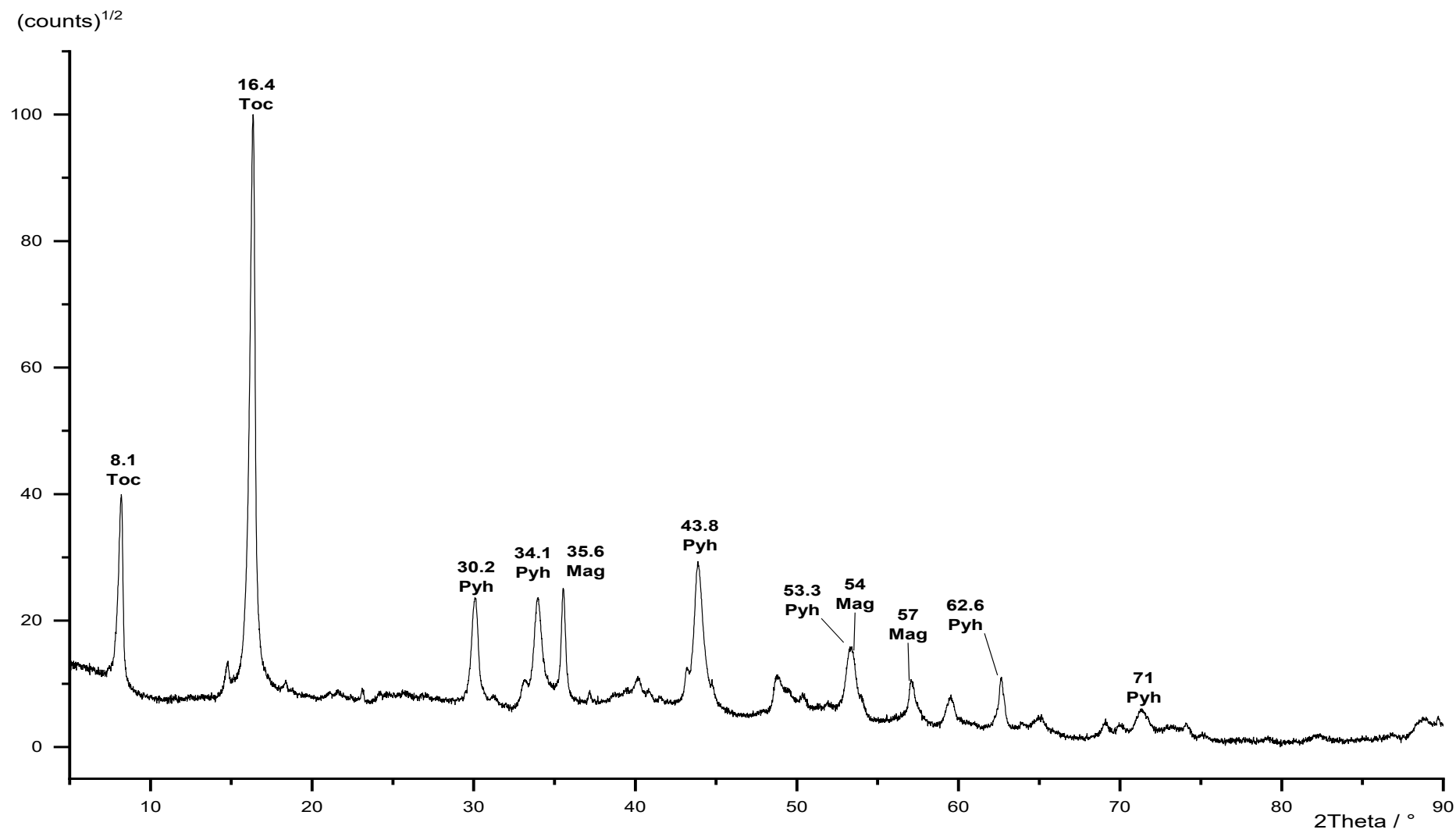


Figure 151: Powder diffraction pattern of TochMgFe\_5. Toc = tochilinite, pyh = pyrrhotite, mag = magnetite, bru = brucite.



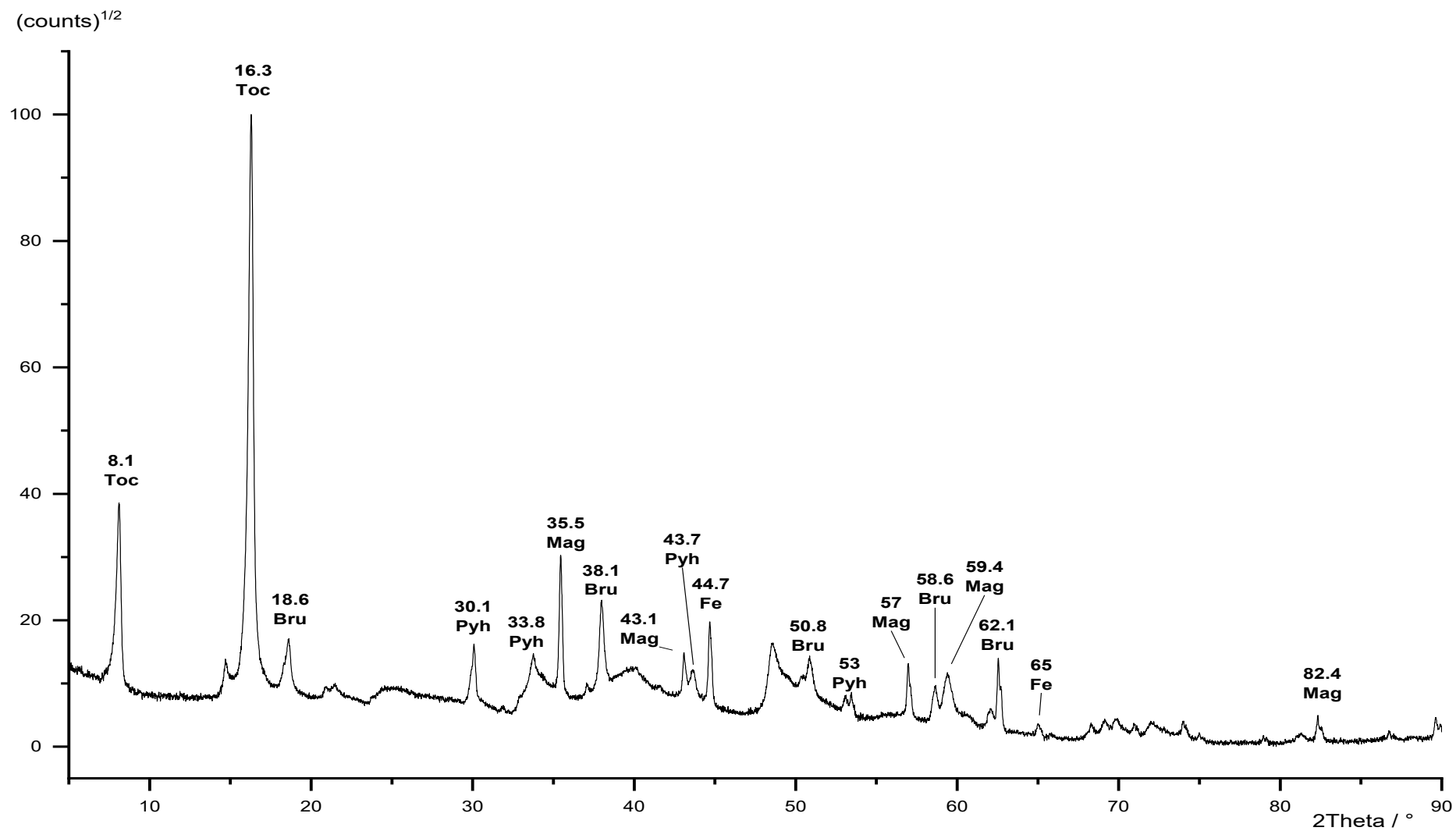


Figure 152: Powder diffraction pattern of TochMgFe\_6. Toc = tochilinite, pyh = pyrrhotite, mag = magnetite, bru = brucite, Fe = iron.

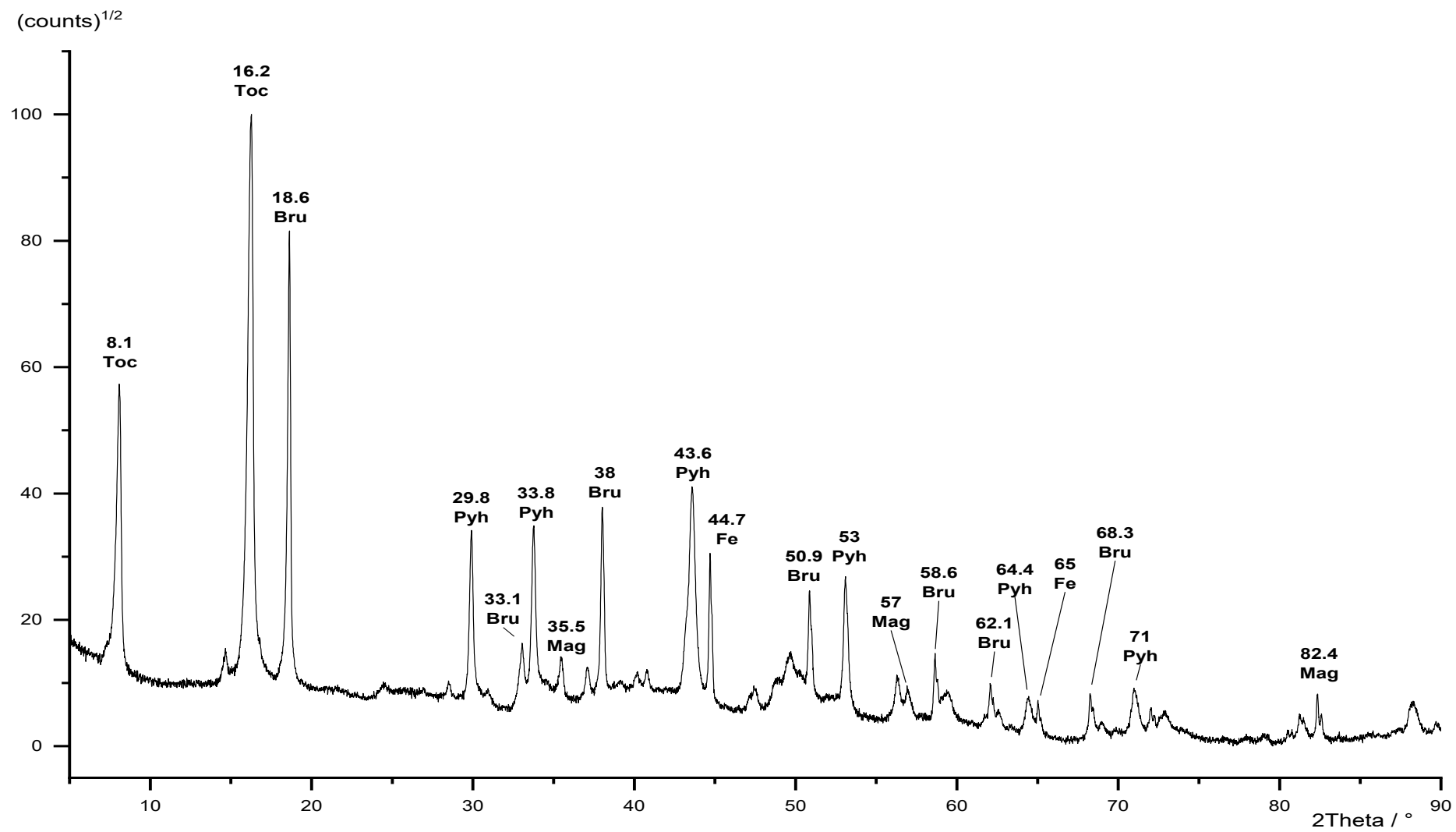


Figure 153: Powder diffraction pattern of TochMgFe\_7. Toc = tochilinite, pyh = pyrrhotite, mag = magnetite, bru = brucite, Fe = iron.

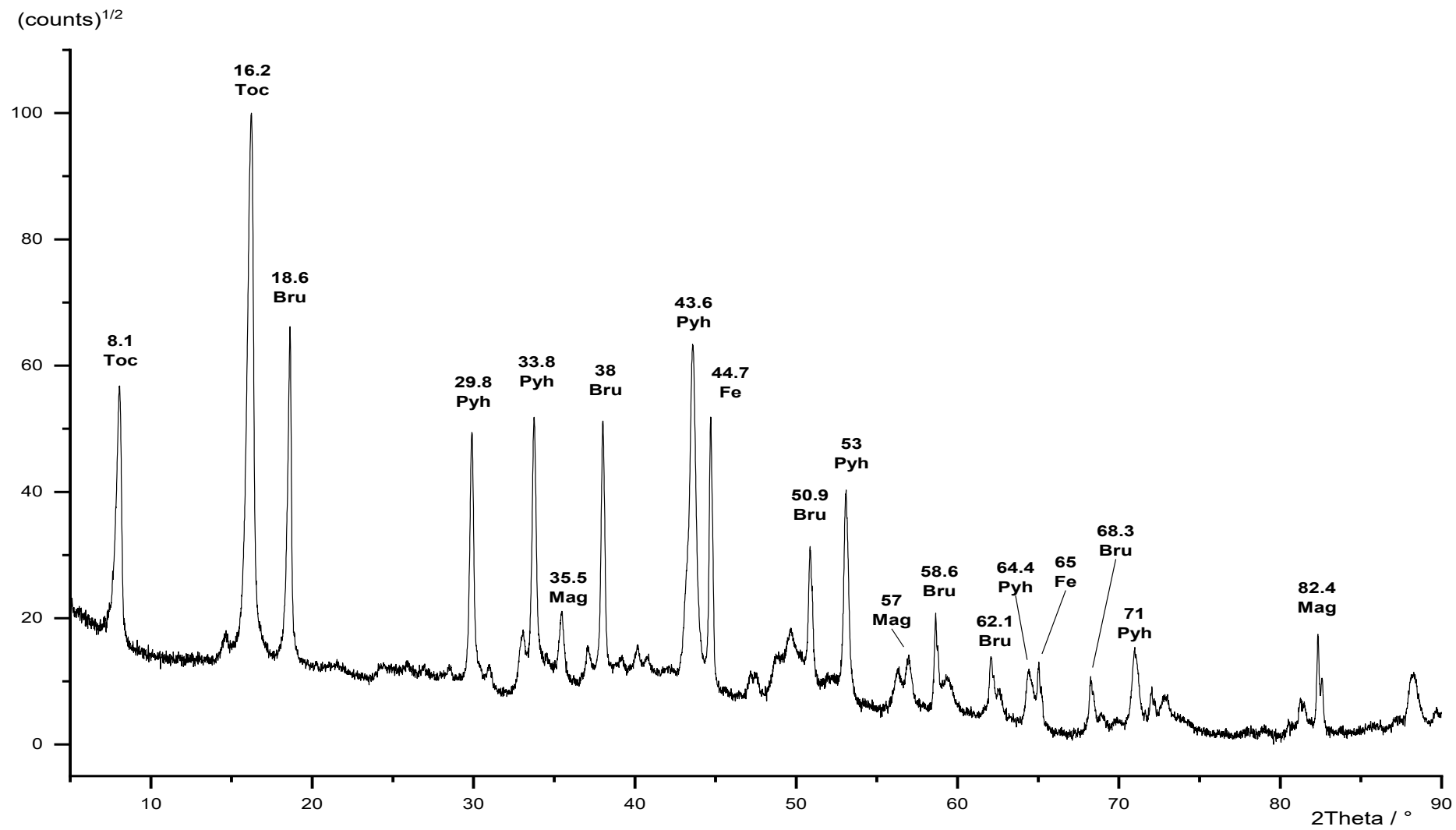


Figure 154: Powder diffraction pattern of TochMgFe<sub>8</sub>. Toc = tochilinite, pyh = pyrrhotite, mag = magnetite, bru = brucite, Fe = iron.

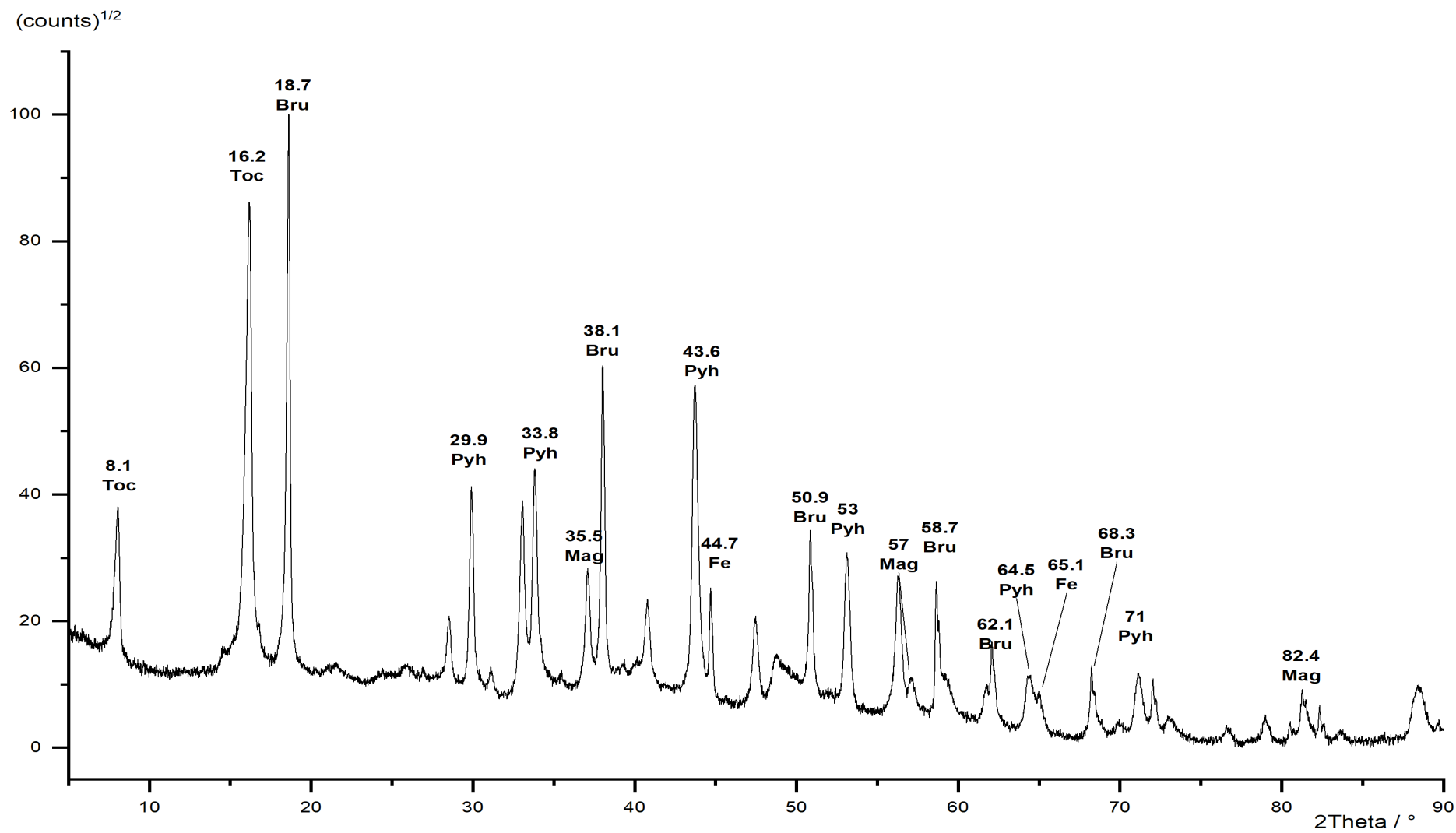


Figure 155: Powder diffraction pattern of TochMgFe\_9. Toc = toichilinite, pyh = pyrrhotite, mag = magnetite, bru = brucite, Fe = iron.

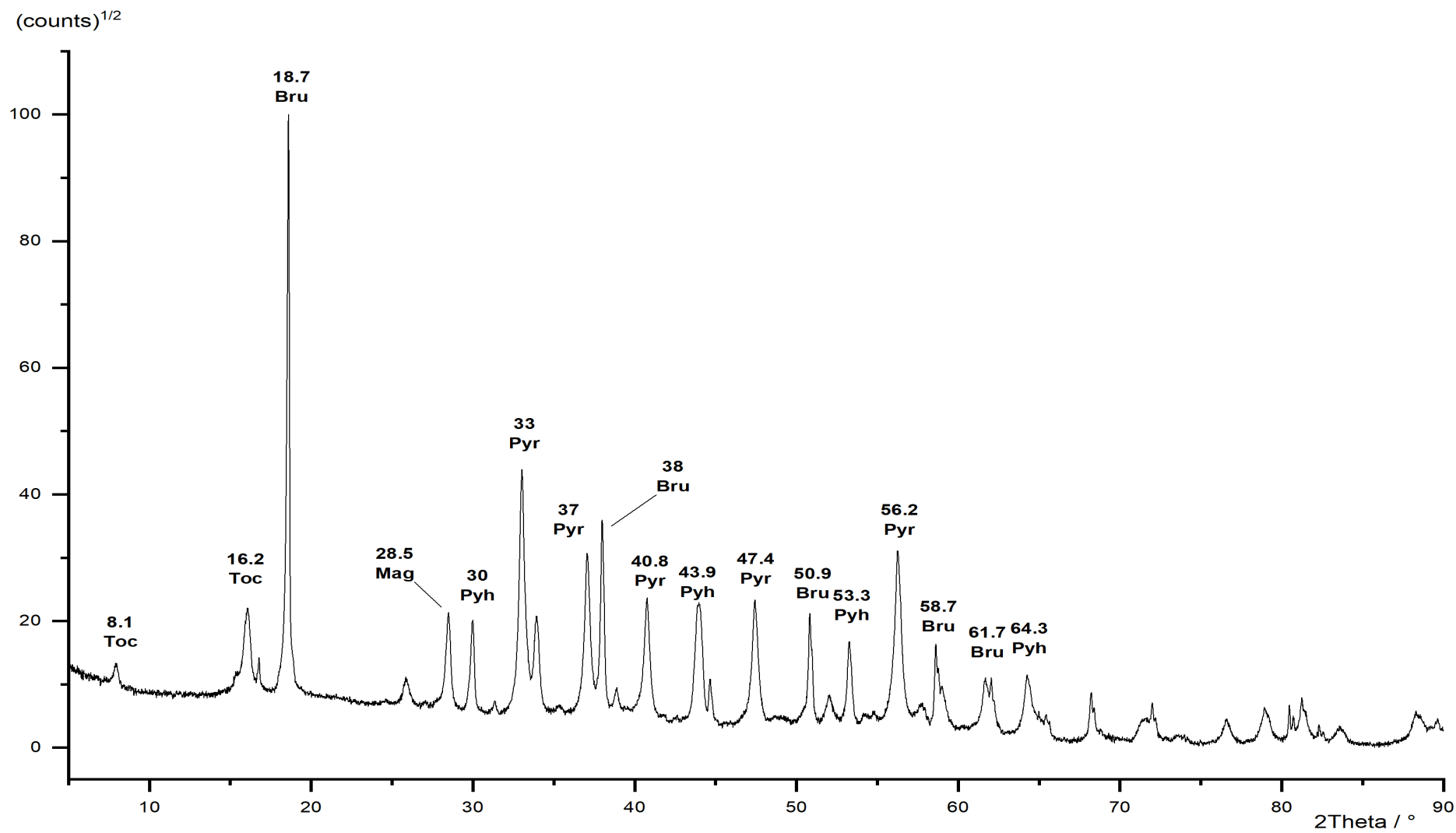


Figure 156: Powder diffraction pattern of TochMgFe\_10. Toc = tochilinite, pyh = pyrrhotite, mag = magnetite, bru = brucite, Pry = pyrite.

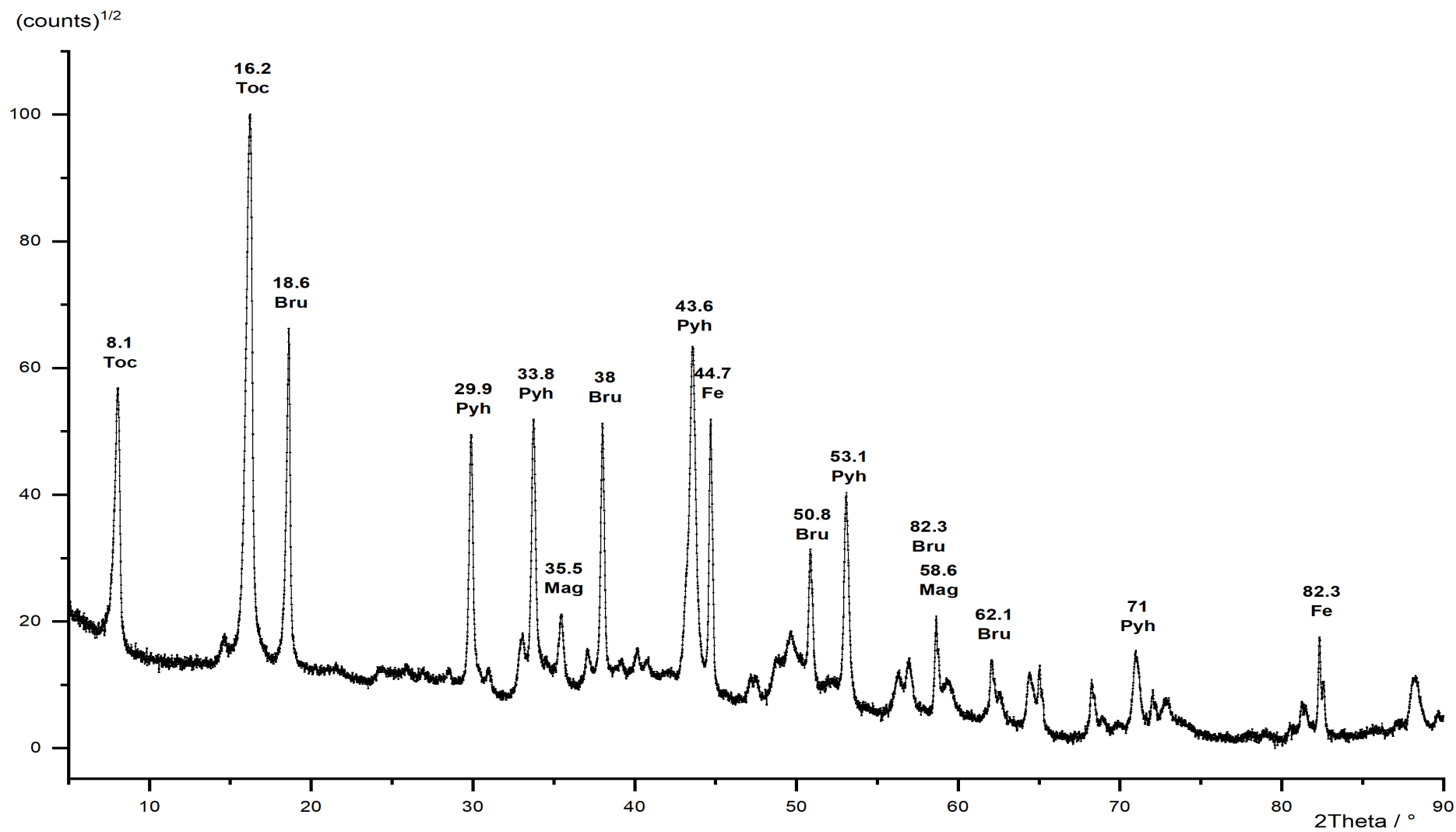


Figure 157: Powder diffraction pattern of TochMgFe\_11. Toc = tochilinite, pyh = pyrrhotite, mag = magnetite, bru = brucite, Fe = iron.

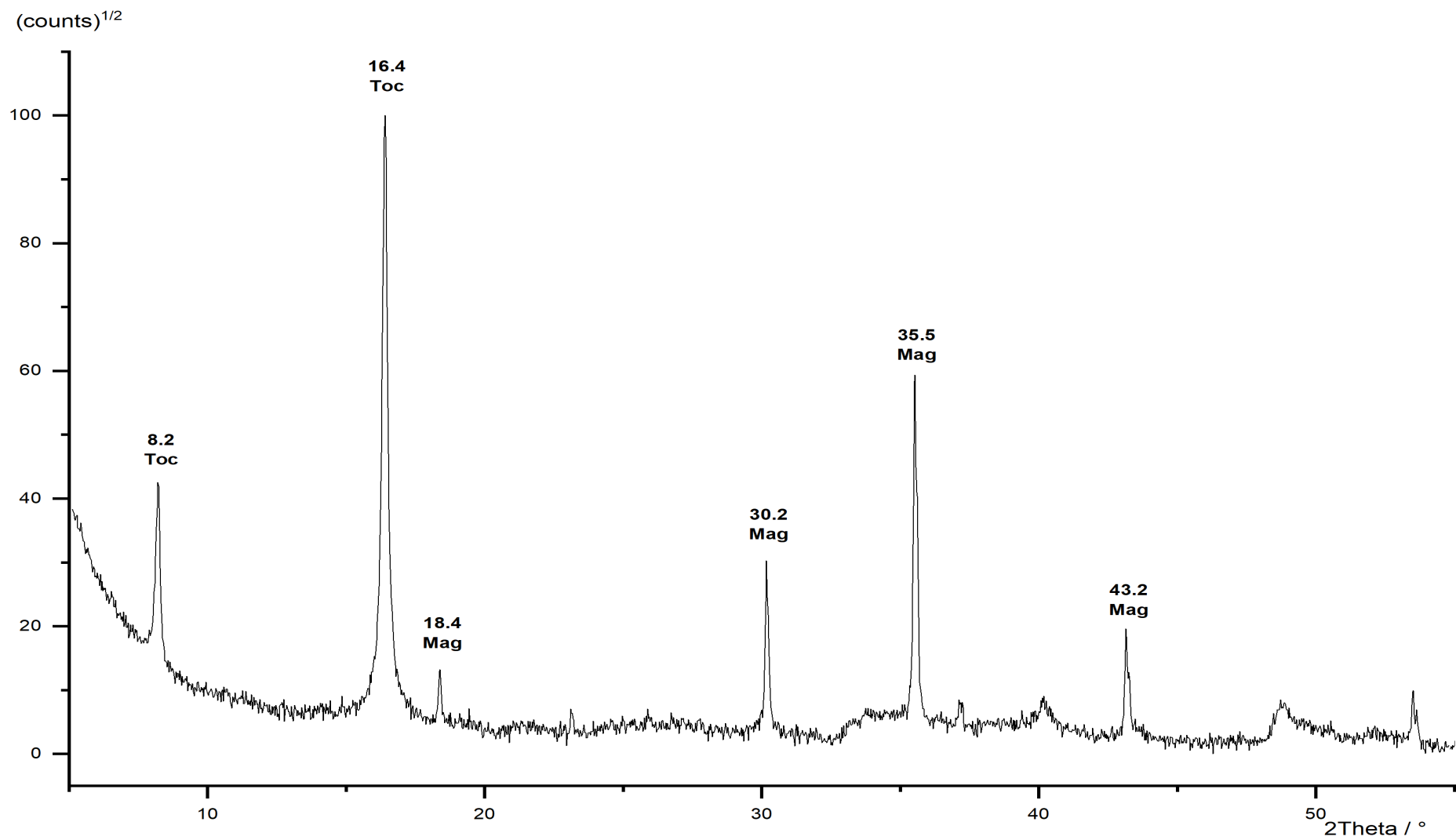


Figure 158: Powder diffraction pattern of TochMgFe\_12. Toc = tochilinite, mag = magnetite.

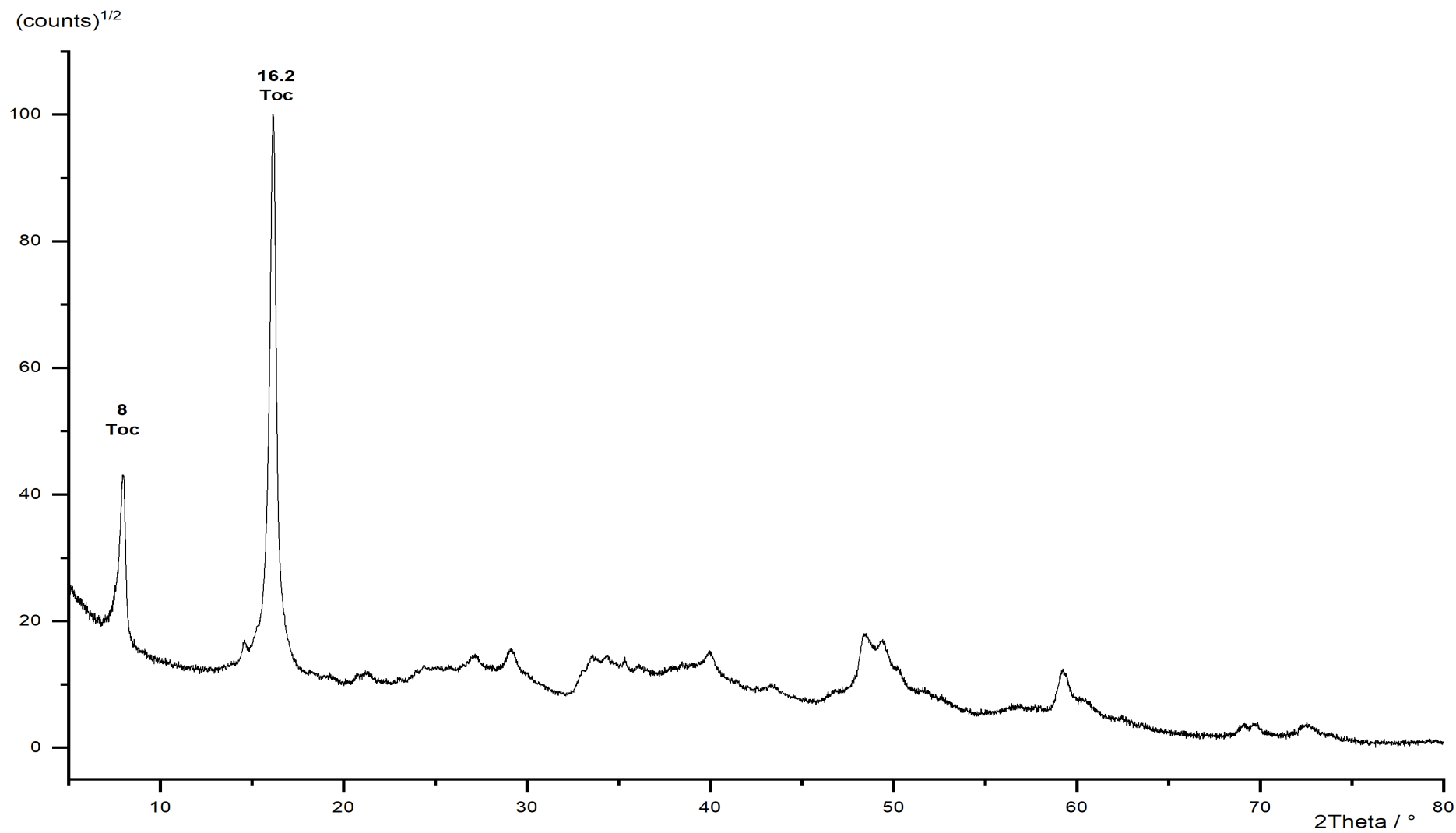


Figure 159: Powder diffraction pattern of TochMgFe<sub>13</sub>. Toc = tochilinite.



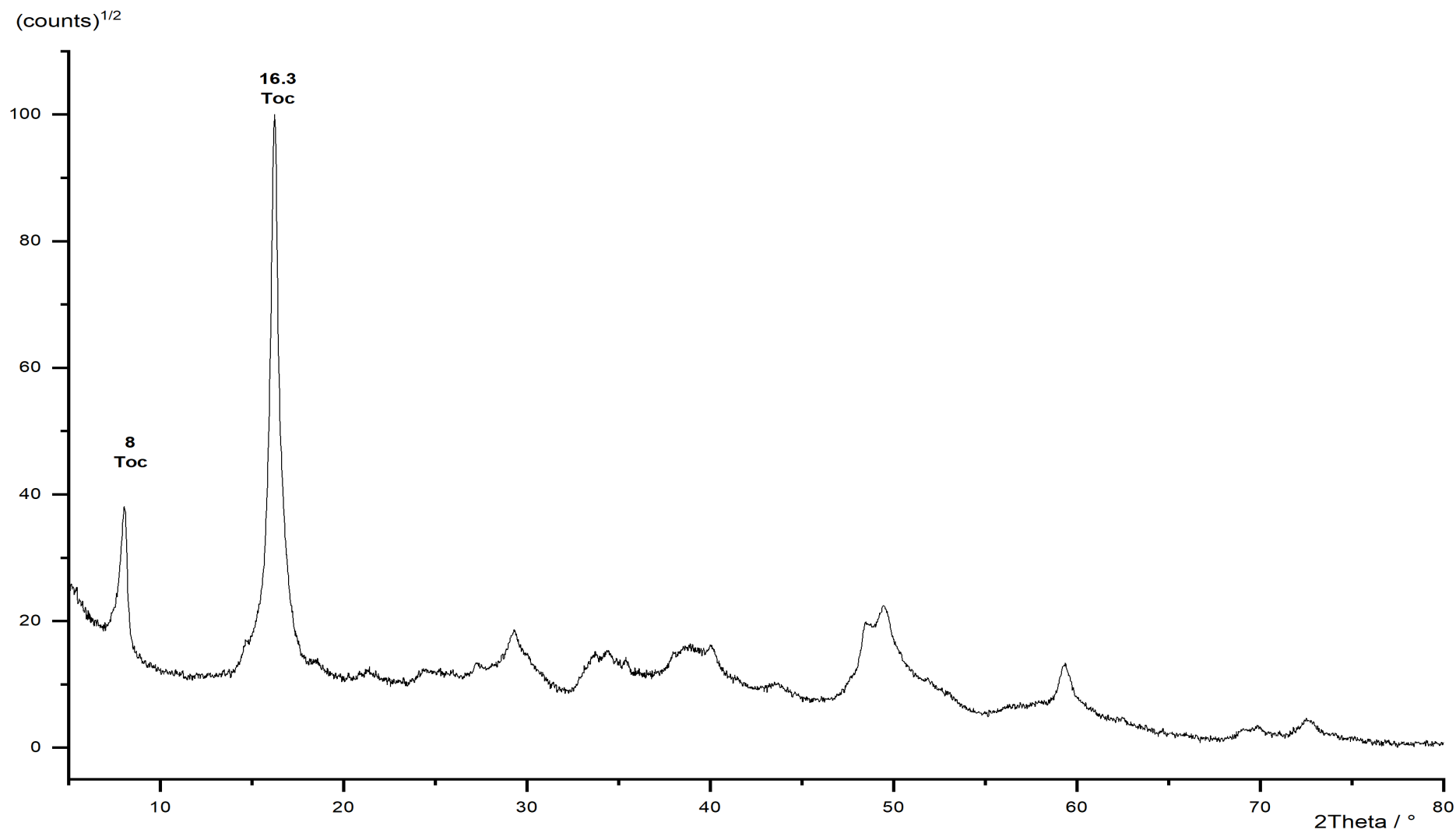


Figure 160: Powder diffraction pattern of TochMgFe<sub>14</sub>. Toc = tochilinite.

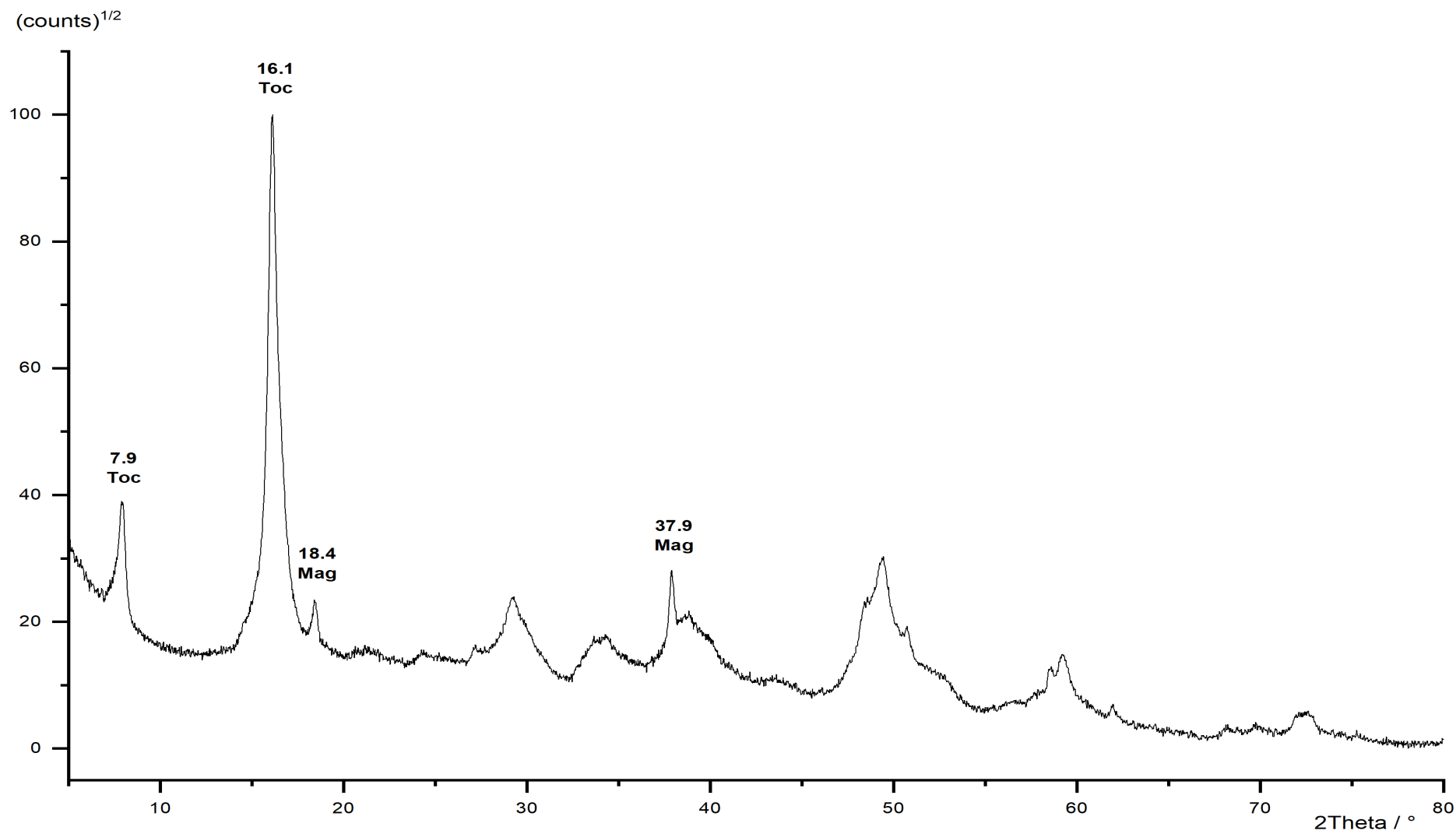


Figure 161: Powder diffraction pattern of TochMgFe<sub>15</sub>. Toc = tochilinite, mag = magnetite.

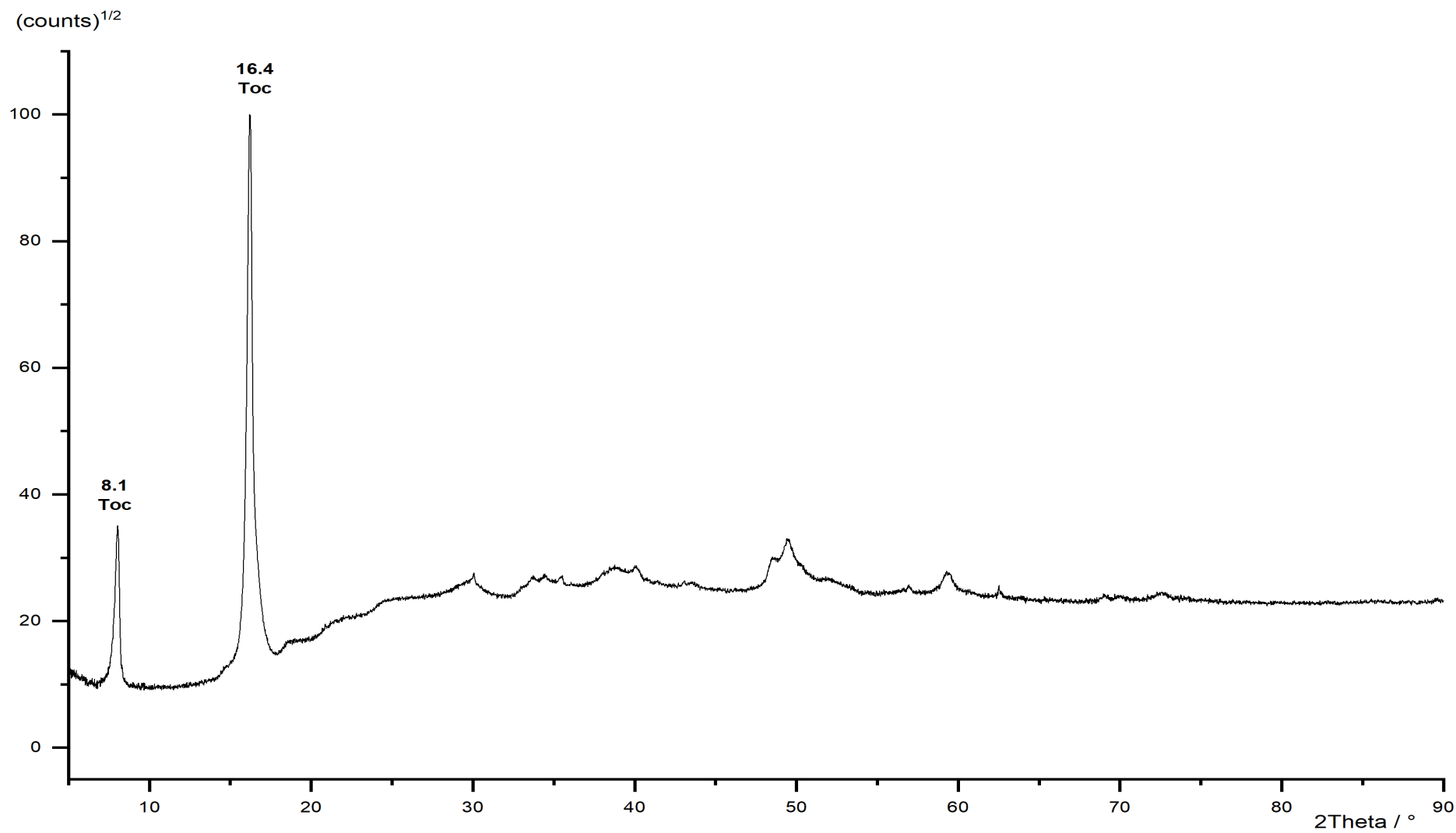


Figure 162: Powder diffraction pattern of TochMgFe<sub>16</sub>. Toc = tochilinite.

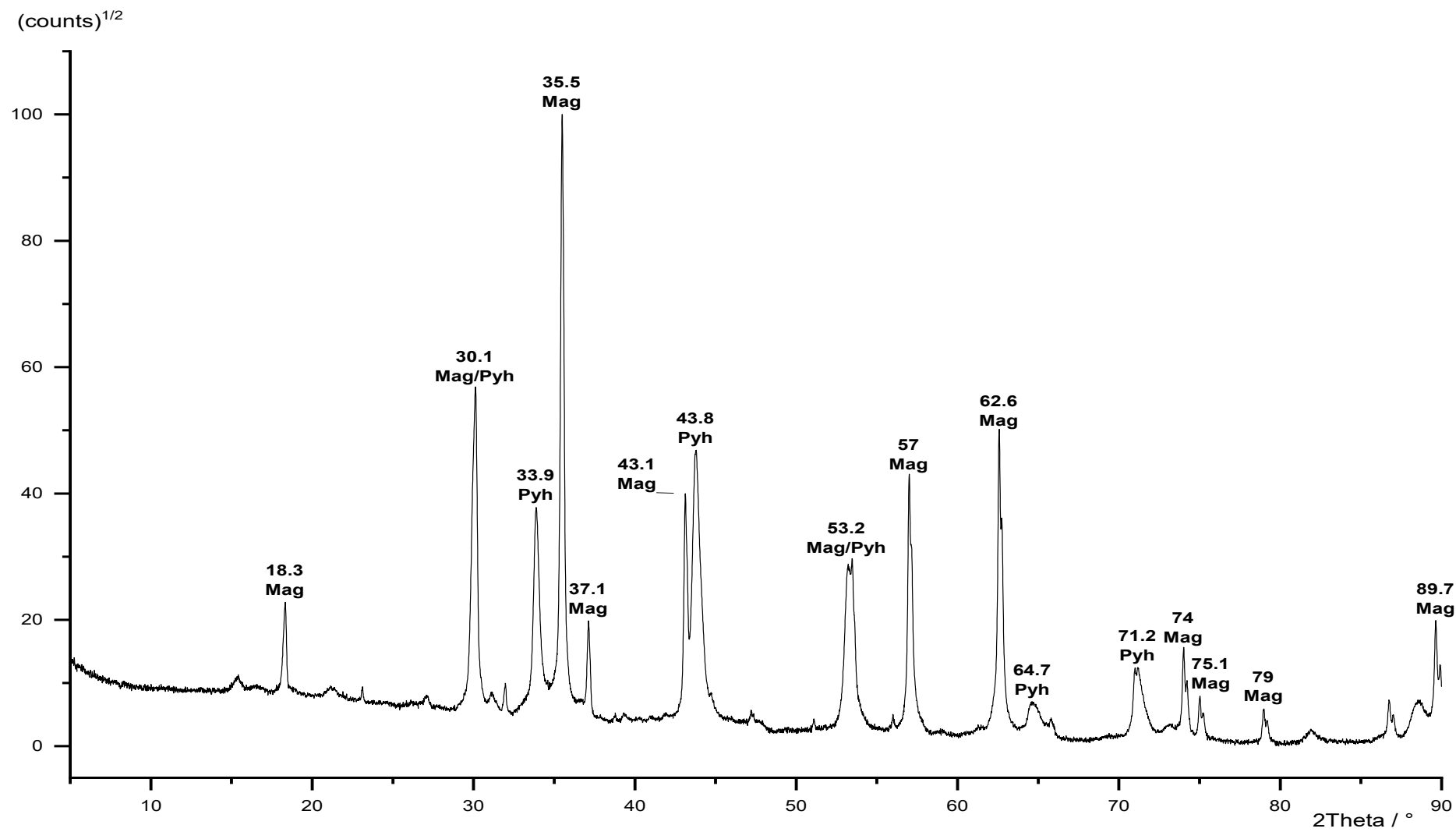


Figure 163: Powder diffraction pattern of TochFeFe\_1. Mag = magnetite, Pyh = pyrrhotite.

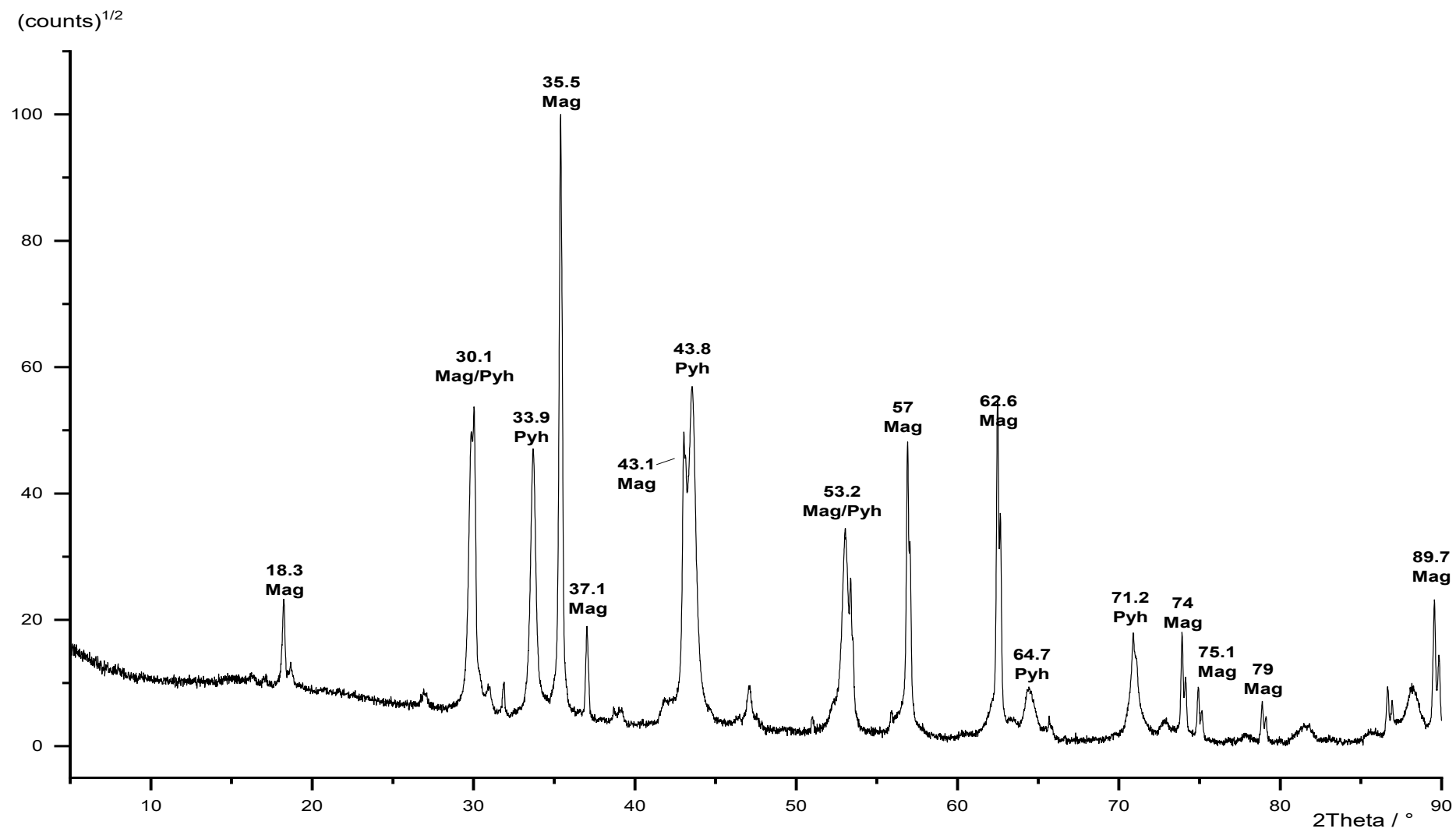


Figure 164: Powder diffraction pattern of TochFeFe\_2. Mag = magnetite, Pyh = pyrrhotite.

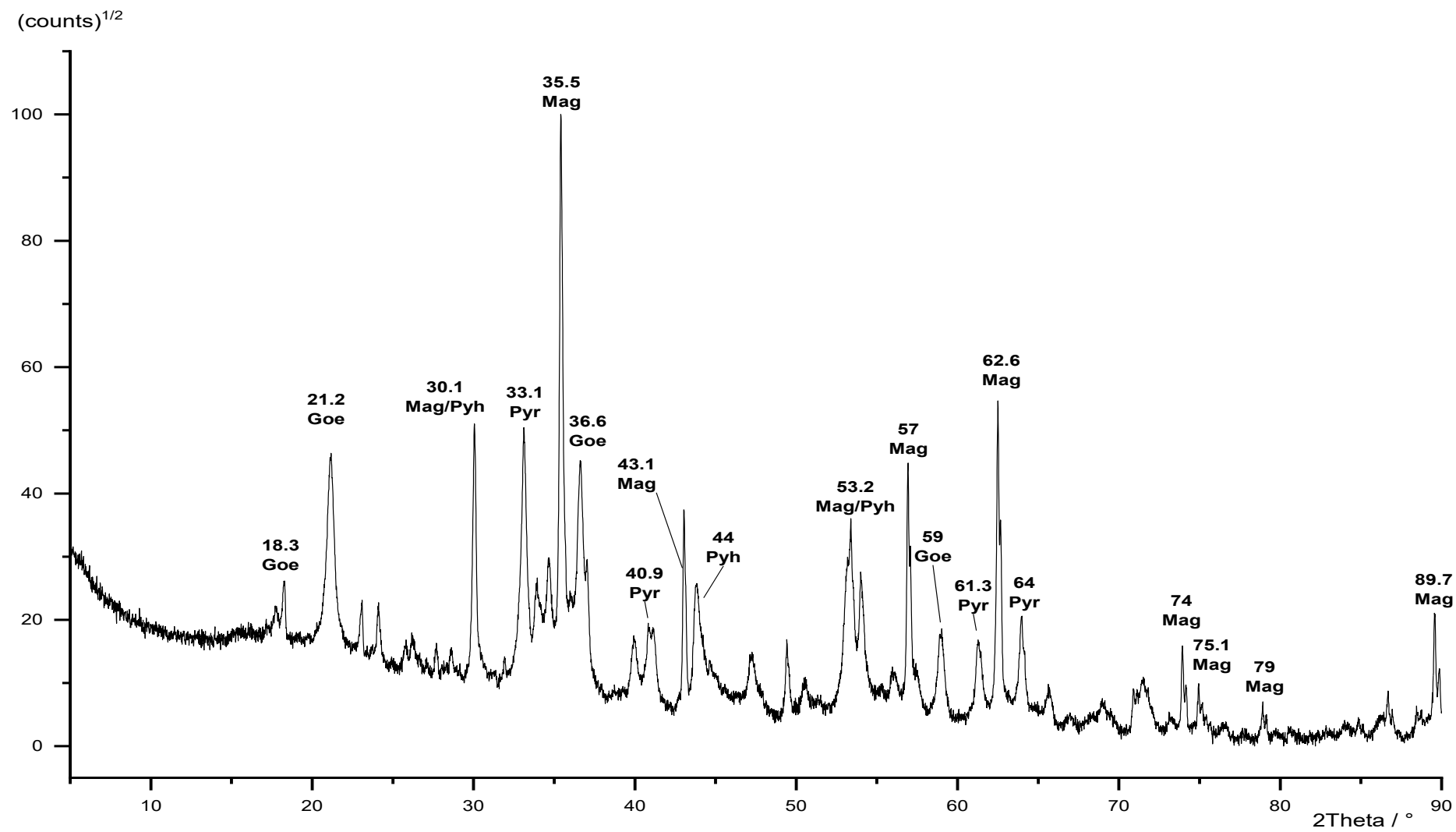


Figure 165: Powder diffraction pattern of TochFeFe\_3. Goe = goethite, Mag = magnetite, Pyh = pyhrrrotite.

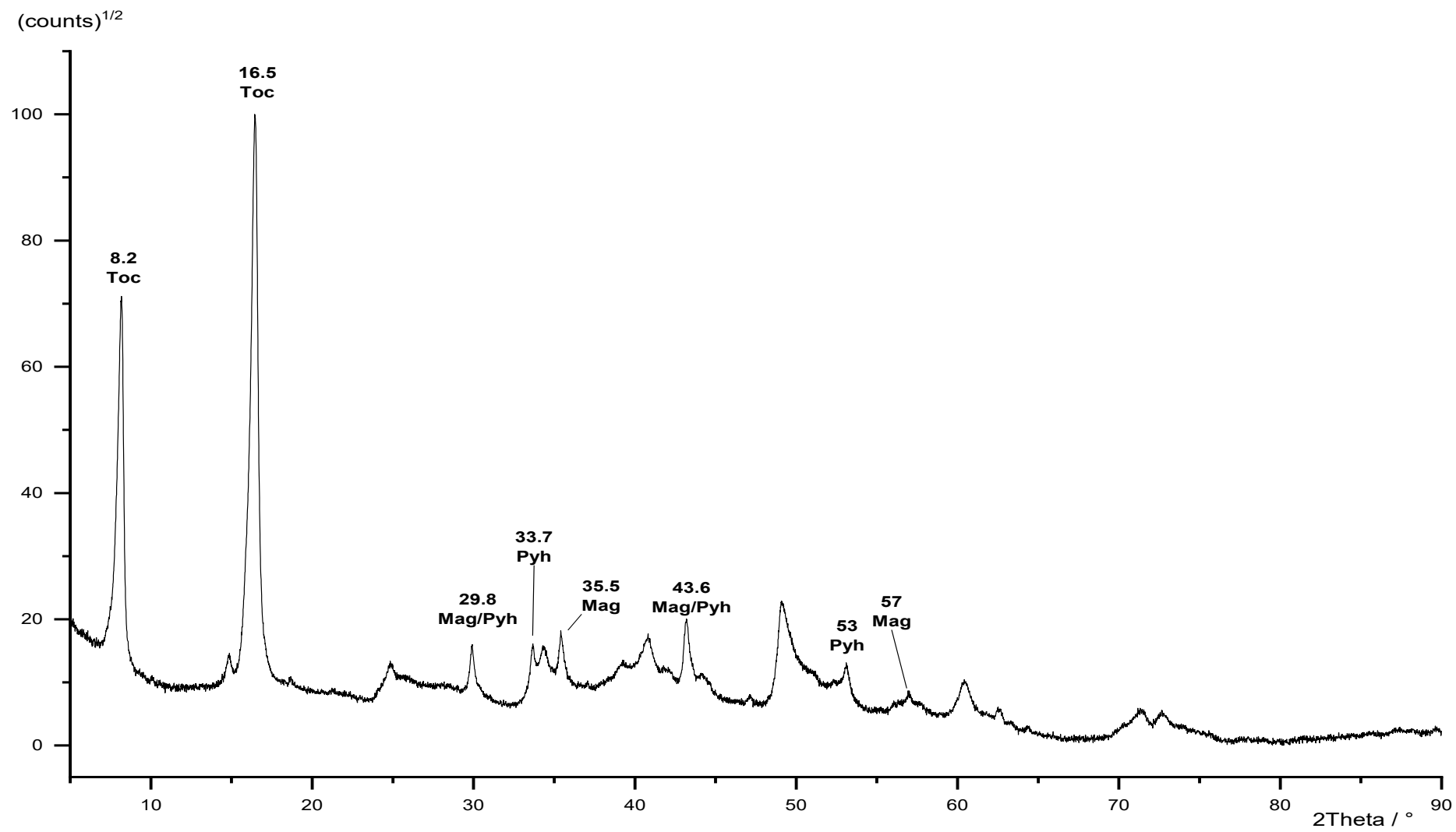


Figure 166: Powder diffraction pattern of TochFeFe\_4. Toc = tochilinite, Mag = magnetite, Pyh = pyhrrrotite.

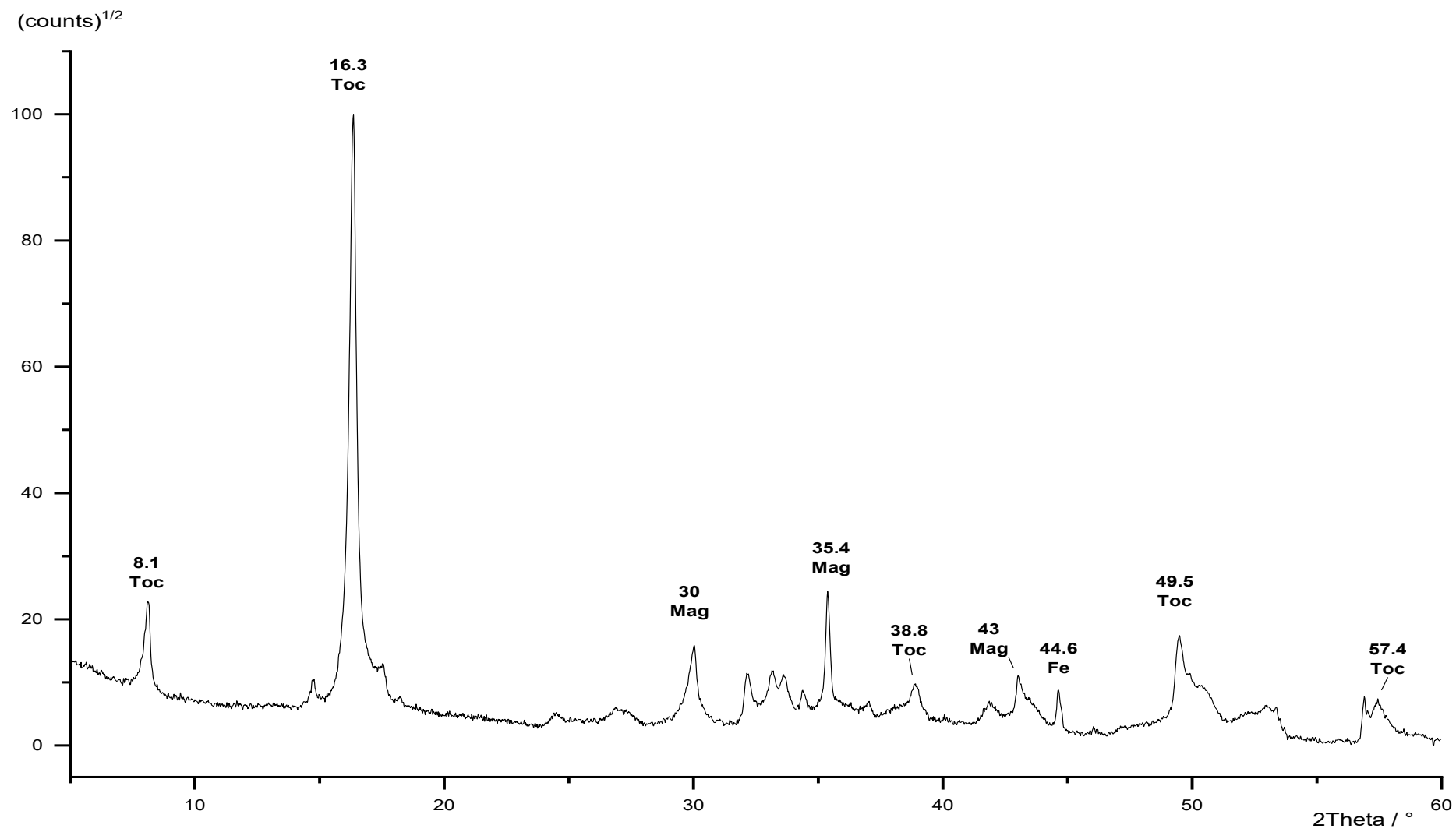


Figure 167: Powder diffraction pattern of TochFeFe\_5. Toc = tochilinite, Mag = magnetite, Pyh = pyhrrrotite.



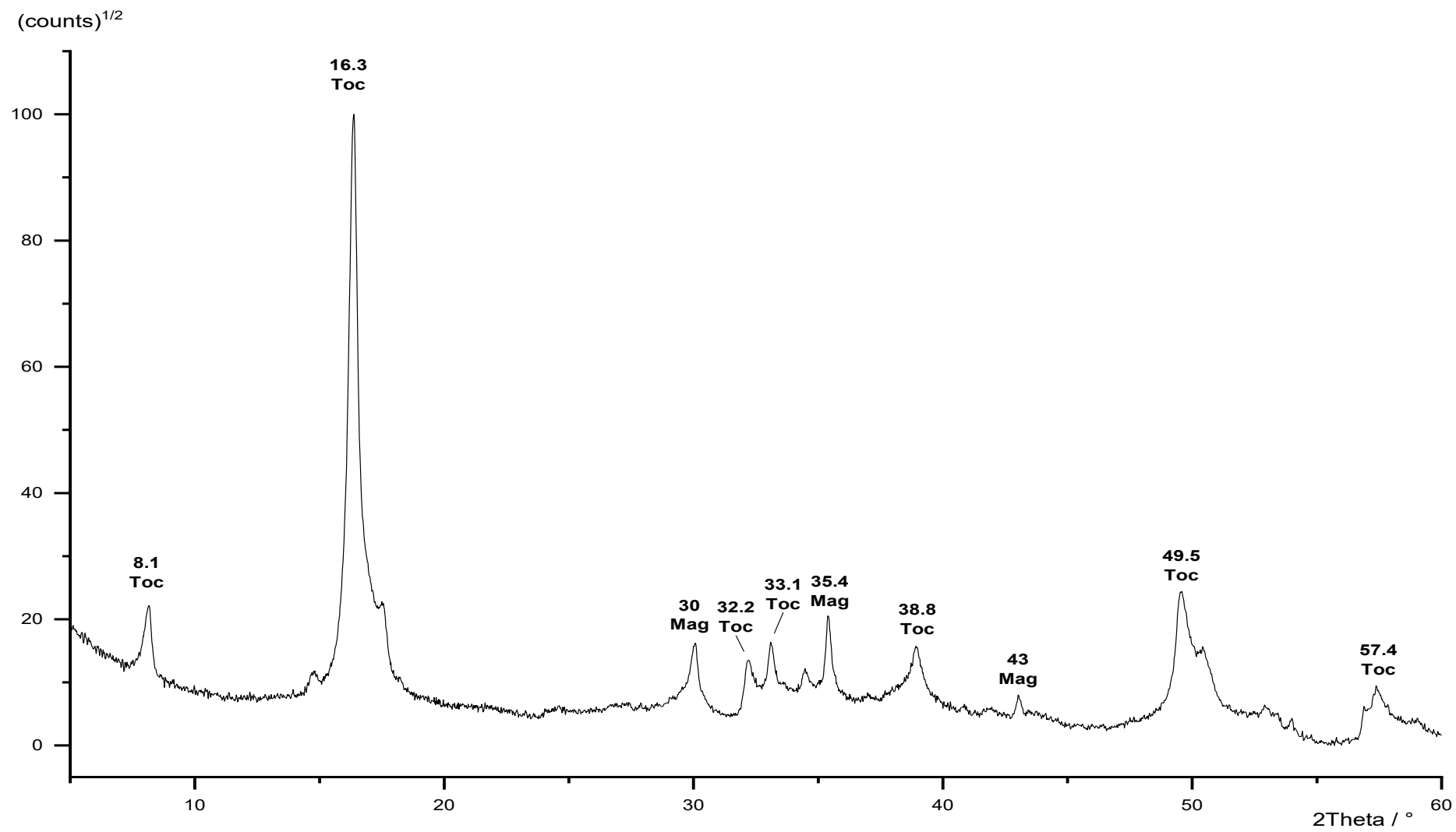


Figure 168: Powder diffraction pattern of TochFeFe<sub>6</sub>. Toc = tochilinite, Mag = magnetite, Pyh = pyhrrrotite.

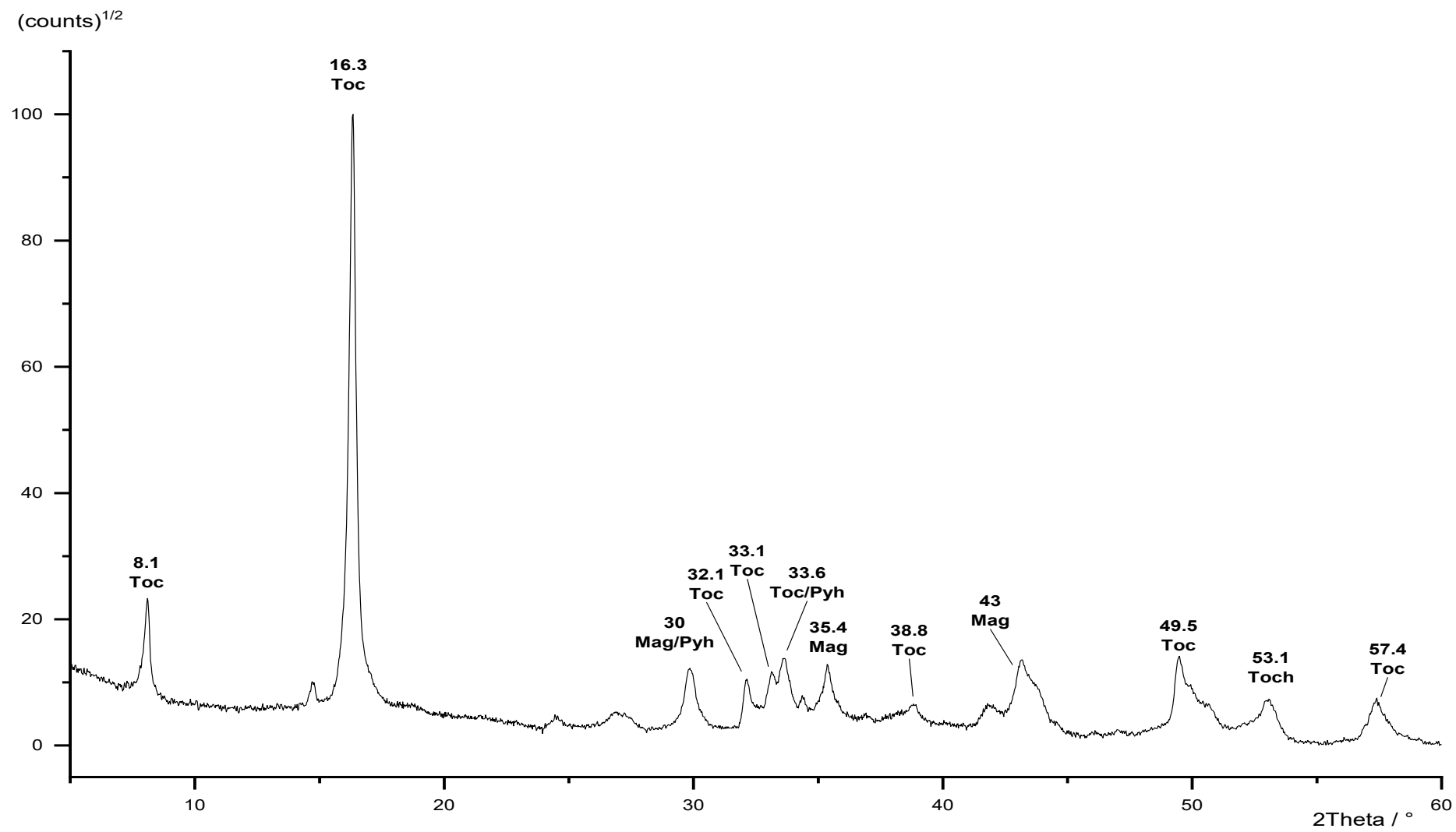


Figure 169: Powder diffraction pattern of TochFeFe\_7. Toc = tochilinite, Mag = magnetite, Pyh = pyhrrrotite.

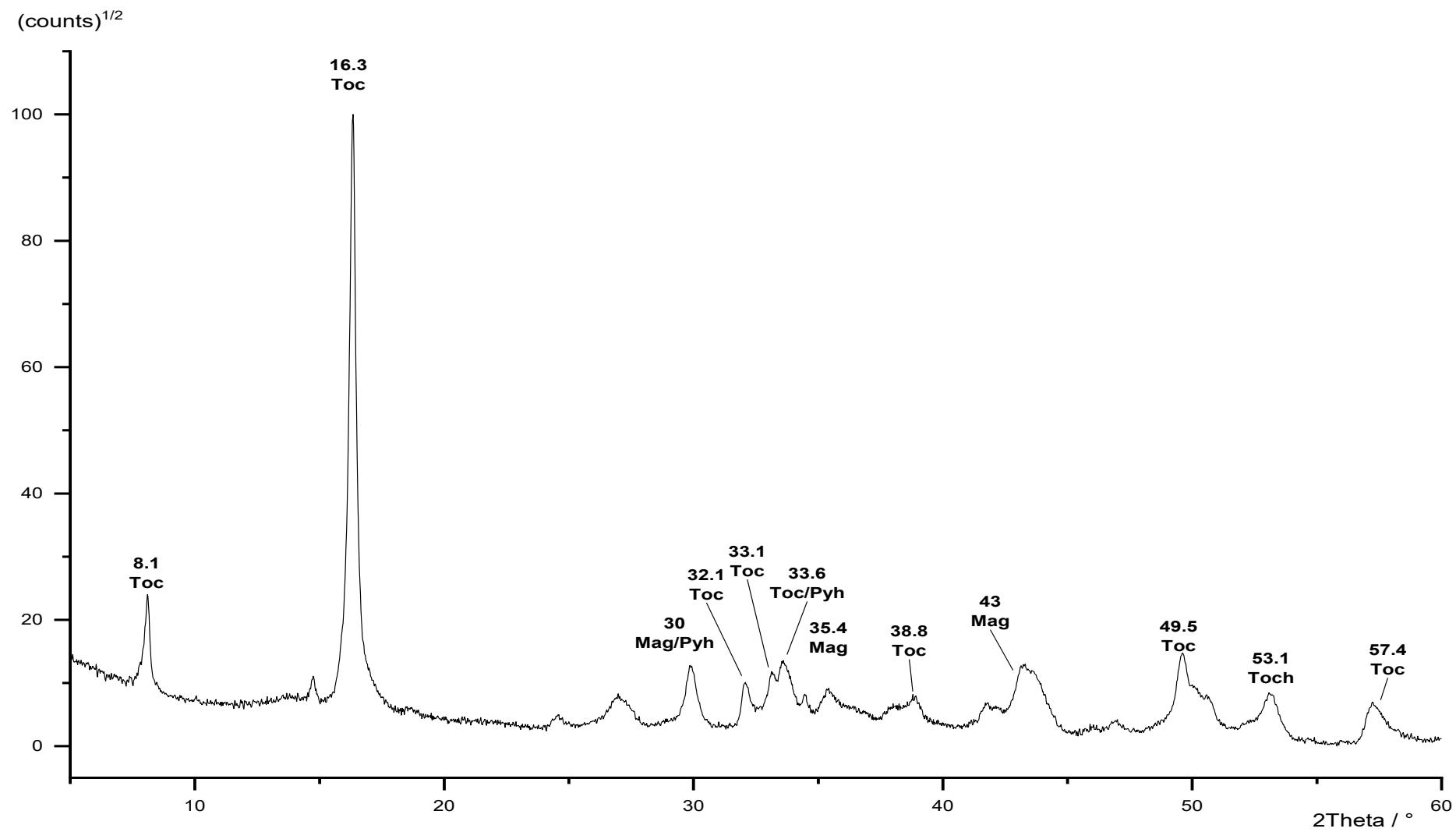


Figure 170: Powder diffraction pattern of TochFeFe<sub>8</sub>. Toc = tochilinite, Mag = magnetite, Pyh = pyhrrrotite.

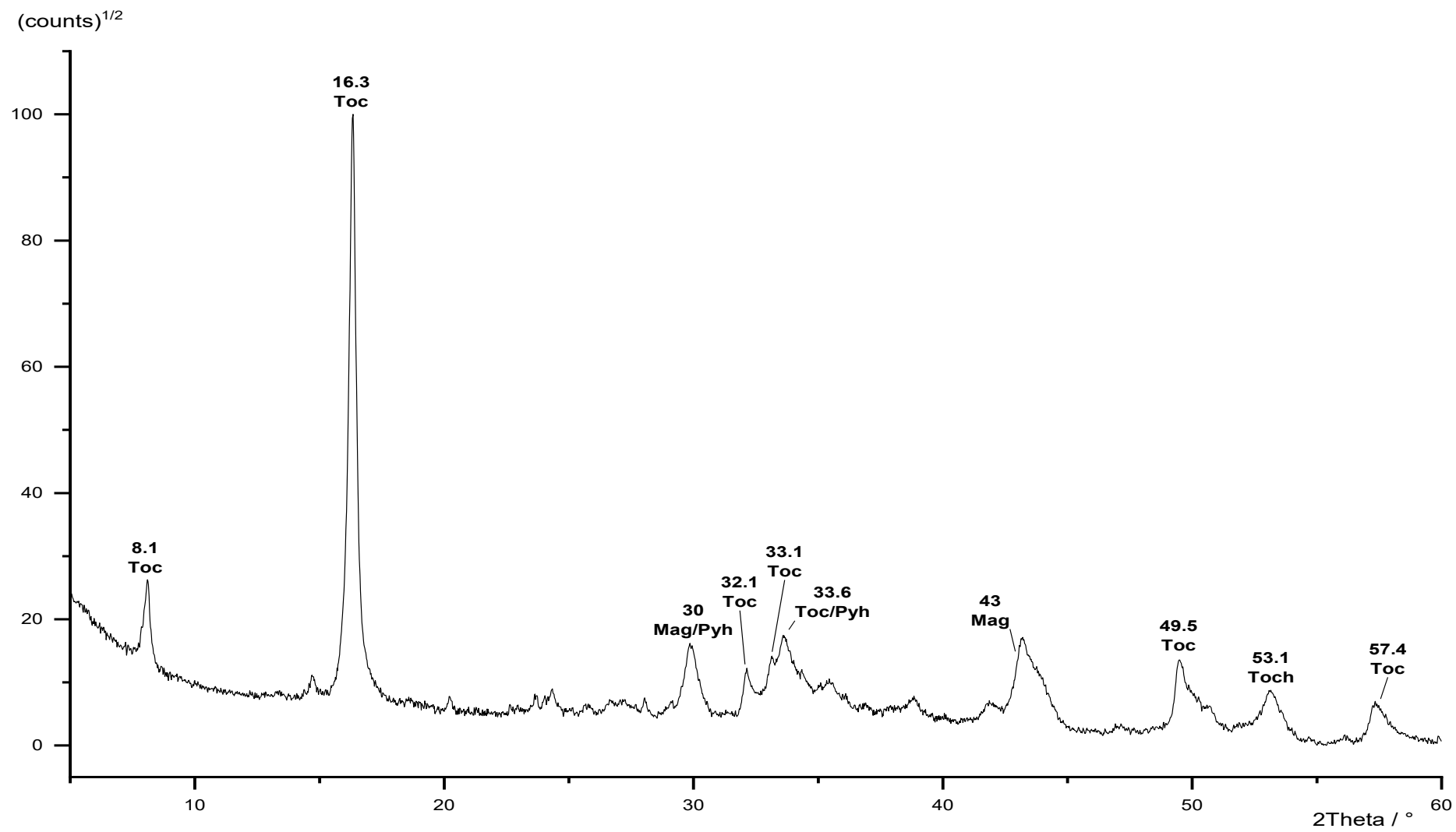


Figure 171: Powder diffraction pattern of TochFeFe\_9. Toc = tochilinite, Mag = magnetite, Pyh = pyhrrrotite.

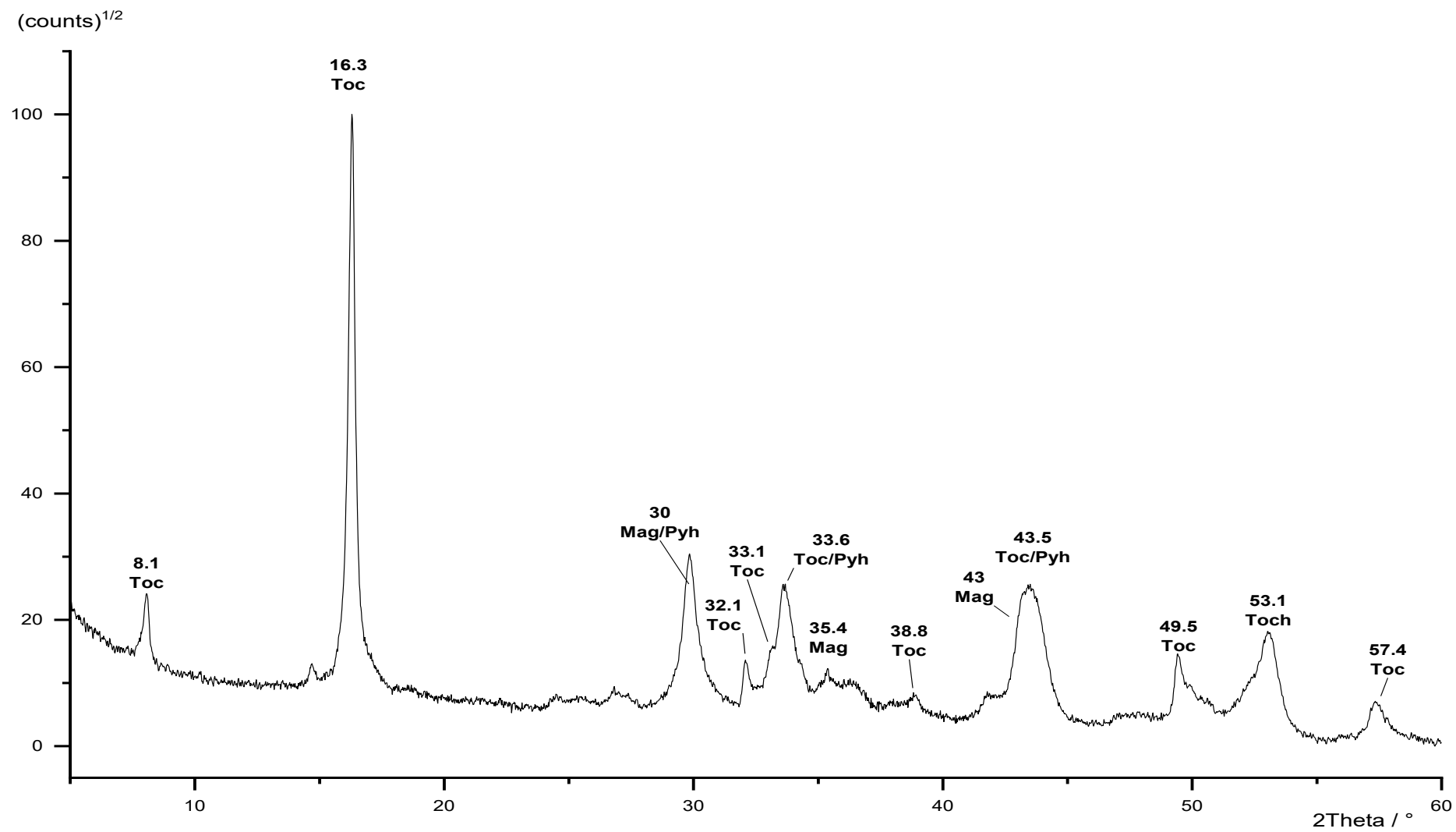


Figure 172: Powder diffraction pattern of TochFeFe\_10. Toc = tochilinite, Mag = magnetite, Pyh = pyrrhotite.

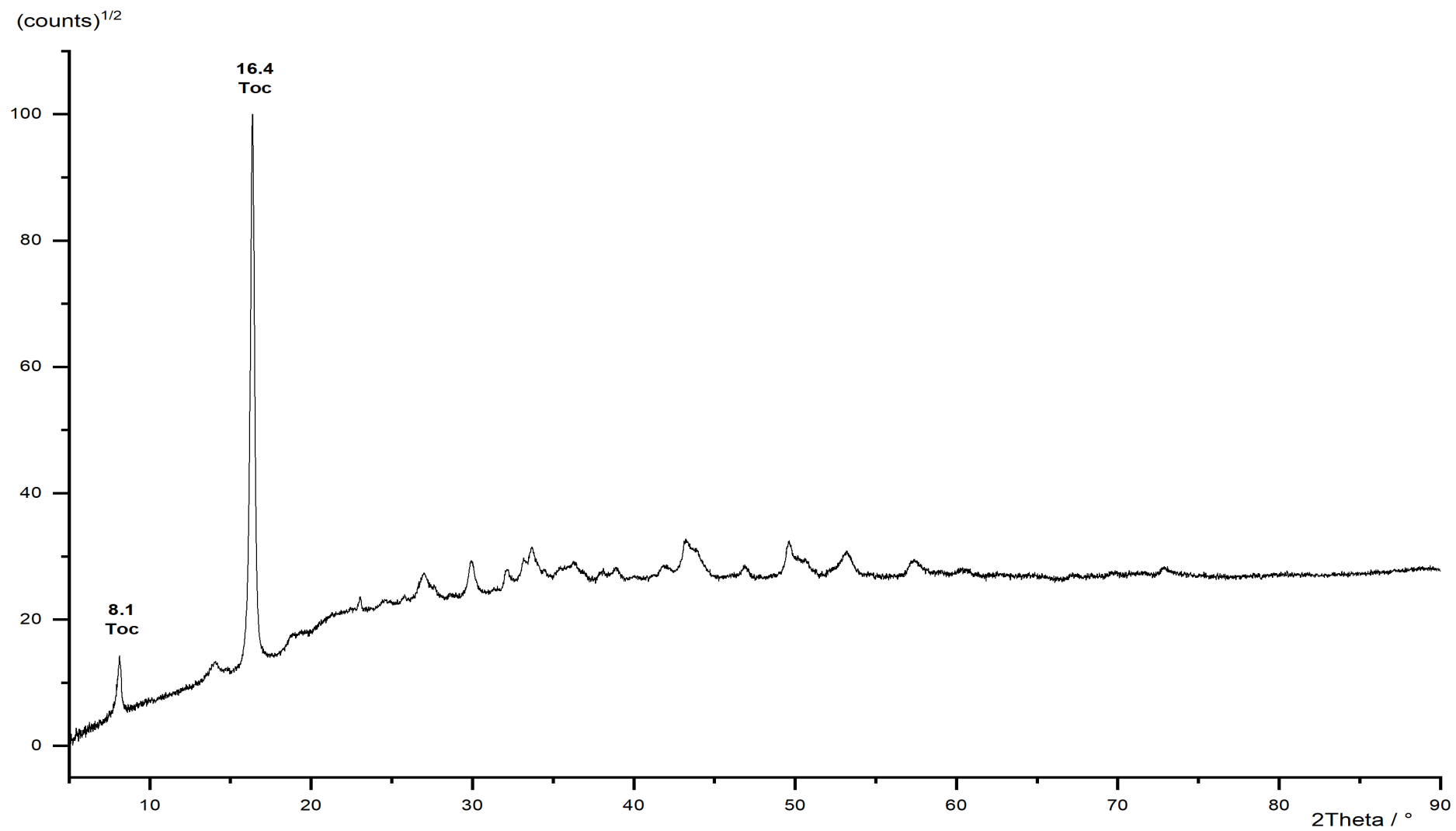


Figure 173: Powder diffraction pattern of TochFeFe\_11. Toc = tochilinite.

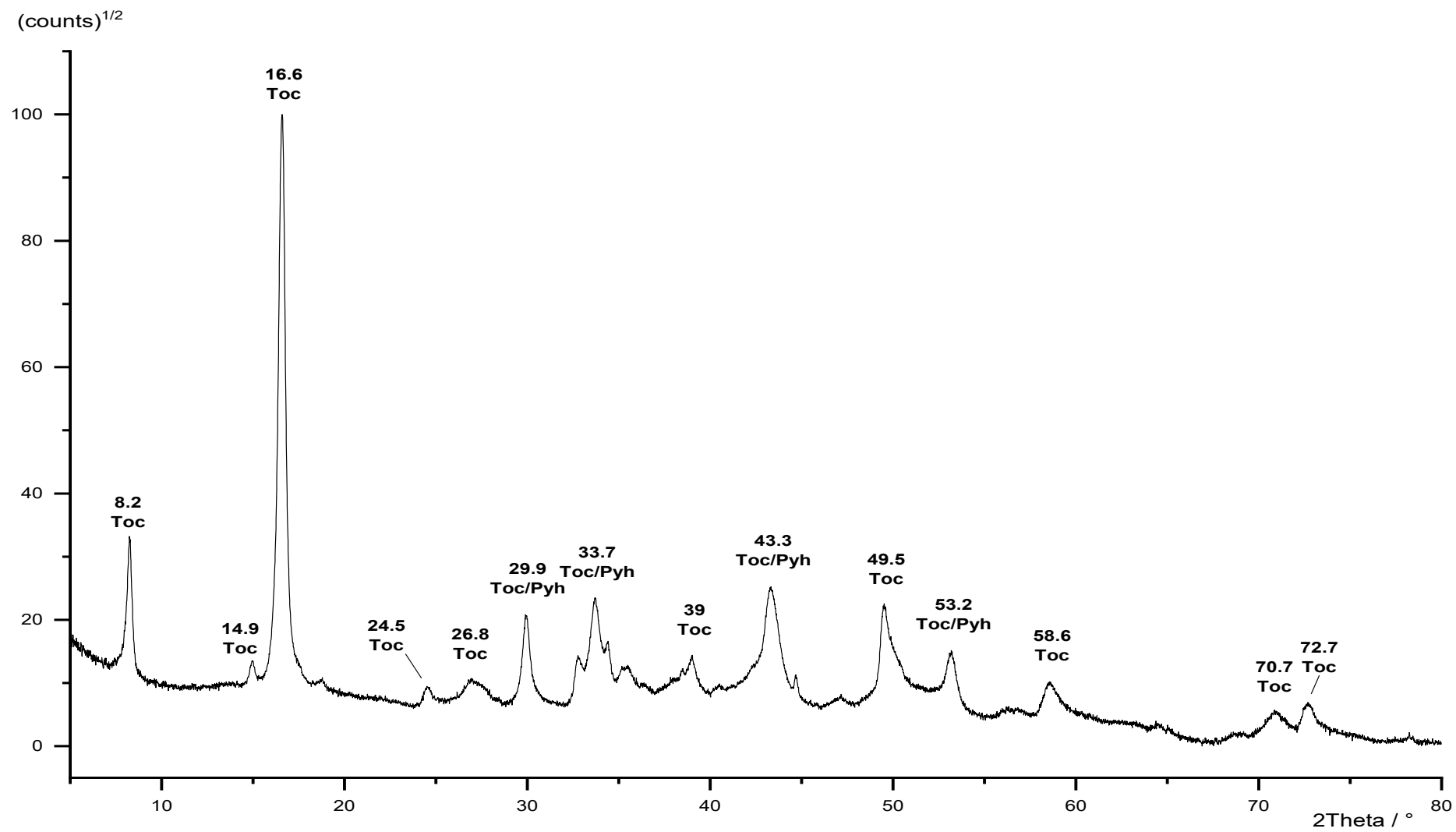


Figure 174: Powder diffraction pattern of TochFeAl<sub>1</sub>. Toc = tochilinite, Pyh = pyrrhotite.

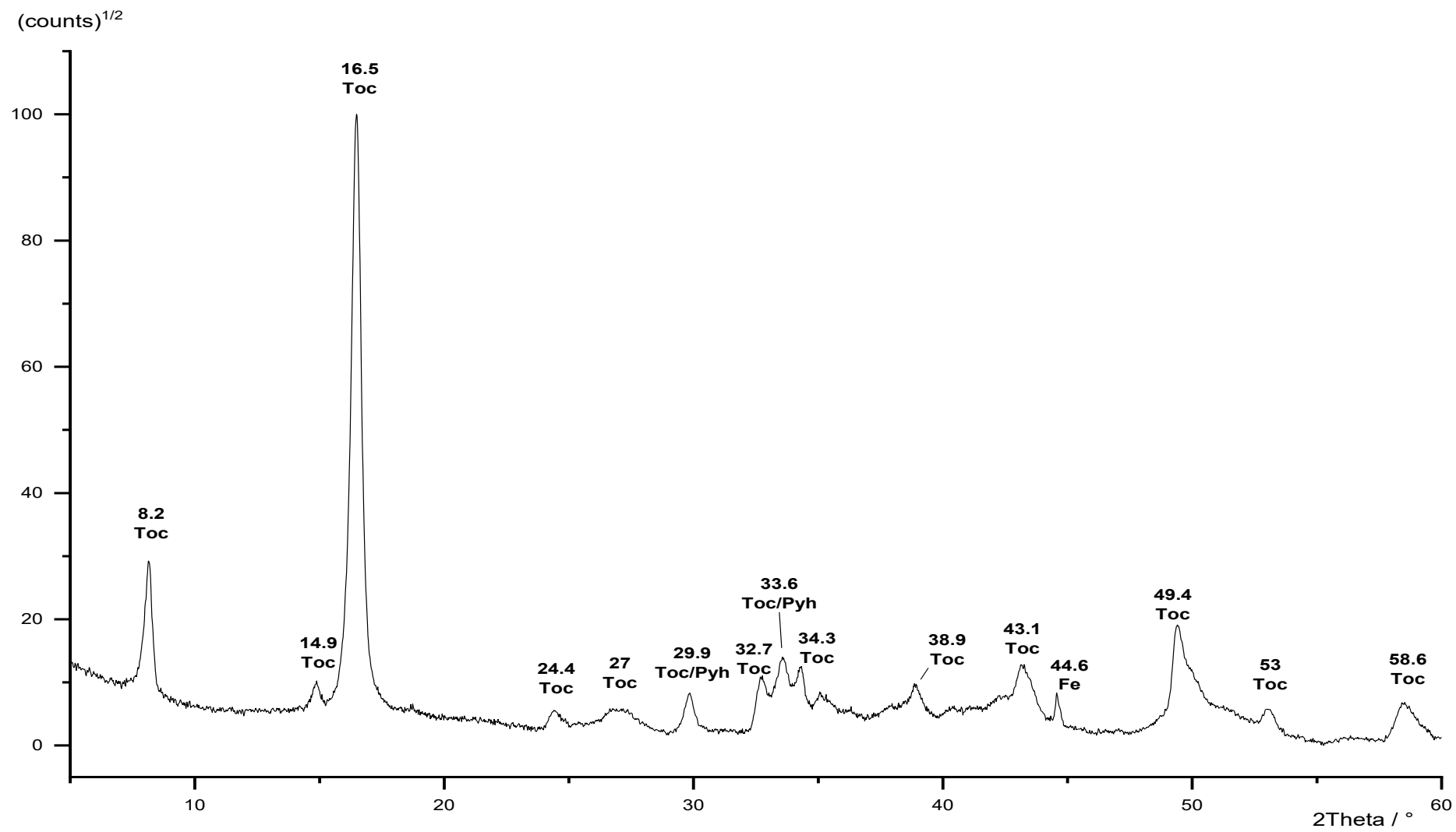


Figure 175: Powder diffraction pattern of TochFeAl<sub>2</sub>. Toc = tochilinite, Pyh = pyrrhotite, Fe = iron.



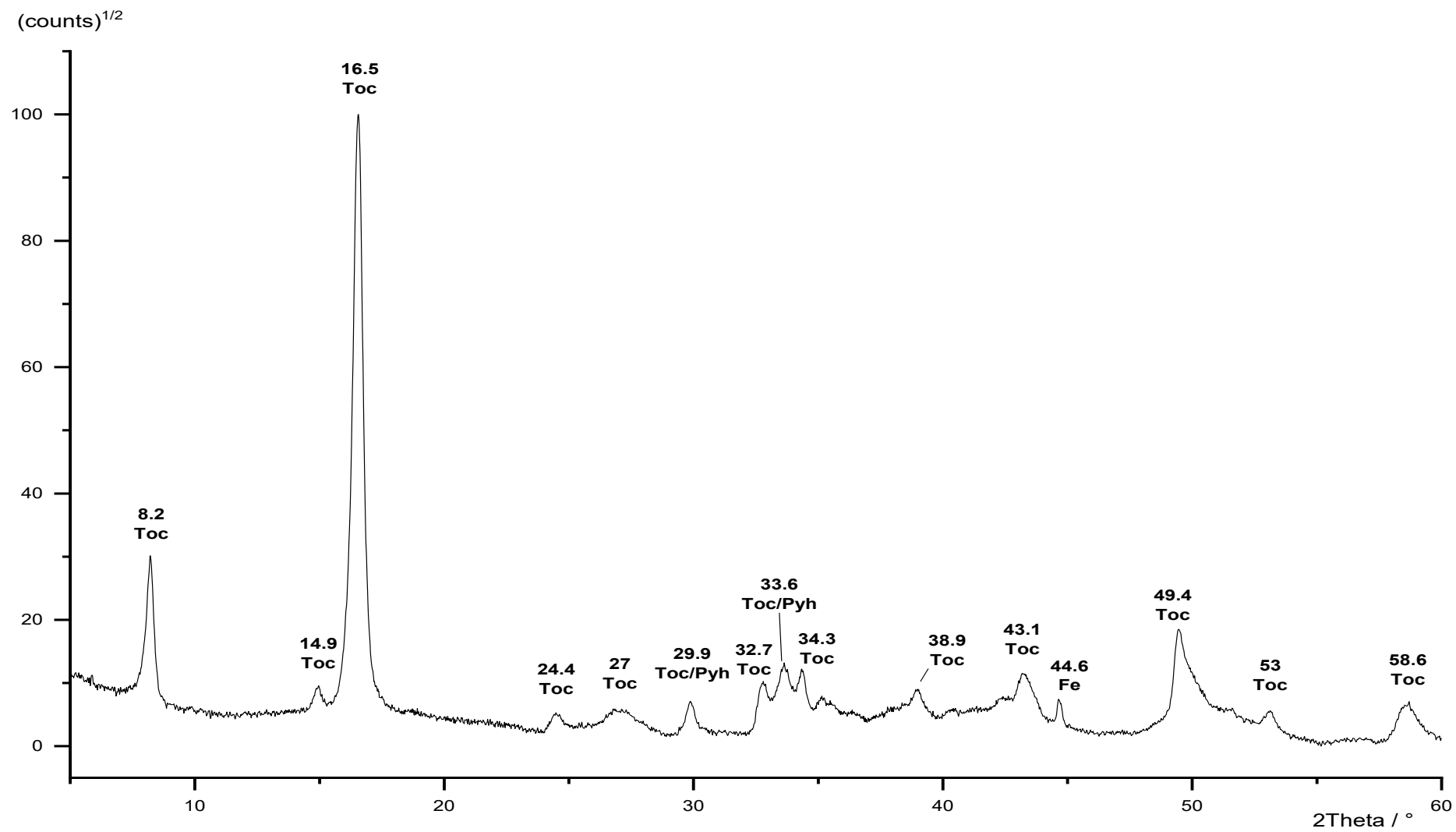


Figure 176: Powder diffraction pattern of TochFeAl<sub>3</sub>. Toc = tochilinite, Pyh = pyrrhotite, Fe = iron.

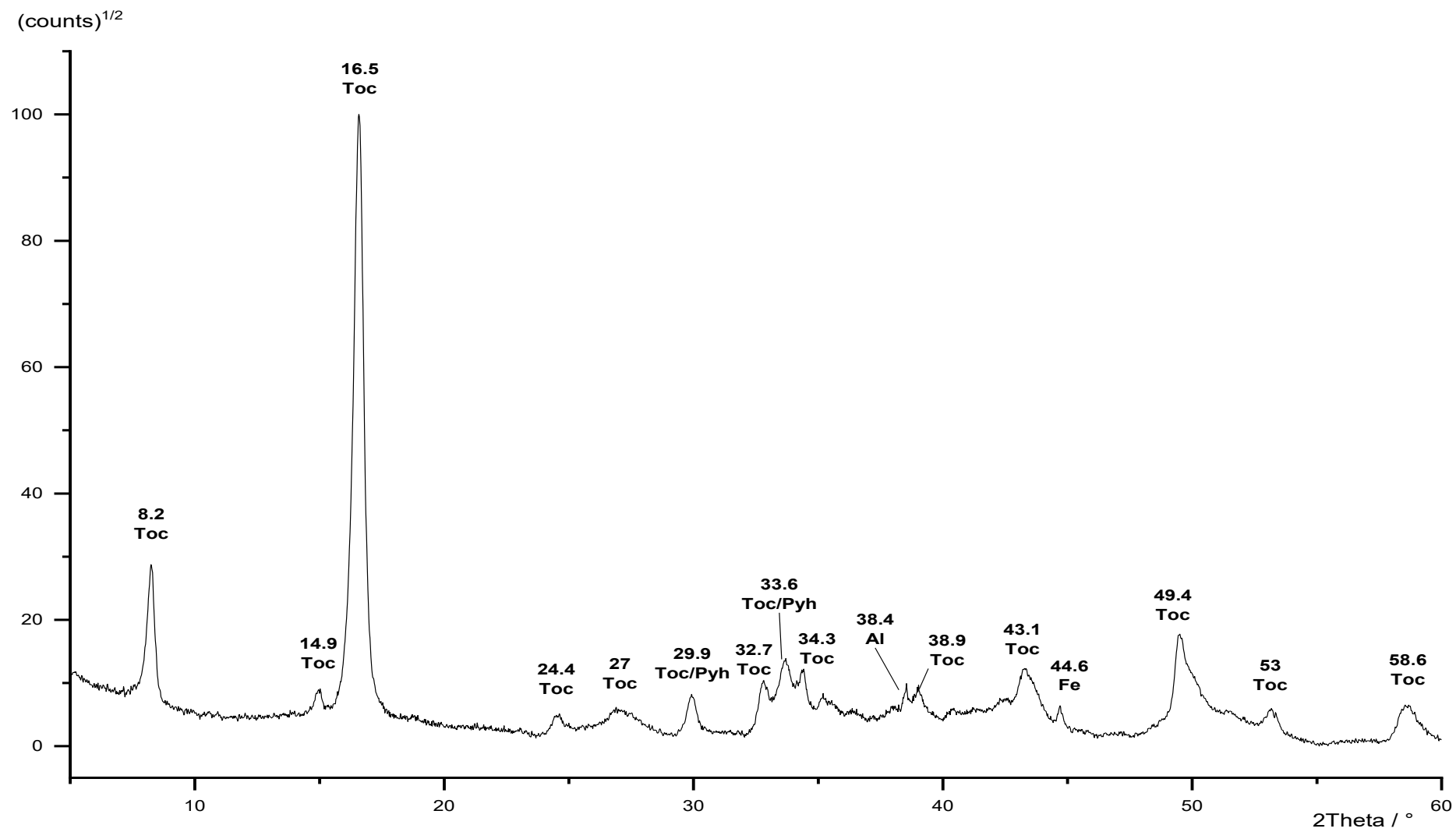


Figure 177: Powder diffraction pattern of TochFeAl<sub>4</sub>. Toc = tochilinite, Pyh = pyrrhotite, Fe = iron, Al = aluminum.

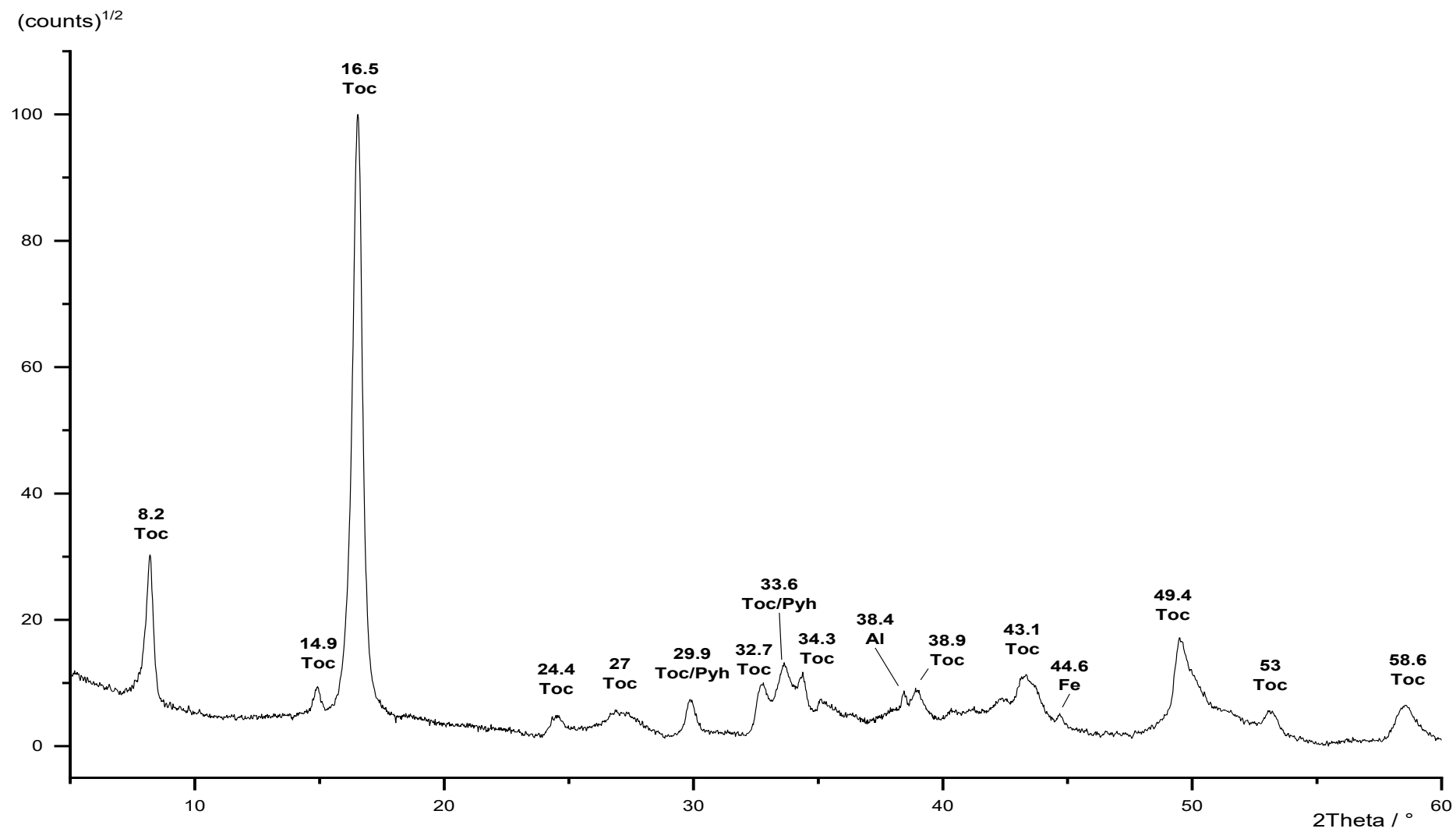


Figure 178: Powder diffraction pattern of TochFeAl<sub>5</sub>. Toc = tochilinite, Pyh = pyrrhotite, Fe = iron, Al = aluminum.

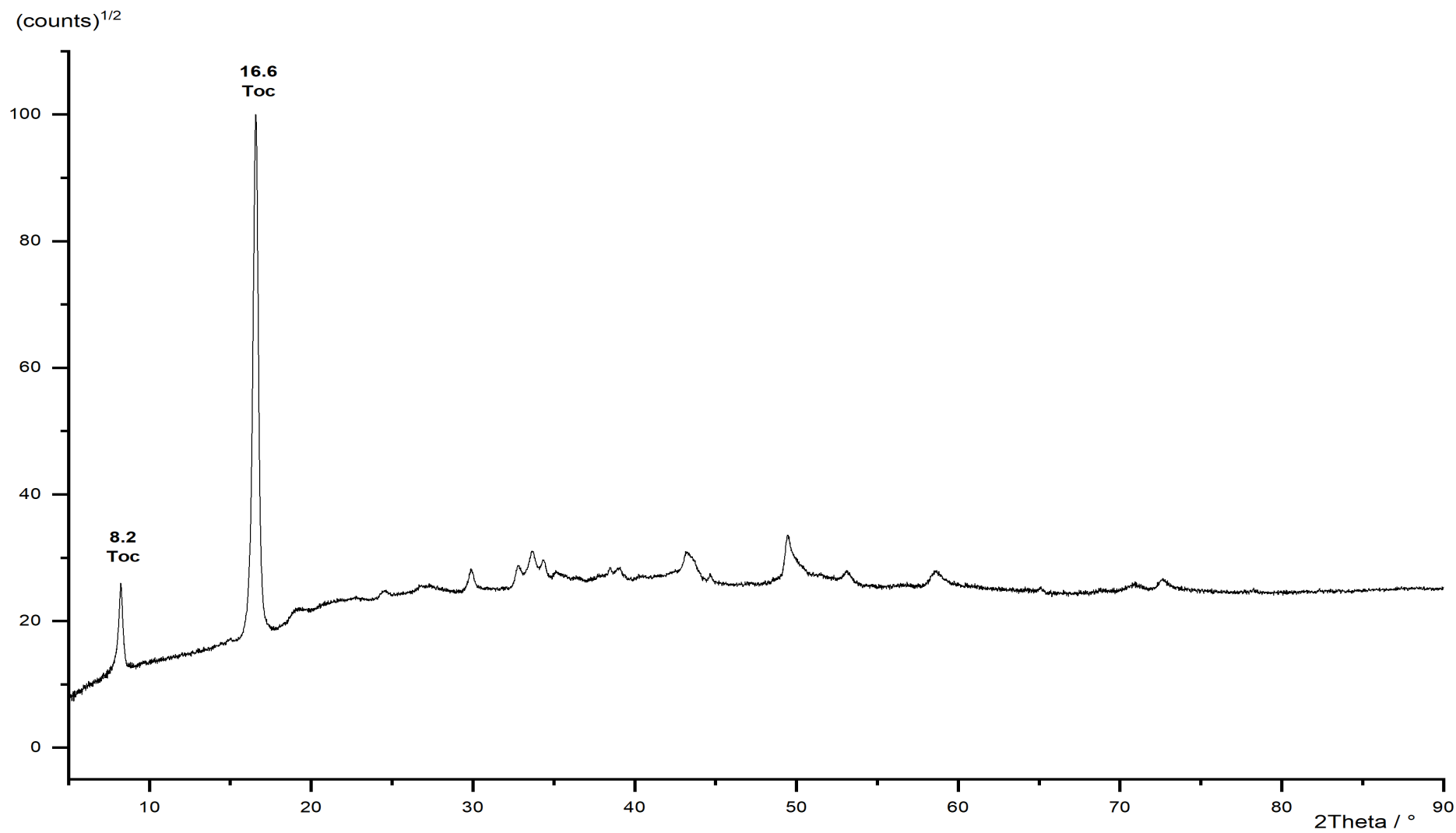


Figure 179: Powder diffraction pattern of TochFeAl<sub>6</sub>. Toc = tochilinite.

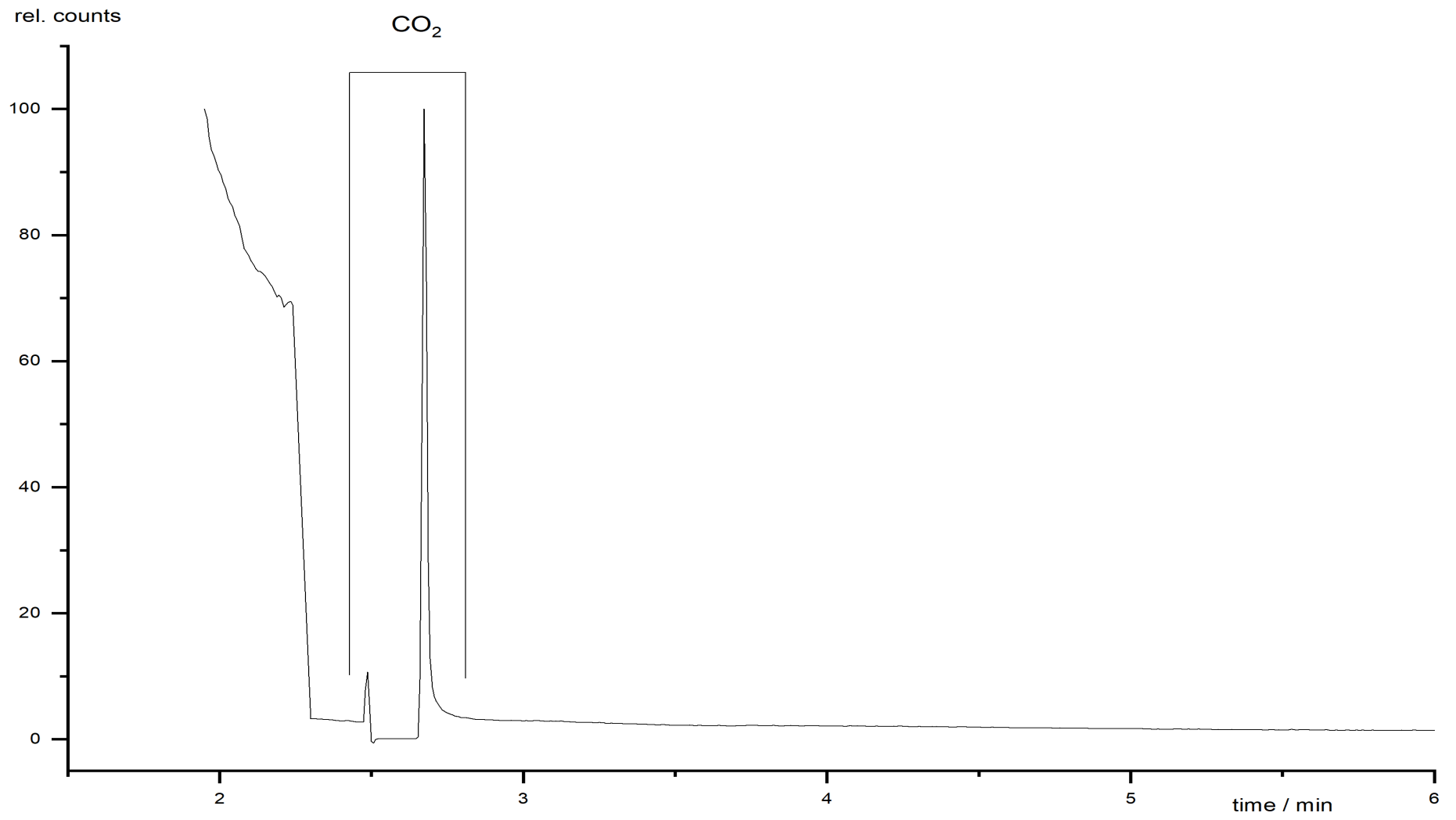


Figure 180: Gas chromatogram of RED\_1.

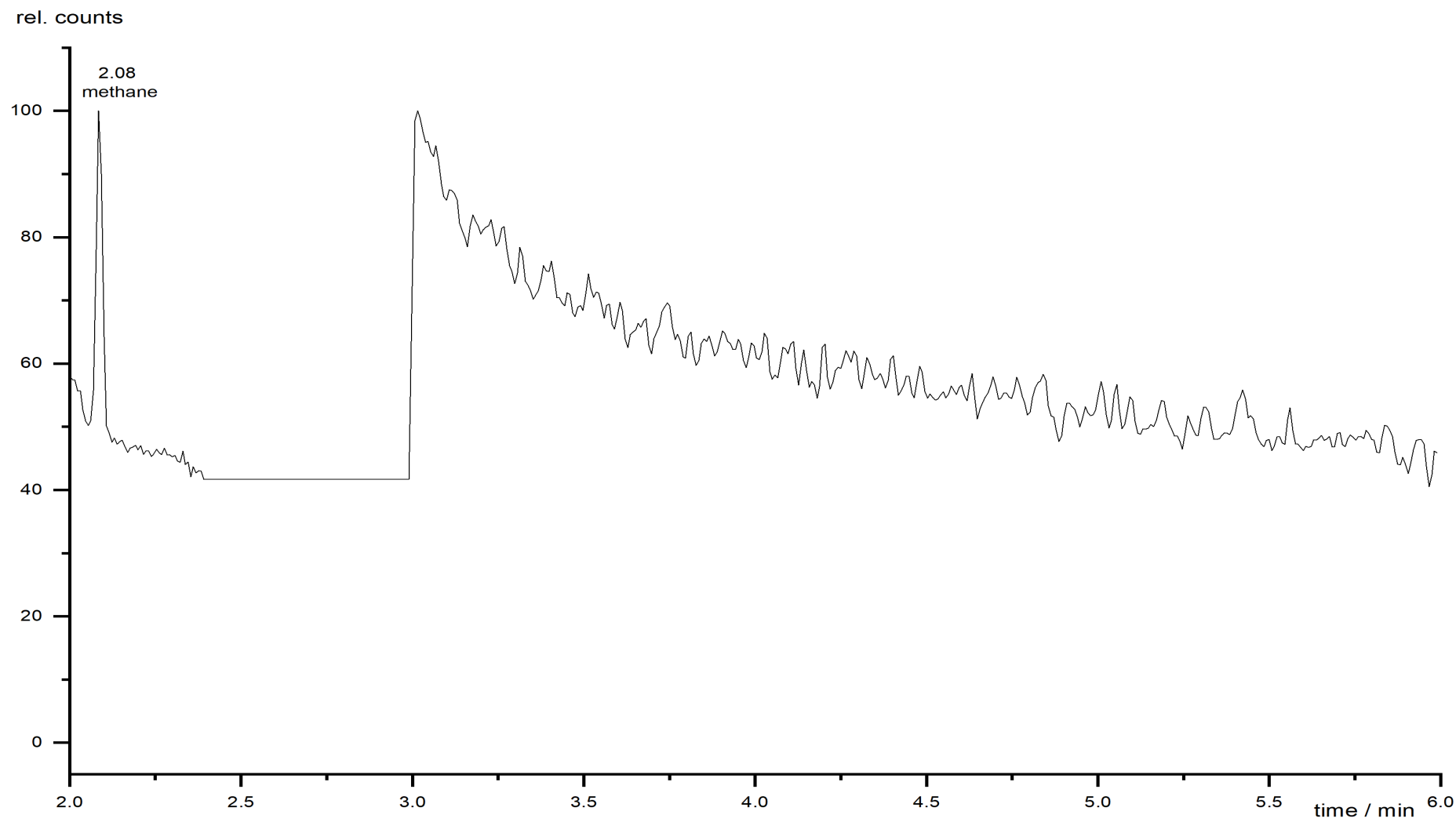


Figure 181: Gas chromatogram of RED\_2.

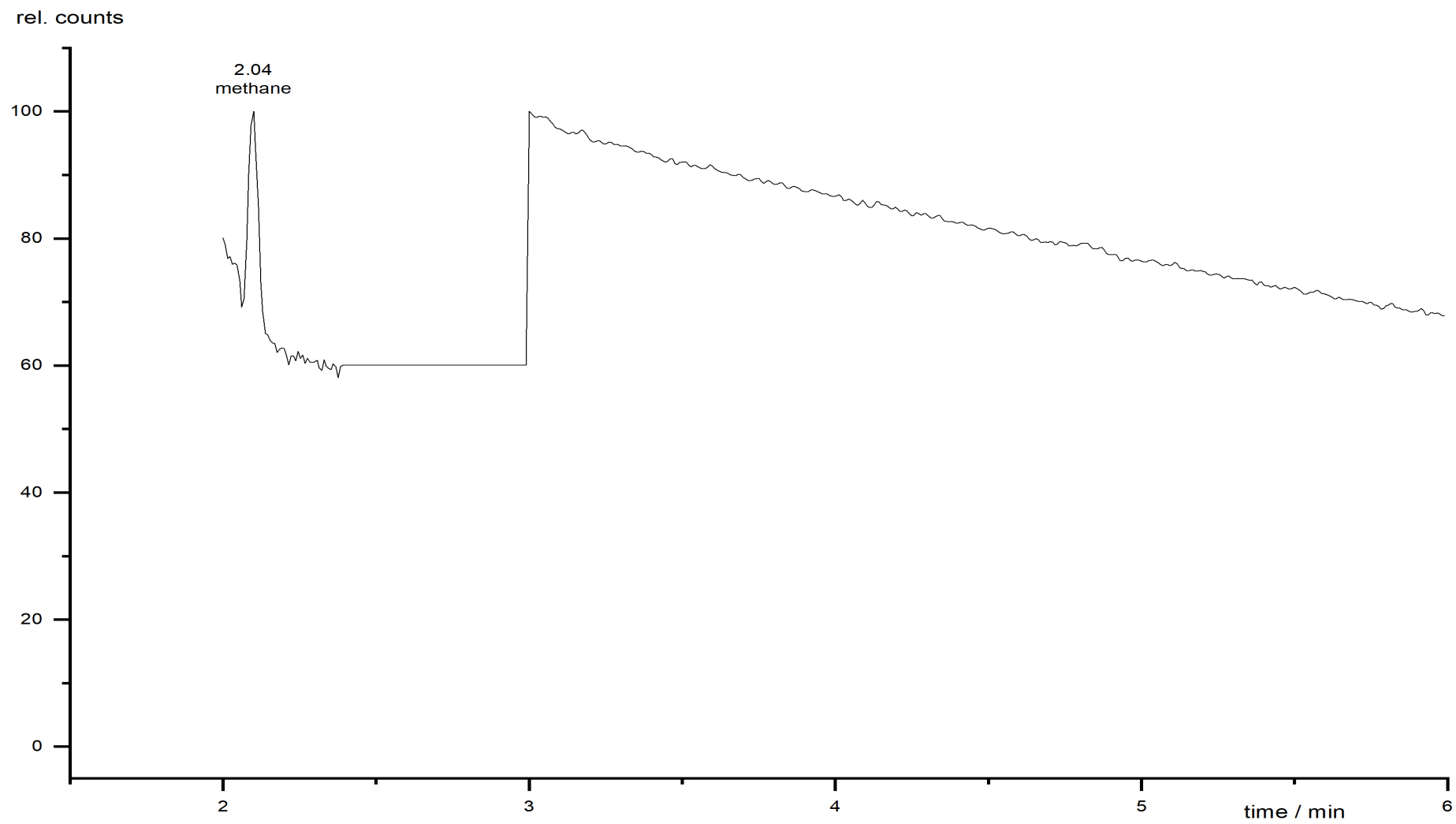


Figure 182: Gas chromatogram of RED\_3.

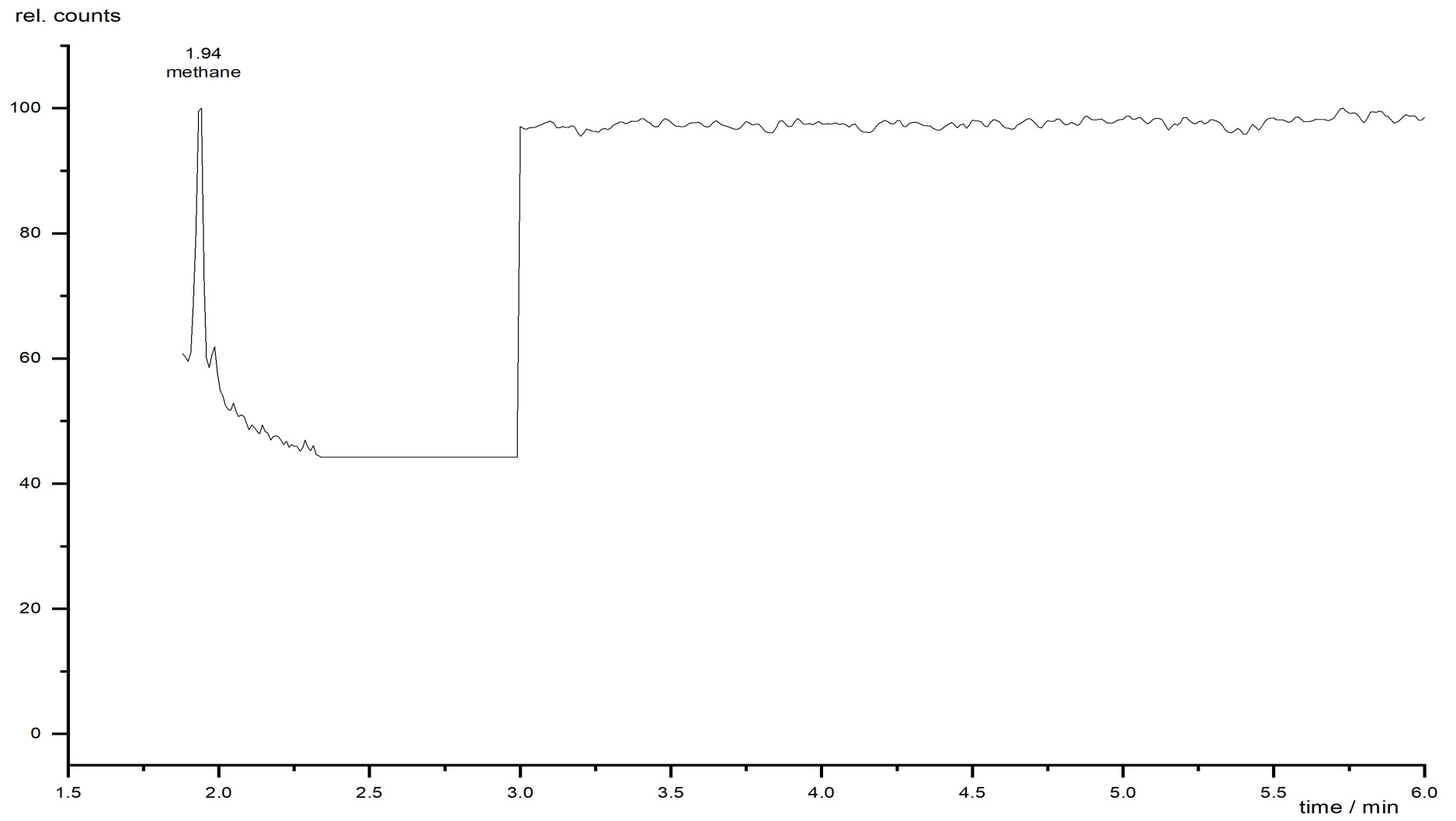


Figure 183: Gas chromatogram of RED\_4.



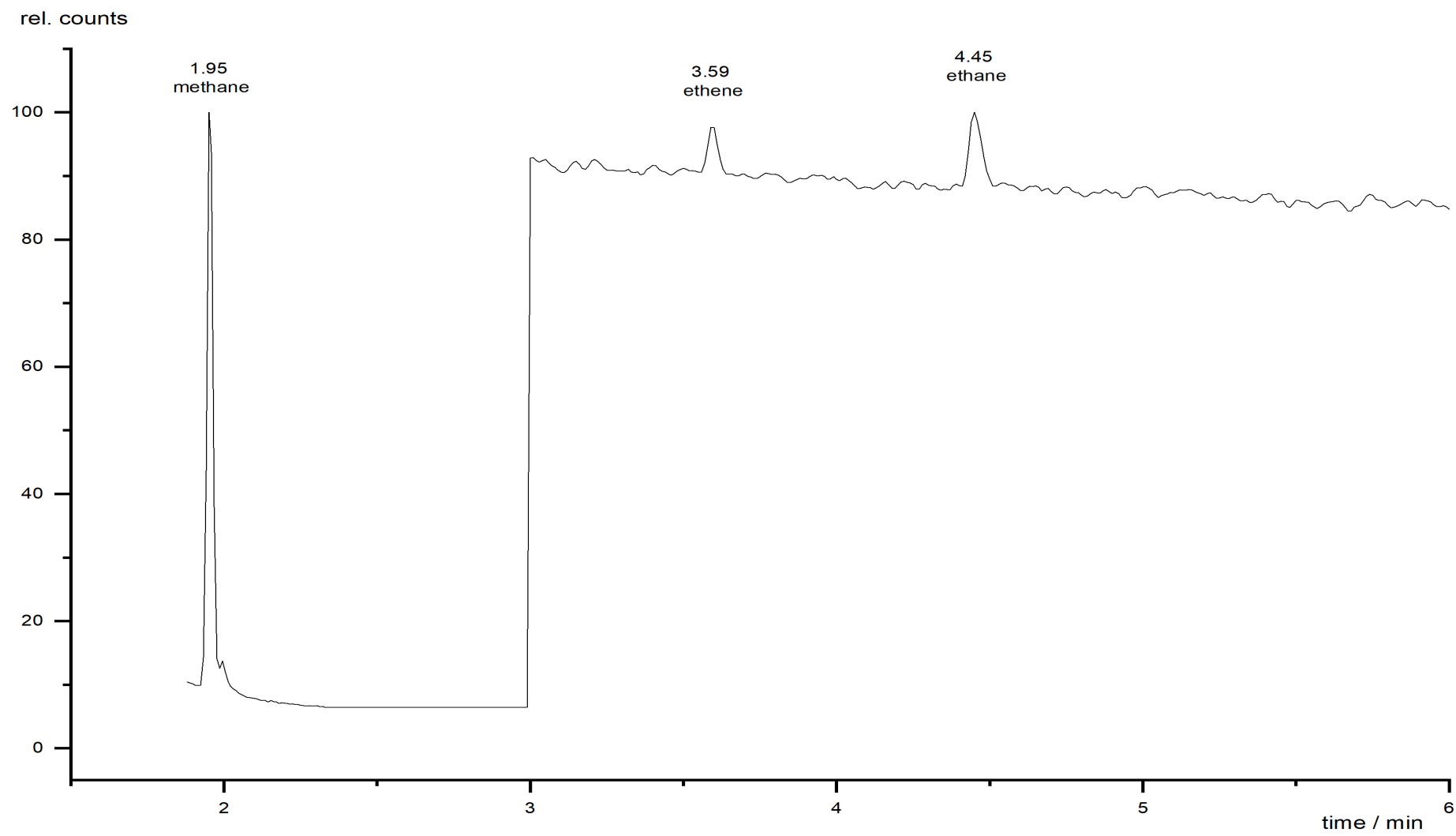


Figure 184: Gas chromatogram of RED\_5.

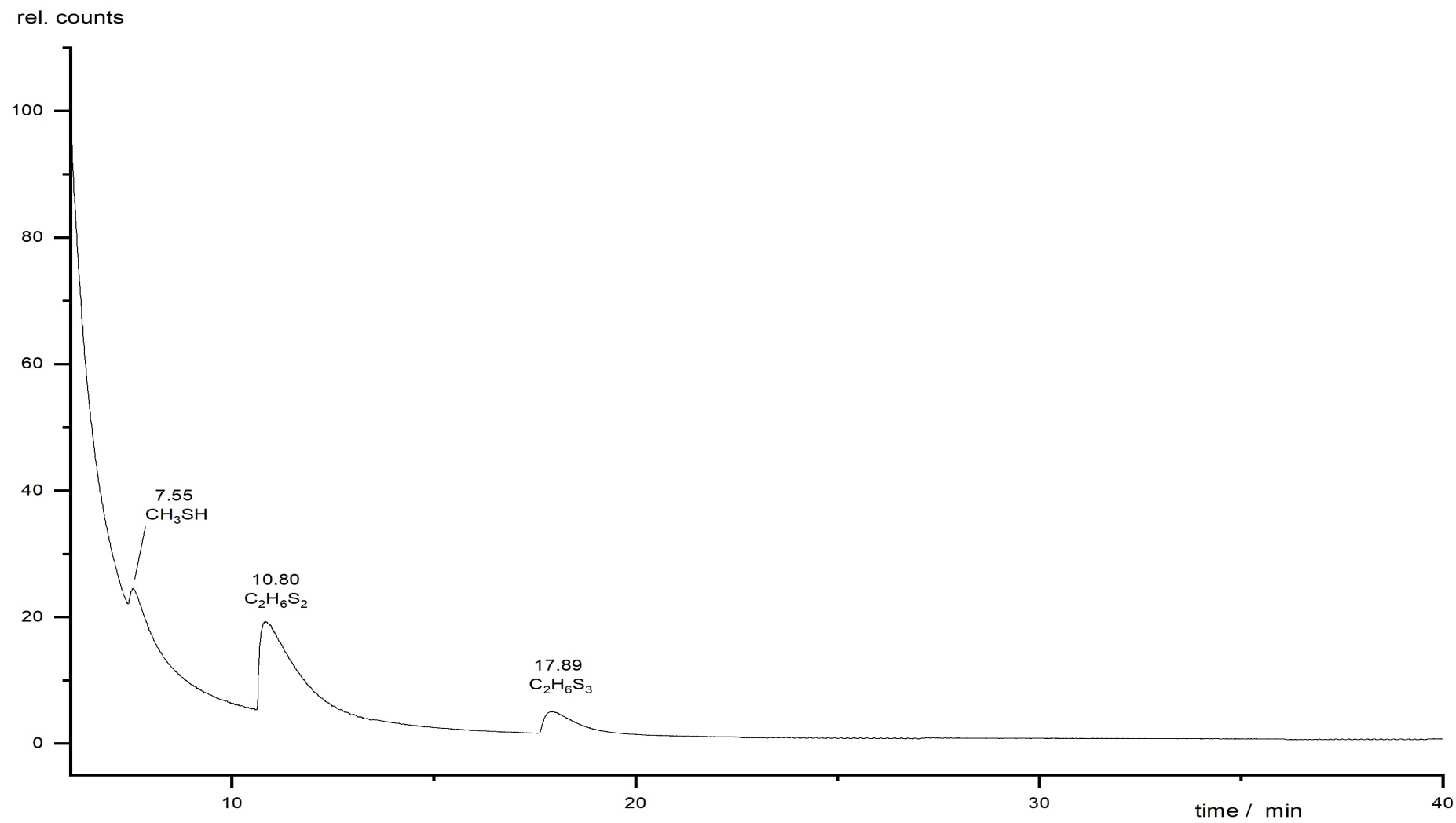


Figure 185: Gas chromatogram of RED\_6.

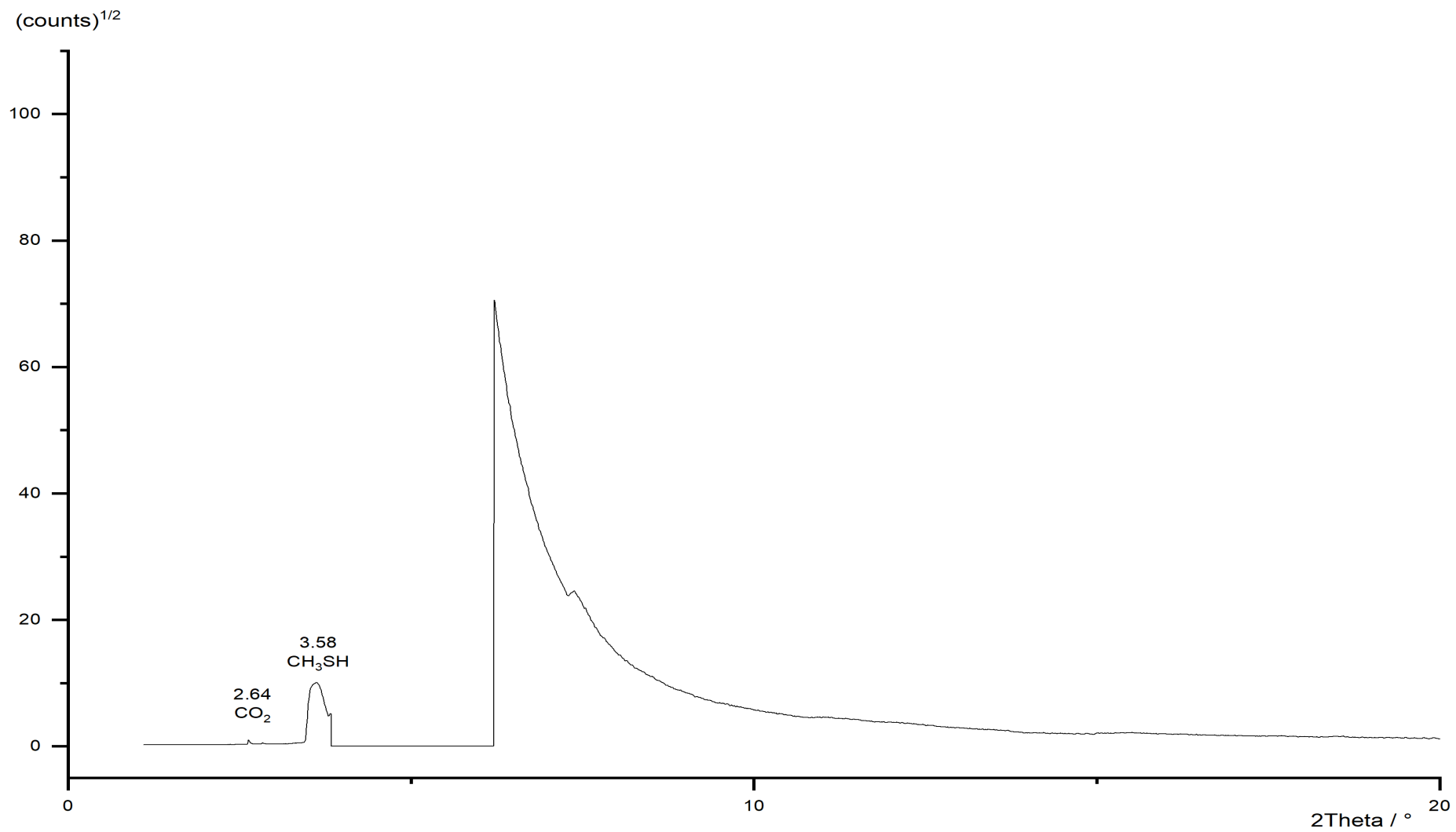


Figure 186: Gas chromatogram of RED\_7.

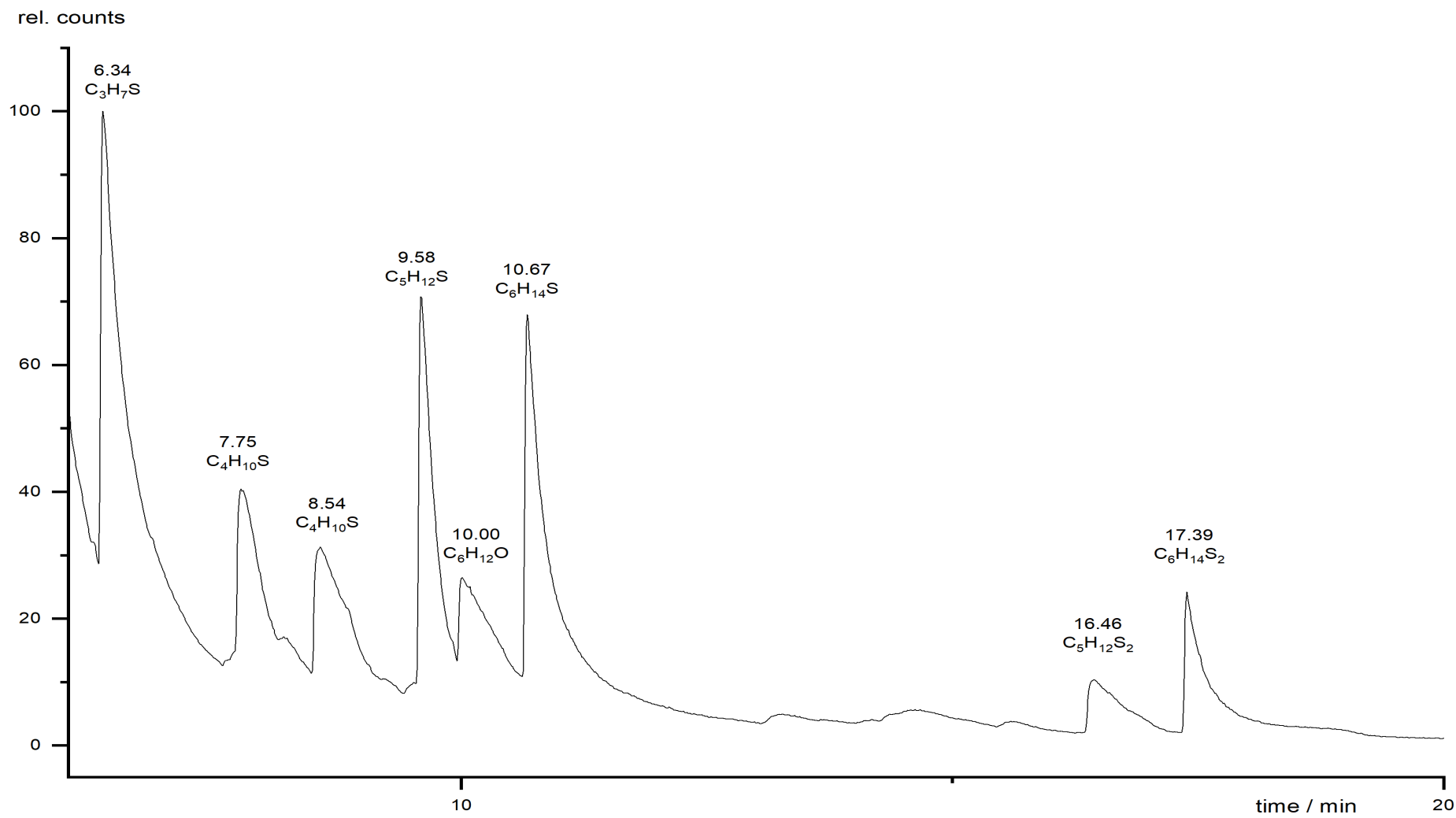


Figure 187: Gas chromatogram of RED\_8.

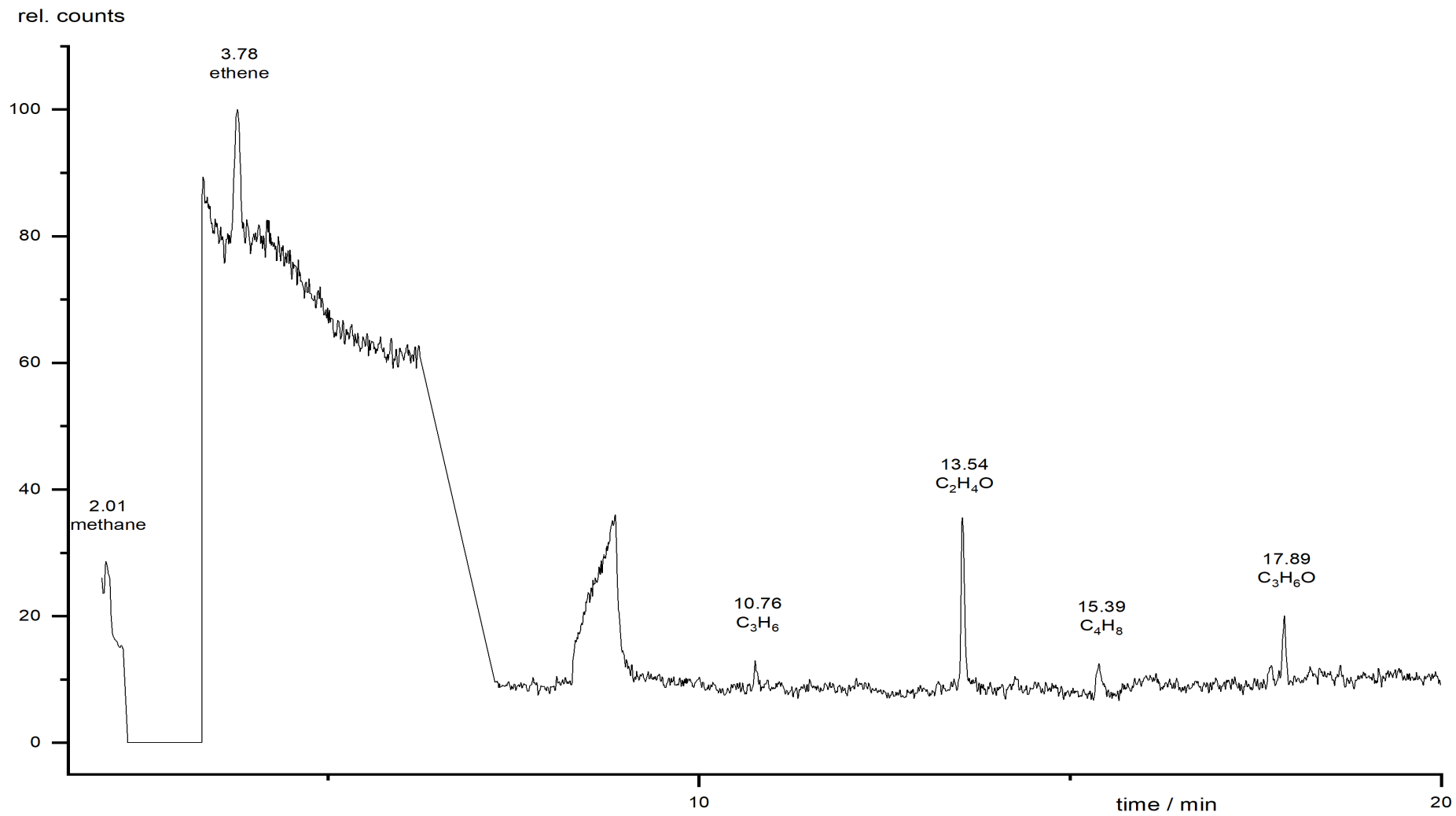


Figure 188: Gas chromatogram of RED\_9.

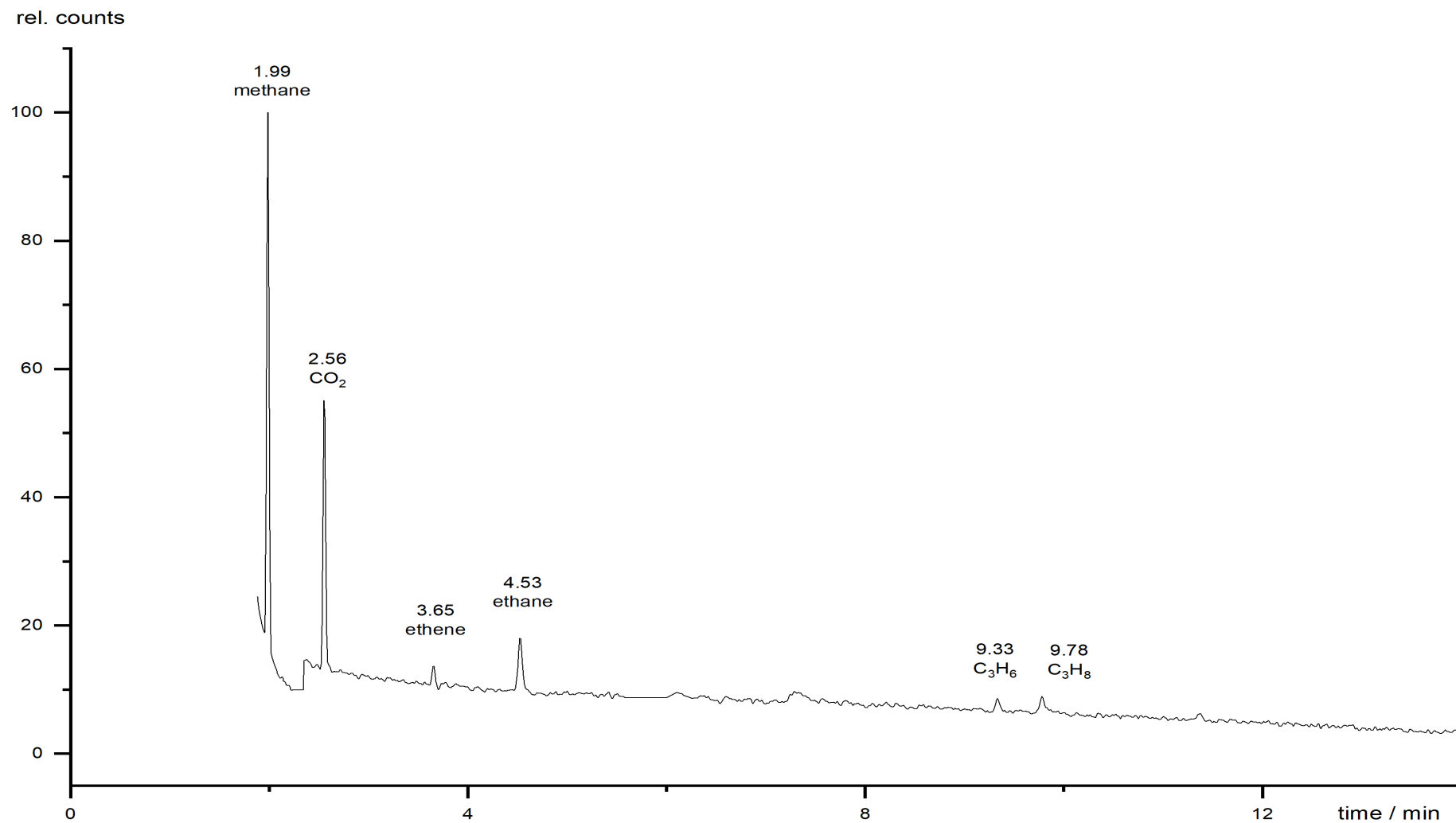


Figure 189: Gas chromatogram of RED\_10.

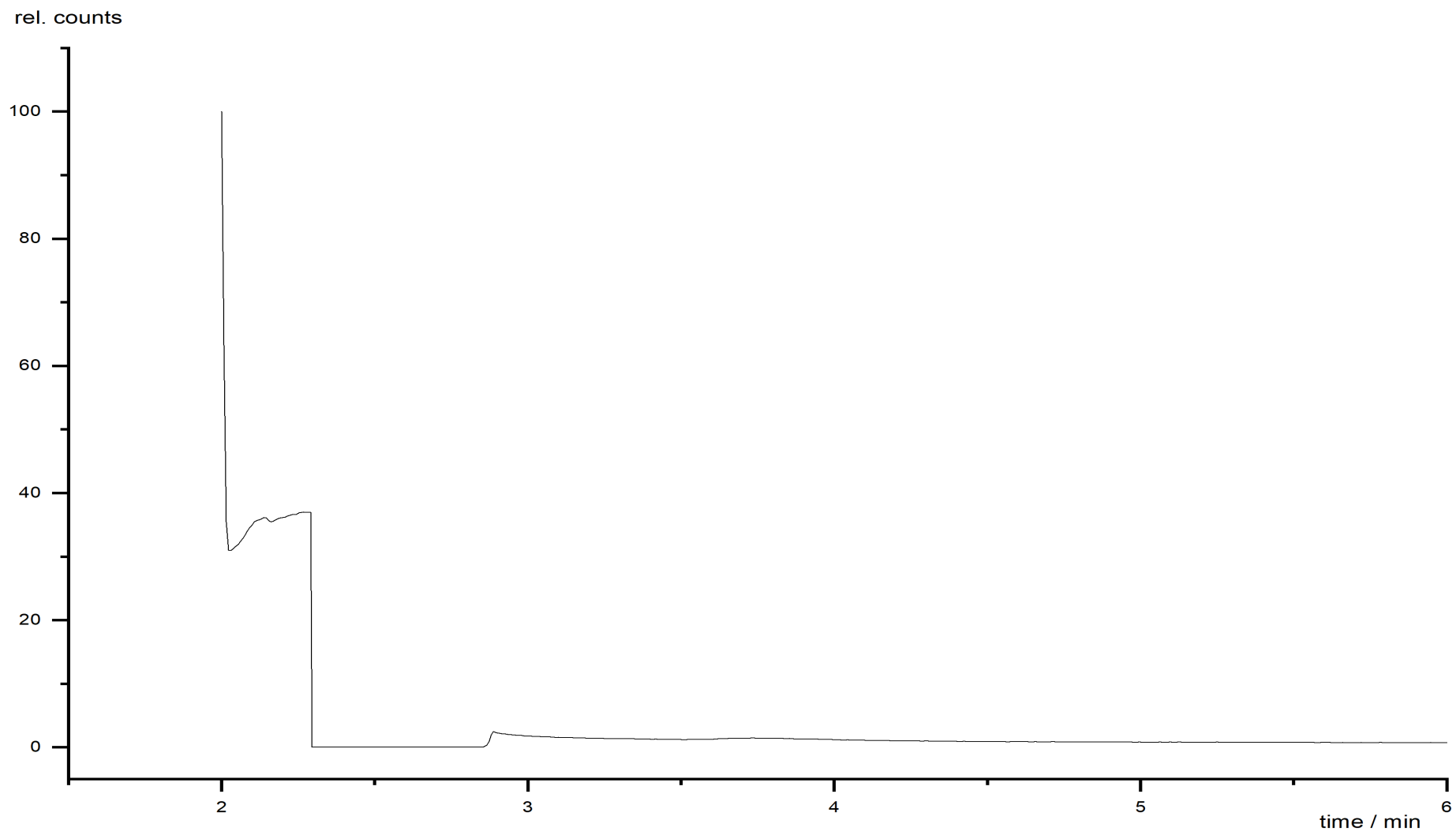


Figure 190: Gas chromatogram of RED\_11.

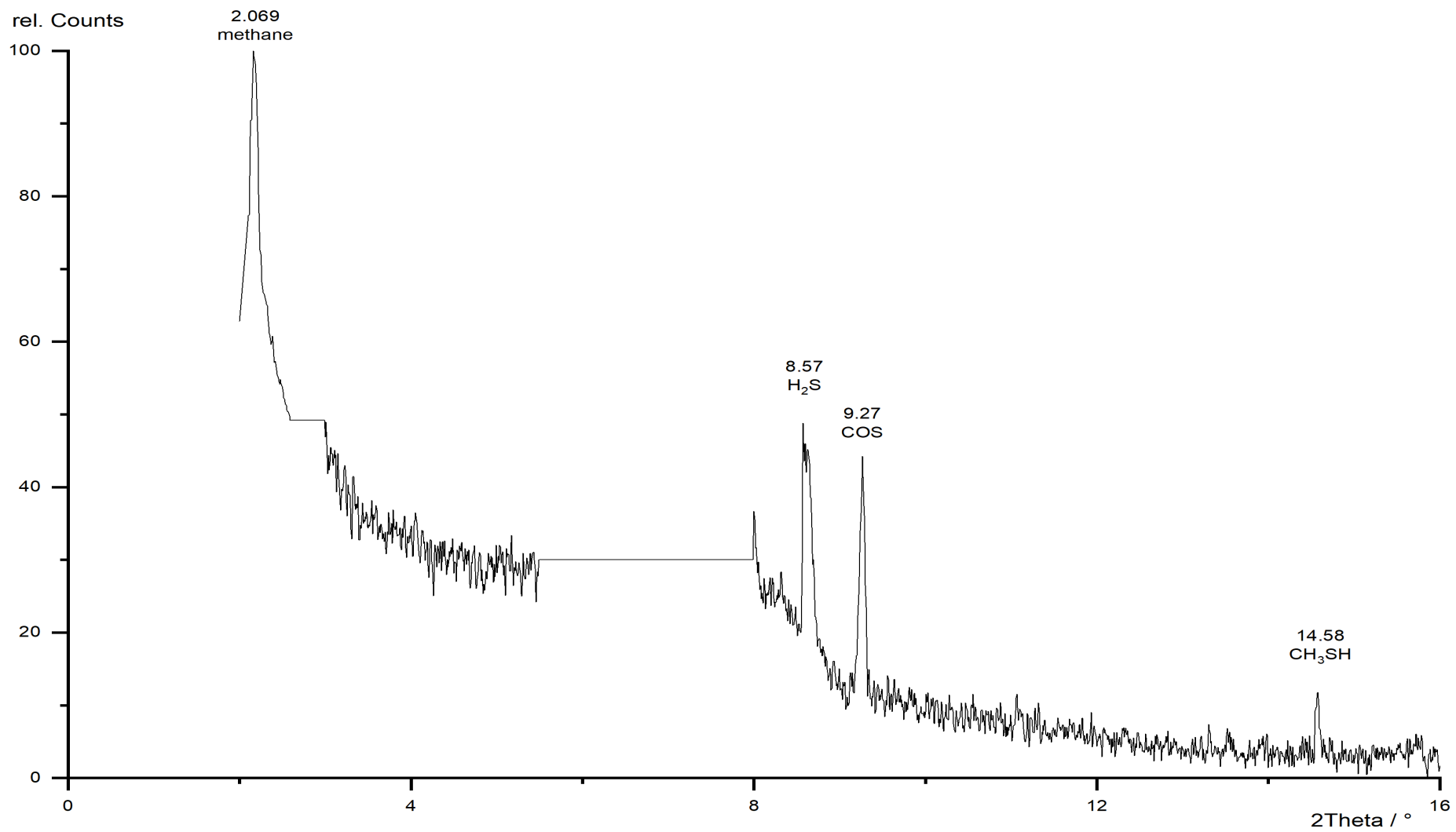


Figure 191: Gas chromatogram of RED\_12.



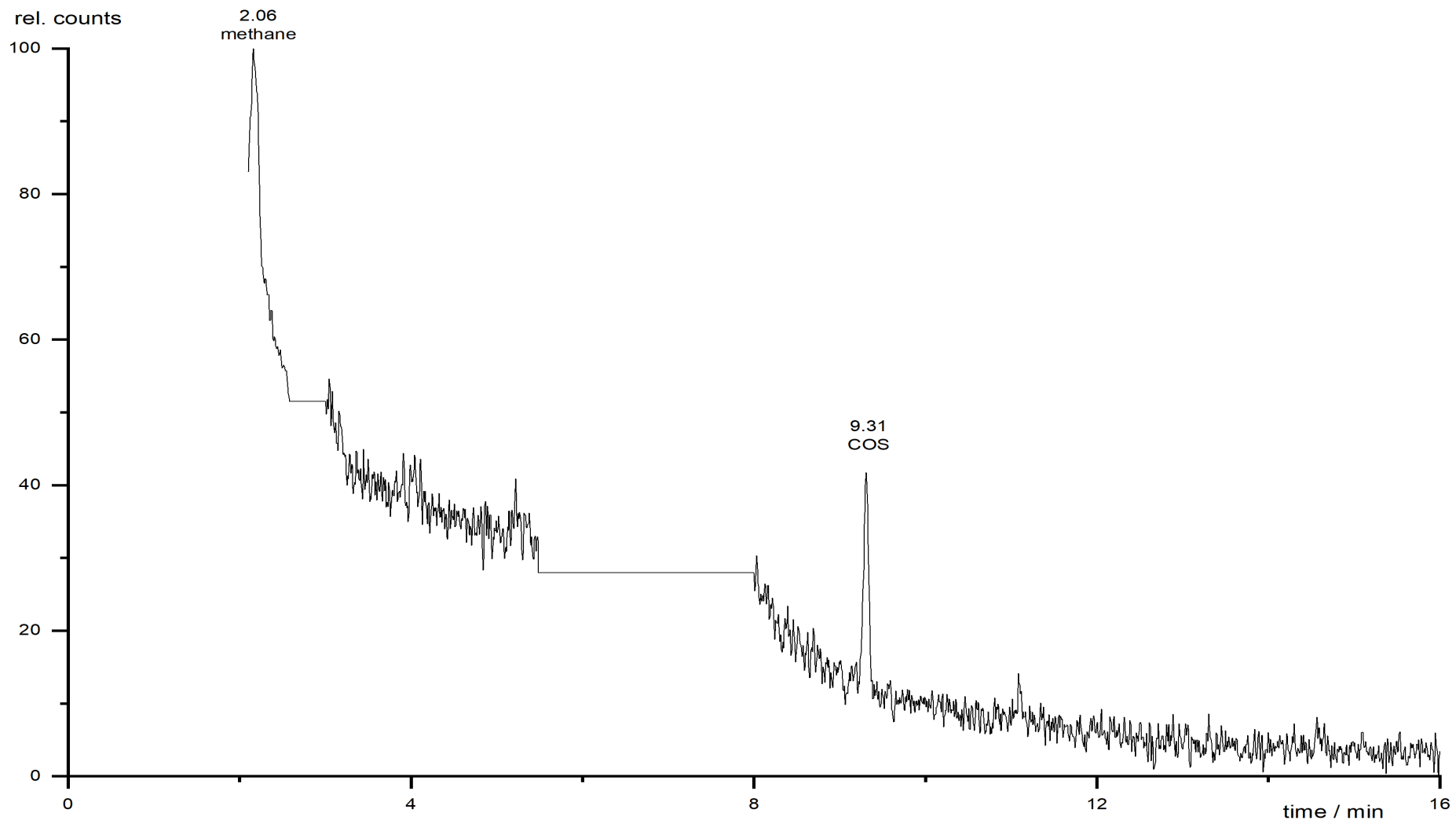


Figure 192: Gas chromatogram of RED\_13.

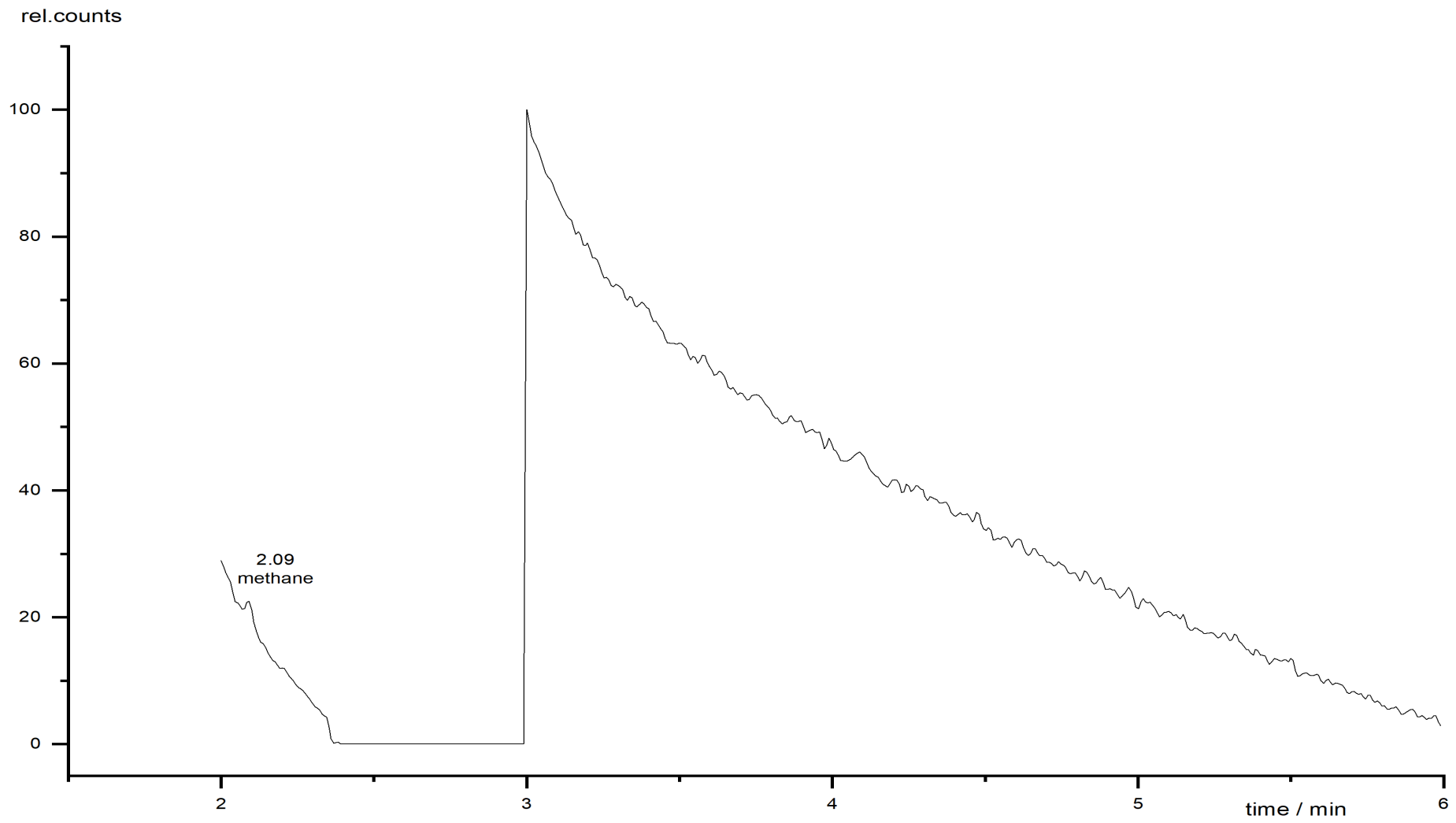


Figure 193: Gas chromatogram of RED\_14.

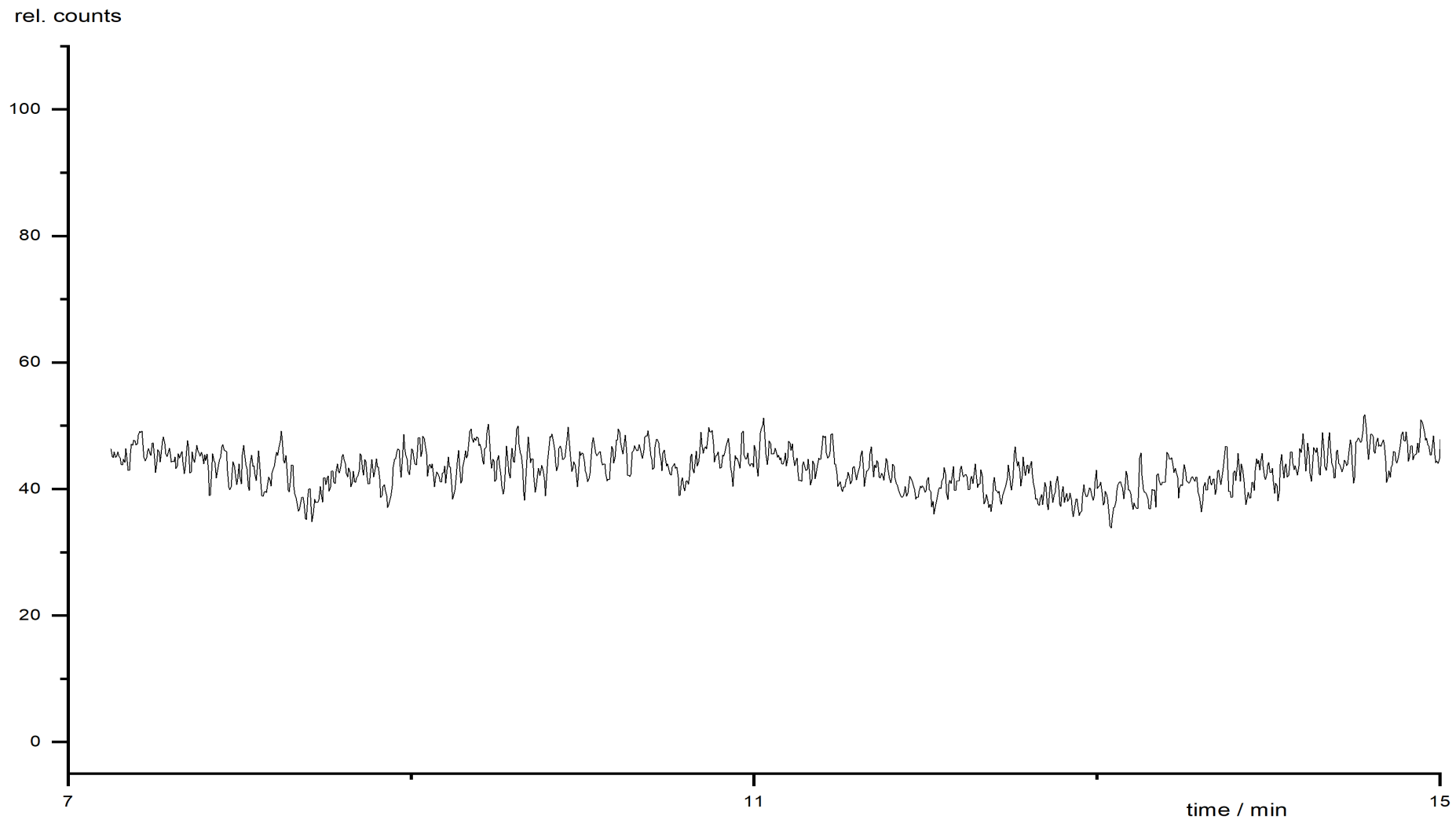


Figure 194: Gas chromatogram of RED\_15.

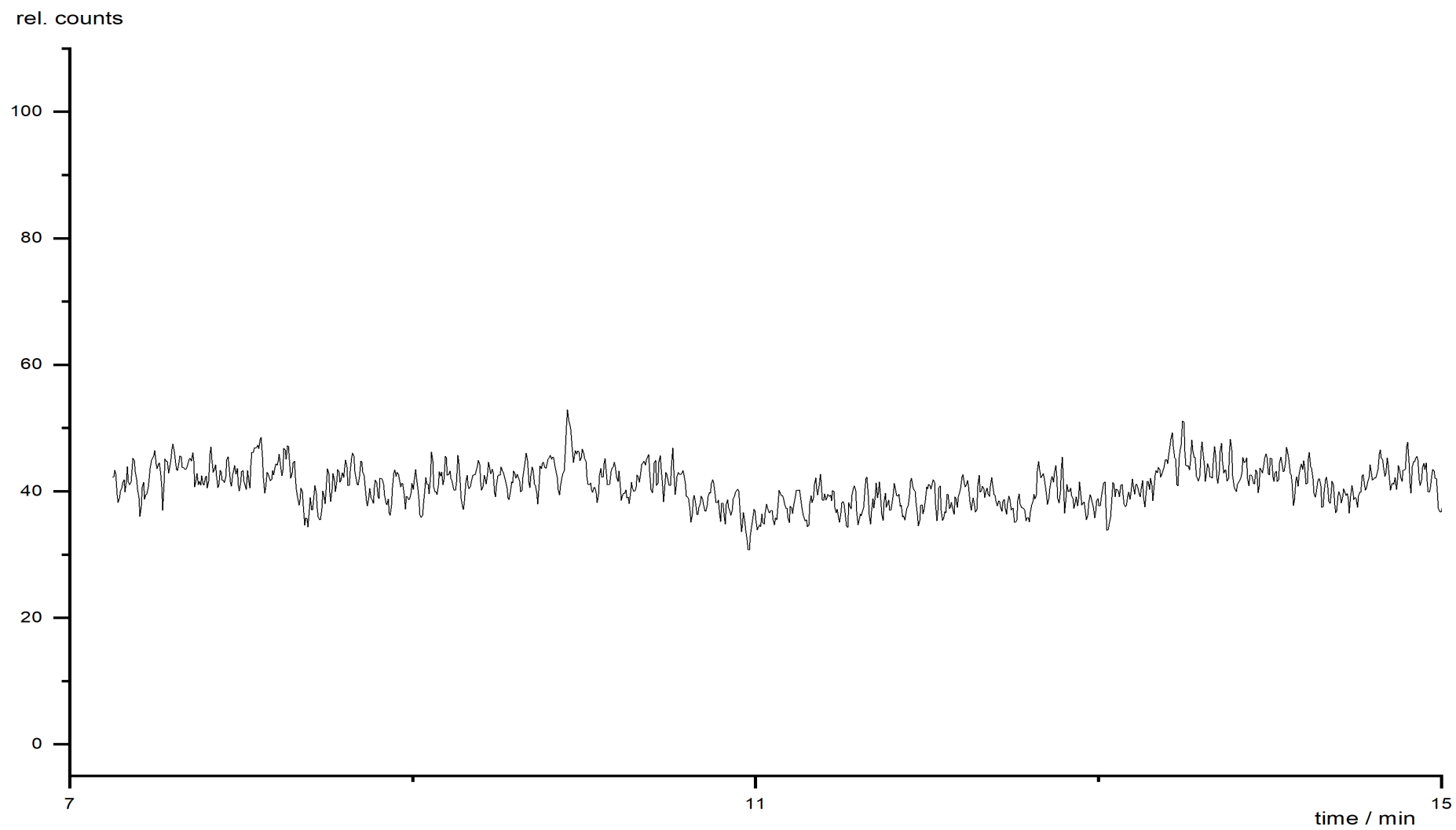


Figure 195: Gas chromatogram of RED\_16.

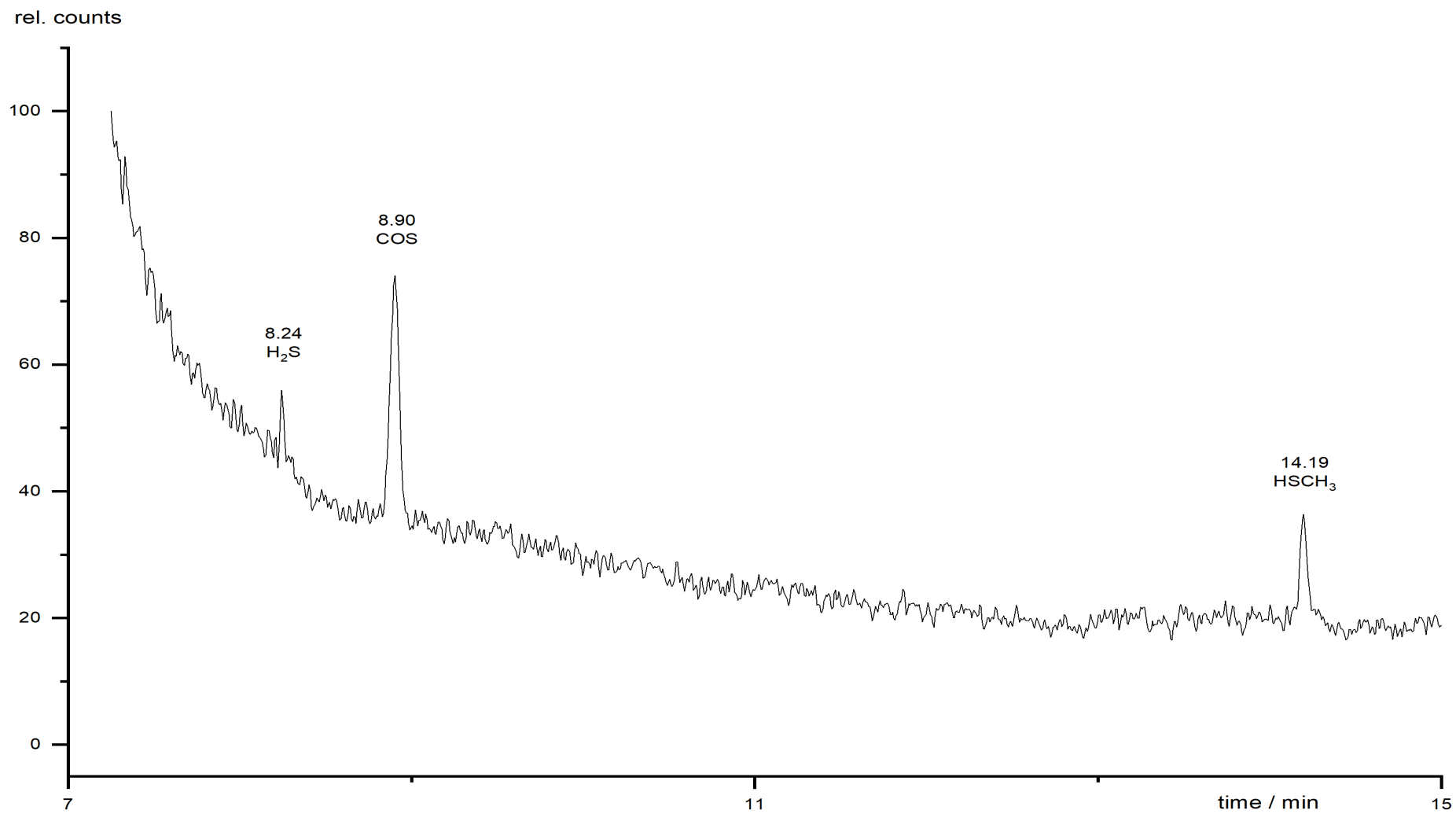


Figure 196: Gas chromatogram of RED\_17.

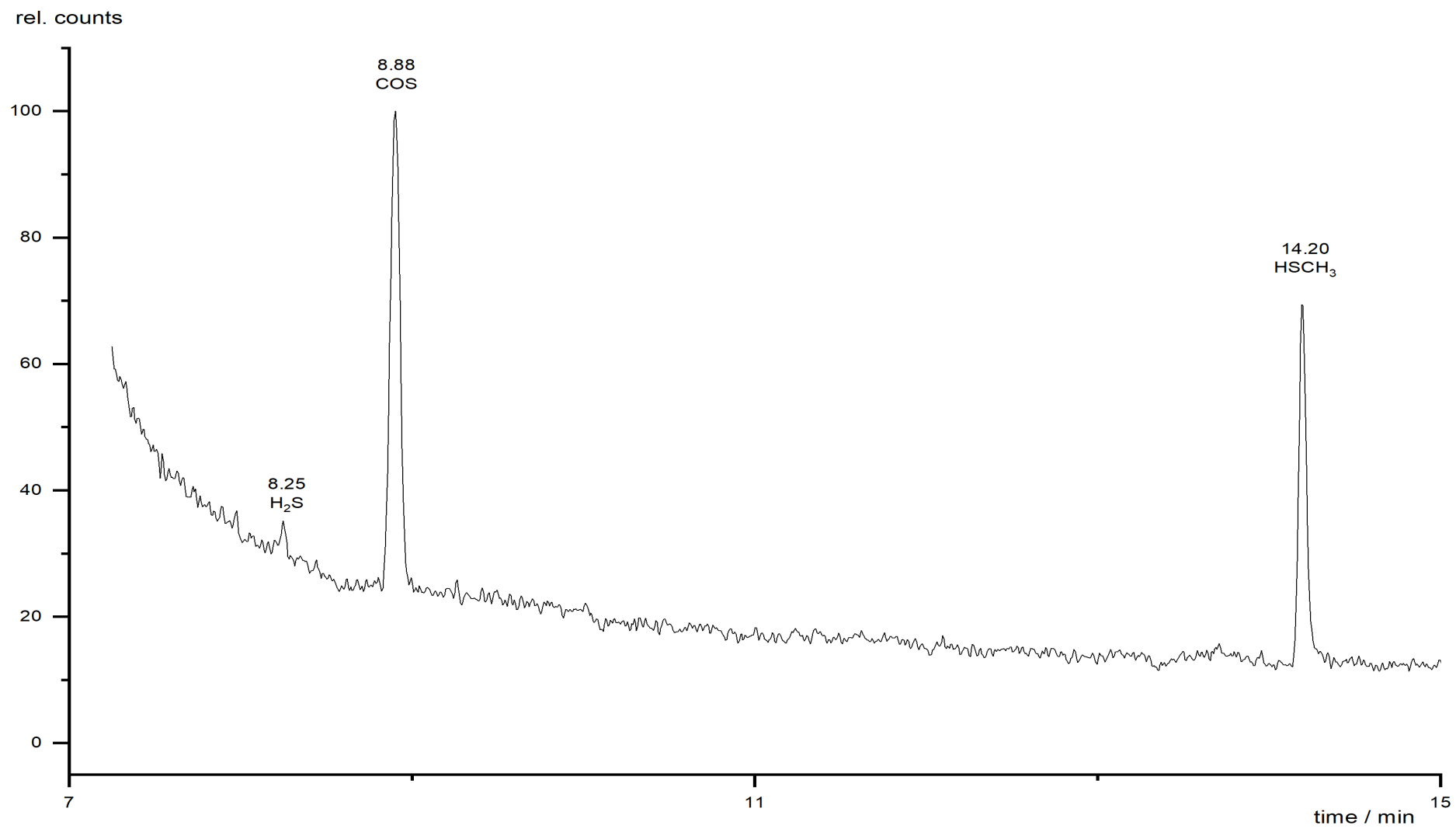


Figure 197: Gas chromatogram of RED\_18.

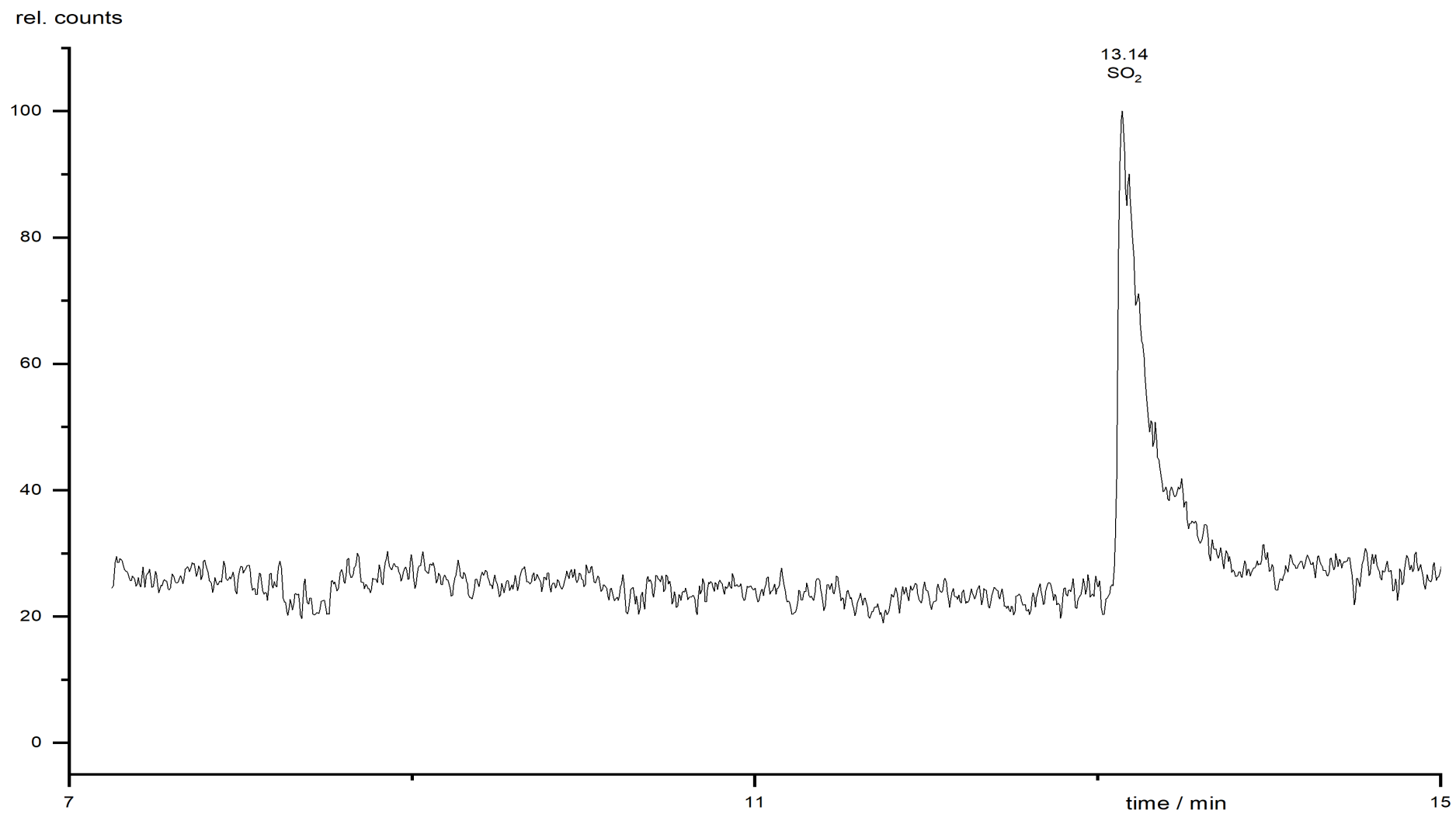


Figure 198: Gas chromatogram of RED\_19.

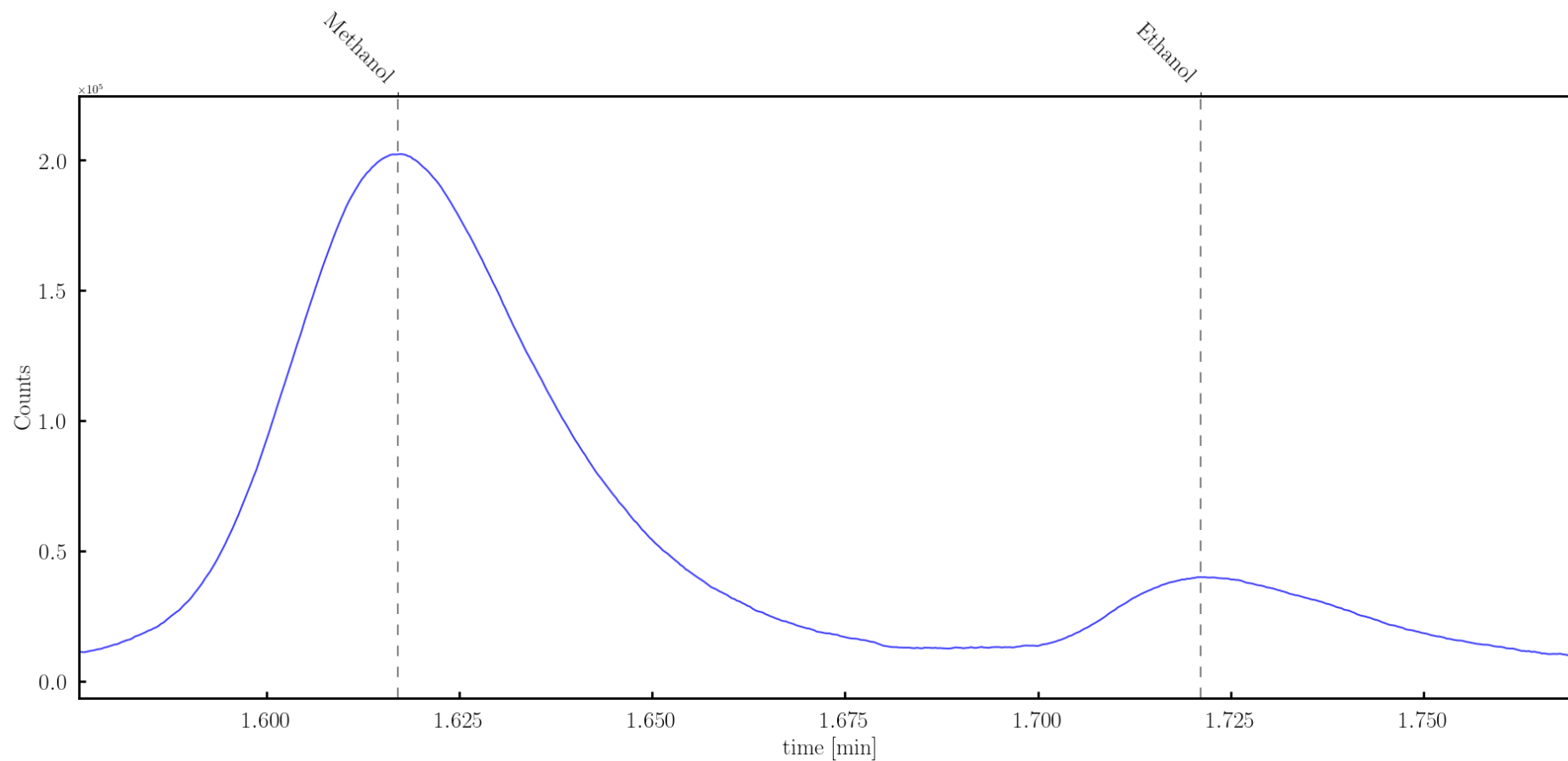


Figure 199: Gas chromatogram of Toch\_Red\_1.



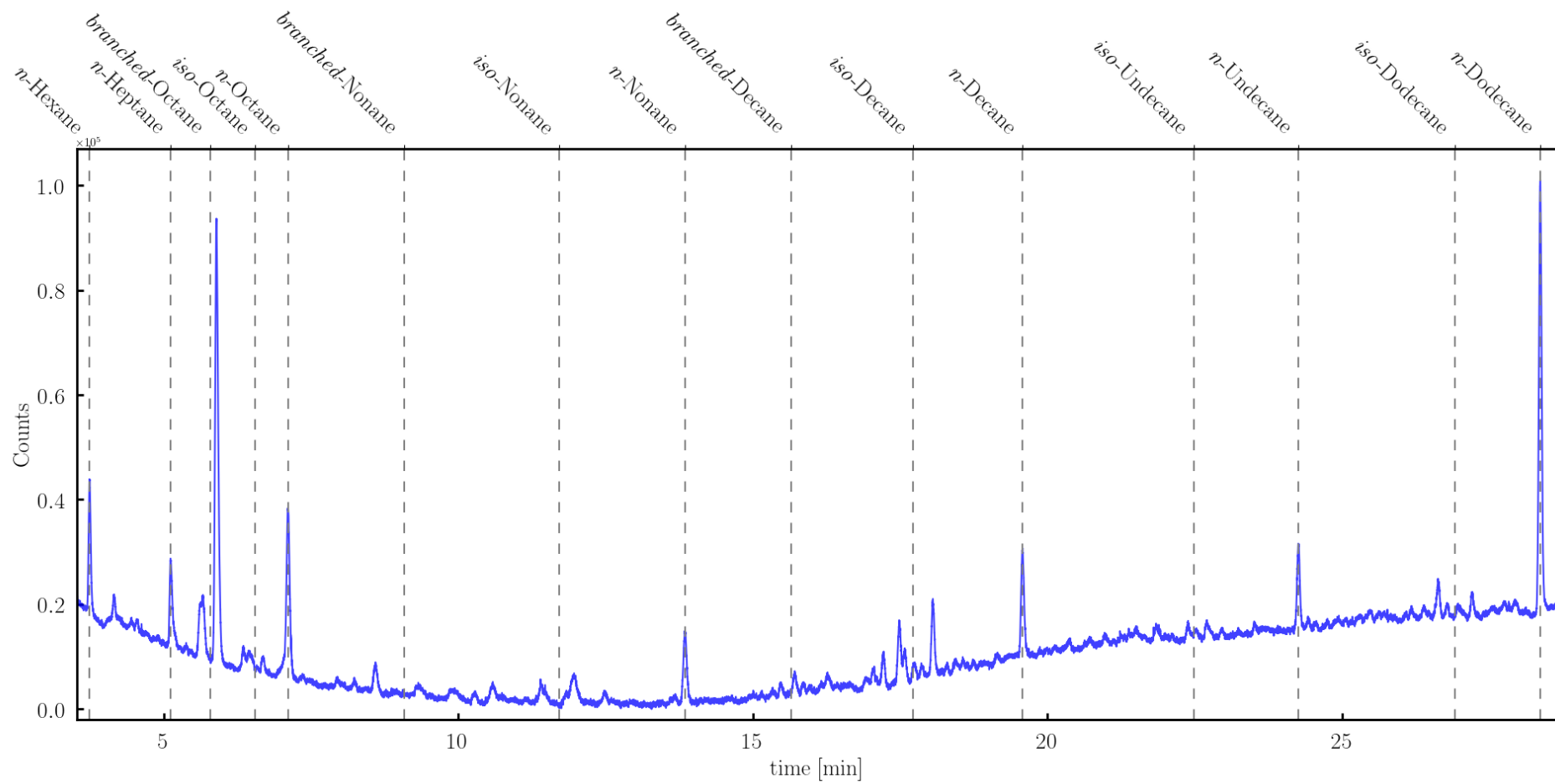


Figure 200: Gas chromatogram of Toch\_Red\_1.

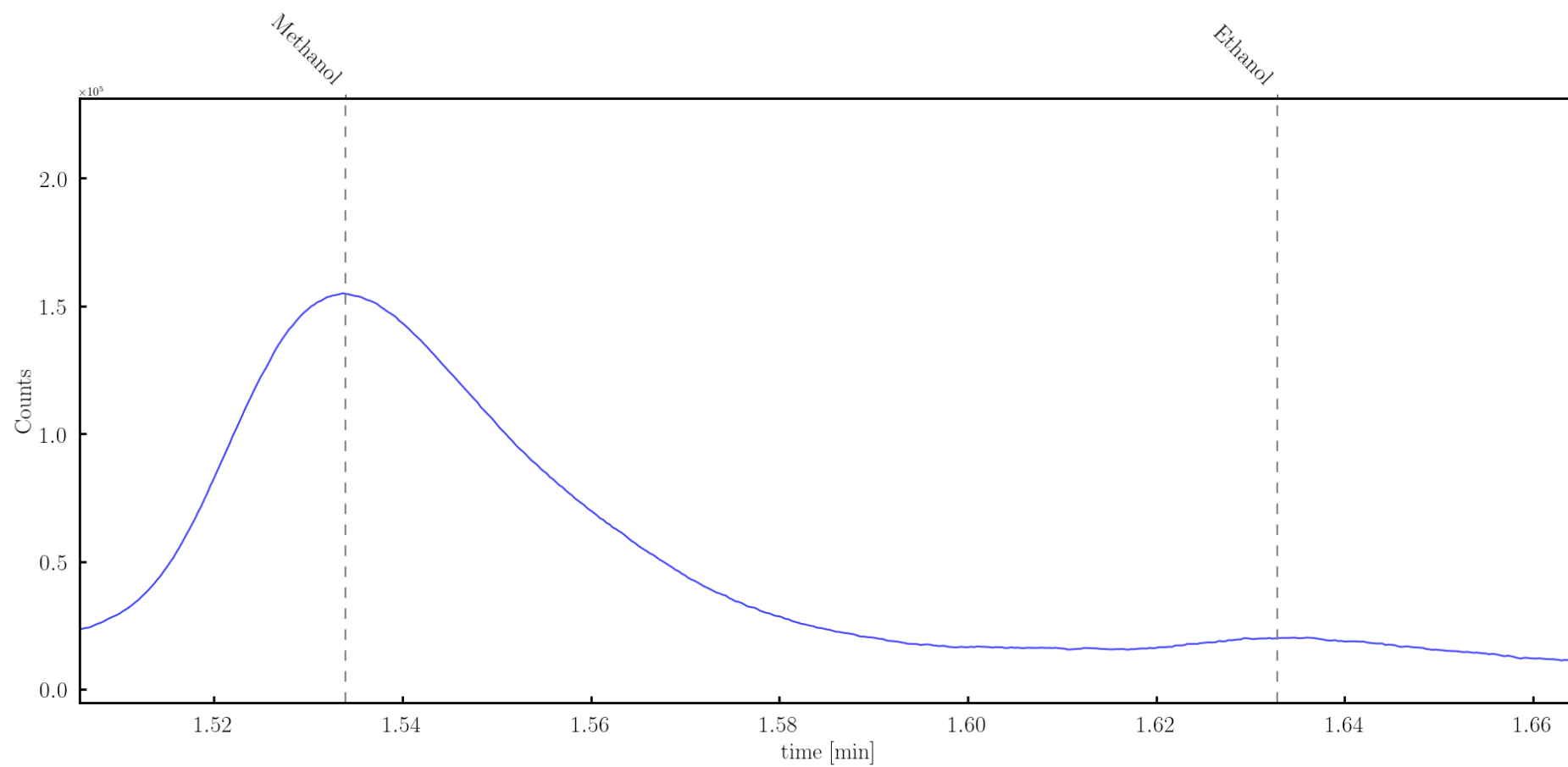


Figure 201: Gas chromatogram of Toch\_Red\_2.

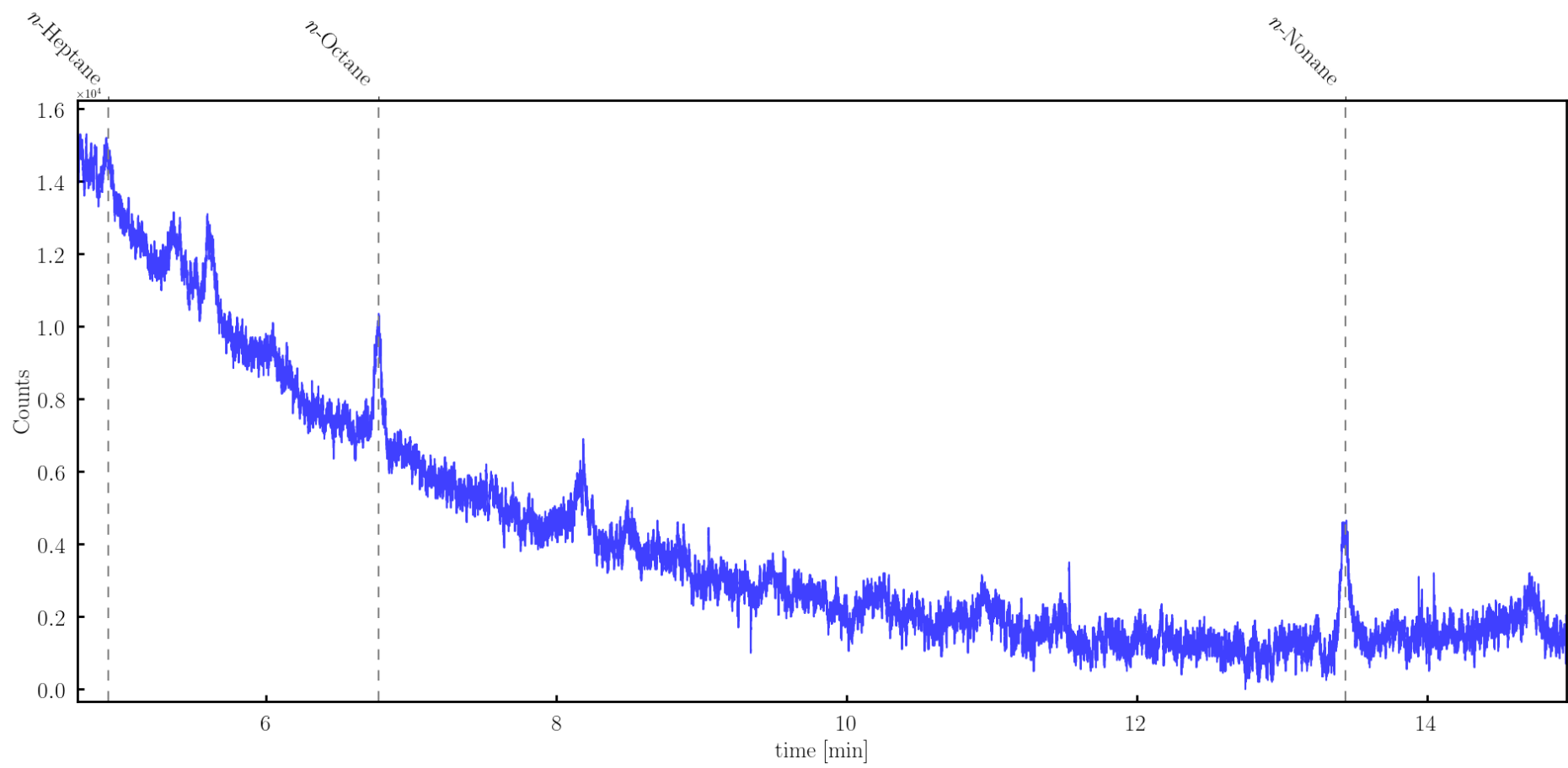


Figure 202: Gas chromatogram of Toch\_Red\_2.

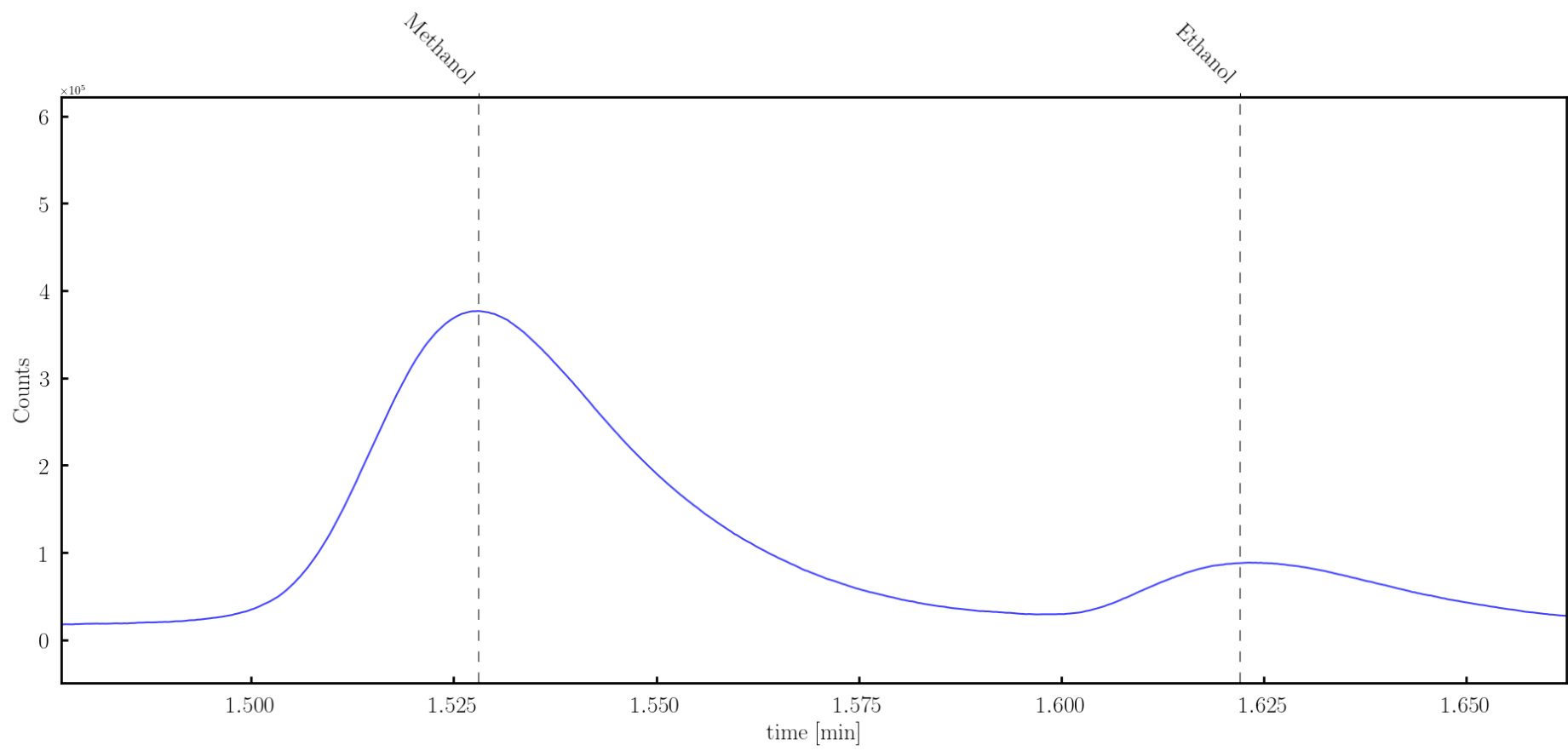


Figure 203: Gas chromatogram of Toch\_Red\_3.

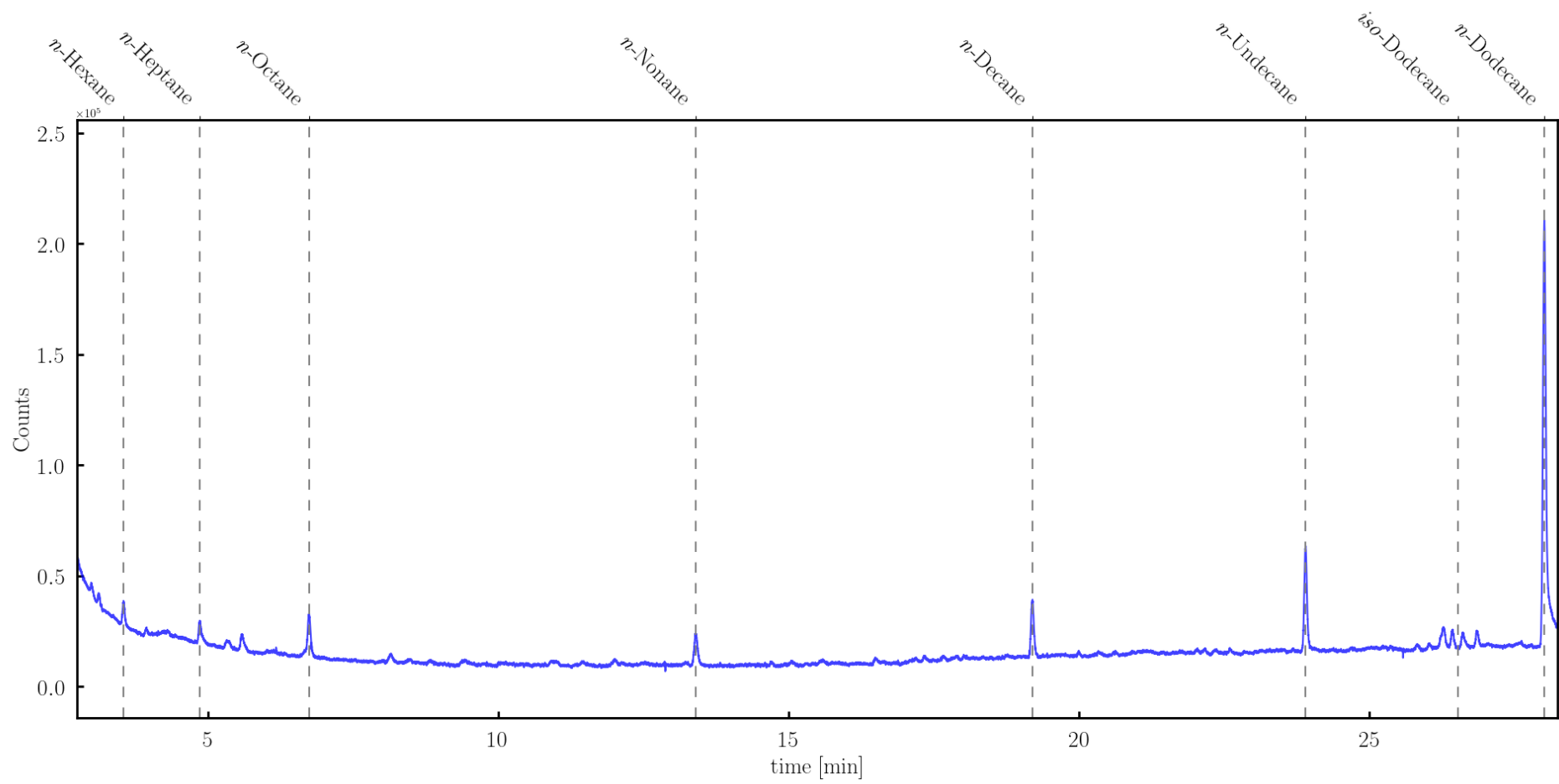


Figure 204: Gas chromatogram of Toch\_Red\_3.

## References

- 1 D. Rickard and G. W. Luther, *Chem. Rev.*, 2007, **107**, 514–562.
- 2 W. Davison, *Aquat. Sci.*, 1991, **53**, 309–329.
- 3 D. Rickard, M. A. A. Schoonen and G. W. Luther III., *Geochemical Transform. Sediment. sulfur.*, 1995, 168–193.
- 4 G. Brostigen, A. Kjekshus, E. E. Astrup, V. Nordal, A. A. Lindberg and J. C. Craig, *Acta Chem. Scand.*, 1969, **23**, 2186–2188.
- 5 M. A. A. Schoonen, *Spec. Pap. 379 Sulfur Biogeochem. - Past Present*, 2007, 117–134.
- 6 E. Drobner, H. Huber, G. Wächtershäuser, D. Rose and K. O. Stetter, *Nature*, 1990, **346**, 742–744.
- 7 D. T. Rickard, M. A. A. Schoonen and G. W. Luther, *Geochemical Transform. Sediment. sulfur.*, 1995, **61**, 168–193.
- 8 A. R. Lennie, S. A. T. Redfern, P. E. Champness, C. P. Stoddart, P. F. Schofield and D. J. Vaughan, *Am. Mineral.*, 1997, **82**, 302–309.
- 9 R. T. Wilkin; H. L. Barnes, *Geochim. Cosmochim. Acta*, 1996, **60**, 4167–4179.
- 10 S. Hunger and L. G. Benning, *Geochem. Trans.*, 2007, **8**, 1–20.
- 11 R. A. D. Patrick, V. S. Coker, M. Akhtar, M. A. Malik, E. Lewis, S. Haigh, P. O'Brien, P. C. Shafer and G. van der Laan, *Mineral. Mag.*, 2017, **81**, 857–872.
- 12 U.-P. Apfel and W. Weigand, *Angew. Chemie Int. Ed.*, 2011, **50**, 4262–4264.
- 13 M. J. Russell and W. Martin, *Trends Biochem. Sci.*, 2004, **29**, 358–363.
- 14 L. M. White, R. Bhartia, G. D. Stucky, I. Kanik and M. J. Russell, *Earth Planet. Sci. Lett.*, 2015, **430**, 105–114.
- 15 A. Roldan, N. Hollingsworth, A. Roffey, H. U. Islam, J. B. M. Goodall, C. R. A. Catlow, J. A. Darr, W. Bras, G. Sankar, K. B. Holt, G. Hogarth and N. H. De Leeuw, *Chem. Commun.*, 2015, **51**, 7501–7504.
- 16 M. Preiner, K. Igarashi, K. B. Muchowska, M. Yu, S. J. Varma, K. Kleinermanns, M. K. Nobu, Y. Kamagata, H. Tüysüz, J. Moran and W. F. Martin, *Nat. Ecol. Evol.*, 2020, **4**, 534–542.
- 17 R. C. Erd, H. T. Evans and D. H. Richter, *Am. Mineral.*, 1957, **42**, 309–333.
- 18 P. Rochette, J. P. Lorand, G. Fillion and V. Sautter, *Earth Planet. Sci. Lett.*, 2001, **190**, 1–12.
- 19 A. R. Lennie, K. E. R. England and D. J. Vaughan, *Am. Mineral.*, 1995, **80**, 960–967.
- 20 J. P. R. De Villiers and D. C. Liles, *Am. Mineral.*, 2010, **95**, 148–152.
- 21 D. M. Roberts, A. R. Landin, T. G. Ritter, J. D. Eaves and C. R. Stoldt, *Sci. Rep.*, 2018, **8**, 1–10.
- 22 R. Skála, I. Císařová and M. Drábek, *Am. Mineral.*, 2006, **91**, 917–921.
- 23 A. R. Lennie, S. A. T. Redfern, P. F. Schofield and D. J. Vaughan, *Mineral. Mag.*, 1995, **59**, 677–683.

- 24 D. Csákberényi-Malasics, J. D. Rodriguez-Blanco, V. K. Kis, A. Rečnik, L. G. Benning and M. Pósfai, *Chem. Geol.*, 2012, **294 + 295**, 249–258.
- 25 J. Zavašnik, N. Stanković, S. M. Arshad and A. Rečnik, *J. Nanoparticle Res.*, , DOI:10.1007/s11051-013-2223-z.
- 26 G. Schmitt, *Corrosion*, 1991, **47**, 285–308.
- 27 Y. Liu, Z. Zhang, N. Bhandari, Z. Dai, F. Yan, G. Ruan, A. Y. Lu, G. Deng, F. Zhang, H. Al-Saiari, A. T. Kan and M. B. Tomson, *Ind. Eng. Chem. Res.*, 2017, **56**, 9016–9027.
- 28 D. Rickard, *Geochim. Cosmochim. Acta*, 2006, **70**, 5779–5789.
- 29 J. A. Bourdoiseau, M. Jeannin, C. Rémazeilles, R. Sabot and P. Refait, *J. Raman Spectrosc.*, 2011, **42**, 496–504.
- 30 M. Mullet, S. Boursiquot, M. Abdelmoula, J. M. Génin and J. J. Ehrhardt, *Geochim. Cosmochim. Acta*, 2002, **66**, 829–836.
- 31 S. Mustafa, D. Misbahud, Y. H. Sammad, M. I. Zaman and K. Sadullah, *Chinese J. Chem.*, 2010, **28**, 1153–1158.
- 32 R. T. Wilkin and D. G. Beak, *Chem. Geol.*, 2017, **462**, 15–29.
- 33 C. A. Coles, S. R. Rao and R. N. Yong, *Environ. Sci. Technol.*, 2000, **34**, 996–1000.
- 34 Y. Lan, A. S. Elwood Madden and E. C. Butler, *Environ. Sci. Process. Impacts*, 2016, **18**, 1266–1273.
- 35 J. Fan, L. Gu, D. Wu and Z. Liu, *Chem. Eng. J.*, 2018, **333**, 657–664.
- 36 D. G. Desai, S. S. Swami, S. K. Dabhade and M. G. Ghagare, *Synth. Commun.*, 2001, **31**, 1249–1251.
- 37 U. Pachmayr, N. Fehn and D. Johrendt, *Chem. Commun.*, 2016, **52**, 194–197.
- 38 X. Zhou, C. Eckberg, B. Wilfong, S. C. Liou, H. K. Vivanco, J. Paglione and E. E. Rodriguez, *Chem. Sci.*, 2017, **8**, 3781–3788.
- 39 Y. Peng, L. Xu, G. Xi, C. Zhong, J. Lu, Z. Meng, G. Li, S. Zhang, G. Zhang and Y. Qian, *Geochim. Cosmochim. Acta*, 2007, **71**, 2858–2875.
- 40 X. Lai, H. Zhang, Y. Wang, X. Wang, X. Zhang, J. Lin and F. Huang, *J. Am. Chem. Soc.*, 2015, **137**, 10148–10151.
- 41 X. Lai, Z. Lin, K. Bu, X. Wang, H. Zhang, D. Li, Y. Wang, Y. Gu, J. Lin and F. Huang, *RSC Adv.*, 2016, **6**, 81886–81893.
- 42 D. D. MacDonald, B. Roberts and J. B. Hyne, *Corros. Sci.*, 1978, **18**, 411–425.
- 43 G.J.Vandentop, M. A. Karolewski and R.G.Cavell, *Surf. Sci.*, 1988, **202**, 457–471.
- 44 M. Jayalakshmi and V. S. Muralidharan, *Corrosion*, 1992, **48**, 918–923.
- 45 N. I. Dowling, *Proc. Int. Symp. Mater. Perform. Sulphur Energy*, 1992, **XXIX**, 1–16.
- 46 P. Marcus and H. Talah, *Corros. Sci.*, 1989, **29**, 455–463.
- 47 R. H. Jones, D. R. Baer, C. F. Windisch Jr. and R. B. Rebak, *NACE - Int. Corros. Conf. Ser.*
- 48 S. H. Jeon, S. T. Kim, I. S. Lee and Y. S. Park, *Corros. Sci.*, 2010, **52**, 3537–3547.
- 49 Z. Liu, X. Gao, L. Du, J. Li, P. Li, X. Bai and R. D. K. Misra, *J. Mater. Eng. Perform.*, 2017,

26, 1010–1017.

- 50 A. J. Bard, R. Parsons and J. Jordan, *Standard Potentials in Aqueous Solution*, New York, 1st edn., 2017.
- 51 D. Renock, T. Gallegos, S. Utsunomiya, K. Hayes, R. C. Ewing and U. Becker, *Chem. Geol.*, 2009, **268**, 116–125.
- 52 J. Zhou, S. Chen, J. Liu and R. L. Frost, *Chem. Eng. J.*, 2018, **354**, 237–244.
- 53 N. Y. Dzade, A. Roldan and N. H. De Leeuw, *Environ. Sci. Technol.*, 2017, **51**, 3461–3470.
- 54 T. Arakaki and J. W. Morse, *Geochim. Cosmochim. Acta*, 1993, **57**, 9–14.
- 55 J. W. Morse and T. Arakaki, *Geochim. Cosmochim. Acta*, 1993, **57**, 3635–3640.
- 56 A. M. WIDLER and T. M. SEWARD, *Geochim. Cosmochim. Acta*, 2002, **66**, 383–402.
- 57 M. Wolthers, L. Charlet, P. R. van Der Linde, D. Rickard and C. H. van Der Weijden, *Geochim. Cosmochim. Acta*, 2005, **69**, 3469–3481.
- 58 O. Yépez, N. Obeyesekere and J. Wylde, *NACE - Int. Corros. Conf. Ser.*, 2017, **8**, 5218–5232.
- 59 J. W. Morse and G. W. Luther, *Geochim. Cosmochim. Acta*, 1999, **63**, 3373–3378.
- 60 B. Hatton and D. Rickard, *Orig. Life Evol. Biosph.*, 2008, **38**, 257–270.
- 61 A. Picard, A. Gartman, J. Cosmidis, M. Obst, C. Vidoudez, D. R. Clarke and P. R. Girguis, *Chem. Geol.*, , DOI:10.1016/j.chemgeo.2019.119343.
- 62 N. Y. Dzade, A. Roldan and N. H. De Leeuw, *J. Chem. Phys.*, , DOI:10.1063/1.4822040.
- 63 E. D. Horowitz, A. E. Engelhart, M. C. Chen, K. A. Quarles, M. W. Smith, D. G. Lynn and N. V. Hud, *Proc. Natl. Acad. Sci. U. S. A.*, 2010, **107**, 5288–5293.
- 64 X. Lai, X. Chen, S. Jin, G. Wang, T. Zhou, T. Ying, H. Zhang, S. Shen and W. Wang, *Inorg. Chem.*, 2013, **52**, 12860–12862.
- 65 H. Lin, R. Z. Kang, L. Kong, X. Y. Zhu and H. H. Wen, *Sci. China Physics, Mech. Astron.*, , DOI:10.1007/s11433-016-0464-3.
- 66 X. Dong, H. Zhou, H. Yang, J. Yuan, K. Jin, F. Zhou, D. Yuan, L. Wei, J. Li, X. Wang, G. Zhang and Z. Zhao, *J. Am. Chem. Soc.*, 2015, **137**, 66–69.
- 67 D. Wu, Z. Guo, N. Liu, L. Zhou, Y. Mao, L. Wan, F. Sun and W. Yuan, *Inorg. Chem. Commun.*, 2018, **91**, 72–76.
- 68 J. Almog, J. E. Baldwin, R. L. Dyer and M. Peters, *J. Am. Chem. Soc.*, 1975, **97**, 226–227.
- 69 C. Huber and G. Wächtershäuser, *Tetrahedron Lett.*, 2003, **44**, 1695–1697.
- 70 D. Rickard, *Geochim. Cosmochim. Acta*, 2006, **70**, A533.
- 71 H. Y. Jeong, J. H. Lee and K. F. Hayes, *Geochim. Cosmochim. Acta*, 2008, **72**, 493–505.
- 72 S. Maruyama, K. Kurokawa, T. Ebisuzaki, Y. Sawaki, K. Suda and M. Santosh, *Geosci. Front.*, 2019, **10**, 1337–1357.
- 73 Y. Peng and Y. Jing, *Earth Planet. Sci. Lett.*, 2014, **408**, 252–262.
- 74 M. R. Lee, B. E. Cohen, A. J. King and R. C. Greenwood, *Geochim. Cosmochim. Acta*, 2019, **264**, 224–244.
- 75 L. B. Browning and W. L. Bourcier, in *Lunar and Planetary Science XXVII*, 1996, pp. 171–



172.

- 76 N. I. Organova, V. A. Drits and A. L. Dmitrik, *Sov. Phys. Crystallogr.*, 1974, **18**, 606–609.
- 77 N. I. Organova, V. A. Drits and A. L. Dmitrik, *Sov. Phys. Crystallogr.*, 1974, **18**, 606–609.
- 78 N. I. Organova, *Am. Mineral.*, 1974, **59**, 190–200.
- 79 M. Mookherjee and L. Stixrude, *Am. Mineral.*, 2006, **91**, 127–134.
- 80 D. C. Harris and D. J. Vaughan, *American Mineral.*, 1972, **57**, 1037–1052.
- 81 J. L. Jambor, *Geol. Surv. Canada*, **76**, 65–69.
- 82 Y. Muramatsu and M. Nambu, *J. Japan. Assoc. Min. Petr. Econ. Geol.*, 1980, **75**, 377–384.
- 83 I. V. Pekov, E. V. Sereba, Y. S. Polekhovskiy, S. N. Britvin, N. V. Chukanov, V. O. Yapaskurt and I. A. Bryzgalov, *Geol. Ore Depos.*, 2013, **55**, 567–574.
- 84 H. T. Evans, *Zeitschrift für Krist. - New Cryst. Struct.*, 1968, **127**, 73–93.
- 85 Y. Moelo, O. Rouer, L. Cario, B. Cervelle and Y. LO Moe Etal, *Mineral. Mag.*, 1999, **63**, 879–889.
- 86 M. Huhma, Y. Vuorelainen, T. A. Häkli and H. Papunen, *Bull. Geol. Soc. Finl.*, 1973, **45**, 103–106.
- 87 I. V. Pekov, V. O. Yapaskurt, Y. S. Polekhovskiy, M. F. Viggasina and O. I. Siidra, *Mineral. Mag.*, 2014, **78**, 663–679.
- 88 W. Wang, S. Wang, X. Ma and J. Gong, *Chem. Soc. Rev.*, 2011, **40**, 3703–3727.
- 89 Y. N. Gao, S. Liu, Z. Zhao, H. C. Tao and Z. Y. Sun, *Wuli Huaxue Xuebao/ Acta Phys. - Chim. Sin.*, 2018, **34**, 858–872.
- 90 M. Ronda-Lloret, G. Rothenberg and N. R. Shiju, *ChemSusChem*, 2019, **12**, 3896–3914.
- 91 L. G. Dodson, M. C. Thompson and J. M. Weber, *Annu. Rev. Phys. Chem.*, 2018, **69**, 231–252.
- 92 K. J. P. Schouten, E. Pérez Gallent and M. T. M. Koper, *J. Electroanal. Chem.*, 2014, **716**, 53–57.
- 93 X. Nie, M. R. Esopi, M. J. Janik and A. Asthagiri, *Angew. Chemie*, 2013, **125**, 2519–2522.
- 94 T. Riedel, G. Schaub, K. W. Jun and K. W. Lee, *Ind. Eng. Chem. Res.*, 2001, **40**, 1355–1363.
- 95 D. Gao, R. M. Arán-Ais, H. S. Jeon and B. Roldan Cuenya, *Nat. Catal.*, 2019, **2**, 198–210.
- 96 J. Zhong, X. Yang, Z. Wu, B. Liang, Y. Huang and T. Zhang, *Chem. Soc. Rev.*, 2020, **49**, 1385–1413.
- 97 J. Halpern, *Adv. Catal.*, 1959, **11**, 301–370.
- 98 D. D. Eley, *Adv. Catal.*, 1948, **1**, 157–199.
- 99 D. Huang, M. Wen, C. Zhou, Z. Li, M. Cheng, S. Chen, W. Xue, L. Lei, Y. Yang, W. Xiong and W. Wang, *Appl. Catal. B Environ.*, 2020, **267**, 1–14.
- 100 W. Martin, M. J. Russell, D. Horner, R. Blankenship, T. Cavalier-Smith and E. Nisbet, in *Philosophical Transactions of the Royal Society B: Biological Sciences*, Royal Society, 2003, vol. 358, pp. 59–85.
- 101 M.J.Russel, A.J.Hall and A. J. B. A.E.Fallick, *Bull. Soc. Econ. Geol.*, 2005, **100**, 419–438.

- 102 E. Camprubí, J. W. de Leeuw, C. H. House, F. Raulin, M. J. Russell, A. Spang, M. R. Tirumalai and F. Westall, *Space Sci. Rev.*, 2019, **215**, 1–53.
- 103 E. L. Shock, *Orig. Life Evol. Biosph.*, 1992, **22**, 67–107, 191–242.
- 104 T. M. McCollom and J. S. Seewald, *Elements*, 2013, **9**, 129–134.
- 105 N. G. Holm, C. Oze, O. Mousis, J. H. Waite and A. Guilbert-Lepoutre, *Astrobiology*, 2015, **15**, 587–600.
- 106 B. Deng, T. J. Campbell and D. R. Burris, *Environ. Sci. Technol.*, 1997, **31**, 1185–1190.
- 107 L. I. Hardy and R. W. Gillham, *Environ. Sci. Technol.*, 2002, **30**, 57–65.
- 108 T. M. McCollom and J. S. Seewald, *Earth Planet. Sci. Lett.*, 2006, **243**, 74–84.
- 109 J. A. Chamberlain, C. R. McLeod, R. J. Traill and G. R. Lachance, *Can. J. Earth Sci.*, 1965, **2**, 188–215.
- 110 E. M. Schwarzenbach, E. Gazel and M. J. Caddick, *Contrib. to Mineral. Petrol.*, 2014, **168**, 1–21.
- 111 L. M. Barge, E. Flores, M. M. Baum, D. G. V. Velde and M. J. Russell, *Proc. Natl. Acad. Sci. U. S. A.*, 2019, **116**, 4828–4833.
- 112 S. J. Varma, K. B. Muchowska, P. Chatelain and J. Moran, *Nat. Ecol. Evol.*, 2018, **2**, 1019–1024.
- 113 N. Kitadai and S. Maruyama, *Geosci. Front.*, 2018, **9**, 1117–1153.
- 114 D. I. Foustoukos and W. E. Seyfried, *Science (80-. )*, 2004, **304**, 1002–1005.
- 115 G. Wächtershäuser, *Prog. Biophys. Mol. Biol.*, 1992, **58**, 85–201.
- 116 I. B. Butler and D. Rickard, *Geochim. Cosmochim. Acta*, 2000, **64**, 2665–2672.
- 117 W. Lubitz, H. Ogata, O. Rüdiger and E. Reiijerse, *Chem. Rev.*, 2014, **114**, 4081–4148.
- 118 E. Camprubi, S. F. Jordan, R. Vasiliadou and N. Lane, *IUBMB Life*, 2017, **69**, 373–381.
- 119 S. W. Ragsdale and M. Kumar, *Chem. Rev.*, 1996, **96**, 2515–2540.
- 120 F. Möller, S. Piontek, R. G. Miller and U. P. Apfel, *Chem. - A Eur. J.*, 2018, **24**, 1471–1493.
- 121 B. M. Hoffman, D. Lukoyanov, Z. Y. Yang, D. R. Dean and L. C. Seefeldt, *Chem. Rev.*, 2014, **114**, 4041–4062.
- 122 F. Zhang and C. Li, *Lect. Notes Energy*, 2016, **32**, 299–317.
- 123 N. Y. Dzade, A. Roldan and N. H. De Leeuw, *Phys. Chem. Chem. Phys.*, 2014, **16**, 15444–15456.
- 124 N. Y. Dzade, A. Roldan and N. H. De Leeuw, *J. Chem. Phys.*, 2015, **143**, 1–8.
- 125 N. Y. Dzade, A. Roldan and N. H. De Leeuw, *J. Chem. Phys.*, , DOI:10.1063/1.4947588.
- 126 D. Rickard, A. Griffith, A. Oldroyd, I. B. Butler, E. Lopez-Capel, D. A. C. C. Manning and D. C. Apperley, *Chem. Geol.*, 2006, **235**, 286–298.
- 127 S. P. Abramov, *J. Alloys Compd.*, 1997, **259**, 212–218.
- 128 W. Heinen and A. M. Lauwers, *Orig. Life Evol. Biosph.*, 1996, **26**, 131–150.
- 129 R. W. Cheary and A. Coelho, *J. Appl. Crystallogr.*, 1992, **25**, 109–121.

- 130 Robert A. Berner, *J. Geol.*, 1964, **72**, 293–306.
- 131 A. Matamoros-Veloza, O. Cespedes, B. R. G. Johnson, T. M. Stawski, U. Terranova, N. H. de Leeuw and L. G. Benning, *Nat. Commun.*, DOI:10.1038/s41467-018-05493-x.
- 132 A. Matamoros-Veloza, T. M. Stawski and L. G. Benning, *Cryst. Growth Des.*, 2018, **18**, 6757–6764.
- 133 R. Guilbaud, I. B. Butler, R. M. Ellam and D. Rickard, *Earth Planet. Sci. Lett.*, 2010, **300**, 174–183.
- 134 M. Wolthers, I. B. Butler and D. Rickard, *Chem. Geol.*, 2007, **236**, 217–227.
- 135 N. G. Harmandas and P. O. Koutsoukos, *J. Cryst. Growth*, 1996, **167**, 719–724.
- 136 N. Lémercy, *Mémoires mathématique Phys. l'Académie R. des Sci.*
- 137 N. Alsen, *Geol. Föreninges*, 1923, **1**, 606–607.
- 138 J.S. Smith and J.D.A. Miller, *Br. Corros. J.*, 1975, **10**, 136–143.
- 139 F. Li, M. An, G. Liu and D. Duan, *Mater. Chem. Phys.*, 2009, **113**, 971–976.
- 140 H. Liu, S. Zhao, Z. Xie, K. Zhu, X. Xu, X. Ding and A. Glowacz, *Powder Technol.*, 2018, **339**, 296–305.
- 141 Z. Asaki and Y. Kondo, *J. Therm. Anal.*, 1989, **35**, 1751–1759.
- 142 Z. Dou, J. C. Jiang, S. P. Zhao, G. B. Mao, M. G. Zhang, L. Wang and Z. R. Wang, *J. Loss Prev. Process Ind.*, 2015, **38**, 156–162.
- 143 S. Boursiquot, M. Mullet, M. Abdelmoula, J.-M. Génin and J. J. Ehrhardt, *Phys. Chem. Miner.*, 2001, **28**, 600–611.
- 144 Z. Asaki, T. Atsumi and Y. Kondo, *Trans. Japan Inst. Met.*, 1986, **27**, 351–360.
- 145 J. Zhu, H. Xian, X. Lin, H. Tang, R. Du, Y. Yang, R. Zhu, X. Liang, J. Wei, H. H. Teng and H. He, *Geochim. Cosmochim. Acta*, 2018, **228**, 259–274.
- 146 H. T. Evans Jr., C. Milton, E. T. Chao, I. Adler, C. Mead, B. Ingram and R. A. Berner, *US Geol. Surv. Prof. Pap.*, 1964, 64–69.
- 147 I. T. Sines, D. D. Vaughn, R. Misra, E. J. Popczun and R. E. Schaak, *J. Solid State Chem.*, 2012, **196**, 17–20.
- 148 D. T. Rickard, *Stock. Contrib. Geol.*, 1969, **20**, 65–95.
- 149 A. R. Lennie, S. A. T. Redfern, P. F. Schofield and D. J. Vaughan, *Mineral. Mag.*, 1995, **59**, 677–683.
- 150 M. Mullet, S. Boursiquot, M. Abdelmoula, J.-M. M. Génin, J.-J. J. Ehrhardt, M. Mullet, J.-J. J. Ehrhardt, J.-M. M. Génin, S. Boursiquot, M. Abdelmoula, J.-M. M. Génin, J.-J. J. Ehrhardt, M. Mullet, J.-J. J. Ehrhardt, J.-M. M. Génin, S. Boursiquot, M. Abdelmoula, J.-M. M. Génin, J.-J. J. Ehrhardt, M. Mullet, J.-J. J. Ehrhardt and J.-M. M. Génin, *Geochim. Cosmochim. Acta*, 2002, **66**, 829–836.
- 151 H. Ohfujii and D. Rickard, *Earth Planet. Sci. Lett.*, 2006, **241**, 227–233.
- 152 J. A. Bourdoiseau, M. Jeannin, R. Sabot, C. Rémazeilles and P. Refait, *Corros. Sci.*, 2008, **50**, 3247–3255.
- 153 D. Rickard, *The chemistry of iron sulphide formation at low temperatures*, 1969, vol. 20.

- 154 M. Wolthers, S. J. Van Der Gaast and D. Rickard, *Am. Mineral.*, 2003, **88**, 2007–2015.
- 155 F. M. Michel, S. M. Antao, P. J. Chupas, P. L. Lee, J. B. Parise and M. A. A. Schoonen, *Chem. Mater.*, 2005, **17**, 6246–6255.
- 156 D. Rickard, A. Griffith, A. Oldroyd, I. B. Butler, E. Lopez-Capel, D. A. C. Manning and D. C. Apperley, *Chem. Geol.*, 2006, **235**, 286–298.
- 157 D. Csákberényi-Malasics, J. D. Rodriguez-Blanco, V. K. Kis, A. Rečnik, L. G. Benning and M. Pósfai, *Chem. Geol.*, 2012, **294–295**, 249–258.
- 158 R. A. Berner, *Science (80-. )*, 1962, **137**, 669.
- 159 Y. Liu, J. Terry and S. Jurisson, *Radiochim. Acta*, 2008, **96**, 823–833.
- 160 S. L. Miller and H. C. Urey, *Science (80-. )*, 1959, **130**, 245–251.
- 161 G. H. Shaw, *Chemie der Erde*, 2008, **68**, 235–264.
- 162 H. Lammer, A. L. Zerkle, S. Gebauer, N. Tosi, L. Noack, M. Scherf, E. Pilat-Lohinger, M. Güdel, J. L. Grenfell, M. Godolt and A. Nikolaou, *Astron. Astrophys. Rev.*, 2018, **26**, 1–72.
- 163 M. J. de Wit and H. Furnes, *Sci. Adv.*, 2016, **2**, 1–12.
- 164 M. J. Russell and A. J. Hall, *Mem. 198 Evol. Early Earth's Atmos. Hydrosphere, Biosph. - Constraints from Ore Depos.*, 2007, **80301**, 1–32.
- 165 W. E. Wallace, in *NIST Chemistry WebBook*, 2021.
- 166 E. J. Levy and W. A. Stahl, *Anal. Chem.*, 1961, **33**, 707–722.
- 167 B. Z. Cvetković, J. Rothardt, A. Büttler, D. Kunz, G. Schlotterbeck and E. Wieland, *Environ. Eng. Sci.*, 2018, **35**, 447–461.
- 168 E. O. Fetisov, M. S. Shah, C. Knight, M. Tsapatsis and J. I. Siepmann, *ChemPhysChem*, 2018, **19**, 512–518.
- 169 L. Leman, L. Orgel and M. R. Ghadiri, *Abstr. Pap. Am. Chem. Soc.*, 2004, **228**, U693.
- 170 G. A. Kakos, T. W. Turney and T. B. Williams, *J. Solid State Chem.*, 1994, **108**, 102–111.
- 171 S. V. Kozerenko, N. I. Organova, V. V. Fadeev, L. O. Magazina, N. N. Kolpakova and L. A. Kopneva, in *Lunar and Planetary Science XXVII*, 1996, pp. 695–696.
- 172 S. V. Kozerenko, V. V. Fadeev, N. I. Chistyakova, N. N. Kolpakova and V. G. Senin, *Exp. Geosci.*, 2001, **10**, 57–58.
- 173 N. I. Chistyakova, T. V Gubaidulina and V. S. Rusakov, *Czechoslov. J. Phys.*, 2006, **56**, 123–131.
- 174 Y. Peng, G. Xi, C. Zhong, L. Wang, J. Lu, X. Sun, L. Zhu, Q. Han, L. Chen, L. Shi, M. Sun, Q. Li, M. Yu and M. Yin, *Geochim. Cosmochim. Acta*, 2009, **73**, 4862–4878.
- 175 L. G. Vacher, L. Truche, F. Faure, L. Tissandier, R. Mosser-Ruck, Y. Marrocchi, R. Mosser-Ruck and Y. Marrocchi, *Meteorit. Planet. Sci.*, 2019, **54**, 1870–1889.
- 176 Z. Guo, F. Sun, B. Han, K. Lin, L. Zhou and W. Yuan, *Phys. Chem. Chem. Phys.*, 2017, **19**, 9000–9006.
- 177 M. E. Zolensky, *Am. Mineral.*, 1986, **71**, 1201–1209.
- 178 C. Schröder, M. Wan, I. B. Butler, A. Tait, S. Pei and C. A. Mccammon, *Minerals*, 2020, **10**,

- 1–13.
- 179 K. Ruiz-Mirazo, C. Briones and A. De La Escosura, *Chem. Rev.*, 2014, **114**, 285–366.
- 180 V. Erastova, M. T. Degiacomi, D. G. Fraser and H. C. Greenwell, *Nat. Commun.*, 2017, **8**, 1–9.
- 181 M. Frenkel-Pinter, M. Frenkel-Pinter, M. Samanta, G. Ashkenasy, L. J. Leman and L. J. Leman, *Chem. Rev.*, 2020, **120**, 4707–4765.
- 182 M. C. Weiss, F. L. Sousa, N. Mrnjavac, S. Neukirchen, M. Roettger, S. Nelson-Sathi and W. F. Martin, *Nat. Microbiol.*, 2016, **1**, 1–8.
- 183 B. Damer, *Life*, , DOI:10.3390/life6020021.
- 184 A. Y. Mulkidjanian, A. Y. Bychkov, D. V. Dibrova, M. Y. Galperin and E. V. Koonin, *Proc. Natl. Acad. Sci. U. S. A.*, 2012, **109**, E821–E830.
- 185 B. H. Patel, C. Percivalle, D. J. Ritson, C. D. Duffy and J. D. Sutherland, *Nat. Chem.*, 2015, **7**, 301–307.
- 186 B. Damer and D. Deamer, *Astrobiology*, 2020, **20**, 429–452.
- 187 A. Omran and M. Pasek, 2020, 1–8.
- 188 M. A. Pasek, 2006.
- 189 M. A. Pasek, *Geosci. Front.*, 2017, **8**, 329–335.
- 190 C. S. Cockell, *Philos. Trans. R. Soc. B Biol. Sci.*, 2006, **361**, 1845–1856.
- 191 P. A. Bland and N. A. Artemieva, *Meteorit. Planet. Sci.*, 2006, **41**, 607–631.
- 192 V. Chevrier, P. Rochette, P. E. Mathé and O. Grauby, *Geology*, 2004, **32**, 1033–1036.
- 193 A. Gronstal, V. Pearson, A. Kappler, C. Dooris, M. Anand, F. Poitrasson, T. P. Kee and C. S. Cockell, *Meteorit. Planet. Sci.*, 2009, **44**, 233–247.
- 194 J. Hernandez and J. Genesca, 2012, 251–258.
- 195 C. Oppenheimer, *J. Volcanol. Geotherm. Res. Elsevier Sci. Publ. B.V*, 1992, **49**, 1–21.
- 196 Y. A. Bogdanov, A. Y. Lein, V. V. Maslennikov, S. Li and A. A. Ul'yanov, *OCEANOLOGY*, 2008, **45**, 679–700.
- 197 G. D. Cody, N. Z. Boctor, T. R. Filley, R. M. Hazen, J. H. Scott, A. Sharma and J. Yoder, *Science (80-. )*, 2000, **289**, 1337–1339.
- 198 G. D. Cody, N. Z. Boctor, J. A. Brandes, T. R. Filley, R. M. Hazen and H. S. Yoder, *Geochim. Cosmochim. Acta*, 2004, **68**, 2185–2196.
- 199 C. Huber, *Science (80-. )*, 2002, **276**, 245–247.
- 200 D. G. Desai, S. S. Swami and R. S. Nandurdikar, *Synth. Commun.*, 2002, **32**, 931–933.
- 201 H. J. Morowitz, *Geochim. Cosmochim. Acta*, 2001, **65**, 3557–3576.
- 202 E. Blöchl, M. Keller, G. Wächtershäuser and K.O.Stetter, *Proc. Natl. Acad. Sci. U. S. A.*, 1992, **89**, 8117–8120.

## Curriculum vitae

- Since 01/2016      PhD student in the field of prebiotic chemistry at the Friedrich-Schiller-Universität, Jena  
Thesis title: Synthesis of mackinawite and tochilinite analogues and investigations on carbon fixation in a prebiotic context.
- 10/2013 – 11/2015      Master's degree in chemistry at the Friedrich-Schiller-Universität, Jena  
Thesis title: Tochilinite in der primordialen Chemie.
- 10/2008 – 03/2012      Bachelor's degree in chemistry at the Technische Universität Darmstadt  
Thesis title: Schlagzähe Polyphthalamide aus Flaschen-PET.